frontiers | Research Topics

Fungal genetics in plant biomass conversion

Edited by
Jiwei Zhang, Guodong Liu and Yu Fukasawa

Published in
Frontiers in Microbiology

ISSN 1664-8714
ISBN 978-2-83251-504-4
DOI 10.3389/978-2-83251-504-4

About Frontiers

Frontiers is more than just an open access publisher of scholarly articles: it is a pioneering approach to the world of academia, radically improving the way scholarly research is managed. The grand vision of Frontiers is a world where all people have an equal opportunity to seek, share and generate knowledge. Frontiers provides immediate and permanent online open access to all its publications, but this alone is not enough to realize our grand goals.

Frontiers journal series

The Frontiers journal series is a multi-tier and interdisciplinary set of open-access, online journals, promising a paradigm shift from the current review, selection and dissemination processes in academic publishing. All Frontiers journals are driven by researchers for researchers; therefore, they constitute a service to the scholarly community. At the same time, the *Frontiers journal series* operates on a revolutionary invention, the tiered publishing system, initially addressing specific communities of scholars, and gradually climbing up to broader public understanding, thus serving the interests of the lay society, too.

Dedication to quality

Each Frontiers article is a landmark of the highest quality, thanks to genuinely collaborative interactions between authors and review editors, who include some of the world's best academicians. Research must be certified by peers before entering a stream of knowledge that may eventually reach the public - and shape society; therefore, Frontiers only applies the most rigorous and unbiased reviews. Frontiers revolutionizes research publishing by freely delivering the most outstanding research, evaluated with no bias from both the academic and social point of view. By applying the most advanced information technologies, Frontiers is catapulting scholarly publishing into a new generation.

What are Frontiers Research Topics?

Frontiers Research Topics are very popular trademarks of the *Frontiers journals series*: they are collections of at least ten articles, all centered on a particular subject. With their unique mix of varied contributions from Original Research to Review Articles, Frontiers Research Topics unify the most influential researchers, the latest key findings and historical advances in a hot research area.

Find out more on how to host your own Frontiers Research Topic or contribute to one as an author by contacting the Frontiers editorial office: frontiersin.org/about/contact

Fungal genetics in plant biomass conversion

Topic editors

Jiwei Zhang — University of Minnesota Twin Cities, United States
Guodong Liu — Shandong University, China
Yu Fukasawa — Tohoku University, Japan

Citation

Zhang, J., Liu, G., Fukasawa, Y., eds. (2023). *Fungal genetics in plant biomass conversion*. Lausanne: Frontiers Media SA. doi: 10.3389/978-2-83251-504-4

Table of contents

frontiers in Microbiology

EDITORIAL
published: 25 March 2022
doi: 10.3389/fmicb.2022.875768

Editorial: Fungal Genetics in Plant Biomass Conversion

Jiwei Zhang[1]*, *Guodong Liu*[2] and *Yu Fukasawa*[3]

[1] Department of Bioproducts and Biosystems Engineering, University of Minnesota, Saint Paul, MN, United States, [2] State Key Laboratory for Microbial Technology, Shandong University, Qingdao, China, [3] Graduate School of Agricultural Sciences, Tohoku University, Miyagi, Japan

Keywords: fungi, gene regulation, plant biomass degradation, genetic mechanisms, fungal metabolism

Editorial on the Research Topic

Fungal Genetics in Plant Biomass Conversion

INTRODUCTION

Fungi in nature evolved distinctive capacities to deconstruct lignocellulose of plant biomass and dominate the carbon turnover process in terrestrial systems. Much of the net carbon sequestered by photosynthesis in land plants (5.6×10^{13} kg C/year) passes through fungi (Gilbertson and Ryvarden, 1987; Berbee et al., 2020). With plants as the reliable carbon and energy sources, lignocellulose-degrading fungi have evolved to survive in highly variable land environments and have become prevalent across the fungal kingdom, primarily in ascomycete and basidiomycete phyla (Kubicek et al., 2014; Rytioja et al., 2014). These fungi are seen as important for maintaining the sustainable ecosystem on our planet, and using them to convert plant biomass for producing advanced biofuels and bioproducts has been deemed as one of the most promising solutions to mitigate anthropogenic issues such as the climate change caused by the extensive use of fossil fuels (Kubicek, 2013).

Fungi use a complex lignocellulose-degrading system including several enzymes most of which are cataloged in the CAZy database (Carbohydrate-Active enZymes; http://www.cazy.org/) to degrade lignocellulose (Lombard et al., 2014). The composition of CAZyme repertories in different fungal species is usually shaped by the lifestyle that allows fungi to adapt to different environments and lignocellulose substrates. On the other hand, to deal with variable biotic (e.g., cooperative and competitive microbes) and abiotic (e.g., C and N source, pH, and light) factors, fungi have also evolved a sophisticated regulatory system to control the synthesis and secretion of these CAZymes precisely (Glass et al., 2013; Kubicek et al., 2014). Regarding this, probing the CAZyme encoding gene resources and dissecting the regulation of these genes are two main aspects of research toward understanding the genetic basis of lignocellulose-degrading fungi. The fast development of systems biology and genetic approaches has dramatically facilitated this research (Floudas et al., 2012; Miyauchi et al., 2020), and it is providing invaluable fundamental knowledge that is transformative for industrial biomass conversion and environmental sustainability.

AIMS AND OBJECTIVES

In this topic, we aim to report the most recent progress related to genetic mechanisms of plant biomass degradation by fungi. This includes original research articles that use traditional genetics and functional genomics to study these fungal mechanisms. With this topic platform, we intend to discuss the current state of: (1) the discovery of crucial plant biomass-converting genetic resources

OPEN ACCESS

Edited and reviewed by:
Daniela Minerdi,
University of Turin, Italy

***Correspondence:**
Jiwei Zhang
zhan3437@umn.edu

Specialty section:
This article was submitted to Fungi and Their Interactions, a section of the journal Frontiers in Microbiology

Received: *14 February 2022*
Accepted: *04 March 2022*
Published: *25 March 2022*

Citation:
Zhang J, Liu G and Fukasawa Y (2022) Editorial: Fungal Genetics in Plant Biomass Conversion. Front. Microbiol. 13:875768. doi: 10.3389/fmicb.2022.875768

by leveraging systems biology approaches and (2) the dissection of the pathways controlling the fungal degradation of plant biomass in pure cultures and during species' interactions.

SIGNIFICANT FINDINGS IN THIS TOPIC

Discovery of genetic resources includes identifying the key pathways involved in fungal interactions during lignocellulose degradation. Interspecies interactions between fungal mycelia affect the degradation process of woody materials as it alters not only fungal community but also fungal physiological activities (Fukasawa et al., 2020). Previous studies have reported elevated CO_2 emissions and oxidase activities in interacting mycelia, leading to a prediction that fungal interaction may activate the degradation of organic matter (Fukasawa et al., 2020). However, measuring the weight loss of wood substrates during fungal competition has been generating discrepancies, begging research for further exploring how fungal interactions would influence lignocellulose-degrading pathways (Fukasawa et al., 2020). In this topic, using multi-omics, Presley et al. explain why the increased enzyme activities are not causing wood degradation during mycelial interaction of two brown rot species. In their study, they found that the secreted enzymes in the interaction zone are dominated by enzymes for fungal cell wall digestion and secondary metabolite production, while plant cell wall-digesting enzymes are mainly found under non-interacting conditions. Given that the fungal decay types are a continuum rather than segregated, as indicated by another paper in this topic (Schilling et al.), it would be helpful to test alternative interactions between fungi with variable decay types to further look at these key lignocellulose-degrading pathways.

Given the extraordinary capacities in degrading recalcitrant wood structures, wood decay fungi were thought of as the natural microbial resource harboring efficient lignocellulose-degrading pathways (Gilbertson and Ryvarden, 1987; Floudas et al., 2012; Miyauchi et al., 2020). To elucidate these in more detail, Kölle et al. compared the genomic sequences of two strains of the brown rot fungus *Rhodonia placenta* with different wood decay rates, and they identified a set of genes and mutations that might contribute to the phenotypic differences. Moreover, using a co-expression gene network, Zhu et al. found a lytic polysaccharide monooxygenase that can cooperate with the oxidative reagents during brown rot.

Fungi from unique environments also harbor valuable lignocellulose-degrading enzymes. Here, Li et al. report 16 cellulolytic fungal species isolated from the unique geographic and climatic environments in the Qinghai-Tibet Plateau. Using comparative transcriptomics, they identified the key mechanism of cellulase production in one of the promising cellulase producers—*Trichoderma harzianum* LZ117. By studying the secretome of the thermophilic fungus *Chaetomium thermophilum*, Jiang et al. found a superior cellobiohydrolase I (CBHI) with higher activity and increased temperature stability compared to *T. reesei* CBHI. From Austrian soils, Hinterdobler et al. isolated 12 new *T. reesei* strains that are highly genetically variable and that produce higher levels of cellulase and xylanase. After SNP verification, the authors propose that their new isolates are unique to European temperate environments and that these would provide biotechnological potential for example for non-GMO strain improvement by species crossing.

The expression of genes encoding lignocellulose-degrading enzymes in filamentous fungi is controlled by complex gene regulatory networks involving transcription factors and protein kinases. These regulators also affect many other cellular metabolic processes, known as cross-pathway regulation (Glass et al., 2013; Kubicek et al., 2014; Rytioja et al., 2014). In this Research Topic, three regulators related to lignocellulose degradation were studied by genetic approaches. Among these, Zhang et al. identified a novel transcription factor in *Talaromyces pinophilus* that negatively regulates the expression of amylolytic and (hemi-)cellulolytic enzyme encoding genes. It was found that the deletion of this regulator also resulted in a reduction in conidiation. In the cellulase producing workhorse *T. reesei*, Beier et al. report the regulatory functions of a putative kinase, USK1, and found that it is required for normal production of both cellulases and a set of secondary metabolites. By a similar approach, but in *Podospora anserina*, Li et al. describe the pleiotropic functions of a conserved kinase, SNF1, in positively regulating the production of cellulases but negatively affecting sterigmatocystin synthesis. These findings highlight the importance of regulatory pathways in fungal degradation of lignocellulose, and also point into an interesting future direction to dissect the regulation balance between primary and secondary metabolism during lignocellulose degradation.

CONCLUSION

The findings reported in this Research Topic are expanding our understanding of fungal mechanisms involved in lignocellulose degradation. We expect these to advance relevant ecological and genetic engineering research and to create effective solutions to current environmental and sustainability challenges.

AUTHOR CONTRIBUTIONS

All authors listed have made a substantial, direct, and intellectual contribution to the work and approved it for publication.

REFERENCES

Berbee, M. L., Strullu-Derrien, C., Delaux, P. M., Strother, P. K., Kenrick, P., Selosse, M.-A., et al. (2020). Genomic and fossil windows into the secret lives of the most ancient fungi. *Nat. Rev. Microbiol.* 18, 717–730. doi: 10.1038/s41579-020-0426-8

Floudas, D., Binder, M., Riley, R., Barry, K., Blanchette, R. A., Henrissat, B., et al. (2012). The Paleozoic origin of enzymatic lignin decomposition reconstructed from 31 fungal genomes. *Science* 336, 1715–1719. doi: 10.1126/science.1221748

Fukasawa, Y., Gilmartin, E. C., Savoury, M., and Boddy, L. (2020). Inoculum volume effects on competitive outcome and wood decay

rate of brown- and white-rot basidiomycetes. *Fungal Ecol.* 45, 100938. doi: 10.1016/j.funeco.2020.100938

Gilbertson, R. L., and Ryvarden, L. (1987). North American Polypores. Volume 1: abortiporus–lindtneria. 433 S., 209 Abb. Oslo 1986. Fungiflora A/S. *J. Basic Microbiol.* 27, 282. doi: 10.1002/jobm.3620270513

Glass, N. L., Schmoll, M., Cate, J. H. D., and Coradetti, S. (2013). Plant cell wall deconstruction by ascomycete fungi. *Annu. Rev. Microbiol.* 67, 477–498. doi: 10.1146/annurev-micro-092611-150044

Kubicek, C. P. (2013). *Fungi and Lignocellulosic Biomass*. Hoboken, NJ: John Wiley and Sons, Inc.

Kubicek, C. P., Starr, T. L., and Glass, N. L. (2014). Plant cell wall-degrading enzymes and their secretion in plant-pathogenic fungi. *Annu. Rev. Phytopathol.* 52, 427–451. doi: 10.1146/annurev-phyto-102313-045831

Lombard, V., Golaconda Ramulu, H., Drula, E., Coutinho, P. M., and Henrissat, B. (2014). The Carbohydrate-active enzymes database (CAZy) in 2013. *Nucleic Acids Res.* 42, 490–495. doi: 10.1093/nar/gkt 1178

Miyauchi, S., Kiss, E., Kuo, A., Drula, E., Kohler, A., Sánchez-García, M., et al. (2020). Large-scale genome sequencing of mycorrhizal fungi provides insights into the early evolution of symbiotic traits. *Nat. Commun.* 11, 5125. doi: 10.1038/s41467-020-1 8795-w

Rytioja, J., Hildén, K., Yuzon, J., Hatakka, A., de Vries, R. P., and Mäkelä, M. R. (2014). Plant-polysaccharide-degrading enzymes from Basidiomycetes. *Microbiol. Mol. Biol. Rev.* 78, 614–649. doi: 10.1128/MMBR.00035-14

Conflict of Interest: The authors declare that the research was conducted in the absence of any commercial or financial relationships that could be construed as a potential conflict of interest.

Publisher's Note: All claims expressed in this article are solely those of the authors and do not necessarily represent those of their affiliated organizations, or those of the publisher, the editors and the reviewers. Any product that may be evaluated in this article, or claim that may be made by its manufacturer, is not guaranteed or endorsed by the publisher.

frontiers in Microbiology

ORIGINAL RESEARCH
published: 13 December 2019
doi: 10.3389/fmicb.2019.02875

Identification of a Novel Transcription Factor TP05746 Involved in Regulating the Production of Plant-Biomass-Degrading Enzymes in *Talaromyces pinophilus*

Ting Zhang, Lu-Sheng Liao, Cheng-Xi Li, Gui-Yan Liao, Xiong Lin, Xue-Mei Luo, Shuai Zhao and Jia-Xun Feng**

State Key Laboratory for Conservation and Utilization of Subtropical Agro-Bioresources, Guangxi Research Center for Microbial and Enzyme Engineering Technology, College of Life Science and Technology, Guangxi University, Nanning, China

OPEN ACCESS

Edited by:
Guodong Liu,
Shandong University, China

Reviewed by:
Weixin Zhang,
Shandong University, China
Guangshan Yao,
Minjiang University, China

***Correspondence:**
Shuai Zhao
shuaizhao0227@gxu.edu.cn
Jia-Xun Feng
jiaxunfeng@sohu.com

Specialty section:
This article was submitted to Fungi and Their Interactions, a section of the journal Frontiers in Microbiology

Received: *04 October 2019*
Accepted: *28 November 2019*
Published: *13 December 2019*

Citation:
Zhang T, Liao L-S, Li C-X, Liao G-Y, Lin X, Luo X-M, Zhao S and Feng J-X (2019) Identification of a Novel Transcription Factor TP05746 Involved in Regulating the Production of Plant-Biomass-Degrading Enzymes in Talaromyces pinophilus. Front. Microbiol. 10:2875. doi: 10.3389/fmicb.2019.02875

Limited information on transcription factor (TF)-mediated regulation exists for most filamentous fungi, specifically for regulation of the production of plant-biomass-degrading enzymes (PBDEs). The filamentous fungus, *Talaromyces pinophilus,* can secrete integrative cellulolytic and amylolytic enzymes, suggesting a promising application in biotechnology. In the present study, the regulatory roles of a Zn2Cys6 protein, TP05746, were investigated in *T. pinophilus* through the use of biochemical, microbiological and omics techniques. Deletion of the gene *TP05746* in *T. pinophilus* led to a 149.6% increase in soluble-starch-degrading enzyme (SSDE) production at day one of soluble starch induction but an approximately 30% decrease at days 2 to 4 compared with the parental strain Δ*TpKu70*. In contrast, the *T. pinophilus* mutant Δ*TP05746* exhibited a 136.8–240.0% increase in raw-starch-degrading enzyme (RSDE) production, as well as a 90.3 to 519.1% increase in cellulase and xylanase production following induction by culturing on wheat bran plus Avicel, relative to that exhibited by Δ*TpKu70*. Additionally, the mutant Δ*TP05746* exhibited accelerated mycelial growth at the early stage of cultivation and decreased conidiation. Transcriptomic profiling and real-time quantitative reverse transcription-PCR (RT-qPCR) analyses revealed that TP05746 dynamically regulated the expression of genes encoding major PBDEs and their regulatory genes, as well as fungal development-regulated genes. Furthermore, *in vitro* binding experiments confirmed that TP05746 bound to the promoter regions of the genes described above. These results will contribute to our understanding of the regulatory mechanism of PBDE genes and provide a promising target for genetic engineering for improved PBDE production in filamentous fungi.

Keywords: transcription factor, plant-biomass-degrading enzymes, mycelial development, conidiation, *Talaromyces pinophilus*

INTRODUCTION

Soil filamentous fungi play crucial roles in terrestrial carbon cycling because they can decay organic matter, including plant biomass (Gougoulias et al., 2014) via secretion of plant-biomass-degrading enzymes (PBDEs), such as cellulase, hemicellulose, and amylase (Bornscheuer et al., 2014). Most of the PBDEs are produced in nature by *Trichoderma*, *Penicillium* and *Aspergillus,* but they generate only low yields (Passos et al., 2018). Therefore, genetic improvement of natural fungal producers such as enzymes needs to be further explored, with an aim of developing strains capable of high production of PBDEs.

In the enzyme market, cellulases and amylases account for the majority of PBDEs. Cellulases are the complexes comprising cellobiohydrolases (EC 3.2.1.91; CBHs), endo-β-1,4-glucanases (EC 3.2.1.4; EGs), and β-1,4-glucosidases (EC 3.2.1.21; BGLs)[1]. Synergistic action among these enzymes is required for cellulose hydrolysis into glucose. During the process, EGs randomly break internal β-1,4-glycosidic bonds in glucan chains to release glucooligosaccharides, resulting in new chain ends. CBHs act on both ends of glucooligosaccharide chains to produce mainly cellobiose. Both soluble glucooligosaccharide and cellobiose are hydrolyzed by BGLs to yield glucose (Bornscheuer et al., 2014).

Comparably, amylases are classified broadly into glucoamylases (EC 3.2.1.3; GLAs), α-amylases (EC 3.2.1.1; AMYs), α-glucosidases (EC 3.2.1.20; AGAs) and 1,4-α-glucan-branching enzymes (EC 2.4.1.18) according to the action principle (see text footnote 1). Among them, GLAs attack α-1,4- or α-1,6-glucosidic bonds at the non-reducing ends of starch chains to release glucose, while AMYs break internal α-1,4-glycosidic bonds of starch chains to generate straight and branched oligosaccharides or maltose. AGAs digest maltose into glucose (Marín-Navarro and Polaina, 2011). Moreover, amylolytic enzymes can show activity toward soluble starch, known as soluble starch-degrading enzymes (SSDEs). Some amylolytic enzymes, known as raw starch-degrading enzymes (RSDEs), can directly hydrolyze raw starch granules below the starch gelatinization temperature (Sun et al., 2010). SSDEs are commonly used for conventional starch processing, including two-step liquefaction and saccharification. During liquefaction, raw starch is first gelatinized at a high temperature (95–105°C) and then liquefied into dextrin via the thermophilic AMYs. Subsequently, GLAs are applied in the saccharification step to hydrolyze the cooled dextrin into glucose at 60–65°C (Sánchez and Cardona, 2008; Görgens et al., 2015). However, the conventional liquefaction step requires high energy input and extra equipment, resulting in a high cost of the starch-derived products.

RSDEs contain the specific starch-binding domain (SBD) that enables them to bind onto the surface of raw starch granules (Sorimachi et al., 1997; Machovic and Janecek, 2006; Xu et al., 2016). RSDE application can reduce the process cost since the liquefaction step would not be needed (Sun et al., 2010; Lee et al., 2012). It was estimated that the application of RSDE in ethanol production, using starch as feedstock, could reduce the fuel cost of the total ethanol product by about 10–20% (Robertson et al., 2006).

Genetic engineering of fungal strains, based on the regulatory network of transcription factors (TFs) and their target genes, is an efficient strategy by which to improve functional enzyme yields. TFs are proteins that control transcription of target genes through binding to specific DNA sequence elements such as promoters, enhancers, etc. TF-mediated transcriptional control is a central regulatory mechanism in all eukaryotic organisms (Weirauch and Hughes, 2011). More than 90 types of TFs in eukaryotes have been identified, including zinc finger (Zn2Cys6, C2H2, GATA, CCHC, DHHC, etc.), helix-turn-helix (HTH), basic leucine zipper (bZIP), APSES and winged helix repressor DNA-binding domain (Weirauch and Hughes, 2011; Carrillo et al., 2017). The regulatory roles of individual TFs vary under different conditions.

Transcriptional expression of genes encoding PBDEs is strictly controlled by specific TFs in filamentous fungi. Since XlnR was first identified to be involved in regulating the expression of genes encoding enzymes involved in degrading plant cell walls in *Aspergillus* (van Peij et al., 1998), several TFs have been found to be expressed in the presence of recalcitrant carbon sources, such as the key activators CLR-2 (Coradetti et al., 2012; Zhao et al., 2016), AmyR (Li et al., 2015), and PoxCxrA (Yan et al., 2017). Among them, CLR-2 and PoxCxrA encode Gal4-like Zn2Cys6 proteins, and play essential roles in the regulation of fungal cellulase gene expression in the presence of cellulose. In *Neurospora crassa*, the expression of *clr-2* is induced by the TF CLR-1 (Coradetti et al., 2012), while it is induced by PoxCxrA in *Penicillium oxalicum* (Liao et al., 2019). The CLR-1 homolog ClrA is less involved in the regulation of cellulase gene expression in *P. oxalicum* (Liao et al., 2019), as well as in *Aspergillus nidulans* (Coradetti et al., 2012; Tani et al., 2014).

The Zn2Cys6 proteins AmyR and/or COL-26 are necessary for amylolytic gene expression in filamentous fungi such as *P. oxalicum*, *N. crassa*, *T. pinophilus*, *Aspergillus* spp., and are required for starch and maltose utilization (Li et al., 2015; Xiong et al., 2017; Zhang et al., 2017). Additionally, AmyR inhibits the expression of cellulase genes and its expression is regulated by *ClrB* in *P. oxalicum* (Li et al., 2015). COL-26 regulates cellulase gene expression and enzyme production, synergistically functioning with the carbon catabolite repressor, CRE-1 (Xiong et al., 2014).

CRE-1 mediates carbon catabolite repression (CCR) that represses cellulase gene expression in the presence of favorable carbon source such as glucose. CRE-1 could directly bind to the promoter regions of major cellulase and xylanase genes and their regulatory genes, such as *clr-2*, resulting in reduction of enzyme yields (Li et al., 2015; Huberman et al., 2016).

The soil fungus *T. pinophilus*, formerly called *Penicillium pinophilus*, produces useful PBDEs such as α-amylase, glucoamylase, cellulase, xylanase, and laccase (Pol et al., 2012; Visser et al., 2013; Kusum et al., 2014; Xian et al., 2015) and medical metabolites such as 3-*O*-methylfunicone and talaromycolides 1–3, 5, and 11. The metabolite 3-*O*-methylfunicone is able to repress mesothelioma cell motility,

[1]http://www.cazy.org/

while talaromycolide kills human-pathogenic methicillin-resistant *Staphylococcus aureus* (Buommino et al., 2012; Zhai et al., 2015). *T. pinophilus* strain 1–95 was isolated in China (Xian et al., 2015), and shown to produce several PBDEs (Li et al., 2017), albeit at low yields.

Comparative transcriptomic profiling and genetic analyses of *T. pinophilus* strain 1–95 identified seven novel regulatory genes that regulate SSDE production. Among them, TpRfx1 (TP06128), positively regulated SSDE production of *T. pinophilus* via binding to the promoter regions of major amylase genes (Liao et al., 2018). Intriguingly, deletion of another candidate regulatory gene *TP05746,* encoding a Zn2Cys6 protein, resulted in a 51.4% increase in SSDE production, compared with the parental strain Δ*TpKu70* when cultured directly on medium containing soluble corn starch (SCS) for 5 days (Liao et al., 2018), but its detailed biological roles are unknown.

In this study, we found that *TP05746* regulated the production of various PBDEs including SSDE, RSDE, cellulase and xylanase of *T. pinophilus*, as well as mycelial growth and conidiation. Experiments further confirmed that TP05746 could bind to the promoter regions of major PBDE genes and their key regulatory genes, and to growth- and development-associated regulatory genes.

MATERIALS AND METHODS

Fungal Strains and Culture Conditions

Talaromyces pinophilus wild-type strain 1–95 (#2645, China General Microbiological Culture Collection, Beijing, China; CGMCC) was isolated from a dry ploughed field in China (Xian et al., 2015). Deletion mutants Δ*TpKu70* and Δ*TP05746* were constructed by knocking out the *TpKu70* gene in strain 1–95 and the *TP05746* gene in Δ*TpKu70*, respectively (Zhang et al., 2017; Liao et al., 2018). The Δ*TpKu70* has no apparent difference in vegetative growth and enzyme production when compared with wild-type strain 1–95 (Zhang et al., 2017). All *T. pinophilus* strains were maintained on potato-dextrose agar (PDA) plates at 4°C or stored in 25% glycerol at -80°C. Cultivation of *Penicillium oxalicum* strains was consistent with the *T. pinophillus* strains. Mutant Δ*PoxKu70* (#3.15650, CGMCC) was derived from the wild-type HP7-1 via deleting gene *PoxKu70* (Zhao et al., 2016).

Asexual spores (conidia) were collected from fungal cells cultured on PDA plates at 28°C for 6 days, resuspended in aqueous 0.2% (v/v) Tween-80, and adjusted to a concentration of 1×10^8 spores mL^{-1}. For mycelial growth for DNA extraction, the fungus was cultured on liquid complete medium (LCM; Liao et al., 2018). Culture conditions for enzyme activity analysis, RNA sequencing, and real-time quantitative reverse transcription-PCR (RT-qPCR) analysis were as described previously (Liao et al., 2018). For RNA sequencing, total RNA was extracted from mycelium harvested after 12-h culture following transfer from glucose into medium containing 1% (w/v) soluble corn starch (SCS; Sigma-Aldrich, St. Louis, MO, United States).

For mycelial growth and observation by light microscopy, standard liquid medium (SLM; Liao et al., 2018) containing 1% (w/v) D-glucose, 1% (w/v) SCS, 2% (w/v) wheat bran plus Avicel [WA; wheat bran: Avicel = 1: 1; (w/w); Sigma-Aldrich, St.] or 2% (w/v) Avicel and/or 0.2% (w/v) 2-deoxy-glucose (2-DG) was inoculated with *T. pinophilus* spores and cultured at 28°C for 12 to 120 h. For phenotypic analyses, 1% (w/v) D-glucose, 1% (w/v) SCS or 2% (w/v) WA were added to solid low-salt minimal medium (LsMM) plates, with PDA being used as a positive control. For measurement of enzymatic activity, *P. oxalicum* strains were cultivated in Avicel medium according to the descried by Yan et al. (2017).

Extraction of Total DNA and RNA From *Talaromyces pinophilus*

Extraction of total DNA and RNA from mycelia of *T. pinophilus* strains was carried out by the method described previously (Yan et al., 2017) with some modifications. In brief, for total DNA extraction, the harvested mycelia were ground in liquid nitrogen and lysate reagent (pH 8.0) was added immediately at a ratio of 10:1 (v: w). Subsequently, an equal volume of a phenol-chloroform mixture was added to the extract to remove proteins, followed by centrifuging at 11,300 × *g* at 4°C for 10 min. Finally, DNA was precipitated using isopropanol at a ratio of 1:1 (v: v).

Total RNA was extracted using TRIzol RNA Kit (Life Technologies, Carlsbad, CA, United States), according to the manufacturer's instructions.

Southern Hybridization Analysis

The only one-site mutation in the mutant Δ*TP05746* was confirmed using Southern hybridization analysis, according to the protocols of the DIG (digoxigenin)-High Prime DNA Labeling & Detection Starter Kit (Life Technologies, Carlsbad, CA, United States). Briefly, genomic DNA from each of the Δ*TpKu70* and the Δ*TP05746* mutants was extracted and digested by *Hin*dIII (TaKaRa Bio Inc., Dalian, China), and then transferred onto a Hybond-N^+ Nylon membrane (GE Healthcare Limited, Amersham, United Kingdom). PCR was used to amplify the hybridization probe, using a specific primer pair TP05746-T-F/TP05746-T-R (**Supplementary Table S1**).

Measurement of PBDE Production and Intracellular Protein Concentration Assays

Plant-biomass-degrading enzymes activities, including SSDE, raw starch-digesting enzymes (RSDE), cellulase and xylanase activities, were assayed as previously described (Liao et al., 2018; Zhang et al., 2019). Briefly, 50 μL of appropriately diluted crude extract produced from the parental strain Δ*TpKu70* or its deletion mutant Δ*TP05746*, were added to 450 μL of 100 mM citrate-phosphate buffer (pH 5.0) containing 1% SCS (Sigma-Aldrich), 1% raw cassava flour (farmer's market, Nanning, China), 1% CMC-Na (Sigma-Aldrich, Darmstadt, Germany), or 1% beechwood xylan (Megazyme International Ireland, Bray, Ireland), and 1 mL of 100 mM citrate-phosphate buffer pH 5.0, containing Whatman No. 1 filter paper (50 mg, 1.0 cm × 6.0 cm; GE Healthcare Limited, Little Chalfont, United Kingdom). The mixture was incubated at 50–60°C for 10–60 min. The reducing

sugars released were determined using the 3,5-dinitrosalicyclic acid method, measuring A_{540} (Miller, 1959). One unit of enzymatic activity (U) was defined as the required amount of enzyme required to produce 1 μmol reducing sugar per minute from the reaction substrates.

The substrates *p*-nitrophenyl-β-D-cellobioside (pNPC) and *p*-nitrophenyl-β-D-glucopyranoside (pNPG) (both from Sigma-Aldrich) were used for measurement of pNPCase and pNPGase activities, respectively. An aliquot (10 μL or 68 μL) of appropriately diluted crude extract from Δ*TpKu70* or Δ*TP05746*, was added into 130 or 72 μL of a mixture containing 14 μL 25 mM pNPG or pNPC, and incubated at 50°C for 15 min. Sodium carbonate (70 μL, 0.4 M) was added to stop the reaction. The *p*-nitrophenol liberated was measured at wavelength of 410 nm, with one unit of enzymatic activity (U) being defined as the amount of enzyme that produced 1 μmol of *p*-nitrophenol per minute from an appropriate substrate. All the assays were performed in three biological replicates.

Protein concentration in extracts of *T. pinophilus* strains was measured using the Bradford assay kit (Pierce Biotechnology, Rockford, IL, United States).

Determination of Mycelial Dry Weight

Mycelial dry weight of *T. pinophilus* strains cultured in SLM containing 1% D-glucose or 1% SCS as the sole carbon source was determined gravimetrically as previously described (Liao et al., 2018). In brief, 1.0×10^8 fresh spores were inoculated into 100 mL of the above medium and shake-cultured at 28°C and 180 rpm for 12 to 84 h. The hyphae were harvested by vacuum suction filtration every 12 h and then dried at 50°C to a constant weight. All the assays were performed in three biological replicates and the mean ± SD of the three replicates is presented.

Light Microscopy Observation

Light microscopy observation of *T. pinophilus* mycelia was performed according to previously described methods (Xiong et al., 2018). The harvested hyphae from *T. pinophilus* strains grown on SLM containing 1% D-glucose, 1% SCS, or 2% WA for 12–36 h was transferred onto microscope slides. The slides were observed under a light microscope (OLYMPUS DP480; Olympus, Tokyo, Japan), and photomicrographs were analyzed using cellSence Dimension digital imaging software (Olympus).

Real-Time Quantitative Reverse Transcription-PCR (RT-qPCR) Analysis

The PrimeScript™ RT Reagent kit (TaKaRa Bio Inc.) was used to synthesize the first-strand cDNA from total RNA of mutant Δ*TpKu70* as the template, according to the manufacturer's instruction. The PCR reaction mixture (20 μL) was composed of 10 μL of SYBR Premix ExTaq II (TaKaRa Bio Inc), 1.6 μL of 10 μM each primer (**Supplementary Table S1**), 2.0 μL of first-strand cDNA and 6.4 μL of sterile water. All the reaction cycles were run as follows: initial denaturation for 3 min at 96°C, followed by 40 cycles of 10 s each at 96°C, and 60°C for 30 s. The fluorescence signals were observed at the end of each extension step at 80°C. The relative expression levels of the tested genes were calculated as described previously (Zhang et al., 2017).

RNA Sequencing

RNA sequencing of *T. pinophilus* strains was performed by BGI, Shenzhen, China, as described by He et al. (2018). A cDNA library was constructed with an average length of 100 bp for each sample and assessed using an Agilent 2100 Bioanalyzer (Agilent Technologies, Santa Clara, CA, United States) and an ABI StepOnePlus real-time PCR system (Applied Biosystems, Foster City, CA, United States), and then sequenced using an Illumina HiSeq 4000 system. Clean reads generated were mapped onto the genome of *T. pinophilus* strain 1–95 (Li et al., 2017) for functional annotation using BWA v0.7.10-r789 (Li and Durbin, 2009) and Bowtie2 v2.1.0 (Langmead and Salzberg, 2012). The gene expression levels (fragments per kilobase of exon per million mapped reads, FPKM) and differentially expressed genes (DEGs) were calculated and screened for, using the software RAEM v1.2.12 (Li and Dewey, 2011) and DESeq (Love et al., 2014), respectively. Genes with $|\log2(\Delta TP05746\_FPKM/\Delta TpKu70\_FPKM)| \geq 1$ and p-value ≤ 0.05 were defined as DEGs.

Overexpression of Gene *TP05746* in *Penicillium oxalicum*

Overexpression of gene *TP05746* was performed in filamentous fungus *P. oxalicum* according to the method for complementary strain construction described by Yan et al. (2017). Briefly, the overexpression cassette comprised of four fragments including approximately 2 kb of left- and right-flanking sequences of gene *POX05007* encoding a aspartic protease (Wang et al., 2018), G418 resistance gene, and gene *TP05746* sequence with a strong promoter pPoxEgCel5B (Wang et al., 2018) and gene *TP05586* terminator, was constructed via fusion PCR. These fragments were amplified using PCR with specific primer pairs (**Supplementary Table S1**). The constructed overexpression cassette was introduced into the fresh protoplasts of the parental strain Δ*PoxKu70* based on the methods previously described (Zhao et al., 2016). The overexpressed transformants were isolated and confirmed via corresponding antibiotics G418 and hygromycin, and PCR with specific confirmation primers (**Supplementary Table S1**).

Recombinant Expression of DNA Fragment Encoding TP05746

A DNA fragment (1002 bp) of *TP05746* was amplified with PCR using primer pairs TP05746-F2/TP05746-R2 (**Supplementary Table S1**). The DNA fragment was cloned into vector pET32a (+) digested with *Sac*I, using ClonExpress® II One Step Cloning Kit (Vazyme Biotech, Nanjing, China). The recombinant plasmid pET32a-TP05746 was introduced into *E. coli* Trans-DE3 cells, and then induced with 0.5 mM isopropyl-beta-D-thiogalactopyranoside (IPTG) and cultured at 16°C for 24 h. The recombinant protein, rTP05746, labeled with Trx-His-S tags, was purified using Ni-nitrilotriacetic acid (Ni-NTA) resin. Trx-His-S fusion

protein and bovine serum albumin (BSA) were used as negative controls.

Electrophoretic Mobility Shift Assay

Electrophoretic mobility shift assay (EMSA) was performed as previously described (Yan et al., 2017). Briefly, DNA fragments approximately 1,000-bp upstream from the ATG start codons of the tested genes were amplified by PCR, using specific primers labeled with 6-carboxyfluorescein (FAM) at the 3′ terminus (**Supplementary Table S1**) as EMSA probes, and a 500-bp DNA sequence upstream from the ATG start codon of *TP10751* encoding β-tubulin (with a FAM label) was used as a control. DNA fragments of the same length but without the FAM label were used as competitive EMSA probes. Approximately 50 ng of DNA probes were mixed with 0, 0.5, 1.0, 1.5, or 2.0 μg of rTP05746 in 2 μL of binding buffer (Liao et al., 2018) and incubated at 25°C for 20 min. In each EMSA reaction, non-specific sheared salmon sperm DNA was added, in order to prevent non-specific binding between protein and probes. For the control, 2.0 μg of BSA or Trx-His-S fusion protein were used. For the competitive EMSA, 2.0 μg of rTP05746 were mixed with 50 ng of DNA probe with the FAM label and 250–2500 ng of competitive EMSA probes. DNA-protein complexes were separated by 4% polyacrylamide Tris–acetic acid–EDTA gel electrophoresis and detected with the Bio-Rad ChemiDoc^{TM} MP Imaging System (Bio-Rad Laboratories, Inc., Hercules, CA, United States) at 489–506 nm.

Phylogenetic Analysis

Proteins homologous to TP05746 were downloaded from NCBI website using BLASTP[2]. The neighbor-joining method and a Poisson correction model were used to construct a phylogenetic tree using software MEGA7.0 (Kumar et al., 2016), with 1000 replicates being used to calculate bootstrap values and gaps, and to handle missing data.

Statistical Analysis

All experimental data associated with enzyme production, intracellular protein concentration, counts by microscopy, gene transcription and biomass were statistically analyzed using Microsoft Excel (Office 2016; Microsoft, Redmond, WA, United States). Summary statistics presented are mean ± SD. Significance analyses ($p \leq 0.05$ or $p \leq 0.01$) among samples were performed using Student's *t* test.

Accession Numbers

The DNA sequence of *TP05746* is available from the GenBank database under accession number MH447996. The transcriptomic data of *T. pinophilus* strains have been deposited in Gene Expression Omnibus (GEO) on NCBI (accession No. GSE131872).

[2]https://blast.ncbi.nlm.nih.gov/Blast.cgi

RESULTS

TP05746 Regulates the Production of PBDEs in *Talaromyces pinophilus*

Previous work had initially found that a deletion mutant Δ*TP05746* of *T. pinophilus* showed a 51.4% increase in SSDE production, compared with the parental strain Δ*TpKu70* cultured directly in medium containing SCS as the sole carbon source (Liao et al., 2018). Protein TP05746, composed of 333 amino acids, contains a conserved Gal4-like domain, also known as a Zn2Cys6 zinc finger domain, at its C-terminus, as identified through NCBI BlastP query (**Figure 1A**). TP05746 shared 87% and 43% of identities with putative C6 transcription factor PMAA_081800 in *Talaromyces marneffei* ATCC 18224 (XP_002147682.1) and AN8177.2 in *Aspergillus nidulans* FGSC A4 (XP 022399897.1), respectively, with the coverage of 100% and 83%, respectively, whereas most of the aligned proteins were selected based on the conserved Zn2Cys6 zinc finger domain at the C-terminus. Additionally, phylogenetic analyses demonstrated that the TP05746 and its homologs were specific to *Talaromyces*, and phylogenetically close to those in the Ajellomycetaceae (**Figure 1B**).

Southern hybridization analysis was employed to confirm the identity of the mutant Δ*TP05746*. The results showed that an expected 6.3-kb band appeared in the transformants of Δ*TP05746*, compared with a 3.2-kb band for Δ*TpKu70* (**Supplementary Figure S1**), confirming that a *TP05746* deletion cassette inserted into only the one correct site in the fungal genome. PCR analysis also confirmed that the deletion cassette replaced the *TP05746* locus (Liao et al., 2018).

Talaromyces pinophilus mutant strain Δ*TP05746* and its parental strain Δ*TpKu70* were then precultured in glucose medium for 24 h, and the same amounts of mycelia were transferred into fresh SLM containing SCS as carbon source and cultured for 1–4 days. Enzyme activity tests indicated that Δ*TP05746* exhibited 149.6% higher SSDE production at day one of SCS induction but then 27.6–33.1% decrease at days 2–4, relative to that exhibited by Δ*TpKu70* ($p < 0.01$, Student's *t*-test; **Figure 2A**). Intriguingly, the RSDE production of Δ*TP05746* increased by 136.8–240.0% over the entire culture period ($p < 0.01$, Student's *t*-test; **Figure 2B**).

In addition to amylase production, cellulase and xylanase production of the Δ*TP05746* were also tested on WA for 2–4 days, using the parental strain Δ*TpKu70* as a control. The results indicated that the production of cellulase, including FPase, CMCase, pNPCase, pNPGase, and xylanase in Δ*TP05746* increased to various degrees, ranging from 90.1 to 519.1%, depending on the enzyme class, compared with those in Δ*TpKu70* ($p < 0.01$, Student's *t*-test; **Figures 2C–G**).

TP05746 Controls Conidiation of *Talaromyces pinophilus*

When both strains, Δ*TP05746* and Δ*TpKu70,* were inoculated onto solid LsMM containing D-glucose, SCS or WA, with PDA being used as a control, colony phenotypes were observed. As shown in **Figure 3A**, no significant difference was found in the

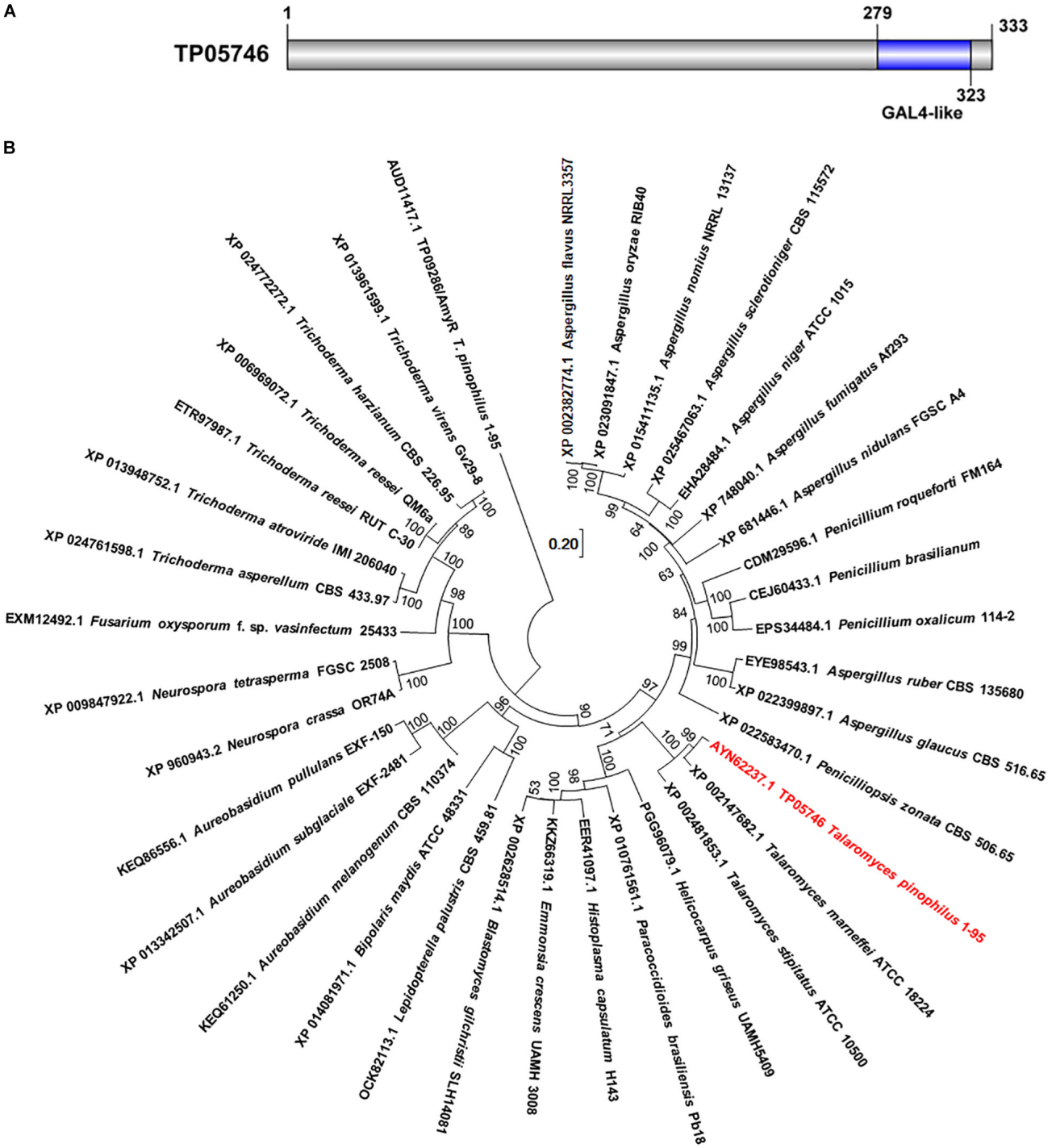

FIGURE 1 | Characterization of TP05746 from *Talaromyces pinophilus*. **(A)** Conserved domain in TP05746. **(B)** Phylogenetic analyses of TP05746 and its homologous proteins. The cladogram was constructed by software MEGA7 based on the neighbor-joining method and a Poisson correction model. Scale bar indicates branch lengths.

colony size between Δ*TP05746* and Δ*TpKu70* on any of the above-mentioned plates, while colony color of Δ*TP05746* was slightly different from that of Δ*TpKu70* on all plates.

Asexual spores (conidia) produced by Δ*TP05746* were then counted following inoculation onto WA plates, using the hemocytometer method (Christensen et al., 2012). The

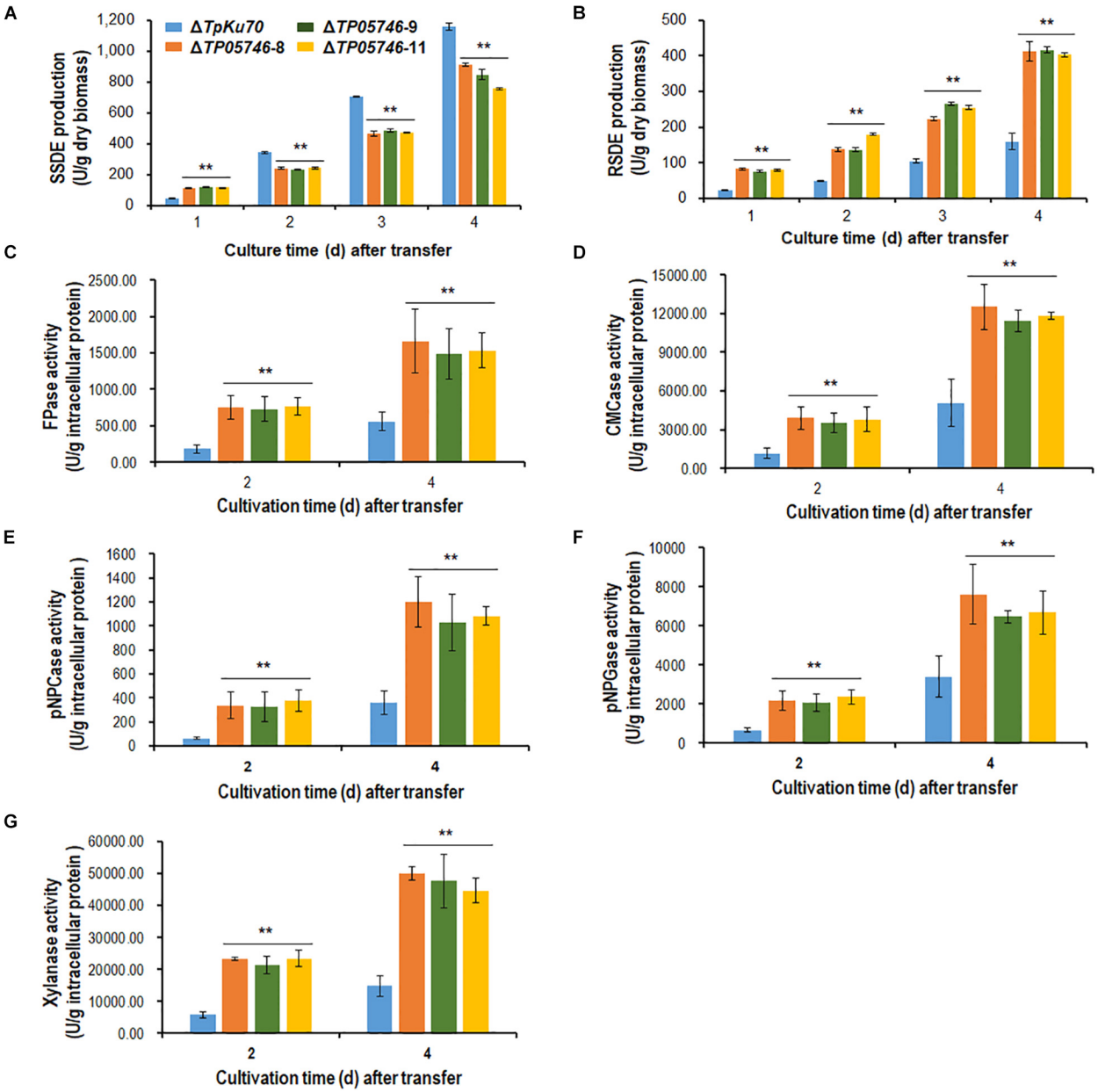

FIGURE 2 | Plant-biomass-degrading enzymes production by *T. pinophilus* mutant Δ*TP05746* and the parental strain Δ*TpKu70*. Crude extracts were produced from *T. pinophilus* strains cultured after a transfer from glucose medium to SCS medium **(A,B)** or WA medium **(C–G)** for 1–4 days. **(A)** SSDE production. **(B)** RSDE production. **(C)** FPase production. **(D)** CMCase production. **(E)** pNPCase production. **(F)** pNPGase production. **(G)** Xylanase production. All experiments were performed with three independent biological replicates. Each data point is mean ± SD. $^{**}p \leq 0.01$ indicates differences between the deletion mutant Δ*TP05746* and the parental strain Δ*TpKu70* by Student's *t*-test. PBDE, plant-biomass-degrading enzymes; SSDE, soluble-starch-degrading enzymes; SCS, soluble corn starch; RSDE, raw-starch-degrading enzymes; FPase, filter paper cellulase; CMCase, carboxymethylcellulase; pNPCase, *p*-nitrophenyl-β-cellobiosidase; pNPGase, *p*-nitrophenyl-β-glucopyranosidase.

results revealed that Δ*TP05746* produced 52.6–61.9% of ($p < 0.01$, Student's *t*-test) spores relative to Δ*TpKu70* at 4–6 days (**Figure 3B**).

As shown in **Figure 3C**, microscopic investigation showed that the mutant Δ*TP05746* exhibited delayed phialide development compared with the parental strain Δ*TpKu70* on WA-supplemented solid LsMM plates.

TP05746 Accelerates Growth of *Talaromyces pinophilus* at Early Stage of SCS or WA Induction but Delays Growth at Later Stages

To investigate whether *TP05746* affected the growth of *Talaromyces pinophilus*, real-time quantitative growth curves in

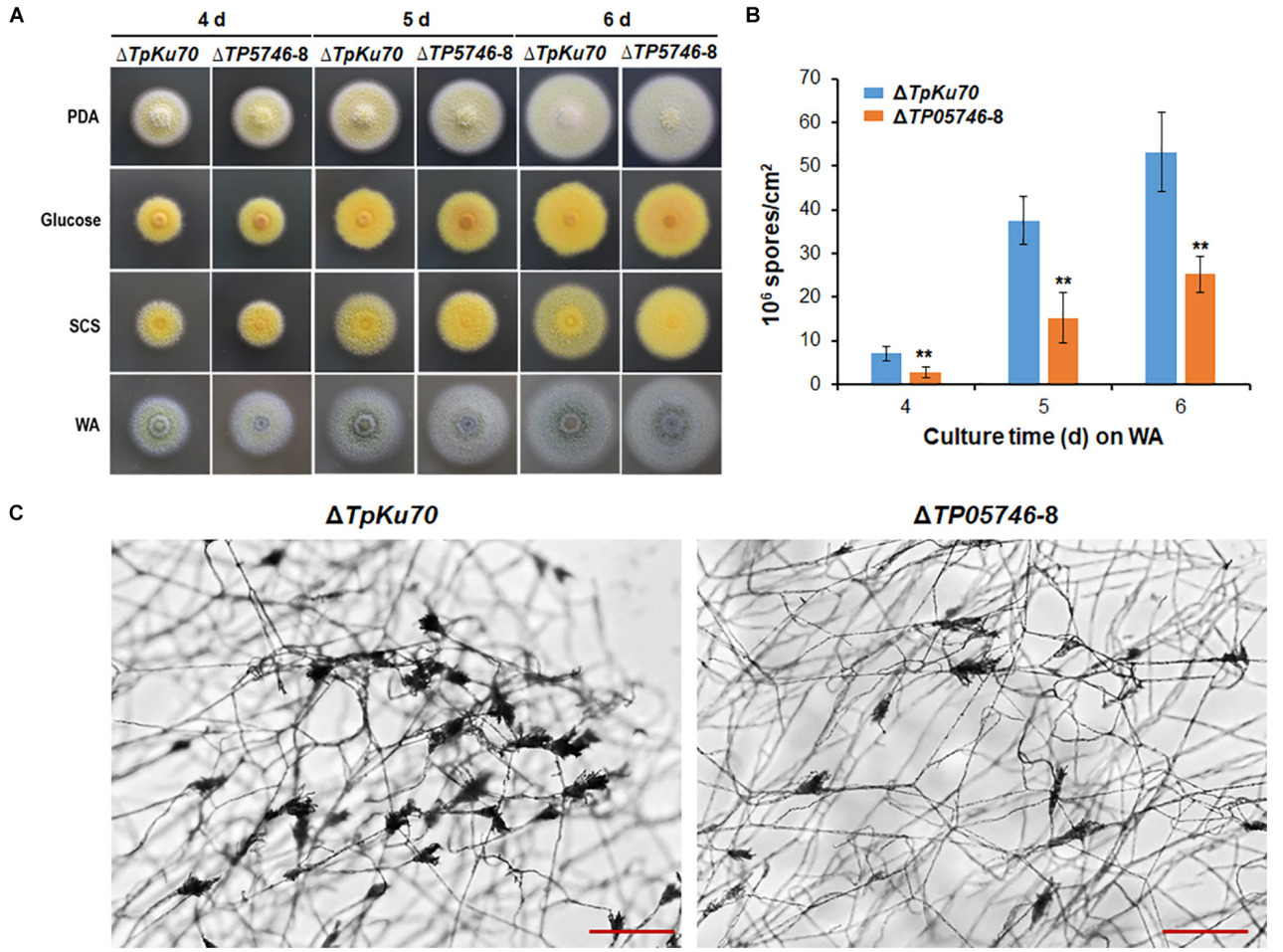

FIGURE 3 | Phenotypic analyses of *T. pinophilus* mutant Δ*TP05746* and the parental strain Δ*TpKu70*. **(A)** Colonies on solid LsMM plates containing glucose, SCS, or WA, with PDA being used for a positive control. Fungal strains were incubated at 28°C for 4–6 days. **(B)** Numbers of asexual spores on WA. Each data point is mean ± SD. $^{**}p < 0.01$ indicates differences between the Δ*TP05746* and parental strain Δ*TpKu70* by Student's *t* test. **(C)** Microscopic investigation of conidiophores. Fungal strains were cultivated on WA at 28°C for 36 h. The mutant Δ*TP05746* exhibited fewer phialides in comparison with the parental strain Δ*TpKu70*. LsMM, low-salt minimal medium; SCS, soluble corn starch; WA, wheat bran plus Avicel; PDA, potato dextrose agar.

the presence of glucose, SCS or WA of both Δ*TP05746* and Δ*TpKu70* were determined and then compared. The results revealed that Δ*TP05746* produced mycelial dry weights similar to Δ*TpKu70* in the glucose medium (**Figure 4A**). When using SCS or WA instead of glucose, however, Δ*TP05746* grew faster ($p < 0.01$, Student's *t*-test) than Δ*TpKu70* at the early induction period (i.e., 24–36 h for WA, and between 24–60 h for SCS) but the growth rate of Δ*TP05746,* compared with Δ*TpKu70*, fell sharply at the later stages ($p < 0.05$, Student's *t*-test; **Figures 4B,C**).

Further microscopic observations revealed that the mutant Δ*TP05746* exhibited significantly more hyphal branching when compared with the parental strain Δ*TpKu70* at 24 and 36 h in both liquid SCS and WA medium, although there was no significant difference at 12 h (**Figure 5**). Moreover, mycelial development of the Δ*TP05746* was the same as that of the Δ*TpKu70* when cultivated on liquid glucose medium (**Supplementary Figure S2**).

Transcriptomic Analyses Reveal That *TP05746* Regulates the Expression of Genes Encoding PBDEs and Their Regulators, and Hyphal Development-Associated Genes in *Talaromyces pinophilus*

The genome-wide mRNA abundance of both the parental strain Δ*TpKu70* and its mutant Δ*TP05746* were measured in cultures grown in SLM containing SCS as the sole carbon source for 12 h. Comparative transcriptomics identified 4429 differentially expressed genes (DEGs) in mutant Δ*TP05746*, using a $|\log2(\text{fold change})| \geq 1$ and *p*-value ≤ 0.05 as thresholds relative to expression in the parental strain Δ*TpKu70* (**Supplementary Table S2**). Among them, the transcripts of 2470 genes were up-regulated and 1959 were down-regulated. Kyoto Encyclopedia of Genes and Genomes (KEGG) annotation revealed that the DEGs were mainly involved in metabolism (47%), with the

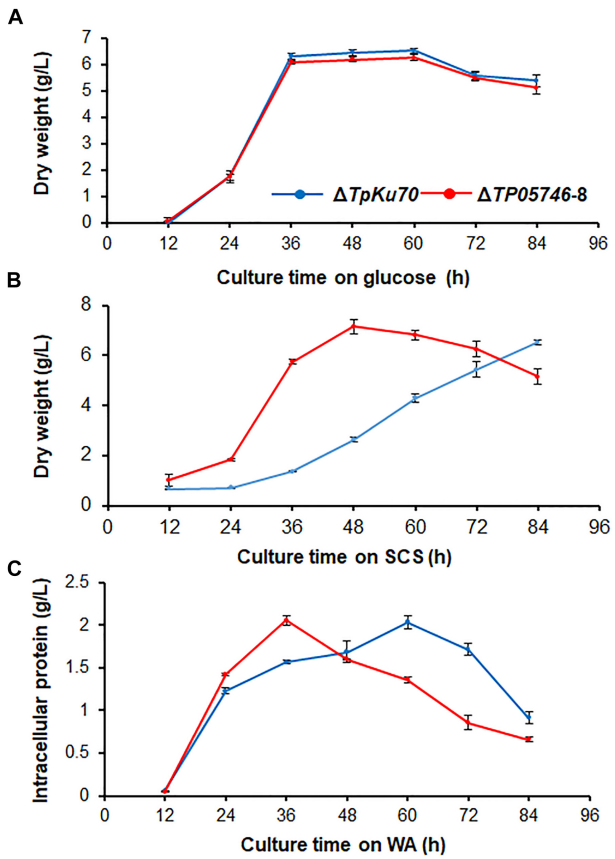

FIGURE 4 | Growth curves of *T. pinophilus* mutant Δ*TP05746* and the parental strain Δ*TpKu70* in SLM containing glucose **(A)**, SCS **(B)**, or WA **(C)** as the sole carbon source for 12–84 h at 28°C, respectively. Three independent experiments were performed as biological replicates. SLM, standard liquid medium; SCS, soluble corn starch; WA, wheat bran plus Avicel.

others being involved in human diseases (15%), organismal systems (15%), environmental information processing (8%), genetic information processing (8%), and cellular processes (7%) (**Figure 6A**). Moreover, the number of up-regulated genes involved in metabolism was greater than that of down-regulated genes (**Supplementary Figure S3**).

Of the DEGs, 14 were involved in starch degradation, including three *amy* genes *TP03368*, *TP04014*/*Amy13A* and *TP07411*, one *gla* gene *TP12319*, and ten *aga* genes *TP00071*, *TP00293*, *TP03337*, *TP03913*, *TP04013*, *TP05120*, *TP09781*, *TP11813*, *TP11464*, and *TP12265*. Comparative analyses revealed that the transcripts of six of these 14 starch-degradation-associated DEGs (*TP03368*, *TP04014*/*Amy13A*, *TP12319*, *TP00071*, *TP04013*, and *TP11464*) were upregulated in Δ*TP05746* in comparison with the expression level in Δ*TpKu70*, with a log2 fold change ranging from 1.27 to 5.90. The other eight DEGs were downregulated, with a log2 fold change ranging from −5.46 to −1.42 (**Figure 6B**).

Interestingly, 44 of the DEGs included in the *TP05746* regulon encoded plant cell wall-degrading enzymes (CWDEs), including one *cbh* gene (*TP09412*/*cbh1*), two *eg* genes (*TP04686* and *TP06957*), and 13 *bgl* genes (*TP01149*, *TP02423*, *TP04716*, *TP05374*, *TP07549*, *TP07716*, *TP07981*, *TP07983*, *TP08074*, *TP09042*, *TP09603*, *TP11082*, and *TP12437*). Of these 44 CWDE-encoding DEGs, 13 genes (*TP01905*, *TP02423*, *TP03145*, *TP03563*, *TP04686*, *TP04716*, *TP06957*, *TP07549*, *TP07888*, *TP10531*, *TP10566*, *TP12748*, and *TP12892*) were upregulated in Δ*TP05746* compared with Δ*TpKu70*, with a log2 fold change ranging from 1.51 to 5.93, whereas the other 31 genes were down-regulated, with a log2 fold change ranging from −7.83 to −1.13 (**Figure 6B**).

In addition to genes encoding carbohydrate-degrading enzymes, the 377 DEGs encoding putative TFs were found, most of which contained Zn2Cys6, C2H2, bZIP, winged helix repressor or homeodomain-like domains, consisting of 159 upregulated ($1.03 < \log2$ fold change < 9.81) and 218 down-regulated ($-10.68 < \log2$ fold change < -1.00) DEGs (**Supplementary Table S2**). Notably, six regulatory genes, known to be involved in controlling the expression of genes encoding PBDEs, were detected, including *TP08849*/*AreA* (log2 fold change = 3.45), *TP09286*/*AmyR* (log2 fold change = 1.10), *TP10486*/*ClrB* (log2 fold change = 5.52), *TP02627*/*XlnR* (log2 fold change = −1.53), *TP00292*/*BglR* (log2 fold change = 3.89), and *TP06351*/*Vib1* (log2 fold change = −3.22) (Li et al., 2017).

Previous work had shown that deletion of *TP05746* resulted in a reduction in asexual spore production, suggesting that *TP05746* controls conidiation of *T. pinophilus*. In the DEGs, 13 genes (*TP04427*/*Bud4*, *TP10226*/*Asp*, *TP10901*/*VosA*, *TP03893*/*FadA*, *TP04237*/*NimX*, *TP05733*/*WetA*, *TP11170*/*FlbA*-like gene, *TP10098*/*FlbA*, *TP03987*/*VeA*, *TP05897*/*RodA*, *TP05092*/*ArpA*, *TP13250*/*ArpA*-like gene, and *TP06809*/*ArpA*-like gene) were observed, which were previously reported to be involved in fungal conidiogenesis (Qin et al., 2013), of which five (*TP04427*/*Bud4*, *TP10226*/*Asp*, *TP10901*/*VosA*, *TP03893*/*FadA*, and *TP04237*/*NimX*) were upregulated ($1.67 < \log2$ fold change < 4.73) and eight were downregulated ($-6.55 < \log2$ fold change < -1.19) in Δ*TP05746* (**Supplementary Table S2**).

RT-qPCR Shows That *TP05746* Dynamically Controls the Expression of Genes Encoding Major PBDE Genes and Their Regulators, and Hyphal Development-Associated Genes in *Talaromyces pinophilus*

RT-qPCR was employed to investigate regulatory dynamics by *TP05746* of the expression of genes involved in the degradation of plant biomass in *T. pinophilus*. On the basis of comparative transcriptomic data, the target genes were identified, including three *amy* genes *TP03368*, *TP04014*/*Amy13A* and *TP07411*, one *gla* gene *TP12319*, and five *aga* genes *TP09781*, *TP11464*, *TP12265*, *TP00071* and *TP04013*, as well as their known regulatory genes *TP09286*/*AmyR* (Zhang et al., 2017), *TP06128*/*Rfx1* (Liao et al., 2018), and *TP00292*/*BglR* (Xiong et al., 2017), and their expression (relative to the levels in the parental strain Δ*TpKu70*) was measured at 12, 24, and 48 h after SCS

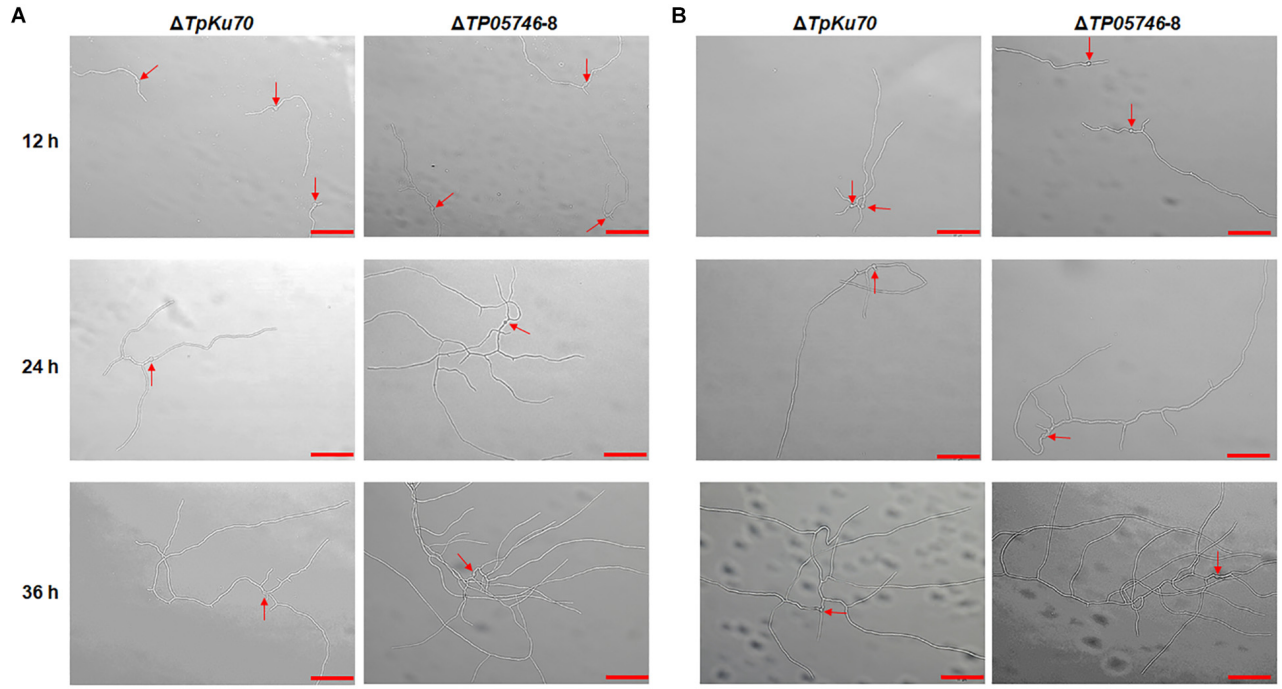

FIGURE 5 | Microscopic investigation of growth of *T. pinophilus* mutant Δ*TP05746* and the parental strain Δ*TpKu70* on SLM containing SCS **(A)** or WA **(B)**. Fungal strains were cultured at 28°C for 12–36 h. The mutant Δ*TP05746* cultured on SCS or WA for 24–36 h showed more hyphal branches than that of the parental strain Δ*TpKu70*. Red arrows indicate the developing conidia. Bar is 50 μm. SLM, standard liquid medium; SCS, soluble corn starch; WA, wheat bran plus Avicel.

induction in the mutant Δ*TP05746*. The results showed that the transcript abundance of these 12 genes was significantly altered in Δ*TP05746* relative to the parental strain. At 12 h after induction, the expression of genes *TP03368*, *TP04014/Amy13A*, *TP12319*, *TP11464*, *TP00071*, *TP04013*, *TP09286/AmyR,* and *TP06128/Rfx1* in the mutant Δ*TP05746* exhibited significant up-regulation, ranging from 1.17- to 87.77-fold, whereas the expression of four genes, *TP07411*, *TP09781*, *TP12265,* and *TP00292/BglR*, was down-regulated by 59.7–81.9% in the mutant Δ*TP05746* ($p < 0.05$, Student's *t*-test). At 24 h, all these targeted genes, except for *TP07411*, *TP12265*, *TP09286/AmyR*, *TP06128/Rfx1,* and *TP00292/BglR*, were significantly upregulated in Δ*TP05746*, the increase ranging from 614.8 to 10108.2% ($p < 0.05$, Student's *t* test). The transcript abundance of *TP09286/AmyR*, *TP06128/Rfx1,* and *TP07411* decreased by 43.7 to 84.0%. By contrast, the transcript abundance of only three genes, namely *TP12319*, *TP09781,* and *TP00071*, continued to increase, by 190.0 to 2142.8% in Δ*TP05746* at 48 h. Six genes, *TP04014*, *TP11464*, *TP12265*, *TP04013*, *TP09286/AmyR,* and *TP06128/Rfx1* showed a 44.2–70.2% decrease in transcript abundance ($p < 0.05$, Student's *t* test; **Figure 7A**).

In addition to starch-degrading enzyme genes, four cellulase and xylanase genes, *TP09412/cbh1*, *TP08514/eg1*, *TP05820/bgl1* and *TP09024/xyn1*, were also selected and their real-time transcription investigated in both Δ*TP05746* and Δ*TpKu70* cultured on WA. The results indicated that the expression of all the cellulase and xylanase genes tested was upregulated to various degrees in Δ*TP05746* relative to Δ*TpKu70* in the early induction period (before 24 h) but downregulated in the later induction period. For example, the transcription levels of all four genes increased by between 228.6% and 29565.0% at 12 h but by between 22.4% and 802.8% at 24 h ($p < 0.05$, Student's *t*-test) in Δ*TP05746* (**Figure 7B**). Conversely, their expression was consistently downregulated by 50.4–75.6% in the mutant at 48 h ($p < 0.05$, Student's *t*-test) (**Figure 7B**).

Five key genes involved in fungal conidiogenesis, namely *TP04427/Bud4*, *TP04237/NimX*, *TP05733/WetA*, *TP10098/FlbA,* and *TP03987/VeA,* were selected for RT-qPCR. The results indicated that, at 12 h, the transcripts of both *TP04237/NimX,* and *TP04427/Bud4* were significantly upregulated, by 54.8% and 143.7%, respectively, while expression of the others was downregulated by 27.5 to 50.0% ($p < 0.01$, Student's *t*-test). At 24 h, the expression of two genes, *TP04237/NimX,* and *TP03987/VeA,* increased by 42.7% and 11.4%, whereas that of *TP04237/NimX*, *TP03987/VeA,* and *TP04427/Bud4* decreased by 23.1 to 40.7% ($p < 0.05$, Student's *t*-test; **Figure 7C**).

TP05746 Binds to the Promoter Regions of Genes Encoding Major PBDEs and Their Regulators *in vitro*, as Well as to Conidiogenesis-Involved Genes

Electrophoretic mobility shift assay was used to confirm whether TP05746 directly or indirectly regulated the expression of target genes. The cDNA of *TP05746* was fused to a DNA fragment encoding Trx-His-S-tags and recombinantly expressed in

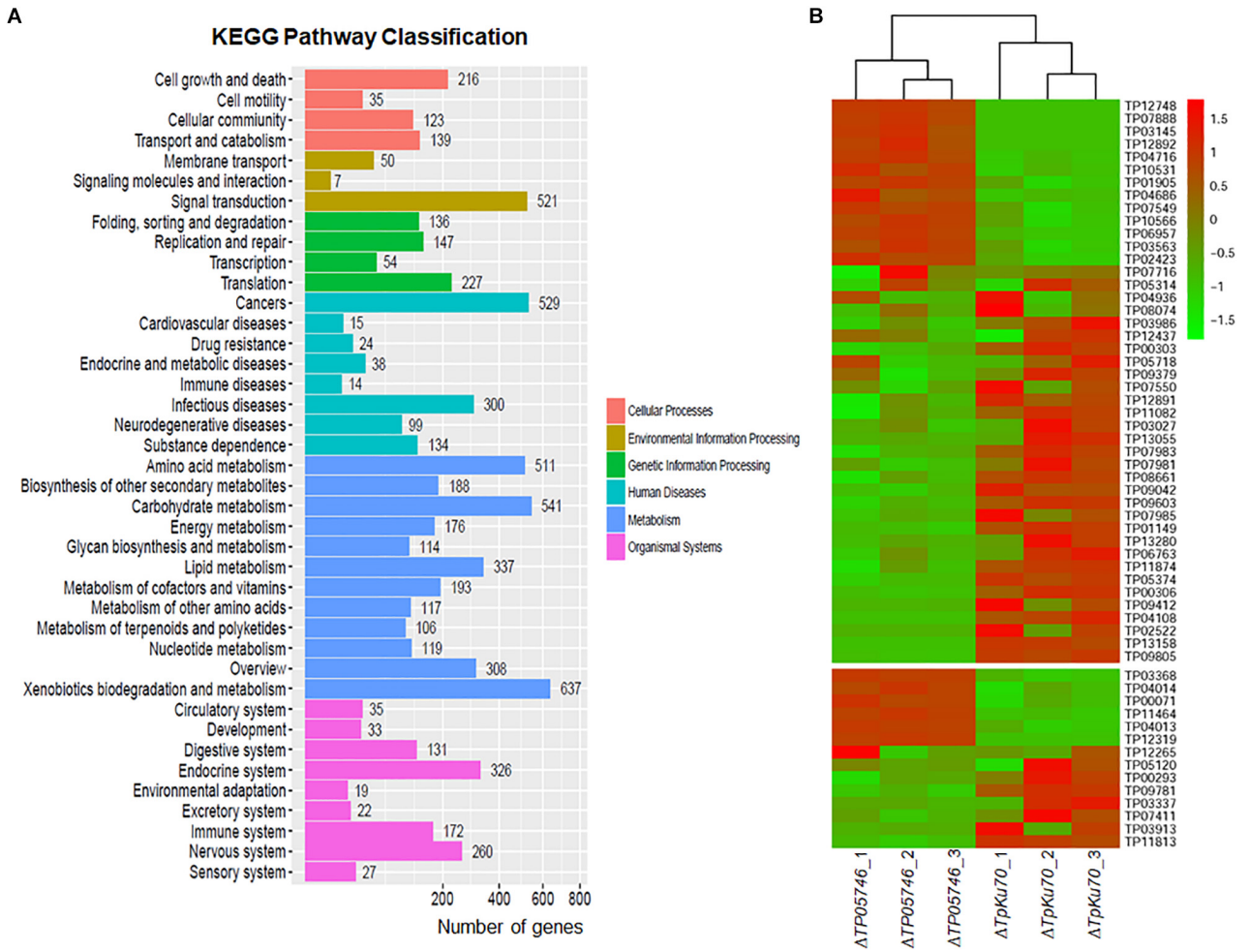

FIGURE 6 | Transcriptomic analysis of *T. pinophilus* mutant Δ*TP05746* and the parental strain Δ*TpKu70* cultured in SLM containing SCS as the sole carbon source for 12 h. **(A)** KEGG pathway classification annotation of 4429 DEGs in the Δ*TP05746* [a | log2(fold change)| $\geq$ 1 and a *p*-value $\leq$ 0.05 as thresholds]. **(B)** Plant cell-wall-degrading enzymes and amylase genes regulated by *TP05746*. SLM, standard liquid medium; SCS, soluble corn starch; KEGG, kyoto encyclopedia of genes and genomes; DEGs: differently expressed genes.

Escherichia coli. The 6-carboxyflurescein (FAM)-tagged DNA probes (∼1,000 bp) in the promoter regions of two α-amylase genes *TP03368*, *TP04014*/*Amy13A*, one glucoamylase gene *TP12319*, three α-glucosidase genes *TP11464*, *TP00071*, *TP04013*, three cellulase genes *TP09412*/*cbh1*, *TP08514*/*eg1*, *TP05820*/*bgl1*, one xylanase gene *TP09024*/*xyn1*, and three regulatory genes *TP00292*/*BglR*, *TP06128*/*Rfx1*, and *TP09286*/*AmyR*, as well as four conidiogenesis-involved genes *TP04427*/*Bud4*, *TP04237*/*NimX*, *TP05733*/*WetA*, and *TP10098*/*FlbA*, were amplified using specific primer pairs (**Supplementary Table S1**). The promoter region of the β-tubulin gene *TP10751*, and either bovine serum albumin (BSA) or the Trx-His-S fusion protein was used as controls. DNA fragments of the same length but without the FAM label, were used as competitive probes. As shown in **Figures 8**, **9**, shifted bands representing rTP05746-DNA complexes in all mixtures of the recombinant protein rTP05746 and EMSA probes of the target genes were observed to various degrees. Moreover, the band size gradually increased along with an increase in rTP05746 amounts (0–2.0 μg), whereas shifted bands did not occur between EMSA probes and either BSA or the Trx-His-S fusion protein, or between rTP05746 and the promoter region of the β-tubulin gene *TP10751*.

Simultaneously, competitive EMSA was performed using the competitive probes, and the results revealed that the concentration of the shifted bands gradually decreased in response to increasing amounts of the competitive probes without the FAM label (**Figures 8**, **9**). However, in fact how interact with these promoters by *TP05746 in vivo* still awaits to be performed.

TP05746 Inhibits the Production of PBDEs in Filamentous Fungus *Penicillium oxalicum*

To further confirm the regulatory roles and potential application of gene *TP05746* in genetic engineering, gene *TP05746* was

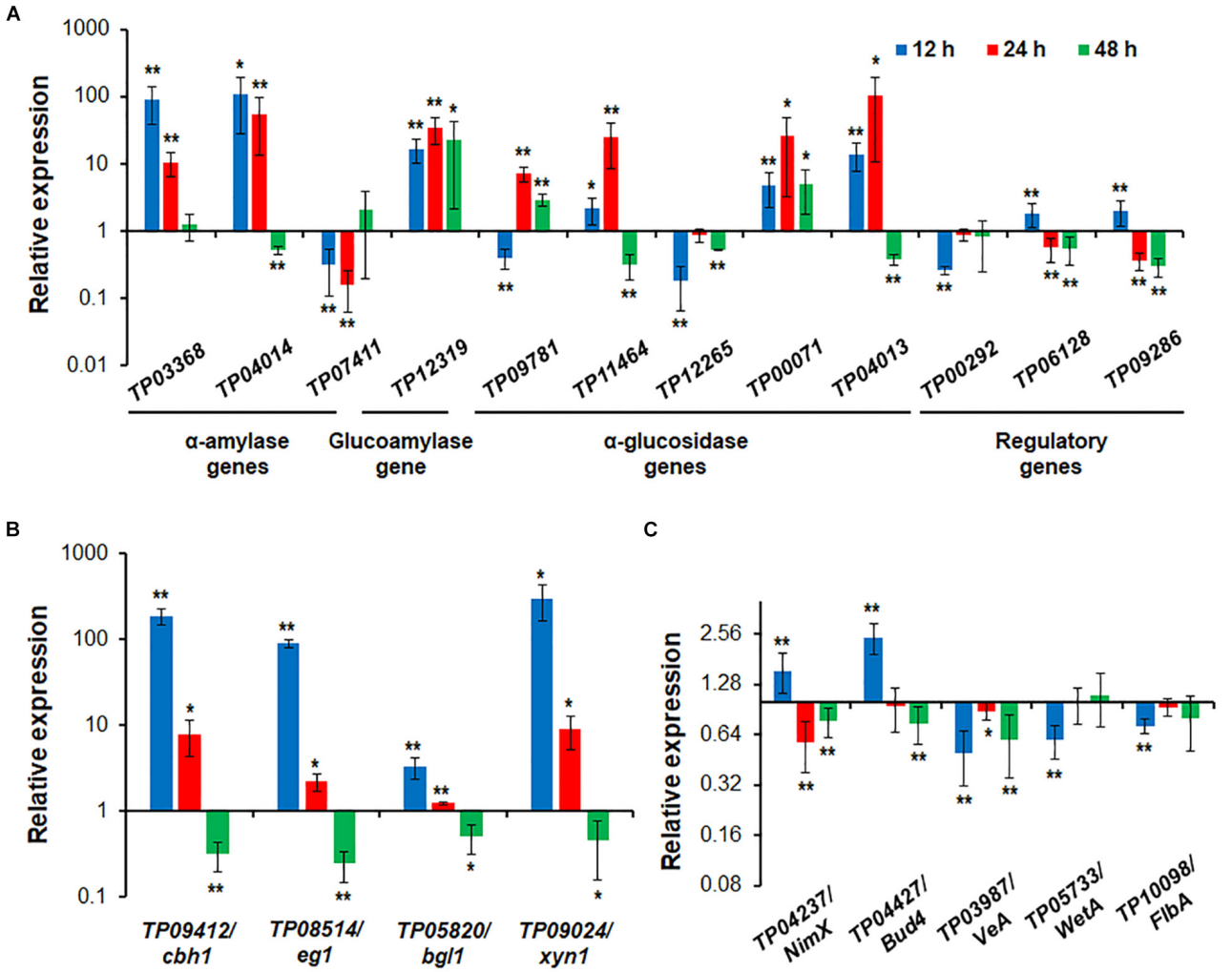

FIGURE 7 | Expressional regulation of enzyme genes and regulatory genes by *TP05746* in *T. pinophilus* as demonstrated by RT-qPCR. **(A)** Amylase genes and their regulatory genes. Total RNA was extracted from fungal strains cultured in medium containing SCS as the carbon source for 12, 24, and 48 h after transfer from glucose. **(B)** Cellulase and xylanase genes. **(C)** Genes involved in conidiogenesis. Fungal cells were cultured on WA for 12, 24, and 48 h after transfer from glucose. Expression levels of the genes tested in the Δ*TP05746* mutant were normalized against the parental strain Δ*TpKu70*. $^{**}p \leq 0.01$ and $^{*}p \leq 0.05$ indicate differences between Δ*TP05746* and Δ*TpKu70* by Student's *t* test. Each experiment contained three biological replicates. RT-qPCR, real-time quantitative reverse transcription PCR; WA, wheat bran plus Avicel.

over-expressed in filamentous fungus *P. oxalicum* parental strain Δ*PoxKu70* (**Supplementary Figure S4**) derived from the wild-type HP7-1 via deleting gene *PoxKu70* (Zhao et al., 2016), and then its production of PBDEs was measured when cultivated on Avicel for 1–3 days. The results indicated the obtained overexpressed strain OX*TP05746_POX* lost 54.4–84.6% of cellulase (FPase, pNPCase and CMCase) and xylanase production, 15.6–49.9% of SSDE and RSDE production, while increased 131.1–275.1% of pNPGase production, compared with the parental strain Δ*PoxKu70* ($p < 0.01$, Student's *t* test; **Figures 10A–G**). Intracellular proteins of strain OX*TP05746_POX* had no significant difference from that of the Δ*PoxKu70* when cultivated on WA for 1 day, but decreased by approximately 70% when for 3 days ($p < 0.01$, Student's *t* test; **Figure 10H**).

DISCUSSION

In this study, we explored regulatory roles of a novel Zn2Cys6 protein, TP05746, that regulated PBDE (i.e., SSDE, RSDE, cellulase, and xylanase) production as well as growth and positively regulated conidiation of *T. pinophilus* through regulating the expression of the associated genes and their regulatory genes (**Figure 11**). TP05746 specifically belonged to *Talaromyces*, and plays an essential regulatory role via a molecular mechanism distinct from that of the known CreA-mediated CCR.

The regulation of *TP05746* on PBDE production is time-dependent, as was expression of their encoded genes. For example, deletion of *TP05746* resulted in an increase in RSDE, cellulase and xylanase activity over the entire induction period, while the level of increasing production tended to fall

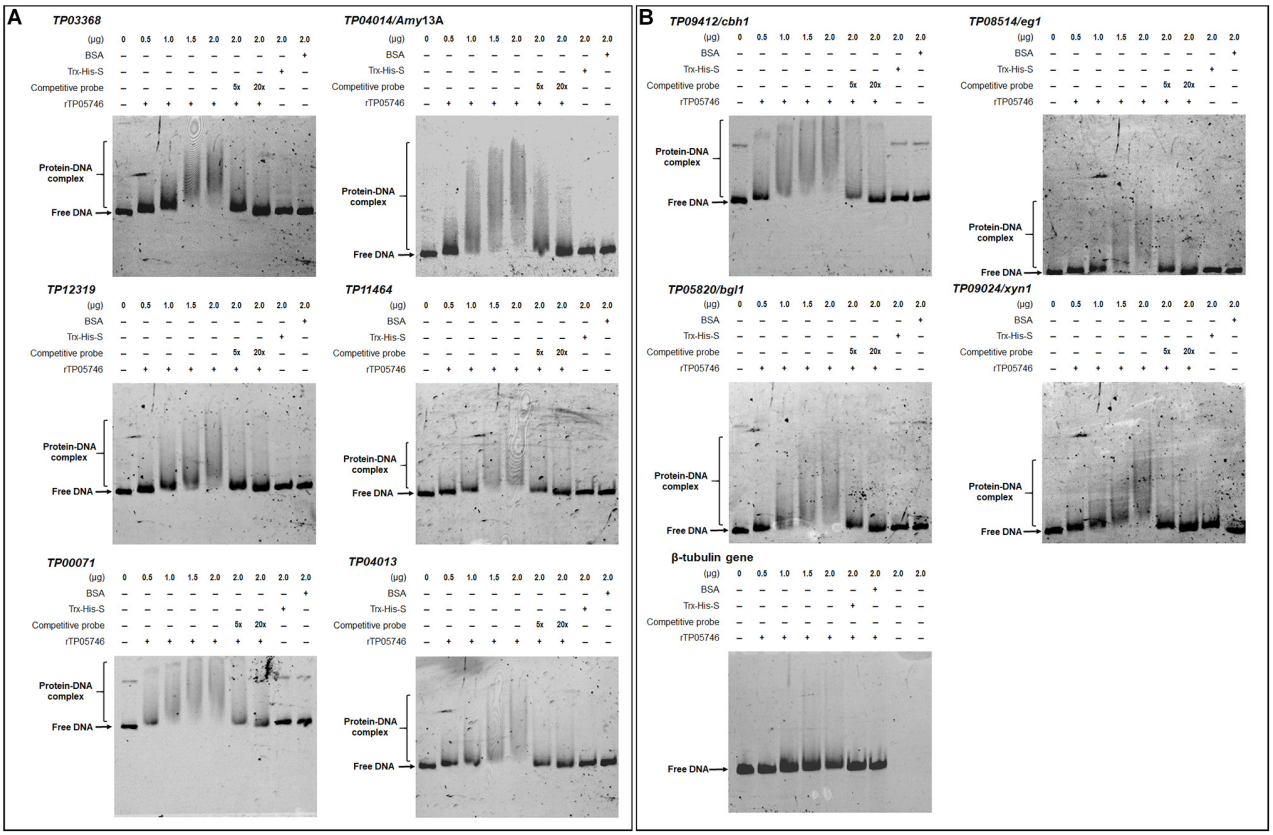

FIGURE 8 | Interaction between TP05746 and genes encoding enzymes as revealed by electrophoretic mobility shift assay (EMSA). **(A)** Amylase genes. **(B)** Cellulase and xylanase genes. The recombinant protein rTP05746 (0–2.0 μg) was mixed with approximately 50 ng of FAM-labeled EMSA probes. EMSA probes lacking the FAM label were used for competitive EMSA. BSA, Trx-His-S fusion protein or the promoter region of the β-tubulin gene alone were used as controls. FAM, 6-carboxyfluorescein; EMSA, electrophoretic mobility shift assay; BSA, bovine serum albumin. In each EMSA reaction, non-specific sheared salmon sperm DNA was added, in order to prevent non-specific binding between protein and probes.

over time, corresponding to dynamic changes in expression of major PBDE genes. The transcripts of *TP03368*-, and *TP04014/Amy13A*-encoding proteins that included SBDs in the mutant Δ*TP05746* first increased and then decreased, while the expression of *TP00071* continued to increase over time. Cellulase and xylanase genes *TP09412/cbh1*, *TP08514/eg1*, *TP05820/bgl1*, and *TP09024/xyn1* were repressed at the early induction stage but activated at later stages.

These observed phenomena are closely associated with substrate induction and a complex regulatory network. Plant biomass is degraded into single sugars via the synergistic action of several PBDEs working at appropriate respective rates, with the most-efficient enzyme mixture being secreted by the fungal cells based on which enzymes are needed in response to specific substrates. To the best of our knowledge, specific inducing substrates are low molecular weight sugars, in-process products of biomass degradation, such as cellobiose, xylobiose and maltose (Amore et al., 2013), but with unstable contents. Additionally, a complex regulatory network, consisting of various TFs and the target genes, are prerequisites to respond to the in-process products. As a note of this complex regulatory network, TP05746 regulates not only the expression of genes encoding specific enzymes, but also that of other TF genes, such as *AmyR*, *TpRfx1,* and *BglR*. AmyR and BglR positively regulate fungal amylase production and negatively control cellulase and xylanase production (Nitta et al., 2012; Li et al., 2015; Xiong et al., 2017; Zhang et al., 2017), whereas TpRfx1 positively mediates PBDE production, including amylase, cellulase and xylanase, in *T. pinopholus* (Liao et al., 2018). However, the actual regulatory mechanism of TP05746 in fungal cells still needs to be further elucidated.

In addition to fungal PBDE production, TP05746 also controls conidiation. Fungal conidiation is governed by the BrlA → AbaA → WetA regulatory cascade in concert with other genes, such as genes encoding FLBs (fluffy low *BrlA* expression) and the velvet family of proteins (Park and Yu, 2016). Here, this study found that deletion of *TP05746* affected the expression of several key conidiation-associated regulatory genes, such as *TP04427/Bud4*, *TP04237/NimX*, *TP05733/WetA*, *TP10098/FlbA* and *TP03987/VeA*. The gene *Bud4* is involved in spectrum formation in hyphal growth and the development of conidiophores in *Aspergillus*, deletion of which resulted in non-production of conidia (Si et al., 2012), as well as *FlbA* (Wieser et al., 1994). *NimX*, also called *cdc2,* encoding

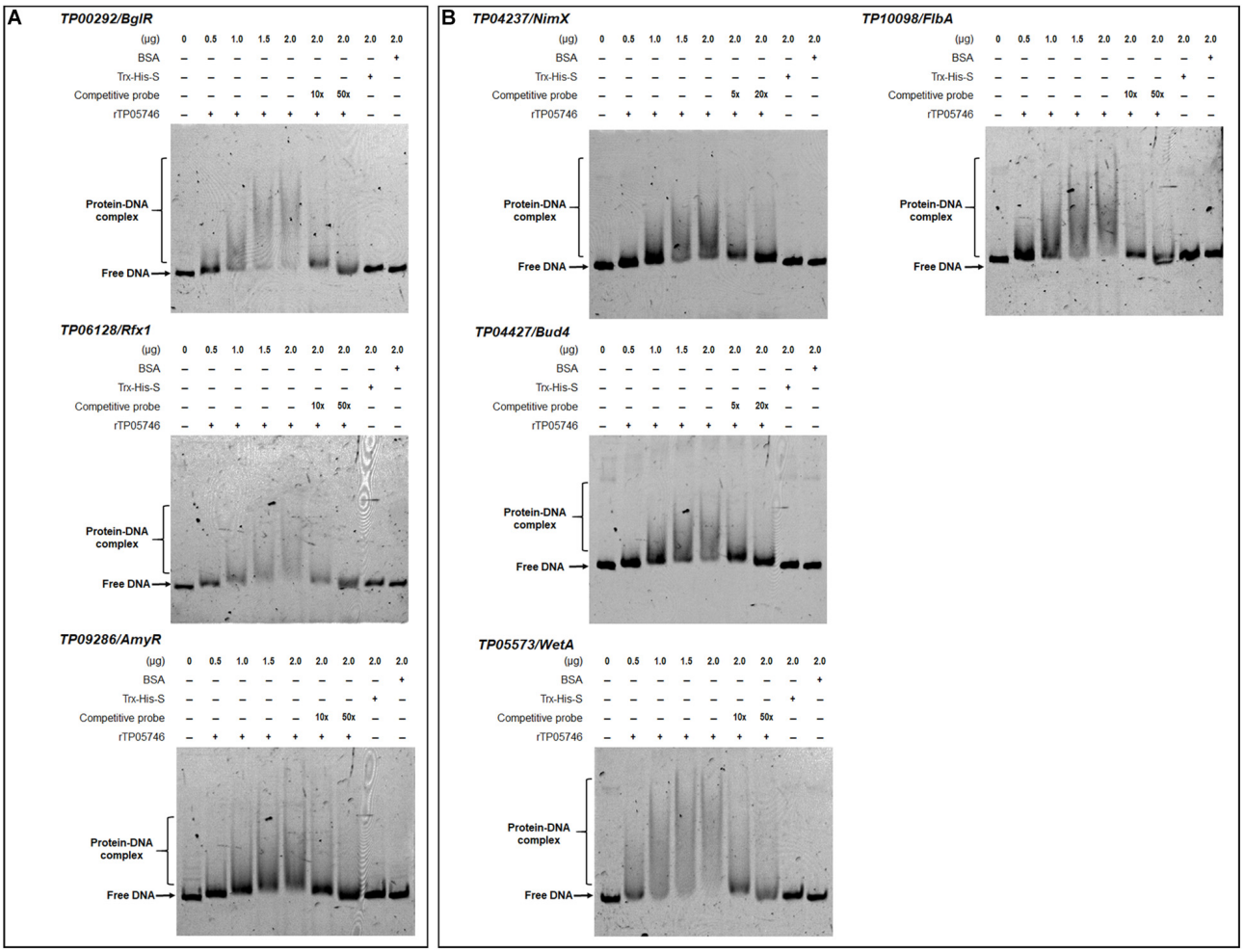

FIGURE 9 | Interaction between TP05746 and regulatory genes revealed by electrophoretic mobility shift assay (EMSA). **(A)** Genes involved in the regulation of PBDE gene expression. **(B)** Genes involved in conidiogenesis. The recombinant protein rTP05746 (0–2.0 μg) was mixed with approximately 50 ng of FAM-labeled EMSA probes. EMSA probes lacking the FAM label were used for competitive EMSA. BSA, Trx-His-S fusion protein or the promoter region of the β-tubulin gene alone were used as controls. FAM, 6-carboxyfluorescein; EMSA, electrophoretic mobility shift assay; BSA: bovine serum albumin; PBDE, plant-biomass-degrading enzymes. In each EMSA reaction, non-specific sheared salmon sperm DNA was added, in order to prevent non-specific binding between protein and probes.

the cyclin-dependent kinase, accelerates hyphal branching and produces abnormal conidiophores at restrictive temperatures in *A. nidulans* (Lin and Momany, 2004). *WetA* is required for the middle to late phases of conidiation, to complete conidiation, and functions in the germination of these asexual spores and the early phase of mycelial growth (Tao and Yu, 2011). The velvet gene *VeA* is essential for proper asexual spore development but exhibits the opposite pattern of conidiation in *Aspergillus fumigatus* according to previous work (Dhingra et al., 2012; Park et al., 2012). Unfortunately, at this point it is not known how *TP03987/VeA* function in *T. pinophilus*. The expression of the above genes regulated by *TP05746* is time-dependent, and reaches a balance, resulting in the phenotypes observed in the mutant Δ*TP05746*. It should be noted that these conidiation-related genes might contribute to the regulation of cellulase and xylanase genes by *TP05746*. For example, the *VeA* ortholog *Vel1* of *T. reesei* positively regulates the expression of key cellulase and xylanase genes (Karimi Aghcheh et al., 2014).

In addition, *TP05746* represses hyphal growth of *T. pinophilus*, which might affect the utilization of nutrients. For example, under SCS induction, the expression of TP05746 is activated, thereby inhibiting the transcription of major amylase genes via a complex regulatory network, resulting in low yields of extracellular amylases. Starch could not be digested into small sugars, including glucose and maltose, to provide energy for the fungal cells.

To the best of our knowledge, few negative TFs have been identified in filamentous fungi to date, deletion of which results in an increase in PBDE production. The best-known repressor is CreA/Cre1/Cre-1, which inhibits almost all fungal genes involved in the degradation of plant biomass in the presence of the preferred carbon source, glucose, including both structural enzyme genes and regulatory genes

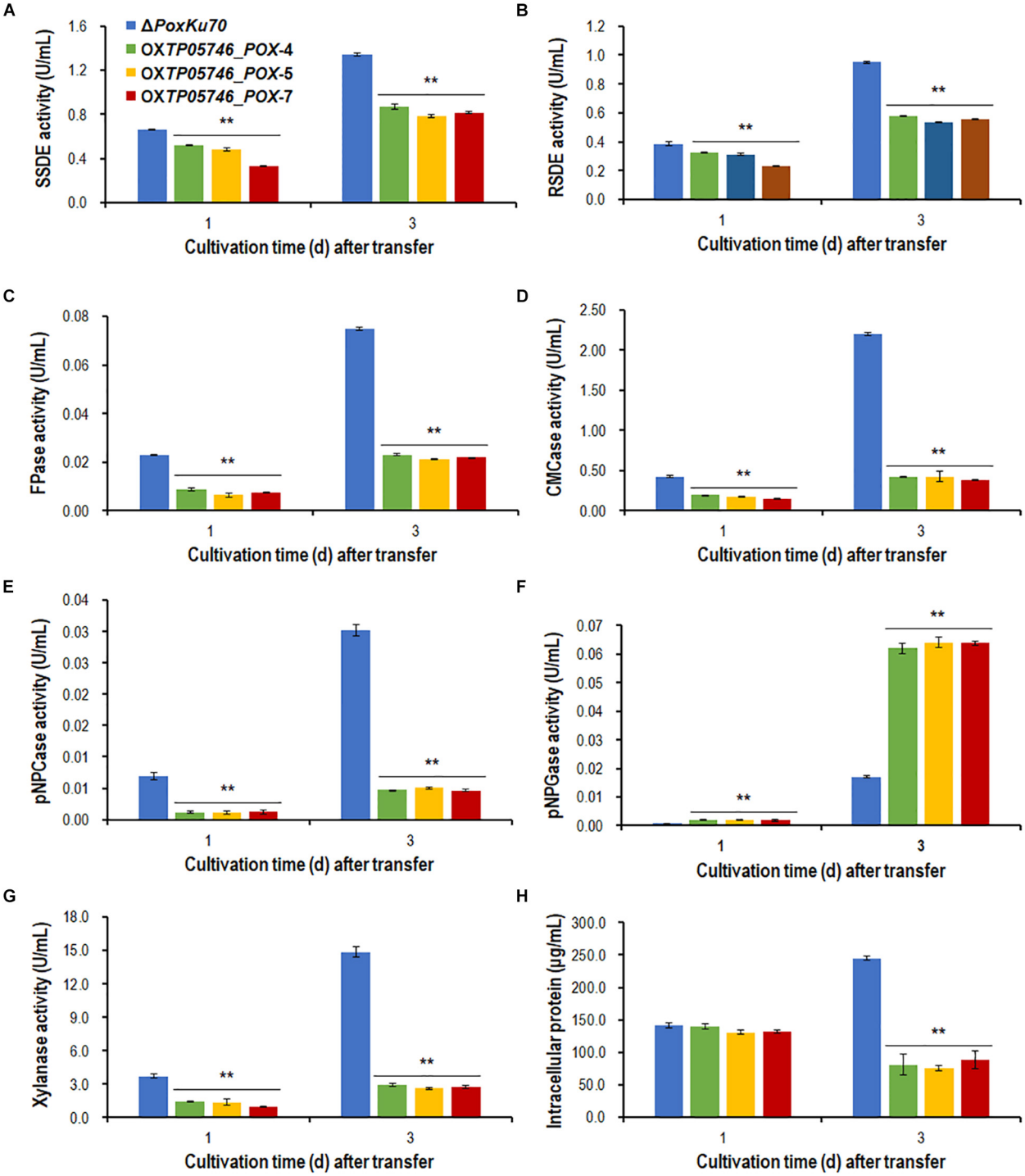

FIGURE 10 | Plant-biomass-degrading enzymes production by overexpression strain OX*TP05746_POX* and the parental strain Δ*PoxKu70*. Crude extracts were produced from *Penicillium oxalicum* strains cultured after a transfer from glucose medium to Avicel medium for 1–3 days. **(A)** SSDE production. **(B)** RSDE production. **(C)** FPase production. **(D)** CMCase production. **(E)** pNPCase production. **(F)** pNPGase production. **(G)** Xylanase production. **(H)** intracellular protein. All experiments were performed independently for three biological replicates. Each data point is mean ± SD. $^{**}p \leq 0.01$ indicates differences between the deletion mutant Δ*TP05746* and the parental strain Δ*TpKu70* by Student's *t* test. PBDE, plant-biomass-degrading enzyme; SSDE, soluble-starch-degrading enzyme; SCS, soluble corn starch; RSDE, raw-starch-degrading enzyme; FPase, filter paper cellulase; CMCase, carboxymethylcellulase; pNPCase, *p*-nitrophenyl-β-cellobiosidase; pNPGase, *p*-nitrophenyl-β-glucopyranosidase.

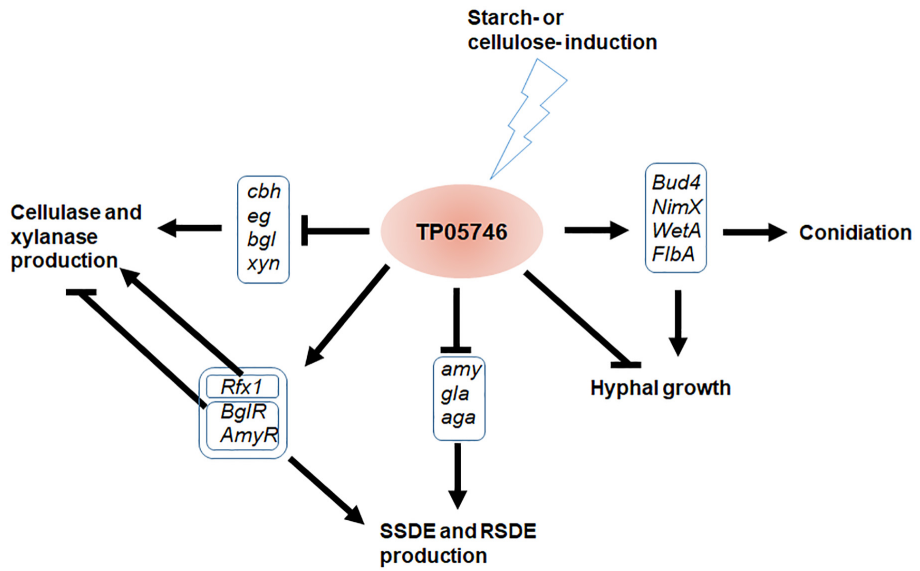

FIGURE 11 | Proposed model of *TP05746* regulation in *T. pinophilus*. *cbh*, cellobiohydrolase gene; *eg*, endo-β-1,4-glucanase gene; *bgl*, β-1,4-glucosidase gene; *gla*, glucoamylase gene; *amy*, α-amylase gene; *aga*, α-glucosidase gene.

(Portnoy et al., 2011; Sun and Glass, 2011; Li et al., 2015). Further experimental data revealed that, in the presence of D-glucose, both SSDE and RSDE production by Δ*TP05746* increased approximately 1.3- to 2.2-fold relative to that of the parental Δ*TpKu70*. In addition, 2-DG could activate CCR in the mutant Δ*TP05746*, leading to insufficient cellulase production, as in Δ*TpKu70* (**Supplementary Figure S5**). These data suggested that TP05746 was not involved in CreA-mediated CCR, suggesting that the mode of action of TP05746 is different from that of CreA.

We tried to construct the complementary strain of the mutant Δ*TP05746* at least four times but failed for unknown reasons. Three randomly chosen knock-out transformants for the gene *TP05746* in *T. pinophilus* were confirmed by both PCR with specific primers and by Southern hybridization analysis. Furthermore, in the enzymatic activity assay, all three randomly chosen transformants showed similar and consistent results, confirming that the obtained phenotype of each transformant was specifically generated by the deletion of the gene *TP05746*. Fortunately, gene *TP05746* was heterologously overexpressed in filamentous fungus *P. oxalicum*. Overexpression of *TP05746* resulted in the reduction of plant-biomass-degrading enzyme production, thereby leading to less accumulation of fungal hyphae. These data also confirmed that *TP05746* plays a negative role in the production of PBDEs.

It should be noted that negatively regulatory genes are potential targets for genetic engineering to achieve increased enzyme production. Deletion of *TP05746* led to a several-fold increase in RSDE production. RSDE application to starch biorefineries to generate biofuels or other biochemical products efficiently saves costs compared with traditional starch processing (Robertson et al., 2006; Görgens et al., 2015).

CONCLUSION

In conclusion, the present study explored the regulatory roles of the novel TF TP05746 in *T. pinophilus* with respect to the control of PBDE production (SSDE, RSDE, cellulase and xylanase), as well as growth and conidiation. Further studies indicated that TP05746 dynamically regulated the expression of the associated genes described above, thereby affecting the corresponding fungal phenotypes. These findings provided novel insights into the regulatory mechanism of fungal PBDE gene expression and identify a potential target for genetic engineering for industrial application.

DATA AVAILABILITY STATEMENT

The datasets generated for this study can be found in the DNA sequence of TP05746 is available from the GenBank database under the accession number MH447996. The transcriptomic data of *T. pinophilus* strains have been deposited in Gene Expression Omnibus (GEO) on NCBI (accession no. GSE131872).

AUTHOR CONTRIBUTIONS

J-XF designed and supervised the study, and involved in data analysis and manuscript revision. SZ co-supervised all the experiments and revised the manuscript. TZ carried out the enzyme activity assay, phenotypic analysis, Southern hybridization analysis, RT-qPCR, and EMSA, and drafted the manuscript. L-SL involved in genomic DNA, RNA, and protein extraction and transcriptomic analysis. C-XL carried out the bioinformatic analysis. G-YL, XL, and X-ML took part in the

preparation of experimental materials and data analysis. All authors read and approved the final manuscript.

FUNDING

This work was financially supported by the grants from the Guangxi Natural Science Foundation (Grant No. 2018GXNSFAA281103), the State Key Laboratory for Conservation and Utilization of Subtropical Agro-Bioresources (SKLCUSA-a201902; SKLCUSA-a201923), Training Program for 1000 Young and Middle-aged Key Teachers in Guangxi at 2019, and the "One Hundred Person" Project of Guangxi.

SUPPLEMENTARY MATERIAL

The Supplementary Material for this article can be found online at: https://www.frontiersin.org/articles/10.3389/fmicb.2019.02875/full#supplementary-material

REFERENCES

Amore, A., Giacobbe, S., and Faraco, V. (2013). Regulation of cellulase and hemicellulase gene expression in fungi. *Curr. Genomics* 14, 230–249.

Bornscheuer, U., Buchholz, K., and Seibel, J. (2014). Enzymatic degradation of (Ligno)cellulose. *Angew. Chem. Int. Ed.* 53, 10876–10893. doi: 10.1002/anie.201309953

Buommino, E., Filippis, A. D., Nicoletti, R., Menegozzo, M., Menegozzo, S., Ciavatta, M. L., et al. (2012). Cell-growth and migration inhibition of human mesothelioma cells induced by 3-O-Methylfunicone from *Penicillium pinophilum* and cisplatin. *Invest. New Drug* 30, 1343–1351. doi: 10.1007/s10637-011-9698-1

Carrillo, A. J., Schacht, P., Cabrera, I. E., Blahut, J., Prudhomme, L., Dietrich, S., et al. (2017). Functional profiling of transcription factor genes in *Neurospora crassa*. *G3* 7, 2945–2956.

Christensen, S., Borrego, E., Shim, W. B., Isakeit, T., and Kolomiets, M. (2012). Quantification of fungal colonization, sporogenesis, and production of mycotoxins using kernel bioassays. *J. Vis. Exp.* 62:3727. doi: 10.3791/3727

Coradetti, S. T., Craig, J. P., Xiong, Y., Shock, T., Tian, C. G., and Glass, N. L. (2012). Conserved and essential transcription factors for cellulase gene expression in ascomycete fungi. *Proc. Natl. Acad. Sci. U.S.A.* 109, 7397–7402. doi: 10.1073/pnas.1200785109

Dhingra, S., Andes, D., and Calvo, A. M. (2012). VeA regulates conidiation, gliotoxin production, and protease activity in the opportunistic human pathogen *Aspergillus fumigatus*. *Eukaryot. Cell* 11, 1531–1543. doi: 10.1128/EC.00222-12

Görgens, J. F., Bressler, D. C., and van Rensburg, E. (2015). Engineering *Saccharomyces cerevisiae* for direct conversion of raw, uncooked or granular starch to ethanol. *Crit. Rev. Biotechnol.* 35, 369–391. doi: 10.3109/07388551.2014.888048

Gougoulias, C., Clark, J. M., and Shaw, L. J. (2014). The role of soil microbes in the global carbon cycle: tracking the below-ground microbial processing of plant-derived carbon for manipulating carbon dynamics in agricultural systems. *J. Sci. Food Agric.* 94, 2362–2371. doi: 10.1002/jsfa.6577

He, Q. P., Zhao, S., Wang, J. X., Li, C. X., Yan, Y. S., Wang, L., et al. (2018). Transcription factor NsdD regulates the expression of genes involved in plant biomass-degrading enzymes, conidiation, and pigment biosynthesis in *Penicillium oxalicum*. *Appl. Environ. Microbiol.* 84:e01039-18. doi: 10.1128/AEM.01039-18

Huberman, L. B., Liu, J., Qin, L. N., and Glass, N. L. (2016). Regulation of the lignocellulolytic response in filamentous fungi. *Fungal Biol. Rev.* 30, 101–111. doi: 10.1016/j.fbr.2016.06.001

Karimi Aghcheh, R., Németh, Z., Atanasova, L., Fekete, E., Paholcsek, M., Sándor, E., et al. (2014). The VELVET A orthologue VEL1 of *Trichoderma reesei* regulates fungal development and is essential for cellulase gene expression. *PLoS One* 9:e112799. doi: 10.1371/journal.pone.0112799

Kumar, S., Stecher, G., and Tamura, K. (2016). MEGA7: molecular evolutionary genetics analysis version 7.0 for bigger datasets. *Mol. Biol. Evol.* 33, 1870–1874. doi: 10.1093/molbev/msw054

Kusum, D., Rahul, J., Sushma, T., and Anita, P. (2014). Prolonged laccase production by a cold and pH tolerant strain of *Penicillium pinophilum* (MCC 1049) isolated from a low temperature environment. *Enzyme Res.* 2014:120708. doi: 10.1155/2014/120708

Langmead, B., and Salzberg, S. L. (2012). Fast gapped-read alignment with Bowtie 2. *Nat. Methods* 9, 357–359. doi: 10.1038/nmeth.1923

Lee, W. S., Chen, I. C., Chang, C. H., and Yang, S. S. (2012). Bioethanol production from sweet potato by co-immobilization of saccharolytic molds and *Saccharomyces cerevisiae*. *Renew. Energ.* 39, 216–222. doi: 10.1016/j.renene.2011.08.024

Li, B., and Dewey, C. N. (2011). RSEM: accurate transcript quantification from RNA-Seq data with or without a reference genome. *BMC Bioinformatics* 12:323. doi: 10.1186/1471-2105-12-323

Li, C. X., Zhao, S., Zhang, T., Xian, L., Liao, L. S., Liu, J. L., et al. (2017). Genome sequencing and analysis of *Talaromyces pinophilus* provide insights into biotechnological applications. *Sci. Rep.* 7:490. doi: 10.1038/s41598-017-00567-0

Li, H., and Durbin, R. (2009). Fast and accurate short read alignment with Burrows-Wheeler transform. *Bioinformatics* 25, 1754–1760. doi: 10.1093/bioinformatics/btp324

Li, Z. H., Yao, G. S., Wu, R. M., Gao, L. W., Kan, Q. B., Liu, M., et al. (2015). Synergistic and dose-controlled regulation of cellulase gene expression in *Pencillium oxalicum*. *PLoS Genet.* 11:e1005509. doi: 10.1371/journal.pgen.1005509

Liao, G. Y., Zhao, S., Zhang, T., Li, C. X., Liao, L. S., Zhang, F. F., et al. (2018). The transcription factor TpRfx1 is an essential regulator of amylase and cellulase gene expression in *Talaromyces pinophilus*. *Biotechnol. Biofuels* 11:276. doi: 10.1186/s13068-018-1276-8

Liao, L. S., Li, C. X., Zhang, F. F., Yan, Y. S., Luo, X. M., Zhao, S., et al. (2019). How an essential Zn2Cys6 transcription factor PoxCxrA regulates cellulase gene expression in ascomycete fungi? *Biotechnol. Biofuels* 12:105. doi: 10.1186/s13068-019-1444-5

Lin, X. R., and Momany, M. (2004). Identification and complementation of abnormal hyphal branch mutants ahbA1 and ahbB1 in *Aspergillus nidulans*. *Fungal Genet. Biol.* 41, 998–1006. doi: 10.1016/j.fgb.2004.07.005

Love, M. I., Huber, W., and Anders, S. (2014). Moderated estimation of fold change and dispersion for RNA seq data with DESeq2. *Genome Biol.* 15:550.

Machovic, M., and Janecek, S. (2006). Starch-binding domains in the post-genome era. *Cell Mol. Life Sci.* 63, 2710–2724. doi: 10.1007/s00018-006-6246-9

Marín-Navarro, J., and Polaina, J. (2011). Glucoamylases: structural and biotechnological aspects. *Appl. Microbiol. Biotechnol.* 89, 1267–1273. doi: 10.1007/s00253-010-3034-0

Miller, G. L. (1959). Use of dinitrosalicylic acid reagent for determination of reducing sugar. *Anal. Chem.* 31, 426–428. doi: 10.1021/ac60147a030

Nitta, M., Furukawa, T., Shida, Y., Mori, K., Kuhara, S., Morikawa, Y., et al. (2012). A new Zn(II)2Cys6-type transcription factor BglR regulates β-glucosidase expression in *Trichoderma reesei*. *Fungal Genet. Biol.* 49, 388–397. doi: 10.1016/j.fgb.2012.02.009

Park, H. S., Bayram, O., Braus, G. H., Kim, S. C., and Yu, J. H. (2012). Characterization of the velvet regulators in *Aspergillus fumigatus*. *Mol. Microbiol.* 86, 937–953. doi: 10.1111/mmi.12032

Park, H. S., and Yu, J. H. (2016). Developmental regulators in *Aspergillus fumigatus*. *J. Microbiol.* 54, 223–231.

Passos, D. D. F., Pereira, N., and Castro, A. M. D. (2018). A comparative review of recent advances in cellulases production by *Aspergillus*, *Penicillium* and *Trichoderma* strains and their use for lignocellulose deconstruction. *Curr. Opin. Green Sustain. Chem.* 14, 60–66.

Pol, D., Laxman, R. S., and Rao, M. (2012). Purifcation and biochemical characterization of endoglucanase from *Penicillium pinophilum* MS. *Indian J. Biochem. Biophys.* 49, 189–194.

Portnoy, T., Margeot, A., Linke, R., Atanasova, L., Fekete, E., Sandor, E., et al. (2011). The CRE1 carbon catabolite repressor of the fungus *Trichoderma reesei*: a master regulator of carbon assimilation. *BMC Genomics* 12:269. doi: 10.1186/1471-2164-12-269

Qin, Y., Bao, L., Gao, M., Chen, M., Lei, Y., Liu, G., et al. (2013). *Penicillium decumbens* BrlA extensively regulates secondary metabolism and functionally associates with the expression of cellulase genes. *Appl. Microbiol. Biotechnol.* 97, 10453–10467. doi: 10.1007/s00253-013-5273-3

Robertson, G. H., Wong, D. W., Lee, C. C., Wagschal, K., Smith, M. R., and Orts, W. J. (2006). Native or raw starch digestion: a key step in energy efficient biorefining of grain. *J. Agric. Food Chem.* 54, 353–365. doi: 10.1021/jf051883m

Sánchez, O. J., and Cardona, C. A. (2008). Trends in biotechnological production of fuel ethanol from different feedstocks. *Bioresour. Technol.* 99, 5270–5295. doi: 10.1016/j.biortech.2007.11.013

Si, H. Y., Rittenour, W. R., Xu, K., Nicksarlian, M., Calvo, A. M., and Harris, S. D. (2012). Morphogenetic and developmental functions of the *Aspergillus nidulans* homologues of the yeast bud site selection proteins Bud4 and Axl2. *Mol. Microbiol.* 85, 252–270. doi: 10.1111/j.1365-2958.2012.08108.x

Sorimachi, K., Le Gal-Coëffet, M. F., Williamson, G., Archer, D. B., and Williamson, M. P. (1997). Solution structure of the granular starch binding domain of *Aspergillus niger* glucoamylase bound to β-cyclodextrin. *Structure* 5, 647–661. doi: 10.1016/s0969-2126(97)00220-7

Sun, H., Zhao, P., Ge, X., Xia, Y., Hao, Z., Liu, J., et al. (2010). Recent advances in microbial raw starch degrading enzymes. *Appl. Biochem. Biotechnol.* 160, 988–1003. doi: 10.1007/s12010-009-8579-y

Sun, J., and Glass, N. L. (2011). Identification of the CRE-1 cellulolytic regulon in *Neurospora crassa*. *PLoS One* 6:e25654. doi: 10.1371/journal.pone.0025654

Tani, S., Kawaguchi, T., and Kobayashi, T. (2014). Complex regulation of hydrolytic enzyme genes for cellulosic biomass degradation in filamentous fungi. *Appl. Microbiol. Biotechnol.* 98, 4829–4837. doi: 10.1007/s00253-014-5707-6

Tao, L., and Yu, J. H. (2011). AbaA and WetA govern distinct stages of *Aspergillus fumigatus* development. *Microbiology* 157, 313–326. doi: 10.1099/mic.0.044271-0

van Peij, N. N., Gielkens, M. M., de Vries, R. P., Visser, J., and de Graaff, L. H. (1998). The transcriptional activator XlnR regulates both xylanolytic and endoglucanase gene expression in *Aspergillus niger*. *Appl. Environ. Microbiol.* 64, 3615–3619.

Visser, E. M., Falkoski, D. L., de Almeida, M. N., Maitan-Alfenas, G. P., and Guimarães, V. M. (2013). Production and application of an enzyme blend from *Chrysoporthe cubensis* and *Penicillium pinophilum* with potential for hydrolysis of sugarcane bagasse. *Bioresour. Technol.* 144, 587–594. doi: 10.1016/j.biortech.2013.07.015

Wang, L., Zhao, S., Chen, X. X., Deng, Q. P., Li, C. X., and Feng, J. X. (2018). Secretory overproduction of a raw starch-degrading glucoamylase in *Penicillium oxalicum* using strong promoter and signal peptide. *Appl. Microbiol. Biotechnol.* 102, 9291–9301. doi: 10.1007/s00253-018-9307-8

Weirauch, M. T., and Hughes, T. R. (2011). A catalogue of eukaryotic transcription factor types, their evolutionary origin, and species distribution. *Subcell. Biochem.* 52, 25–73. doi: 10.1007/978-90-481-9069-0_3

Wieser, J., Lee, B. N., Fondon, J. W. III, and Adams, T. H. (1994). Genetic requirements for initiating asexual development in *Aspergillus nidulans*. *Curr. Genet.* 27, 62–69.

Xian, L., Wang, F., Luo, X., Feng, Y. L., and Feng, J. X. (2015). Purification and characterization of a highly efficient calcium-independent alpha-amylase from *Talaromyces pinophilus* 1-95. *PLoS One* 10:e121531. doi: 10.1371/journal.pone.0121531

Xiong, Y., Sun, J. P., and Glass, N. L. (2014). VIB1, a link between glucose signaling and carbon catabolite repression, is essential for plant cell wall degradation by *Neurospora crassa*. *PLoS Genet.* 10:e1004500. doi: 10.1371/journal.pgen.1004500

Xiong, Y., Wu, V. W., Lubbe, A., Qin, L., Deng, S., Kennedy, M., et al. (2017). A fungal transcription factor essential for starch degradation affects integration of carbon and nitrogen metabolism. *PLoS Genet.* 13:e1006737. doi: 10.1371/journal.pgen.1006737

Xiong, Y. R., Zhao, S., Fu, L. H., Liao, X. Z., Li, C. X., Yan, Y. S., et al. (2018). Characterization of novel roles of a HMG-box protein PoxHmbB in biomass-degrading enzyme production by *Penicillium oxalicum*. *Appl. Microbiol. Biotechnol.* 102, 3739–3753. doi: 10.1007/s00253-018-8867-y

Xu, Q. S., Yan, Y. S., and Feng, J. X. (2016). Efficient hydrolysis of raw starch and ethanol fermentation: a novel raw starch-digesting glucoamylase from *Penicillium oxalicum*. *Biotechnol. Biofuels* 9:216.

Yan, Y. S., Zhao, S., Liao, L. S., He, Q. P., Xiong, Y. R., Wang, L., et al. (2017). Transcriptomic profiling and genetic analyses reveal novel key regulators of cellulase and xylanase gene expression in *Penicillium oxalicum*. *Biotechnol. Biofuels* 10:279. doi: 10.1186/s13068-017-0966-y

Zhai, M. M., Niu, H. T., Li, J., Xiao, H., Shi, Y. P., Di, D. L., et al. (2015). Talaromycolides A-C, novel phenyl-substituted phthalides isolated from the green chinese onion-derived fungus *Talaromyces pinophilus* AF-02. *J. Agric. Food Chem.* 63, 9558–9564. doi: 10.1021/acs.jafc.5b04296

Zhang, M. Y., Zhao, S., Ning, Y. N., Fu, L. H., Li, C. X., Wang, Q., et al. (2019). Identification of an essential regulator controlling the production of raw-starch-digesting glucoamylase in *Penicillium oxalicum*. *Biotechnol. Biofuels* 12:7. doi: 10.1186/s13068-018-1345-z

Zhang, T., Zhao, S., Liao, L. S., Li, C. X., Liao, G. Y., and Feng, J. X. (2017). Deletion of *TpKu70* facilitates gene targeting in *Talaromyces pinophilus* and identification of *TpAmyR* involvement in amylase production. *World J. Microbiol. Biotechnol.* 33:171. doi: 10.1007/s11274-017-2331-5

Zhao, S., Yan, Y. S., He, Q. P., Yang, L., Yin, X., Li, C. X., et al. (2016). Comparative genomic, transcriptomic and secretomic profiling of *Penicillium oxalicum* HP7-1 and its cellulase and xylanase hyper-producing mutant EU2106, and identification of two novel regulatory genes of cellulase and xylanase gene expression. *Biotechnol. Biofuels* 9:203. doi: 10.1186/s13068-016-0616-9

Conflict of Interest: The authors declare that the research was conducted in the absence of any commercial or financial relationships that could be construed as a potential conflict of interest.

frontiers in Microbiology

ORIGINAL RESEARCH
published: 20 May 2020
doi: 10.3389/fmicb.2020.00974

The Kinase USK1 Regulates Cellulase Gene Expression and Secondary Metabolite Biosynthesis in *Trichoderma reesei*

*Sabrina Beier, Wolfgang Hinterdobler, Alberto Alonso Monroy, Hoda Bazafkan and Monika Schmoll**

Center for Health and Bioresources, AIT Austrian Institute of Technology GmbH, Tulln, Austria

The complex environment of fungi requires a delicate balance between the efforts to acquire nutrition, to reproduce, and to fend off competitors. In *Trichoderma reesei*, an interrelationship between regulation of enzyme gene expression and secondary metabolism was shown. In this study, we investigated the physiological relevance of the unique YPK1-type kinase USK1 of *T. reesei*. *Usk1* is located in the vicinity of the SOR cluster and is involved in regulation of several genes from this secondary metabolite cluster as well as dihydrotrichotetronine and other secondary metabolites. Moreover, USK1 is required for biosynthesis of normal levels of secondary metabolites in liquid culture. USK1 positively influences cellulase gene regulation, secreted cellulase activity, and biomass formation upon growth in constant darkness on cellulose. Positive effects of USK1 on transcript abundance of the regulator of secondary metabolism, *vel1*, and the carbon catabolite repressor gene *cre1* are in agreement with these functions. In summary, we found that with USK1, *T. reesei* comprises a unique kinase that adds an additional layer of regulation to the connection of secondary metabolism and enzyme production in fungi.

Keywords: *Trichoderma reesei*, *Hypocrea jecorina*, sorbicillin, dihydrotrichotetronin, secondary metabolism, plant cell wall degradation, signal transduction

OPEN ACCESS

Edited by:
Guodong Liu,
Shandong University, China

Reviewed by:
Fengming Lin,
Southeast University, China
Ting-Fang Wang,
Academia Sinica, Taiwan

****Correspondence:***
Monika Schmoll
monika.schmoll@ait.ac.at

Specialty section:
This article was submitted to Fungi and Their Interactions, a section of the journal Frontiers in Microbiology

Received: *15 November 2019*
Accepted: *22 April 2020*
Published: *20 May 2020*

Citation:
Beier S, Hinterdobler W, Monroy AA, Bazafkan H and Schmoll M (2020) The Kinase USK1 Regulates Cellulase Gene Expression and Secondary Metabolite Biosynthesis in Trichoderma reesei. Front. Microbiol. 11:974. doi: 10.3389/fmicb.2020.00974

INTRODUCTION

Trichoderma reesei (syn. *Hypocrea jecorina*) represents one of the most important filamentous fungi for industrial applications (Bischof et al., 2016). *T. reesei* is a model organism for regulation of plant cell wall degradation due to its efficient machinery for regulation and secretion of carbohydrate active enzymes (Saloheimo and Pakula, 2012; Gupta et al., 2016; Paloheimo et al., 2016). Plant cell wall degrading enzymes are largely co-regulated in *T. reesei* (Foreman et al., 2003) and their expression is regulated by a network of transcription factors (Benocci et al., 2017), of which XYR1, ACE3, and the carbon catabolite repressor CRE1 are most important. Besides transcription factors, also several signal transduction pathways impact cellulase regulation and especially light as a signal has a profound influence on enzyme expression (Schmoll, 2018).

Trichoderma reesei has a long tradition of application in industry and received generally regarded as safe (GRAS) status (Nevalainen et al., 1994). Recently, the safety of *T. reesei* as an industrial producer of food and feed enzymes has been re-assessed with a very low level of risk for contamination with harmful toxins (Frisvad et al., 2018). In recent years, secondary metabolism of *T. reesei* became an interesting field of investigation and also some interconnections with enzyme production became obvious, highlighting the importance

of secondary metabolite screening done routinely for industrial production strains.

Sorbicillinoids represent a group of secondary metabolites produced by filamentous fungi, for which anti-inflamatory and antimicrobial functions are reported (Cram, 1948; Maskey et al., 2005) and potential anticancer and anti-HIV applications are discussed (Bringmann et al., 2003; Yao et al., 2015). The biosynthetic genes responsible for production were first elucidated in *Penicillium chrysogenum* (Salo et al., 2016; Guzman-Chavez et al., 2017). In *T. reesei*, the production of sorbicillin compounds was investigated at the molecular level. The gene cluster responsible for production of the respective yellow pigments (SOR cluster) is regulated by the two transcription factors YPR1 and YPR2 as well as the carbon catabolite repressor CRE1 and the secondary metabolism regulator LAE1 (Derntl et al., 2016, 2017a; Monroy et al., 2017). The cluster arose in early Hypocreales and lateral gene transfer led to the structure in the *T. reesei* genome (Druzhinina et al., 2016). The produced sorbicillinoids exert a growth limiting effect on other microbes (Derntl et al., 2017a). Regulation of the SOR cluster is altered in response to the carbon source (Derntl et al., 2016; Dattenböck et al., 2018; Hitzenhammer et al., 2019) and on cellulose a negative feedback cycle is obvious upon growth in light and a positive cycle in darkness (Monroy et al., 2017). Previously, also high level constitutive production of sorbicillinoids was achieved by random mutagenesis of *T. reesei* RutC30 (Li et al., 2018). However, the regulatory basis for this effect remains to be investigated.

Phosphate residues, attached to and removed from regulatory proteins in a precisely orchestrated manner, represent the currency of signaling processes within the cell. Thereby, biological activity, subcellular localization, half-life, and posttranscriptional modifications as well as interactions with other proteins are regulated (Cohen, 2000; Kosti et al., 2010; Turra et al., 2014). In fungi, diverse physiological functions are known for protein kinases and protein phosphatases including modulation of development, expression of plant cell wall degrading enzymes, secondary metabolism, as well as circadian rhythmicity and light response (Diernfellner and Schafmeier, 2011; Park et al., 2011; Ghosh et al., 2014; de Assis et al., 2015; Winkelströter et al., 2015). Recently, an involvement of different protein phosphatases in many of these mechanisms was shown for *T. reesei* as well (Rodriguez-Iglesias and Schmoll, 2019). The genome of *T. reesei* comprises 103 predicted protein kinase genes (Schmoll et al., 2016). Phosphoproteomic analysis of the reaction of *T. reesei* to inducing conditions provided insights into a complex signaling network, with phosphorylation changes in proteins associated with light-mediated cellulase regulation, carbon sensing, and osmoregulation as well as in the glycolytic pathway (Nguyen et al., 2016).

Here we investigated a kinase with similarity to YPK1 type kinases, which turned out to be unique in *Trichoderma* spp. With functions in regulation of genes within the SOR cluster, but also in cellulase gene expression, this kinase may represent an interesting evolutionary adaptation of *T. reesei* to the need of balanced resource distribution between nutrient acquisition and reaction to competitors.

RESULTS

A Unique AGC Family Protein Kinase in the Vicinity of the SOR Cluster

Searching for signaling factors modulating expression of the SOR cluster, we found an AGC family serine/threonine protein kinase represented by the gene model TR_53776 in its vicinity (scaffold 1:478516-479682; 2.3 kb upstream of TR_73618/*pks11*), which may regulate transcription factor activity or influence enzyme stability by phosphorylation. A recent study on protein phosphorylation in *T. reesei* (Nguyen et al., 2016) revealed phosphorylation of the transporter within the SOR cluster (TR_43701), which impacts secondary metabolite levels (Monroy et al., 2017). TR_53776 is related to YPK1 type kinases (protein domain cd11651), which are essential for cell growth in yeast and play a role in endocytosis and cell wall integrity. The *ypk1* homolog in *Neurospora crassa* (NCU07280) was found to be essential (Park et al., 2011), but analyses of conditional mutants in *Aspergillus nidulans* showed functions in growth, hyphal morphogenesis, and delivery of cell membrane and cell wall constituents to the hyphal apex (Colabardini et al., 2013). TR_53776 comprises one potential PEST motif (amino acids 6–24) in its sequence, which indicates regulation of protein stability by phosphorylation (Rechsteiner and Rogers, 1996) as well as eight poor PEST motifs. TargetP 2.0, NetNES 1.1, and WoLF PSORT were used for prediction of localization; however, no targeting sequences to the nucleus or other cellular compartments were detected. Evaluation of available transcriptome data revealed that TR_53776 is regulated in an induction specific manner (Stappler et al., 2017a), but no significant regulation was observed by light, photoreceptors or CRE1 (Tisch et al., 2011b; Tisch and Schmoll, 2013; Monroy et al., 2017).

We further found that the genomic localization of TR_53776 close to the SOR cluster is not syntenic in other fungi such as *Aspergillus niger* or *P. chrysogenum*. Accordingly, bidirectional best hit analysis showed that the best blast hits of TR_53776 in these fungi were related to kinases other than TR_53776. Therefore, we performed a phylogenetic analysis of TR_53776 and its most closely related kinases in *T. reesei* using the best hits of related fungi along with putative homologs from more distantly related fungi. This analysis showed that TR_53776 is not conserved in fungi, not even in closely related *Trichoderma* spp. like *Trichoderma harzianum* (**Figure 1**). Only for *Trichoderma atroviride*, a homolog was detected. Consequently, we named TR_53776 *u*nique *S*OR cluster *k*inase 1 (*usk1*).

Evaluation of a Relevance of *usk1* for Growth

While *usk1* is not an ortholog of the well characterized *ypk1* kinases, its close relationship still made us evaluate whether there are functional similarities by deleting *usk1* in QM6a. In contrast to YPK1 homologs in *N. crassa* and *A. nidulans*, *T. reesei* USK1 is not essential for growth. Strains lacking *usk1* are viable and analyses of hyphal extension on solid media with

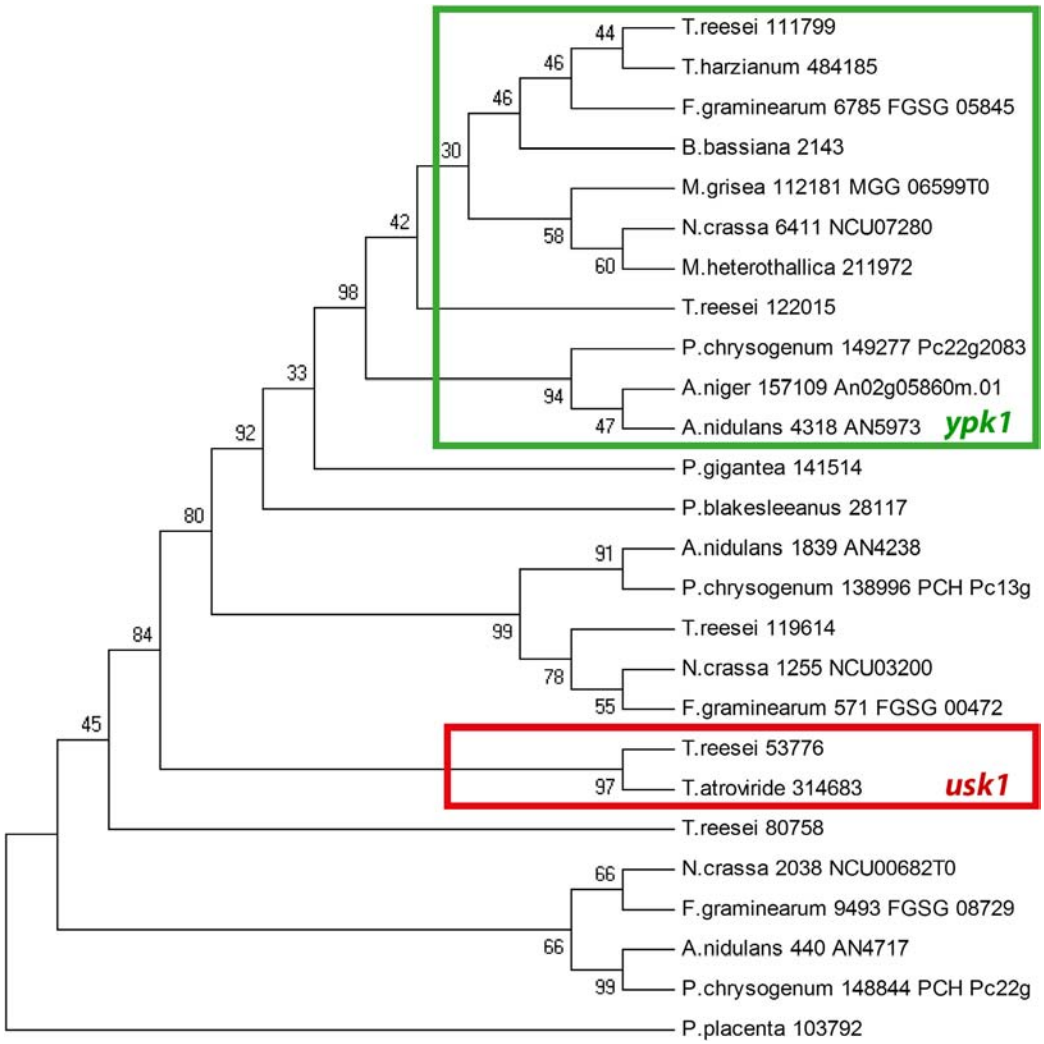

FIGURE 1 | Phylogenetic analysis of *usk1* in fungi. The phylogenetic tree was obtained using MEGA4.0 with the maximum parsinomy method. Numbers at branches indicate bootstrap support values. Protein IDs or locus IDs are provided along with species names for sequences originating from *Trichoderma reesei*, *Trichoderma harzianum*, *Fusarium graminearum*, *Beauveria bassiana*, *Magnaporthe grisea*, *Neurospora crassa*, *Myceliophthora heterothallica*, *Penicillium chrysogenum*, *Aspergillus niger*, *Aspergillus nidulans*, *Phlebiopsis gigantea*, *Phycomyces blakesleeanus*, and *Postia placenta*.

malt extract, cellulose, or glucose did not show any growth defect (**Supplementary Figures S1, S2**). We also tested the relevance of USK1 for dealing with osmotic stress including ion stress (minimal media with 1 M NaCl or 1 M sorbitol) upon growth in the presence of cellulose or glucose in light and darkness. However, also under these conditions, no significant alterations in growth compared to wild-type was observed (**Supplementary Figures S1, S2**).

USK1 Positively Impacts Cellulase Gene Expression

Transcript levels of *usk1* are upregulated in an induction specific manner (Stappler et al., 2017a). Therefore, we evaluated a relevance of this kinase for regulation of cellulase gene expression. Analysis of transcript levels of *cbh1* upon growth on minimal medium with cellulose as carbon source revealed a positive impact of USK1 on *cbh1* transcript abundance in darkness (**Figure 2A**), but not in light (**Figure 2B**). Accordingly, biomass formation of Δ*usk1* in liquid media with cellulose as carbon source decreased considerably in darkness (**Figure 2C**) and specific secreted endo-β-1,4-glucanase activity dropped (**Figure 2D**). Accordingly, also liberation of reducing sugars from cellulose, representing cellulase activity, decreased (**Figure 2E**). However, β-glucosidase activity remained largely unchanged in.Δ*usk1* (**Figure 2F**). In light only a minor alteration in biomass formation (83 ± 5.4%) was observed between mutant and wildtype. Specific endo-β-1,4-glucanase activity representing cellulase activity remained below detection limits in the deletion strain, as in the wildtype upon growth in constant light.

Since CRE1 was previously shown to impact the SOR cluster (Monroy et al., 2017) besides its function as a carbon catabolite

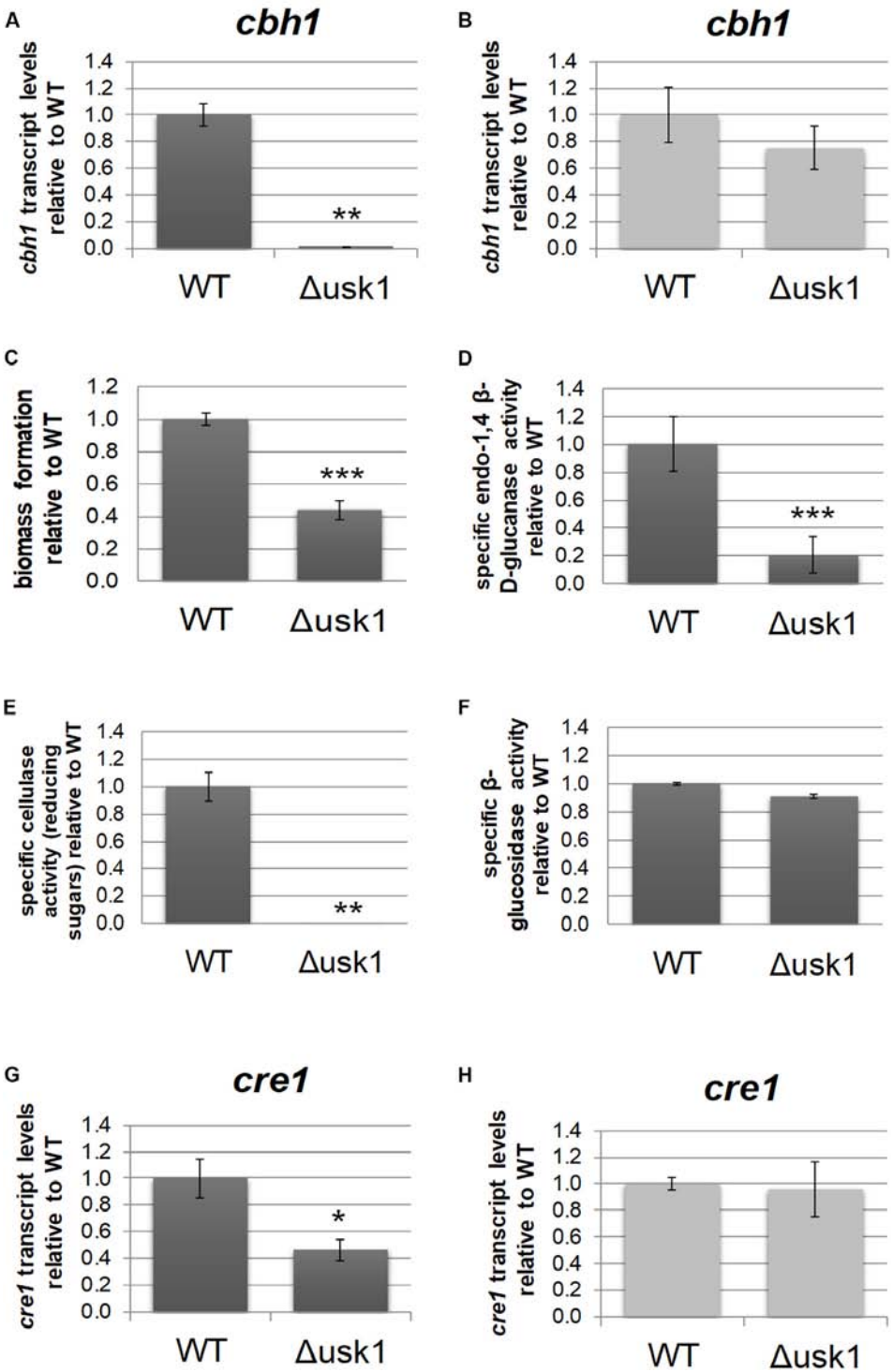

FIGURE 2 | Regulatory impact of USK1 on cellulase regulation and on CRE1. Transcript levels of cellobiohydrolase 1 (*cbh1*) as representative cellulase are shown for growth on microcrystalline cellulose in constant darkness (**A**; DD) and constant light (**B**; LL). **(C)** Biomass formation upon growth on microcrystalline cellulose in constant darkness. **(D)** Specific endo-1,4 β-D-glucanase activity upon growth on cellulose in darkness. **(E)** Specific cellulase activity (reducing sugars) upon growth on cellulose in darkness. **(F)** Specific β-glucosidase activity upon growth on cellulose in darkness. **(G,H)** Transcript abundance of *cre1* upon growth on cellulose in constant darkness **(G)** or constant light **(H)**. Error bars indicate standard deviations of three biological replicates. Asterisks indicate statistically significant differences compared to wildtype (**p*-value < 0.05, ***p*-value < 0.01, ****p*-value < 0.001).

repressor (Strauss et al., 1995), we tested an influence of USK1 on transcript abundance of *cre1*. In darkness, we observed a positive effect of USK1 (about twofold) on transcript levels of *cre1* on cellulose (**Figure 2G**), while no effect was seen in light (**Figure 2H**).

USK1 Is Involved in Regulation of Secondary Metabolism

Due to its genomic position close to the SOR cluster, we analyzed a potential influence of USK1 on gene regulation of secreted metabolites in general, of those in the SOR cluster and the impact on production of known secondary metabolites produced by *T. reesei*.

First we tested for a general regulation of secreted metabolite patterns by analysis of secreted compounds during cultivation on minimal medium with cellulose as carbon source by high performance thin layer chromatography (HPTLC) (Hinterdobler et al., 2019). This method provides an informative visual overview on abundance of metabolites in multiple samples and represents a valuable alternative to mass spectrometry, particularly for organisms with only few compounds already known and characterized like *T. reesei* (Frisvad et al., 2018; Hinterdobler et al., 2019). We found a clear decrease in overall abundance of metabolites upon growth in liquid culture with cellulose as carbon source in darkness in Δ*usk1* (**Figures 3A–D**), but no changes in light compared to wildtype under the same conditions (**Figures 3E,F**). Although biosynthesis of yellow pigments, largely representing sorbicillinoids, is at a low level under these conditions, the positive effect of USK1 on production of individual compounds of this group is still visible (**Figures 3C,D**). Accordingly, analysis of the supernatant for absorbance at 370 nm, representing part of the sorbicillinoids, is decreased (**Figure 3G**).

Quantification of selected secondary metabolites in the supernatant of cellulose grown cultures by mass spectrometry with internal standards revealed decreased levels for the sorbicillin derivative dihydrotrichotetronine (syn. bislongiquinolide or bisorbibutenolide, Shirota et al., 1997; a major product of the SOR cluster, Monroy et al., 2017), alamethicine, orsellinic acid, and paracelsin (**Figure 3H**). Consequently, USK1 does not only impact sorbicilline compounds associated with the SOR cluster, such as dihydrotrichotetronine, but also other compounds, which is in agreement with HPTLC analysis. Hence, this putative kinase is not specifically targeting sorbicillin production, but presumably impacts regulation of multiple secondary metabolite gene clusters to modulate secondary metabolism more broadly.

In order to gain insight into the regulatory basis of the effect of USK1 on secondary metabolite production, we analyzed its impact on transcript abundance of the general regulator of secondary metabolism, *vel1*, and the two transcription factor genes associated with the SOR cluster, *ypr1* and *ypr2*. We found that USK1 positively regulates transcript abundance of *vel1* in darkness, but slightly negatively in light (**Figures 4A,B**). For *ypr1*, we found negative regulation by USK1 in light and darkness (**Figures 4C,D**), but no effect on *ypr2* (**Figures 4E,F**).

Screening for an influence of USK1 on transcript abundance of SOR cluster genes (**Figures 4G–P**) showed a negative effect USK1 on *sor1* (TR_73618), *sor5* (TR_73623), and TR_73631 in light and darkness. The gene encoding the transporter SOR4 (TR_43701) is positively regulated in darkness by USK1 (**Figure 4O**). While USK1 appears to exert a negative effect on transcript levels of several SOR cluster genes, the decreased abundance of secondary metabolites associated with this cluster in the culture filtrate as shown in **Figures 3C,D,G** may be due to the decreased levels of the transporter TR_43701 (**Figure 4O**).

DISCUSSION

As one of the most important biotechnological workhorses among filamentous fungi, the physiology of *T. reesei* and particularly its secondary metabolism are of high interest to industry. It is of utmost importance to ensure the lack of harmful secondary metabolites in food and feed products from fungal fermentations. Therefore, investigation of regulators and the conditions under which they are operative is crucial to understand secondary metabolism in *T. reesei*.

Protein kinases generally have broad functions in fungi, including regulation of pathogenicity and virulence, stress response, circadian rhythmicity, development, and metabolism (Dickman and Yarden, 1999; Diernfellner and Schafmeier, 2011; Brown et al., 2014; Turra et al., 2014; Manfiolli et al., 2019). The kinomes of fungi share similarity, albeit domain distribution and density of kinomes are suggested to reflect taxonomy (Kosti et al., 2010). In *A. nidulans*, protein kinases were shown to impact secondary metabolism, particularly the group of mitogen activated protein kinases (De Souza et al., 2013). MAPkinases impact secondary metabolism also in *Podospora anserina* (Bidard et al., 2012) and *N. crassa* (Park et al., 2008). USK1 is related to YPK-type protein kinases (particularly to YPK2) which are essential for cell growth and maintenance of cell wall integrity (Chen et al., 1993; Roelants et al., 2002). Saccharomyces *cerevisiae* YPK2 is subject to phosphorylation by TOR kinases, thereby impacting actin polarization (Kamada et al., 2005). Moreover, YPK2 is implicated in the sphingolipid mediated signaling pathway which targets multiple physiological functions like endocytosis, ubiquitin dependent proteolysis, regulation of nutrient uptake, the cell cycle, translation, and heat stress response (Chung et al., 2001; Cowart and Obeid, 2007). The *N. crassa* kinase most closely related to USK1 is NCU07280/STK50, which is an essential gene in this fungus (Park et al., 2011) and only shows minor regulation in response to phytosphingosine (Videira et al., 2009). A function in glucose starvation was reported for the fission yeast kinase related to USK1, GAD8 (Saitoh et al., 2015). Also in *A. nidulans*, the most closely related kinase AN5973 is an essential gene required for polar axis establishment and germling growth (Colabardini et al., 2013; De Souza et al., 2013).

Although USK1 is closely related to these kinases, our analyses revealed that it represents a unique kinase in *Trichoderma* spp. Accordingly, deletion of *usk1* also was not fatal and growth characteristics of Δ*usk1* were largely normal. Nevertheless, USK1

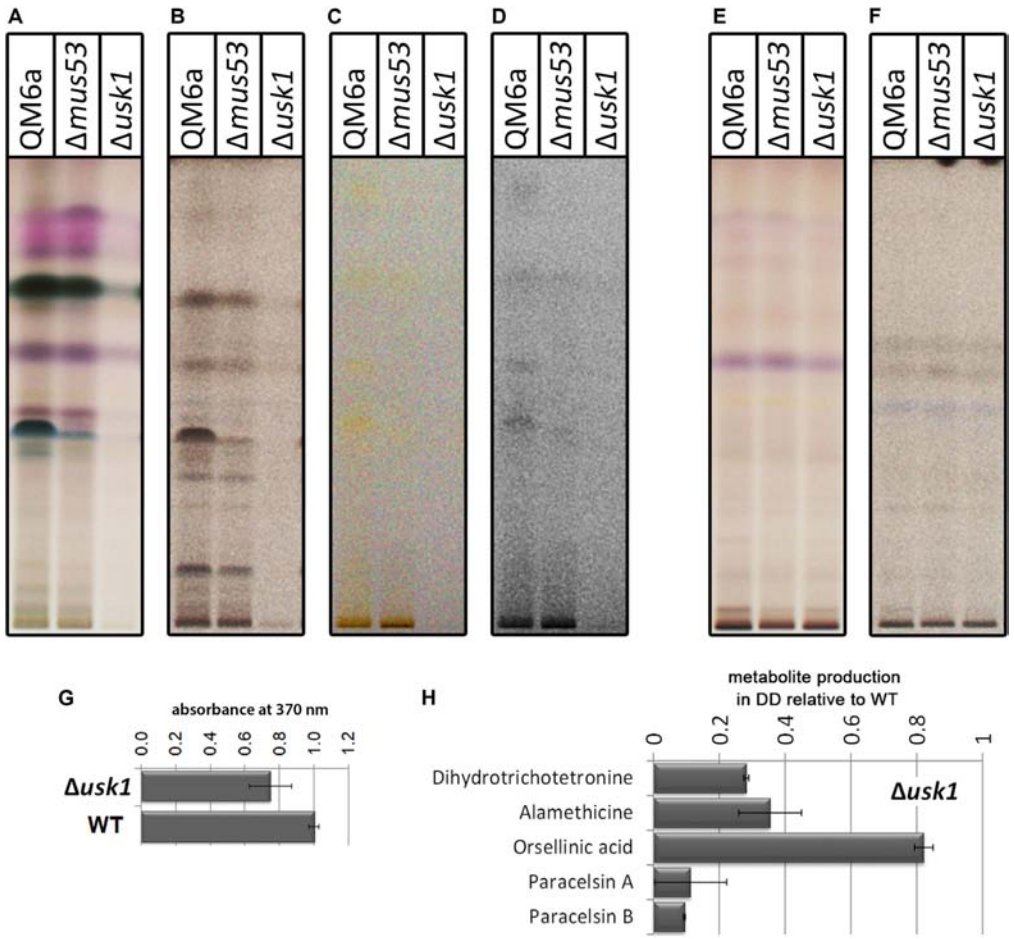

FIGURE 3 | Impact of USK1 on production of secondary metabolites and their regulators. Wildtype QM6a, parental strain QM6aΔ*mus53* and Δ*usk1* were grown on minimal medium in constant light (LL; **E,F**) or constant darkness (DD; **A–D**) with cellulose as carbon source. The individual panels show different visualization techniques showing different sets of secondary metabolites of substance classes responsive to the respective technique. **(A,E)** show visualization at visible light after derivatization with anisaldehyde solution. **(B,F)** show absorption at 254 nm after development. **(C,D)** show visualization at visible light after development. For better visibility of the yellow compounds shown in **(C)** in the saturation was lowered in **(D)**. Analyses were done in biological triplicates and are related to biomass values. **(G)** Determination of absorbance at 370 nm in the supernatant in relation to the wildtype in constant darkness. Analysis was done in biological triplicates. **(H)** Quantitative analyses by mass spectrometry with internal standards were performed from strains grown on cellulose in darkness. Abundance of the mentioned metabolites is shown in relation to the wildtype. Values are normalized to biomass.

is highly relevant for expression of cellulolytic enzymes and impacts regulation of genes of the SOR cluster, which is in its genomic vicinity. In Trichoderma *parareesei*, with the closest homology to *T. reesei* this localization is conserved, but already in *Trichoderma citrinoviride*, the locus of *usk1* and the SOR cluster is altered as it is in *T. atroviride* and *Trichoderma gamsii*. This is in agreement with the SOR cluster being only present in the section Longibrachiatum (Druzhinina et al., 2016). Consequently, the regulatory impact of USK1 on the SOR cluster could have been a beneficial event after acquisition by lateral gene transfer.

Cellulase gene expression is regulated in response to diverse environmental cues, the most important of them being the kind of carbon source and its abundance as well as the impact of light. This regulation is influenced broadly by components of different signal transduction pathways, which are known to be subject to modifications in activity levels by phosphorylation (Bazafkan et al., 2014; Paloheimo et al., 2016; Schmoll, 2018). Transcript levels of *usk1* are decreased upon growth in darkness on glucose compared to cellulose in QM6a (Beier, Hinterdobler, and Schmoll, unpublished). Additionally, *usk1* showed induction specific regulation (Stappler et al., 2017a). Considering the substantial impact of USK1 on biomass formation and cellulase production upon growth on cellulose, it can be assumed that the major function of USK1 is in nutrient signal transduction and potentially in its coordination with regulation of secondary metabolism. Thereby, the impact of USK1 is not limited to the genes of the cluster and the compounds associated with the SOR cluster. With a relevance of USK1 also to the production of alamethicine and paracelsine, a broader function of USK1 on secondary metabolism is obvious, which is also reflected in considerably

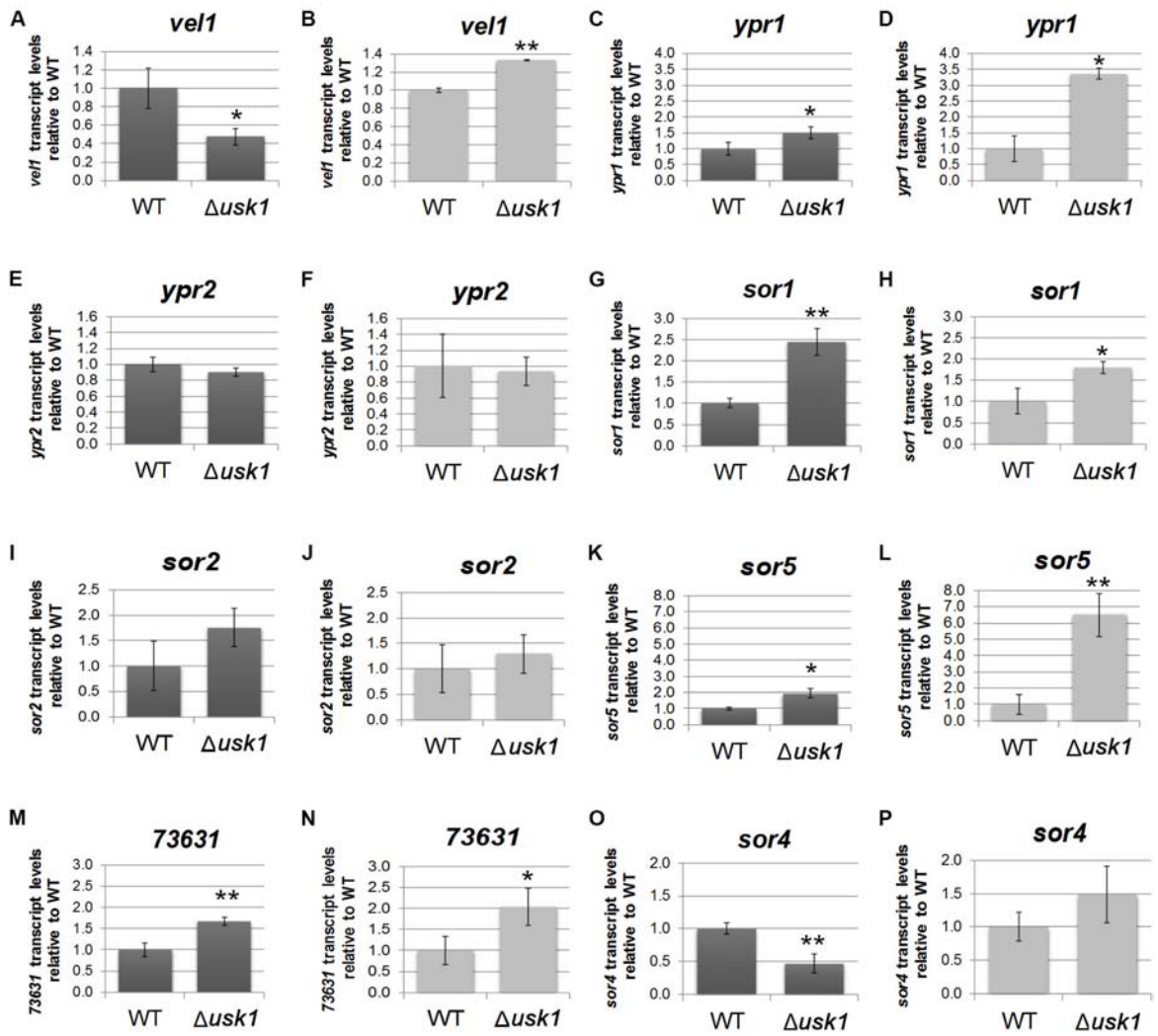

FIGURE 4 | Influence of USK1 on regulators of secondary metabolism and the SOR cluster. Evaluation of the impact of USK1 on known regulators of secondary metabolism. Transcript abundance of *vel1* **(A,B)**, *ypr1* **(C,D)**, and *ypr2* **(E,F)** upon growth on cellulose in constant darkness (DD; **A,C,E**) or constant light (LL; **B,D,F**). **(G–P)** Impact of USK1 on SOR cluster genes. Transcript levels of sor1 (TR_73618; **G,H**), sor2 (TR_73621; **I,J**), sor5 (TR_73623; **K,L**), TR_73631 **(M,N)**, and sor4 (TR_43701; **O,P**) are shown for growth on microcrystalline cellulose in constant darkness (DD; **G,I,K,M,O**) and constant light (LL; **H,J,L,N,P**). Error bars indicate standard deviations of three biological replicates. Asterisks indicate statistically significant differences compared to wildtype (*p-value < 0.05, **p-value < 0.01).

decreased levels of secreted metabolites detected in the HPTLC analysis (**Figure 3**). These findings are in agreement with previous reports, showing that alterations in the levels SOR cluster compounds are often accompanied with modulations of further metabolites associated with other secondary metabolite clusters (Bazafkan et al., 2017; Monroy et al., 2017; Dattenböck et al., 2018). Also for the transcription factor YPR2, which regulates the SOR cluster (Derntl et al., 2016; Monroy et al., 2017), regulation of multiple genes involved in secondary metabolism was shown (Hitzenhammer et al., 2019). For the transcription factor XPP1, which exerts functions in primary and secondary metabolism, a broad impact on both quantity and diversity of secreted metabolites was shown as well (Derntl et al., 2017b). While the actual target(s) of USK1 remain to be elucidated, it can be assumed that in agreement with the results for YPR2 and XPP1, regulation of secondary metabolism is governed by a flat hierarchical network that targets gene regulation broadly rather than specifically, hence establishing a complex network of interdependent regulatory effects. The modulating function of USK1 on the SOR cluster genes and their products as well as on enzyme production moreover add further support for a crosstalk between enzyme expression and secondary metabolism in *T. reesei*.

MATERIALS AND METHODS

Strains and Cultivation Conditions

QM6a (ATCC13631) (Martinez et al., 2008) and QM6aΔ*mus53* (Steiger et al., 2011) was used in this study. For analysis of

gene regulation by USK1, strains were cultivated in constant darkness (to exclude interference by circadian rhythmicity) on malt extract agar plates for 14 days to produce conidia for inoculation.

For liquid cultures 10^8 conidia/L were used for inoculation. Strains grown in Mandels Andreotti minimal medium (Mandels and Andreotti, 1978) with 1% (w/v) cellulose (avicel, SERVA, Alfa Aesar, Karlsruhe, Germany) in constant light (1700 lux, Osram L18W/835 fluorescent bulbs) or in constant darkness at 28°C at 200 r/min. Mycelia and supernatants were harvested after 96 h. Red safety light (darkroom lamp, Philips PF712E, red, E27, 15 W) was applied to avoid random light pulses during harvesting of dark grown cultures.

Hyphal extension was investigated on plates in constant light or constant darkness on the carbon sources mentioned with the experiment and three biological replicates were used. Sexual development was analyzed with strains grown on malt extract media at 22°C in dark-light cycles as described previously (Schmoll, 2013).

Construction of Δ*usk1*

Deletion of *usk1* was done in QM6aΔ*mus53* (deficient in non-homologous end joining) using the streamlined procedure described previously (Schuster et al., 2012) with the *hph* marker cassette. Transformation was done by protoplasting (Gruber et al., 1990). Successful deletion was confirmed by PCR using primers 53776RTF and 53776RTR. Sequences of all primers used in this study are given in **Supplementary Table S1**. Copy number determination for integration of the deletion cassette in to the genome of *T. reesei* was performed as described previously (Tisch and Schmoll, 2013). This analysis showed integration of one single copy of the *usk1* deletion cassette into the genome and hence confirmed homologous integration (**Supplementary Figure S3**).

Nucleic Acid Manipulation and Analysis

Isolation of total RNA, quality control, and RTqPCR were done as described previously (Tisch et al., 2011a; Bazafkan et al., 2017). *Sar1* was used as reference gene for RT-qPCR as it was shown to be generally very stable across different conditions (Bazafkan et al., 2017). We considered three biological and three technical replicates for analysis using the CFX Maestro analysis software (Biorad, Hercules, CA, United States). Primers used for analysis are listed in **Supplementary Table S1**.

Enzyme Assays

Endo-1,4-β-glucanase activity in culture filtrates was determined using azo-CM-cellulose (S-ACMC-L, Megazyme, Wicklow, Ireland) according to the manufacturers instructions.

Cellulase activity as represented by reducing sugars was measured using the pHBAH (*p*-hydroxybenzoic acid hydrazide) assay as described previously (Mellitzer et al., 2012). Therefore, 1% (w/v) cellulose (Alfa Aesar, Karlsruhe, Germany) served as sole carbon source in the substrate suspension. The absorbance at 410 nm was determined in 96-well flat bottom plates (Greiner Bio One, Kremsmünster, Austria) using a BioTek Synergy™ Mx microplate reader.

Analysis of β-glucosidase was performed using the chromogenic substrate 4-nitrophenyl-β-D-glucopyranosid as described previously (da Silva Delabona et al., 2017).

Biomass for determination of specific enzyme activity was measured in the presence of insoluble cellulose with intracellular protein content as representative criterium as described previously (Schuster et al., 2011; Stappler et al., 2017b). Three biological replicates and technical triplicates were analyzed.

Bioinformatic Analysis

Phylogenetic analysis was performed as described previously (Bazafkan et al., 2015) using the software packages ClustalX1.82 and MEGA4 (Tamura et al., 2007). Therefore, sequences were obtained from JGI Mycocosm. Homology and BLAST searches were performed on the JGI Mycocosm platform[1]. Screening for PEST domains (Rechsteiner and Rogers, 1996) was done using the online resource ePESTFIND[2] with default settings. TargetP 2.0 (Emanuelsson et al., 2007), NetNES 1.1 (la Cour et al., 2004), and WoLF PSORT (Horton et al., 2007) were applied to analyze protein characteristics. For detection of conserved domains, the conserved domain search at NCBI[3] (Marchler-Bauer et al., 2017). Statistical significance of values was evaluated by *t*-test in RStudio (compare_means, ggpubr).

Analysis of Secondary Metabolites Secreted by *T. reesei*

High performance thin layer chromatography was performed as described previously from culture supernatants of cellulose grown mycelia by extraction with chloroform (Monroy et al., 2017; Hinterdobler et al., 2019). Measurements are related to biomass abundance for every sample.

Abundance of selected secondary metabolites was analyzed by mass spectrometry with internal standards as described previously (Malachova et al., 2014; Monroy et al., 2017).

DATA AVAILABILITY STATEMENT

All datasets relevant for this study are included in the article/**Supplementary Material**.

AUTHOR CONTRIBUTIONS

SB contributed to analysis of growth and cellulase production. WH contributed to analysis of secondary metabolite production. AM participated in secondary metabolite analysis and cultivation. HB constructed the recombinant strain. SB and

[1]https://mycocosm.jgi.doe.gov/mycocosm/home

[2]http://emboss.bioinformatics.nl/cgi-bin/emboss/epestfind

[3]https://www.ncbi.nlm.nih.gov/Structure/cdd/wrpsb.cgi?

WH participated in drafting the manuscript. MS conceived of the study, participated in analysis and interpretation of results, and wrote the final version of the manuscript. All authors read and agreed to publication of the final manuscript.

FUNDING

Work of SB, HB, and AM was supported by the Austrian Science Fund (FWF; projects P26935; P24350 to MS). Work of WH was supported by the NFB (Science Fund of Lower Austria; Grant LC16-04 to MS). The funding agencies had no role in study design or publication.

ACKNOWLEDGMENTS

We want to thank Julia Scholda for technical assistance with HPTLC analysis and Marlene Stiegler, Michael Sulyok, and Stefan Böhmdorfer for technical assistance and the possibility to access analytic equipment.

SUPPLEMENTARY MATERIAL

The Supplementary Material for this article can be found online at: https://www.frontiersin.org/articles/10.3389/fmicb.2020.00974/full#supplementary-material

REFERENCES

Bazafkan, H., Beier, S., Stappler, E., Böhmdorfer, S., Oberlerchner, J. T., Sulyok, M., et al. (2017). SUB1 has photoreceptor dependent and independent functions in sexual development and secondary metabolism in *Trichoderma reesei*. *Mol. Microbiol.* 106, 742–759. doi: 10.1111/mmi.13842

Bazafkan, H., Dattenböck, C., Böhmdorfer, S., Tisch, D., Stappler, E., and Schmoll, M. (2015). Mating type dependent partner sensing as mediated by VEL1 in *Trichoderma reesei*. *Mol. Microbiol.* 96, 1103–1118. doi: 10.1111/mmi.12993

Bazafkan, H., Tisch, D., and Schmoll, M. (2014). "Regulation of glycoside hydrolase expression in *Trichoderma*," in *Biotechnology and Biology of Trichoderma*, eds V. K. Gupta, M. Schmoll, A. Herrera-Estrella, I. Druzhinina, and M. G. Tuohy (Oxford: Elsevier), 291–307.

Benocci, T., Aguilar-Pontes, M. V., Zhou, M., Seiboth, B., and de Vries, R. P. (2017). Regulators of plant biomass degradation in ascomycetous fungi. *Biotechnol. Biofuels* 10:152. doi: 10.1186/s13068-017-0841-x

Bidard, F., Coppin, E., and Silar, P. (2012). The transcriptional response to the inactivation of the PaMpk1 and PaMpk2 MAP kinase pathways in *Podospora anserina*. *Fungal Genet. Biol.* 49, 643–652. doi: 10.1016/j.fgb.2012.06.002

Bischof, R. H., Ramoni, J., and Seiboth, B. (2016). Cellulases and beyond: the first 70 years of the enzyme producer *Trichoderma reesei*. *Microb. Cell Fact.* 15:106. doi: 10.1186/s12934-016-0507-6

Bringmann, G., Lang, G., Muhlbacher, J., Schaumann, K., Steffens, S., Rytik, P. G., et al. (2003). Sorbicillactone A: a structurally unprecedented bioactive novel-type alkaloid from a sponge-derived fungus. *Prog. Mol. Subcell Biol.* 37, 231–253. doi: 10.1007/978-3-642-55519-0_9

Brown, N. A., Ries, L. N. A., and Goldman, G. H. (2014). How nutritional status signalling coordinates metabolism and lignocellulolytic enzyme secretion. *Fungal Genet. Biol.* 72, 48–63. doi: 10.1016/j.fgb.2014.06.012

Chen, P., Lee, K. S., and Levin, D. E. (1993). A pair of putative protein kinase genes (YPK1 and YPK2) is required for cell growth in *Saccharomyces cerevisiae*. *Mol. Gen. Genet.* 236, 443–447. doi: 10.1007/bf00277146

Chung, N., Mao, C., Heitman, J., Hannun, Y. A., and Obeid, L. M. (2001). Phytosphingosine as a specific inhibitor of growth and nutrient import in *Saccharomyces cerevisiae*. *J. Biol. Chem.* 276, 35614–35621. doi: 10.1074/jbc.M105653200

Cohen, P. (2000). The regulation of protein function by multisite phosphorylation – a 25 year update. *Trends Biochem. Sci.* 25, 596–601. doi: 10.1016/s0968-0004(00)01712-6

Colabardini, A. C., Brown, N. A., Savoldi, M., Goldman, M. H., and Goldman, G. H. (2013). Functional characterization of *Aspergillus nidulans ypkA*, a homologue of the mammalian kinase SGK. *PLoS ONE* 8:e57630. doi: 10.1371/journal.pone.0057630

Cowart, L. A., and Obeid, L. M. (2007). Yeast sphingolipids: recent developments in understanding biosynthesis, regulation, and function. *Biochim. Biophys. Acta* 1771, 421–431. doi: 10.1016/j.bbalip.2006.08.005

Cram, D. J. (1948). Mold metabolites; the structure of sorbicillin, a pigment produced by the mold *Penicillium notatum*. *J. Am. Chem. Soc.* 70, 4240–4243. doi: 10.1021/ja01192a077

da Silva, Delabona, P., Rodrigues, G. N., Zubieta, M. P., Ramoni, J., Codima, C. A., et al. (2017). The relation between xyr1 overexpression in *Trichoderma harzianum* and sugarcane bagasse saccharification performance. *J. Biotechnol.* 246, 24–32. doi: 10.1016/j.jbiotec.2017.02.002

Dattenböck, C., Tisch, D., Schuster, A., Monroy, A. A., Hinterdobler, W., and Schmoll, M. (2018). Gene regulation associated with sexual development and female fertility in different isolates of *Trichoderma reesei*. *Fungal Biol. Biotechnol.* 5:9. doi: 10.1186/s40694-018-0055-4

de Assis, L. J., Ries, L. N., Savoldi, M., Dinamarco, T. M., Goldman, G. H., and Brown, N. A. (2015). Multiple phosphatases regulate carbon source-dependent germination and primary metabolism in *Aspergillus nidulans*. *G3 (Bethesda)* 5, 857–872. doi: 10.1534/g3.115.016667

De Souza, C. P., Hashmi, S. B., Osmani, A. H., Andrews, P., Ringelberg, C. S., Dunlap, J. C., et al. (2013). Functional analysis of the *Aspergillus nidulans* kinome. *PLoS ONE* 8:e58008. doi: 10.1371/journal.pone.0058008

Derntl, C., Guzman-Chavez, F., Mello-de-Sousa, T. M., Busse, H. J., Driessen, A. J. M., Mach, R. L., et al. (2017a). In Vivo study of the sorbicillinoid gene cluster in *Trichoderma reesei*. *Front. Microbiol.* 8:2037. doi: 10.3389/fmicb.2017.02037

Derntl, C., Kluger, B., Bueschl, C., Schuhmacher, R., Mach, R. L., and Mach-Aigner, A. R. (2017b). Transcription factor Xpp1 is a switch between primary and secondary fungal metabolism. *Proc. Natl. Acad. Sci. U.S.A.* 114, E560–E569. doi: 10.1073/pnas.1609348114

Derntl, C., Rassinger, A., Srebotnik, E., Mach, R. L., and Mach-Aigner, A. R. (2016). Identification of the main regulator responsible for synthesis of the typical yellow pigment produced by *Trichoderma reesei*. *Appl. Environ. Microbiol.* 82, 6247–6257. doi: 10.1128/AEM.01408-16

Dickman, M. B., and Yarden, O. (1999). Serine/threonine protein kinases and phosphatases in filamentious fungi. *Fungal Genet. Biol.* 26, 99–117. doi: 10.1006/fgbi.1999.1118

Diernfellner, A. C., and Schafmeier, T. (2011). Phosphorylations: making the *Neurospora crassa* circadian clock tick. *FEBS Lett.* 585, 1461–1466. doi: 10.1016/j.febslet.2011.03.049

Druzhinina, I. S., Kubicek, E. M., and Kubicek, C. P. (2016). Several steps of lateral gene transfer followed by events of 'birth-and-death' evolution shaped a fungal sorbicillinoid biosynthetic gene cluster. *BMC Evol. Biol.* 16:269. doi: 10.1186/s12862-016-0834-6

Emanuelsson, O., Brunak, S., von Heijne, G., and Nielsen, H. (2007). Locating proteins in the cell using TargetP, SignalP and related tools. *Nat. Protoc.* 2, 953–971. doi: 10.1038/nprot.2007.131

Foreman, P. K., Brown, D., Dankmeyer, L., Dean, R., Diener, S., Dunn-Coleman, N. S., et al. (2003). Transcriptional regulation of biomass-degrading enzymes in the filamentous fungus *Trichoderma reesei*. *J. Biol. Chem.* 278, 31988–31997. doi: 10.1074/jbc.M304750200

Frisvad, J. C., Moller, L. L. H., Larsen, T. O., Kumar, R., and Arnau, J. (2018). Safety of the fungal workhorses of industrial biotechnology: update on the mycotoxin and secondary metabolite potential of *Aspergillus niger, Aspergillus oryzae,* and *Trichoderma reesei*. *Appl. Microbiol. Biotechnol.* 102, 9481–9515. doi: 10.1007/s00253-018-9354-1

Ghosh, A., Servin, J. A., Park, G., and Borkovich, K. A. (2014). Global analysis of serine/threonine and tyrosine protein phosphatase catalytic subunit genes in *Neurospora crassa* reveals interplay between phosphatases and the p38 mitogen-activated protein kinase. *G3 (Bethesda)* 4, 349–365. doi: 10.1534/g3.113.008813

Gruber, F., Visser, J., Kubicek, C. P., and de Graaff, L. H. (1990). The development of a heterologous transformation system for the cellulolytic fungus *Trichoderma reesei* based on a *pyrG* -negative mutant strain. *Curr. Genet.* 18, 71–76. doi: 10.1007/bf00321118

Gupta, V. K., Steindorff, A. S., de Paula, R. G., Silva-Rocha, R., Mach-Aigner, A. R., Mach, R. L., et al. (2016). The post-genomic era of *Trichoderma reesei*: what's next? *Trends Biotechnol.* 34, 970–982. doi: 10.1016/j.tibtech.2016.06.003

Guzman-Chavez, F., Salo, O., Nygard, Y., Lankhorst, P. P., Bovenberg, R. A. L., and Driessen, A. J. M. (2017). Mechanism and regulation of sorbicillin biosynthesis by *Penicillium chrysogenum*. *Microb. Biotechnol.* 10, 958–968. doi: 10.1111/1751-7915.12736

Hinterdobler, W., Schuster, A., Tisch, D., Ozkan, E., Bazafkan, H., Schinnerl, J., et al. (2019). The role of PKAc1 in gene regulation and trichodimerol production in *Trichoderma reesei*. *Fungal Biol. Biotechnol.* 6:12. doi: 10.1186/s40694-019-0075-8

Hitzenhammer, E., Büschl, C., Sulyok, M., Schuhmacher, R., Kluger, B., Wischnitzki, E., et al. (2019). YPR2 is a regulator of light modulated carbon and secondary metabolism in *Trichoderma reesei*. *BMC Genomics* 20:211. doi: 10.1186/s12864-019-5574-8

Horton, P., Park, K. J., Obayashi, T., Fujita, N., Harada, H., Adams-Collier, C. J., et al. (2007). WoLF PSORT: protein localization predictor. *Nucleic Acids Res.* 35, W585–W587. doi: 10.1093/nar/gkm259

Kamada, Y., Fujioka, Y., Suzuki, N. N., Inagaki, F., Wullschleger, S., Loewith, R., et al. (2005). Tor2 directly phosphorylates the AGC kinase Ypk2 to regulate actin polarization. *Mol. Cell Biol.* 25, 7239–7248. doi: 10.1128/MCB.25.16.7239-7248.2005

Kosti, I., Mandel-Gutfreund, Y., Glaser, F., and Horwitz, B. A. (2010). Comparative analysis of fungal protein kinases and associated domains. *BMC Genomics* 11:133. doi: 10.1186/1471-2164-11-133

la Cour, T., Kiemer, L., Molgaard, A., Gupta, R., Skriver, K., and Brunak, S. (2004). Analysis and prediction of leucine-rich nuclear export signals. *Protein Eng. Des. Sel.* 17, 527–536. doi: 10.1093/protein/gzh062

Li, C., Lin, F., Sun, W., Yuan, S., Zhou, Z., Wu, F. G., et al. (2018). Constitutive hyperproduction of sorbicillinoids in *Trichoderma reesei* ZC121. *Biotechnol. Biofuels* 11:291. doi: 10.1186/s13068-018-1296-4

Malachova, A., Sulyok, M., Beltran, E., Berthiller, F., and Krska, R. (2014). Optimization and validation of a quantitative liquid chromatography-tandem mass spectrometric method covering 295 bacterial and fungal metabolites including all regulated mycotoxins in four model food matrices. *J. Chromatogr. A* 1362, 145–156. doi: 10.1016/j.chroma.2014.08.037

Mandels, M., and Andreotti, R. (1978). Problems and challenges in the cellulose to cellulase fermentation. *Proc. Biochem.* 13, 6–13.

Manfiolli, A. O., Siqueira, F. S., Dos Reis, T. F., Van Dijck, P., Schrevens, S., Hoefgen, S., et al. (2019). Mitogen-activated protein kinase cross-talk interaction modulates the mroduction of Melanins in *Aspergillus fumigatus*. *mBio* 10, e215–e219. doi: 10.1128/mBio.00215-19

Marchler-Bauer, A., Bo, Y., Han, L., He, J., Lanczycki, C. J., Lu, S., et al. (2017). CDD/SPARCLE: functional classification of proteins via subfamily domain architectures. *Nucleic Acids Res.* 45, D200–D203. doi: 10.1093/nar/gkw1129

Martinez, D., Berka, R. M., Henrissat, B., Saloheimo, M., Arvas, M., Baker, S. E., et al. (2008). Genome sequencing and analysis of the biomass-degrading fungus *Trichoderma reesei* (syn. *Hypocrea jecorina*). *Nat. Biotechnol.* 26, 553–560. doi: 10.1038/nbt1403

Maskey, R. P., Grun-Wollny, I., and Laatsch, H. (2005). Sorbicillin analogues and related dimeric compounds from *Penicillium notatum*. *J. Nat. Prod.* 68, 865–870. doi: 10.1021/np040137t

Mellitzer, A., Glieder, A., Weis, R., Reisinger, C., and Flicker, K. (2012). Sensitive high-throughput screening for the detection of reducing sugars. *Biotechnol. J.* 7, 155–162. doi: 10.1002/biot.201100001

Monroy, A. A., Stappler, E., Schuster, A., Sulyok, M., and Schmoll, M. (2017). A CRE1- regulated cluster is responsible for light dependent production of dihydrotrichotetronin in *Trichoderma reesei*. *PLoS ONE* 12:e0182530. doi: 10.1371/journal.pone.0182530

Nevalainen, H., Suominen, P., and Taimisto, K. (1994). On the safety of *Trichoderma reesei*. *J. Biotechnol.* 37, 193–200.

Nguyen, E. V., Imanishi, S. Y., Haapaniemi, P., Yadav, A., Saloheimo, M., Corthals, G. L., et al. (2016). Quantitative site-specific phosphoproteomics of *Trichoderma reesei* signaling pathways upon induction of hydrolytic enzyme production. *J. Proteome Res.* 15, 457–467. doi: 10.1021/acs.jproteome.5b00796

Paloheimo, M., Haarmann, T., Mäkinen, S., and Vehmaanperä, J. (2016). "Production of industrial enzymes in *Trichoderma reesei*," in *Gene Expression Systems in Fungi: Advancements and Applications*, eds M. Schmoll and C. Dattenböck (Heidelberg: Springer International), 23–58.

Park, G., Pan, S., and Borkovich, K. A. (2008). Mitogen-activated protein kinase cascade required for regulation of development and secondary metabolism in *Neurospora crassa*. *Eukaryot. Cell* 7, 2113–2122. doi: 10.1128/EC.00466-07

Park, G., Servin, J. A., Turner, G. E., Altamirano, L., Colot, H. V., Collopy, P., et al. (2011). Global analysis of serine-threonine protein kinase genes in *Neurospora crassa*. *Eukaryot. Cell* 10, 1553–1564. doi: 10.1128/EC.0514011

Rechsteiner, M., and Rogers, S. W. (1996). PEST sequences and regulation by proteolysis. *Trends Biochem. Sci.* 21, 267–271.

Rodriguez-Iglesias, A., and Schmoll, M. (2019). Protein phosphatases regulate growth, development, cellulases and secondary metabolism in *Trichoderma reesei*. *Sci. Rep.* 9:10995. doi: 10.1038/s41598-019-47421-z

Roelants, F. M., Torrance, P. D., Bezman, N., and Thorner, J. (2002). Pkh1 and Pkh2 differentially phosphorylate and activate Ypk1 and Ykr2 and define protein kinase modules required for maintenance of cell wall integrity. *Mol. Biol. Cell* 13, 3005–3028. doi: 10.1091/mbc.e02-04-0201

Saitoh, S., Mori, A., Uehara, L., Masuda, F., Soejima, S., and Yanagida, M. (2015). Mechanisms of expression and translocation of major fission yeast glucose transporters regulated by CaMKK/phosphatases, nuclear shuttling, and TOR. *Mol. Biol. Cell* 26, 373–386. doi: 10.1091/mbc.E14-11-1503

Salo, O., Guzman-Chavez, F., Ries, M. I., Lankhorst, P. P., Bovenberg, R. A., Vreeken, R. J., et al. (2016). Identification of a polyketide synthase involved in sorbicillin biosynthesis by *Penicillium chrysogenum*. *Appl. Environ. Microbiol.* 82, 3971–3978. doi: 10.1128/AEM.0035016

Saloheimo, M., and Pakula, T. M. (2012). The cargo and the transport system: secreted proteins and protein secretion in *Trichoderma reesei* (*Hypocrea jecorina*). *Microbiology* 158(Pt 1), 46–57. doi: 10.1099/mic.0.053132-0

Schmoll, M. (2013). "Sexual development in *Trichoderma* – scrutinizing the aspired phenomenon," in *Trichoderma: Biology and Applications*, eds P. K. Mukherjee, B. A. Horwitz, U. S. Singh, M. Mukherjee, and M. Schmoll (Wallingford: CAB International), 67–86.

Schmoll, M. (2018). Regulation of plant cell wall degradation by light in *Trichoderma*. *Fungal Biol. Biotechnol.* 5:10. doi: 10.1186/s40694-018-0052-7

Schmoll, M., Dattenböck, C., Carreras-Villasenor, N., Mendoza-Mendoza, A., Tisch, D., Aleman, M. I., et al. (2016). The genomes of three uneven siblings: footprints of the lifestyles of three *Trichoderma* species. *Microbiol. Mol. Biol. Rev.* 80, 205–327. doi: 10.1128/MMBR.00040-15

Schuster, A., Bruno, K. S., Collett, J. R., Baker, S. E., Seiboth, B., Kubicek, C. P., et al. (2012). A versatile toolkit for high throughput functional genomics with *Trichoderma reesei*. *Biotechnol. Biofuels* 5:1. doi: 10.1186/1754-6834-5-1

Schuster, A., Kubicek, C. P., and Schmoll, M. (2011). Dehydrogenase GRD1 represents a novel component of the cellulase regulon in *Trichoderma reesei* (*Hypocrea jecorina*). *Appl. Environ. Microbiol.* 77, 4553–4563. doi: 10.1128/AEM.00513-11

Shirota, O., Pathak, V., Chowdhury, F. H., Setsuko, S., Takatori, K., and Satake, M. (1997). Structural elucidation of trichotetronines: polyketides possessing a bicyclo [2.2.2] octane skeleton with a tetronic acid moiety isolated from *Trichoderma* spp. *J. Chem. Soc. Perkin Trans.* 1, 2961–2964.

Stappler, E., Dattenböck, C., Tisch, D., and Schmoll, M. (2017a). Analysis of light- and carbon-specific transcriptomes implicates a class of G-protein-coupled receptors in cellulose sensing. *mSphere* 2:e89-17. doi: 10.1128/mSphere.00089-17

Stappler, E., Walton, J. D., and Schmoll, M. (2017b). Abundance of secreted proteins of *Trichoderma reesei* is regulated by light of different intensities. *Front. Microbiol.* 8:2586. doi: 10.3389/fmicb.2017.02586

Steiger, M. G., Vitikainen, M., Uskonen, P., Brunner, K., Adam, G., Pakula, T., et al. (2011). Transformation system for *Hypocrea jecorina* (*Trichoderma reesei*) that favors homologous integration and employs reusable bidirectionally selectable markers. *Appl. Environ. Microbiol.* 77, 114–121. doi: 10.1128/AEM.02100-10

Strauss, J., Mach, R. L., Zeilinger, S., Hartler, G., Stoffler, G., Wolschek, M., et al. (1995). Cre1, the carbon catabolite repressor protein from *Trichoderma reesei*. *FEBS Lett.* 376, 103–107. doi: 10.1016/0014-5793(95)01255-5

Tamura, K., Dudley, J., Nei, M., and Kumar, S. (2007). MEGA4: molecular evolutionary genetics analysis (MEGA) software version 4.0. *Mol. Biol. Evol.* 24, 1596–1599. doi: 10.1093/molbev/msm092

Tisch, D., Kubicek, C. P., and Schmoll, M. (2011a). New insights into the mechanism of light modulated signaling by heterotrimeric G-proteins: ENVOY acts on *gna1* and *gna3* and adjusts cAMP levels in *Trichoderma reesei* (*Hypocrea jecorina*). *Fungal Genet. Biol.* 48, 631–640. doi: 10.1016/j.fgb.2010.12.009

Tisch, D., Kubicek, C. P., and Schmoll, M. (2011b). The phosducin-like protein PhLP1 impacts regulation of glycoside hydrolases and light response in *Trichoderma reesei*. *BMC Genomics* 12:613. doi: 10.1186/1471-2164-12-613

Tisch, D., and Schmoll, M. (2013). Targets of light signalling in *Trichoderma reesei*. *BMC Genomics* 14:657. doi: 10.1186/1471-2164-14-657

Turra, D., Segorbe, D., and Di Pietro, A. (2014). Protein kinases in plant-pathogenic fungi: conserved regulators of infection. *Annu. Rev. Phytopathol.* 52, 267–288. doi: 10.1146/annurev-phyto-102313-050143

Videira, A., Kasuga, T., Tian, C., Lemos, C., Castro, A., and Glass, N. L. (2009). Transcriptional analysis of the response of *Neurospora crassa* to phytosphingosine reveals links to mitochondrial function. *Microbiology* 155(Pt 9), 3134–3141. doi: 10.1099/mic.0.029710-0

Winkelströter, L. K., Dolan, S. K., Fernanda Dos, Reis, T., Bom, V. L., Alves, et al. (2015). Systematic global analysis of genes encoding protein phosphatases in *Aspergillus fumigatus*. *G3 (Bethesda)* 5, 1525–1539. doi: 10.1534/g3.115.016766

Yao, Y., Li, J., Jiang, C. S., Zhao, X. X., Miao, Z. H., Liu, H. T., et al. (2015). Trichodimerol and sorbicillin induced apoptosis of HL-60 cells is mediated by reactive oxygen species. *Pharmazie* 70, 394–398.

Conflict of Interest: The authors declare that the research was conducted in the absence of any commercial or financial relationships that could be construed as a potential conflict of interest.

frontiers in Microbiology

ORIGINAL RESEARCH
published: 10 June 2020
doi: 10.3389/fmicb.2020.01038

Involvement of *PaSNF1* in Fungal Development, Sterigmatocystin Biosynthesis, and Lignocellulosic Degradation in the Filamentous Fungus *Podospora anserina*

*Yuanjing Li[1], Pengfei Yan[2], Xiaojie Lu[1], Yanling Qiu[1], Shang Liang[1], Gang Liu[1], Shuangfei Li[1], Lin Mou[1] and Ning Xie[1]**

[1] Shenzhen Key Laboratory of Microbial Genetic Engineering, College of Life Sciences and Oceanography, Shenzhen University, Shenzhen, China, [2] Key Laboratory of Functional Inorganic Material Chemistry (MOE), School of Chemistry and Materials Science, Heilongjiang University, Harbin, China

OPEN ACCESS

Edited by:
Guodong Liu,
Shandong University, China

Reviewed by:
Shuai Zhao,
Guangxi University, China
Robert Debuchy,
Centre National de la Recherche Scientifique (CNRS), France

***Correspondence:**
Ning Xie
ning.xie@szu.edu.cn

Specialty section:
This article was submitted to Fungi and Their Interactions, a section of the journal Frontiers in Microbiology

Received: *29 December 2019*
Accepted: *27 April 2020*
Published: *10 June 2020*

Citation:
Li Y, Yan P, Lu X, Qiu Y, Liang S, Liu G, Li S, Mou L and Xie N (2020) Involvement of PaSNF1 in Fungal Development, Sterigmatocystin Biosynthesis, and Lignocellulosic Degradation in the Filamentous Fungus Podospora anserina. Front. Microbiol. 11:1038. doi: 10.3389/fmicb.2020.01038

The sucrose non-fermenting 1/AMP-activated protein kinase (SNF1/AMPK) is a central regulator of carbon metabolism and energy production in the eukaryotes. In this study, the functions of the *Podospora anserina* SNF1 (PaSNF1) ortholog were investigated. The Δ*PaSNF1* mutant displays a delayed development of mycelium and fruiting bodies and fails to form ascospores. The expression of the *PaSNF1* gene in the strain providing female organs in a cross is sufficient to ensure fertility, indicating a maternal effect. Results of environmental stress showed that Δ*PaSNF1* was hypersensitive to stress, such as osmotic pressure and heat shock, and resistant to fluconazole. Interestingly, the knockout of *PaSNF1* significantly promoted sterigmatocystin (ST) synthesis but suppressed cellulase [filter paperase (FPA), endoglucanase (EG), and β-glucosidase (BG)] activity. Further, transcriptome analysis indicated that *PaSNF1* made positive regulatory effects on the expression of genes encoding cellulolytic enzymes. These results suggested that *PaSNF1* may function in balancing the operation of primary and secondary metabolism. This study suggested that SNF1 was a key regulator concerting vegetative growth, sexual development, and stress tolerance. Our study provided the first genetic evidence that SNF1 was involved in the ST biosynthesis and that it may also be a major actor of lignocellulose degradation in *P. anserina*.

Keywords: *Podospora anserina*, sucrose non-fermenting 1, sexual development, stress tolerance, secondary metabolism, lignocellulose degradation

INTRODUCTION

Lignocellulose is one of the most abundant renewable resources on earth, mainly composed of cellulose, hemicellulose, and lignin (Jonsson et al., 2013). It can be converted into different carbohydrates, including glucose, xylose, and aromatic monomer compounds, which could be applied for the production of ethanol, carbohydrates, and aromatic products (Ragauskas et al., 2014; Kawaguchi et al., 2016; Wu et al., 2018). It has promising applications in food, paper,

and textile industries as well as the production of biofuels and other chemicals (Paulova et al., 2015; Kubicek and Kubicek, 2016; Yenkie et al., 2016). However, the commercial applications of lignocellulosic degradation in the production of biofuels and chemicals were limited by its complex structure, biological obstinacy, low efficiency, and high cost, thus hindering the effective utilization of the raw material in green technology (Weng et al., 2008; Paulova et al., 2015). Biodegradation of lignocellulose into fermentable sugars with cellulase [including Carbohydrate-Active Enzymes (CAZy)] has been an environmental-friendly approach (Gupta et al., 2016). Filamentous fungi were considered as promising candidates for producing lignocellulolytic enzymes (Couturier et al., 2016).

Filamentous fungi and their enzymes show great potential in the degradation of tough lignocellulose (Bomble et al., 2017). Some ascomycetes such as *Trichoderma reesei* and *Aspergillus nidulans* have been commonly applied in the industrial production of cellulase and hemicellulase (de Assis et al., 2015; Bischof et al., 2016). Many cellulose and lignin degradation-associated enzymes were found in the filamentous fungus *Podospora anserina*, making this fungus a model to elucidate the enzymatic decomposition of plant biomass (Couturier et al., 2016). Recent studies have shown that catalase, laccase, and bilirubin oxidase participated in the degradation of cellulose in *P. anserina* (Bourdais et al., 2012; Xie et al., 2014, 2015). The regulation mechanism of cellulase and hemicellulase gene expression has been extensively investigated (Benocci et al., 2017). In cellulolytic fungi, several key transcriptional activators as well as repressors have being involved in this regulation. For example, the transcription factor XlnR/XYR1 regulated the expression of cellulase and hemicellulase genes in *Aspergillus niger*, *Neurospora crassa*, and *T. reesei*, respectively (Stricker et al., 2008; Sun et al., 2012; Dos Santos, Castro et al., 2016). In addition, the transcription factors CLR-1 and CLR-2 were essential for growth on cellulose in *N. crassa* (Coradetti et al., 2012). Recent studies have shown that the CLR-4 acted as a positive activator of cellulase expression by directly binding to the promoters of CLR-1 and CLR-2 (Liu et al., 2019). CLR-3 repressed the cellulolytic response through CLR-1 (Huberman et al., 2017). The conserved zinc-finger transcription factor Cre1/CreA was the key factor in mediating carbon catabolite repression (CCR), an important mechanism for suppressing cellulase production during growth on favorably metabolized carbon source, such as glucose (Sun and Glass, 2011; Lichius et al., 2014). Deletion of Cre1/CreA alleviated some aspects of CCR for cellulolytic enzyme expression in *Penicillium decumbens* and *N. crassa* (Sun and Glass, 2011; Liu et al., 2013). Therefore, transcriptional activation or de-repression via nutrient sensing pathways has also been essential for inducing the lignocellulolytic response.

Sucrose non-fermenting 1/AMP-activated protein kinase (SNF1/AMPK kinases) was regarded as an important regulator that participated in the development of fungi and activation of catabolite-repressed genes (Lee et al., 2009; Ghillebert et al., 2011). In yeast, as a heterotrimer kinase complex, SNF1 contained α-subunit encoded by *SNF1*; β-subunits encoded by *GAL83*, *SIP1*, and *SIP2*; and γ-subunit encoded by *SNF4*. The SNF1 complex can be activated by three upstream kinases (Sak1, Elm1, and Tos3) via phosphorylation (Hedbacker and Carlson, 2008), whereas it could also be inactivated by Reg1-Glc7 protein phosphatase (Sanz et al., 2000). The regulation of SNF1 activity played a central role in the alleviation of CCR, for both *Saccharomyces cerevisiae* and the majority of filamentous fungi (Brown et al., 2013). In yeast, under the glucose starvation, Mig1 was phosphorylated by SNF1, inducing the de-repression of glucose repressed genes. Studies have shown that the CCR mechanism was different in filamentous fungi and yeast. CreA, a Mig1 homolog, was a critical regulator of carbon catabolism inhibition in the lignocellulolytic fungus *A. nidulans* and the orthologous SNF1 kinase was essential for CreA/Cre1 de-repression (Brown et al., 2013). However, homologous proteins of Cre1 could not be phosphorylated by homologous proteins of SNF1 in *T. reesei* (Cziferszky et al., 2003). Overall, it was unclear whether there was a conserved mechanism for *SNF1* to regulate carbon catabolite in filamentous fungi. Little was known about the functions of *SNF1* in the fungal development and lignocellulosic degradation.

Besides, SNF1 complex participated in a wide variety of physiological processes, such as fungal meiosis, spore formation, filamentous growth, and biofilm formation (Lee et al., 2009; Ghillebert et al., 2011). It was also involved in the response to environmental stresses, such as salt stress, heat shock, alkaline pH, and endoplasmic reticulum stress (Hahn and Thiele, 2004; Hong and Carlson, 2007; Casamayor et al., 2012; Ferrer-Dalmau et al., 2015). For many pathogenic filamentous fungi, *SNF1* genes showed critical roles in fungal development and virulence, such as *Magnaporthe oryzae* (Yi et al., 2008), *Gibberella zeae* (Lee et al., 2009), *Verticillium dahlia* (Tzima et al., 2011), *Penicillium digitatum* (Zhang et al., 2013), *Beauveria bassiana* (Wang et al., 2014), *Leptosphaeria maculans* (Feng et al., 2014), and *Fusarium virguliforme* (Islam et al., 2017). The lack of *SNF1* led to inhibitory expression of cell-wall-degrading enzymes, damage of sporulation, and spore germination; thus, its virulence on the hosts would be impaired.

Biosynthesis of secondary metabolites (SMs) may be tightly regulated. Their expression was often triggered by chemical or environmental stimuli and coordinated with the development and morphogenesis of the producing organism. Sterigmatocystin (ST) was one of the ultimate precursors in the biosynthesis of the aflatoxins. The gene cluster responsible for the ST biosynthesis was identified in *A. nidulans* by Brown et al. (1996). A similar cluster of genes was found in *P. anserina* (Slot and Rokas, 2011). ST was detected in cultures of a freshly isolated *P. anserina* strain (Bills and Gloer, 2016). The ST biosynthetic gene cluster was regulated by the cluster-specific AflR transcription factor, which functioned downstream of glucose sensing (Fernandes et al., 1998). Overexpression of *PaAflR* led to a ST overproduction and a female sterility phenotype in *P. anserina* (Shen et al., 2019). Additionally, LaeA also regulated the ST biosynthetic gene cluster in an AflR-dependent manner. The Δ*LaeA* mutation abolishes AflR expression and subsequently the production of ST and other SMs (Bok and Keller, 2004). Interestingly, Cre1, which regulated cellulase production, was also involved in the synthesis of SMs (Monroy et al., 2017). However, the importance of *SNF1* and their functional connections in regulating SMs have been unknown.

Elucidating the physiological functions of *SNF1* contributed to understanding the mechanisms of filamentous fungi sense nutrition and cellular energetic status, which was paramount for the industrial production of cellulase. In this study, we identified a homolog of *SNF1* in the genome of *P. anserina*. With the use of a homologous recombination strategy, the disruption mutant of *P. anserina* SNF1 (*PaSNF1*) was constructed, and the effects of *PaSNF1* in fungal development and lignocellulosic degradation were characterized. Δ*PaSNF1* was characterized for defects in sexual reproduction (e.g., fruiting body formation), colony formation, ascospore germination, and stress responses. Our study provided the first genetic evidences that *SNF1* was involved in the ST biosynthesis. Enzymology and transcriptome analysis confirmed that *PaSNF1* played important roles in cellulose degradation.

MATERIALS AND METHODS

Strains and Culture Conditions

All strains of *Podospora anserina* applied in this study were derived from the "S" wild-type (WT) strain, which was sequenced for obtaining the genome of the *P. anserina* (Espagne et al., 2008; Grognet et al., 2014; Silar et al., 2019). The standard culture protocol of *P. anserina* could be found at http://podospora.igmors.u-psud.fr/methods.php. The Δ*mus51:Hygro* mutant strain differed from the S WT reference strain by a single deletion of the *mus-51* gene, in which frequency of targeted gene replacement was increased (El-Khoury et al., 2008).

Phylogenetic Analysis

The putative SNF1 genes of *P. anserina* were identified by BLAST at the *P. anserina* website by retrieving various fungal SNF1[1]. In this study, the putative SNF1 encoded by *Pa_2_770* was named as PaSNF1. The alignment was manually refined, and sites with ambiguous alignment were removed from the dataset. The phylogenetic tree was reconstructed using a neighbor-joining method, and an alignment was produced with the CLUSTALW algorithm in the MEGA5 software (Wang et al., 2014), in which the numbers at nodes indicated bootstrap values with 1,000 replications.

Generation of Deletion Mutants and Complementation

A deletion cassette for the *SNF1* (*Pa_2_770*) gene was constructed with a geneticin resistance cassette as previously reported (Xie et al., 2014, 2015, 2018). The Δ*mus51:Hygro* protoplasts were transformed by the PCR products with geneticin cassette. Transformants were screened on selective medium containing 100 μg/ml of geneticin and 75 μg/ml of hygromycin. Putative deleted mutants were firstly selected by PCR. The PCR amplified specific junctions to the replaced locus, with two primers that annealed at one end of the selectable resistance gene and upstream of the proximal flank in the deletion cassette (**Supplementary Table S1**). Homologous recombination of the deletion cassette allowed amplification of a predictable fragment on each side of the selectable resistance gene. Three candidate transformants would be genetically purified by crossing them with WT. It aimed to eliminate the potential untransformed nuclei and then segregate out the Δ*mus-51* mutation. Mat- and mat + geneticin-R and hygromycin-S strains were identified from each progeny, and one transformant was subjected to Southern blot analysis for final validation (**Supplementary Figure S2**). Only purified transformants verified by Southern blot would be selected as stock deletion mutants for subsequent studies.

To ensure that the relevant *PaSNF1* gene was inactivated in the derived phenotypes, the complementation procedure was done by ectopic insertion of corresponding gene under the control of its native promoter. The WT with complete CDS and the 5′ (500 bp) and 3′ (200 bp) flanking regions were amplified by PCR using a high-fidelity polymerase and primers of PaSNF1-cF and PaSNF1-cR (**Supplementary Table S1**). The DNA fragment was cloned into the pBC-Nourseo (Lalucque et al., 2012) at the *Not*I and *Bam*HI sites to yield pBC-Nours-*PaSNF1* plasmid. This plasmid was transformed into the protoplasts of the Δ*PaSNF1* mutant strain. Transformants (CP*PaSNF1*) were screened on selective medium with 40 μg/ml of nourseothricin (Xie et al., 2018). The presence of the WT allele was also verified by PCR.

Growth and Development in Standard Conditions

To determine the roles of *PaSNF1* in fungal physiology, both the deleted mutant and WT were incubated separately on M_2 medium at 27°C. Colony morphology, pigmentation, perithecium formation, ascospore production, ascospore dispersal, and germination were observed during the vegetative growth and sexual cycle. Three plates were set for each treatment, and the experiment was repeated once.

Stress Sensitivity Assays

In this study, mat + mating type strains were used unless specified. For evaluating the stress sensitivity, WT, Δ*PaSNF1*, and CP*PaSNF1* were incubated separately on M_2 medium, supplemented with osmotic stress reagents (0.5 M of NaCl, 0.5 M of KCl, 0.5 M of sorbitol, and 0.75 M of glycerol), oxidative reagents (0.01% H_2O_2 and 50 μM of menadione), cell wall inhibitors [0.02% Congo red and 0.05% sodium dodecyl sulfate (SDS)], and cell membrane inhibitor (2.5 μg/ml of fluconazole). The menadione was obtained from Macklin, and fluconazole was purchased from Aladdin. Fresh mycelium was incubated at 45°C in water bath for 2 h. Equal volume of mycelium was inoculated on M2. Equal volume of mycelium without heat shock served as control. All cultures were incubated at 27°C for 3 days, colony size was measured, three plates were set for each treatment, and the experiment was repeated once.

[1] http://podospora.i2bc.paris-saclay.fr/

Detection of Secondary Metabolites by High-Performance Liquid Chromatography

To analyze the SMs, both WT and Δ*PaSNF1* (mat + mating type) strains were incubated separately in 100 ml of liquid medium (in 250-ml triangle bottle) at 27°C, shaking at 150 rpm for 7 days. Mycelium and the liquid phase were separated by centrifugation. The supernatant was extracted for three times with an equal volume of ethyl acetate. The organic phase was transferred for evaporation to yield a concentrated residue. The residue was re-suspended in 1 ml of methanol and then centrifuged at 12,000 rpm for 10 min. The obtained supernatant was filtered with 0.22-μm Millipore filter and then analyzed with high-performance liquid chromatography (HPLC) (Waters e2695 separations Module) with 2998 PDA detector with ultimate XB-C18 column (4.6 × 250 mm, Welch Materials, Inc.). The conditions for HPLC were as follows: flow rate was 1 ml/min, column temperature was 30°C, and the solvent gradients were solvent A (H_2O) and solvent B (methanol). The sample was detected for 20 min using a linear gradient of 10–90% (0–20 min), 100% MeOH (20.01–30 min), and 10% MeOH (30.01–30 min). The wavelength of UV detector was set at 254 nm.

Characterization of Sterigmatocystin Synthesis in Δ*PaSNF1* Mutant

For the purification of these compounds, Δ*PaSNF1* mutant (mat + mating type) were cultured in 5 l of liquid medium at 27°C, shaken at 150 rpm for 7 days. Culture media were Solution 1 0.5% (v/v), Solution 2 0.5% (v/v), Solution 3 0.5% (v/v), Solution 4 0.5% (v/v), biotin 0.05% (v/v), thiamine 0.05% (v/v), microelement 0.1% (v/v), yeast extract 0.5% (m/v), and dextrin blonde 0.55% (m/v). The standard culture protocol of *P. anserina* could be found at http://podospora.igmors.u-psud.fr/methods.php. The culture was extracted with ethyl acetate for three times. The organic phase was evaporated to obtain the crude residue (1.3 g). The residue was separated on silica gel column with a stepped gradient elution of CH_2Cl_2–MeOH (100:0–0:100) to yield 6 subfractions (Fr. 1–Fr. 6). Fr. 1 (a total of 105.4 mg) was further purified by semi-preparative HPLC, and ST was gained (at 18.5 min). Nuclear magnetic resonance (NMR) spectra were performed on a Bruker Avance III 500 spectrometer (600 MHz). DMSO-d_6 was applied as the solvent for analyzing ST (Pachler et al., 1976; Oleinikova et al., 2012).

Cellulose Degradation and Enzyme Assays

For evaluating the activity of cellulase, both WT and Δ*PaSNF1* (mat + mating type) were cultured. The mycelium agar pieces (2 × 2 mm) from actively growing WT and mutant strains were transferred to Petri dishes with cellophane placed on M2 medium, and then the mycelia were incubated at 27°C for 2 days (Xie et al., 2015). The harvested mycelium was smashed in 200 μl of extraction buffer (sodium citrate buffer 50 mM, pH7.0) by FastPrep (4.0) for 20 s. All the samples were centrifuged at 10,000 rpm for 10 min to obtain the supernatants. The activity of FPA and EG were measured by the 3,5-dinitrosalicylic acid (DNS) method with filter paper and carboxymethyl cellulose as substrates (Liao et al., 2018). The activity of BG and exo-1,4-β-glucanase (CBH) was determined using *p*-nitrophenyl-β-D-glucopyranoside (pNPG) and *p*-nitrophenol-D-cellobioside (pNPC) as the substrates, respectively (Li et al., 2016). Protein concentration was quantified with Bradford method (Bradford, 1976). All the determinations were performed in triplicate. To evaluate the cellulose degradation, the M2 standard minimal synthetic medium contains dextrin (0.5%) as carbon source. Dextrins were replaced with microcrystalline cellulose (MCC; 0.5%) from Sigma and 0.5 g/plate straw materials. Fragmented mycelia from mat + and mat- strains of WT or Δ*PaSNF1* were mixed and then inoculated in the center of the plate under constant light illumination. Photographs were taken after 7 days of incubation.

Transcriptome Analysis

The mycelia of WT and Δ*PaSNF1* grown in cellulose (3 days) were harvested by filtration and immediately frozen in liquid nitrogen. The culture medium was a fungal liquid culture medium. An equivalent amount of carbon source dextrin was replaced with microcrystalline cellulose. The composition of the medium was as follows: Solution 1 0.5% (v/v), Solution 2 0.5% (v/v), Solution 3 0.5% (v/v), Solution 4 0.5% (v/v), biotin 0.05% (v/v), thiamine 0.05% (v/v), microelement 0.1% (v/v), yeast extract 0.5% (m/v), and Avicel (Sigma) 0.55% (m/v). Total RNA was extracted using TRIzol® RNA reagent (Invitrogen, Carlsbad, CA, United States) and further purified using DNase I (RNeasy Mini kit, Qiagen, Hilden, Germany). NanoDrop and agarose gel electrophoresis were used to check RNA integrity and concentration.

Qualified RNA with an OD260/OD280 > 1.8 and RNA integrity number (RIN) > 7.0 was prepared according to Majorbio (Shanghai, China) standard protocols and sequenced on an Illumina HiSeq 2000/2500 platform (San Diego, CA, United States). All data in this study were generated by sequencing two independent duplicate samples. Total clean reads were mapped against predicted transcripts from the WT *P. anserina* strain genome[2] to assess sequence homology and functional annotation. Read mapping and counting using TopHat (version 2.1.1) and hisat2 (version 2.1.0) were performed. RSEM (version 1.3.1) software was used to analyze gene expression levels with the fragments per kilobase of exon per million mapped reads (FPKM) method. Differentially expressed genes (DEGs) were screened using the DESeq2 (version 1.24.0) with fold change of more than 1.5 and p-value ≤ 0.05 as thresholds. The dataset was also manually screened for the genes encoding carbohydrate active enzymes. Hierarchical clustering analysis was performed using the pheatmap package in R (version 3.6.1)[2]. RNA-Seq data were deposited in the National Center for Biotechnology Information (NCBI) Sequence Read Archive (SRA) under accession number PRJNA597840.

[2]https://www.ncbi.nlm.nih.gov/genome/?term=txid5145[orgn],

[3]http://www.r-project.org

Quantitative RT-PCR

The mycelia of WT and Δ*PaSNF1* grown in cellulose (3 days) were harvested by filtration and immediately frozen in liquid nitrogen. Total RNA was extracted using TRIzol® RNA reagent (Invitrogen, Carlsbad, CA, United States) for total RNA extraction. All total RNA samples were reversely transcribed into cDNAs and then assessed for the transcript levels of 20 genes via RT-qPCR with paired primers (**Supplementary Table S1**). All RT-qPCR experiments with three cDNA samples of each strain were performed under the action of SYBR® Premix Ex TaqTM (TaKaRa, Dalian, China). Initially, three reference genes were used for normalization: *GPD* (glyceraldehyde 3-phosphate dehydrogenase, formally *Pa_3_5110*), *PDF2* (protein phosphatase PP2A regulatory subunit A, *Pa_7_6690*), and *UBC* (ubiquitin, *Pa_4_7790*). All three were stably expressed; comparatively speaking, *PDF2* has the best stability, and in RNA-Seq data, the difference between the FPKM of *PaPDF2* in WT and Δ*PaSNF1* was not significant. Thus, only the *PaPDF2* gene was used as a reference gene to normalize gene expression results. The ratio of each gene transcript in Δ*PaSNF1* over that in WT was converted to log2 for comparison with the corresponding log2 ratio from the RNA-Seq data.

Microscopic Observations

The perithecia of mycelia grown on agar were observed and captured with a homemade microscope, combining a camera [monochromatic 1/3″ complementary metal–oxide–semiconductor (CMOS) sensor with a resolution of 1,280 × 960 pixels] and a telecentric objective (4 × magnification and 65-mm focal length). Pictures of squashed perithecia and ascospore were captured with a Nikon eclipse Ni-V microscope and analyzed with ImageJ.

RESULTS

Identification of SNF1 Homolog in *Podospora anserina* and Phylogenetic Analysis

The genome of *Podospora anserina* has been sequenced[4]. SNF1 protein sequences of yeast and two filamentous fungi *Neurospora crassa* and *Hypocrea jecorina* were used as a query to identify the homolog in *P. anserina* genome. A homologous protein was found in *P. anserina*, presenting the highest identity with *N. crassa*, *H. jecorina*, and yeast, which was 75.64, 83.63, and 41%, respectively, and designated as SNF1 (Protein ID: CAP72646.1; Pa_2_770). The open reading frame (ORF) of SNF1 in *P. anserina* was predicted to be 2,127 bp in length, encoding a peptide of 708 amino acids with a predicted molecular weight of ∼79.91 kDa (**Supplementary Figure S1A**). SMART analysis[5] of SNF1 suggested that this protein contained a serine/threonine (Ser/Thr) kinase catalytic domain (KD) (residues 67–318) and a two C-terminal domain (CTD) (residues 532–628 and residues 633–704). KD with the identity of 78.17% exhibited a high similarity to the SNF1 Ser/Thr catalytic domain in *Saccharomyces cerevisiae*. The degree of similarity was even lower at the CTD (25% identity), and only a few blocks showed identical residues (**Supplementary Figures S1,C**). Maximum likelihood method was applied to analyze the similarities among above 11 proteins, and a phylogenetic tree was constructed (**Figure 1**). The predicted amino acid sequence of *PaSNF1* shared an identity of 75.64% with NcSNF1 of *N. crassa* (CAD70761), 64.67% with HjSNF1 of *H. jecorina* (AF291845) (Cziferszky et al., 2003), 67.73% with FoSNF1 of *Fusarium oxysporum* (AAN32715) (Ospina-Giraldo et al., 2003), 66.06% with BbSNF1 of *Beauveria bassiana* (EJP66968) (Wang et al., 2014), 63.41% with PmSNF1 of *Pestalotiopsis microspora* (AUW40141) (Wang et al., 2018), 57.53% with MgSNF1 of *Magnaporthe grisea* (ABF48563) (Yi et al., 2008), 57.94% with SsSNF1 of *Sclerotinia sclerotiorum* (CAB40826) (Vacher et al., 2003), 44.35% with PdSNF1 of *Penicillium digitatum* (AFS18464) (Zhang et al., 2013), and 43.43% with CcSNF1 of *Cochliobolus carbonum* (AAD43341) (Tonukari et al., 2000). PaSNF1 protein showed lower homology with SNF1 protein from *S. cerevisiae*, which was 42%. SNF1 orthologs showed that PaSNF1 from different fungi clustered together, whereas yeast homologs formed a separate cluster (**Figure 1**).

Creation of *PaSNF1* Knockout and Complementation Mutants

PaSNF1 disruption mutant was generated by replacing a coding sequence of *PaSNF1* with the genetic resistance gene. The *PaSNF1* disruption mutant without additional ectopic integrations of the replacement cassette sequence mutants was confirmed by PCR and Southern blot (**Supplementary Figure S2**). For the complementation CP*PaSNF1*, a functional *PaSNF1* ORF was introduced into the Δ*PaSNF1* mutant, and the obtained complementation mutants were screened on a selective medium containing nourseothricin and geneticin and then confirmed by PCR.

Effects of *PaSNF1* on Growth and Development of *Podospora anserina* in Standard Conditions

To investigate the effects of SNF1 in the development of *P. anserina*, the *PaSNF1* mutant (Δ*PaSNF1*), complementation mutants (CP*PaSNF1*), and the WT strains were cultured under the optimal conditions for growth and sexual reproduction (on M2 minimal medium at 27°C, in the presence of light). Then the detailed phenotypic analysis was performed. The knockout of *PaSNF1* gene led to the growth and developmental defects of *P. anserina*. Compared with that of WT, the growth of the mutant Δ*PaSNF1* was significantly decreased. Colony size of Δ*PaSNF1* was 77% of WT after 3 days of incubation (**Figures 2A,F**). The fruiting bodies of WT strain began to develop after 5 days. There were numerous viable ascospores expelled after 2 days (**Figure 2B**). Δ*PaSNF1* mat + x Δ*PaSNF1* mat- led to a defect in perithecium production and ascospore formation. Compared with WT, there was a 62% reduction

[4]http://podospora.i2bc.paris-saclay.fr/index.php

[5]http://smart.embl-heidelberg.de/

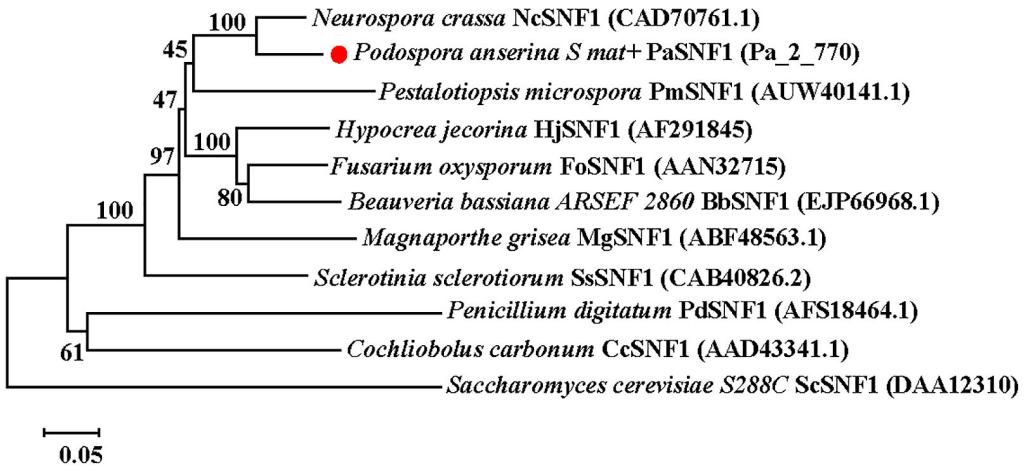

FIGURE 1 | Phylogenetic analysis of *PaSNF1* and SNF1 orthologs identified in other organisms. The phylogenetic tree was reconstructed using a neighbor-joining method. Numbers at nodes indicate bootstrap values with 1,000 replications. GenBank accession number of a given SNF1-coding gene was parenthesized following the name of each fungal species. Distance scale: scale that represents the number of differences between sequences (e.g., 0.05 means 5% differences between two sequences). SNF1, sucrose non-fermenting 1; *PaSNF1*, *Podospora anserina* SNF1.

in the production of perithecia (**Figure 2G**). Surprisingly, no ascospore was expelled from perithecia in Δ*PaSNF1* mutant (**Figures 2B,E**). Microscopic observation of perithecia showed that the ascus shells produced by WT and mutants were similar, without significant difference in diameter. The ascus shell of the mutant also differentiated into a normal neck (**Figure 2C**). Microscopic observations of squashed perithecia were made in order to observe produced ascospores and asci. Typical rosettes of asci with four ascospores were observed in WT strain crosses. Usual rosettes were composed of mature ascospores, which were dark green owing to accumulation of melanin, and not fully ripened ascospores, which were light green. However, transparent asci were observed and failed to form intact ascospores in the Δ*PaSNF1* (**Figure 2D**). These observations indicate that the lack of ascospore release in the Δ*PaSNF1* was due to a defect in ascospore formation rather than a defect in the mechanism of forcible ascospore discharge.

To further analyze the role of the *PaSNF1* gene in sexual development, we investigated the behavior of Δ*PaSNF1* strain as male and female partners in crosses with a WT strain. Plates with Δ*PaSNF1* mat + and WT mat- mycelia were covered with 1.5 ml of sterile water, which spread male gametes from one mycelium on the other and allowed these spermatia to fertilize female organs (**Figure 3**). WT mat- female organs fertilized by Δ*PaSNF1* mat + spermatia produced ascospores, indicating that the deletion of *PaSNF1* is not dominant and can be complemented by the functional *PaNSF1* gene present in the WT female strain. In contrast, Δ*PaSNF1* mat + female organs fertilized by WT mat- spermatia did not produce ascospores, indicating that Δ*PaSNF1* has a maternal effect; that is, the presence of a functional *PaSNF1* gene in the male nuclei cannot complement the absence of this gene in the female organ. Crosses on plates with Δ*PaSNF1* mat- and WT mat + indicated that the maternal effect of Δ*PaSNF1* is not mating-type dependent. In addition, *SNF1* knockout resulted in a red–orange pigment deposition of the mutant Δ*PaSNF1*, compared with WT on solid M2 plates (**Figure 2B**). To further confirm that the phenotypic changes observed in the mutant resulted from the deletion of *PaSNF1* instead of other unknown genetic mutations, we conducted complementation analyses of Δ*PaSNF1*. The defects of Δ*PaSNF1* in mycelial growth, sexual development, and pigmentation were complemented by genetic complementation. Our results indicated that *PaSNF1* not only affected mycelial growth but also regulated fruit body formation and developmental maturation.

The Roles of *SNF1* in the Environmental Stress Tolerance

To determine the roles of *PaSNF1* in response to stress conditions, the growth of the strains under different stress conditions was analyzed (**Figure 4**). The growth of the Δ*PaSNF1* mutant was significantly inhibited by 0.5 M of NaCl, 0.5 M of KCl, and 0.75 M of glycerol, compared with that of WT and CP*PaSNF1*, whereas the result was different for sorbitol. This result suggested that *PaSNF1* may be necessary for the cellular responses of *P. anserina* to osmotic pressure. In contrast, the Δ*PaSNF1* mutant was insensitive to 0.01% H_2O_2. However, on plates supplemented with 50 μM of oxidant menadione, the growth rate of Δ*PaSNF1* mutant was obviously slower, implying the roles of *SNF1* in its tolerance to this stress. The Δ*PaSNF1* mutant showed similar sensitivity to heat shock, presented with slower growth, and significantly increased inhibition rate. Particularly interestingly, the resistance of the Δ*PaSNF1* mutant to the fungicide fluconazole was significantly increased after knocking out of the *SNF1* gene; compared with WT and CP*PaSNF1* strains, the growth of Δ*PaSNF1* mutant was significantly increased while the inhibition rate was reduced. These results indicated that the *PaSNF1* gene in *P. anserina* played an important role in its response to osmotic stress, oxidative stress, and heat shock.

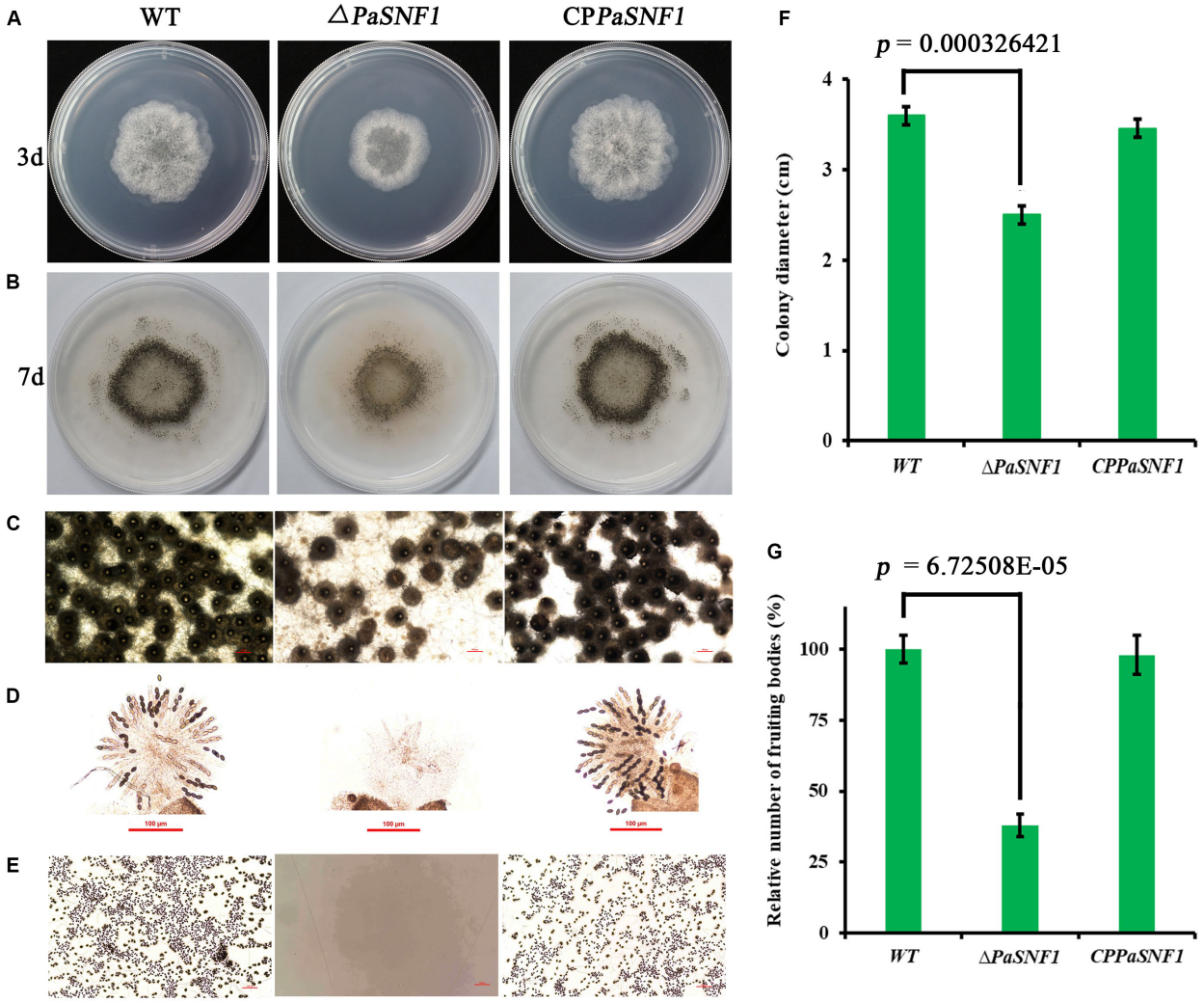

FIGURE 2 | Growth and development of WT and mutants on M2 medium. **(A)** Colony size of WT and Δ*PaSNF1* after 3 days of incubation. **(B)** Fertility on M_2 medium developed after 5 days. Perithecia are visible as small black dots. All the strains produced the usual ring of mature perithecia in the center of the Petri dish. **(C)** Microscopic observation of perithecia of WT and Δ*PaSNF1*. **(D)** Microscopic observation of ascospores inside perithecia. **(E)** Microscopic observation of ascospores erupting from fruiting bodies. **(F,G)** Colony diameter and fruiting bodies number, respectively; fruiting body number was expressed with respect to that of WT considered as 100%. Error bars are standard deviations of triplicate samples. Differences in the data were assessed by the *T*-test. WT, wild type; *PaSNF1*, *Podospora anserina* SNF1.

The Regulation of *SNF1* for Sterigmatocystin Biosynthesis

In fungi, SMs were generally associated with the developmental processes in response to various abiotic or biotic external stimuli (Yin et al., 2012). To examine the regulation effects of *SNF1* in biosynthesis of SMs in *P. anserina*, the profile of secondary compounds in Δ*PaSNF1* cultures was analyzed by HPLC. We found that the profile of SMs was significantly altered after the deletion of *PaSNF1* (**Figure 5A**). Based on HPLC profiling, peak of SM 1 (at 18.5 min) in Δ*PaSNF1* was 50% higher than that of WT (**Figures 5A,C**). To further identify the compound at 18.5 min, large-scale fermentation was performed; the metabolites were further isolated and purified. The compound was identified as ST by NMR (**Figure 5B** and **Supplementary Figures S3**, **S4**). The result suggested that the biosynthesis of ST was negatively regulated by *PaSNF1*. The above results demonstrated that *PaSNF1* was a regulator of SMs and may be involved in either activation or silencing of certain gene clusters in *P. anserina*.

Knockout of *SNF1* Led to Impaired Cellulose-Utilizing Ability

To investigate whether the PaSNF1 kinase participated in the production of cellulase, the cellulase activity and cellulose-utilizing ability of WT and Δ*PaSNF1* were detected. The cellulase activity of WT and Δ*PaSNF1* was further compared, including FPA, EG, CBH, and BG (**Figure 6A**). After 3 days of culture on M2 medium, the activities of FPA, EG, and BG were significantly

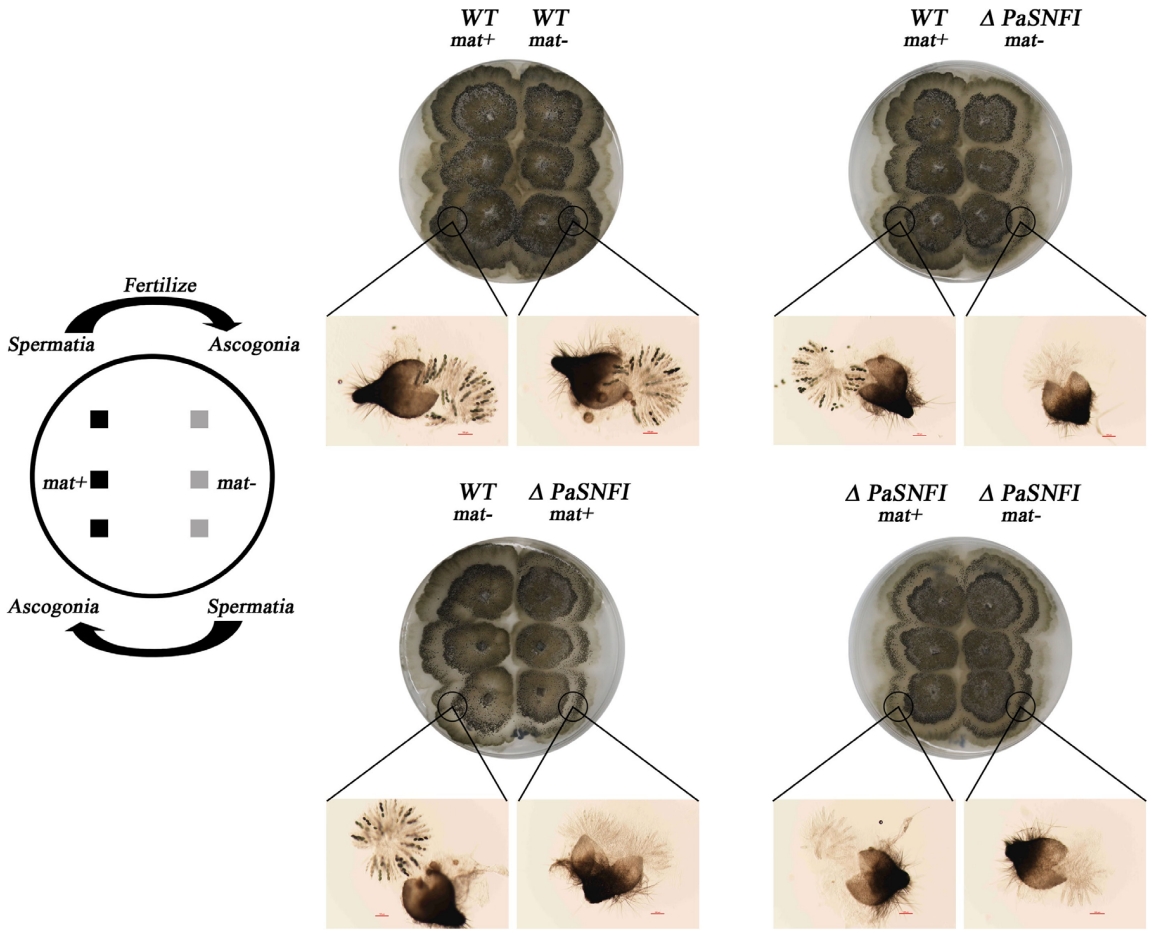

FIGURE 3 | Spreading experiments. *Podospora anserina* is a heterothallic species with two mating types called mat+ and mat-. Each mating type differentiates male and female organs. Male organs (spermatia) are single cells that can be spread by water all over the plate. They are recognized by female organs of opposite mating type, which fuse with the male cells and subsequently differentiate in mature fruiting bodies. Crosses were made by inoculating the strains 1.5 cm apart. After 3 days of growth, 1.5 ml of water was added and spread all over the plate. The pictures were taken 4 days after fertilization.

lower than those of WT, which were reduced to 17.2, 27.4, and 50.3%, respectively, of WT (**Figure 6A**). After 7 days of culture on MCC agar medium (with microcrystalline cellulose as carbon source instead of dextrin), the fruit body formation of Δ*PaSNF1* mutant was significantly reduced, and similar phenotypes were observed on straw medium (**Figure 6B**). Therefore, *PaSNF1* was considered as critical for the cellulose-utilizing ability of *P. anserina*.

SNF1 Regulated the Expression of the Carbohydrate-Active Enzymes Genes and Transporters in *Podospora anserina*

The results described above confirmed that *SNF1* made effects on cellulase and hemicellulase expression of *P. anserina*; however, these effects could not be validated solely from growth data. To determine whether the defect in cellulase secretion and activity in the Δ*PaSNF1* mutant was due to the failure to induce cellulase gene expression versus a defect in cellulase secretion, we assessed genome-wide expression differences via RNA-Seq between the WT and Δ*PaSNF1* strains in medium containing Avicel. Transcriptome results showed that significant expression differences in 468 genes were observed in Δ*PaSNF1* compared with WT; DEGs accounted for 4.3% of all genetic data, among which 129 genes were up-regulated and 339 genes were down-regulated (**Figure 7A** and **Supplementary Table S2**). Among these genes, 41 of 471 CAZyme encoding genes were detected (Carbohydrate Active Enzymes database[6]), 24 genes were significantly down-regulated, 17 genes were significantly up-regulated (**Figure 7B** and **Supplementary Table S3**), and the DEGs accounted for 8.7% of all CAZyme-encoding genes. To verify whether the CAZyme-encoding genes were enriched and overexpressed, we used Log2FC(Δ*PaSNF1*/WT) to perform statistical analysis (*T*-test) on up-regulated and down-regulated genes between CAZyme-encoding genes and non-CAZyme-encoding genes in DEGs. The results indicate that the differences of up-regulated (p value = 0.219811) and down-regulated genes (p-value = 0.740564) between CAZyme-encoding genes and

[6]http://www.cazy.org/

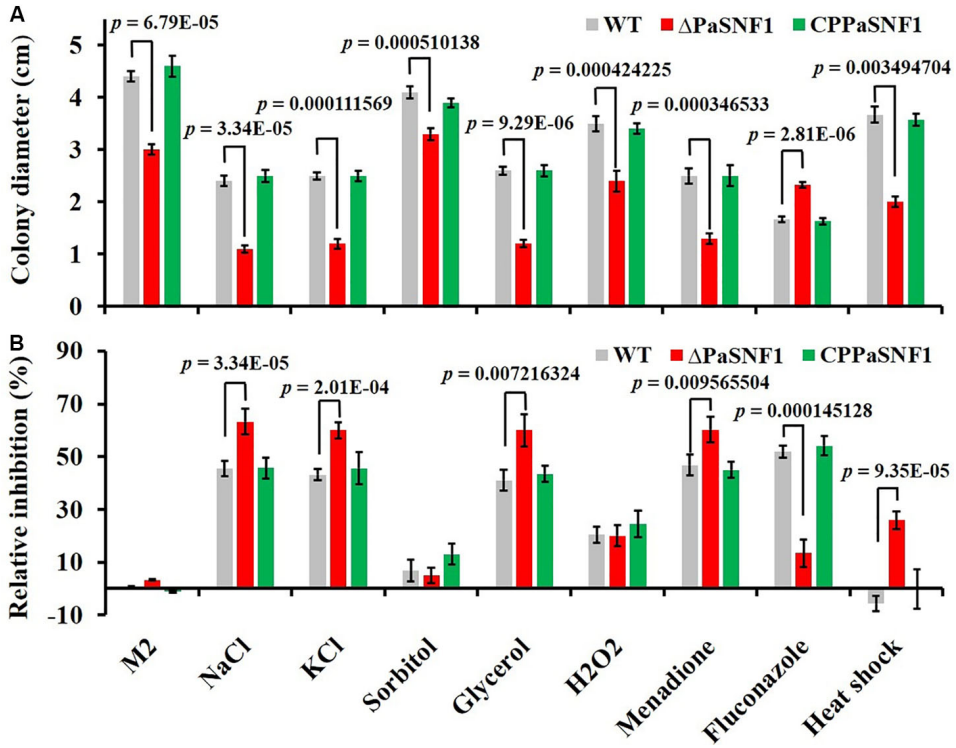

FIGURE 4 | Tolerance analysis to environmental stresses. **(A)** Colony sizes of WT, Δ*PaSNF1*, and CP*PaSNF1* were incubated separately on M2 medium, supplemented with one of the osmotic stress reagents (0.5 M of NaCl, 0.5 M of KCl, 0.5 M of sorbitol, and 0.75 M of glycerol), oxidative reagents (0.01% H_2O_2 and 50 μM of menadione), and 2.5 μg/ml of fluconazole; and fresh mycelium was incubated at 45°C in water bath for 2 h. M2 medium without the supplements was served as the control. **(B)** Relative inhibition rate. All cultures were incubated at 27°C for 3 days, and colony size was measured. Three plates were set for each treatment, and the experiment was repeated once. Error bars are standard deviations of triplicate samples. Differences in the data were assessed by the *T*-test. WT, wild type; *PaSNF1*, *Podospora anserina* SNF1.

non-CAZyme-encoding genes were not significant. However, the proportion (41/468 × 100% = 8.76%) of CAZyme-encoding genes in DEGs was doubled as compared with the proportion (471/10,888 × 100% = 4.33%) of all CAZyme-encoding genes in the genome, and these results suggest to some extent that more CAZyme-encoding genes were induced to be activated, although CAZyme-encoding genes are not overrepresented in the DEGs in Δ*PaSNF1*. These down-regulated genes encoded CAZymes in the glycoside hydrolase family (GH2, GH3, GH5, GH13, GH17, GH37, GH55, GH76, GH81, and GH94), laccase (AA1 and Lac), cellobiose dehydrogenases (AA3 and CDH), and lytic polysaccharide monooxygenases (LPMO, AA9, and AA11); however, in the Δ*PaSNF1* mutant, FPKM of LPMOs was very small, and the FPKM of AA9 and AA11 is 0.665 and 3.83, respectively (**Figure 7C** and **Supplementary Table S3**). The majority of which comprised glycosyl hydrolases (GHs) participated in cellulose and hemicellulose degradation. These findings implied that expression of most of the cellulolytic and hemicellulolytic genes was affected by the deletion of *PaSNF1*. Down-regulated genes also contained some glycosidase activity against various side chains in hemicellulose, such as endo-1,6-alpha-mannosidase (PODANS_1_19460), β-galactosidase (PODANS_1_18330), chitin deacetylase (PODANS_1_4780), and α,α-trehalase (PODANS_1_2050). The reduced expression of various glycosidase genes was also reflected in the decreased ability to grow on their oligosaccharide substrates (**Supplementary Figure S5**). The majority of up-regulated genes encoded CAZymes are the glycoside hydrolase family (GH6, GH7, GH11, GH18, and GH53) and LPMOs (AA9: PODANS_1_21900, PODANS_2_4860, PODANS_3_2580, PODANS_5_10760, PODANS_6_11370, and PODANS_6_11470). FPKM of LPMOs was significantly increased, which reached 69% in up-regulated genes encoded CAZymes in Δ*PaSNF1*, 2.5 times that of WT (**Figure 7D**), which may be related to the increase of H_2O_2 in the mutant. In addition, 23 transporters were found to be down-regulated in the Δ*PaSNF1* strain compared with WT, and nine of these genes encoded proteins that belong to the major facilitator superfamily (MFS) permeases (**Figure 7E** and **Supplementary Table S4**). Four sugar transporters were included: *PODANS_5_4520* (*SPT1*) encoded sugar and polyol transporter 1 (SPT1) (Schilling and Oesterhelt, 2007), *PODANS_4_9820* (*Hgt-1*) was identified as a high-affinity glucose transporter (Baruffini et al., 2006), and *PODANS_5_480* and *PODANS_1_22840* (*MstA*) showed the capability of transporting monosaccharides including xylose (Jorgensen et al., 2007). However, none of the transcription factors known to directly regulate cellulase gene expression exhibited altered expression. Interestingly, two

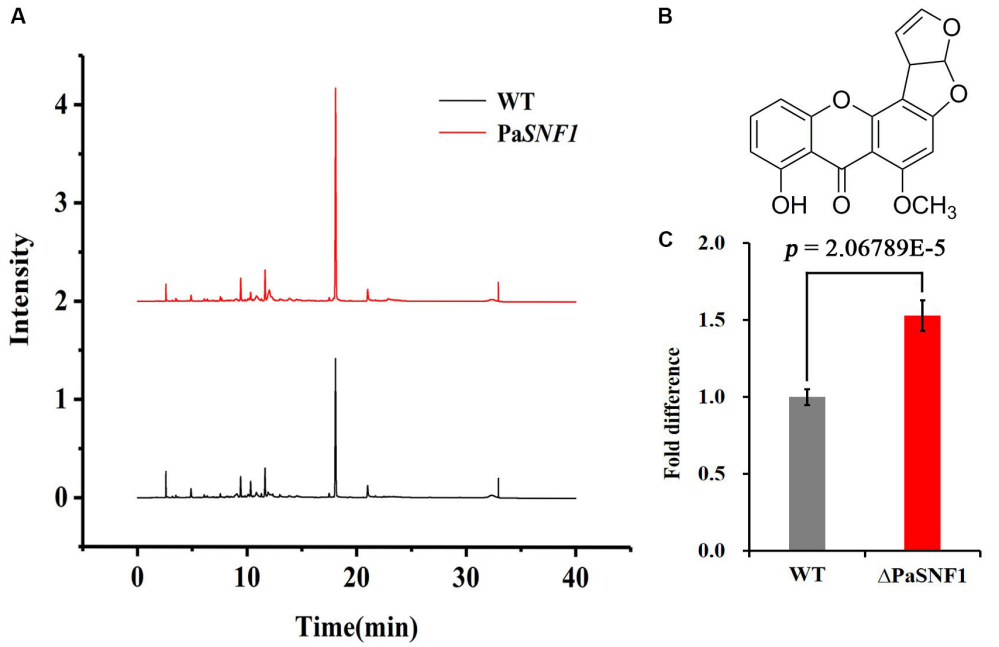

FIGURE 5 | Identification and analysis of ST. **(A)** HPLC analysis of SM production with WT and Δ*PaSNF1* mutant. The strains were grown on M_2 media for 7 days. **(B)** The chemical structure of ST by NMR. **(C)** Relative amounts of ST in Δ*PaSNF1* strain compared with WT. Error bars are standard deviations of triplicate samples. Differences in the data were assessed by the *T*-test. ST, sterigmatocystin; HPLC, high-performance liquid chromatography; SM, secondary metabolite; WT, wild type; *PaSNF1*, *Podospora anserina* SNF1; NMR, nuclear magnetic resonance.

genes (*PODANS_3_3440* and *PODANS_5_12360*) encoding secondary metabolic regulators LAE1 were significantly down-regulated (**Supplementary Table S2**), which was a homolog of methyltransferase LAE1 of *Trichoderma reesei*. It was involved in cellulase gene expression regulations (Seiboth et al., 2012), suggesting an indirect relationship between SNF1 and cellulase expression. To validate the DEGs identified from RNA-Seq data, transcript levels of 10 up-regulated (*PODANS_1_9380*, *PODANS_1_5230*, *PODANS_1_12700*, *PODANS_4_5380*, *PODANS_5_9670*, *PODANS_6_2530*, *PODANS_7_8775*, *PODANS_4_5370*, *PODANS_2_7185*, and *PODANS_1_990*) and 10 down-regulated genes (*PODANS_3_1840*, *PODANS_6_9965*, *PODANS_7_150*, *PODANS_5_3595*, *PODANS_3_2688*, *PODANS_3_780*, *PODANS_6_10085*, *PODANS_5_11880*, *PODANS_1_19460*, and *PODANS_7_8100*) in the mycelium cells of Δ*PaSNF1* and WT were assessed via RT-qPCR with paired primers (**Supplementary Table S1**) and compared with those in the RNA-Seq data. As a result, all the gene transcripts assessed in RT-qPCR showed the same up-regulated or down-regulated trends as determined by the RNA-Seq analysis for DEGs identification (**Figure 7F**).

DISCUSSION

Organisms would suffer a variety of nutritional conditions during their life cycle. Complex signaling networks have been evolved in microbes to identify and prioritize the utilization of available energy sources, such as the CCR system. The CCR system would prevent the utilization of difficultly metabolizable carbon sources for ensuring the preferential utilization of easily metabolizable carbon sources such as D-glucose. For many fungi, several genes involved in the carbon catabolism were regulated by CCR, including the genes encoding carbohydrate-degrading enzymes such as cellulase, amylase, and xylanase. The SNF1/AMPK was highly conserved among eukaryotic organisms, which was a key regulator in both carbon metabolism and energy homeostasis. The regulation of SNF1 activity played a central role in the alleviation of CCR (Brown et al., 2013). During the absence of glucose, *SNF1* regulated the expression of metabolic genes by controlling transcriptional activators and repressors (Carlson, 1999). In *Saccharomyces cerevisiae*, *SNF1* acted as an activator for more than 400 glucose-repressing genes, some of which were involved in alternative carbon source utilization pathways (Young et al., 2003). In this study, the function of *PaSNF1* was explored. Our results demonstrated that *PaSNF1* played important roles in regulating vegetative growth, sexual development, stress responses, and biosynthesis of SMs in *Podospora anserina* and then confirmed that it was a major actor of lignocellulose degradation in *P. anserina*.

The PaSNF1 protein consisted of a serine/threonine (Ser/Thr) kinase catalytic domain (KD) (residues 67–318) and a two CTD (residues 532–628 and 633–704), showing the same structure with the SNF1s identified in many other organisms (Zhang et al., 2013; Islam et al., 2017). In addition, the PaSNF1 protein generally shared a high sequence identity with the SNF1s of other organisms, especially the catalytic domain (Cziferszky et al., 2003; Ospina-Giraldo et al., 2003; Wang et al., 2014, 2018).

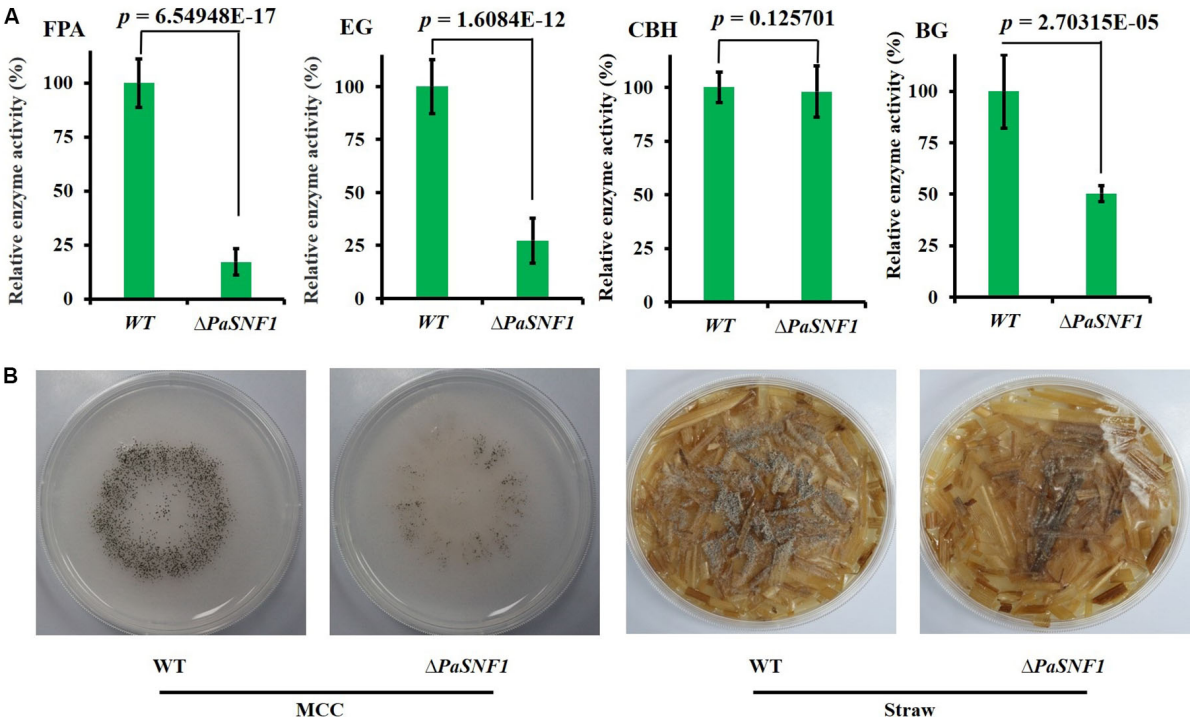

FIGURE 6 | Knockdown of *PaSNF1* led to defects in cellulose-utilizing ability. **(A)** Enzyme assays in WT and Δ*PaSNF1* mutant. The mycelia of 2-day-old cultures grown on M2 medium of the indicated strains were harvested and smashed in proper extraction buffer. Activity was expressed with respect to that of WT considered as 100%. Error bars are standard deviations of triplicate samples. Differences in the data were assessed by the *T*-test. **(B)** Fertility of WT and Δ*PaSNF1* on medium with MCC and straw medium. Fertility was measured by counting the number of mature perithecia on plates containing MCC and straw medium as sole carbon source. Pictures of mycelia of WT and Δ*PaSNF1* mutant were taken after 7 days of growth. Fruiting bodies (perithecia) are visible as small black dots. *PaSNF1*, *Podospora anserina* SNF1; WT, wild type; MCC, microcrystalline cellulose.

Phylogenetic analysis of SNF1 homologous proteins from filamentous fungi and yeasts formed a separate cluster. Results of phylogenetic analysis indicated that PaSNF1 was much more closely related to the SNF1 orthologs from the filamentous ascomycetous fungi than those from ascomycetous yeasts, plants, or mammals (**Figure 1**). Among the SNF1s in the filamentous fungi, the PaSNF1 was closest to the SNF1 ortholog identified in *Neurospora crassa*, *Hypocrea jecorina*, *Fusarium oxysporum*, and *Beauveria bassiana* (**Figure 1**).

The essential role of *SNF1* in filamentous fungi was the regulation of vegetative growth and sexual development. The ability to form the perithecia and ascospores was affected in *GzSNF1* deletion mutants (Lee et al., 2009), conidiation was also affected by the loss of *PdSNF* (Zhang et al., 2013), and the ablation of *LmSNF1* would result in impaired sporulation and spore germination (Feng et al., 2014). In Δ*MoSNF1* mutant, the sporulation ability was abolished (Yi et al., 2008), and the *PmSNF1* also played a critical role in conidiation and vegetative growth in *Pestalotiopsis microspora* NK17 (Wang et al., 2018). Deletion of *SNF1* in *Fusarium graminearum* led to defects in vegetative growth and sexual reproduction (Yu et al., 2014). Our observations were consistent with the above results; the knockout of *PaSNF1* gene led to the growth and developmental defects of *P. anserina*. The *PaSNF1* did not only affect mycelial growth but also regulate fruit body formation and developmental maturation (**Figure 2**). This finding suggested that *PaSNF1* could trigger the expression of genes required for the formation of fruit body and ascospores. Mechanisms underlying these functions may be associated with the inadequate or unbalanced nutrients (Lee et al., 2009).

In yeast, the SNF1 protein kinase has been necessary for its response to various environmental stresses such as sodium and lithium salts, alkaline pH, heat shock, and hyperosmolarity (Hong and Carlson, 2007). Treatment with high concentrations of salts (0.8 M of KCl and 1 M of NaCl), 1 M of sorbitol, and 2 mM of oxidant H_2O_2 could dramatically inhibit vegetative growth of the Δ*PmSNF1* mutant strain (Wang et al., 2018). However, the response of the *SNF1* mutant of *Cryptococcus neoformans* to osmotic, salt, and oxidative stresses was not significantly different from that of the WT (Hu et al., 2008). Our results showed that the growth of the Δ*PaSNF1* mutant would be significantly inhibited by 0.5 M of NaCl, 0.5 M of KCl, and 0.75 M of glycerol; however, Δ*PaSNF1* mutant was not sensitive to 0.5 M of sorbitol. A comparable function for *SNF1* in the *C. neoformans* JEC21 has been reported (Yang et al., 2010). Our data clearly demonstrated the crucial roles of *PaSNF1* in the tolerance of fungus to heat shock; the mycelium of the Δ*PaSNF1* mutant was sensitive to heat shock of 45°C. This function of SNF1 has been previously reported in other fungi, such as *C. neoformans* and *Pestalotiopsis microspora* (Yang et al., 2010; Wang et al., 2018).

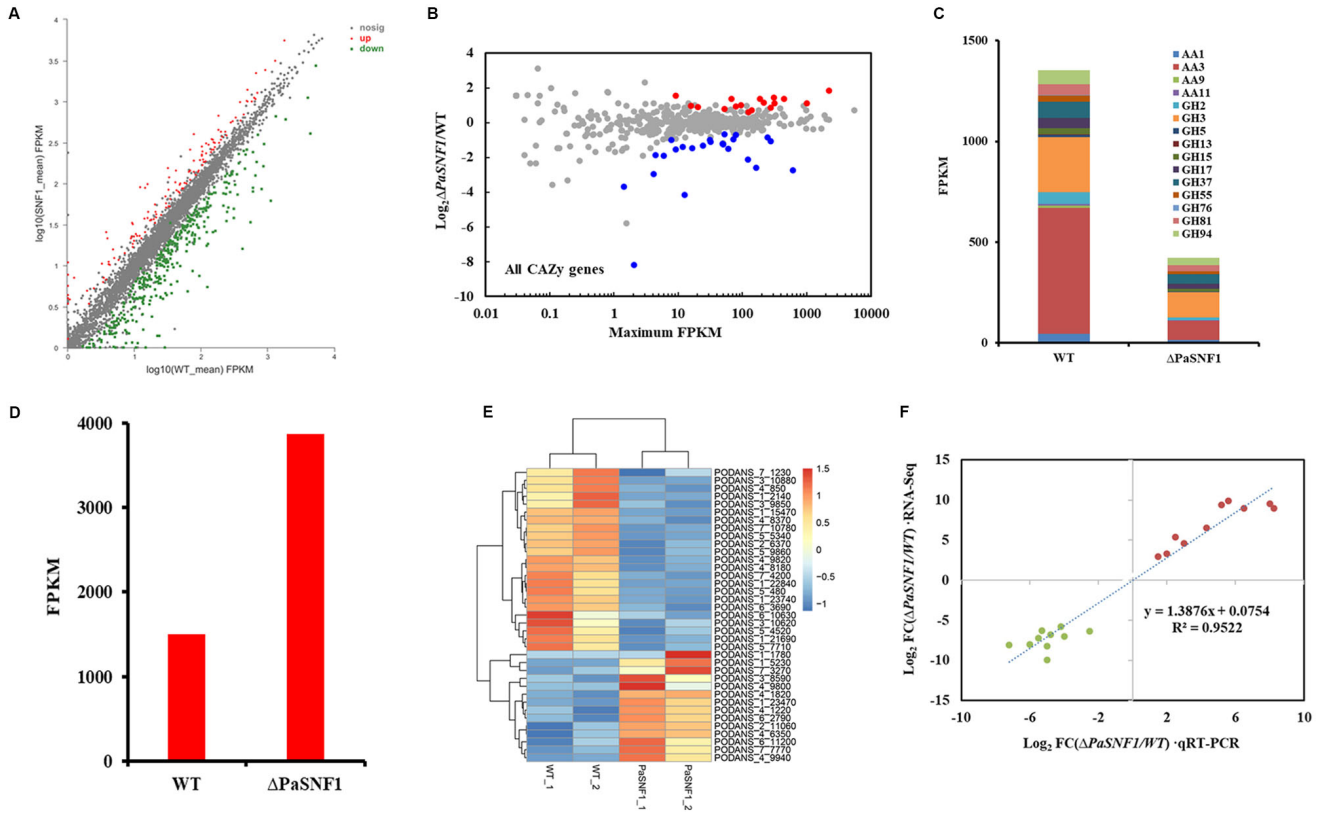

FIGURE 7 | Comparative transcriptomics analysis between Δ*PaSNF1* and WT grown in Avicel medium. **(A)** Differentially expressed genes in the mutant Δ*PaSNF1* relative to WT. The expression profile was calculated for conditions including Avicel. Genes that showed differential expression identified by DESeq2 package are shown. Up-regulated and down-regulated genes are shown in red and green, respectively. **(B)** Relative mRNA abundance of all CAZy genes in Δ*PaSNF1* mutant versus WT. The significantly up-regulated genes are shown in red, whereas down-regulated genes are shown in blue (based on adjusted *p*-value). **(C)** Total expression of genes encoding major cellulases from RNA-Seq data in WT and Δ*PaSNF1* strains. **(D)** Total expression of genes encoding LPMO from RNA-Seq data in WT and Δ*PaSNF1* strains. **(E)** Regulation of putative transporter genes by *PaSNF1*. Values in heatmaps were calculated by log2 (Gene_FPKM in Δ*PaSNF1*/Gene_FPKM in WT). FPKM mapped. **(F)** Expression level validation of DEGs using RT-qPCR. Comparisons of log2 ratios of 10 up-regulated and 10 down-regulated genes from the RNA-Seq data and RT-qPCR experiments with paired primers (**Supplementary Table S1**). *PaSNF1*, *Podospora anserina* SNF1; WT, wild type; CAZy, Carbohydrate-Active Enzymes; DEG, differentially expressed genes.

Moreover, after the knockout of *SNF1* gene, the resistance of the Δ*PaSNF1* mutant to the fungicide fluconazole would be significantly increased, whereas the sensitivity to fluconazole was not varied in Δ*CnSNF1* mutant (Hu et al., 2008). It indicated the remarkable functional deviation between *PaSNF1* and *CnSNF1*, although the underlying mechanism remained to be identified.

Ascomycete genomes code for on average 40 biosynthetic gene clusters with crucial importance in SM synthesis (Pusztahelyi et al., 2015). Genome analyses in aspergilli suggest between 39 and 80 biosynthetic gene clusters per species (Inglis et al., 2013). Sequence analysis of the *P. anserina* genome revealed its ability to produce 40 putative SMs including 18 polyketide synthases (PKSs) (Espagne et al., 2008). However, until now, only limited chemical investigations have been conducted, and plenty of SMs were yet to be discovered. Recent studies have shown that ABR1 was involved in biosynthesis of DHN melanin, which colored ascospores; and knockout of ABR1 led to decreased ascospore pigmentation accompanied by lowered ascospore germination rate (Xie et al., 2018). Shen et al. (2019) reported that *PaStcA* and *PaAflR* were key genes necessary for the biosynthesis of ST in *P. anserina*, deletion of *PaStcA* that blocked the ST pathway, and overexpression of *PaAflR* that resulted in the excessive accumulation of ST, thus leading to a female sterility phenotype. In this study, to identify the metabolites regulated by *PaSNF1*, the large-scale fermentation of the Δ*PaSNF1* mutant was performed, and the structures of metabolites with unique peaks were characterized. This result suggested that *PaSNF1* may have negative effects on the biosynthesis of ST. The general pattern of the peaks for ST was significantly increased in the HPLC profile of Δ*PaSNF1* mutant compared with WT (**Figure 5**). Correspondingly, the deletion of *PaSNF1* led to a defect in perithecium production and ascospore formation. Moreover, *OE-PaAflR* displayed overproduction of ST, and overexpression of *PaAflR* also led to sterility (Shen et al., 2019). These results indicated that ST was closely related to the development of fungi and spore formation. To our knowledge, this has been the first report of SNF's regulation effects on ST biosynthesis.

In addition to regulating ST synthesis, SNF1 also played a critical role in regulating cellulose degradation. We showed that a Δ*PaSNF1* mutant displayed severe growth defects on cellulose, and similar phenotypes were observed on straw medium (**Figure 6B**), which was correlated with a lack of cellulolytic enzyme activity. Indeed, the enzyme activities of FPA, EG, and BG in Δ*PaSNF1* mutant were significantly reduced (**Figure 6A**). The defects in *PaSNF1* would lead to the reduced (or impaired) production of such enzymes, thus inhibiting the degradation of lignocellulose and utilization of carbon sources. Consistent with this phenotype, the expression of the many CAZymes genes of *P. anserina* was significantly decreased in the Δ*PaSNF1* mutant compared with WT (**Figure 7**). Following the extracellular degradation of the lignocellulose, the uptake of the soluble breakdown products has been a key process to regulate the transcription of cellulases and related genes. The transporters played an important role, some of which exhibited the ability to sense the breakdown products during their passage through the cell membrane (Novy et al., 2019). Transcriptome analysis showed that the genes coding for MFS permeases were also highly repressed in the Δ*PaSNF1* mutant, including four putative sugar transporters. These findings suggested that *PaSNF1* played an important role in positively regulating the expression of genes encoding cellulolytic enzymes. Interestingly, our data revealed that the main transcription factors that regulated the expression of cellulases in *P. anserina* showed no change of expression in the mutant strain relative to WT strain. For example, the expression of XYR1, CLR1, and CLR2 was not significantly varied in mutant strains, especially CRE1, which was the key protein of CCR and the direct target protein of SNF1. The expression of cellulosic biomass degrading enzyme genes was regulated by various global regulators. The protein methyltransferase LAE1 was one global regulator of SM gene clusters such as ST formation, which regulated sexual and asexual developmental processes in Ascomycota (Tani et al., 2014). LAE1 also played an important role in regulating the expression of cellulase, polysaccharide hydrolases, and xyr1 in *Trichoderma reesei* (Seiboth et al., 2012). Our results showed that two putative LAE1 (*PODANS_3_3440; PODANS_5_12360*) expressions were significantly down-regulated in the Δ*PaSNF1*. This result suggested a refined dual mechanism that controlled the expression of cellulase genes through the modulation of transcription factors.

SNF1 promoted feeding on lignocellulose and reduced the synthesis of ST. There may be a balance between feeding and fighting competitors on the basis of anticorrelated effects on each pathway. In our study, negative correlation was observed based on the data of enzyme activity and metabolite map. In a previous study, analysis of the genome revealed that CAZymes of *T. reesei* were often observed in clusters along with genes involved in SM (Martinez et al., 2008). It was considered as a means to fend off competitors for nutrients. Fungi constantly faced the challenge to outcompete other organisms in complex ecosystems. Therefore, they developed powerful enzyme systems for degradation of substrates, which provided for fast growth and efficient colonization of their environment (van den Brink and de Vries, 2011). However, fungi also evolved the ability to kill, or at least inhibit the growth of their competitors, by producing a versatile array of SMs (Demain and Fang, 2000). The application of these different survival utilities should be tightly controlled in order to balance the assignment of resources for feeding to succeed by superior growth or fighting to decrease the chances of survival for competitors. This study supported this hypothesis of coordination of substrate degradation and competition. This may be a mechanism via which fungi evolved to balance the operation of primary and secondary metabolism during its life cycle. Thus, an economic distribution of resources for feeding (enzyme production) and fighting (SM production) would be reasonable.

CONCLUSION

In conclusion, in this work, the roles of *PaSNF1* in vegetative growth, sexual development, and lignocellulose degradation in *Podospora anserina* were investigated. Our study clearly suggested that SNF1 played a critical regulation role in growth, development, and stress response. Importantly, SNF1 can function as a critical global regulator for the SM biosynthesis and cellulase production. In the future, proteomics analysis and ChIP-seq on PaSNF1 would be performed to identify the interaction partners of PaSNF1. This will be crucial to develop deeper understanding on the cellulase-regulating signal transduction processes and the SNF1-mediated regulation mechanism of lignocellulose degradation in *P. anserina*, as well as its effects on growth and development.

DATA AVAILABILITY STATEMENT

The datasets generated for this study can be found in the SRA database: https://www.ncbi.nlm.nih.gov/sra/PRJNA597840, accession number PRJNA597840.

AUTHOR CONTRIBUTIONS

YL, PY, and NX designed the study. YL, XL, YQ, and SL performed the experiments. YL, GL, SL, and LM analyzed the data. YL and NX wrote the manuscript. All authors reviewed the results and approved the final version of the manuscript.

FUNDING

This study was supported jointly by the National Natural Science Foundation of China (No. 31601014), the Shenzhen Science and Technology Key Project (No. JSGG20171013091238230), the

Science and Technology Project of Shenzhen City, the Shenzhen Bureau of Science, Technology and Information (No. JCYJ20180305123659726), and Science and Technology Application Demonstration Project (Shenzhen Government, No. KJYY20180201180253571).

SUPPLEMENTARY MATERIAL

The Supplementary Material for this article can be found online at: https://www.frontiersin.org/articles/10.3389/fmicb.2020.01038/full#supplementary-material

REFERENCES

Baruffini, E., Goffrini, P., Donnini, C., and Lodi, T. (2006). Galactose transport in *Kluyveromyces lactis*: major role of the glucose permease Hgt1. *FEMS Yeast Res.* 6, 1235–1242. doi: 10.1111/j.1567-1364.2006.00107.x

Benocci, T., Aguilar-Pontes, M. V., Zhou, M., Seiboth, B., and de Vries, R. P. (2017). Regulators of plant biomass degradation in ascomycetous fungi. *Biotechnol. Biofuels* 10:152. doi: 10.1186/s13068-017-0841-x

Bills, G. F., and Gloer, J. B. (2016). Biologically active secondary metabolites from the fungi. *Microbiol. Spectr.* 4:FUNK-0009-2016.

Bischof, R. H., Ramoni, J., and Seiboth, B. (2016). Cellulases and beyond: the first 70 years of the enzyme producer *Trichoderma reesei*. *Microb. Cell Fact.* 15:106. doi: 10.1186/s12934-016-0507-6

Bok, J. W., and Keller, N. P. (2004). LaeA, a regulator of secondary metabolism in *Aspergillus* spp. *Eukaryot. Cell* 3, 527–535. doi: 10.1128/ec.3.2.527-535.2004

Bomble, Y. J., Lin, C. Y., Amore, A., Wei, H., Holwerda, E. K., Ciesielski, P. N., et al. (2017). Lignocellulose deconstruction in the biosphere. *Curr. Opin. Chem. Biol.* 41, 61–70. doi: 10.1016/j.cbpa.2017.10.013

Bourdais, A., Bidard, F., Zickler, D., Berteaux-Lecellier, V., Silar, P., and Espagne, E. (2012). Wood utilization is dependent on catalase activities in the filamentous fungus *Podospora anserina*. *PLoS One* 7:e29820. doi: 10.1371/journal.pone.0029820

Bradford, M. M. (1976). A rapid and sensitive method for the quantitation of microgram quantities of protein utilizing the principle of protein-dye binding. *Anal. Biochem.* 72, 248–254. doi: 10.1016/0003-2697(76)90527-3

Brown, D. W., Yu, J. H., Kelkar, H. S., Fernandes, M., Nesbitt, T. C., Keller, N. P., et al. (1996). Twenty-five coregulated transcripts define a sterigmatocystin gene cluster in *Aspergillus nidulans*. *Proc. Natl. Acad. Sci. U.S.A.* 93, 1418–1422. doi: 10.1073/pnas.93.4.1418

Brown, N. A., de Gouvea, P. F., Krohn, N. G., Savoldi, M., and Goldman, G. H. (2013). Functional characterisation of the non-essential protein kinases and phosphatases regulating *Aspergillus nidulans* hydrolytic enzyme production. *Biotechnol. Biofuels* 6:91. doi: 10.1186/1754-6834-6-91

Carlson, M. (1999). Glucose repression in yeast. *Curr. Opin. Microbiol.* 2, 202–207. doi: 10.1016/s1369-5274(99)80035-6

Casamayor, A., Serrano, R., Platara, M., Casado, C., Ruiz, A., and Arino, J. (2012). The role of the Snf1 kinase in the adaptive response of *Saccharomyces cerevisiae* to alkaline pH stress. *Biochem. J.* 444, 39–49. doi: 10.1042/BJ20112099

Coradetti, S. T., Craig, J. P., Xiong, Y., Shock, T., Tian, C., and Glass, N. L. (2012). Conserved and essential transcription factors for cellulase gene expression in ascomycete fungi. *Proc. Natl. Acad. Sci. U.S.A.* 109, 7397–7402. doi: 10.1073/pnas.1200785109

Couturier, M., Tangthirasunun, N., Ning, X., Brun, S., Gautier, V., Bennati-Granier, C., et al. (2016). Plant biomass degrading ability of the coprophilic ascomycete fungus *Podospora anserina*. *Biotechnol. Adv.* 34, 976–983. doi: 10.1016/j.biotechadv.2016.05.010

Cziferszky, A., Seiboth, B., and Kubicek, C. P. (2003). The Snf1 kinase of the filamentous fungus *Hypocrea jecorina* phosphorylates regulation-relevant serine residues in the yeast carbon catabolite repressor Mig1 but not in the filamentous fungal counterpart Cre1. *Fungal Genet. Biol.* 40, 166–175. doi: 10.1016/s1087-1845(03)00082-3

de Assis, L. J., Ries, L. N., Savoldi, M., Dos Reis, T. F., Brown, N. A., and Goldman, G. H. (2015). *Aspergillus nidulans* protein kinase A plays an important role in cellulase production. *Biotechnol. Biofuels* 8:213. doi: 10.1186/s13068-015-0401-1

Demain, A. L., and Fang, A. (2000). The natural functions of secondary metabolites. *Adv. Biochem. Eng. Biotechnol.* 69, 1–39.

Dos Santos, Castro, L., de Paula, R. G., Antonieto, A. C., Persinoti, G. F., Silva-Rocha, R., et al. (2016). Understanding the role of the master regulator XYR1 in *Trichoderma reesei* by global transcriptional analysis. *Front. Microbiol.* 7:175. doi: 10.3389/fmicb.2016.00175

El-Khoury, R., Sellem, C. H., Coppin, E., Boivin, A., Maas, M. F., Debuchy, R., et al. (2008). Gene deletion and allelic replacement in the filamentous fungus *Podospora anserina*. *Curr. Genet.* 53, 249–258. doi: 10.1007/s00294-008-0180-3

Espagne, E., Lespinet, O., Malagnac, F., Da Silva, C., Jaillon, O., Porcel, B. M., et al. (2008). The genome sequence of the model ascomycete fungus *Podospora anserina*. *Genome Biol.* 9:R77. doi: 10.1186/gb-2008-9-5-r77

Feng, J., Zhang, H., Strelkov, S. E., and Hwang, S. F. (2014). The *LmSNF1* gene is required for pathogenicity in the canola blackleg pathogen *Leptosphaeria maculans*. *PLoS One* 9:e92503. doi: 10.1371/journal.pone.0092503

Fernandes, M., Keller, N. P., and Adams, T. H. (1998). Sequence-specific binding by *Aspergillus nidulans* AflR, a C6 zinc cluster protein regulating mycotoxin biosynthesis. *Mol. Microbiol.* 28, 1355–1365. doi: 10.1046/j.1365-2958.1998.00907.x

Ferrer-Dalmau, J., Randez-Gil, F., Marquina, M., Prieto, José, A., and Casamayor, A. (2015). Protein kinase Snf1 is involved in the proper regulation of the unfolded protein response in *Saccharomyces cerevisiae*. *Biochem. J.* 468, 33–47. doi: 10.1042/bj20140734

Ghillebert, R., Swinnen, E., Wen, J., Vandesteene, L., Ramon, M., Norga, K., et al. (2011). The AMPK/SNF1/SnRK1 fuel gauge and energy regulator: structure, function and regulation. *FEBS J.* 278, 3978–3990. doi: 10.1111/j.1742-4658.2011.08315.x

Grognet, P., Bidard, F., Kuchly, C., Tong, L. C., Coppin, E., Benkhali, J. A., et al. (2014). Maintaining two mating types: structure of the mating type locus and its role in heterokaryosis in *Podospora anserina*. *Genetics* 197, 421–432. doi: 10.1534/genetics.113.159988

Gupta, V. K., Kubicek, C. P., Berrin, J. G., Wilson, D. W., Couturier, M., Berlin, A., et al. (2016). Fungal enzymes for bio-products from sustainable and waste biomass. *Trends Biochem. Sci.* 41, 633–645. doi: 10.1016/j.tibs.2016.04.006

Hahn, J.-S., and Thiele, D. J. (2004). Activation of the *Saccharomyces cerevisiae* heat shock transcription factor under glucose starvation conditions by Snf1 protein kinase. *J. Biol. Chem.* 279, 5169–5176. doi: 10.1074/jbc.M311005200

Hedbacker, K., and Carlson, M. (2008). SNF1/AMPK pathways in yeast. *Front. Biosci.* 13, 2408–2420. doi: 10.2741/2854

Hong, S. P., and Carlson, M. (2007). Regulation of snf1 protein kinase in response to environmental stress. *J. Biol. Chem.* 282, 16838–16845. doi: 10.1074/jbc.M700146200

Hu, G., Cheng, P. Y., Sham, A., Perfect, J. R., and Kronstad, J. W. (2008). Metabolic adaptation in *Cryptococcus neoformans* during early murine pulmonary infection. *Mol. Microbiol.* 69, 1456–1475. doi: 10.1111/j.1365-2958.2008.06374.x

Huberman, L. B., Coradetti, S. T., and Glass, N. L. (2017). Network of nutrient-sensing pathways and a conserved kinase cascade integrate osmolarity and carbon sensing in *Neurospora crassa*. *Proc. Natl. Acad. Sci. U.S.A.* 114, E8665–E8674. doi: 10.1073/pnas.1707713114

Inglis, D. O., Binkley, J., Skrzypek, M. S., Arnaud, M. B., Cerqueira, G. C., Shah, P., et al. (2013). Comprehensive annotation of secondary metabolite biosynthetic genes and gene clusters of *Aspergillus nidulans*, *A. fumigatus*, *A. niger* and *A. oryzae*. *BMC Microbiol.* 13:91. doi: 10.1186/1471-2180-13-91

Islam, K. T., Bond, J. P., and Fakhoury, A. M. (2017). FvSNF1, the sucrose non-fermenting protein kinase gene of *Fusarium virguliforme*, is required for cell-wall-degrading enzymes expression and sudden death syndrome development in soybean. *Curr. Genet.* 63, 723–738. doi: 10.1007/s00294-017-0676-9

Jonsson, L. J., Alriksson, B., and Nilvebrant, N. O. (2013). Bioconversion of lignocellulose: inhibitors and detoxification. *Biotechnol. Biofuels* 6:16. doi: 10.1186/1754-6834-6-16

Jorgensen, T. R., vanKuyk, P. A., Poulsen, B. R., Ruijter, G. J., Visser, J., and Iversen, J. J. (2007). Glucose uptake and growth of glucose-limited chemostat cultures of *Aspergillus niger* and a disruptant lacking MstA, a high-affinity

glucose transporter. *Microbiology* 153(Pt 6), 1963–1973. doi: 10.1099/mic.0.2006/005090-0

Kawaguchi, H., Hasunuma, T., Ogino, C., and Kondo, A. (2016). Bioprocessing of bio-based chemicals produced from lignocellulosic feedstocks. *Curr. Opin. Biotechnol.* 42, 30–39. doi: 10.1016/j.copbio.2016.02.031

Kubicek, C. P., and Kubicek, E. M. (2016). Enzymatic deconstruction of plant biomass by fungal enzymes. *Curr. Opin. Chem. Biol.* 35, 51–57. doi: 10.1016/j.cbpa.2016.08.028

Lalucque, H., Malagnac, F., Brun, S., Kicka, S., and Silar, P. (2012). A non-Mendelian MAPK-generated hereditary unit controlled by a second MAPK pathway in *Podospora anserina*. *Genetics* 191, 419–433. doi: 10.1534/genetics.112.139469

Lee, S. H., Lee, J., Lee, S., Park, E. H., Kim, K. W., Kim, M. D., et al. (2009). GzSNF1 is required for normal sexual and asexual development in the ascomycete *Gibberella zeae*. *Eukaryot. Cell* 8, 116–127. doi: 10.1128/EC.00176-08

Li, C., Lin, F., Li, Y., Wei, W., Wang, H., Qin, L., et al. (2016). A beta-glucosidase hyper-production *Trichoderma reesei* mutant reveals a potential role of cel3D in cellulase production. *Microb. Cell Fact.* 15:151. doi: 10.1186/s12934-016-0550-3

Liao, G. Y., Zhao, S., Zhang, T., Li, C. X., Liao, L. S., Zhang, F. F., et al. (2018). The transcription factor TpRfx1 is an essential regulator of amylase and cellulase gene expression in *Talaromyces pinophilus*. *Biotechnol. Biofuels* 11:276. doi: 10.1186/s13068-018-1276-8

Lichius, A., Seidl-Seiboth, V., Seiboth, B., and Kubicek, C. P. (2014). Nucleo-cytoplasmic shuttling dynamics of the transcriptional regulators XYR1 and CRE1 under conditions of cellulase and xylanase gene expression in *Trichoderma reesei*. *Mol. Microbiol.* 94, 1162–1178. doi: 10.1111/mmi.12824

Liu, G., Zhang, L., Qin, Y., Zou, G., Li, Z., Yan, X., et al. (2013). Long-term strain improvements accumulate mutations in regulatory elements responsible for hyper-production of cellulolytic enzymes. *Sci. Rep.* 3:1569. doi: 10.1038/srep01569

Liu, Q., Li, J., Gao, R., Li, J., Ma, G., and Tian, C. (2019). CLR-4, a novel conserved transcription factor for cellulase gene expression in ascomycete fungi. *Mol. Microbiol.* 111, 373–394. doi: 10.1111/mmi.14160

Martinez, D., Berka, R. M., Henrissat, B., Saloheimo, M., Arvas, M., Baker, S. E., et al. (2008). Genome sequencing and analysis of the biomass-degrading fungus *Trichoderma reesei* (syn. *Hypocrea jecorina*). *Nat. Biotechnol.* 26, 553–560. doi: 10.1038/nbt1403

Monroy, A. A., Stappler, E., Schuster, A., Sulyok, M., and Schmoll, M. (2017). A CRE1- regulated cluster is responsible for light dependent production of dihydrotrichotetronin in *Trichoderma reesei*. *PLoS One* 12:e0182530. doi: 10.1371/journal.pone.0182530

Novy, V., Nielsen, F., Seiboth, B., and Nidetzky, B. (2019). The influence of feedstock characteristics on enzyme production in *Trichoderma reesei*: a review on productivity, gene regulation and secretion profiles. *Biotechnol. Biofuels* 12:238. doi: 10.1186/s13068-019-1571-z

Oleinikova, G., Denisenko, V., Slinkina, N., and Afiyatullov, S. H. (2012). Secondary metabolites of the marine fungus *Aspergillus ustus* KMM 4640. *Chem. Nat. Compd.* 48, 467–469. doi: 10.1007/s10600-012-0276-3

Ospina-Giraldo, M. D., Mullins, E., and Kang, S. (2003). Loss of function of the *Fusarium oxysporum SNF1* gene reduces virulence on cabbage and *Arabidopsis*. *Curr. Genet.* 44, 49–57. doi: 10.1007/s00294-003-0419-y

Pachler, K. G., Steyn, P. S., Vleggaar, R., and Wessels, P. L. (1976). Carbon-13 nuclear magnetic resonance assignments and biosynthesis of aflatoxin B 1 and sterigmatocystin. *J. Chem. Soc. Perkin 1* 11, 1182–1189.

Paulova, L., Patakova, P., Branska, B., Rychtera, M., and Melzoch, K. (2015). Lignocellulosic ethanol: technology design and its impact on process efficiency. *Biotechnol. Adv.* 33, 1091–1107. doi: 10.1016/j.biotechadv.2014.12.002

Pusztahelyi, T., Holb, I. J., and Pócsi, I. (2015). Secondary metabolites in fungus-plant interactions. *Front. Plant Sci.* 6:573. doi: 10.3389/fpls.2015.00573

Ragauskas, A. J., Beckham, G. T., Biddy, M. J., Chandra, R., Chen, F., Davis, M. F., et al. (2014). Lignin valorization: improving lignin processing in the biorefinery. *Science* 344:1246843. doi: 10.1126/science.1246843

Sanz, P., Alms, G. R., Haystead, T. A. J., and Carlson, M. (2000). Regulatory interactions between the Reg1-Glc7 protein phosphatase and the Snf1 protein kinase. *Mol. Cell. Biol.* 20, 1321–1328. doi: 10.1128/Mcb.20.4.1321-1328.2000

Schilling, S., and Oesterhelt, C. (2007). Structurally reduced monosaccharide transporters in an evolutionary conserved red alga. *Biochem. J.* 406, 325–331. doi: 10.1042/bj20070448

Seiboth, B., Karimi, R. A., Phatale, P. A., Linke, R., Hartl, L., Sauer, D. G., et al. (2012). The putative protein methyltransferase LAE1 controls cellulase gene expression in *Trichoderma reesei*. *Mol. Microbiol.* 84, 1150–1164. doi: 10.1111/j.1365-2958.2012.08083.x

Shen, L., Poree, F. H., Gaslonde, T., Lalucque, H., Chapeland-Leclerc, F., and Ruprich-Robert, G. (2019). Functional characterization of the sterigmatocystin secondary metabolite gene cluster in the filamentous fungus *Podospora anserina*: involvement in oxidative stress response, sexual development, pigmentation and interspecific competitions. *Environ. Microbiol.* 21, 3011–3026. doi: 10.1111/1462-2920.14698

Silar, P., Dauget, J. M., Gautier, V., Grognet, P., Chablat, M., Hermann-Le Denmat, S., et al. (2019). A gene graveyard in the genome of the fungus *Podospora comata*. *Mol. Genet. Genomics* 294, 177–190. doi: 10.1007/s00438-018-1497-3

Slot, J. C., and Rokas, A. (2011). Horizontal transfer of a large and highly toxic secondary metabolic gene cluster between fungi. *Curr. Biol.* 21, 134–139. doi: 10.1016/j.cub.2010.12.020

Stricker, A. R., Mach, R. L., and de Graaff, L. H. (2008). Regulation of transcription of cellulases- and hemicellulases-encoding genes in *Aspergillus niger* and *Hypocrea jecorina* (*Trichoderma reesei*). *Appl. Microbiol. Biotechnol.* 78, 211–220. doi: 10.1007/s00253-007-1322-0

Sun, J., and Glass, N. L. (2011). Identification of the CRE-1 cellulolytic regulon in *Neurospora crassa*. *PLoS One* 6:e25654. doi: 10.1371/journal.pone.0025654

Sun, J., Tian, C., Diamond, S., and Glass, N. L. (2012). Deciphering transcriptional regulatory mechanisms associated with hemicellulose degradation in *Neurospora crassa*. *Eukaryot. Cell* 11, 482–493. doi: 10.1128/EC.05327-11

Tani, S., Kawaguchi, T., and Kobayashi, T. (2014). Complex regulation of hydrolytic enzyme genes for cellulosic biomass degradation in filamentous fungi. *Appl. Microbiol. Biotechnol.* 98, 4829–4837. doi: 10.1007/s00253-014-5707-6

Tonukari, N. J., Scott-Craig, J. S., and Walton, J. D. (2000). The *Cochliobolus carbonum SNF1* gene is required for cell wall-degrading enzyme expression and virulence on maize. *Plant Cell* 12, 237–247. doi: 10.1105/tpc.12.2.237

Tzima, A. K., Paplomatas, E. J., Rauyaree, P., Ospina-Giraldo, M. D., and Kang, S. (2011). *VdSNF1*, the sucrose nonfermenting protein kinase gene of *Verticillium dahliae*, is required for virulence and expression of genes involved in cell-wall degradation. *Mol. Plant Microbe Interact.* 24, 129–142. doi: 10.1094/MPMI-09-09-0217

Vacher, S., Cotton, P., and Fèvre, M. (2003). Characterization of a SNF1 homologue from the phytopathogenic fungus *Sclerotinia sclerotiorum*. *Gene* 310, 113–121. doi: 10.1016/s0378-1119(03)00525-0

van den Brink, J., and de Vries, R. P. (2011). Fungal enzyme sets for plant polysaccharide degradation. *Appl. Microbiol. Biotechnol.* 91, 1477–1492. doi: 10.1007/s00253-011-3473-2

Wang, D., Li, Y., Wang, H., Wei, D., Akhberdi, O., Liu, Y., et al. (2018). The AMP-activated protein kinase homolog Snf1 concerts carbon utilization, conidia production and the biosynthesis of secondary metabolites in the taxol-producer *Pestalotiopsis microspora*. *Genes* 9:E59. doi: 10.3390/genes9020059

Wang, X. X., He, P. H., Feng, M. G., and Ying, S. H. (2014). *BbSNF1* contributes to cell differentiation, extracellular acidification, and virulence in *Beauveria bassiana*, a filamentous entomopathogenic fungus. *Appl. Microbiol. Biotechnol.* 98, 8657–8673. doi: 10.1007/s00253-014-5907-0

Weng, J. K., Li, X., Bonawitz, N. D., and Chapple, C. (2008). Emerging strategies of lignin engineering and degradation for cellulosic biofuel production. *Curr. Opin. Biotechnol.* 19, 166–172. doi: 10.1016/j.copbio.2008.02.014

Wu, X., Fan, X., Xie, S., Lin, J., Cheng, J., Zhang, Q., et al. (2018). Solar energy-driven lignin-first approach to full utilization of lignocellulosic biomass under mild conditions. *Nat. Catal.* 1, 772–780. doi: 10.1038/s41929-018-0148-8

Xie, N., Chapeland-Leclerc, F., Silar, P., and Ruprich-Robert, G. (2014). Systematic gene deletions evidences that laccases are involved in several stages of wood degradation in the filamentous fungus *Podospora anserina*. *Environ. Microbiol.* 16, 141–161. doi: 10.1111/1462-2920.12253

Xie, N., Ruprich-Robert, G., Silar, P., and Chapeland-Leclerc, F. (2015). Bilirubin oxidase-like proteins from *Podospora anserina*: promising thermostable enzymes for application in transformation of plant biomass. *Environ. Microbiol.* 17, 866–875. doi: 10.1111/1462-2920.12549

Xie, N., Ruprich-Robert, G., Silar, P., Herbert, E., Ferrari, R., and Chapeland-Leclerc, F. (2018). Characterization of three multicopper oxidases in the filamentous fungus *Podospora anserina*: a new role of an ABR1-like protein in fungal development? *Fungal Genet. Biol.* 116, 1–13. doi: 10.1016/j.fgb.2018.04.007

Yang, J., Li, D., Liu, X., Pan, J., Yan, B., and Zhu, X. (2010). Regulation of virulence factors, carbon utilization and virulence by SNF1 in *Cryptococcus neoformans* JEC21 and divergent actions of SNF1 between cryptococcal strains. *Fungal Genet. Biol.* 47, 994–1000. doi: 10.1016/j.fgb.2010.08.002

Yenkie, K. M., Wu, W., Clark, R. L., Pfleger, B. F., Root, T. W., and Maravelias, C. T. (2016). A roadmap for the synthesis of separation networks for the recovery of bio-based chemicals: matching biological and process feasibility. *Biotechnol. Adv.* 34, 1362–1383. doi: 10.1016/j.biotechadv.2016.10.003

Yi, M., Park, J. H., Ahn, J. H., and Lee, Y. H. (2008). MoSNF1 regulates sporulation and pathogenicity in the rice blast fungus *Magnaporthe oryzae*. *Fungal Genet. Biol.* 45, 1172–1181. doi: 10.1016/j.fgb.2008.05.003

Yin, W. B., Amaike, S., Wohlbach, D. J., Gasch, A. P., Chiang, Y. M., Wang, C. C., et al. (2012). An *Aspergillus nidulans* bZIP response pathway hardwired for defensive secondary metabolism operates through aflR. *Mol. Microbiol.* 83, 1024–1034. doi: 10.1111/j.1365-2958.2012.07986.x

Young, E. T., Dombek, K. M., Tachibana, C., and Ideker, T. (2003). Multiple pathways are co-regulated by the protein kinase Snf1 and the transcription factors Adr1 and Cat8. *J. Biol. Chem.* 278, 26146–26158. doi: 10.1074/jbc.M301981200

Yu, J., Son, H., Park, A. R., Lee, S. H., Choi, G. J., Kim, J. C., et al. (2014). Functional characterization of sucrose non-fermenting 1 protein kinase complex genes in the Ascomycete *Fusarium graminearum*. *Curr. Genet.* 60, 35–47. doi: 10.1007/s00294-013-0409-7

Zhang, T., Sun, X., Xu, Q., Zhu, C., Li, Q., and Li, H. (2013). *PdSNF1*, a sucrose non-fermenting protein kinase gene, is required for *Penicillium digitatum* conidiation and virulence. *Appl. Microbiol. Biotechnol.* 97, 5433–5445. doi: 10.1007/s00253-012-4593-z

Conflict of Interest: The authors declare that the research was conducted in the absence of any commercial or financial relationships that could be construed as a potential conflict of interest.

frontiers in Microbiology

ORIGINAL RESEARCH
published: 12 June 2020
doi: 10.3389/fmicb.2020.01288

Using Wood Rot Phenotypes to Illuminate the "Gray" Among Decomposer Fungi

Jonathan S. Schilling[1], Justin T. Kaffenberger[2], Benjamin W. Held[3], Rodrigo Ortiz[4] and Robert A. Blanchette[3]*

[1] Department of Plant & Microbial Biology, University of Minnesota, Saint Paul, MN, United States, [2] Department of Bioproducts & Biosystems Engineering, University of Minnesota, Saint Paul, MN, United States, [3] Department of Plant Pathology, University of Minnesota, Saint Paul, MN, United States, [4] Escuela de Construcción Civil, Facultad de Ingeniería, Universidad de Valparaíso, Valparaíso, Chile

OPEN ACCESS

Edited by:
Yu Fukasawa, Tohoku University, Japan

Reviewed by:
Ari Mikko Hietala, Norwegian Institute of Bioeconomy Research (NIBIO), Norway
Abbot Okotie Oghenekaro, University of Manitoba, Canada
Bonnie Grace Waring, Utah State University, United States

***Correspondence:**
Jonathan S. Schilling
schillin@umn.edu

Specialty section:
This article was submitted to Fungi and Their Interactions, a section of the journal Frontiers in Microbiology

Received: *12 March 2020*
Accepted: *20 May 2020*
Published: *12 June 2020*

Citation:
Schilling JS, Kaffenberger JT, Held BW, Ortiz R and Blanchette RA (2020) Using Wood Rot Phenotypes to Illuminate the "Gray" Among Decomposer Fungi. Front. Microbiol. 11:1288. doi: 10.3389/fmicb.2020.01288

Wood-decomposing fungi use distinct strategies to deconstruct wood that can significantly vary carbon release rates and fates. White and brown rot-type fungi attack lignin as a prerequisite to access carbohydrates (white rot) or selectively remove carbohydrates (brown rot). Soft rot fungi use less well-studied mechanisms to deconstruct wood (e.g., cavitation and erosion). These fungi often co-exist in nature, creating a balance in carbon turnover that could presumably "tip" in a changing climate. There is no simple genetic marker, however, to distinguish fungi by rot types, and traditional black and white distinctions (brown and white, in this case) cannot explain a spectrum of "gray" carbon loss possibilities. In this study, we tested 39 wood-degrading fungal strains along this spectrum of rot types. We tracked wood mass loss and chemical changes in aspen blocks in early- to mid-decay stages, including three signatures of fungal nutritional mode measured from wood rather than from fungus: dilute alkali solubility, water-soluble monosaccharides, and lignin loss (%) relative to density loss (%) (L/D). Results were then plotted relative to rot types and correlated with gene counts, combining new data with past results in some cases. Results yielded a novel distinction in soluble monosaccharide patterns for brown rot fungi, and reliable distinctions between white and brown rot fungi, although soft rot fungi were not as clearly distinguished as suggested in past studies. Gene contents (carbohydrate-active enzymes and peroxidases) also clearly distinguished brown and white rot fungi, but did not offer reliable correlation with lignin vs. carbohydrate selectivity. These results support the use of wood residue chemistry to link fungal genes (with known or unknown function) with emergent patterns of decomposition. Wood signatures, particularly L/D, not only confirm the rot type of dominant fungi, but they offer a more nuanced, continuous variable to which we can correlate genomic, transcriptomic, and secretomic evidence rather than limit it to functional categories as distinct "bins."

Keywords: gray rot, brown rot, white rot, soft rot, decomposer, peroxidase, CAZY, decay

INTRODUCTION

Fungi are Earth's dominant forest decomposers, and they release carbon from our largest pool of aboveground biomass – wood. Fungal wood decay mechanisms, given their variable capacities to unlock carbohydrates embedded within lignin, dictate the flow of recycled carbon in forests and promise gene targets for industries. Harnessing fungal DNA information to predict decay rates and wood chemical changes is thus a critical need. Reliable predictions of wood decay using DNA-based information, however, remains both a priority (Keenan et al., 2013) and a challenge (e.g., Song et al., 2017 vs. Cline et al., 2018).

Connecting fungal genomes to their emergent wood decomposition functions is an inexact science, largely due to biological variability. Fungal nutritional strategies for deconstructing wood are not functionally redundant – they vary in ways that can have major implications in ecosystems and on greenhouse gas emissions. White rot-type fungi target lignin with enzymes such as peroxidases (PODs) to unsheathe carbohydrates and gain access for carbohydrate-active enzymes (CAZYs) such as glycosyl hydrolases (GHs) targeting hemicellulose and cellulose. Brown rot fungi instead use reactive oxygen species (ROS) mechanisms to loosen wood cell wall components before selectively extracting carbohydrates, using a contracted set of GHs expressed at higher levels (Zhang et al., 2019). A third group, soft rot fungi, use less well-studied cavitation or erosion mechanisms to mine carbohydrates from the lignocellulose matrix (Eriksson et al., 1990; Daniel and Nilsson, 1998; Blanchette et al., 2010). These decay types, particularly the lignin in residues, will influence the succession of wood decay and soil community assembly and function (Zeikus, 1981; Cornwell et al., 2008; Talbot et al., 2015). These various fungal nutritional modes also alter wood solubility (Cowling, 1961; Worrall et al., 1997; Schilling et al., 2015), lignin methylation (Filley et al., 2002), and strength (Brischke et al., 2008) in unique ways. These unique pathways steer carbon toward different fates that could significantly alter CO_2 emissions from a given forest.

Within and among these distinct rot types, there is a great deal of gray that confounds the binary brown vs. white approach to rot type classification. One well-known example is among white rot fungi, where some species exhibit a selective lignin degradation mode and others a simultaneous degradation of all wood structural bio-polymers (Blanchette, 1984, 1991). Some individual white rot species are capable of exhibiting either selective or simultaneous decay, depending on substrate and environmental conditions (Otjen et al., 1987). This kind of variability and plasticity can have great consequence on the amounts and rates of carbon released from wood. We have also learned that wood-degrading fungi greatly differ in the type and number of enzymes at their disposal for lignocellulosic degradation (Eastwood et al., 2011; Floudas et al., 2012; Riley et al., 2014), in some cases without clear genomic explanations for observed lignocellulolytic capacity. Brown rot fungi do not appear to show this degree of mechanistic diversity (Kaffenberger and Schilling, 2014), but in many ways resemble soft rot fungi in terms of carbohydrate selective mechanisms and cubical checking during wood decay (Eriksson et al., 1990; Blanchette et al., 2004; Abdel-Azeem et al., 2019).

From the inadequacy of these rot type categories (bins), the concept of "gray rot" has emerged, particularly in reference to the inadequacy of the brown vs. white rot paradigm (Riley et al., 2014). However, the meaning of the word "gray" is regularly used to denote two different things: (1) inadequate gene-to-function linkages (for example, fungus lacks POD genes but degrades lignin) and (2) a gradient of carbohydrate selectivity rather than a binary distinction (degrades lignin selectively vs. degrades lignin simultaneously with carbohydrates). The former represents an unknown – the latter represents a gradient. In the case of the latter carbohydrate selectivity gradient, a significant body of research developed in a pre-molecular era exists to demonstrate this phenotypic variability. This has not been well-linked to the former, the inadequate gene-to-functional linkages, despite its potential to correlate with genomic information and its direct link to carbon utilization.

In this study, we made phenotype rather than genotype a primary focus for our fungal wood decay trials, with the intent to establish several things we believe are useful for genomics research. First, we wanted to expand the number of isolates used in Worrall et al. (1997) and in Schilling et al. (2015) to confirm a broad distinction in carbohydrate selectivity among brown and white rot fungi. Second, we wanted to test several other wood residue qualities, specifically alkali solubility and free sugar content, that might also distinguish rot type, given the lack of reliable genetic information to do so. Third, we wanted to assess the potential for relative lignin selectivity, a continuous variable, to delineate the "gray" spectrum of rot types and offer an independent variable to correlate with gene contents. Our results demonstrate reliable distinctions between white and brown rots with all three variables (solubility, sugars, and lignin selectivity), but a need to combine tests is necessary if soft rot fungi are evaluated. In terms of gene content patterns, however, there was poor correlation between lignolytic gene content and lignolysis by white rot fungi. These results offer a useful tool that is measurable as a compiled history of rot types in the wood residues, and it can help better link fungal genes to the phenotypic traits related to functions of interest.

MATERIALS AND METHODS

Fungal Cultures

Many fungi used in this study were field isolates collected across North and South America by the authors, and several strains were obtained from culture collections (**Table 1**). Isolates were originally selected to represent a range of nutritional types of interest in plant biomass conversion, and included 14 brown rot species, 22 white rot species, and 3 species that have an unknown decay type. All isolates are publically available through the Forest Mycology Culture Collection (University of Minnesota). Strain identity was determined or verified by DNA amplification and ITS sequencing (ITS1 and ITS4), matching with Genbank BLASTn database as previously

TABLE 1 | Isolate information for fungi tested in microcosms for this study, including % mass loss (±standard error) from aspen wood decomposed 2 or 4 weeks by each fungus in soil-block microcosms.

Fungus *Genus species*	Rot type	Source	UMN code	GenBank accession	2-wk mass loss (%)	4-wk mass loss (%)
Antrodia sp.	Brown	United States	202A	KC514838	0.48 (0.06)	7.10 (0.97)
Antrodia carbonica	Brown	FPL	753 FPL	KC514806	0.42 (0.20)	1.04 (0.15)
Laetiporus squalidus	Brown	Chile	ChBrnRt1	KC514808	3.63 (1.38)	17.55 (7.64)[b]
Laetiporus squalidus	Brown	Chile	Ten. #91	KC514814	3.04 (2.15)	12.33 (2.95)[b]
Laetiporus squalidus	Brown	Chile	Ach. #46	KC514825	2.44 (0.40)	16.57 (4.42)[b]
Postia sp.	Brown	United States	PC2-2	KC514831	0.06 (0.05)	0.13 (0.09)
Fistulina hepatica	Brown	United States	FP-103444-T	KC514826	0.12 (0.11)	0.24 (0.04)
Fomitopsis cajanderi	Brown	United States	33A	KC514811	0.56 (0.14)	0.50 (0.31)
Fomitopsis cajanderi	Brown	MN	TAB 83	KC514827	6.78 (4.17)[b]	22.01 (0.01)[b]
Gloeophyllum sepiarium	Brown	United States	206A	KC514817	6.11 (0.06)[b]	15.61 (6.05)[b]
Neolentinus lepideus	Brown	United States	751	KC514815	2.30 (1.64)	30.48 (0.02)[b]
Oligoporus balsaminus	Brown	United States	212A	KC514830	0.43 (0.29)	7.28 (0.14)
Phaeolus schweinitzii	Brown	United States	209	KC514818	1.62 (0.30)	14.31 (0.35)[b]
Pyrofomes demidoffii	Brown	AZ	PJ-1	KC514835	0.33 (0.00)	1.17 (0.01)
Conferticium ravum	White	MN	BY1	KC514809	1.88 (0.50)	4.60 (1.55)
Ceriporiopsis subvermispora[a]	White	United States	105725 FPL	KC514810	0.80 (0.53)	9.48 (4.55)[b]
Aurantiporus sp.	White	United States	Tyro292	KC514840	1.56 (0.41)	5.62 (1.04)
Dichomitus squalens[a]	White	United States	4C	KC514837	2.08 (0.33)	21.32 (3.85)[b]
Ganoderma sessile	White	MN	GL-MN1	KC514839	9.13 (1.92)[b]	23.17 (2.94)[b]
Ganoderma sessile	White	MN	HoneyL1	KC514812	8.97 (0.24)[b]	21.29 (0.83)[b]
Ganoderma tsugae[a]	White	WI	WI-7C	KC514828	1.34 (0.16)	10.64 (3.35)[b]
Hymenochaete corrugata	White	MN	H-2 MN	KC514813	2.67 (1.15)	14.44 (0.06)[b]
Inonotus dryophilus[a]	White	MN	ID1	KC589014	0.18 (0.05)	3.74 (0.46)
Irpex lacteus	White	MN	34A	KC514829	9.97 (0.17)[b]	19.58 (0.32)[b]
Peniophorella praetermissa	White	Chile	Ten. #74	KC514832	0.06 (0.11)	0.10 (0.08)
Perenniporia subacida[a]	White	United States	11A	KC514821	4.63 (0.25)[b]	9.37 (0.01)[b]
Phellinus arctostaphyli	White	AZ	PM-1	KC589015	0.38 (0.04)	2.48 (0.47)
Phellinus pini[a]	White	MN	TAB 19	KC514836	0.37 (0.01)	1.67 (0.38)
Phlebia brevispora	White	United States	64C	KC514833	0.93 (0.21)	8.00 (0.96)
Phlebia chrysocreas	White	Chile	604	KC514834	4.38 (0.43)[b]	9.58 (4.08)[b]
Phlebia sp.	White	Chile	Park #82	KC514819	−0.20 (0.05)	5.00 (0.96)
Phlebia tremellosa[a]	White	FPL	PRL 2845	KC514820	0.64 (0.50)	8.17 (5.14)[b]
Baltazaria sp.[a]	White	NH	B360	KC514822	−0.08 (0.10)	6.68 (1.52)
Stereum hirsutum	White	Chile	Calem #67	KC514824	1.31 (0.17)	12.34 (2.93)[b]
Trametes betulina	White	United States	611A	KC514816	0.83 (0.08)	3.52 (0.26)
Kretzschmaria hedjaroudei	White	WI	303B	KC514841	0.44 (0.06)	1.12 (0.28)
Jaapia argillacea	Unk	Antar	Di44-5	KC514904	0.49 (0.52)	1.79 (0.40)
Sistotrema brinkmannii	Unk	Chile	Quin. 25A	KC514823	0.24 (0.12)	0.39 (0.24)
Sistotrema coronilla	Unk	Can	WBR-1	KC514807	0.11 (0.05)	0.07 (0.06)

[a]*Known to selectively degrade lignin.* [b]*Indicates significantly greater mass loss than corresponding control (Dunnett's multiple comparison, family error rate = 0.05). Control mass loss (no fungus added) for aspen averaged 0.1%. FPL, USDA Forest Products Laboratory Collection (Madison, WI, United States). All others available in University of Minnesota Forest Mycology Collection (St. Paul, MN, United States). AZ, NH, MN, and WI, State designators, United States; Can, Canada; Antar, Antarctica.*

described (Arenz et al., 2006). Isolates were maintained on 2% (w/v) potato dextrose agar (PDA) plates.

Wood Chemical Characterization

Aspen (*Populus tremuloides*) densities pre- and post-decay were measured in solid wood using dry weights (g; 100°C for 48 h) per fresh/green volumes (cm^3). Aspen was selected again with a focus on plant biomass conversion. Sound and decayed wood was chemically characterized as in Sluiter and Sluiter (2010), without protein analysis. Substrates were Wiley-milled to 40 mesh with a Wiley Mill, and characterization of resulting powder was replicated four times. The sum of fractions (carbohydrates + lignin + ash + extractives + uronic acids + acetyl) averaged 94.6%, nearing mass closure of 100% of constituents accounted.

Acid-insoluble (Klason) was measured gravimetrically using 72% sulfuric acid as solvent, and acid-soluble lignin was quantified by spectrometer at a wavelength of 240 nm and with a extinction coefficient of 30, as recommended by Sluiter et al. (2008). Carbohydrates measured included glucan,

largely representative of cellulose, as well as the hemicellulosic structural carbohydrates (xylan, galactan, arabinan, and mannan). These analyses included free monosaccharides that were soluble in water pre- and post-decay by fungi, which were as high as 2.11% of the total wood mass in decayed samples. Monosaccharides were separated via HPLC using an Aminex HPX-87P analytical column (Bio-Rad) and two in-line guard columns: Micro-guard Carbo-P and Micro-guard De-ashing (Bio-Rad). Mobile phase was degassed HPLC-grade deionized water (Sigma Aldrich) at an operating flow rate of 0.4 mL min^{-1}. Operating column temperature was at 85°C, injection volume was 20 μL, and refractive index was used for detection. Standard response calibration curves were developed with reagent grade glucose, arabinose (Sigma Aldrich), galactose, xylose, and mannose (Acros Organics).

Aspen Decomposition by Fungi

The intent of this study was not to demonstrate mass loss potential, but to capture early decay stages to match soluble sugar patterns with alkali solubility and, by design, accessibility for cellulases (data not shown). Aspen as 19 mm^3 cubes were exposed to one of the 39 tested fungi for 2 or 4 weeks following the soil block test (American Society for Testing and Materials [ASTM], 1994), using one block per jar and five replicates per treatment as suggested by power analysis. Controls were placed in sterile soil jars for 2 or 4 weeks. Equal parts by volume of peat moss, potting soil, and vermiculite were wetted with distilled water and thoroughly mixed, adding 250 g of this mixture, lightly packed in 473 mL glass jars. Birch feeder strips (40 mm × 10 mm × 2 mm) were water-soaked under vacuum for 10 min and placed in parallel on top of the soil in each jar before autoclave-sterilization (twice at 121°C, 16 psi; 1 h, each run). Two fungal plugs were sterilely placed on the ends of each feeder strip and allowed to grow for two weeks before substrate addition. Treatments were doubled for 2 and 4 week destructive harvesting. Initial and final oven-dried mass was recorded after drying at 100°C for 48 h.

Rot Type Indicators

Lignin loss relative to density loss (L/D, using %s) has been shown, as in Worrall et al. (1997) and Schilling et al. (2015), to be a useful index of carbohydrate selectivity (lower L/D; brown and soft rot) vs. lignin selectivity (higher L/D; white rot) among wood-degrading fungi. Worrall et al. (1997) used a soil-block design with 20 mm × 10 mm × 5 mm blocks, and Schilling et al. (2015) used wafers exposed inside petri plates over agar, with L/D calculated by the same methods. These L/D distinctions are only reliable when limited to wood within wood/bole decay classes II and IIII using Sollins (1982) and following Harmon et al. (2008) – a rot type cannot be assigned in class I when there is little discernable rot. In our case, this reduced the number of isolates from each study used in a composite of 78 isolates from this study combined with Worrall et al. (1997) and Schilling et al. (2015). A common threshold is 0.8 to distinguish brown and soft rot (<0.8) from white rot (>0.8).

Wood dilute alkali solubility (DAS) increases more during brown rot than during white or soft rot due to a combination of both lignin modifications and carbohydrate depolymerization (discussed in Schilling et al., 2015). We measured DAS for wood powder in 0.2 M sodium hydroxide as described by Shortle et al. (2010). The alkali solubility of degraded woody biomass offers a quick method of determining likely decay type and was used as a metric of decay type for samples degraded by unknown species based on our previous work (Schilling et al., 2015). This analysis, similar to L/D, is best done in decay class II/III if used in isolation to identify rot type, and the threshold of mass losses for significant DAS distinctions between rot types is often higher than the class I/II transition (Schilling et al., 2015). Instead of using DAS in isolation for rot type distinctions, we used this analysis across the entire range of mass losses to root best fits and demonstrate overall patterns of solubility.

Based on preliminary data from monosaccharide contents in decayed wood, the soluble sugar fractions for glucan and xylan were also measured with the hypothesis that higher soluble monosaccharides would be present during brown rot than during white rot. This hypothesis is at odds with Jurgensen et al. (1989) from field sampling performed at six conifer forest locations, but is in line with laboratory results noted by Cowling (1961). Cowling found in lab trials that brown-rotted sweetgum wood tended to have a greater concentration of "available reducing substances" than white-rotted wood in its hot water extractives, which would include water-soluble saccharides.

Statistics

Statistical significance of mass loss was determined by comparing week 2 and week 4 samples with corresponding controls using Dunnett's multiple comparison test ($\alpha = 0.05$). Significance of differences in the progression of chemical component losses between white rot and brown rot was determined by first selecting a model fit for the loss of the chemical component as a function of total mass loss for both groups. Total mass loss was used as the independent variable in lieu of exposure time to control for variability among species in growth rate. Comparisons between the residual sum of squares (SS) from each group and the SS resulting from analysis when all data were pooled were made using F tests as described by Motulsky and Ransnas (1987). For all components, a linear model fit was deemed sufficient, as additional terms were not significant.

For DAS, a modified Michaelis–Menten equation offered the best model fit. This equation is described as follows:

$$DAS = DAS_{sound} + \frac{\theta_1 \times m_{loss}}{\theta_2 + m_{loss}}$$

Where DAS_{sound} is the DAS of the undecayed controls, m_{loss} is the mass loss of the sample, and θ_1 and θ_2 to vary, with θ_1 representing the asymptotic maximum DAS and θ_2 representing the mass loss at which the DAS is at half of this maximum asymptote. Both decay type groups were separately fit to this equation by minimizing the residual SS while allowing θ_1 and θ_2 to vary. The same DAS_{sound} constant was used for both groups. After establishing the best fit equation for each groups, the equality of the variance about the decay type specific designated model fit was determined using Levene's test. Likewise, Levene's test was used to compare decay types for variance

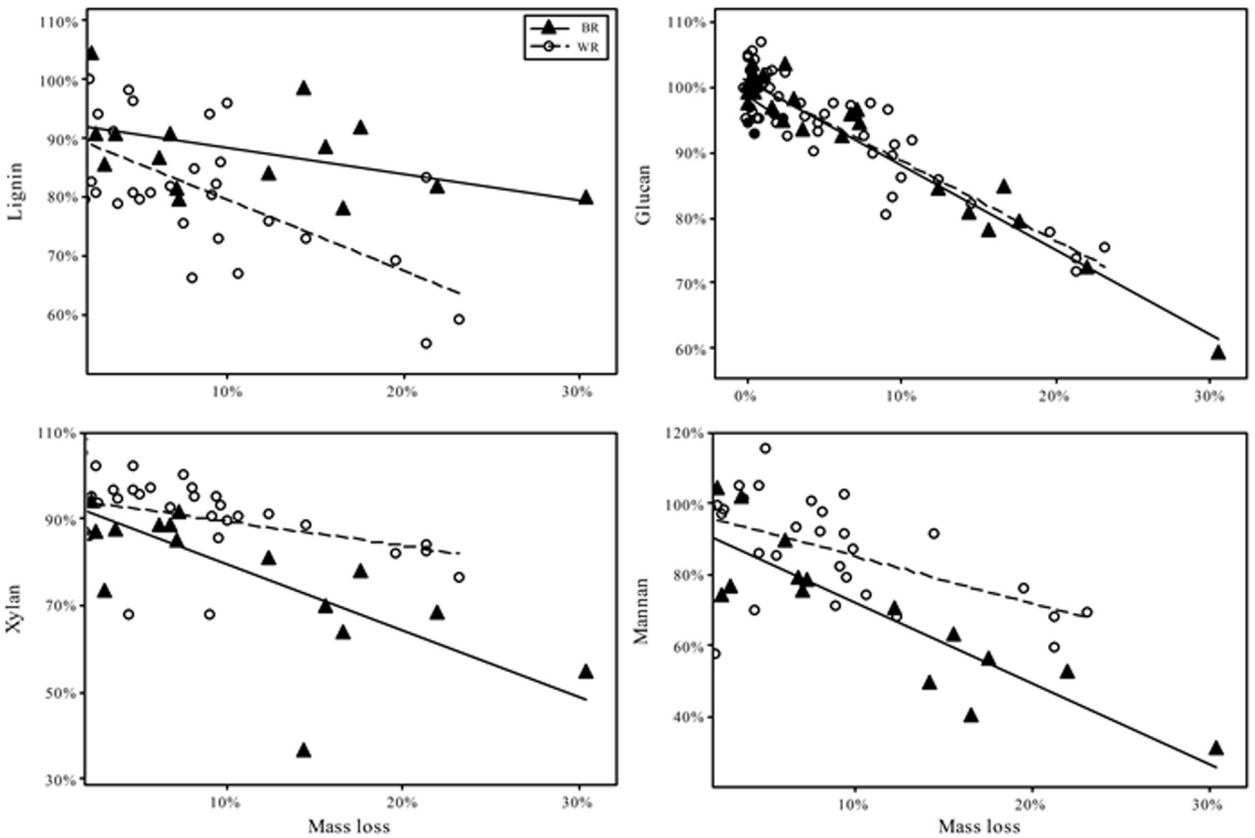

FIGURE 1 | Percentage of chemical component remaining after fungal degradation to the indicated mass loss. Remaining percentage is based on the amount of component present in sound aspen. Trend fits are linear. Initial contents were, as % of dry mass (Standard error): Lignin 20.4% (0.2); Glucan 44.2% (1.1); Xylan 15.8% (0.2); Mannan 2.8% (0.2).

TABLE 2A | Linear ($Y = M \times X + B$) model fit coefficients, standard error (S), and the coefficient of determination (R^2) for the% of component remaining in aspen wood as a function of mass loss after degradation by tested brown rot and white rot fungi.

	Brown rot				White rot				*T*-test			Levene's test	
Component	***M***	***B***	***S***	R^2	***M***	***B***	***S***	R^2	***T***	***P***	***DF***	***F***	***P***
Glucan	−1.335	1.009	0.023	0.970	−1.228	1.009	0.038	0.805	0.50	0.619	69	6.84	0.011
Xylan	−1.459	0.987	0.032	0.953	−0.938	1.016	0.030	0.813	2.65	0.010	58	0.24	0.625
Mannan	−2.253	0.965	0.061	0.922	−1.565	1.020	0.111	0.449	1.17	0.244	67	0.25	0.620
Lignin	−0.118	0.877	0.070	0.258	−1.395	0.945	0.090	0.497	−4.44	0.000	65	1.46	0.231

Results of two sample t-tests comparing the effect of brown rot and white rot on the rate of loss and Levene's test for equal variances about the model fits between the two decay types are also included.

TABLE 2B | Linear ($Y = M \times X + B$) model fit coefficients, standard error (S), and the coefficient of determination (R^2) for the% of component remaining in aspen wood as a function of mass loss after degradation by known selective white rot species and all other tested white rot fungi.

	Selective white rot				Other white rot				*T*-test		
Component	***M***	***B***	***S***	R^2	***M***	***B***	***S***	R^2	***T***	***P***	***DF***
Glucan	−1.116	0.994	0.038	0.77	−1.273	1.016	0.040	0.809	−0.76	0.457	23
Xylan	−0.115	0.906	0.051	0.021	−0.867	0.987	0.097	0.248	2.01	0.053	31
Mannan	−1.285	0.970	0.148	0.224	−1.334	0.992	0.135	0.286	−0.06	0.951	20
Lignin	−1.976	0.940	0.093	0.636	−0.930	0.906	0.084	0.333	2.13	0.046	20

Additionally, the results of two sample t-tests comparing the effect of selective and other white rot species on rate of loss for each component are provided.

differences among the fit residuals for chemical component and sugar yield analyses.

A generalized linear regression model was used to assess the significance of the role of decay type in the release of free sugar over the course of degradation. Xylose and glucose yields were tested as response variables. Mass loss, decay type, and their interaction term were factors included in the model.

RESULTS AND DISCUSSION

Mass Loss

Overall, wood mass losses were in line with the relatively short incubation period and generally confined results to early decay stages, as planned. Of the 39 isolates tested in initial screening with aspen wood, 24 caused a mean mass loss in excess of 5% after 4 weeks (**Table 1**). Seven isolates (2 BR and 5 WR) caused statistically greater mass loss than controls ($P < 0.05$) after 2 weeks and 18 isolates (7 BR, 11 WR) caused significant mass loss after 4 weeks. Eleven isolates, including those of unclear or unknown decay type (*Jaapia argillacea* and the two *Sistotrema* species), produced mean mass losses less than 2% after 4 weeks. Lignin selectivity metrics, which require a more strict threshold ($\geq$9% per aspen; Schilling et al., 2015), restricted L/D further to 13 isolates from this study that could be composited with previous data to pool L/D for 78 isolates, total.

Wood Chemistry and Patterns of Decay

Aspen chemical composition analyses approached 95%, nearing full mass closure. Lignin content (wt%) was 20.4% (±0.2), glucan 44.2% (±0.2), and hemicellulose 22.7% (±0.2; xylan 15.8%). Uronic acid content was 3.0% (±0.0) and acetyl 4.2% (±0.0). Extractives were 3.0% (±0.3) and ash 0.2% (±0.0). This composition is comparable to previously described values for hardwoods/angiosperms (Rowell, 1984; Saddler and Mackie, 1990; Wang et al., 2012). Typical of hardwoods, hemicelluloses were predominantly composed of xylan and a relatively small proportion of mannan (2.8%, ±0.2), unlike a softwood like pine. Uronic acids and acetyl groups were abundant, also unlike pine, and ash and extractives contents were lower than what would be expected in non-woody grasses.

As test fungi decayed aspen, wood component loss patterns generally were characteristic of decay type for brown and white rot strains (**Figure 1**). White rot species removed lignin at a significantly faster rate than brown rot (11.8× faster) ($t(65) = 4.44$, $P < 0.0001$), and showed a collective pattern in line with simultaneous white rot. However, white rot species known to selectively degrade lignin ($n = 8$; noted in **Table 1**) caused lignin loss at a rate that was more than twice that of the other tested white rot fungi (**Table 2A**). These selective delignifying fungi also appeared to cause a slower rate of xylan loss than the other white rot fungi ($P = 0.053$), though these data were poorly fit by the model equation ($R^2 = 0.021$).

As often observed, brown rot hemicellulose losses tended to outpace white rot (Cowling, 1961; Kirk and Highley, 1973). Xylan and mannan loss rates in brown rot were 55 and 44% greater than white rot, respectively, but only the difference in the rate of xylan loss was statistically significant (**Table 2B**). Galactan was not present in an appreciable amount and arabinan loss was highly variable because of its minor contribution to overall mass of the wood. The rate of glucan loss was statistically identical in both decay types, but the variance about the linear fit for white rot was significantly greater than that for brown rot based on Levene's test, with $P = 0.0011$ (**Table 2B**). Variance about model fits for other components also tended to be greater in white rot based on standard error, but the difference as compared with brown rot were not statistically significant.

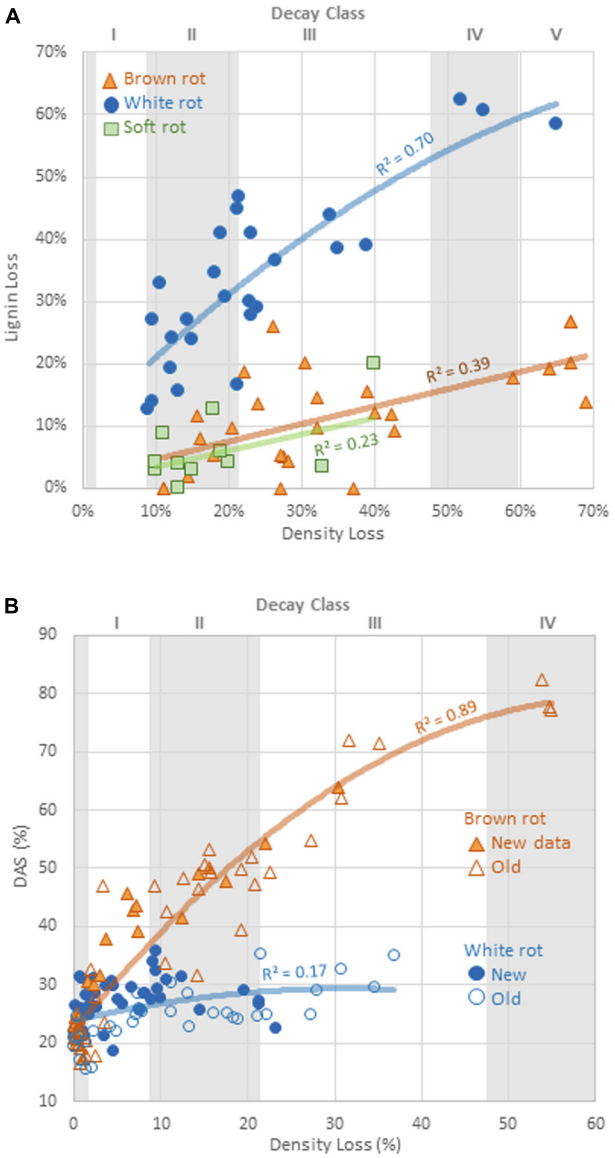

FIGURE 2 | Comparison of **(A)** the rate of lignin loss and **(B)** change in dilute alkali solubility (DAS) relative to the rate of total mass loss for distinct decay types. Line fits are linear or exponential, showing best fits. Decay classes shown for wood substrates are specificto aspen, using Harmon et al. (2008) appendices.

TABLE 3 | Soluble glucose and xylose after treatment with the indicated fungus for 2 or 4 weeks. Yields are expressed as a percentage of soluble sugar relative to the xylan or glucan content of untreated aspen.

Species	Accession #	Decay type	Xylose (%)		Glucose (%)	
			2 weeks	4 weeks	2 weeks	4 weeks
Control	–	–	0.06	0.09	0.09	0.03
Aurantiporus sp.	KC514840	W	0.11	2.11[a]	0.23	1.17[a]
L. squalidus	KC514808	B	0.19	1.85[a]	0.15	1.01[a]
L. squalidus	KC514825	B	0.10	0.52	0.10	0.71[a]
P. schweinitzii	KC514818	B	0.00	1.81[a]	0.00	0.69[a]
N. lepideus	KC514815	B	0.00	1.10	0.17	0.66
F. cajanderi	KC514827	B	0.18	0.50	0.13	0.59
L. squalidus	KC514814	B	0.10	0.89	0.12	0.53
G. sepiarium	KC514817	B	0.36	0.43	0.25	0.50
G. sessile	KC514812	W	0.08	0.42	0.21	0.33
P. tremellosa	KC514820	W	0.00	0.77	0.00	0.25
Antrodia sp.	KC514838	B	0.00	0.21	0.03	0.20
J. argillacea	KC514904	?	0.00	0.75	0.00	0.19
D. squalens	KC514837	W	0.05	0.22	0.15	0.16
H. corrugata	KC514813	W	0.00	0.12	0.10	0.15
C. ravum	KC514809	W	1.57	0.59	0.41	0.13
I. lacteus	KC514829	W	0.85	0.00	0.17	0.10
P. chrysocreas	KC514834	W	0.25	0.00	0.20	0.08
Phlebia sp.	KC514819	W	0.00	0.21	0.03	0.07
O. balsaminus	KC514830	B	0.01	0.22	0.01	0.07
S. hirsutum	KC514824	W	0.13	0.46	0.05	0.06
S. coronilla	KC514807	?	0.00	0.00	0.24	0.05
P. subacida	KC514821	W	0.00	0.20	0.00	0.04
C. subvermispora	KC514810	W	0.00	0.21	0.00	0.03
Postia sp.	KC514831	B?	2.15[a]	0.00	0.52	0.00
P. arctostaphyli	KC589015	W	1.15	0.00	0.26	0.00
F. hepatica	KC514826	B	0.90	0.00	0.23	0.00
P. praetermissa	KC514832	W	0.99	0.00	0.19	0.00
I. dryophilus	KC589014	W	0.02	0.00	0.16	0.00
Baltazaria sp.	KC514822	W	0.00	0.00	0.15	0.00
P. pini	KC514836	W	0.00	0.00	0.12	0.00
T. betulina	KC514816	W	0.00	0.00	0.11	0.00
P. demidoffii	KC514835	W	0.00	0.00	0.07	0.00
K. hedjaroudei	KC514841	W	0.01	0.00	0.04	0.00
G. sessile	KC514839	W	0.02	0.00	0.03	0.00
G. tsugae	KC514828	W	0.04	0.00	0.01	0.00
P. brevispora	KC514833	W	0.00	0.00	0.01	0.00
A. carbonica	KC514806	B	0.00	0.00	0.00	0.00
F. cajanderi	KC514811	B	0.00	0.00	0.00	0.00
S. brinkmanii	KC514823	?	0.00	0.00	0.00	0.00

[a] *Indicates significantly greater mass loss than corresponding control (Dunnett's multiple comparison, family error rate = 0.05).*

Fungal Rot Type Indicators

Dilute Alkali Solubility

Alkali solubility of brown-rotted wood typically increases in early decay relative to the DAS of sound wood, while white-rotted wood typically exhibits modest DAS increases (Cowling, 1961; Shortle et al., 2010). Schilling et al. (2015) showed for birch this threshold of distinction to be a DAS of 40%, a value that would vary by wood species and decay stage, but that held true for our isolates. Values for parameters θ_1 and θ_2 obtained by the fit of both decay types to a modified Michaelis-Menten equation were compared. Added to the initial DAS value (DAS of sound wood), θ_1 represents the asymptotic maximum DAS, while θ_2 represents the mass loss at which the DAS is at half of this maximum asymptote. Brown rot exhibited a significantly greater ($P = 0.018$) theoretical maximum DAS ($\theta_1 = 0.54$, vs. 0.06 for white rot).

Overall, the potential for DAS to distinguish brown from white rot was confirmed (**Figure 2**), and the patterns may be very useful for obtaining rot type information from isolates with poor BLAST

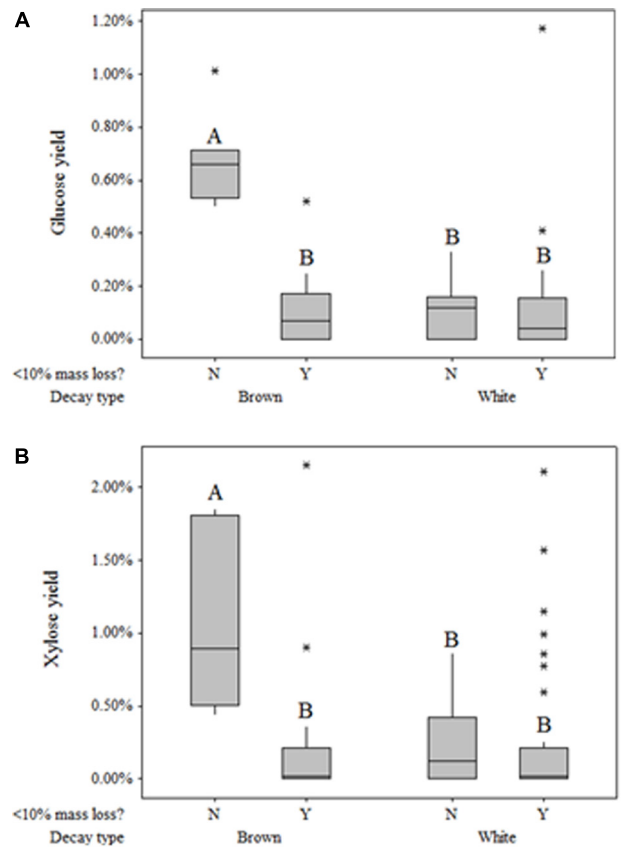

FIGURE 3 | Box plots of glucose **(A)** and xylose **(B)** yield based on original glucan and xylan content, respectively, following pretreatment but preceding enzymatic hydrolysis, with respect to decay type and extent of decay (>10%). Plots within the same graph sharing the same letter are not significantly different based on Tukey's *post hoc* comparisons.

query fits (<95% confidence) or that are complete unknowns. Using DAS, however, does bear caveats in the lab and in the field. First, we still lack data on soft rot alkali solubility effects, excepting a few targeted species tested over a half century ago (e.g., Savory and Pinion, 1958; Seifert, 1966; Henningsson, 1967). The screen by Worrall et al. (1997) is the only exception, giving the strongest indication that DAS is low for both soft and white rot fungi, but these studies have often been limited in scope by low wood mass losses. The second caveat, specific to field studies, is that early increases in DAS by brown rot fungi leave a signature in wood that cannot be erased in later stages, termed "legacy bias" in Schilling et al. (2015). These caveats, however, can be overcome by tracking lignin loss patterns as a complementary analysis, explained next.

Soluble Monosaccharides

Fungi degrading wood also solubilized monomeric sugars beyond those present in sound aspen at levels dependent on rot type (**Table 3**). Glucose and xylose yields resulting solely from fungal degradation were as high as 2.15 and 1.17%, respectively. General linear regression indicated that neither the main effect of decay type nor the interaction term between decay type and mass loss were significant factors in modeling xylose yield ($P = 0.926$, $P = 0.053$, respectively). For glucose yield, however, the interaction term between mass loss and decay type was highly significant ($P < 0.001$), though the main effect of decay type was not significant ($P = 0.547$). The significance of this interaction term was driven by the large difference in glucose yield between brown-rotted samples that exhibited more than 10% mass loss and those that did not exceed 10% mass loss. This mass loss distinction had no effect on either xylose or glucose yields of white rot (**Figures 3A,B**). As with glucose, xylose yield for brown rot was substantially higher than that of white rot when mass loss exceeded 10%.

This observation in "free" sugar patterns has rarely been identified, and results in the field have contradicted those in single-strain trials. Cowling (1961) found that brown-rotted sweetgum tended to have a greater concentration of "available reducing substances" than white-rotted sweetgum in all stages of decay when testing hot water extractives, which would include water-soluble saccharides. This observation of higher free monosaccharide in brown-rotted wood contradicts Jurgensen et al. (1989), who noted differences in soluble sugar concentrations for brown-rot and white-rot of native logs from six conifer forests. This distinction between lab and field may indicate a role for sugars released during brown rot in excess of the concentrations during white rot. Free sugar "cascade" effects on microbial communities have been observed in various other environments, including the microbiomes in the human digestive tract (Sonnenberg et al., 2010), soils (Luo et al., 2008; Chen et al., 2008), and forest litter (Scheu and Schaefer, 1998). These interactions have not been explored in wood decomposer communities, and may limit the ecological niche of brown rot fungi, given their diffuse ROS strategy for deconstructing wood.

Lignin Loss/Density Loss

The relative selectivity of lignin removal from aspen was high for white rot fungi and low for brown rot fungi in this study, with soft rot patterns similar to brown rot (**Figure 2**). Data were combined with data from previous studies ($n = 78$, total) to demonstrate the binary distinction between white and brown rot (**Figure 4**), although it should be noted that *Daldinia* and *Hypoxylon* genera in the Ascomycota and designated as soft rot fungi have previously been shown to remove lignin more like white than brown rot fungi (Nilsson et al., 1989). White rot fungi that decayed aspen to Class II/III decay in our study were unanimously above the 0.8 threshold for L/D proposed by Worrall et al. (1997) and confirmed by Schilling et al. (2015). These new data build an even stronger case for using L/D to determine rot type outcomes in wood decay studies (Seifert, 1966; Schilling et al., 2015), but coupling with DAS for soft rot identification (Worrall et al., 1997). Although rot type is integrated into trait-focused DNA high-throughput sequencing tools such as FunGuild (Nguyen et al., 2016), the extrapolation of a functional wood decay outcome from operational taxonomic units (OTUs) remains limited by abundance quantification caveats and the assumption that the current snapshot of community can explain the history of rot. Measuring wood

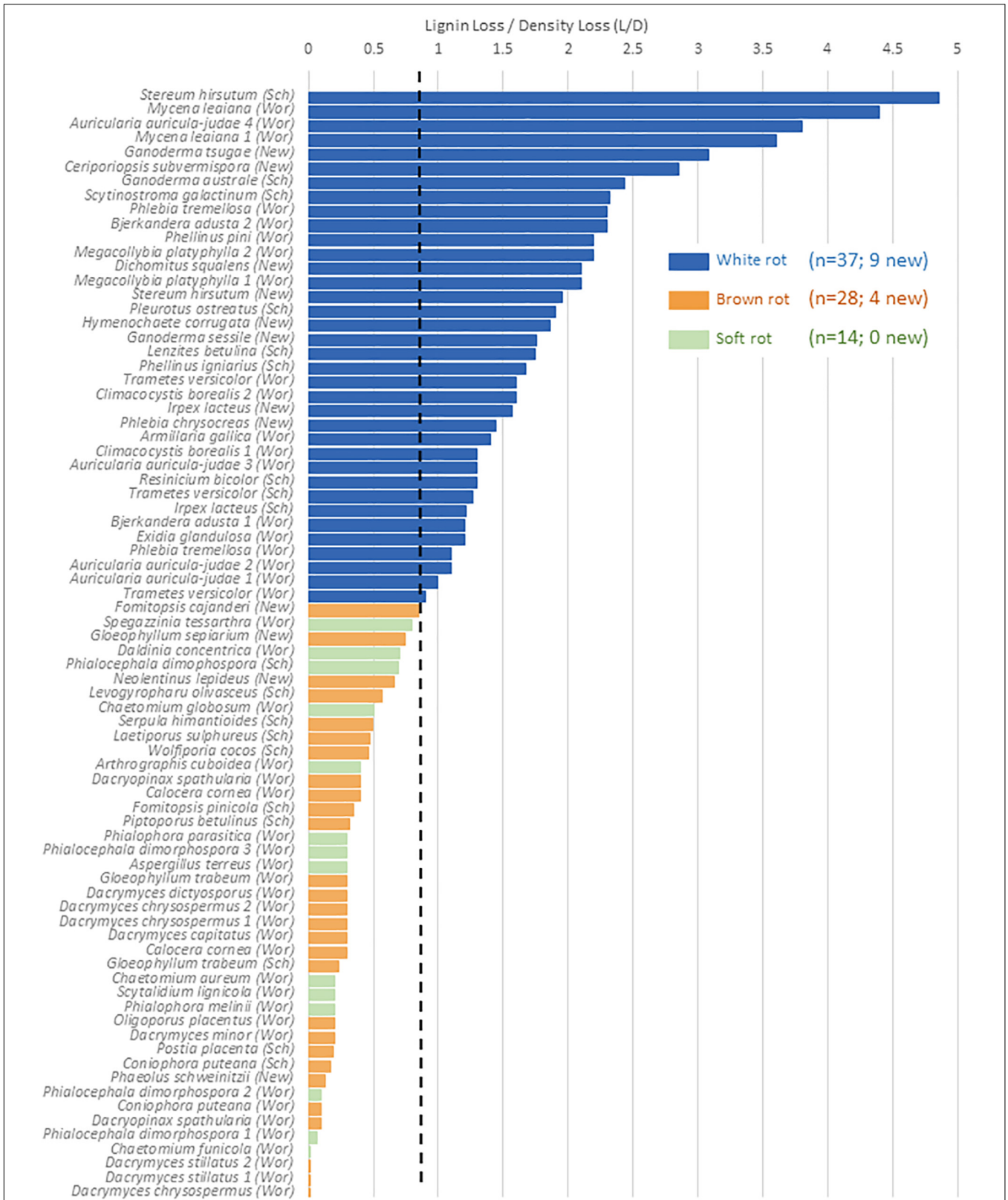

FIGURE 4 | %Lignin loss relative to%Density loss (L/D) in aspen wood decayed by fungi with distinct nutritional modes, restricted to Class II/III decay. A O.S threshold (dashed line) distinguishing brown and white rot proposed by Worrall et al. (1997; "Wor"), and validated in Schilling et al. (2015; "Sch"), is complemented in this study ("New"). Gene count correlations with L/D are shown for the sum of genes from **Table 2**, including a separate correlation for PODs.

TABLE 4 | Gene contents, and corresponding lignin selectivity values (L/D), in annotated strains of brown and white rot fungal isolates used in this study.

Fungus *Genus species* *annotations noted, Table 1	Rot Type	GH5	GH6	GH7	Total GH	CBM_1	AA1_1 Lac	AA2 POD	AA3_2	AA5_1	AA9 LPMO	Total ALL	L/D
Coniophora puteana	Brown	21	2	2	25	2	6	0	13	6	10	87	0.2
Postia placenta	Brown	17	0	0	17	0	2	1	24	3	2	66	0.2
Gloeophyllum trabeum	Brown	9	0	0	9	1	4	0	20	2	4	49	0.3
Fomitopsis betulina	Brown	18	0	0	18	0	2	1	17	4	3	63	0.3
Fomitopsis pinicola	Brown	19	0	0	19	0	5	1	16	4	4	68	0.3
Calocera cornea	Brown	23	0	0	23	1	0	0	13	3	0	63	0.4
Laetiporus sulphureus	Brown	20	0	2	22	0	7	1	26	5	2	85	0.5
Serpula himantiodes	Brown	25	1	0	26	6	5	0	14	5	5	87	0.5
Wolfipora cocos	Brown	18	0	0	18	0	3	1	8	4	2	54	0.5
Leucogyrophana olivasceus	Brown	26	1	1	28	8	6	0	9	5	12	96	0.6
Neolentinus lepideus	Brown	23	0	0	23	0	4	0	23	2	4	79	0.7
Exidia glandulosa	White	53	1	6	60	59	0	36	36	10	39	300	1.2
Trametes versicolor	White	22	1	4	27	23	7	26	17	9	18	154	1.3
Armillaria gallica	White	20	2	4	26	13	25	8	65	5	19	187	1.4
Irpex lacteus	White	26	1	4	31	26	0	10	21	7	16	142	1.4
Bjerkandera adusta	White	19	1	5	25	32	1	20	30	7	28	168	1.8
Auricularia subglabra	White	41	2	6	49	48	0	19	38	9	19	231	1.8
Trametes betulina	White	21	1	3	25	21	8	16	21	7	13	136	1.8
Pleurotus ostreatus	White	21	3	16	40	33	11	9	23	16	29	201	1.9
Dichomitus squalens	White	19	1	4	24	17	11	12	27	9	15	139	2.1
Ceriporiopsis subvermispora	White	18	0	3	21	16	9	17	17	3	9	113	2.9
Stereum hirsutum	White	20	1	3	24	17	15	6	40	8	16	150	3.5

Gene counts accessed using JGI MycoBank.

residues, directly, compiles the history of successional rot type dominance and offers a timely, useful complement to high-throughput sequencing.

The continuous nature of the L/D, however, offers an even bigger reward for linking molecular data to functional outcomes in two key ways: (1) by resolving the "gray" gradient of a rot type spectrum, and (2) by producing a continuous variable (from 0 to 5) with which to correlate other –omics data such as gene contents (**Table 4**). It essentially shifts data analyses from a bar graph with rot type as the independent variable on the *X* axis to enabling correlations along an L/D continuum. This gradient among the 78 isolate composite (**Figure 4**) shows the breadth of carbohydrate selectivity among wood degrading fungi that matches gene content in some, but not all cases. The continuous L/D also enables correlation of POD counts with lignin selectivity, also with a negative relationship (r^2 = 0.23). These line fits are relatively poor and not shown here in Figures, but the lack of positive correlation is interesting, and the concept of linear regression with a direct measure of carbon release strategies should be very useful for future genomic studies.

CONCLUSION

The data generated in this study validate wood residue chemistry as a valuable tool for determining fungal rot type dominance and for linking omics information to a measurable outcome. Specifically, a continuous gradient of "gray rot" can be resolved by analysis of lignin selectivity (as L/D). This spectrum has a convenient division of brown (L/D $<$ 0.8) from white rot (L/D $>$ 0.8) that we reconfirmed here, and it can be used in tandem with a simple wood solubility test (as DAS) to help distinguish a third decay strategy, soft rot. These data offer a time-tested, but often overlooked quality control tool when attempting to extrapolate function from fungal gene contents, consequence from re-assembled secretomes in planta, or species dominance in field samples relying on relative OTU abundance estimates. Being able to tie genomic information and OTU tables to a consequence, measured in the wood, can greatly enable the promise of trait-based approaches trying to link the characteristics of fungi to their emergent roles.

DATA AVAILABILITY STATEMENT

The raw data supporting the conclusions of this article will be made available by the authors, without undue reservation.

AUTHOR CONTRIBUTIONS

JS, JK, BH, and RB designed the experiment. BH, RB, and RO collected, maintained and supplied isolates, with life history

information, for lab trials. JS and JK performed the lab trials and analyses with the isolates. JK compiled information. JK and JS created the figures, tables, and manuscript, which was edited by all authors. All authors contributed to the article and approved the submitted version.

FUNDING

This work was supported by University of Minnesota Institute on the Environment (IonE) awards (RC-00008–11; RS-0010-12), as well as generous support from the Buckman Foundation through a Bioproducts and Biosystems Engineering (BBE) fellowship and a Doctoral Dissertation Fellowship from the Graduate School at the University of Minnesota.

ACKNOWLEDGMENTS

We thank José Navarrette from Universidad de Bio Bio, Concepcion, Chile, for his help in obtaining isolates used in this study.

REFERENCES

Abdel-Azeem, A., Held, B. W., Richards, J. E., Davis, S. L., and Blanchette, R. A. (2019). Assessment of biodegradation in ancient archaeological wood from the middle cemetery at abydos, Egypt. *PLoS One* 14:e0213753. doi: 10.1371/journal.pone.0213753

American Society for Testing and Materials [ASTM] (1994). "Standard method of accelerated laboratory test of natural decay resistance of woods (D 1413-76)," in *Proceeding of the 1994 Annual Book of Standards*, Vol. 04.10 (Philadelphia, PA: American Society for Testing and Materials), 218–224.

Arenz, B. E., Held, B. E., Jurgens, J. A., Farrell, R. L., and Blanchette, R. A. (2006). Fungal diversity in soils and historic wood from the ross sea region of Antarctica. *Soil Biol. Biochem.* 38, 3057–3064. doi: 10.1016/j.soilbio.2006.01.016

Blanchette, R. A. (1984). Screening wood decayed by white rot fungi for preferential lignin degradation. *Appl. Environ. Microbiol.* 48, 647–653. doi: 10.1128/aem.48.3.647-653.1984

Blanchette, R. A. (1991). Delignification by wood-decay fungi. *Annu. Rev. Phytopathol.* 29, 381–398.

Blanchette, R. A., Held, B. W., Arenz, B. E., Jurgens, J. A., Baltes, N. J., Duncan, S. M., et al. (2010). An antarctic hot spot for fungi at Shackleton's historic hut on cape royds. *Micr. Ecol.* 60, 29–38. doi: 10.1007/s00248-010-9664-z

Blanchette, R. A., Held, B. W., Jurgens, J. A., and Haight, J. E. (2004). Wood deterioration in chacoan great houses of the southwestern United States. *Conserv. Manag. Archaeol. Sites* 6, 204–212. doi: 10.1179/135050304793137775

Brischke, C., Welzbacher, C. R., and Huckfeldt, T. (2008). Influence of fungal decay by different basidiomycetes on the structural integrity of Norway spruce wood. *Holz Roh Werkst.* 66, 433–438. doi: 10.1007/s00107-008-0257-1

Chen, J., Huijun, X., Xuliang, Z., Guoqiang, Z., Zhihui, B., and Hongxun, Z. (2008). Substrate-induced changes in microbial community-level physiological profiles and their application to discriminate microbial communities. *J. Environ. Sci.* 20, 725–731. doi: 10.1016/s1001-0742(08)62119-1

Cline, L., Schilling, J. S., Menke, J., Fleischauer, E., and Kennedy, P. G. (2018). Ecological and functional effects of fungal endophytes on wood decomposition. *Func. Ecol.* 32, 181–191. doi: 10.1111/1365-2435.12949

Cornwell, W. K., Cornelissen, J. H. C., Amatangelo, K., Dorrepaal, E., Eviner, V. T., Godoy, O., et al. (2008). Plant species traits are the predominant control on litter decomposition rates within biomes worldwide. *Ecol. Lett.* 11, 1065–1071. doi: 10.1111/j.1461-0248.2008.01219.x

Cowling, E. B. (1961). Comparative biochemistry of the decay of sweetgum sapwood by white-rot and brown-rot fungi. *U.S. Dept. Agric. Tech. Bull.* 1258, 1–79.

Daniel, G., and Nilsson, T. (1998). "Developments in the study of soft rot and bacterial decay," in *Forest Products Biotechnology*, eds A. Bruce, and J. W. Palfreyman (London: Taylor & Francis), 37–62.

Eastwood, D. C., Floudas, D., Binder, M., Majcherczyk, A., Schneider, P., Aerts, A., et al. (2011). The plant cell wall decomposing machinery underlies the functional diversity of forest fungi. *Science* 333, 762–765.

Eriksson, K.-E., Blanchette, R. A., and Ander, P. (1990). *Microbial and Enzymatic Degradation of Wood and Wood Components*. Berlin: Springer.

Filley, T. R., Cody, G. D., Goodell, B., Jellison, J., Noser, C., and Ostrofsky, A. (2002). Lignin demethylation and polysaccharide decomposition in spruce sapwood degraded by brown rot fungi. *Organ. Geochem.* 33, 111–124. doi: 10.1016/s0146-6380(01)00144-9

Floudas, D., Binder, M., Riley, R., Barry, K., Blanchette, R. A., Henrissat, B., et al. (2012). The Paleozoic origin of enzymatic lignin decomposition reconstructed from 31 fungal genomes. *Science* 336, 1715–1719.

Harmon, M. E., Woodall, C. W., Fasth, B., and Sexton, J. (2008). *Woody Detritus Density and Density Reduction Factors for Tree Species in the United States: A synthesis*. Gen. Tech. Rep. NRS-29. Newtown Square, PA: USDA.

Henningsson, B. (1967). Changes in impact bending strength, weight and alkali solubility following fungal attack on birch wood. *Stud. For. Suec.* 41, 1–20.

Jurgensen, M. F., Larsen, M. J., Wolosiewicz, M., and Harvey, A. E. (1989). A comparison of dinitrogen fixation rates in wood litter decayed by white-rot and brow-rot fungi. *Plant Soil* 115, 117–122. doi: 10.1007/bf02220701

Kaffenberger, J. T., and Schilling, J. S. (2014). Comparing lignocellulose physiochemistry after decomposition by brown rot fungi with distinct evolutionary origins. *Environ. Microbiol.* 17, 4885–4897. doi: 10.1111/1462-2920.12615

Keenan, T. F., Davidson, E. A., Munger, J. W., and Richardson, A. D. (2013). Rate my data: quantifying the value of ecological data for the development of models of the terrestrial carbon cycle. *Ecol. Appl.* 23, 273–286. doi: 10.1890/12-0747.1

Kirk, T. K., and Highley, T. L. (1973). Quantitative changes in structural components of conifer woods during decay by white-and brown rot fungi. *Phytopathology* 63, 1338–1342.

Luo, W., D'Angelo, E. M., and Coyne, M. S. (2008). Organic carbon effects on aerobic polychlorinated biphenyl removal and bacterial community composition in soils and sediments. *Chemosphere* 70, 364–373. doi: 10.1016/j.chemosphere.2007.07.022

Motulsky, H. J., and Ransnas, L. A. (1987). Fitting curves to data using nonlinear regression: a practical and nonmathematical review. *FASEB J.* 1, 365–374. doi: 10.1096/fasebj.1.5.3315805

Nguyen, N. H., Song, Z., Bates, S. T., Branco, S., Menke, J., Schilling, J. S., et al. (2016). FunGuild: an open annotation tool for parsing fungal community datasets by ecological guild. *Fungal Ecol.* 20, 241–248. doi: 10.1016/j.funeco.2015.06.006

Nilsson, T., Daniel, G., Kirk, T. K., and Obst, J. R. (1989). Chemistry and microscopy of wood decay by some higher ascomycetes. *Holzforschung* 43, 11–18. doi: 10.1515/hfsg.1989.43.1.11

Otjen, L., Blanchette, R. A., Effland, M., and Leatham, G. (1987). Assessment of 30 white rot basidiomycetes for selective lignin degradation. *Holzforschung* 41, 343–349. doi: 10.1515/hfsg.1987.41.6.343

Riley, R., Salamov, A. A., Brown, D. W., Nagy, L. G., Floudas, D., Held, B. W., et al. (2014). Extensive sampling of basidiomycete genomes demonstrates inadequacy of the white-rot/brown-rot paradigm for wood decay fungi. *Proc. Natl. Acad. Sci. U.S.A.* 111, 9923–9928. doi: 10.1073/pnas.1400592111

Rowell, R. (ed.) (1984). *The Chemistry of Solid Wood*. Washington DC: American Chemical Society.

Saddler, J. N., and Mackie, K. (1990). Bioconversion of lignocellulosics. *Biomass* 22, 293–305. doi: 10.1016/0144-4565(90)90024-e

Savory, J. G., and Pinion, L. C. (1958). Chemical aspects of decay of beech wood by Chaetomium globosum. *Holzforschung* 12, 99–103. doi: 10.1515/hfsg.1958.12.4.99

Scheu, S., and Schaefer, M. (1998). Bottom-up control of the soil macrofauna community in a beechwood on limestone: manipulation of food resources. *Ecology* 79, 1573–1585. doi: 10.1890/0012-9658(1998)079[1573:bucots]2.0.co;2

Schilling, J. S., Kaffenberger, J. T., Liew, F. J., and Song, Z. (2015). Signature modifications reveal decomposer community history. *PLoS One* 10:e0120679. doi: 10.1371/journal.pone.0120679

Seifert, K. (1966). Chemical changes in the beech cell wall by soft-rot (*Chaetomium globosum* Kunze). *Hols Roh Werkstoff* 24, 185–189. doi: 10.1007/bf02610268

Shortle, W. C., Dudzik, K. R., and Smith, K. T. (2010). Development of wood decay in wound-initiated discolored wood of eastern red cedar. *Holzforschung* 64, 529–536.

Sluiter, A., Hames, B., Ruiz, R., Scarlata, C., Sluiter, J., Templeton, D., et al. (2008). *Determination of Structural Carbohydrates and Lignin in Biomass*. NREL/TP-510-42618 Technical Report. Golden, CO: National Renewable Energy Laboratory.

Sluiter, J., and Sluiter, A. (2010). *Summative Mass Closure – LAP Review and Integration: Feedstocks*. NREL/TP-510-48087 Technical Report. Golden, CO: National Renewable Energy Laboratory.

Sollins, P. (1982). Input and decay of coarse woody debris in coniferous stands in western Oregon and Washington. *Can. J. For. Res.* 12, 18–28. doi: 10.1139/x82-003

Song, Z., Kennedy, P. G., Liew, F. J., and Schilling, J. S. (2017). Fungal endophytes as priority colonizers during wood decomposition. *Func. Ecol.* 31, 407–418. doi: 10.1111/1365-2435.12735

Sonnenberg, E. D., Zheng, H., Joglekar, P., Higginbottom, S. K., Firbank, S. J., Bolam, D. N., et al. (2010). Specificity of polysaccharide use in intestinal *Bacteroides* species determines diet-induced microbiota alterations. *Cell* 141, 1241–1252. doi: 10.1016/j.cell.2010.05.005

Talbot, J. M., Martin, F., Kohler, A., Henrissat, B., and Peay, K. (2015). Functional guild classification predicts the enzymatic role of fungi in litter and soil biogeochemistry. *Soil Biol. Biochem.* 88, 441–456. doi: 10.1016/j.soilbio.2015.05.006

Wang, Z. J., Zhu, J. Y., Zalesny, R. S. Jr., and Chen, K. F. (2012). Ethanol production from poplar wood through enzymatic saccharification and fermentation by dilute acid and SPORL pretreatments. *Fuel* 95, 606–614. doi: 10.1016/j.fuel.2011.12.032

Worrall, J. J., Anagnost, S. E., and Zabel, R. A. (1997). Comparison of wood decay among diverse lignicolous fungi. *Mycologia* 89, 199–219. doi: 10.1080/00275514.1997.12026772

Zeikus, J. G. (1981). Lignin Metabolism and the Carbon Cycle. In *Advances in Microbial Ecology* ed. M. Alexander (New York, NY: Springer), 211–243. doi: 10.1007/978-1-4615-8306-6_5

Zhang, J., Figueroa, M., Castaño, J. D., Silverstein, K., and Schilling, J. S. (2019). Gene regulation shifts shed light on fungal adaptation in plant biomass decomposers. *mBio* 10:e2176-19. doi: 10.1128/mBio.02176-19

Conflict of Interest: The authors declare that the research was conducted in the absence of any commercial or financial relationships that could be construed as a potential conflict of interest.

frontiers in Microbiology

ORIGINAL RESEARCH
published: 18 June 2020
doi: 10.3389/fmicb.2020.01338

Degradative Capacity of Two Strains of *Rhodonia placenta*: From Phenotype to Genotype

Martina Kölle[1], Maria Augusta Crivelente Horta[2], Minou Nowrousian[3], Robin A. Ohm[4], J. Philipp Benz[2,5] and Annica Pilgård[1,6]*

[1] Chair of Wood Science, TUM School of Life Sciences Weihenstephan, Technical University of Munich, Munich, Germany, [2] Professorship for Wood Bioprocesses, TUM School of Life Sciences Weihenstephan, Technical University of Munich, Freising, Germany, [3] Department of Molecular and Cellular Botany, Ruhr University Bochum, Bochum, Germany, [4] Department of Biology, Microbiology, Utrecht University, Utrecht, Netherlands, [5] Institute of Advanced Study, Technical University of Munich, Garching, Germany, [6] Biobased Materials, Bioeconomy, RISE Research Institutes of Sweden, Borås, Sweden

Brown rot fungi, such as *Rhodonia placenta* (previously *Postia placenta*), occur naturally in northern coniferous forest ecosystems and are known to be the most destructive group of decay fungi, degrading wood faster and more effectively than other wood-degrading organisms. It has been shown that brown rot fungi not only rely on enzymatic degradation of lignocellulose, but also use low molecular weight oxidative agents in a non-enzymatic degradation step prior to the enzymatic degradation. *R. placenta* is used in standardized decay tests in both Europe and North America. However, two different strains are employed (FPRL280 and MAD-698, respectively) for which differences in colonization-rate, mass loss, as well as in gene expression have been observed, limiting the comparability of results. To elucidate the divergence between both strains, we investigated the phenotypes in more detail and compared their genomes. Significant phenotypic differences were found between the two strains, and no fusion was possible. MAD-698 degraded scots pine more aggressively, had a more constant growth rate and produced mycelia faster than FPRL280. After sequencing the genome of FPRL280 and comparing it with the published MAD-698 genome we found 660,566 SNPs, resulting in 98.4% genome identity. Specific analysis of the carbohydrate-active enzymes, encoded by the genome (CAZome) identified differences in many families related to plant biomass degradation, including SNPs, indels, gaps or insertions within structural domains. Four genes belonging to the AA3_2 family could not be found in or amplified from FPRL280 gDNA, suggesting the absence of these genes. Differences in other CAZy encoding genes that could potentially affect the lignocellulolytic activity of the strains were also predicted by comparison of genome assemblies (e.g., GH2, GH3, GH5, GH10, GH16, GH78, GT2, GT15, and CBM13). Overall, these mutations help to explain the phenotypic differences observed between both strains as they could interfere with the enzymatic activities, substrate binding ability or protein folding. The investigation of the molecular reasons that make these two strains distinct contributes to the understanding of the development of this important brown rot reference species and will help to put the data obtained from standardized decay tests across the globe into a better biological context.

Keywords: *Rhodonia placenta*, *Postia placenta*, brown rot, genome comparison, standardized decay tests, wood degradation, hydrolytic enzymes

OPEN ACCESS

Edited by:
Jiwei Zhang,
University of Minnesota, United States

Reviewed by:
Asaf Salamov,
Joint Genome Institute, United States
Byoungnam Min,
Joint Genome Institute, United States

****Correspondence:***
J. Philipp Benz
benz@hfm.tum.de

Specialty section:
This article was submitted to Fungi and Their Interactions, a section of the journal Frontiers in Microbiology

Received: *17 March 2020*
Accepted: *25 May 2020*
Published: *18 June 2020*

Citation:
Kölle M, Horta MAC, Nowrousian M, Ohm RA, Benz JP and Pilgård A (2020) Degradative Capacity of Two Strains of Rhodonia placenta: From Phenotype to Genotype. Front. Microbiol. 11:1338. doi: 10.3389/fmicb.2020.01338

INTRODUCTION

Brown rot fungi such as *Rhodonia placenta* (Fr.) *Niemelä, K.H. Larss. & Schigel* (previously *Postia placenta*) naturally occur in the northern forest ecosystems and are known to be the most destructive species, albeit representing only a small group within wood decay fungi (Zabel and Morrell, 1992; Goodell, 2003; Vanden Wymelenberg et al., 2010). It has been suggested that this is because brown rot fungi circumvent the lignin, leaving it behind in a highly modified state (Cowling, 1961; Kleman-Leyer et al., 1992; Suzuki et al., 2006; Schwarze, 2007; Arantes et al., 2011; Yelle et al., 2011; Schilling et al., 2015). Brown rot fungi do not only rely on enzymatic degradation of lignocellulose but use low molecular weight oxidative agents prior to the enzymatic degradation (Goodell et al., 1997; Arantes et al., 2012; Arantes and Goodell, 2014).

It is still not fully understood how the non-enzymatic oxidative degradation phase proceeds in detail. The currently most accepted theory is that brown rot fungi secrete oxalic acid, which diffuses into the lumen, where it sequesters Fe^{3+} as a chelator (Goodell et al., 1997; Eastwood et al., 2011; Arantes et al., 2012). Fe^{2+} is then formed through reduction by hydroquinones and other reducing agents, while additionally hydrogen peroxide (H_2O_2) is formed; likely through a reaction between hydroquinones and oxygen (Paszczynski et al., 1999; Jensen et al., 2001; Eastwood et al., 2011; Arantes et al., 2012; Melin et al., 2015). Hydroxyl radicals are then generated through the reaction of H_2O_2 and Fe^{2+} (Fenton reaction), causing cellulose and hemicellulose depolymerization and lignin modification (Fenton, 1894; Baldrian and Valášková, 2008; Arantes et al., 2012). Oligosaccharides, solubilized during this process, diffuse through the cell walls into the lumen, where they become accessible to cellulases and hemicellulases (Martinez et al., 2005; Goodell et al., 2017).

The number of genes encoding lignin-related enzymes is typically extremely reduced in the genomes of brown rot fungi. Most do not encode class II lignin-modifying peroxidases (AA2) (Riley et al., 2014) and laccase genes are either completely missing, as in *Gloeophyllum trabeum* (Floudas et al., 2012), or very limited in number in *R. placenta* (Martinez et al., 2009; Wei et al., 2010). Cellobiohydrolases, belonging to the GH families 6 and 7, attack cellulose and are often accompanied by a carbohydrate-binding module (mostly CBM1). In most brown rot fungi (including *Rhodonia placenta*) cellobiohydrolases are either absent or lacking a CBM1 domain (Lombard et al., 2013; Riley et al., 2014). Moreover cellobiose dehydrogenases (family AA3_1) are absent in the majority of brown rot fungi, and genes from cellulolytic families (GH5, GH12, GH44, GH45) are reduced. Still they are able to depolymerize and degrade polysaccharides from the wood cell wall (Martinez et al., 2009; Eastwood et al., 2011; Floudas et al., 2012; Riley et al., 2014). It is noteworthy that the number of enzymes active on hemicelluloses is not reduced to the same extent as cellulose-active enzymes (Martinez et al., 2009; Wei et al., 2010).

The dikaryotic strain MAD-698 of *Rhodonia placenta* was first sequenced by Martinez et al. (2009). Since then, there have been several studies on transcriptomics, proteomics and expression of single genes likely involved in wood decay (Vanden Wymelenberg et al., 2010; Ryu et al., 2011; Ringman et al., 2014; Alfredsen et al., 2016a; Zhang et al., 2016; Pilgård et al., 2017; Zhang and Schilling, 2017; Beck et al., 2018). The results of these studies imply that there is a time-wise and spatial separation between the non-enzymatic oxidative and the enzymatic degradation phase. Especially genes involved in the non-enzymatic oxidative degradation are significantly upregulated during early decay. Later decay stages are dominated by expression of GH family genes (Zhang et al., 2016). The transition from non-enzymatic oxidative to enzymatic degradation is triggered by the release of inducer molecules, particularly cellobiose (Zhang and Schilling, 2017). Investigations of the secretome seemed to confirm these trends (Presley et al., 2018). Findings by us and others (Ringman et al., 2014; Alfredsen et al., 2016a,b; Ringman et al., 2016; Pilgård et al., 2017; Kölle et al., 2019; Ringman et al., 2020), also imply that there might be additional mechanisms in the regulation of the non-enzymatic degradation beyond the cellobiose switch (Zhang and Schilling, 2017).

Since brown rot fungi can cause massive damage in a short period of time, wood products and wood protection systems need to be vigorously tested prior to permission for commercial use. This is performed according to national standardized tests (Cowling, 1961; Filley et al., 2002; Niemenmaa et al., 2007; Arantes et al., 2012; Arantes and Goodell, 2014). In standardized decay tests, *R. placenta* is used as a representative brown rot fungus. Two widely used strains of *R. placenta* are MAD-698 and FPRL280. MAD-698 is the recommended strain in the US American Wood-preservers' Association Standard (AWPA E10-16, 2016), while FPRL280 is the recommended strain in the European standard EN 113 (CEN EN 113, 1996).

Differences in mass loss, colonization-rate, as well as in gene expression between the *R. placenta* MAD-698 and the FPRL280 strains have been observed (Thaler et al., 2012), leading to the assumption that there might be significant differences in either the genome, gene regulation, or in post-transcriptional mechanisms involved in the degradation process. Importantly, these observations raise fundamental concerns about the comparability of results obtained with these two strains.

While the corresponding monokaryotic strain to MAD-698, MAD-SB12, was sequenced more recently (Gaskell et al., 2017), the genome of the monokaryotic *R. placenta* strain FPRL280 has not been analyzed so far. To investigate the degradative capacity of the "European" *R. placenta* strain FPRL280 in comparison with the "American" *R. placenta* strain MAD-698/MAD-SB12, we thus sequenced its genome and performed parallel standardized decay tests, aiming to identify differences between the two strains that might help to explain the observed variances in phenotype. Comparisons of the genomes of different *Rhodonia* strains has to our knowledge not been performed before. In this study, our goal was to deliver solid genomic data on differences between MAD-SB12 and FPRL280 that can be used for further functional analysis. While contributing to a better understanding of the species' lineage and hopefully providing a

reference for future studies using either one of the two strains, the knowledge gained may also be of great interest for new biomass conversion technologies (Mester et al., 2004; Goodell et al., 2008; Schilling et al., 2012).

MATERIALS AND METHODS

Strains

An isolate of *Rhodonia placenta* (Fr.) Niemelä, K.H. Larss. & Schigel (previously *Postia placenta*) FPRL280 was used in this study. MAD-698 is a dikaryotic strain (Martinez et al., 2009) and was used for phenotype tests and phenotype comparisons. MAD-SB12, a monokaryotic strain (Gaskell et al., 2017), was used for a fusion test, mapping of the FPRL280 sequence and for genotype comparisons. FPRL280 is a monokaryotic strain and was used for phenotype tests, sequencing as well as for genotype comparisons.

Phenotype Analysis

Growth Test and Appearance

To investigate growth speed and growth behavior, 4% malt agar plates were inoculated with either *R. placenta* FPRL280 or *R. placenta* MAD-698. Measurement of the growth progress started on day two and the hyphal front was measured daily until the mycelium reached the edges of the plate (8 days). The diameter was measured in two directions, and a mean was calculated. Growth appearance of *R. placenta* strain FPRL280 and MAD-698 was observed and evaluated subjectively, when growing either on 4% malt agar dishes or on wood samples.

Mass Loss Test

The mass loss test was done according to the method presented by Bravery (Bravery, 1979). Sterile nets were placed on 4% malt agar petri dishes and inoculated with either *R. placenta* FPRL280 or *R. placenta* MAD-698. When the plates were completely overgrown, miniblock wood samples (10 mm × 5 mm × 30 mm) of scots pine (*Pinus sylvestris* L.) were placed on top of the nets. Samples were harvested after 1, 2, 3, 4, 5, 6, and 7 weeks of incubation at 22°C and 70% relative humidity, dried and weighted.

Fusion Test

Possible fusion between *R. placenta* strain FPRL280 and strains MAD-698 and MAD-SB12 was tested on 4% malt agar petri dishes.

Genotype Analysis

Sequencing, Mapping, and *de novo* Assembly

Rhodonia placenta (Fr.) FPRL280 was cultivated on 4% malt agar plates for 14 days at room temperature (25°C). The DNA was extracted following the protocol by Traeger et al. (2013) (see Appendix). Library prep was done using the Illumina TruSeq PCR free kit (insert size 350 bp), according to the TruSeq DNA Sample Preparation Guide (Part #15036187, Rev.D, June 2015). The DNA libraries were paired-end (2 × 126) sequenced on an Illumina HiSeq2500 equipment. Paired-end reads were quality-trimmed to remove reads with undefined bases and trim reads from the 5′ and 3′ends until a base with phred-quality ≥ 10 was reached, with minimum length 60 bp.

The reads were mapped against the dikaryotic *R. placenta* MAD-698 genome, but the described comparison was done with the monokaryotic *R. placenta* MAD-SB12 genome[1] (Gaskell et al., 2017) using Bowtie 2 (Langmead and Salzberg, 2012) version 2.2.6 for comparison, and SAMtools version 1.4 (Li et al., 2009) and BCFtools version 1.4 for variant calling. The reads were also *de novo* assembled using SPAdes (Bankevich et al., 2012) version 3.10. Gene prediction on SPAdes assembly was done with Maker (Cantarel et al., 2008). The following options were set in the CTL file of maker: protein2genome = 1, always_complete = 1. Maker was run with the [-RM_off] option, otherwise default parameters were used.The assembly was annotated based on the combined predicted proteins from the previously published assembly (Martinez et al., 2009; Gaskell et al., 2017). The predicted proteins from the *de novo* annotation were used for prediction of the 11,486 orthologous genes using reciprocal blast analysis and MAD-SB12 (Gaskell et al., 2017) as reference genome.

Annotation of CAZy-Encoding Genes

The public CAZy list determined by Gaskell et al. (2017) with 317 CAZy genes was used to find the corresponding CAZy genes in the *de novo* assembly of FPRL280. The CAZy gene sequences in coding sequences (CDSs) from MAD-SB12 were used to find the corresponding gene sequences within the entire set of CDSs from FPRL280, and only the best hits were selected, based on *e*-value, score and identity (**Supplementary Data Sheet 1**). A total of 298 genes were identified this way and another 16 sequences were when searching against the full *de novo* genome assembly. For four CAZy genes from MAD-SB12 no significant *e*-values could be retrieved by both methods, indicating that these genes do not exist in the FPRL280 *de novo* genome assembly (POSPLADRAFT_1141676, POSPLADRAFT_1141705, POSPLADRAFT_1042744, and POSPLADRAFT_1121407).

Validation of Genome Assembly

Polymerase chain reaction (PCR)-based Sanger sequencing of seven CAZy-encoding genes was performed to validate the differences found in the *de novo* assembled FPRL280 genome compared to MAD-SB12. Primers were designed based on the FPRL280 *de novo* assembly, and the sequences from the PCR product of the gDNA amplification were compared with the published sequence of MAD-SB12 (**Supplementary Table 1** and **Supplementary Figure 2**). Sequences were compared using CLC Genomics Workbench 20.0 (QIAGEN, Aarhus, Denmark). For those genes which were not found in the FPRL280 *de novo* assembly, primers were designed based on MAD-SB12 sequence and used to probe for the corresponding genes in the gDNA of both strains.

The whole genome project has been deposited in the Sequence Read Archive (SRA) of NCBI under accession numbers PRJNA606481 and SAMN14091738 to the sample reads and to the assembly.

[1] https://mycocosm.jgi.doe.gov/PosplRSB12_1/PosplRSB12_1.home.html

Phylogenetic Analysis

The species phylogeny was reconstructed using highly conserved gene products of the previously published genome annotations of the species indicated in **Figure 5** (Martinez et al., 2009; Eastwood et al., 2011; Fernandez-Fueyo et al., 2012; Floudas et al., 2012; Olson et al., 2012; Suzuki et al., 2012; Tang et al., 2012; Binder et al., 2013; Ohm et al., 2014; Nagy et al., 2015; Miettinen et al., 2016; Wu et al., 2018; Casado López et al., 2019). BUSCO v2 (dataset "fungi_odb9") was used to select 179 highly conserved proteins for the species phylogeny (Simão et al., 2015). These sequences were concatenated and aligned with MAFFT 7.307 (Katoh and Standley, 2013) and well-aligned regions were identified with Gblocks 0.91b (Talavera and Castresana, 2007). This resulted in 86,531 amino acid positions. RAxML version 8.1.16 was used for the phylogenetic tree reconstruction using the PROTGAMMAWAG similarity matrix and 100 bootstraps (Stamatakis, 2014). The phylogenetic tree was visualized and rooted on the outgroups *S. lacrymans* and *H. annosum* using Dendroscope (Huson and Scornavacca, 2012).

RESULTS

Phenotypic Comparison Between FPRL280 and MAD-698

When incubated on malt extract agar plates, MAD-698 was found to grow faster during the first 5 days, whereas FPRL280 started its growth delayed, but accelerated and caught up with MAD-698 between days 5 and 6 (**Figure 1**).

Differences were also observed in the general appearance, when growing on petri dishes with 4% malt agar. MAD-698 grew more multidirectional than FPRL280, which also grew closer to the surface of the medium, directed to the edges of the plates (**Figures 2**, **4**). The mycelium of MAD-698 produced more aerial hyphae growing upwards, giving the mycelium a more voluminous appearance (**Figures 2**, **4**). When growing on wood samples, there were also differences between the two fungi. MAD-698 clearly produced more mycelium during the 8-week degradation test (**Figure 2**).

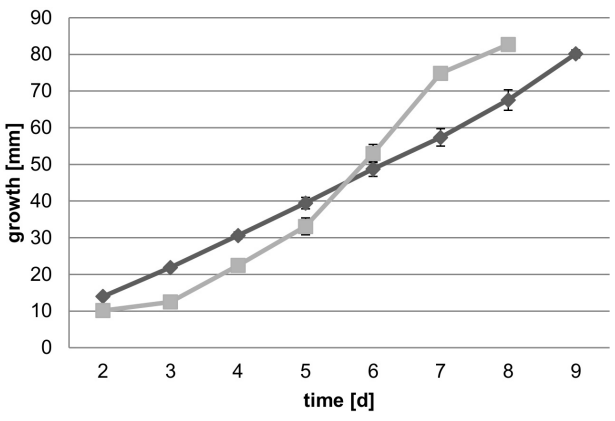

FIGURE 1 | Growth speed of both strains on 4% malt agar plates over 9 days (n = 5). Average daily growth rates of FPRL280 (gray squares) and MAD-698 (black diamonds) are shown with standard deviations in the graph and imply that MAD is starting growth earlier and grows more evenly than FPRL.

To determine differences in wood degradation capacity a mass loss test on wooden miniblock samples was performed over 7 weeks (**Figure 3**). Despite showing a delayed growth phenotype on malt agar, FPRL280 started degrading the wood earlier than MAD-698 but then slowed down. After 6 and 7 weeks, mass loss by MAD-698 was significantly stronger, suggesting that MAD-698 is degrading the wood in a more aggressive manner than FPRL280 in the long term.

Fusion Test

To test whether FPRL280 and MAD-698 are able to fuse, the strains were confronted with each other on the same plate. A border was immediately built up between the two *R. placenta* strains when the mycelia met, which both fungi did not overgrow (**Figure 4A**). The same was observed for FPRL280 and the corresponding monokaryotic strain of MAD, MAD-SB12 (**Supplementary Figure 3**). Further days of investigation showed that even on the edges of the plates, the fungi grew upwards, but not over the demarcation line. After several weeks, there was a broad band of mycelium looking like a wall built up between the two strains (**Figure 4B**).

Sequencing of FPRL280 and Comparison With MAD-SB12

Next, we sequenced the genome of *R. placenta* strain FPRL280. Since the genome assembly of strain MAD-698 is much more fragmented and gap-rich than the more recent MAD-SB12 assembly, mapping rates of the genome reads of FPRL280 were much lower, reducing the quality of downstream variant analysis (**Table 1**). We therefore decided to focus our genomic comparison on the monokaryotic strain MAD-SB12 and a *de novo* assembly. *In* the *de novo* genome assembly, 12,997 genes were predicted for FPRL280, which is about the same number as reported for MAD-SB12 (12,541), 11,486 of these being putative orthologs (**Supplementary Data Sheet 1** and **Table 2**).

A comparison with the MAD-SB12 genome showed an overall identity of 98.4% with 660,566 SNPs and 25,837 indels, translating roughly into one difference per 60 basepairs on average (**Table 3** and **Supplementary Data Sheet 2**). In addition, precise classification is presented in **Supplementary Data Sheet 2**, showing the affected genes, changes in amino acid sequences, the position and the kind of variance. An overview on how the SNPs are distributed over introns, exons, UTRs, or if they occur in intergenic regions can be found in **Supplementary Figure 4**. A total of 686,402 variants were detected within the whole genome (introns included), 16,299 variants (2.37%) residing in CAZy genes. A phylogenetic tree based on 179 highly conserved gene products shows that both *R. placenta* strains are closely related. The evolutionary distance between them is similar to the distance between strains of *Lentinus tigrinus* and *Dichomitus squalens* (**Figure 5**).

Next, we compared all detected variants between FPRL280 and MAD-SB12 vs. variants that are present in predicted CAZyme genes (**Table 4** and **Supplementary Data Sheet 3**). **Table 4**

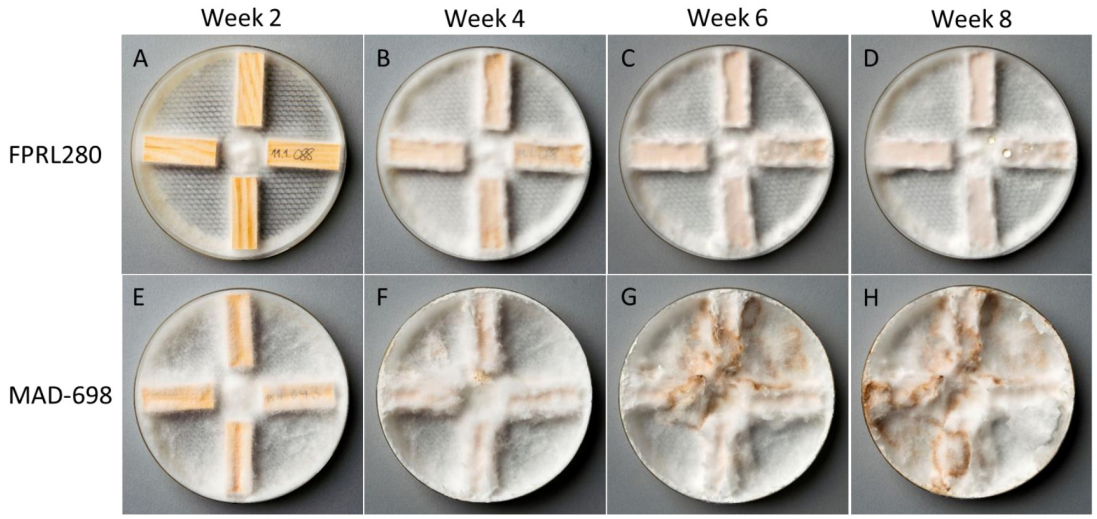

FIGURE 2 | Wood degradation test to observe appearance of both strains (FPRL280 and MAD-698) when growing on miniblock wood samples. **(A–D)** Show growth of FPRL280 after 2–8 weeks. **(E–H)** Show growth of MAD-698 after 2–8 weeks. Clear differences can be seen in these pictures, not only in appearance of the mycelium, but also in growth speed and mycelium production.

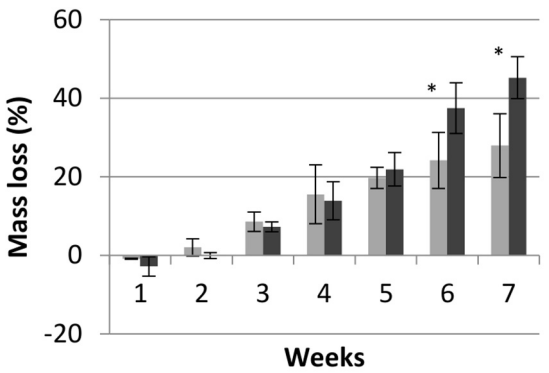

FIGURE 3 | Mass loss of pine wood samples over time when incubated with FPRL280 (gray) and MAD-698 (black). Data show means of biological ($n = 4$) and technical replicates ($n = 8$) with standard deviations, showing that MAD is causing a higher mass loss than FPRL after 6 weeks. *T*-test was used to determine the significance, with $p < 0.05$. "*" means significant differenced between the strains ($p < 0.05$).

presents results for the variant analysis between FPRL280 and MAD-SB12 as well as the number of coding sequences (CDS) and CAZy genes being affected. Within the CDS, we found a total of 10,027 genes with amino acid changes (AACs), of which 69% had between one and ten AACs and 1.2% having more than 50 AACs. Of all CAZy-encoding genes, almost all (92.43%) had at least one AAC, including 46 AAs, 136 GHs and 24 CBMs. Additionally, 17 genes with deletions, 30 with insertions and 20 frame shifts through indels were detected within the CAZy genes. Thirty-three CAZy genes were identified that had variants in consensus splice sites (VCSSs), the largest group here being the AA3_2 subfamily with eight genes and the GH5_5 subfamily with two genes. Overall, insertions appeared in 9.46% and deletions in 5.36% of all CAZy genes. Summarized results of the variant analysis, considering the sizes of the CAZy subfamilies, can be seen in **Figures 6A,B**. For an overview of variants in all CAZy families see **Supplementary Figure 1**.

Of all genes having AACs, 162 genes (1.67%) had $\geq$ 50 instances and 17 (0.18%) even $\geq$ 100 (**Figure 7**). Genes with 50 and more AACs were looked at in more detail, which showed that 23 of these were affected over more than 10% of their length, 107 genes were affected between 5 and 10% and 29 genes $\leq$ 5%. The GO terms regarding the annotated molecular functions of the genes were investigated and grouped. Proteins with associated functions that might contribute the observed phenotypic differences were present in this group. For example, 15 genes had RNA-, DNA or nucleic acid binding functions, based on UniProt search of the respective *R. placenta* MAD-SB12 homologs, or WD-repeat regions involved in a wide range of protein-protein interactions in signal transduction processes, cell division, RNA processing and so on (Yu et al., 2000; Smith, 2008; Stirnimann et al., 2010). The list furthermore was enriched for F-box-domain containing proteins (further referred to as F-box proteins; eight of a total of 164 predicted in the genome; p-value $< 5 \times 10^{-3}$), and showed an overrepresentation of proteins with kinase function (15 out of a predicted total of 398; p-value $< 5 \times 10^{-4}$). Further alignment of the protein sequences showed that the domains of two F-box proteins, four protein kinases as well as two WD-repeats regions are heavily affected (**Table 5**). Screening all variants showed four genes which had additional variants besides AACs: FPRL280_424_1 (POSPLADRAFT_1046092) had three VCSSs as well as a one-base insertion leading to a frameshift; FPRL280_272 (POSPLADRAFT_1065282) had an additional VCSS, FPRL280_188_6 (POSPLADRAFT_1035374) showed one five-base, one one-base and one two-base deletion, leading to frameshifts, three one-base and two four-base insertions, also leading to frameshifts as well as one VCSS. Further

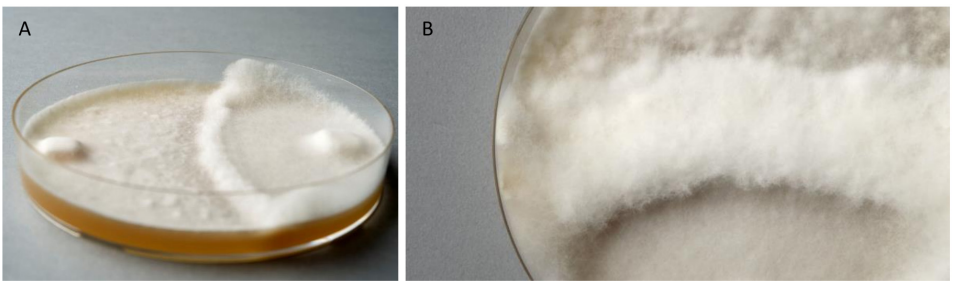

FIGURE 4 | Fusion test of the two *Rhodonia placenta* strains growing on one plate. **(A)** FPRL280 (left side) and MAD-698 (right side), 2 weeks after incubation, clearly showing the formation of a barrier, which is not overgrown. **(B)** The barrier got thicker and neither of the fungi overgrew it.

FPRL280_104_5 (POSPLADRAFT_1046501) had additionally two VCSSs and a three-base insertion, not leading to a frameshift.

Identification and Validation of Variants in CAZyme-Encoding Genes

Genomic regions of selected genes from GH31, AA3_2, GH16, CBM18, GH5, and CE15 family members were amplified and sequenced to verify the observed variances in the FPRL280 genome (**Supplementary Data Sheet 4**). All mentioned genes are consecutively numbered and shown in **Table 6** with corresponding IDs for MAD-SB12 and FPRL280, as well as the predicted effects of the variants. The regions tested by PCR amplification are indicated in **Figure 8**.

Within the GH31 domain of gene FPRL280_88_4, as well as in the cellulose domain of gene FPRL280_14_15 several SNPs and AACs could be confirmed (**Figures 8A,B**). Thirteen SNPs were verified to exist in gene FPRL280_46_15, a predicted oxidoreductase (AA3_2; PFAM00732/PFAM05199) with putative cellobiose dehydrogenase or alcohol oxidase activity (EC 1.1.99.18 or EC 1.1.3.13), in a small region of the domain (**Figure 7C**) and the RicinB_lectin domain (PFAM14200) of gene FPRL280_3_68 (**Figure 7D**). High number of variants were furthermore detected in gene FPRL280_327_3, with predicted 4-O-methyl-glucuronoyl methylesterase activity (EC 3.1.1) in a region close to the functional domain (**Figure 7E**), predict to allow the frameshift.

In addition to the selected genes shown in **Figure 7**, it was possible to confirm SNPs (including two AACs) within CBM13 domain-containing gene, and further AACs in CBM18, CBM21, CBM48, and CBM50 genes (**Table 5** and **Supplementary Data Sheet 3**). Other CBM13-encoding genes (FPRL280_235_10 and FPRL280_174_14) presented variances in consensus splice sites and insertions/deletions leading to putative frameshifts. Mutations leading to frameshifts were also detected in genes belonging to the CAZy families CBM21 and CBM50, as well as members of GH95, GH31, GH30_3, GH71, GH47, GH79, GH18, and GH16 (**Table 5** and **Supplementary Data Sheet 3**). Fourteen GH families were affected by mutations within predicted consensus splice sites: GH10; GH12; GH128; GH16; GH2; GH28; GH3; GH30_3; GH47; GH5_5; GH5_9; GH55; GH92; GH95 (**Table 5**).

Four genes (POSPLADRAFT_1141676, POSPLADRAFT_1141705, POSPLADRAFT_1042744, and POSPLADRAFT_1121407) present in the MAD-SB12 genome could not be detected in or amplified from the FPRL280 genome. All four genes belong to the CAZy subfamily AA3_2 (**Supplementary Figure 2**).

TABLE 1 | Comparison of genome assemblies for MAD-698 (Martinez et al., 2009), MAD-SB12 (Gaskell et al., 2017), and FPRL280.

	MAD-698 assembly	SB12 assembly	FPRL280
Assembly size (Mb)	90.9	42.5	36.3
No. of scaffolds	1243	549	1848
No. of gaps within scaffolds	10184	897	192
Total size of gaps (Mb)	21.9	2.6	0.007
% of scaffold length in gaps	24.1	6.1	0.02
Mapping rate of FPRL280 reads (%)	64	80	NA

TABLE 2 | Assembly and annotation features for *R. placenta* FPRL280.

Feature	Value
Genome assembly size (Mbp)	39
No. of contigs	3,158
No. of scaffolds	2,948
No. of scaffolds ≥ 1000 bp	1,848
Scaffold N50	74 kb
Gene models	12,997

TABLE 3 | Overview of the variant analysis between FPRL280 and MAD-SB12 genomes.

	All variants	Variants in CAZy genes
Total no. of variants	686, 403 (100%)	16, 299 (2.37%)
SNPs	660, 566 (96.24%)	15, 888 (2.40%)
Indels	25, 837 (3.76%)	411 (1.61%)

DISCUSSION

In the present study, we performed a direct comparison of both phenotype and genotype of two commonly used strains of *R. placenta*, FPRL280 and MAD-698 (or MAD-SB12,

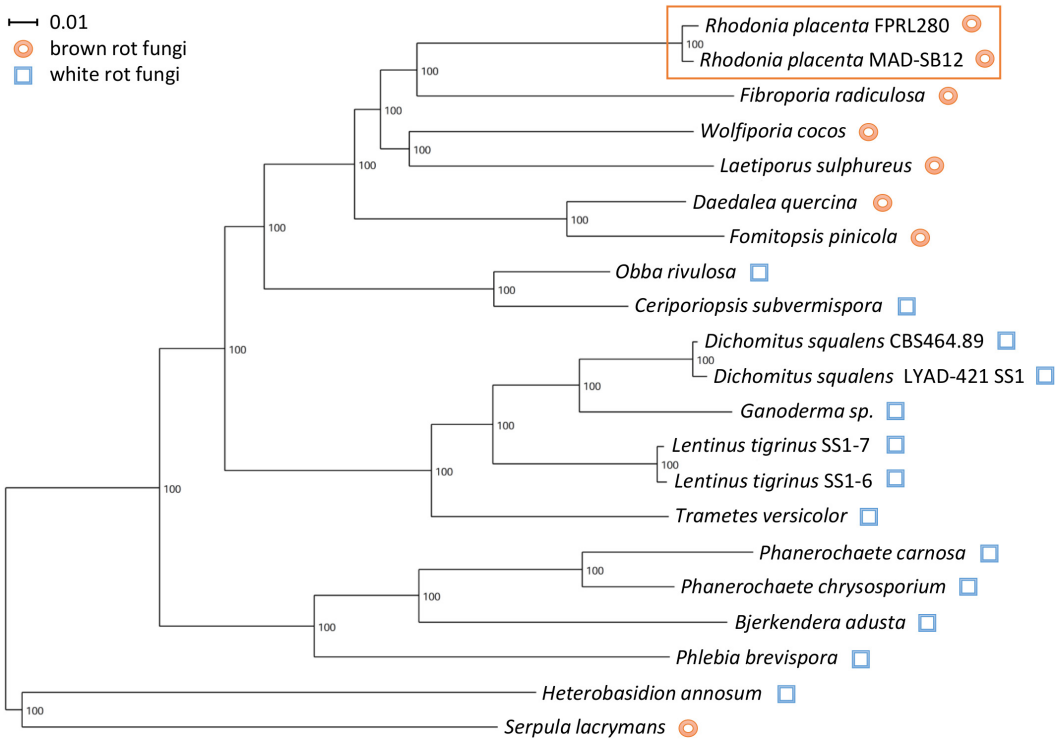

FIGURE 5 | Phylogenetic tree of members of the order Polyporales based on 179 highly conserved proteins. *S. lacrymans* (order Russulales) and *H. annosum* (order Boletales) were used as outgroup to root the tree. The strains of *R. placenta* cluster closely together, as expected for closely related strains (orange box).

TABLE 4 | Detailed variant analysis and number of affected genes with corresponding percentage according to total number of CDS genes (all variants) or total number of CAZy genes (variants in CAZy genes).

	All variants		Variants in CAZy genes	
	Total No. of variants	**No. of genes**	**Total No. of variants**	**No. of genes**
AACs (in CDS)	115,302	10, 027 (79.95%)	3,301	293 (92.43%)
Deletions (in CDS)	1,177	929 (7.41%)	20	17 (5.36%)
Insertions (in CDS)	2,123	1, 233 (9.83%)	48	30 (9.48%)
Frameshifts through indels	1,499	954 (7.61%)	25	20 (7.89%)
VCSSs (in CDS)	1,194	984 (7.85%)	38	33 (10.41%)

respectively). We chose to directly compare the phenotypes of MAD-698 (a dikaryon) and FPRL280 (which, suggested by the genome assembly and by absence of microscopically visible clamps, is a monokaryon), since these are the two strains being used in laboratories in the US and Europe for standardized decay test of wood products (AWPA E10-16, 2016). However, for the genome comparison with FPRL280, we chose to use the monokaryotic MAD-SB12 genome. The genome size determined for FPRL280 was much closer to that of MAD-SB12 and mapping efficiencies were substantially higher (**Table 1**). Since the genome of MAD-SB12 was isolated from a basidiospore of the fruiting dikaryon MAD-698, the genome is as close to the formely reported genome of MAD-698 as possible (Gaskell et al., 2017).

Differences in growth behavior, wood decomposition effectiveness and mycelial appearance were observed and quantified as well as vegetative incompatibility between the strains. Since it has been shown that monokaryons and dikaryons of *Trametes versicolor* have similar decay rate, combative ability and ligninolytic enzymes production (Hiscox et al., 2010), we assume that this does not account as a major influencing factor in *R. placenta* as well. While the observed vegetative incompatibility might have been caused by the different nuclear status nevertheless, this behavior was also seen for FPRL280 and MAD-SB12 (the respective monokaryon; **Supplementary Figure 3**), which indicates that the incompatibility depends on genetic differences rather than on differences in nuclear status.

One to two percent of the gene products in eukaryotic organisms belong to the GT family (Lairson et al., 2008), which are necessary, among others, for the biosynthesis of the fungal cell wall (Klutts et al., 2006). GTs are enzymes that utilize an activated sugar substrate, containing a phosphate leaving group (Lairson et al., 2008) and catalyze the transfer of sugar moieties from

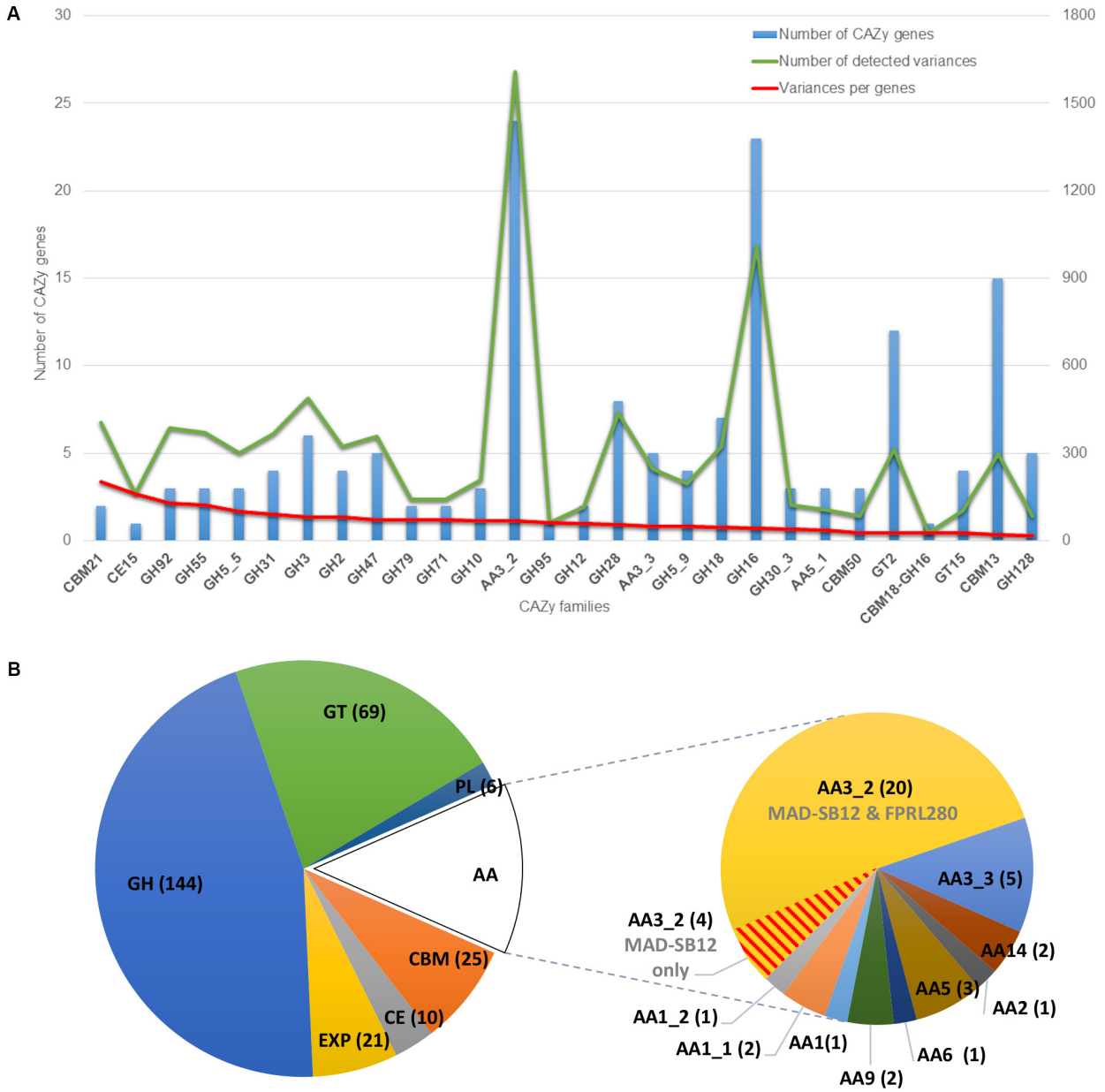

FIGURE 6 | CAZy classification. **(A)** Variant analysis of CAZy genes of FPRL280 compared to MAD-SB12 (only CDS). The graphic only shows CAZy families mentioned in the text, a graphic with results for all CAZy families can be found as **Supplementary Figure 1**. The blue bar shows the number of CAZy genes with variants within the CAZy subfamilies. The green line shows the number of all variants occurring in the CAZy subfamilies. The red line shows the variances within the CAZy subfamilies normalized to their size. **(B)** Entire classification of CAZy-encoding genes in both genomes, highlighting class AA, with the subfamily AA3_2, in which many variants were found and four genes were missing in FPRL280 vs. MAD-SB12 (red line pattern). The piecharts contain CAZy families AA, CBM, CE, GH, GT, and PL, as well as expansins (EXP).

donor molecules to specific acceptors, leading to the formation of glycosidic bonds (Campbell et al., 1997; Coutinho et al., 2003). Five putative GT genes were found having AACs in FPRL280. Potentially therefore, these mutations could be part of the reason why the MAD-698 mycelia have a different appearance than FPRL280. However, since the GTs include 110 families and we don't know which effects the VCSS have on the enzymes (Lairson et al., 2008), this remains speculative until further analysis.

The differences in phenotype make the comparison interesting both in terms of genomic research and industrial applications. Mutations in important genes are one explanation for the differences seen in phenotype between the two species, but also regulatory mechanisms are likely having a powerful impact. The two genomes are closely related with a total identity of 98.4% and as confirmed by a phylogenetic analysis (**Figure 5**). The results of the variant analysis nevertheless showed a high number of

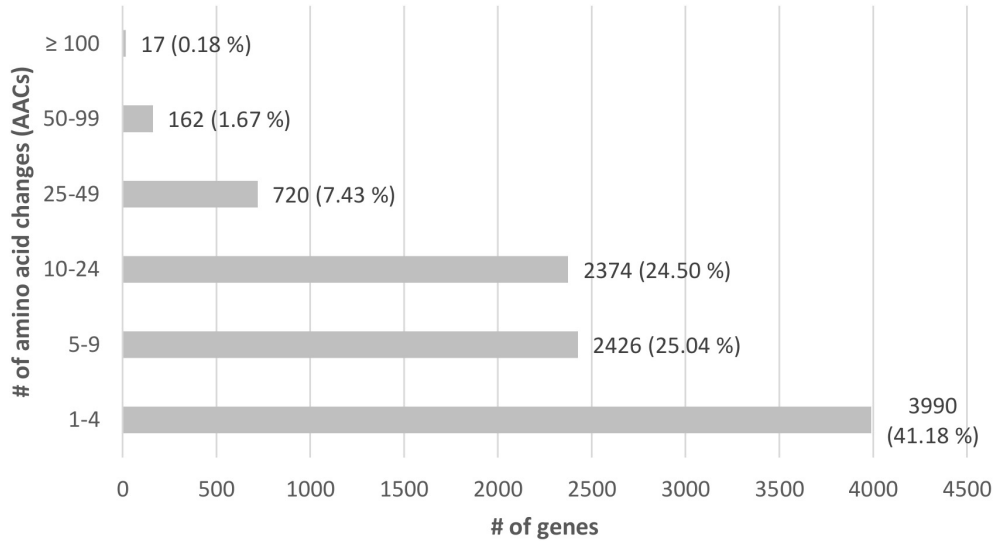

FIGURE 7 | All genes with amino acid changes (AACs) after comparing MAD-SB12 and FPRL280, according to amount of AACs (*y*-axis) and number of genes with corresponding percentage (*x*-axis).

TABLE 5 | Genes with ≥ 50 AACs, which were looked at in more detail due to their predicted effect on the phenotype.

Protein	Affected genes	Avg. degree of affection (% of the gene length)	No. of AACs (Avg.)
F-Box protein	8	10.24	69.25
Kinases	15	6.13	62.4
WD repeats	3	7.75	107.7
DNA binding	7	4.87	56.43
Nucleic acid binding	4	5.92	71
RNA binding	4	5.01	66

The table includes the percentage of bases affected, relative to the total protein length and the number of AACs, as well as the protein.

potentially impactful differences between the two strains. For example, amino acid changes (AAC) were found in 92% of all predicted CAZy genes, as well as deletions in 5% and insertions in 9%. Moreover, variants in consensus splicing sites (VCSS) were found in 10% of all CAZys. Overall, a higher percentage of AACs and VCSSs were found in CAZy genes compared to the entire complement of CDSs (**Table 2**), often affecting structural domains. We also found that four genes belonging to the CAZy family AA3_2 could not be detected in the FPRL280 genome, potentially explaining part of the observed differences regarding wood decay rates (see also below).

Brown rot fungi possess less GHs than white-rot fungi, but they seem to compensate this by secreting higher amounts of their remaining GHs (Presley et al., 2018). Brown rot fungi generally lack processive cellobiohydrolases and instead rely more on endoglucanases, which are thought to cleave cellulose randomly (Eriksson et al., 1990; Vanden Wymelenberg et al., 2010). Putative endo-acting cellulases belong to the CAZy families GH5 and GH12 (Ryu et al., 2011; Floudas et al., 2012; Lombard et al., 2013). Zhang et al. (2016) found only three endoglucanases (GH5 and GH12) and one putative endoglucanase (GH12) in *R. placenta*. We found mutations in the well-characterized endo-1,4-β-D-glucanase PpCel5A (FPRL280_14_15; Ppl1| 115648; POSPLADRAFT_1164613; XP_024344095) belonging to the GH5 family and including the endo-1,4-β-glucanase FPRL280_142_19 (Ppl1| 52805/Ppl1| 112669; POSPLADRAFT_1050186; XP_024333913) belonging to the GH12 family in FPRL280. Mutations were also found in several putative hemicellulases, such as the β-mannosidase FPRL280_NODE_261 (Ppl1| 57564; POSPLADRAFT_1043339; XP_024342514), the α-1,2-mannosidase FPRL280_294_2 (Ppl1| 62385; POSPLADRAFT_1043572; XP_024342867) and the β-xylosidase FPRL280_9_74 (Ppl1| 127469; POSPLADRAFT_1069652; XP_024341044). In addition, we found that several putative β-glucosidase-encoding genes in FPRL280 have mutations (**Supplementary Data Sheet 3**).

Hemicellulases can be found in several GH families and are often co-operating to break down complex hemicelluloses (Ryu et al., 2011; Brigham et al., 2018). Moreover, β-glucosidases are relatively non-specific in brown rot fungi (Herr et al., 1978; Valášková and Baldrian, 2006). It could be hypothesized that the detected mutations in hemicellulases and β-glucosidases will not affect the decay capability of FPRL280 as much as mutations in the endoglucanases since several β-glucosidases have been found in *R. placenta* (Martinez et al., 2009) and only three to four endoglucanases (Zhang et al., 2016). The sequence variances seen in GH family enzymes, in particularly the endoglucanases, could thus be one part of a possible explanation to the overall lower decomposition rate by FPRL280 compared to MAD-698, since these enzymes are responsible for the depolymerization of the structural carbohydrates in the wood cell wall (Ryu et al., 2011; Floudas et al., 2012; Lombard et al., 2013).

TABLE 6 | All genes mentioned in the results are numbered with both IDs (MAD-SB12 and FPRL280), the CAZy family these genes belong to and the predicted effects of variances, causing AACs, VCSSs or frameshifts.

ID MAD-SB12 "POSPLADRAFT_"	ID FPRL280 "FPRL280_"	CAZy family	Predicted effect
1050820	88_4	GH31	AAC (positions 480 and 553) in coding protein XP_024333100.1, mutations, leading to frameshifts
1164613	14_15	GH5_5	AAC (positions 72 and 126) in protein XP_024344095.1, VCSS
1048102	46_15	AA3_2	4 AACs (positions 272, 308, 312, and 332) in protein XM_024479440.1
1044277	3_68	CBM13	AAC (positions 30 and 90) in protein XP_024341629.1
1065808	327_3	CE15	Mutations, leading to frameshifts
1046599	156_2	GH95	Mutations, leading to frameshifts, VCSS
1057601	47_16	GH30_3	Mutations, leading to frameshifts, VCSS
1066962	238_7	GH71	Mutations, leading to frameshifts, deletion (4 bases) in EC 3.2.1.59
1138061	218_2	GH47	Mutations, leading to frameshifts, insertion (8 bases) and deletion (4 bases) in enzyme-encoding region (EC 3.2.1.113); VCSS
1155254	318_2	GH79	Mutations, leading to frameshifts
1168110	279_6	GH18	Mutations, leading to frameshifts
1181115	252_4	GH16	Mutations, leading to frameshifts
1064814	264_7	GH10	VCSS
1050186	142_19	GH12	VCSS
1183855	4_136	GH128	VCSS
1142572	640_1	GH16	VCSS
1043339	NODE_261	GH2	VCSS
1049546	348_3	GH28	VCSS
1174812	49_4	GH3	VCSS
1042537	14_27	GH5_5	VCSS
1181612	432_1	GH5_9	VCSS
1131418	269_3	GH55	VCSS
1043572	294_2	GH92	VCSS

During early stages of brown rot decay, CEs are required for hemicellulose removal, for example to remove acetyl groups from xylan in hardwoods (Cowling, 1961; Puls, 1997). Presley et al. (2018) found an increased spectrum of genes attributed to CEs in brown rot secretomes, particularly in early stages of decay. In one protein putatively belonging to the CE15 family (POSPLADRAFT_1065808/FPRL280_327_2; XP_024339306) we found a high number of AACs in the FPRL280 ortholog compared to MAD-SB12 and VCSSs. These mutations might affect the hemicellulose depolymerization in FPRL280 negatively.

As mentioned above, brown rot fungi rely on non-enzymatic break-down of lignocellulose using low molecular weight compounds, such as H_2O_2, Fe^{2+} and oxalate for Fenton chemistry (Goodell et al., 1997; Arantes et al., 2009; Arantes and Goodell, 2014), for an efficient lignocellulose degradation. The genomes of brown rot fungi suggest the presence of a number of AA enzymes that are known to generate H_2O_2. Among these are AA3 GMC oxidoreductases and AA5 copper radical oxidases (Floudas et al., 2012; Levasseur et al., 2013). AA3 are a family of flavoenzymes that oxidize aliphatic alcohols, aryl alcohols and mono- and disaccharides. This oxidation is coupled with the reduction of a variety of electron acceptors, including O_2 (resulting in the formation of H_2O_2), quinones and other enzymes. Enzymes belonging to the AA3_2 subfamily include two closely related FAD-dependent enzymes, aryl-alcohol oxidase and glucose-1-oxidase (Levasseur et al., 2013; Sützl et al., 2018). Flavoproteins, such as GMC oxidoreductases, form the base of a wide array of biological processes, for example removal of radicals, which contribute to oxidative stress adaptation. The CAZy group with the highest number of variances in FPRL280 was the AA3_2 subfamily. We found eight putative genes with VCSS in the FPRL280 genome. In addition to this, four AA3_2-encoding genes were missing in the FPRL280 genome. Taking into account the suggested importance of hydroquinones for the H_2O_2 production, mutations in AA3_2 proteins, or the absence of entire proteins, could thus have severe effects on the degradation capacity of FPRL280. Enzymes belonging to the AA5 family are copper radical oxidases and are known to be a major constituent of the secretome of several brown rot fungi (Kersten and Cullen, 2014). AA5s oxidize a variety of substrates resulting in the production of H_2O_2 via the reduction of O_2 (Jensen et al., 2002). The AA5 family includes two subfamilies, AA5_1 containing characterized glyoxal oxidase and AA5_2 containing galactose oxidase, raffinose oxidase and alcohol oxidase enzymes (Ito et al., 1991). In a copper radical oxidase (Ppl1| 56703

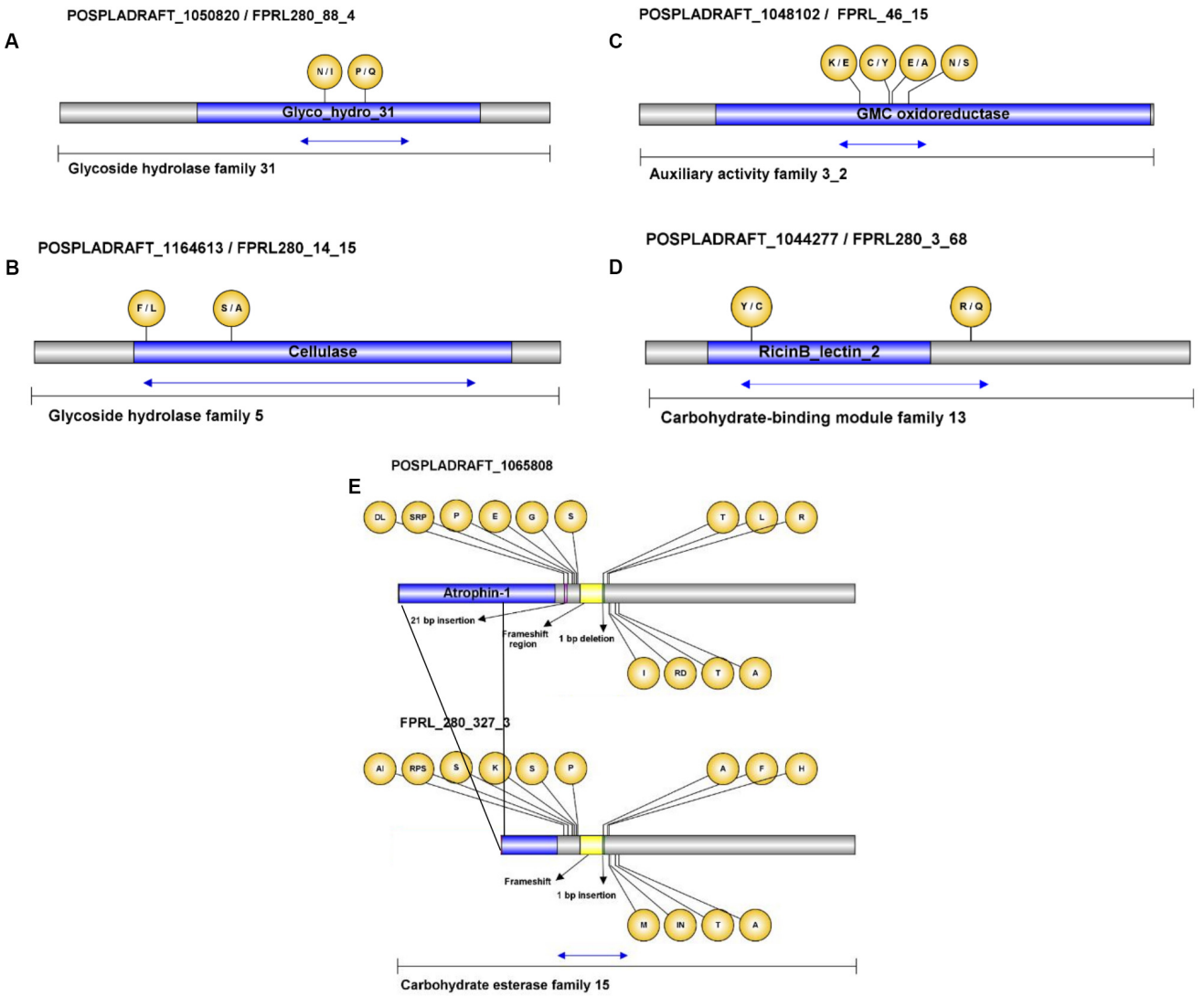

FIGURE 8 | Visualization of variances and amino acid changes in selected CAZy genes. The differences were confirmed by gDNA amplification of FPRL280 followed by comparison with the published MAD-SB12 gene sequence and the FPRL280 *de novo* genome assembly. The amino acid changes are shown in the bubbles, MAD-SB12/FPRL280 **(A–D)**, and as indicated **(E)**. The blue arrows indicate the partial sequences verified by Sanger sequencing. The black lines in **(E)** represent the region that is missing in the FPRL280 homolog.

POSPLADRAFT_1046361/FPRL280_259_1; XP_024339806) belonging to the subfamily AA5_2, we found VCSS. The fact that four AA3_2 genes are missing in FPRL280 and that parts of the domains are missing in enzymes in both AA3_2 and AA5_2, in addition to high numbers of gaps and point mutations, also in VCSS, might lead to changes with possible effects on the protein functions. Since members of the AA3 family do not directly act on polymeric constituents of lignocellulosic material, but support degradation by reducing low-molecular weight components, with one of the main products being H_2O_2 (Sützl et al., 2018), changes in AA3_2 genes could affect this support substantially. The effect of this might be a less effective Fenton reaction in FPRL280 compared to MAD-698, which could explain the phenotypical findings that MAD-698 is more potent during prolonged decay, producing higher mass losses than FPRL280. Brown rot fungi have most likely a fine-tuned complex network of gene products working together to deliver radicals via the Fenton reaction. Perhaps even small changes in these gene products could lead to measurable effects. Whether this is indeed the case, however, needs to be verified by future experiments.

A proportionally large part of the variances found in FPRL280 are located in regulatory genes which could have a huge impact on the phenotype far beyond the mere differences of the two genomes.

Nucleic acid binding proteins, for example, are important factors involved in gene expression (Latchman, 1997). Zinc-finger proteins belonging to this group can act as transcription factors and form one of the largest families if transcriptional

regulators in eukaryotes, with an enormous functional diversity (Miller et al., 1985; MacPherson et al., 2006). One representative (POSPLADRAFT_1155119/FPRL280_66_2) was found to be affected by more than 50 AACs in this study. Mutations in genes coding for these proteins are therefore likely to contribute to the overall complexity of the phenotypes of both strains, since their functional differences will affect entire downstream regulons.

Kinases, mediating phosphorylation reactions of proteins and other cellular constituents, are another example of important regulatory proteins involved in many signaling cascades. Within the pool of proteins found to have > 50 AACs between FPRL280 and MAD-SB12, kinases were found to be overrepresented (p-value $< 5 \times 10^{-4}$) indicating that the function of several signaling pathways might be affected. However, the diversity of kinases is immense, and future efforts are necessary to identify exactly which pathways these are.

F-box motifs, also found to be overrepresented (p-value $< 5 \times 10^{-3}$), function as a site of protein-protein interaction and the respective proteins are key factors involved in protein ubiquination proteasomal degradation (Jonkers and Rep, 2009). As part of the Skp, Cullin, F-box containing complex (SCF complex; a multi-protein E3 ubiquitin ligase), F-box proteins have several target proteins, which suggests that mutations may also have a pleiotropic effect on the phenotype. In filamentous fungi, F-box proteins can be involved in several cellular processes, including control of the cell division cycle, sugar sensing, mitochondrial connectivity, and control of the circadian clock (Jonkers and Rep, 2009). The proteolytic function of the ubiquitin-proteasome system is furthermore important for virulence regulation in pathogenic fungi (Liu and Xue, 2011) and the variations in F-box domains in some proteins in FPRL280 might thus contribute to the lower virulence seen in FPRL280 compared to MAD-698.

Besides AACs, frame shift mutations and VCSSs can potentially have even more drastic effects on the amino acid sequences of proteins. However, for most CAZy genes we looked at in more detail, there variances did not affect the conserved functional domains. Moreover, splicing can be better observed by a transcriptional analysis. This is currently ongoing, including a gene expression regulation analysis, and will be part of another manuscript.

We limited the scope of this paper to a comparative genome study, since we wanted to highlight the phenotypic differences between the two *R. placenta* strains and the underlying genomes. A careful genomics analysis is very important, as it forms the basis for further research. However, genome analysis can clearly explain the differences between the strains only partially, and functional genomics studies, including transcription, translation, gene regulation and protein-protein-interactions, need to be included in the future for a more profound comparison.

CONCLUSION

The initial reason for comparing the two strains was to gain insight into the genetic differences between two economically relevant strains of *R. placenta* (FPRL280 and MAD-698) showing different phenotypes. The specific mutations discussed in this paper might contribute to these observed differences as they are found in relevant domains of many potentially important genes especially regulatory genes, and thus might affect the function of the respective proteins. However, with 98.4% overall identity, the genomic variances cannot explain all observations. Differences in regulatory mechanisms (signaling cascades etc.) are likely also present and impactful, and therefore need to be further investigated.

The results from this paper show the importance of a united strain selection of decay fungi in standardized decay tests. Two strains of one species can behave differently even though the genomes appear similar. The investigation of the reasons that make these two strains distinct is useful for the understanding of the degradation mechanisms employed by brown rot fungi and the development of this important brown rot reference species.

DATA AVAILABILITY STATEMENT

The datasets generated for this study can be found in the NCBI databank under BioProject number PRJNA606481, and BioSample SAMN14091738.

AUTHOR CONTRIBUTIONS

AP, MK, JB, and MH initiated and designed the research. MK, MN, RO, and MH performed the analyses. AP, MK, JB, and MH co-wrote the manuscript with support of MN and RO. All authors were included in the interpretation of the data, read and approved the final manuscript.

FUNDING

This work was supported by the Swedish Research Council Formas 942-2015-530 to AP; DFG project NO407/7-1 to MN.

ACKNOWLEDGMENTS

MK and AP gratefully acknowledge financial support from The Swedish Research Council and MN from the DFG. We gratefully acknowledge excellent technical assistance by Petra Arnold (TUM). Thanks also to Dan Cullen for providing us a sample of the *Rhodonia placenta* MAD-SB12 strain for laboratory tests.

SUPPLEMENTARY MATERIAL

The Supplementary Material for this article can be found online at: https://www.frontiersin.org/articles/10.3389/fmicb.2020.01338/full#supplementary-material

REFERENCES

Alfredsen, G., Fossdal, C. G., Nahy, N. E., Jellison, J., and Goodell, B. (2016a). Furfurylated wood: impact on *Postia placenta* gene expression and oxalate crystal formation. *Holzforschung* 70:947. doi: 10.1515/hf-2015-0203

Alfredsen, G., Pilgård, A., and Fossdal, C. G. (2016b). Characterisation of *Postia placenta* colonisation during 36 weeks in acetylated southern yellow pine sapwood at three acetylation levels including genomic DNA and gene expression quantification of the fungus. *Holzforschung* 70, 1055–1065. doi: 10.1515/hf-2016-0009

Arantes, V., and Goodell, B. (2014). "Current understanding of brown-rot fungal biodegradation mechanisms: a review," in *Deterioration and Protection of Sustainable Biomaterials*, eds T. P. Schultz, B. Goodell, and D. D. Nicholas (Washington, DC: American Chemical Society), 3–21. doi: 10.1021/bk-2014-1158.ch001

Arantes, V., Jellison, J., and Goodell, B. (2012). Peculiarities of brown-rot fungi and biochemical Fenton reaction with regard to their potential as a model for bioprocessing biomass. *Appl. Microbiol. Biotechnol.* 94, 323–338. doi: 10.1007/s00253-012-3954-y

Arantes, V., Milagres, A. M. F., Filley, T. R., and Goodell, B. (2011). Lignocellulosic polysaccharides and lignin degradation by wood decay fungi: the relevance of nonenzymatic Fenton-based reactions. *J. Ind. Microbiol. Biotechnol.* 38, 541–555. doi: 10.1007/s10295-010-0798-2

Arantes, V., Qian, Y., Milagres, A. M. F., Jellison, J., and Goodell, B. (2009). Effect of pH and oxalic acid on the reduction of Fe3+ by a biomimetic chelator and on Fe3+ desorption/adsorption onto wood: implications for brown-rot decay. *Int. Biodeterior. Biodegradation* 63, 478–483. doi: 10.1016/j.ibiod.2009.01.004

AWPA E10-16 (2016). *Laboratory Method for Evaluating the Decay Resistance of Wood-Based Materials Against Pure Basidiomycete Cultures: Soil/Block Test*. Birmingham, AL: AWPA.

Baldrian, P., and Valášková, V. (2008). Degradation of cellulose by basidiomycetous fungi. *FEMS Microbiol. Rev.* 32, 501–521. doi: 10.1111/j.1574-6976.2008.00106.x

Bankevich, A., Nurk, S., Antipov, D., Gurevich, A. A., Dvorkin, M., Kulikov, A. S., et al. (2012). SPAdes: a new genome assembly algorithm and its applications to single-cell sequencing. *J. Comput. Biol.* 19, 455–477. doi: 10.1089/cmb.2012.0021

Beck, G., Hegnar, O. A., Fossdal, C. G., and Alfredsen, G. (2018). Acetylation of Pinus radiata delays hydrolytic depolymerisation by the brown-rot fungus *Rhondonia placenta*. *Int. Biodeterior. Biodegradation* 135, 39–52. doi: 10.1016/j.ibiod.2018.09.003

Binder, M., Justo, A., Riley, R., Salamov, A., Lopez-Giraldez, F., Sjökvist, E., et al. (2013). Phylogenetic and phylogenomic overview of the Polyporales. *Mycologia* 105, 1350–1373. doi: 10.3852/13-003

Bravery, A. F. (1979). "A miniaturised wood-block test for the rapid evaluation of preservative fungicides. In: Screening Techniques for Potential Wood Preservative Chemicals," in *Proceedings of a Special Seminar Held in Association with the 10th Annual Meeting of IRG, Peebles 1978*, South Hill, VA: Peebles.

Brigham, J. S., Adney, W. S., and Himmel, M. E. (2018). "Hemicellulases: diversity and applications," in *Handbook on Bioethanol - Production and Utilization*, ed. C. Wyman (Washington, DC: Taylor & Francis).

Campbell, J. A., Davies, G. J., Bulone, V., and Henrissat, B. (1997). A classification of nucleotide-diphospho-sugar glycosyltransferases based on amino acid sequence similarities. *Biochem. J.* 326(Pt 3), 929–939. doi: 10.1042/bj3260929u

Cantarel, B. L., Korf, I., Robb, S. M. C., Parra, G., Ross, E., Moore, B., et al. (2008). MAKER: an easy-to-use annotation pipeline designed for emerging model organism genomes. *Genome Res.* 18, 188–196. doi: 10.1101/gr.6743907

Casado López, S., Peng, M., Daly, P., Andreopoulos, B., Pangilinan, J., Lipzen, A., et al. (2019). Draft genome sequences of three Monokaryotic isolates of the white-rot basidiomycete fungus *Dichomitus squalens*. *Microbiol. Resour. Announc.* 8:e00264-19.

CEN EN 113 (1996). *Wood Preservatives. Test method for determining the protective effectiveness against wood destroying Basidiomycetes. Determination of the Toxic Values*. Brussels: European Committee for Standardisation.

Coutinho, P. M., Deleury, E., Davies, G. J., and Henrissat, B. (2003). An evolving hierarchical family classification for glycosyltransferases. *J. Mol. Biol.* 328, 307–317. doi: 10.1016/s0022-2836(03)00307-3

Cowling, E. B. (1961). *Comparative Biochemistry of the Decay of Sweetgum Sapwood by White-Rot and Brown-Rot Fungi*. Washington, DC: United States Department of Agriculture.

Eastwood, D. C., Floudas, D., Binder, M., Majcherczyk, A., Schneider, P., Aerts, A., et al. (2011). The plant cell wall–decomposing machinery underlies the functional diversity of forest fungi. *Science* 333, 762–765.

Eriksson, K., Blanchette, R. A., and Ander, P. (1990). *Microbial and Enzymatic Degradation of Wood and Wood Components*. Berlin: Springer.

Fenton, H. (1894). Oxidation of tartaric acid in the presence of iron. *J. Chem. Soc. Trans.* 65, 899–910. doi: 10.1039/ct8946500899

Fernandez-Fueyo, E., Ruiz-Dueñas, F. J., Ferreira, P., Floudas, D., Hibbett, D. S., Canessa, P., et al. (2012). Comparative genomics of *Ceriporiopsis subvermispora* and *Phanerochaete chrysosporium* provide insight into selective ligninolysis. *Proc. Natl. Acad. Sci. U.S.A.* 109, 5458–5463.

Filley, T. R., Cody, G. D., Goodell, B., Jellison, J., Noser, C., and Ostrofsky, A. (2002). Lignin demethylation and polysaccharide decomposition in spruce sapwood degraded by brown rot fungi. *Organ. Geochem.* 33, 111–124. doi: 10.1016/s0146-6380(01)00144-9

Floudas, D., Binder, M., Riley, R., Barry, K., Blanchette, R. A., Henrissat, B., et al. (2012). The paleozoic origin of enzymatic lignin decomposition reconstructed from 31 fungal genomes. *Science* 336, 1715–1719.

Gaskell, J., Kersten, P., Larrondo, L. F., Canessa, P., Martinez, D., Hibbett, D. S., et al. (2017). Draft genome sequence of a monokaryotic model brown-rot fungus *Postia (Rhodonia) placenta* SB12. *Genomics Data* 14, 21–23. doi: 10.1016/j.gdata.2017.08.003

Goodell, B. (2003). "Brown-rot fungal degradation of wood: our evolving view," in *Wood Deterioration and Preservation: Advances in Our Changing World*, eds B. Goodell, D. D. Nicholas, and T. P. Schultz (Washington, DC: ACS Publications).

Goodell, B., Jellison, J., Liu, J., Daniel, G., Paszczynski, A., Fekete, F., et al. (1997). Low molecular weight chelators and phenolic compounds isolated from wood decay fungi and their role in the fungal biodegradation of wood. *J. Biotechnol.* 53, 133–162. doi: 10.1016/s0168-1656(97)01681-7

Goodell, B., Qian, Y., and Jellison, J. (2008). "Fungal decay of wood: soft rot - brown rot - white rot. Development of commercial wood preservatives," in *ACS Symposium Series*, ed. T. E. A. Schultz (Washington, DC: American Chemical Society).

Goodell, B., Zhu, Y., Kim, S., Kafle, K., Eastwood, D. C., Daniel, G., et al. (2017). Modification of the nanostructure of lignocellulose cell walls via a non-enzymatic lignocellulose deconstruction system in brown rot wood-decay fungi. *Biotechnol. Biofuels* 10:179.

Herr, D., Baumer, F., and Dellweg, H. (1978). Purification and properties of an extracellular veta-glucosidase from *Lenzites trabea*. *Eur. J. Appl. Microbiol. Biotechnol.* 5, 29–36. doi: 10.1007/bf00515684

Hiscox, J., Hibbert, C., Rogers, H., and Boddy, L. (2010). Monokaryons and dikaryons of *Trametes versicolor* have similar combative, enzyme and decay ability. *Fungal Ecol.* 3, 347–356. doi: 10.1016/j.funeco.2010.02.003

Huson, D. H., and Scornavacca, C. (2012). Dendroscope 3: an interactive tool for rooted phylogenetic trees and networks. *Syst. Biol.* 61, 1061–1067. doi: 10.1093/sysbio/sys062

Ito, N., Phillips, S. E. V., Stevens, C., Ogel, Z. B., Mcpherson, M. J., Keen, J. N., et al. (1991). Novel thioether bond revealed by a 1.7 Å crystal structure of galactose oxidase. *Nature* 350, 87–90. doi: 10.1038/350087a0

Jensen, K., Ryan, Z., Marty, A., Cullen, D., and Hammel, K. E. (2002). An NADH:quinone oxidoreductase active during biodegradation by the brown-rot basidiomycete *Gloeophyllum trabeum*. *Appl. Environ. Microbiol.* 68, 2699–2703. doi: 10.1128/aem.68.6.2699-2703.2002

Jensen, K. A., Houtman, C. J., Ryan, Z. C., and Hammel, K. E. (2001). Pathways for extracellular Fenton chemistry in the brown rot basidiomycete *Gloeophyllum trabeum*. *Appl. Environ. Microbiol.* 67, 2705–2711. doi: 10.1128/aem.67.6.2705-2711.2001

Jonkers, W., and Rep, M. (2009). Lessons from fungal F-box proteins. *Eukaryot. Cell* 8, 677–695. doi: 10.1128/ec.00386-08

Katoh, K., and Standley, D. M. (2013). MAFFT multiple sequence alignment software version 7: improvements in performance and usability. *Mol. Biol. Evol.* 30, 772–780. doi: 10.1093/molbev/mst010

Kersten, P., and Cullen, D. (2014). Copper radical oxidases and related extracellular oxidoreductases of wood-decay Agaricomycetes. *Fungal Genet. Biol.* 72, 124–130. doi: 10.1016/j.fgb.2014.05.011

Kleman-Leyer, K., Agosin, E., Conner, A. H., and Kirk, T. K. (1992). Changes in molecular size distribution of cellulose during attack by white rot and brown rot fungi. *Appl. Environ. Microbiol.* 58, 1266–1270. doi: 10.1128/aem.58.4.1266-1270.1992

Klutts, J., Yoneda, A., Reilly, M., Bose, I., and Doering, T. (2006). Glycosyltransferases and their products: Cryptococcal variations on fungal themes. *FEMS Yeast Res.* 6, 499–512. doi: 10.1111/j.1567-1364.2006.00054.x

Kölle, M., Ringman, R., and Pilgård, A. (2019). Initial *Rhodonia placenta* gene expression in acetylated wood: group-wise upregulation of non-enzymatic oxidative wood degradation genes depending on the treatment level. *Forests* 10:1117. doi: 10.3390/f10121117

Lairson, L. L., Henrissat, B., Davies, G. J., and Withers, S. G. (2008). Glycosyltransferases: structures, functions, and mechanisms. *Annu. Rev. Biochem.* 77, 521–555. doi: 10.1146/annurev.biochem.76.061005.092322

Langmead, B., and Salzberg, S. L. (2012). Fast gapped-read alignment with Bowtie 2. *Nat. Methods* 9, 357–359. doi: 10.1038/nmeth.1923

Latchman, D. S. (1997). Transcription factors: an overview. *Int. J. Biochem. Cell Biol.* 29, 1305–1312.

Levasseur, A., Drula, E., Lombard, V., Coutinho, P. M., and Henrissat, B. (2013). Expansion of the enzymatic repertoire of the CAZy database to integrate auxiliary redox enzymes. *Biotechnol. Biofuels* 6:41. doi: 10.1186/1754-6834-6-41

Li, H., Handsaker, B., Wysoker, A., Fennell, T., Ruan, J., Homer, N., et al. (2009). The Sequence Alignment/Map format and SAMtools. *Bioinformatics* 25, 2078–2079. doi: 10.1093/bioinformatics/btp352

Liu, T.-B., and Xue, C. (2011). The ubiquitin-proteasome system and f-box proteins in pathogenic fungi. *Mycobiology* 39, 243–248. doi: 10.5941/myco.2011.39.4.243

Lombard, V., Golaconda Ramulu, H., Drula, E., Coutinho, P. M., and Henrissat, B. (2013). The carbohydrate-active enzymes database (CAZy) in 2013. *Nucleic Acids Res.* 42, D490–D495.

MacPherson, S., Larochelle, M., and Turcotte, B. (2006). A fungal family of transcriptional regulators: the zinc cluster proteins. *Microbiol. Mol. Biol. Rev.* 70, 583–604. doi: 10.1128/MMBR.00015-06

Martinez, Á. T., Speranza, M., Ruiz-Dueñas, F. J., Ferreira, P., Camarero, S., Guillén, F., et al. (2005). Biodegradation of lignocellulosics: microbial, chemical, and enzymatic aspects of the fungal attack of lignin. *Int. Microbiol.* 8, 195–204.

Martinez, D., Challacombe, J., Morgenstern, I., Hibbett, D. S., Schmoll, M., Kubicek, C., et al. (2009). Genome, transcriptome, and secretome analysis of wood decay fungus *Postia placenta* supports unique mechanisms of lignocellulose conversion. *Proc. Natl. Acad. Sci. U.S.A.* 106, 1954–1959.

Melin, V., Henríquez, A., Freer, J., and Contreras, D. (2015). Reactivity of catecholamine-driven Fenton reaction and its relationships with iron(III) speciation. *Redox Rep.* 20, 89–96. doi: 10.1179/1351000214y.0000000119

Mester, T., Varela, E., and Tien, M. (2004). "Wood degradation by brown-rot and white-rot fungi," in *Genetics and Biotechnology*, ed. U. Kück (Berlin: Springer), 355–368. doi: 10.1007/978-3-662-07426-8_17

Miettinen, O., Riley, R., Barry, K., Cullen, D., De Vries, R. P., Hainaut, M., et al. (2016). Draft genome sequence of the white-rot fungus *Obba rivulosa* 3A-2. *Genome Announc.* 4:e00976-16.

Miller, J., Mclachlan, A. D., and Klug, A. (1985). Repetitive zinc-binding domains in the protein transcription factor IIIA from Xenopus oocytes. *EMBO J.* 4, 1609–1614. doi: 10.1002/j.1460-2075.1985.tb03825.x

Nagy, L. G., Riley, R., Tritt, A., Adam, C., Daum, C., Floudas, D., et al. (2015). Comparative genomics of early-diverging mushroom-forming fungi provides insights into the origins of lignocellulose decay capabilities. *Mol. Biol. Evol.* 33, 959–970. doi: 10.1093/molbev/msv337

Niemenmaa, O., Uusi-Rauva, A., and Hatakka, A. (2007). Demethoxylation of [O14CH3]-labelled lignin model compounds by the brown-rot fungi *Gloeophyllum trabeum* and *Poria (Postia) placenta*. *Biodegradation* 19, 555–565. doi: 10.1007/s10532-007-9161-3

Ohm, R. A., Riley, R., Salamov, A., Min, B., Choi, I.-G., and Grigoriev, I. V. (2014). Genomics of wood-degrading fungi. *Fungal Genet. Biol.* 72, 82–90. doi: 10.1016/j.fgb.2014.05.001

Olson, Å., Aerts, A., Asiegbu, F., Belbahri, L., Bouzid, O., Broberg, A., et al. (2012). Insight into trade-off between wood decay and parasitism from the genome of a fungal forest pathogen. *New Phytol.* 194, 1001–1013. doi: 10.1111/j.1469-8137.2012.04128.x

Paszczynski, A., Crawford, R., Funk, D., and Goodell, B. (1999). De novo synthesis of 4,5-dimethoxycatechol and 2, 5-dimethoxyhydroquinone by the brown rot fungus *Gloeophyllum trabeum*. *Appl. Environ. Microbiol.* 65, 674–679. doi: 10.1128/aem.65.2.674-679.1999

Pilgård, A., Schmöllerl, B., Risse, M., Fossdal, C. G., and Alfredsen, G. (2017). "Profiling *Postia placenta* colonisation in modified wood - microscopy, DNA quantification and gene expression," in *Proceedings of the Wood Science and Engineering*, Copenhagen, 17–18.

Presley, G. N., Panisko, E., Purvine, S. O., and Schilling, J. S. (2018). Coupling Secretomics with enzyme activities to compare the temporal processes of wood metabolism among white and brown rot fungi. *Appl. Environ. Microbiol.* 84:e00159-18.

Puls, J. (1997). Chemistry and biochemistry of hemicelluloses: relationship between hemicellulose structure and enzymes required for hydrolysis. *Macromol. Symp.* 120, 183–196. doi: 10.1002/masy.19971200119

Riley, R., Salamov, A. A., Brown, D. W., Nagy, L. G., Floudas, D., Held, B. W., et al. (2014). Extensive sampling of basidiomycete genomes demonstrates inadequacy of the white-rot/brown-rot paradigm for wood decay fungi. *Proc. Natl. Acad. Sci. U.S.A.* 111, 9923–9928. doi: 10.1073/pnas.1400592111

Ringman, R., Pilgård, A., Kölle, M., Brischke, C., and Richter, K. (2016). Effects of thermal modification on *Postia placenta* wood degradation dynamics: measurements of mass loss, structural integrity and gene expression. *Wood Sci. Technol.* 50, 385–397. doi: 10.1007/s00226-015-0791-z

Ringman, R., Pilgård, A., and Richter, K. (2014). Effect of wood modification on gene expression during incipient *Postia placenta* decay. *Int. Biodeterior. Biodegradation* 86, 86–91. doi: 10.1016/j.ibiod.2013.09.002

Ringman, R., Pilgård, A., and Richter, K. (2020). Brown rot gene expression and regulation in acetylated and furfurylated wood: a complex picture. *Holzforschung* 74, 391–399. doi: 10.1515/hf-2019-0031

Ryu, J. S., Shary, S., Houtman, C. J., Panisko, E. A., Korripally, P., St John, F. J., et al. (2011). Proteomic and functional analysis of the cellulase system expressed by *Postia placenta* during brown rot of solid wood. *Appl. Environ. Microbiol.* 77, 7933–7941. doi: 10.1128/aem.05496-11

Schilling, J. S., Ai, J., Blanchette, R. A., Duncan, S. M., Filley, T. R., and Tschirner, U. W. (2012). Lignocellulose modifications by brown rot fungi and their effects, as pretreatments, on cellulolysis. *Bioresour. Technol.* 116, 147–154. doi: 10.1016/j.biortech.2012.04.018

Schilling, J. S., Kaffenberger, J. T., Liew, F. J., and Song, Z. (2015). Signature wood modifications reveal decomposer community history. *PLoS One* 10:e0120679. doi: 10.1371/journal.pone.0120679

Schwarze, F. W. M. R. (2007). Wood decay under the microscope. *Fungal Biol. Rev.* 21, 133–170. doi: 10.1016/j.fbr.2007.09.001

Simão, F. A., Waterhouse, R. M., Ioannidis, P., Kriventseva, E. V., and Zdobnov, E. M. (2015). BUSCO: assessing genome assembly and annotation completeness with single-copy orthologs. *Bioinformatics* 31, 3210–3212. doi: 10.1093/bioinformatics/btv351

Smith, T. F. (2008). "Diversity of WD-repeat proteins," in *The Coronin Family of Proteins: Subcellular Biochemistry*, eds C. S. Clemen, L. Eichinger, and V. Rybakin (New York, NY: Springer), 20–30.

Stamatakis, A. (2014). RAxML version 8: a tool for phylogenetic analysis and post-analysis of large phylogenies. *Bioinformatics* 30, 1312–1313. doi: 10.1093/bioinformatics/btu033

Stirnimann, C. U., Petsalaki, E., Russell, R. B., and Müller, C. W. (2010). WD40 proteins propel cellular networks. *Trends Biochem. Sci.* 35, 565–574. doi: 10.1016/j.tibs.2010.04.003

Sützl, L., Laurent, C. V. F. P., Abrera, A. T., Schütz, G., Ludwig, R., and Haltrich, D. (2018). Multiplicity of enzymatic functions in the CAZy AA3 family. *Appl. Microbiol. Biotechnol.* 102, 2477–2492. doi: 10.1007/s00253-018-8784-0

Suzuki, H., Macdonald, J., Syed, K., Salamov, A., Hori, C., Aerts, A., et al. (2012). Comparative genomics of the white-rot fungi, *Phanerochaete carnosa* and *P. chrysosporium*, to elucidate the genetic basis of the distinct wood types they colonize. *BMC Genomics* 13:444. doi: 10.1186/1471-2164-13-444

Suzuki, M. R., Hunt, C. G., Houtman, C. J., Dalebroux, Z. D., and Hammel, K. E. (2006). Fungal hydroquinones contribute to brown rot of wood. *Environ. Microbiol.* 8, 2214–2223. doi: 10.1111/j.1462-2920.2006.01160.x

Talavera, G., and Castresana, J. (2007). Improvement of phylogenies after removing divergent and ambiguously aligned blocks from protein sequence alignments. *Syst. Biol.* 56, 564–577. doi: 10.1080/10635150701472164

Tang, J. D., Perkins, A. D., Sonstegard, T. S., Schroeder, S. G., Burgess, S. C., and Diehl, S. V. (2012). Short-read sequencing for genomic analysis of the brown rot fungus Fibroporia radiculosa. *Appl. Environ. Microbiol.* 78, 2272–2281. doi: 10.1128/aem.06745-11

Thaler, N., Alfredsen, G., and Fossdal, C. G. (2012). "Variation in two *Postia placenta* strains, MAD-698-R and FPRL280 - mass loss, DNA content and gene expression," in *Proceedings of the IRG Annual Meeting, IRG/WP 12-10781*, Kuala Lumpur.

Traeger, S., Altegoer, F., Freitag, M., Gabaldon, T., Kempken, F., Kumar, A., et al. (2013). The genome and development-dependent transcriptomes of *Pyronema confluens*: a window into fungal evolution. *PLoS Genet.* 9:e1003820. doi: 10.1371/journal.pgen.1003820

Valášková, V., and Baldrian, P. (2006). Degradation of cellulose and hemicelluloses by the brown rot fungus Piptoporus betulinus – production of extracellular enzymes and characterization of the major cellulases. *Microbiology* 152, 3613–3622. doi: 10.1099/mic.0.29149-0

Vanden Wymelenberg, A., Gaskell, J., Mozuch, M., Sabat, G., Ralph, J., Skyba, O., et al. (2010). Comparative transcriptome and secretome analysis of wood decay fungi *Postia placenta* and *Phanerochaete chrysosporium*. *Appl. Environ. Microbiol.* 76, 3599–3610. doi: 10.1128/aem.00058-10

Wei, D., Houtman, C. J., Kapich, A., Hunt, C., Cullen, D., and Hammel, K. E. (2010). Laccase and its role in production of extracellular reactive oxygen species during wood decay by the brown rot basidiomycete *Postia placenta*. *Appl. Environ. Microbiol.* 76, 2091–2097. doi: 10.1128/aem.02929-09

Wu, B., Xu, Z., Knudson, A., Carlson, A., Chen, N., Kovaka, S., et al. (2018). Genomics and development of *Lentinus tigrinus*: a white-rot wood-decaying mushroom with dimorphic fruiting bodies. *Genome Biol. Evol.* 10, 3250–3261. doi: 10.1093/gbe/evy246

Yelle, D. J., Wei, D., Ralph, J., and Hammel, K. E. (2011). Multidimensional NMR analysis reveals truncated lignin structures in wood decayed by the brown rot basidiomycete *Postia placenta*. *Environ. Microbiol.* 13, 1091–1100. doi: 10.1111/j.1462-2920.2010.02417.x

Yu, L., Gaitatzes, C., Neer, E., and Smith, T. F. (2000). Thirty-plus functional families from a single motif. *Protein Sci.* 9, 2470–2476. doi: 10.1110/ps.9.12.2470

Zabel, R., and Morrell, J. J. (1992). *Wood Microbiology: Decay and its Prevention*. San Diego, CA: Academic Press.

Zhang, J., Presley, G. N., Hammel, K. E., Ryu, J.-S., Menke, J. R., Figueroa, M., et al. (2016). Localizing gene regulation reveals a staggered wood decay mechanism for the brown rot fungus *Postia placenta*. *Proc. Natl. Acad. Sci. U.S.A.* 113, 10968–10973. doi: 10.1073/pnas.1608454113

Zhang, J., and Schilling, J. (2017). Role of carbon source in the shift from oxidative to hydrolytic wood decomposition by *Postia placenta*. *Fungal Genet. Biol.* 106, 1–8. doi: 10.1016/j.fgb.2017.06.003

Conflict of Interest: The authors declare that the research was conducted in the absence of any commercial or financial relationships that could be construed as a potential conflict of interest.

frontiers in Microbiology

ORIGINAL RESEARCH
published: 24 June 2020
doi: 10.3389/fmicb.2020.01389

OPEN ACCESS

Edited by:
J. Philipp Benz, Technical University of Munich, Germany

Reviewed by:
Dongsheng Wei, Nankai University, China
Andre Ferraz, University of São Paulo, Brazil

***Correspondence:**
Barry Goodell
bgoodell@umass.edu

Specialty section:
This article was submitted to Fungi and Their Interactions, a section of the journal Frontiers in Microbiology

Received: *15 April 2020*
Accepted: *29 May 2020*
Published: *24 June 2020*

Citation:
Zhu Y, Plaza N, Kojima Y, Yoshida M, Zhang J, Jellison J, Pingali SV, O'Neill H and Goodell B (2020) Nanostructural Analysis of Enzymatic and Non-enzymatic Brown Rot Fungal Deconstruction of the Lignocellulose Cell Wall. Front. Microbiol. 11:1389. doi: 10.3389/fmicb.2020.01389

Nanostructural Analysis of Enzymatic and Non-enzymatic Brown Rot Fungal Deconstruction of the Lignocellulose Cell Wall†

*Yuan Zhu[1], Nayomi Plaza[2], Yuka Kojima[3], Makoto Yoshida[3], Jiwei Zhang[4], Jody Jellison[5], Sai Venkatesh Pingali[6], Hugh O'Neill[6] and Barry Goodell[7]**

[1] School of Materials Science and Engineering, Central South University of Forestry and Technology, Changsha, China, [2] Forest Products Laboratory, USDA Forest Service, Madison, WI, United States, [3] Department of Environmental and Natural Resource Science, Tokyo University of Agriculture and Technology, Fuchu, Japan, [4] Department of Bioproducts and Biosystems Engineering, University of Minnesota, Saint Paul, MN, United States, [5] Center for Agriculture, Food and the Environment, University of Massachusetts, Amherst, MA, United States, [6] Biology and Soft Matter Division, Oak Ridge National Laboratory, Oak Ridge, TN, United States, [7] Department of Microbiology, Morrill Science Center IV-N, University of Massachusetts, Amherst, MA, United States

Brown rot (BR) decay mechanisms employ carbohydrate-active enzymes (CAZymes) as well as a unique non-enzymatic chelator-mediated Fenton (CMF) chemistry to deconstruct lignocellulosic materials. Unlike white rot fungi, BR fungi lack peroxidases for lignin deconstruction, and also lack some endoglucanase/cellobiohydrolase activities. The role that the CMF mechanism plays in "opening up" the wood cell wall structure in advance of enzymatic action, and any interaction between CMF constituents and the selective CAZyme suite that BRs possess, is still unclear. Expression patterns for CMF redox metabolites and lytic polysaccharide monooxygenase (LPMO–AA9 family) genes showed that some LPMO isozymes were upregulated with genes associated with CMF at early stages of brown rot by *Gloeophyllum trabeum*. In the structural studies, wood decayed by the *G. trabeum* was compared to CMF-treated wood, or CMF-treated wood followed by treatment with either the early-upregulated LPMO or a commercial CAZyme cocktail. Structural modification of decayed/treated wood was characterized using small angle neutron scattering. CMF treatment produced neutron scattering patterns similar to that of the BR decay indicating that both systems enlarged the nanopore structure of wood cell walls to permit enzyme access. Enzymatic deconstruction of cellulose or lignin in raw wood samples was not achieved via CAZyme cocktail or LPMO enzyme action alone. CMF treatment resulted in depolymerization of crystalline cellulose as attack progressed from the outer regions of individual crystallites. Multiple pulses of CMF treatment on raw wood showed a progressive increase in the spacing between the cellulose elementary fibrils (EFs), indicating the CMF eroded the matrix outside the EF bundles, leading to less tightly packed EFs. Peracetic acid delignification treatment enhanced subsequent CMF treatment effects, and allowed both enzyme systems to further increase spacing of the EFs. Moreover, even after a single pulse of CMF treatment, both enzymes were apparently able to penetrate the

cell wall to further increase EF spacing. The data suggest the potential for the early-upregulated LPMO enzyme to work in association with CMF chemistry, suggesting that *G. trabeum* may have adopted mechanisms to integrate non-enzymatic and enzymatic chemistries together during early stages of brown rot decay.

Keywords: brown rot of lignocellulose, wood decay fungi, non-enzymatic activity, LPMO upregulated enzyme expression, chelator-mediated Fenton (CMF) degradation, biorefinery, CAZymes, SANS (small-angle neutron scattering)

INTRODUCTION

Nature has developed various systems for wood degradation (Eastwood et al., 2011; Cragg et al., 2015; Daniel, 2016; Goodell, 2020). In general, biomass-degrading fungi rely on complex degradative machineries that basically catalyze two types of processes: (1) generation of oxidative species (e.g., radicals) that act directly on the biomass; and (2) direct enzymatic depolymerization, for example by glycoside hydrolases. In most white rot fungi, the mode of attack is primarily enzymatic, but cell wall-degrading enzymes are too large to penetrate the intact wood cell wall, so in simultaneous white rots, erosion of the cell wall proceeds only from exposed lignocellulose surfaces. Brown rot (BR) fungi have been recognized as evolving from the predecessors of current white rot fungi and, as part of this evolutionary process, lignolytic enzyme systems and crucial types of cellulases in BRs have been lost (Hibbett and Donoghue, 2001; Floudas et al., 2012). In BRs, a chelator-mediated Fenton (CMF) system has evolved to replace at least some of the cellulolytic enzymatic machinery possessed by progenitor white rot fungi. The replacement of physiologically expensive extracellular enzymes with a low-molecular weight system that permits the efficient deconstruction of both holocellulose and lignin has been considered to confer an evolutionary advantage to brown rot fungi in exploiting some types of woody tissue (Goodell et al., 1997; Eastwood et al., 2011; Arantes et al., 2012; Floudas et al., 2012).

Efficiency is gained in brown rot attack because low molecular weight metabolites can diffuse deep within the wood cell wall to catalyze depolymerization at more internal cell wall sites than are accessible to larger enzymes (Goodell, 2020). The CMF system is unique among all biological systems in being the only substrate deconstruction system known based on oxygen radical chemistry that permits non-enzymatic deconstruction at a considerable distance (several microns) from the organism (Goodell et al., 2014). Generation of an oxidative mechanism deep within the wood cell wall, and apart from the fungal hyphae, is important for a number of reasons not the least of which is that, generation of an indiscriminate ROS oxidative mechanism must occur in a manner that does not cause damage either to the fungus or to the extracellular enzymes secreted by the fungus. Prior research has demonstrated that many extracellular hydrolytic carbohydrate-active enzymes (CAZymes) are expressed in later stages of BR decay (delayed temporal expression) after the cell wall structure has been non-enzymatically modified to permit enzyme access (Zhang et al., 2016, 2019; Presley and Schilling, 2017). Although this has been discussed as a mechanism to avoid ROS damage to enzymes, our research has also demonstrated that because of differing micro-environmental conditions, pH shifts, and other parameters, ROS generation by CMF action would occur only within the wood cell wall, which is inaccessible to enzymes (Goodell et al., 1997; Arantes and Goodell, 2014). Therefore, we propose that delayed temporal expression of most CAZymes in brown rot fungi is due primarily to the fact that secretion of most enzymes at early decay stages would not result in depolymerization of the cell wall. Instead, the delayed expression of CAZymes permits these enzymes to have maximal effectiveness after the cell wall structure has been opened by non-enzymatic CMF action, in a type of energy investment strategy to permit CAZyme digestion of holocellulose within the cell walls at this later stage (Zhang et al., 2019).

The brown rot non-enzymatic CMF mechanism has been explored only in a limited manner for use in biomimetic industrial/biorefinery applications (Goodell et al., 2017; Kent et al., 2018; Liu et al., 2020). Prior work with Fenton chemistry alone has in many cases not taken into account the short half-life of hydroxyl radicals generated. Thus, in some cases, Fenton-type treatments for industrial processing have been designed without an understanding that reactants must be allowed to sequentially penetrate and then react within the cell wall to efficiently generate hydroxyl radicals where needed for cell wall depolymerization (Goodell et al., 2014). In our previous work, results show that the CMF-iron treatment was highly efficient in opening up the pore structure of wood, and indicate that a single-stage treatment modifies wood in a manner similar to that achieved by a moderate level of decay by brown rot fungi. However, fungal metabolism of sugars does not occur with CMF treatment, and the resulting sugars and oligosaccharides produced can potentially be used in downstream fermentation or other industrial processes (Goodell et al., 2017). Furfurals and hydroxymethyl furfurals are typically not generated using Fenton chemistries with biomass substrates unless high heat is used, and further, Fenton chemistries have been used to reduce the amount of furfurals generated in biomass deconstruction (Yang et al., 2014, 2019).

Lytic polysaccharide monooxygenase (LPMO) enzymes are known to be the only redox enzyme which can depolymerize crystalline cellulose in delignified cell walls directly. LPMOs previously had been considered to use oxygen as an electron acceptor in the catalytic reactions; however, in more recent studies hydrogen peroxide, which is also well-known as a component of the CMF system, has been recognized to be a more efficient electron acceptor with the catalytic efficiency of LPMO with hydrogen peroxide being significantly higher than that with molecular oxygen (Bissaro et al., 2017; Forsberg et al., 2019).

Although research on the actual role of LPMO in lignified wood has been limited, high molecular weight (HMW) lignin and low molecular weight (LMW) lignin have been reported to serve as electron donors for LPMO9 (Muraleedharan et al., 2018), resulting in enhanced LPMO efficiency in cellulose deconstruction. Because CMF chemistry fragments lignin (Goodell et al., 2017), and this lignin also serves to donate electrons which reduce iron (Tamaru et al., 2019), this suggests that *G. trabeum* LPMO activity might be enhanced by CMF activity in a manner not yet understood. The manner in which the CMF mechanism may "open up" the structure of wood cell walls in advance of enzymatic action also is unknown, as is the mode of LPMO action on lignocellulose either with or without CMF treatment.

In the current study, we explored potential pathways for the biosynthesis of iron-reducing chelators produced by *G. trabeum* involved in CMF chemistry. This mechanistic expression analysis was done with the aim of helping to integrate our current understanding of both non-enzymatic and enzymatic brown rot decay mechanisms with nanostructural data and to characterize changes that occur when wood is treated with various systems to mimic brown rot decay processes. We also then conducted a nanostructural analysis, where experiments with the CMF system modeled using different levels of treatment were conducted, and we compared treatments with and without CAZyme treatment. In some samples, peracetic acid was used to remove lignin prior to treatment and permit better understanding of attack on the cellulose structure. These treatments were used as baseline, or reference treatments, for comparison to the CMF and enzyme treatments and compared to wood decayed by *G. trabeum*. Additional undecayed wood samples were treated using either CMF chemistry, or CMF chemistry followed by treatment with either a recombinant AA9-LPMO cloned from *G. trabeum* (GtLPMO9A-2), which was reported to show activity not only for cellulose but also for some hemicelluloses such as xyloglucan and glucomannan (Kojima et al., 2016), or by a CAZyme cocktail (a commercial blend of cellulases/xylanases). Modification of the structure of wood cell walls was characterized using small angle neutron scattering (SANS). Enhancing understanding of brown rot degradative mechanisms will lead to better solutions to address recalcitrance problems associated with lignin encrustation of cellulose in the pretreatment of biomass in biorefinery applications.

MATERIALS AND METHODS

Figure 1 provides a schematic summary of the procedures used in this research.

Gene Expression Patterns

To explore the interaction between LPMO and CMF in terms of expression timing, gene expression levels were retrieved from RNA-seq datasets obtained by measuring mRNA levels from *G. trabeum* in decayed thin aspen wood wafers (Gene Expression Omnibus number GSE108189) (Zhang et al., 2019). In this work, a 'thin wood wafer design' was used to promote fungal growth along a strip of wood, which was then sequentially sectioned to allow the different decay stages to be assessed using temporal transcriptomics for brown rot decay (Zhang et al., 2016). Specifically an American Society for Testing and Materials soil microcosm chamber was used to culture *G. trabeum* (Zhang et al., 2016). The soil medium was composed of a 1:1:1 mixture of soil, peat, and vermiculite, hydrated to 40–45% (wt/vol) moisture content as specified in the standard. Sterilized aspen (*Populus* sp.) wood wafers (2.5 mm thick × 25 mm wide × 60 mm long) were placed at an angle in the microcosm chambers with the 25 mm edge resting on the soil surface, for colonization from the base by hyphae. Wafers were harvested after the advancing hyphal front had colonized 50 mm up the length of a wafer. The wafers were then sectioned into 5-mm sections along their entire length, using advancing hyphal front as the starting point (0 mm), and short wafer sections the cut from the 0–5 mm, 15–20 mm and 30–35 mm zones. These zones were then sampled for transcriptomic analysis, representing early-, mid-, and late-decay stages of brown rot, respectively.

Expression levels in Reads Per Kilobase of transcript per Million mapped (RPKM) of genes relating to hydroquinone, oxalate and LPMO synthesis were studied for their temporal expression patterns, as brown rot decay by *G. trabeum* progressed. A key metabolite family of interest in early stages of BR wood decay is the low molecular weight (LMW) hydroquinone family of metabolites including 2,5-dimethoxyhydroquinone (DMHQ) and 4,5-dimethoxy-1,2-benzenediol (DMC) (Goodell et al., 1997; Kerem et al., 1999; Paszczynski et al., 1999).

A *de novo* synthesis pathway was built in brown rot fungi according to previous studies on aromatic metabolites in wood-decaying fungi, and the key pathway genes involved in hydroquinone synthesis were identified via a BlastP search of the relevant homologs in the *G. trabeum* genome (Hattori et al., 1999; Lapadatescu et al., 2000; Meganathan, 2001).

Nanostructural Characterization

Wood Samples

Southern yellow pine (SYP - *Pinus* spp.) sapwood wood shavings (110–160 μm thick) were prepared using a commercial wood-shop planer. Alternately, SYP sapwood disks (19 mm diameter, 0.5 mm ∼ 0.6 mm thick) were cut using a sledge microtome. Samples are referred to as "shavings" or "disks" in this research. Disks were used for chemical (CMF), delignification and enzyme treatments. Shavings were used for decay treatments because disks lost structural integrity rapidly in decay tests and it was not possible to transfer them into the SANS sample holders for analysis.

Peracetic Acid (PAA) – Delignification Treatments

PAA solution (30% wt/wt) was prepared using deionized (DI) water, and 1 g of air-dried SYP wood disks were saturated with 10 mL PAA solution in a shaker bath at 100 rpm and 25°C for 24 h (Chang and Holtzapple, 2000). Delignified SYP disks were then washed five times each with 40 ml DI water, and dried at 60°C for 24 h. PAA treatment and washing were repeated 3X to remove

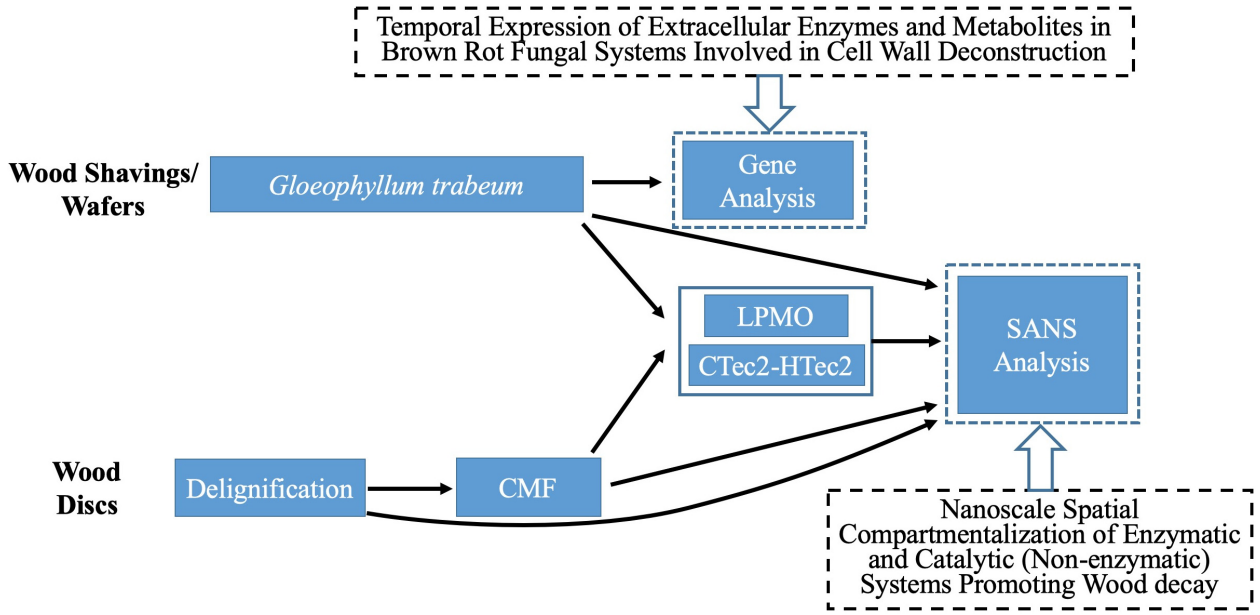

FIGURE 1 | Flow chart of materials, treatments and analyses used in our procedures.

lignin. Mass loss for all samples averaged 29 ± 5% after 3 PAA treatment cycles. No shaving samples were treated with PAA.

Chelator-Mediated Fenton (CMF) Treatments

For CMF treatment, three replicate wood disks each, with/without PAA-delignification, were treated with 50 mM iron (III) chloride hexahydrate ($FeCl_3.6H_2O$) in acetate buffer (pH 4.0, 1M) at a loading of 0.2 g wood/5 ml buffered iron (III) solution. Sample materials were thoroughly mixed for 10 min to allow the iron to penetrate and bind to cellulose deep within the wood cell wall, and then dried at 120°C for 2 h to remove moisture prior to the addition of the redox chelator. 2,3-dihydroxybenzoic acid (2, 3-DHBA) 50 mM was then added as the redox chelator at 25°C with shaking for 30 min using an equal volume to the initial iron (III) solution. The same volume of H_2O_2 (final molarity of 0.5 M) was then added with hand mixing for 5 min followed by water bath shaking (125 rpm) at 40°C overnight. Samples were then drained of all solutions, and another fresh batch of 0.5 M H_2O_2 was added again. After 24 h of incubation (25°C, 125 rpm), the H_2O_2 was drained from the samples. These procedures were repeated 2X or 4X (designated as 2x or 4x pulses) to produce the CMF treated samples (**Table 1**), which were stored frozen for additional treatment or further analysis. Note: PAA-delignified wood disks were unable to go through 4-pulses of CMF treatment as the wood was solubilized at that point.

Decay Treatment

Decay treatment was the same as that described previously (Goodell et al., 2017). Wood shavings were incubated with mycelium from liquid cultures of *G. trabeum* for either 18 or 42 days (2 replicates each), designated as 18dGt and 42dGt, respectively. After incubation, samples were carefully transferred into the titanium cells for SANS analysis.

Enzyme Treatment

A recombinant LPMO (GtLPMO9A-2) was cloned from *G. trabeum*, and heterologously expressed in the yeast *Pichia pastoris* as detailed previously (Kojima et al., 2016). This enzyme has activity on cellulose, carboxymethylcellulose and broad activity on hemicelluloses such as glucomannan and xyloglucans (Kojima et al., 2016). The use of the LPMO on samples in this research was compared to use of a combination of commercial enzymes (CTec2 and HTec2 – Novozymes, Bagsvaerd, Denmark) mixed in a cocktail.

LPMO treatments were applied at a rate of 1 μM (final concentration), and the CTec2 and HTec2 mixture (at a ratio of 4:1) was applied at a final concentration 10-12FPU/g wood in 50 mM acetate buffer (pH 5). The activity of the CTec2 and HTec2 enzymes was assessed prior to use via a filter paper activity assay (Bailey, 1981). Enzymes were used to treat wood disks or wood shavings either without pretreatment

TABLE 1 | Mass losses comparing unmodified wood or wood that was PAA-delignified and then treated with either 1, 2, or 4 pulses of the CMF system.

Samples	CMF	Mass loss
Unmodified Wood	1-pulse	4%
	2-pulses	16%
	4-pulses	78%
Delignified wood	1-pulse	33%
	2-pulses	36%

Only single samples were available for the mass loss measurements.

(reference treatments) or after samples were pretreated using the PAA treatment for delignification, CMF treatment, or by decay with *G. trabeum* as detailed in **Table 2**. All enzyme treatments were conducted in a water bath shaker for 72 h (45°C, 100 rpm). Samples were then subsequently washed with DI water before oven-drying.

SANS Analysis

Terminology

For appropriate interpretation, it is helpful to define the following terms used in SANS data analysis. These definitions are very brief, appropriate for this research, and they are not intended to provide a detailed understanding of SANS data analysis:

Low-q, mid-q, and high-q. These terms represent regions of the *x*-axis (scattering vector q) of the SANS curves which are associated with the size of features in the sample contributing to the scattering. Low-q extends from 0.001 – 0.01 [$Å^{-1}$], mid-q from 0.01 – 0.1 [$Å^{-1}$], and high-q from 0.1–0.3 [$Å^{-1}$].

Power Law Exponent. This is a number that describes the shape of the different sections of the SANS curves; specifically, the low-q and mid-q sections. In our research, the shape of the SANS curves varies as changes occur in the samples, and the mid-q Power Law Exponent generally increases as separation of EFs, and other angstrom and nanoscale separations, occur.

Radius of gyration (R_g). This term defines the average characteristic size of a nanoscale feature as the average radius/distance from the center of mass of the feature taking into account aspect ratio. Here, the R_g may correspond to a space or a gap which may change in size with treatments, but it also may show how the size of polymeric agglomerates (repolymerized lignin fragments) may be changing in response to treatments.

Methodology

After being treated as described in **Table 2**, D_2O saturated samples were loaded into titanium cells, with quartz windows and a 0.5 mm aluminum spacer. Once the titanium holder was screw-sealed, it was filled with D_2O and all air bubbles were removed. To the extent possible, both disks and shavings were aligned inside the titanium cells so that the wood grain was oriented vertically (**Figures 2A,B**). Overlapping and/or misalignments inside the titanium cells were observed for some of the delignified wood disks and wood shavings (**Figures 2C,D**). Misalignments inside the wood cell wall likely decreased the sharpness of the diffraction peak in the aligned scattering from these samples, consequently, increasing the polydispersity and uncertainty in the measured values of the elementary fibril spacing of samples exposed to more severe treatment like DW-CMF-2 or DW-LPMO.

SANS measurements were performed on the Bio-SANS beam line at the High Flux Isotope Reactor facility in the Oak Ridge National Laboratory (Oak Ridge, TN, United States). All scattering patterns were acquired using a neutron wavelength λ of 6 Å, with a wavelength spread ($\Delta\lambda/\lambda$) of 13%. To achieve a broad scattering vector range (from 0.003 to 0.27 $Å^{-1}$) two sample-to-detector distances (1.7 and 14.5 m) were necessary. The shorter sample-to-detector distance provided the higher q data, and the longer distance was used to acquire the lowest *q* values. Circular aperture diameters of 40 and 14 mm were used for the source and sample, respectively. The radial distance

TABLE 2 | Treatments of all wood samples analyzed by SANS.

Labels	PAA delignification	CMF	*G. trabeum*	Enzyme
UW	–	–	–	–
UW-CMF-1	–	+	–	–
UW-CMF-2	–	++	–	–
UW-CMF-4	–	++++	–	–
UW-LPMO	–	–	–	LPMO
UW-CMF-1-LPMO	–	+	–	LPMO
UW-CMF-2-LPMO	–	++	–	LPMO
UW-CTec2-HTec2	–	–	–	CTec2-HTec2
UW-CMF-1-CTec2-HTec2	–	+	–	CTec2-HTec2
UW-CMF-2-CTec2-HTec2	–	++	–	CTec2-HTec2
0 dGt	–	–	–	–
18 dGt	–	–	18 dGt	–
42 dGt	–	–	42 dGt	–
18 dGt-LPMO	–	–	18 dGt	LPMO
42 dGt-LPMO	–	–	42 dGt	LPMO
18 dGt-CTec2-HTec2	–	–	18 dGt	CTec2-HTec2
42 dGt-CTec2-HTec2	–	–	42 dGt	CTec2-HTec2
DW-CMF-1	+	+	–	–
DW-CMF-2	+	++	–	–
DW-LPMO	+	–	–	LPMO
DW-CTec2-HTec2	+	–	–	CTec2-HTec2

For CMF-treated wood: +, single pulse; ++, double pulse; ++++, 4-pulse CMF treatment.

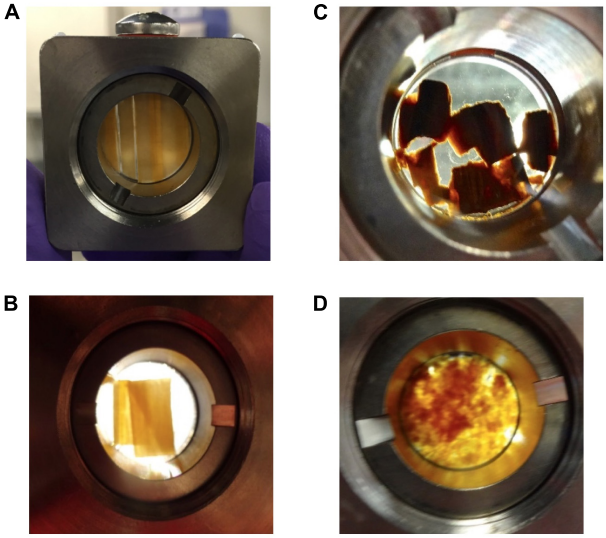

FIGURE 2 | D_2O saturated samples loaded into titanium cells for SANS analysis showing the differences in sample alignment inside those cells. The majority of the **(A)** wood disks and **(B)** wood shavings were aligned vertically inside the titanium cells, whereas a few of the **(C)** delignified disks were less well oriented and the **(D)** decayed wood shavings were randomly oriented.

from the beam-center to the edge of the detector images was converted into the reciprocal space scattering vector q, which describes the relationship between the neutron wavelength λ and the scattering angle θ as $q = 4\pi\sin(\theta)/\lambda$. The detector images were normalized to the incident beam monitor counts, and corrected for pixel sensitivity, dark current and background contributions. Then, the images were transformed into polar reciprocal space to reduce the data anisotropically into two profiles: aligned and amorphous. If no anisotropy was observed (**Figure 3C**), then the image was reduced isotropically into one scattering curve. Features with strong preferential orientation such as the regularly packed cellulose elementary fibrils (EFs) in the S2 cell wall layer contributed to the anisotropic scattering in the aligned sector (**Figure 3A**), whereas scattering from all the lesser organized wood polymers contributed to the isotropic or amorphous scattering. This reduction was implemented using the IgorPro macros provided at the beamline. **Figure 3** shows the typical scattering patterns observed in this study, and the corresponding 1D scattering profiles obtained from the data reduction.

SANS 1D profiles were analyzed using the IRENA package implemented in IgorPro (Ilavsky and Jemian, 2009). Based on the different structural features observed in our study, we fitted the data using an empirical model consisting of a low-q power law, a mid-q unified fit level and a Gaussian peak. While several models have been used to fit scattering data from wood, including (a) empirical models (Fernandes et al., 2011; Thomas et al., 2014; Plaza et al., 2016), (b) variations of the Unified fit (Goodell et al., 2017), and (c) cylinder-based models (Jakob et al., 1996; Penttila et al., 2019), in our current research we chose an empirical model in order to detect the changes caused by the various treatments without making assumptions about the cellulose microfibril arrangement in the wood cell wall. Some of our treatments caused lignin to be modified, and a model appropriate for changes which occur in both lignin and cellulose must be considered. However, even though the empirical model was the best suited for analyzing our work, the trends reported are not model-dependent and to the best of our knowledge, would not change if a different model was used to fit the data.

For the wood disks, which mostly scattered anisotropically, the peak was enhanced by subtracting the amorphous profiles from the aligned curves, which removed the mid-q scattering contribution. These subtracted curves were fitted with only two structural levels to extract the low-q power law (P_1) and the peak position (q_0), which has been used to measure the spacing between elementary fibrils (EFs) in wood using the following equation $2\pi/q_0$ (Fernandes et al., 2011; Thomas et al., 2014; Plaza et al., 2016). Then, the amorphous profiles were fitted using the model with three structural levels to extract the mid-q radius of gyration (R_g) and power law exponent (P_2). For the wood shavings, which scattered isotropically, the reduced scattering profiles exhibited weak features, and the data were fitted using the model with the three structural levels, though for these samples, differences were only observed in the mid-q scattering region. All uncertainties reported reflect both the natural variability and polydispersity of the structural features in wood, as well as the goodness of the fit, which in our case was calculated in IRENA as the range satisfied by this condition: $\chi^2_{fit} < 1.06\chi^2_{critical}$. It should be noted that SANS is a bulk measurement technique and thus, while each scattering profile is obtained from a single sample, all structural features within the accessible length scale range contribute to the measured profile.

RESULTS AND DISCUSSION

Hypothesized Gene Expression Pathways for DMHQ and Related LMW Redox Metabolites, With Proposed Interaction Between CMF and LPMO Genes

LMW metabolites play important roles in CMF chemistry, among which catechol/hydroquinone derivatives (Goodell et al., 1997; Paszczynski et al., 1999) (e.g., 2,5-dimethoxy-1,4-benzenediol [hydroquinone] – DMHQ and 4,5-dimethoxy-1,2-benzenediol – DMC) (Kerem et al., 1999) and related LMW compounds (Eastwood et al., 2011) (e.g., variegatic acid) have been most commonly reported. The ability of these compounds to reduce iron to Fe^{2+} has been validated by several groups, and H_2O_2 produced through redox cycling has also been proposed (Varela and Tien, 2003). At least three independent brown rot lineages are known to produce these LMW catecholate/hydroquinones and related iron-reducing compounds (Floudas et al., 2012; Eastwood, 2014), which are here referred to simply as "chelators."

In this research we found that the genes associated with hydroquinone chelator synthesis pathways were more likely upregulated at early brown rot stages in *G. trabeum*

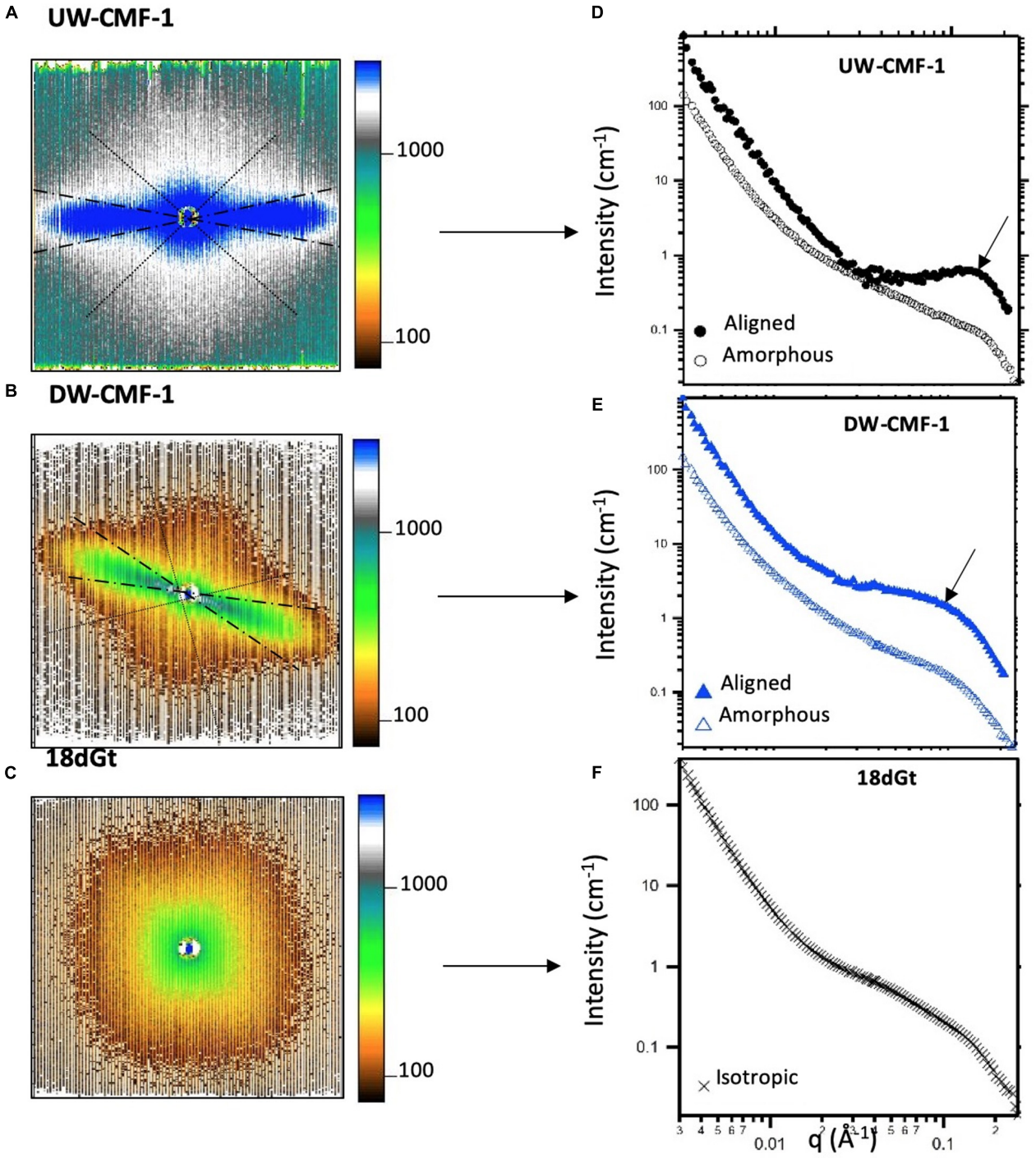

FIGURE 3 | Uncorrected SANS 2D detector images from **(A)** an unmodified wood disk treated with one pulse of CMF, **(B)** a delignified wood disk treated with one pulse of CMF, and **(C)** wood shavings decayed by *G. trabeum* for 18 days. The aligned sectors used in the data reduction are shown between the dashed radians, and the amorphous sector is enclosed within the dotted lines. All patterns were measured at a sample-to-detector distance of 1.7 m. **(D–F)** Scattering profiles reduced from the anisotropic and isotropic scattering patterns showing the aligned (closed symbols), amorphous (open symbols) and isotropic curves (crosses). Arrows in d and e show the location where the diffraction peak is observed.

(**Figures 4A,B**), indicating the roles of these metabolites in non-enzymatic cell wall deconstruction during the incipient stage of brown rot. This is in line with our previous report that showed several genes encoding LMW metabolites were upregulated early during brown rot. Our previous data also showed that most of the CAZymes, including many cellulases, were upregulated late

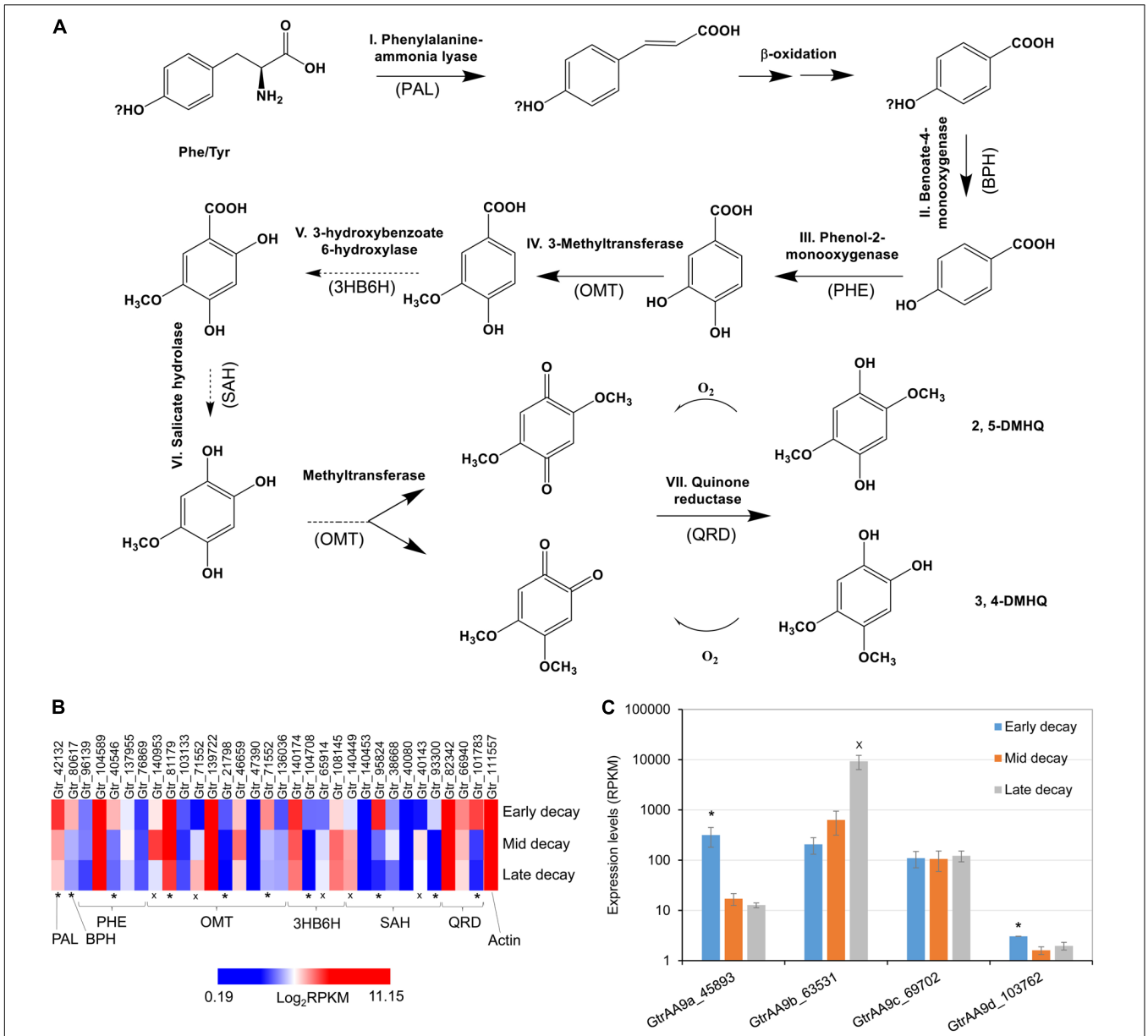

FIGURE 4 | Co-expression of LPMO and LMW hydroquinone pathways at an early brown rot stage in *G. trabeum*. **(A)** The hydroquinone chelator synthesis pathway and the enzyme homologs catalyzing each step are proposed based on standard pathways. Genes that were significantly upregulated (*, FDR < 0.05 by RNA-seq) in early brown rot basically covered all the required key enzyme components of the pathway, although several OMT, 3HB6H and SAH genes were clearly upregulated at late decay stages (x, FDR < 0.05) **(B)**. Expression timing of *G. trabeum* LPMO genes showed that AA9a was significantly upregulated in early brown rot stages, and these were co-expressed with genes for metabolites produced in proposed pathway for hydroquinone synthesis. **(C)** Expression levels for GtrAA9 genes during early-, mid- and late-decay stages.

and the expression pattern for AA9b (JGI protein ID 63531; **Figure 4C**) is in agreement with this. Conversely however, two LPMO genes AA9a (45893, designated GtLPMO9A) and AA9d (103762, designated GtLPMO9D) were found to be upregulated significantly at early decay stages. GtLPMO9A-2, which is one of the splicing variants transcribed from the AA9a gene, was reported to show activity not only against cellulosic substrates but also against hemicellulosic substrates such as glucomannan (Kojima et al., 2016), which is one of the primary hemicelluloses in softwood. Considering the relatively high expression levels of the AA9a gene at an early decay stage (**Figure 4C**), we propose that this enzyme may play an important role in the degradation of the wood cell wall ahead of hydrolytic enzymes such as cellulases. Moreover, co-expression of the AA9a gene with the genes involved in the synthesis of hydroquinones indicates that GtLPMO9A might potentially work cooperatively with hydroquinones in the reaction process of the non-enzymatic chelators produced by *G. trabeum* and

associated with CMF chemistry. There have been no prior reports on the enzymatic characteristics of GtLPMO9D, but we found very low expression levels of the AA9d gene (RPKM < 10) suggesting perhaps only limited association of the GtLPMO9D enzyme with LMW chelators.

We also observed that several catechol *o*-methyltransferase (OMT), 3-hydroxybenzoate 6-hydroxylase (3HB6H), and *s*-adenosyl-l-homocysteine (SAH) genes were upregulated in late decay stages (**Figure 4B**). We propose that this is related to detoxification and polymerization of low levels of soluble lignin which would have been released into the extracellular fungal matrix (ECM) which surrounds the fungal hyphae, as the lignin was being initially depolymerized by CMF attack during decay. OMT and 3HB6H can act on phenolic fragments to modify and detoxify them, while SAH prevents methylation of phenolics. Preventing methylation of lignin monomer fragments (by *S*-adenosyl methionine) potentially would promote additional repolymerization of lignin radical monomers which would be consistent with the nature of brown rotted lignin.

Nanostructural Characterization

Effects of Pulsed CMF Treatments and G. *trabeum* Decay on Wood Cell Walls

Two-dimensional scattering patterns from the CMF treated disks were anisotropic, and featured strong, aligned scattering sectors. Whereas all decay treated shaving samples exhibited isotropic scattering, due to their random orientation inside the cell. Reducing the patterns into one-dimensional profiles allowed us to compare the effects of the treatment on the wood nanostructure (**Figure 5**). For CMF-treated samples, we observed that increasing the CMF pulse number led to an increase in the mid-q scattering and a shift toward lower q in the diffraction peak. This indicates that multiple pulses of CMF treatment on raw wood promoted a progressive increase in the spacing between cellulose chains as the outer portion of the bundles of EFs was being depolymerized and eroded by CMF oxidation. A similar increase in cellulose chain spacing (in the 200 crystal plane) was also observed previously in brown rot decay (Howell et al., 2011). For decayed samples in our current work, the diffraction peak was not observable in the isotropic curves, which interestingly exhibited nearly identical features to the amorphous curves from the CMF-treated samples.

The similarity between scattering profiles of the decay-treated samples and the CMF-treated samples supports the hypothesis that CMF-treatment causes similar nanostructural changes to those caused by early stage fungal decay. The shift in the diffraction peak indicates that the spacing between elementary fibrils increased as the CMF treatment depolymerized and eroded the outer regions of the cellulose microfibrils as suggested previously in brown rotted wood (Howell et al., 2011). Scattering in the mid-q region also may support the formation of nodules of repolymerized lignin as decay progresses, as has previously been reported in brown rotted wood (Goodell et al., 2017). The overlap observed in the high-q scattering region suggests that the diameter of the cellulose EFs is likely unaffected by the CMF treatment, and we propose that these EFs likely change configuration (i.e., they become more loosely packed) and expand

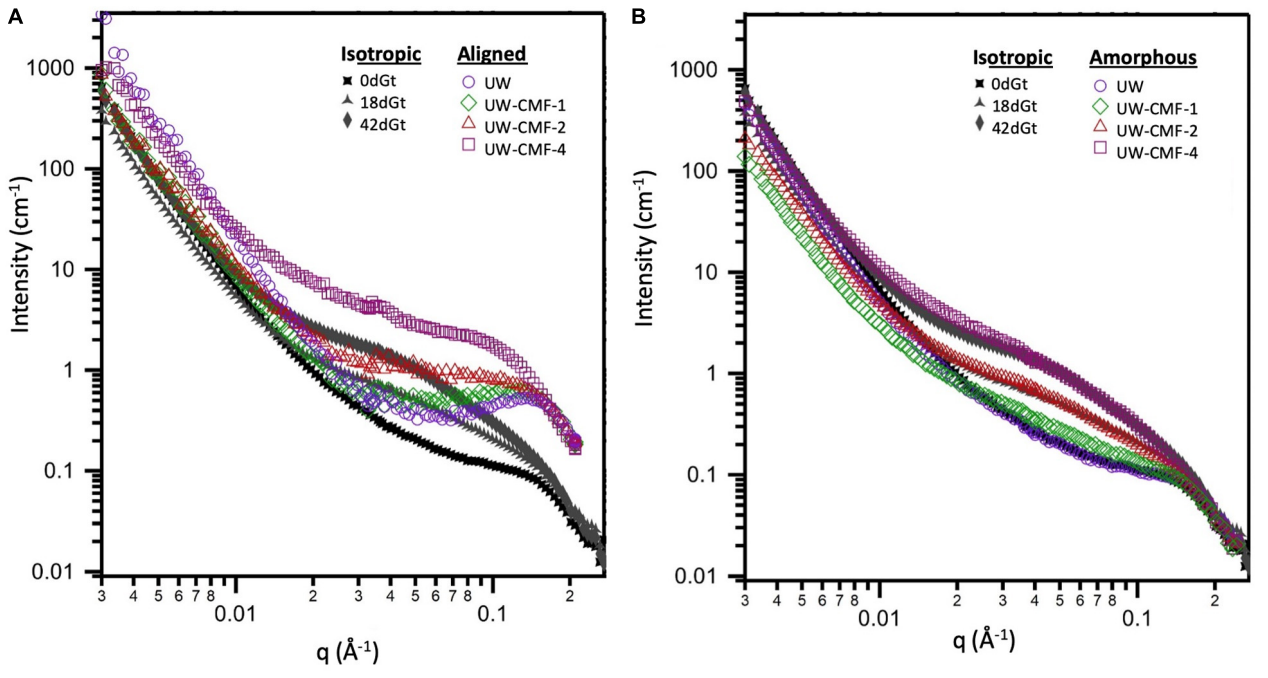

FIGURE 5 | Comparison of the effect of CMF treatment on sound wood, and decay by *G. trabeum*, on the wood's nanostructure. Both **(A,B)** plots show the isotropic scattering profiles of the decayed samples which are plotted together with either: **(A)** the aligned scattering curves from the pulsed CMF-treated samples or **(B)** the amorphous scattering profiles from the pulsed CMF-treated samples.

slightly as the cellulose outer layers are also being eroded, supporting an earlier observation in brown rotted wood using X-ray diffraction (Howell et al., 2011). Experiments that probe beyond the q-range achieved in this study would further confirm how CMF modifies the cellulose crystalline structure.

By fitting the data to a model with three structural levels, we quantified the changes caused by the treatments (**Table 3**). For the CMF-treated samples, changes were observed across the entire q-range. At low-q, the power law exponent decreased with increasing pulses meaning that the treatment led to an increase in the surface roughness of structures that were larger than 200 nm, such as the cellulose microfibril lamellar structure in the S2 cell wall layer and larger re-polymerized lignin particles (Goodell et al., 2017). In the mid-q region, the R_g particle size decreased as the CMF-pulse number increased probably reflecting cellulose EFs fragment length, as well as fragments from depolymerized lignin and/or hemicelluloses, while the power law exponents were similar to those from the decay treated samples. For the decay treated samples the most significant changes were observed in the mid-q scattering region, as the low and high-q regions were fixed while fitting the data. For the untreated control sample, scattering from the long EFs gave rise to power law scattering with an exponent of 1. As the samples were decayed, the mid-q power law exponent increased to 2.5, which corresponds to scattering from mass fractals (Beaucage, 1996). The mid-q characteristic dimension R_g remained constant beyond 18 days. Scattering in this region has been previously attributed to scattering from lignin aggregates (Pingali et al., 2014; Goodell et al., 2017). Here, we observe that the average size of the aggregates decreased with an increase in CMF pulses. Interestingly, with increasing treatment severity, the mid-q Rg (6 nm) is about double the Rg of spruce lignin monomers in aqueous media reported from computational studies (Vermaas et al., 2019) which we attribute to re-polymerization of the modified lignin in our work. At high-q, changes in the EFs spacing were not detectable in the decay-treated samples, but for the CMF-treated samples an increase of 50% was observed from 1 to 4 pulses.

CMF treatment with an increasing number of pulses was compared to decay by *G. trabeum* over several weeks, and neutron scattering patterns were found to be similar as the severity of treatments increased (**Figure 5** and **Table 3**). Although enzymatic action also likely came into play during decay by *G. trabeum*, the ability of CMF treatment to mimic the degradation of the wood cell wall and achieve similar mid-q characteristic sizes to those generated by brown rot fungal decay is a unique finding. This data suggests that the extracellular CAZymes secreted by *G. trabeum* may largely support CMF action by the fungus in early- to mid-stages of decay, and also supports the finding reported earlier (Goodell et al., 2017) that the function of at least some extracellular CAZymes in the brown rot decay of softwoods is to digest oligosaccharides as they diffuse from the wood cell wall into the lumen space, with limited penetration of enzymes into the wood cell wall. The mechanism may be different in hardwoods as the pattern of attack of the wood cell wall by brown rot fungi has been observed to be different in hardwoods compared to softwoods, with greater cell wall porosity developing in hardwood than in softwood cell walls (Daniel, 2016; Goodell et al., 2017). This suggests a basis for the differential preference of some decay fungi in attacking different woody tissue types (gymnosperm vs. angiosperm) (Riley et al., 2014; Goodell et al., 2017; Krah et al., 2018). *G. trabeum* is a unique brown rot fungus because it has the capacity to also degrade grasses (Kaffenberger and Schilling, 2013; Presley et al., 2018). Prior research has suggested that feruloyl esterases secreted by *G. trabeum* are important in allowing *G. trabeum*, but not the other brown rot fungi included in the analyses, to degrade grasses (Presley et al., 2018). We suggest that the low molecular weight CMF mechanism may also play a role in the selective degradation of grasses by brown rot fungi particularly because enzymes, including feruloyl esterases, would be unable to penetrate deeply in lignified cell walls. CMF factors that may play a role in the selective degradation of grass cell wall material potentially would include: (a) the type of chelator produced by the fungus [hydroquinone/catechol (Paszczynski et al., 1999) vs. variegatic acid (Eastwood et al., 2011) and potentially other chelator structures]; (b) the levels of oxalate produced within the fungal ECM, and the differential pH between the ECM and the plant cell wall; (c) the capacity of the lignin and cellulose in the grass species to bind iron; and (d) the redox capacity of the fungal chelators and cell wall lignin monomers to redox cycle to permit H_2O_2 generation within the wood cell wall.

TABLE 3 | Comparison between CMF and *G. trabeum* (Gt) decay treatments.

Sample	Low-q	Mid-q		High-q
	P_1	R_g (nm)	P_2	EF spacing (nm)
UW	3.91 ± 0.16*	–	–	4.66 ± 0.23*
UW-CMF-1	3.72 ± 0.16*	9 ± 1.3	1.6 ± 0.1	5.11 ± 0.17*
UW-CMF-2	3.57 ± 0.21*	7.9 ± 0.5	2.1 ± 0.1	6.40 ± 0.44*
UW-CMF-4	3.40 ± 0.31*	6 ± 1.1	2.5 ± 0.1	7.70 ± 0.15*
0 dGt	4.1 ± 0.07	–	1.2 ± 0.1	5.07 ± 0.24
18 dGt	3.6**	8 ± 2.2	1.8 ± 0.4	7**
42 dGt	3.6**	8 ± 0.7	2.4 ± 0.3	7**

**Parameters were fitted using the anisotropic curve and fixed while fitting the amorphous curve. **Parameters were fixed while fitting the isotropic curves due to weak features and/or limited q-range.*

Interaction Between the CMF Treatment or Fungal Decay Followed by Enzyme Treatment

Scattering patterns from unmodified wood samples pre-treated solely with a cellulolytic enzymatic cocktail, as expected, did not exhibit any new features, and wood shavings scattered isotropically while disks scattered anisotropically. Both the cloned LMPO and commercial CAZyme enzymatic treatments slightly increased the EF spacing of wood samples following CMF treatment (**Table 4**). While, it is conceivable that the *G. trabeum* would have a similar effect on the EF spacing, it is not clear from our data if the decay by *G. trabeum* increased EF spacing prior to enzymatic treatment. Because of weak nature of the diffraction peak in the scattering from the

TABLE 4 | Comparison between CMF/*G. trabeum* (Gt) decay and enzymes.

Sample	Low-q		Mid-q	High-q
	P_1	R_g (nm)	P_2	EFs spacing (nm)
18 dGt	3.6**	8.0 ± 2.2	1.8 ± 0.44	7**
18 dGt-LPMO	3.6**	8 ± 1.1	1.8 ± 0.19	7**
18 dGt-CTec2-Htec2	3.6**	7 ± 1.6	2 ± 0.5	7**
42 dGt	3.6**	8.0 ± 0.7	2.4 ± 0.30	7**
42 dGt-LPMO	3.6**	7.25 ± 1.38	2.2 ± 0.54	7**
42 dGt-CTec2-Htec2	3.6**	7 ± 1.41	2.1 ± 0.45	7**
UW CMF-1	3.72 ± 0.16*	9 ± 1.3	1.6 ± 0.14	5.11 ± 0.17*
UW-CMF-1-LPMO	3.72 ± 0.18*	6.38 ± 0.69	2.03 ± 0.31	5.35 ± 0.29*
UW-CMF-1-CTec2	3.87 ± 0.22*	9 ± 1.2	1.56 ± 0.15	5.30 ± 0.14*
UW CMF-2	3.57 ± 0.21*	7.89 ± 0.48	2.1 ± 0.13	6.4 ± 0.44*
UW-CMF-2-LPMO	3.5 ± 0.2*	6.94 ± 0.69	2.2 ± 0.2	7.22 ± 0.62*
UW-CMF-2-CTec2-Htec2	3.55 ± 0.12*	7.27 ± 0.92	2.18 ± 0.26	6.85 ± 0.44*

**Parameters were fitted using the anisotropic curve and fixed while fitting the amorphous curve. **Parameters were fixed while fitting the isotropic curves due to weak features and/or limited q-range.*

TABLE 5 | Impact of pre-delignification on CMF and enzymatic treatments.

Sample	Low-q	Mid-q		High-q
	P_1	R_g (nm)	P_2	EFs spacing (nm)
DW	3.5 ± 0.2*	10 ± 1.6	1.9 ± 0.2	16 ± 1.8*
DW-CMF-1	3.65 ± 0.1*	3.6 ± 0.4	2.8 ± 0.4	34 ± 4.6*
DW-CMF-2	3*	5.3 ± 0.4	2.7 ± 0.2	–
DW-LPMO	1.43 ± 0.1 (aligned) 3.1 ± 0.2 (amorphous)	4.5 ± 0.3	2.9 ± 0.2	41.6 ± 19*
DW-Ctect2-Htec2	3*	4.4 ± 0.5	2.8 ± 0.4	–
UW	3.9 ± 0.16*	–	–	4.66 ± 0.23*
UW-LPMO	4.11 ± 0.14*	16 ± 4.1	1.3 ± 0.08	4.88 ± 0.12*
UW-CTec2-Htec2	4.59 ± 0.39*	21 ± 4.8	1.5 ± 0.09	4.96 ± 0.11*

**Parameters were fitted using the anisotropic curve and fixed while fitting the amorphous curve.*

wood shavings, the EF values were fixed when fitting those curves (**Table 4**). We observed that the CMF treatment allowed the cloned LMPO and the commercial CAZyme treatment to further increase spacing of the EFs; however, because of the weak diffraction peak in the wood shaving samples, it remains unclear if decay by *G. trabeum* followed by enzyme treatment also permitted further increase in the EFs. After CMF treatment, LPMO activity demonstrated an equal or better treatment effect compared to that of the commercial CAZyme cocktail, but because comparison of different types of enzymes is difficult based solely on addition of similar amounts of protein, a direct comparison is not possible. These results are important because they show that a recombinant LPMO from a brown rot organism has similar capacity in wood deconstruction compared to commercial enzymes produced by other microorganisms. The findings are also unique in that supplemental enzymatic treatment is able to open the structure of the wood cell wall beyond the levels promoted by CMF treatment. It further suggests that cyclic CMF pretreatment integrated with enzymatic treatment, potentially at low dosages than typically used, may be a more effective way to open the structure of the wood cell wall in biorefinery applications, as opposed to single pretreatments followed by enzymatic treatment.

Impact of Pre-delignification on CMF and Enzymatic Treatments

Access of enzymes to wood components has been known to be limited by the presence of recalcitrant lignin. The data above suggest that CMF treatment, and potentially brown rot fungal action, can improve the efficiency of subsequent enzyme action on wood through modification and redistribution of the lignin. This is supported by the similarity of the mid-q scattering features, namely the characteristic size R_g and the power law exponent, measured in the CMF-treated samples and the PAA delignified wood samples (**Table 5**). In the current work, PAA treatment was also used as a reference pretreatment, and specifically for comparison to the ways that lignin was depolymerized/displaced by both the CMF treatment and/or by the enzymatic treatments (the later because of loss of cellulose). It should be noted that the Rg of unmodified Kraft lignin macromolecules in aqueous solution has been observed to be in the range of 40 nm (Sabaghi and Fatehi, 2019), which is similar to

the sizes of openings that we observed between elementary fibrils. Moreover, electron microscopy studies on thermochemically treated wood have shown the spacing between microfibrils (bundles of elementary fibrils) to be in the order of 20 nm (Ciesielski et al., 2013), which is similar to the elementary fibril spacing measured in our delignified wood samples. The removal of lignin using PAA was designed to help better distinguish the modes of attack, specifically on cellulose structure. It is conceivable that by delignifying the cell wall with PAA and also by depolymerization of lignin using the CMF treatment, that the regular packing of the elementary fibrils was altered because the constraints of the lignin matrix were removed. This change may have allowed us to observe the naturally polydisperse size of the cellulose microfibrils.

SUMMARY/CONCLUSION

In this research we explored the role that the CMF mechanism plays in the initial decay process by brown rot fungi, "opening up" the wood cell wall structure in advance of enzymatic action. We also explored any potential interaction between CMF constituents and a unique LPMO enzyme. The *G. trabeum*, brown rot LPMO was found to be upregulated early during initiation of brown rot decay, together with genes for a proposed pathway associated with the production of hydroquinones involved in the CMF mechanism.

SANS was used to assess changes in the size and spacing of the nanostructure of wood decayed by the *G. trabeum* and these data were compared to that from wood that was CMF-treated, or CMF-treated wood followed by treatment with either the early-upregulated LPMO or a commercial CAZyme cocktail. PAA delignification treatment, used as a reference, opened the structure of cellulose, and subsequent CMF treatment then further enhanced the effects of the PAA treatment to allow both the CAZyme cocktail and LPMO enzymes to then further increase the spacing between the elementary fibrils.

As expected, neither the LPMO nor the CAZyme cocktail produced structural changes in unmodified wood samples that had not been otherwise pretreated, and the cellulose microfibrils remained unaltered. The CMF treatment of unmodified wood produced neutron scattering patterns similar to that observed in the *G. trabeum* decayed wood, indicating that both brown rot decay and the CMF treatment enlarged the nanopore structure of wood cell walls to permit apparent enzyme access. Even after only a single pulse of CMF treatment, both the LPMO and the commercial CAZyme cocktail enzymes were able to penetrate the cell wall and further increase elementary fibril spacing. Further, our SANS data support that lignin was depolymerized, concurrent with cellulose elementary fibril deconstruction, by CMF action to allow cellulose elementary fibrils to separate, and the lignin was then re-deposited as nanoscale particles (nodules) as previously reported.

Our data suggest that CMF treatment resulted in the oxidation of accessible cellulose fibrils with a concomitant reduction in the size of their cellulose crystallites as attack progressed from the outer regions of cellulose microfibrils. This is similar, and consistent with, the previous scattering data for the pattern of attack observed in brown rotted wood and also similar to prior data on brown rotted wood generated by X-ray diffraction. Multiple pulses of CMF treatment with unmodified wood also produced a progressive increase in elementary fibril spacing, indicating erosion of the cellulose microfibrils by CMF oxidation.

This research confirms earlier work and suggests the potential for the early-upregulated LPMO enzyme from *G. trabeum* to work in association with early-stage CMF chemistry. We propose that *G. trabeum* may have adopted mechanisms to integrate non-enzymatic CMF chemistry and early-upregulated LPMO enzymatic chemistries together during initial stages of brown rot decay.

AUTHOR'S NOTE

A portion of this research required the use of Neutron scattering instrumentation, and was conducted at the Bio-SANS facility at the High Flux Isotope Reactor (HFIR Project #IPTS-13888); a DOE Office of Science User Facility operated by the Oak Ridge National Laboratory.

DATA AVAILABILITY STATEMENT

RNA-seq data for this article are deposited at: https://www.ncbi.nlm.nih.gov/geo/query/acc.cgi?acc=GSE108189. The data for the recombinant LPMO enzyme cloned from *Gloeophyllum trabeum* (GtLPMO9A-2) accession number LC157848, is deposited in the DDBJ database: https://www.ddbj.nig.ac.jp/index-e.html. The Small Angle Neutron Scattering (SANS) data can be accessed at: http://doi.org/10.5281/zenodo.3755828.

AUTHOR CONTRIBUTIONS

YZ, MY, JJ, and BG developed the experimental design for nanostructural analysis. YZ and MY performed the treatments and SANS analysis with SP and HO'N. BG conceptualized the research, obtained the research support, brought together the research team, and integrated the data analyses. JZ performed the gene expression analysis, metabolite pathway modeling and data workup for the gene expression work, and edited the manuscript. MY and YK provided the information to JZ on properties of the cloned LPMO. SP and HO'N facilitated use and set-up of the SANS beam line, and coordinated with YZ, NP, MY, and BG. NP and SP conducted the bulk of the SANS data analysis with support from YZ. YZ developed the initial draft, and with BG coordinated subsequent drafts. YK and MY provided the LPMO enzyme, input on LPMO use and the write-up on LPMOs. All team members contributed to the final data analysis and writing of the manuscript.

FUNDING

YZ appreciates support from the National Natural Science Foundation of China (No. 31890772). We also acknowledge support from the National Institute of Food and Agriculture, U.S. Department of Agriculture, the UMass Center for Agriculture, Food and the Environment under project number S1075 – MAS00503. The contents are solely the responsibility of the authors and do not necessarily represent the official views of the USDA or NIFA. MY and YK were supported by grant funding from JSPS KAKENHI 18H02252. DOE co-authors were funded by the DOE Office of Science, Office of Biological and Environmental Research under the Genomic Science Program (FWP ERKP752).

ACKNOWLEDGMENTS

We thank Novozymes Bioenergy for the gift of the Cellic® CTec2 and HTec2 – Enzymes.

REFERENCES

Arantes, V., and Goodell, B. (2014). "Current understanding of brown-rot fungal biodegradation mechanisms: a review," in *Deterioration and Protection of Sustainable Biomaterials*, eds T. P. Schultz, B. Goodell, and D. D. Nicholas (Washington, DC: American Chemical Society), 3–21. doi: 10.1021/bk-2014-1158.ch001

Arantes, V., Jellison, J., and Goodell, B. (2012). Peculiarities of brown-rot fungi and biochemical Fenton reaction with regard to their potential as a model for bioprocessing biomass. *Appl. Microbiol. Biotechnol.* 94, 323–338. doi: 10.1007/s00253-012-3954-y

Bailey, M. J. (1981). The effect of β-glucosidase on some assays for cellulolytic enzymes. *Biotechnol. Lett.* 3, 695–700. doi: 10.1007/bf00134846

Beaucage, G. (1996). Small-angle scattering from polymeric mass fractals of arbitrary mass-fractal dimension. *J. Appl. Crystallogr.* 29, 134–146. doi: 10.1107/s0021889895011605

Bissaro, B., Rohr, A. K., Muller, G., Chylenski, P., Skaugen, M., Forsberg, Z., et al. (2017). Oxidative cleavage of polysaccharides by monocopper enzymes depends on H2O2. *Nat. Chem. Biol.* 13, 1123–1128. doi: 10.1038/nchembio.2470

Chang, V. S., and Holtzapple, M. T. (2000). "Fundamental factors affecting biomass enzymatic reactivity," in *Proceedings of the Twenty-First Symposium On Biotechnology For Fuels And Chemicals*, Fort Collins.

Ciesielski, P. N., Matthews, J. F., Tucker, M. P., Beckham, G. T., Crowley, M. F., Himmel, M. E., et al. (2013). 3D electron tomography of pretreated biomass informs atomic modeling of cellulose microfibrils. *ACS Nano* 7, 8011–8019. doi: 10.1021/nn4031542

Cragg, S. M., Beckham, G. T., Bruce, N. C., Bugg, T. D. H., Distel, D. L., Dupree, P., et al. (2015). Lignocellulose degradation mechanisms across the Tree of Life. *Curr. Opin. Chem. Biol.* 29, 108–119. doi: 10.1016/j.cbpa.2015.10.018

Daniel, G. (2016). "Fungal degradation of wood cell walls," in *Secondary Xylem Biology; Origins, Functions, and Applications*, Chap. 8, eds Y. S. Kim, R. Funada, and A. P. Singh (Amsterdam: Elsevier).

Eastwood, D. C. (2014). "Evolution of fungal wood decay," in *Deterioration and Protection of Sustainable Biomaterials, ACS Symposium. Series*, eds T. P. Schultz, B. Goodell, and D. D. Nicholas (Washington, DC: Amercian Chemical Society), 93–112. doi: 10.1021/bk-2014-1158.ch005

Eastwood, D. C., Floudas, D., Binder, M., Majcherczyk, A., Schneider, P., Aerts, A., et al. (2011). The plant cell wall-decomposing machinery underlies the functional diversity of forest fungi. *Science* 333, 762–765.

Fernandes, A. N., Thomas, L. H., Altaner, C. M., Callow, P., Forsyth, V. T., Apperley, D. C., et al. (2011). Nanostructure of cellulose microfibrils in spruce wood. *Proc. Natl. Acad. Sci. U.S.A.* 108, E1195–E1203.

Floudas, D., Binder, M., Riley, R., Barry, K., Blanchette, R. A., Henrissat, B., et al. (2012). The Paleozoic origin of enzymatic lignin decomposition reconstructed from 31 fungal genomes. *Science* 336, 1715–1719.

Forsberg, Z., Sorlie, M., Petrovic, D., Courtade, G., Aachmann, F. L., Vaajekolstad, G., et al. (2019). Polysaccharide degradation by lytic polysaccharide monooxygenases. *Curr. Opin. Struct. Biol.* 59, 54–64.

Goodell, B. (2020). "Fungi Involved in the Biodeterioration and Bioconversion of lignocellulose substrates.(Chapter)," in *The Mycota Vol. II: Genetics and Biotechnology, 3rd edition (in press)*, eds J. P. Benz and K. Schipper (Cham: Springer).

Goodell, B., Jellison, J., Liu, J., Daniel, G., Paszczynski, A., Fekete, F., et al. (1997). Low molecular weight chelators and phenolic compounds isolated from wood decay fungi and their role in the fungal biodegradation of wood. *J. Biotechnol.* 53, 133–162. doi: 10.1016/s0168-1656(97)01681-7

Goodell, B., Nakamura, M., and Jellison, J. (2014). "The chelator mediated Fenton system in the brown rot fungi: details of the mechanims, and reasons why it has been ineffective as a biomimetic treatment in some biomass applications. A review," in *Proceedings: International Research Group on Wood Protection. IRG-WP*, St George, UT.

Goodell, B., Zhu, Y., Kim, S., Kafle, K., Eastwood, D. C., Daniel, G., et al. (2017). Modification of the nanostructure of lignocellulose cell walls via a non-enzymatic lignocellulose deconstruction system in brown rot wood-decay fungi. *Biotechnol. Biofuels* 10:179.

Hattori, T., Nishiyama, A., and Shimada, M. (1999). Induction of L-phenylalanine ammonia-lyase and suppression of veratryl alcohol biosynthesis by exogenously added L-phenylalanine in a white-rot fungus *Phanerochaete chrysosporium*. *FEMS Microbiol. Lett.* 179, 305–309. doi: 10.1016/s0378-1097(99)00427-9

Hibbett, D. S., and Donoghue, M. J. (2001). Analysis of character correlations among wood decay mechanisms, mating systems, and substrate ranges in homobasidiomycetes. *Syst. Biol.* 50, 215–242. doi: 10.1080/10635150151125879

Howell, C., Hastrup, A. C. S., Jara, R., Larsen, F. H., Goodell, B., and Jellison, J. (2011). Effects of hot water extraction and fungal decay on wood crystalline cellulose structure. *Cellulose* 18, 1179–1190. doi: 10.1007/s10570-011-9569-0

Ilavsky, J., and Jemian, P. R. (2009). Irena : tool suite for modeling and analysis of small-angle scattering. *J. Appl. Crystallogr.* 42, 347–353. doi: 10.1107/s0021889809002222

Jakob, H. F., Tschegg, S. E., and Fratzl, P. (1996). Hydration dependence of the wood-cell wall structure in picea abies. a small-angle X-ray scattering study. *Macromolecules* 29, 8435–8440. doi: 10.1021/ma9605661

Kaffenberger, J. T., and Schilling, J. S. (2013). Using a grass substrate to compare decay among two clades of brown rot fungi. *Appl. Microbiol. Biotechnol.* 97, 8831–8840. doi: 10.1007/s00253-013-5142-0

Kent, M. S., Zeng, J., Rader, N., Avina, I. C., and Sale, K. L. (2018). Efficient conversion of lignin into a water-soluble polymer by a chelator-mediated fenton reaction: optimization of H2O2 use and performance as a dispersant. *Green Chem.* 20, 3024–2037.

Kerem, Z., Jensen, K. A., and Hammel, K. E. (1999). Biodegradative mechanism of the brown rot basidiomycete *Gloeophyllum trabeum*: evidence for an extracellular hydroquinone-driven fenton reaction. *FEBS Lett.* 446, 49–54. doi: 10.1016/s0014-5793(99)00180-5

Kojima, Y., Varnai, A., Ishida, T., Sunagawa, N., Petrovic, D., Igarashi, K., et al. (2016). A lytic polysaccharide monooxygenase with broad xyloglucan specificity from the brown-rot fungus *Gloeophyllum trabeum* and its action on cellulose-xyloglucan complexes. *Appl. Environ. Microbiol.* 82, 6557–6572. doi: 10.1128/aem.01768-16

Krah, F. S., Bassler, C., Heibl, C., Soghigian, J., Schaefer, H., and Hibbett, D. S. (2018). Evolutionary dynamics of host specialization in wood-decay fungi. *BMC Evol. Biol.* 18:119. doi: 10.1186/s12862-018-1229-7

Lapadatescu, C., Ginies, C., Quere, J. L., and Bonnarme, P. (2000). Novel scheme for biosynthesis of aryl metabolites from L-phenylalanine in the fungus *Bjerkandera adusta*. *Appl. Environ. Microbiol.* 66, 1517–1522. doi: 10.1128/aem.66.4.1517-1522.2000

Liu, J., Zhu, Y., Wang, C., Goodell, B., and Esker, A. R. (2020). Chelator-mediated biomimetic degradation of cellulose and chitin. *Int. J. Biol. Macromol.* 153, 433–440. doi: 10.1016/j.ijbiomac.2020.02.262

Meganathan, R. (2001). Ubiquinone biosynthesis in microorganisms. *FEMS Microbiol. Lett.* 203, 131–139. doi: 10.1111/j.1574-6968.2001.tb10831.x

Muraleedharan, M. N., Zouraris, D., Karantonis, A., Topakas, E., Sandgren, M., Rova, U., et al. (2018). Effect of lignin fractions isolated from different biomass sources on cellulose oxidation by fungal lytic polysaccharide monooxygenases. *Biotechnol. Biofuels* 11, 1–15.

Paszczynski, A., Crawford, R., Funk, D., and Goodell, B. (1999). De novo synthesis of 4, 5-dimethoxycatechol and 2, 5-dimethoxyhydroquinone by the brown rot fungus *Gloeophyllum trabeum*. *Appl. Environ. Microbiol.* 65, 674–679. doi: 10.1128/aem.65.2.674-679.1999

Penttila, P. A., Rautkari, L., Osterberg, M., and Schweins, R. (2019). Small-angle scattering model for efficient characterization of wood nanostructure and moisture behaviour. *J. Appl. Crystallogr.* 52, 369–377. doi: 10.1107/s1600576719002012

Pingali, S. V., O'Neill, H. M., Nishiyama, Y., He, L., Melnichenko, Y. B., Urban, V., et al. (2014). Morphological changes in the cellulose and lignin components of biomass occur at different stages during steam pretreatment. *Cellulose* 21, 873–878. doi: 10.1007/s10570-013-0162-6

Plaza, N. Z., Pingali, S. V., Qian, S., Heller, W. T., and Jakes, J. E. (2016). Informing the improvement of forest products durability using small angle neutron scattering. *Cellulose* 23, 1593–1607. doi: 10.1007/s10570-016-0933-y

Presley, G. N., Ndimba, B. K., and Schilling, J. S. (2018). Brown rot-type fungal decomposition of sorghum bagasse: variable success and mechanistic implications. *Hindawi Intern. J. Microbiol.* 2018:4961726.

Presley, G. N., and Schilling, J. S. (2017). Distinct growth and secretome strategies for two taxonomically divergent brown rot fungi. *Appl. Environ. Microbiol.* 83:e02987-16.

Riley, R., Salamov, A. A., Brown, D. W., Nagy, L. G., Floudas, D., Held, B. W., et al. (2014). Extensive sampling of basidiomycete genomes demonstrates inadequacy of the white-rot/brown-rot paradigm for wood decay fungi. *Proc. Natl. Acad. Sci. U.S.A.* 111, 9923–9928. doi: 10.1073/pnas.1400592111

Sabaghi, S., and Fatehi, P. (2019). Phenomenological changes in lignin following polymerization and its effects on flocculating clay particles. *Biomacromolecules* 20, 3940–3951. doi: 10.1021/acs.biomac.9b01016

Tamaru, Y., Yoshida, M., Eltis, L. D., and Goodell, B. (2019). Multiple iron reduction by methoxylated phenolic lignin structures and the generation of reactive oxygen species by lignocellulose surfaces. *Intern. J. Biol. Macromol.* 128, 340–346. doi: 10.1016/j.ijbiomac.2019.01.149

Thomas, L. H., Forsyth, V. T., Martel, A., Grillo, I., Altaner, C. M., and Jarvis, M. C. (2014). Structure and spacing of cellulose microfibrils in woody cell walls of dicots. *Cellulose* 21, 3887–3895. doi: 10.1007/s10570-014-0431-z

Varela, E., and Tien, M. (2003). Effect of pH and oxalate on hydroquinone-derived hydroxyl radical formation during brown rot wood degradation. *Appl. Environ. Microbiol.* 69, 6025–6031. doi: 10.1128/aem.69.10.6025-6031.2003

Vermaas, J. V., Dellon, L. D., Broadbelt, L. J., Beckham, G. T., and Crowley, M. F. (2019). Automated transformation of lignin topologies into atomic structures with lignin builder. *ACS Sustain. Chem. Eng.* 7, 3443–3453. doi: 10.1021/acssuschemeng.8b05665

Yang, C., Wang, D., and Tang, Q. (2014). Pretreatment of furfural industrial wastewater by Fenton, electro-Fenton and Fe(II)-activated peroxydisulfate processes: a comparative study. *Water Sci. Technol.* 70, 414–421. doi: 10.2166/wst.2014.242

Yang, M., Jin, C., Shuang, E., Liu, J., Zhang, S., Liu, Q., et al. (2019). Fenton reaction-modified corn stover to produce value-added chemicals by ultralow enzyme hydrolysis and maleic acid and aluminum chloride catalytic conversion. *Energy Fuels* 33, 6429–6435. doi: 10.1021/acs.energyfuels.9b00983

Zhang, J., Presley, G. N., Hammel, K. E., Ryu, J.-S., Menke, J. R., Figueroa, M., et al. (2016). Localizing gene regulation reveals a staggered wood decay mechanism for the brown rot fungus *Postia placenta*. *Proc. Natl. Acad. Sci. U.S.A.* 113, 10968–10973. doi: 10.1073/pnas.1608454113

Zhang, J., Silverstein, K. A. T., Castano, J. D., Figueroa, M., and Schilling, J. S. (2019). Gene regulation shifts shed light on fungal adaption in plant biomass decomposers. *mBio* 10:e2176-19.

Conflict of Interest: The authors declare that the research was conducted in the absence of any commercial or financial relationships that could be construed as a potential conflict of interest.

frontiers in Microbiology

ORIGINAL RESEARCH
published: 14 July 2020
doi: 10.3389/fmicb.2020.01633

Improved Production of Majority Cellulases in *Trichoderma reesei* by Integration of *cbh1* Gene From *Chaetomium thermophilum*

Xianzhang Jiang[1†], Jiawen Du[1†], Ruonan He[1], Zhengying Zhang[1], Feng Qi[1], Jianzhong Huang[1] and Lina Qin[1,2]**

[1] National Joint Engineering Research Center of Industrial Microbiology and Fermentation Technology, College of Life Sciences, Fujian Normal University, Fuzhou, China, [2] Provincial University Key Laboratory of Cellular Stress Response and Metabolic Regulation, College of Life Sciences, Fujian Normal University, Fuzhou, China

OPEN ACCESS

Edited by:
Jiwei Zhang,
University of Minnesota, Twin Cities, United States

Reviewed by:
Xu Fang,
Shandong University, China
Hao Fang,
Northwest A&F University, China
Gen Zou,
Shanghai Academy of Agricultural Sciences, China

***Correspondence:**
Jianzhong Huang
hjz@fjnu.edu.cn
Lina Qin
qinln@fjnu.edu.cn

† These authors have contributed equally to this work

Specialty section:
This article was submitted to Fungi and Their Interactions, a section of the journal Frontiers in Microbiology

Received: *14 March 2020*
Accepted: *23 June 2020*
Published: *14 July 2020*

Citation:
Jiang X, Du J, He R, Zhang Z, Qi F, Huang J and Qin L (2020) Improved Production of Majority Cellulases in Trichoderma reesei by Integration of cbh1 Gene From Chaetomium thermophilum. Front. Microbiol. 11:1633. doi: 10.3389/fmicb.2020.01633

Lignocellulose is an abundant waste resource and has been considered as a promising material for production of biofuels or other valuable bio-products. Currently, one of the major bottlenecks in the economic utilization of lignocellulosic materials is the cost-efficiency of converting lignocellulose into soluble sugars for fermentation. One way to address this problem is to seek superior lignocellulose degradation enzymes or further improve current production yields of lignocellulases. In the present study, the lignocellulose degradation capacity of a thermophilic fungus *Chaetomium thermophilum* was firstly evaluated and compared to that of the biotechnological workhorse *Trichoderma reesei.* The data demonstrated that compared to *T. reesei, C. thermophilum* displayed substantially higher cellulose-utilizing efficiency with relatively lower production of cellulases, indicating that better cellulases might exist in *C. thermophilum*. Comparison of the protein secretome between *C. thermophilum* and *T. reesei* showed that the secreted protein categories were quite different in these two species. In addition, to prove that cellulases in *C. thermophilum* had better enzymatic properties, the major cellulase cellobiohydrolase I (CBH1) from *C. thermophilum* and *T. reesei* were firstly characterized, respectively. The data showed that the specific activity of *C. thermophilum* CBH1 was about 4.5-fold higher than *T. reesei* CBH1 in a wide range of temperatures and pH. To explore whether increasing CBH1 activity in *T. reesei* could contribute to improving the overall cellulose-utilizing efficiency of *T. reesei*, *T. reesei cbh1* gene was replaced with *C. thermophilum cbh1* gene by integration of *C. thermophilum cbh1* gene into *T. reesei cbh1* gene locus. The data surprisingly showed that this gene replacement not only increased the cellobiohydrolase activities by around 4.1-fold, but also resulted in stronger induction of other cellulases genes, which caused the filter paper activities, Azo-CMC activities and β-glucosidase activities increased by about 2.2, 1.9, and 2.3-fold, respectively. The study here not only provided new resources of superior cellulases genes and new strategy to improve the cellulase production in *T. reesei,* but also contribute to opening the path for fundamental research on *C. thermophilum.*

Keywords: *Trichoderma reesei*, thermophilic fungi, *Chaetomium thermophilum*, cellobiohydrolase I, lignocellulase, biomass, cellulase

INTRODUCTION

Plant biomass from agriculture and forestry is one of the most abundant resources on the earth and it has been considered as a promising material for producing renewable biofuels and other value-added bio-products (Himmel et al., 2007). One of the bottlenecks of this process is the enzymatic degradation of biomass-derived polysaccharides. Currently, the filamentous fungi *Trichoderma*, *Aspergillus,* and *Penicillium* species are the most commonly used producer for lignocellulases in industry (Kubicek et al., 2014). However, the optimum temperature of enzymes from these species is normally from 30 to 50°C at which the efficiency of biomass polysaccharides saccharification is very low. Many thermophilic fungi can secrete thermostable biomass-degrading enzymes including lignocellulases, proteases, amylases, laccases, chitinases, lipases, and esterases, which holds a great promise in industrial applications (DeCastro et al., 2016). However, due to the lack of genetic tools for strain engineering in thermophilic species, progress toward the improvement of their enzyme production has been hampered. One way to overcome these drawbacks is the introduction of lignocellulases encoding genes from thermophilic fungi into mesophilic species, in which a variety of genetic tools have been developed, to combine the advantages of mesophilic and thermophilic properties.

The soft-rot fungus *Trichoderma reesei* is a model organism for plant biomass degradation and widely used in industry for the production of cellulases and xylanases due to the large capacity of hydrolytic enzymes secretion (Bischof et al., 2016). After rounds of random mutagenesis, several industrial strains can secrete lignocellulases over 100 g/L culture (Cherry and Fidantsef, 2003). Besides its large protein secretion capacity, *T. reesei* naturally has the ability to form disulfide bonds and to glycosylate proteins (Singh et al., 2015). In addition, *T. reesei* can grow on inexpensive substrate such as lignocellulosic waste materials and many secreted enzymes from *T. reesei* are under the GRAS status (Generally Recognized as Safe) (Sewalt et al., 2016). These properties have promoted efforts to develop *T. reesei* as an excellent host for production of lignocellulases and recombinant proteins. Many studies have shown that the lignocellulose degradation ability could be improved by recombinant expression of biomass degrading enzymes from different organisms in *T. reesei* (Zhang et al., 2010; Dashtban and Qin, 2012; Treebupachatsakul et al., 2015).

Chaetomium thermophilum, an ascomycete thermophilic species, commonly exists in the heating phase of composts with an optimum growth temperature around 50°C (Kellner et al., 2016). The release of *C. thermophilum* genome database (Bock et al., 2014) and several biotechnological studies indicate that there are valuable biomass degradation associated enzymes existed in *C. thermophilum* (Voutilainen et al., 2008; Li et al., 2010). However, the secreted enzyme components and their properties in *C. thermophilum* have been rarely studied. In the present study, the capability of lignocellulose degradation of *C. thermophilum* was evaluated and compared to that of *T. reesei*. Besides, the enzyme properties of the major cellulase cellobiohydrolase I (CBH1) from *T. reesei* and *C. thermophilum* were compared. Moreover, to explore whether increasing CBH1 activities in *T. reesei* cellulases complex could contribute to improving the cellulose degradation efficiency, the native *T. reesei cbh1* gene was replaced with *C. thermophilum cbh1* gene in *T. reesei*. The CBH activities, filter paper activities, endoglucanases activities, and β-glucosidase activities, along with the transcriptional levels of several cellulases genes including *eg1*, *eg2*, *cbh2*, and *bgl1*, as well as the transcriptional factors (TFs) *xyr1*, *cre1*, and *ace3* of the resultant strains have been investigated. This study may provide a new resource of superior cellulases genes and a new strategy to improve the efficiency of biomass saccharification by *T. reesei*.

Abbreviations: ATCC, American type culture collection; CBH1, cellobiohydrolase I gene; CGMCC, China general microbiological culture collection center; FDR, false discovery rate; FPA, filter paper assay; HPAEC-PAD, ultra-high performance liquid chromatography coupled tandem mass spectroscopy; MM, minimal medium; pNPG, 4-nitrophenyl -D-glucopyranoside; SD, standard deviation; TFs, transcriptional factors; UPLC-MS/MS, ultra-high performance liquid chromatography coupled tandem mass spectroscopy; VMM, Vogel's minimal medium; YPD, media containing 1% yeast extract, 2% peptone, 1% dextrose.

MATERIALS AND METHODS

Microbial Strains and Growth Conditions

Escherichia coli Trans1-T1 used for recombinant plasmid construction was bought from TransGen Biotech. *T. reesei* Tu6 strain (ATCC MYA-256) was used as control to evaluate lignocellulose degradation efficiency of *C. thermophilum*. *T. reesei* Tu6Δ*ku70* strain used as host strain to construct indicated recombinant strains was kindly provided by Dr. Monika Schmoll (AIT Austrian Institute of Technology, Austria). *T. reesei* strains Tr-cT*cbh1*, Tr-cC*cbh1*, and Tr-Ct*cbh1* were constructed in this study and described below. *C. thermophilum* (CGMCC 3.17990) was provided by China general microbiological culture collection center. *T. reesei* strains were grown for 5 to 6 days at 28°C on potato dextrose agar plates (PDA) or PDA supplemented with 5 mM uridine when necessary. Minimal medium (Penttilä et al., 1987) was applied as a selective medium for the screening of *T. reesei* transformants. *C. thermophilum* strain was grown for 5–7 days at 50°C on PDA slants.

For protein secretion and enzyme activities analysis, *T. reesei* conidia were firstly inoculated into 100 mL liquid minimal medium with 2% glucose as the carbon source (MM+2% glucose) at 10^6 conidia/mL and grown at 28°C on a rotary shaker for 48 h at 200 rpm, the mycelia were then filtered through 200 mesh sifter (30 μm pore diameter) and washed twice with carbon-free medium. About 2.2 g of this wet mycelia was added into 50 mL of fresh cellulase-inducing minimal medium in which 2% glucose (w/v) was substituted with 2% Avicel or 2% sugarcane bagasse and grown at 200 rpm at 28°C in consistent dark. For analysis of *C. thermophilum*, 7 days of *C. thermophilum* culture grown on a slant (18 mm × 180 mm) was scraped and first inoculated into *Neurospora* Vogel's minimal medium (VMM) (Vogel, 1956) with 2% glucose as carbon source and grown at 50°C on a rotary shaker (200 rpm) for 36 h. The cultures were then filtered and about 2.2 g of the wet mycelia was respectively transferred into 50 mL VMM media with 2% Avicel or 2% sugarcane bagasse as

carbon source and grown at 50°C on a rotary shaker (200 rpm) for indicated time in the natural light.

Transformation of *T. reesei* Strains by Electroporation

The electroporation transformation method was based on the protocol described in Schuster et al. (2012) with some optimization. In brief, fresh *T. reesei* conidia (within 7 days) grown on a 90 mm agar plate was harvested and washed three times using 1.1 M ice cold sorbitol to make conidia suspension at the concentration of 10^8 conidia/mL. A total of 1–2 μg of transformed DNA in a final volume of 10 and 90 μL of sorbitol washed conidia suspension was put into pre-chilled electroporation cassette. Gene Pulser Xcell electroporation system (Bio-Rad, United States) was used for electroporation with the set of 1.6 kV, 600 Ω, 25 μF. After electroporation, 900 μL of 1.1 M icy cold sorbitol was immediately added into the electroporation reaction mix before transferring into 9 mL of YPD (1% yeast extract, 2% peptone, 1% dextrose). The whole mixture was incubated for 12 h at 30°C and centrifuged at 2000 × g for 5 min. The electroporated conidia were re-suspended in 500 μL of YPD and added with 14 mL of top MM agar media. The whole mixture was spread over 2–3 bottom MM agar plates and incubated at 30°C for 5–7 days.

Construction of *T. reesei* Recombinant Strains

C*pyr4* series strains were constructed by transforming strain Tu6Δ*ku70* with plasmid pSK-*pyr4* (Qin et al., 2012).

Tr-cT*cbh1* was constructed by transforming strain Tu6Δ*ku70* with a DNA fragment including *pyr4* gene expression cassette and cDNA1 promoter (936 bp upstream of the start codon of cDNA1 gene) flanked with 2 kb upstream of *cbh1* promoter (1.5 kb upstream of the start codon of *cbh1* gene) and 2 kb downstream of *cbh1* promoter. The plasmid pTrcT*cbh1* used for generating Tr-cT*cbh1* transformants was constructed by ligation of the above fragments into a backbone from plasmid pBluescript SK (+). The primer pair pTrcT*cbh1*-F1F/R was used for amplifying 2 kb fragment of the upstream of *cbh1* promoter. The primer pair pTrcT*cbh1*-F2F/R was used to amplify the *pyr4* gene expression cassette. The primer pair pTrcT*cbh1*-F3F/R was used for amplifying cDNA1 promoter. The primer pair pTrcT*cbh1*-F4F/R was used for amplifying 2 kb downstream of *cbh1* promoter. The primer pair pTrcT*cbh1*-F5F/R was used for amplifying the vector backbone from plasmid pBluescript SK (+).

Tr-cC*cbh1* strain was generated by transforming strain Tu6Δ*ku70* with a fragment containing the expression cassette of *pyr4* gene, cDNA1 promoter and cDNA sequence of *C. thermophilum cbh1* gene (Accession No: AM711862.1), flanked with 2 kb upstream of the *cbh1* promoter and 2 kb downstream of *T. reesei cbh1* gene (Accession No: XM_006969162). The plasmid pTrcC*cbh1* used for generating Tr-cC*cbh1* transformants was constructed by ligation of the fragments of cDNA sequence of *C. thermophilum cbh1* gene and 2 kb downstream of *T. reesei cbh1* gene into the vector backbone from the plasmid pTrcT*cbh1*. The primer pair pTrcC*cbh1*-F1F/R was used for amplifying cDNA sequence of *C. thermophilum cbh1* gene. The primer pair pTrcC*cbh1*-F2F/R was used for amplifying the fragment of 2 kb downstream of *T. reesei cbh1* gene. The primer pair pTrcC*cbh1*-F3F/R was used for amplifying the vector backbone which included 2 kb fragment of the upstream of *cbh1* promoter, *pyr4* gene expression cassette, and cDNA1 promoter.

Tr-Ct*cbh1* was created by co-transforming strain Tu6Δ*ku70* with linearized plasmid pSK-*pyr4* (Qin et al., 2018) and a fragment including cDNA sequence of *C. thermophilum cbh1* gene, flanked with 2 kb upstream and downstream of *T. reesei cbh1* gene. The plasmid pTrCt*cbh1* used for generating Tr-Ct*cbh1* transformants was constructed by ligation of 2 kb upstream of *T. reesei cbh1* gene and cDNA sequence of *C. thermophilum cbh1* gene into the vector backbone from plasmid pTrcC*cbh1*. The primer pair pTrCt*cbh1*-F1F/R was used for amplifying 2 kb upstream of *T. reesei cbh1* gene. The primer pair pTrCt*cbh1*-F2F/R was used for amplifying cDNA sequence of *C. thermophilum cbh1* gene. The primer pair pTrCt*cbh1*-F3F/R was used for amplifying the vector backbone from plasmid pTrcC*cbh1* which included 2 kb downstream of *T. reesei cbh1* gene.

All types of transformants were selected on minimal media without adding uridine and tested for genotypes by diagnostic PCR. The sequence of all the primers used in this study was listed in the **Supplementary Table S1**.

Determination of Biomass in Culture Including Insoluble Cellulose

As described before (Stappler et al., 2017), the abundance of biomass accumulation in the culture containing insoluble cellulose was determined by the measurement of the intracellular protein concentration of mycelia. The mycelia in culture were filtered using a vacuum filter system and added 1 mL 0.1 M NaOH and lysed using a mini-bead beater (Biospec Products, Bartlesville, OK, United States) with 0.5 mm diameter glass beads. The mixture was incubated for 1 h at room temperature and centrifuged for 5 min at 12,000 rpm and the supernatants were transferred to new tubes. The protein concentration in the supernatants was measured by using the Bradford Protein Assay.

Protein Concentration and Enzyme Activities

Protein concentration in supernatants of all cultures was determined by Bradford method by following the instruction (Bio-Rad Protein Assay). Cellobiohydrolase (CBH) activities of Tr-cT*cbh1*, Tr-cC*cbh1*, and C*pyr4* series strains under glucose were measured using 1 mM soluble 4-methylumbelliferyl-b-D-cellobiose (MUC, Sigma) as a substrate following methods described in Wu et al. (2017). In brief, 10 μL of culture supernatant and 40 μL of 1 mM MUC in 50 mM sodium acetate buffer (pH 5) were incubated together at 50°C for 15 min by using thermocycler. After 15 min, the temperature was raised to 95°C for 5 min to deactivate the enzyme. After cooling down to room temperature, the fluorescence was measured at 445 nm with excitation with 365 nm. CBH activities of Tr-Ct*cbh1* and C*pyr4* series strains under cellulose were measured using the same substrate, but the method was as described as in Bailey and Tähtiharju (2003). CBH1 activity was calculated by subtraction

of β-glucosidase and endoglucanase activity. One unit of CBH activity was defined as the amount of enzyme necessary to release 1 μmol methyl umbelliferone in one minute. The total cellulase activities in the supernatants were measured by filter paper activity using Whatman No. 1 filter paper as the substrate (Ghose, 1987). Endoglucanase activity was determined by using azo-carboxymethyl cellulose (Azo-CM-Cellulose; Megazyme) as the substrate and following the manufacturer's specifications. β-glucosidase activity was measured by using 4-nitrophenyl -D-glucopyranoside (pNPG) as the substrate and following the method described in Tian et al. (2009). In brief, 50 μL of 10 × diluted culture supernatant was added into 200 μL of 500 μM pNPG in 50 mM sodium acetate buffer, pH 5.0. The mixture was incubated at 50°C for 10 min and terminated by adding 750 μL of 1 M Na_2CO_3. After cooling down to room temperature, the absorbance at 400 nm was measured. One unit of β-glucosidase activity was defined as the amount of enzyme necessary to release 1 μmol p-nitrophenol in 1 min.

Optimal pH and Temperature Analysis of the Recombinant CBH1

The optimum pH was determined by measuring the enzyme activities using Glycine-HCl (pH 2.0–3.0, 50 mM), Citric buffer (pH 3.0–6.0, 50 mM), phosphate buffer (pH 6.0–8.0, 200 mM) and Glycine-NaOH (pH 9.0–10.0, 50 mM) at 50°C. A total of 25 μL of filtered culture supernatant was added into 75 μL of the each of the above buffers with 1 mM MUC as substrate and incubated at 50°C for 1 h and then transferred to 95°C for 5 min to deactivate the enzyme. The enzyme activities were calculated by the absorbance under 445 nm emission and 365 nm excitation after incubation. The pH stability was assayed by incubating the enzyme at different pH range from pH 2.0–9.0 for 2 h at room temperature. Then the samples were diluted 10-fold in 50 mM citric buffer, pH 4.0 before measuring the residual activity. The optimum temperature of recombinant CBH1 was determined between 20 and 80°C in 50 mM citric buffer, pH 4.0. Thermal stability was investigated by incubating the enzyme at a different temperature ranging from 20 to 80°C for 30 min in 50 mM citric buffer, pH 4.0. The remaining activities were measured under standard conditions.

Secretory Protein Analysis by Liquid Chromatography-Mass Spectrometry

The supernatants of 120 h of *C. thermophilum* and *T. reesei* culture under Avicel were used to run SDS-PAGE firstly. The SDS-PAGE gels were subsequently cut and digested by trypsin and then analyzed using an EASY-nLC 1000 liquid chromatograph which was connected in line with an Orbitrap Fusion Tribrid mass spectrometer equipped with a nanoelectrospray ionization (nanoESI) source (Thermo Fisher Scientific, Waltham, MA, United States). The peptides were loaded onto a trap column (C18, 5 μm particles, 100 μm ID, 3 cm length, Dr. Maisch GmbH) and separated using an analytical column (C18, 3 μm particles, 75 μm ID, 15 cm length, Dr. Maisch GmbH) at a flow rate of 400 nL/min with a 60 min LC gradient composed of Solvent A [0.1% formic acid (v/v)] and Solvent B [acetonitrile, 0.1% formic acid (v/v)]. The gradient was 3–8% B for 3 min, 8–23% B for 45 min, 23–35% B for 9 min, 35–80% B for 2 min, and finally 80% B for 1 min. Full-scan mass spectra were acquired in the positive-ion mode over the m/z range from 350 to 1550 using the Orbitrap mass analyzer in profile format with a mass resolution setting of 120,000. In the data-dependent mode, the top-speed mode was selected with the most intense ions exceeding an intensity threshold of 5000 counts from each full-scan mass spectrum for tandem mass spectrometry (MS/MS) analysis using HCD activation type with 33% collision energy. MS/MS spectra were acquired in centroid format using an ion trap detector. Real-time charge state screening was enabled to exclude unassigned and 1+ charge states from MS/MS analysis. The exclusion duration in dynamic exclusion was set as 20 s. Raw data were searched against the amino acid sequences of *T. reesei* or *C. thermophilum* using Mascot software (version 2.5).

HPAEC-PAD Analysis of Released Glucose and Cellobiose From Filter Paper

A total of 500 μL of appropriately diluted hydrolysates from filter paper was analyzed on a Thermo Scientific Dionex ICS-5000 high-performance liquid chromatography (Dionex Corporation, Sunnyvale, CA, United States) instrument equipped with a CarboPac PA100 guard column (4 × 50 mm) and an analytical column (4 × 250 mm) with a flow rate as 1 mL/min at 22°C. The samples were resolved in a mobile phase of 100 mM NaOH. Glucose and cellobiose were used as standards.

Quantitative RT-PCR Analysis

An aliquot of 2 × 10^6 mL of *T. reesei* conidia were first inoculated into 100 mL MM+2% glucose media and grown at 28°C on a rotary shaker for 48 h at 200 rpm, the mycelia were then filtered through 200 mesh sifter (30 μm pore diameter) and washed twice with carbon-free MM media. A total of 2.2 g of the filtered wet mycelia were transferred to MM+1% Avicel medium and cultured at 28°C in the constant dark at 200 rpm for 48 h. Biological triplicates were prepared for each strain. Total RNA was isolated from samples taken at 12, 24, and 48 h of shift using zirconia/silica beads and a Mini-Beadbeater with 1 mL TRIzol reagent (from Invitrogen). RNA purification and DNase I treatment were performed using Easy Pure RNA Purification Kit (from TransGen Biotech). qRT-PCR was performed using TransScript Green One-Step qRT-PCR SuperMixKit (from TransGen Biotech) on the LightCycler 96 instrument (from Roche Life Science). Primer sequences used for amplification are described in **Supplementary Table S1**. The relative transcriptional levels of the tested genes were normalized to the expression level of the actin gene and calculated by $2^{-\Delta Ct}$ as a relative expression level.

Statistical Significance Tests

For all the experiments, three biologically replicated strains and three technical replicates for each strain were set for statistical analysis. Statistical significance was determined by *t*-test analysis by the false discovery rate (FDR) approach by using the Prism GraphPad software.

RESULTS

Chaetomium thermophilum Displayed Greater Lignocellulose Utilization Ability Compared to *T. reesei*

To search for thermophilic lignocellulases with outstanding enzyme properties, the cellulose degradation capacity of the thermophilic fungus *C. thermophilum* was evaluated and compared to that of *T. reesei*. To alleviate potential effects caused by differential spore germination efficiency, *C. thermophilum* CGMCC 3.17990 and *T. reesei* strain Tu6 were firstly grown in medium containing glucose as the sole carbon source and the same amount of wet mycelia (about 2.2 g) were then transferred into medium containing Avicel or sugarcane bagasse as the carbon source. The biomass accumulation, the extracellular protein concentration, and the filter paper activities in the supernatant were measured at different time points. The abundance of biomass accumulation in the culture containing insoluble carbon source Avicel or sugarcane was determined by the measurement of the intracellular protein concentration of mycelia.

The data shown in **Figure 1A** demonstrated that the biomass accumulation in *C. thermophilum* was significantly faster than

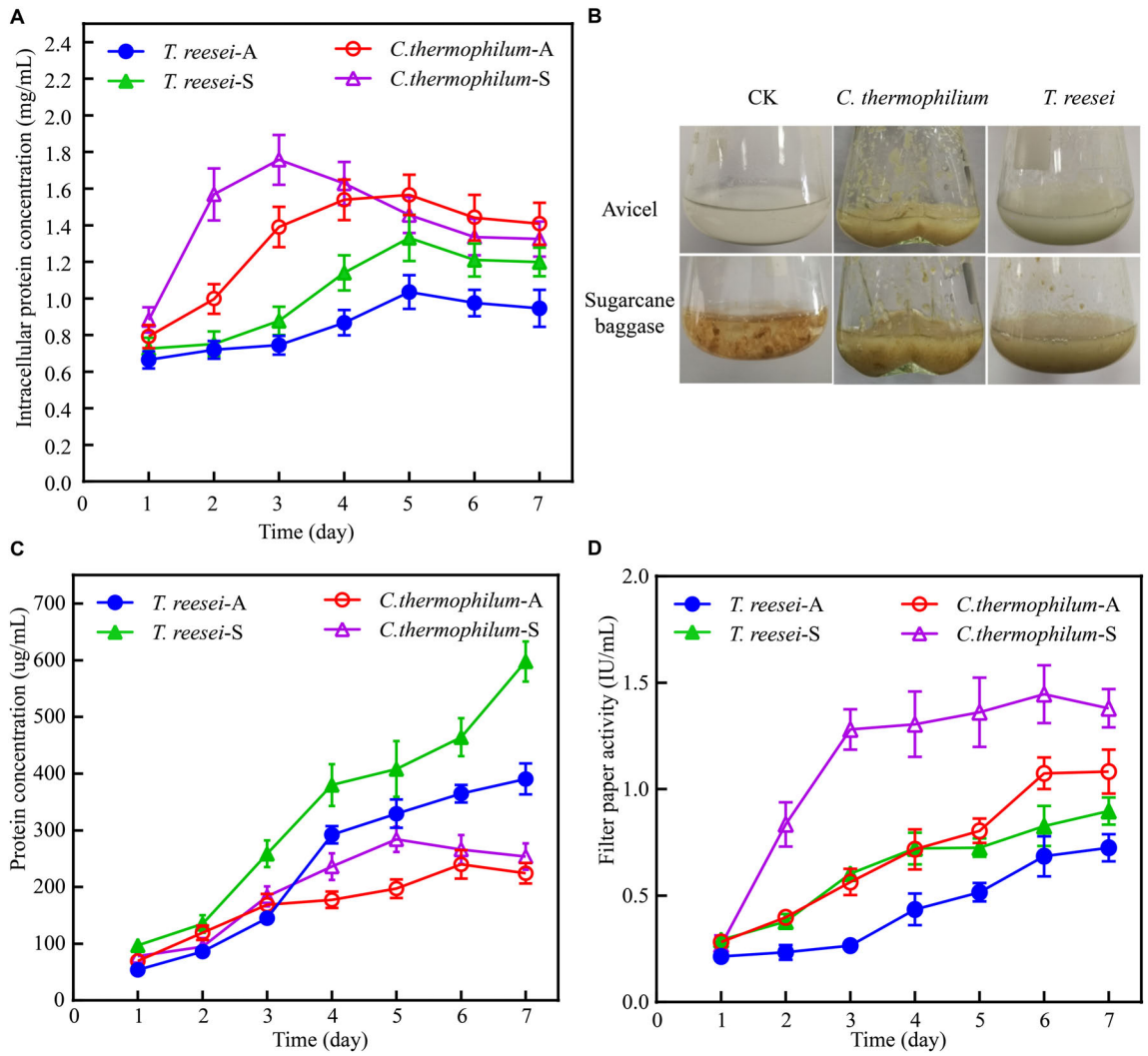

FIGURE 1 | Phenotypic analysis of *C. thermophilum* and *T. reesei* when response to cellulose. **(A)** The intracellular protein concentration of *C. thermophilum* and *T. reesei* mycelia collected from the culture under Avicel or sugarcane bagasse after transferring from the glucose culture. **(B)** Growth phenotype of *C. thermophilum* and *T. reesei* under Avicel or sugarcane bagasse. About 2.2 g wet mycelia of *C. thermophilum* and *T. reesei* were collected and transferred into Avicel or sugarcane bagasse media from glucose contained media and cultivated for 48 h. **(C)** Total secreted protein levels in the supernatants of *C. thermophilum* and *T. reesei* in Avicel or sugarcane bagasse media at different time points. **(D)** Filter paper activities of the supernatants of *C. thermophilum* and *T. reesei* in Avicel or sugarcane bagasse media at different time points. Shown in **(A,C,D)** are the mean values of three biological replicates. Error bars show the standard deviations between these replicates. *T. reesei*-A, *T. reesei*-S, *C. thermophilum*-A, and *C. thermophilum*-S respectively indicates *T. reesei* grown on Avicel (A) or sugarcane bassage (S) and *C. thermophilum* grown on Avicel (A) or sugarcane bassage (S). Shown in **(B)** is one of the three represents.

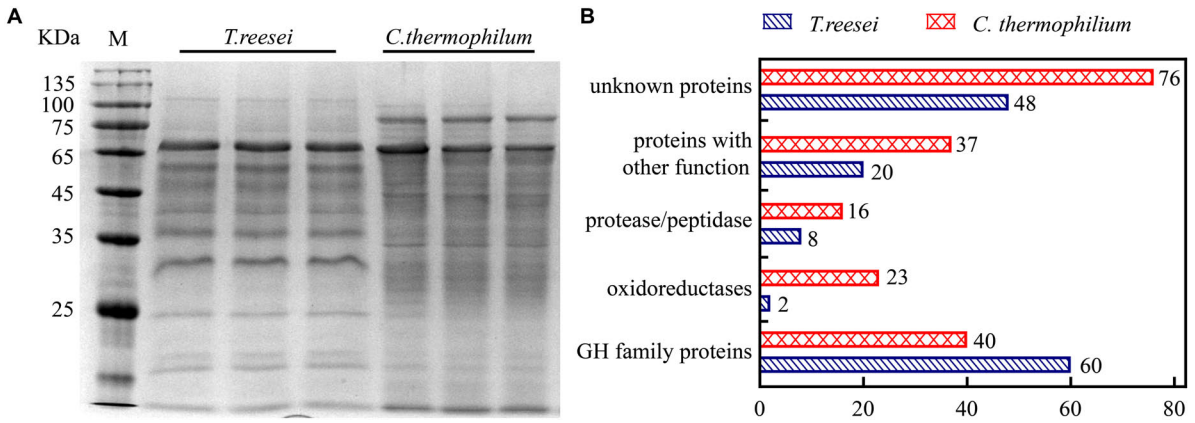

FIGURE 2 | The extracellular protein categories in the supernatants of cellulose cultures were different between *C. thermophilum* and *T. reesei*. **(A)** SDS-PAGE analysis of the secreted proteins in the supernatant of *C. thermophilum* and *T. reesei* in 120-h Avicel cultures after transferring from glucose cultures. **(B)** Major protein categories of the secretome of *C. thermophilum* and *T. reesei* under Avicel. The data was collected by UPLC-MS/MS analysis and the detailed information was listed in **Supplementary Tables S2–S7**.

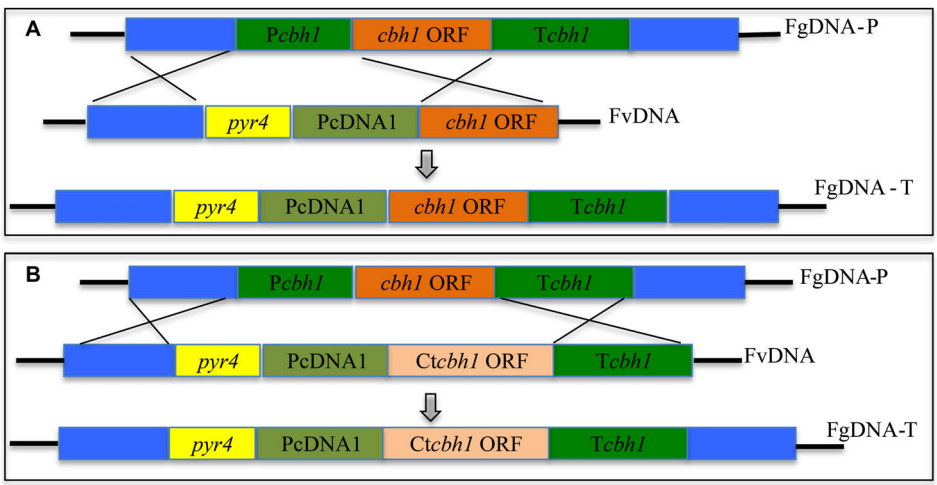

FIGURE 3 | Expression of Tr-CBH1 and Ct-CBH1 in *T. reesei* using cellulase-free background system. **(A)** Schematic diagram of the construction of recombinant strain Tr-c*Tcbh1*. **(B)** Schematic diagram of the construction of recombinant strain Tr-c*Cctbh1*. FgDNA-P indicates fragments in the parental strain. FvDNA indicates Fragment from plasmid vector constructed for the generation of the indicated recombinant strain. FgDNA-T indicates DNA fragments in the generated transformant strain.

that in *T. reesei* under both Avicel and sugarcane bagasse. Under 48 h of the after-transferring culture, *C. thermophilum* showed obvious growth phenotype under both Avicel and sugarcane bagasse compared to *T. reesei* (**Figure 1B**), suggesting higher utilization efficiency of cellulose materials in *C. thermophilum* relative to that in *T. reesei*. Further analysis of the extracellular protein levels (**Figure 1C**) in the culture supernatants of *C. thermophilum* and *T. reesei* showed that under Avicel, the levels of secreted proteins in *C. thermophilum* were slightly higher than that in *T. reesei* in the first 3 days. However, after 3 days, the extracellular protein levels in *T. reesei* were significantly higher than those in *C. thermophilum*. Under sugarcane bagasse, the extracellular protein levels in *T. reesei* were higher than that in *C. thermophilum* in all the tested time points and similar to the observed phenotype under Avicel, the difference of secreted protein levels between *C. thermophilum* and *T. reesei* significantly enlarged after 3 days. These data suggested that the secreted protein levels in the supernatants of *C. thermophilum* were considerably less than those in *T. reesei* when response to both Avicel and sugarcane bagasse. However, analysis of the filter paper activities in the culture supernatants (**Figure 1D**) showed that consistent with the growth phenotype, *C. thermophilum* exhibited significantly higher filter paper activities compared to *T. reesei* in all the tested time points and under both celluloses carbon sources. This observed phenomenon indicated that *C. thermophilum* might contain cellulases with better specific activities or have better enzyme complex system for cellulose degradation.

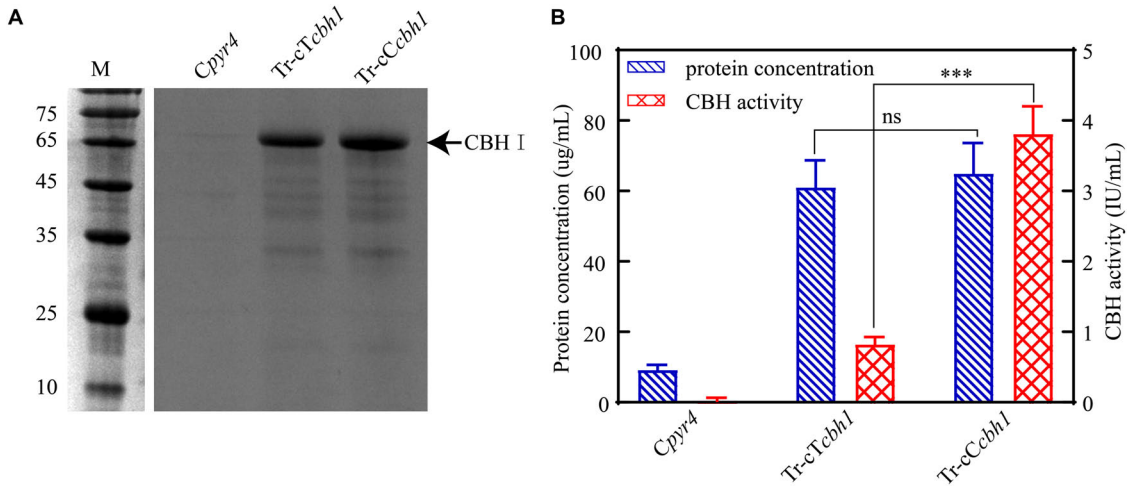

FIGURE 4 | Ct-CBH1 showed higher specific activity compared to Tr-CBH1. **(A)** SDS-PAGE analysis of the secreted proteins in the supernatant of the recombinant *T. reesei* strains C*pyr4*, Tr-cT*cbh1*, and Tr-cC*cbh1*. A suspension of 10^6 conidia/mL was inoculated into MM media with glucose as the only carbon source and cultivated for 48 h. A total of 20 μL of the supernatant was used for SDS-PAGE analysis. **(B)** Total secreted protein levels and CBH activities in the supernatants of the indicated *T. reesei* strains. The samples used in **(B)** were as same as in **(A)**. Shown are the mean values of three biological replicates. Error bars show the standard deviations between these replicates. The significance of differences between Tr-cT*cbh1* and Tr-cC*cbh1* strains was based on *t*-test analysis by the FDR approach. Asterisks indicate significant differences (***$P < 0.001$). ns, not significant.

Chaetomium thermophilum Contained More Extracellular Protein Categories Compared to *T. reesei*

To further investigate the mechanism behind the higher cellulose degradation efficiency in *C. thermophilum*, the supernatants of *C. thermophilum* and *T. reesei* cultures under Avicel were analyzed by SDS-PAGE. The data shown in **Figure 2A** indicated that the bands pattern of the secreted proteins in *C. thermophilum* was quite different from that in *T. reesei.* Although the total extracellular protein levels in *T. reesei* were more than that in *C. thermophilum,* it was worth noting that compared to *T. reesei*, there were more protein bands in the supernatants of *C. thermophilum* cellulose culture, indicating *C. thermophilum* might secrete more protein categories.

Based on the SDS-PAGE analysis, the components and the relative abundances of the extracellular proteins in the supernatants were subsequently evaluated by performing ultra-high performance liquid chromatography coupled tandem mass spectroscopy (UPLC-MS/MS). The data shown in **Figure 2B** and **Supplementary Table S2**–S7 further confirmed that the extracellular protein categories were quite different between *C. thermophilum* and *T. reesei.* In *C. thermophilum,* 192 proteins were identified from the UPLC-MS/MS analysis, including 40 glycoside hydrolase proteins, 23 oxidoreductases, 16 protein degradation associated proteins (protease or peptidase) as well as 113 proteins with unknown function or other functions. While in *T. reesei,* 138 proteins were identified including 60 glycoside hydrolase proteins, 8 protease and peptidases, 2 oxidoreductases, and 68 proteins with unknown function or other functions. Unlike *T. reesei*, in which most of the secreted proteins were glycoside hydrolase proteins, *C. thermophilum* contained fewer glycoside hydrolase proteins and much more oxidoreductases, proteases, and peptidases. Considering that most lignocellulases belongs to glycoside hydrolase family proteins, *C. thermophilum* might contain fewer lignocellulases compared to *T. reesei*. Beside containing cellulases with higher specific activities, the different secreted protein categories in *C. thermophilum* might also play an important role in its high-efficiency of degrading celluloses.

Cellobiohydrolase I From *C. thermophilum* Showed Relatively Higher Specific Activity Compared to *T. reesei* CBH1

To investigate if *C. thermophilum* contain superior cellulases relative to *T. reesei,* one of the major cellulases, CBH1, from *C. thermophilum* and *T. reesei* were first characterized and compared. To prevent the effects caused by other cellulases on the measurement of CBH1 activities, a cellulase-free background system (Uzbas et al., 2012) was applied to respectively express *C. thermophilum* CBH1 (Ct-CBH1) and *T. reesei* CBH1 (Tr-CBH1) using cDNA1 promoter in *T. reesei* strain Tu6Δ*ku70* under glucose. For the construction of Tr-CBH1 expression strain, the promoter of *cbh1* gene in Tu6Δ*ku70* was replaced with cDNA 1 promoter via homologous recombination (**Figure 3A**), while for expressing Ct-CBH1, the DNA region including both *cbh1* promoter and the ORF of *cbh1* gene was replaced with cDNA 1 promoter and the cDNA of Ct-CBH1 (**Figure 3B**). The generated strains were named as Tr-cT*cbh1* and Tr-cC*cbh1*, respectively. Since in the transformants of Tr-cT*cbh1* and Tr-cC*cbh1*, the uridine auxotrophy of Tu6Δ*ku70* strains were complemented by the *pyr4* gene, meanwhile, a uridine complementary strain

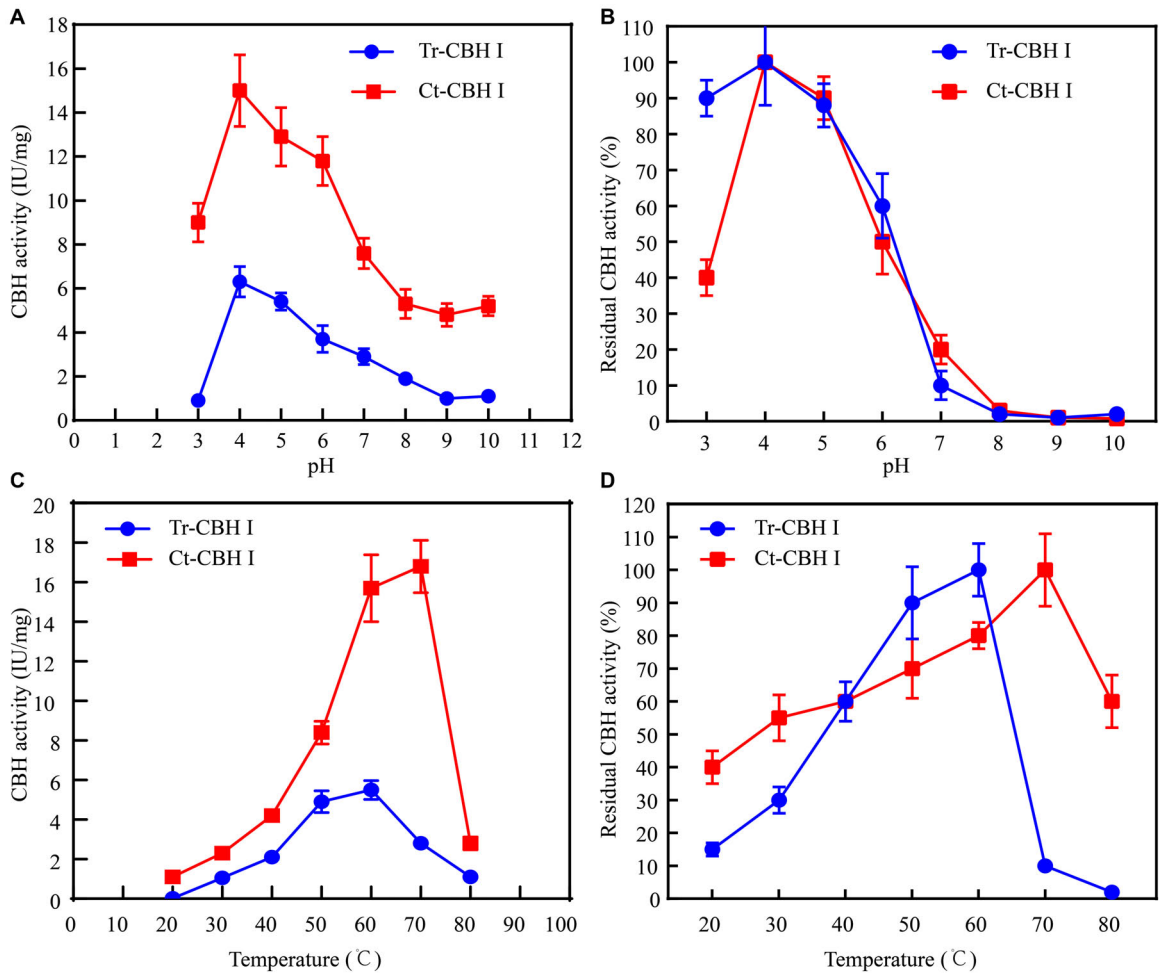

FIGURE 5 | Ct-CBH1 showed higher optimum temperature and better temperature stability compared to Tr-CBH1. **(A)** Optimum pH determination of Tr-CBH1 and Ct-CBH1. **(B)** pH stability analysis of Tr-CBH1 and Ct-CBH1. **(C)** Optimum temperature determination of Tr-CBH1 and Ct-CBH1. **(D)** Temperature stability analysis of Tr-CBH1 and Ct-CBH1. Shown are the mean values of three biological replicates. Error bars show the standard deviations between these replicates.

C*pyr4* was thus constructed by transforming the plasmid pSK-*pyr4* (Qin et al., 2018) into Tu6Δ*ku70* and used as a control for analysis of CBH1 expression.

Three independent strains of each Tr-cT*cbh1*, Tr-cC*cbh1*, and C*pyr4* transformants were respectively cultivated in shake flasks with glucose as the only carbon source. The supernatants of 48 h post-inoculation culture were used for analyzing the secreted protein concentration, CBH activities, as well as SDS-PAGE analysis. As shown in **Figure 4A**, compared to C*pyr4* strains, Tr-cT*cbh1* and Tr-cC*cbh1* strains showed a significantly additional band about 65 kDa. The protein concentration in the supernatants of Tr-cT*cbh1* and Tr-cC*cbh1* cultures was also significantly higher (**Figure 4B**). Additional enzyme activity analysis (**Figure 4B**) further confirmed that the recombinant *cbh1* gene from both *C. thermophilum* and *T. reesei* were successfully expressed in *T. reesei* under glucose, in which the expression of the native cellulases genes was largely repressed due to the regulation of carbon catabolite repression (CCR). It is worth noting that the expression levels of Ct-CBH1 in Tr-cC*cbh1* strains were slightly higher than Tr-CBH1 in Tr-cT*cbh1* strains (**Figure 4A**). However, the CBH activity in Tr-cC*cbh1* strains was about 4.7-fold higher than that in Tr-cT*cbh1* strains (**Figure 4B**). The data that CBH1 activities normalized by total proteins in the supernatant indicated that the relative specific activities of CBH1 from *C. thermophilum* were about 4.5-fold higher than CBH1 from *T. reesei*. Although whether other cellulases in *C. thermophilum* have higher specific activities still needed to be characterized, the existence of CBH1 with higher specific activity at least confirmed that *C. thermophilum* indeed contains superior cellulase.

Chaetomium thermophilum CBH1 Showed Higher Optimum Temperature Compared to *T. reesei* CBH1

Considering that *C. thermophilum* is a thermophilic fungus, whose optimum growth temperature is around 50°C (Kellner et al., 2016), the optimum temperature of Ct-CBH1 and its

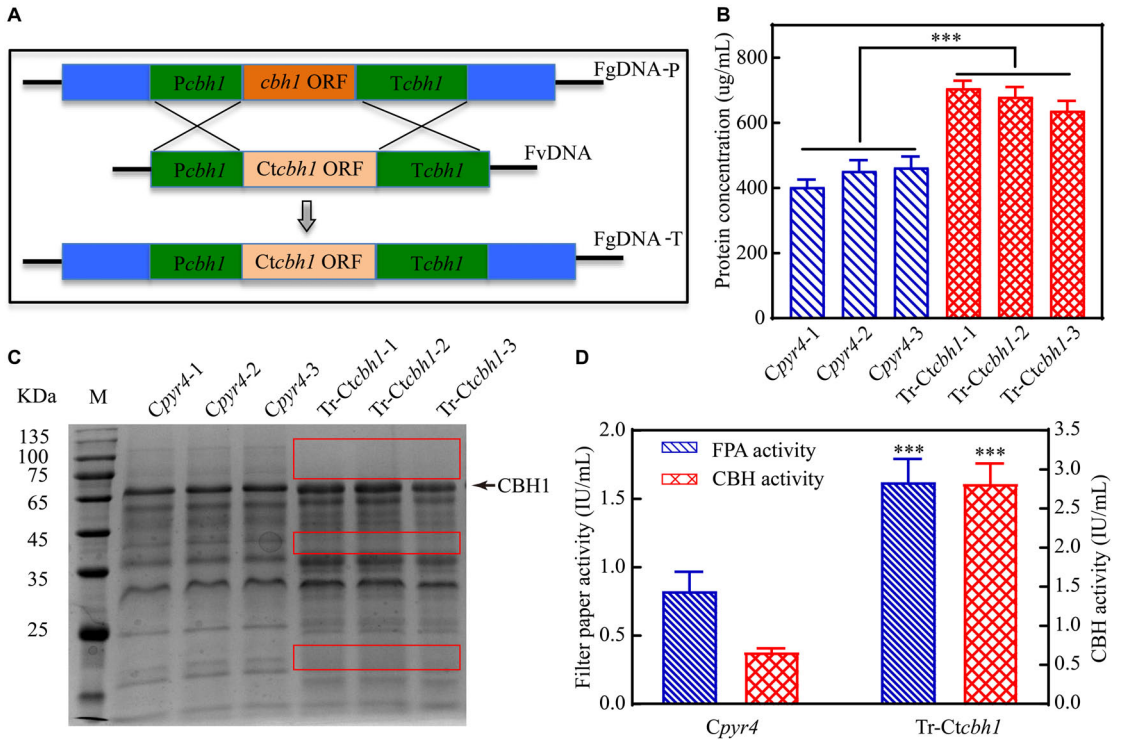

FIGURE 6 | Replacement of Tr-*cbh1* with Ct-*cbh1* gene in *T. reesei* increased the production of cellulases. **(A)** Schematic diagram of the construction of recombinant *T. reesei* strain Tr-Ct*cbh1*. FgDNA-P indicates the fragment in the parental strain. FvDNA indicates the fragment from plasmid vector constructed for generation of the indicated recombinant strain. FgDNA-T indicates DNA fragment in the generated transformant strain. **(B)** Total secreted protein levels of three independent C*pyr4* and Tr-Ct*cbh1* transformants in the supernatant of 120-h Avicel cultures after transferring from glucose cultures. Shown are the mean values of three technical replicates. Error bars show the standard deviations between these replicates. **(C)** SDS-PAGE analysis of the extracellular proteins of C*pyr4* and Tr-Ct*cbh1* strains. The protein bands highlighted with the red frame line indicates proteins in Tr-Ct*cbh1* strains were less than that in C*pyr4* strains. **(D)** Filter paper activities and CBH activities of C*pyr4* and Tr-Ct*cbh1* strains. The samples used in **(C,D)** were as same as in **(B)**. Error bars in **(D)** show the standard deviations between the biological replicates shown in **(C)**. The significance of differences between C*pyr4* and Tr-Ct*cbh1* strains was based on *t*-test analysis by the FDR approach. Asterisks indicate significant differences (***$P < 0.001$). ns, not significant.

temperature stability were subsequently measured and compared with Tr-CBH1. To make sure that the assay for temperature activity curve was carried under the appropriate pH condition, the optimum pH and pH stability for both Ct-CBH1 and Tr-CBH1 were first determined at 50°C. As shown in **Figures 5A,B**, the optimal pH for both Ct-CBH1 and Tr-CBH1 was pH 4.0, and both Ct-CBH1 and Tr-CBH1 displayed the best residual activities at pH 4.0, suggesting pH 4.0 was the optimum condition for CBH1 activity measurement. The assays for optimum temperature were thus carried at pH 4.0, and at seven different temperatures (20–80°C), by using MUC as the substrate. The result shown in **Figure 5C** demonstrated that the optimum temperature of Ct-CBH1 was 70°C, while the optimum temperature of Tr-CBH1 was 60°C, and among all the temperatures, Ct-CBH1 displayed higher activities than Tr-CBH1. For the temperature stability analysis (**Figure 5D**), Tr-CBH1 was stable between 50 and 60°C, the remaining activity dropped dramatically below 50°C or above 60°C. However, Ct-CBH1 was more stable at most of the tested temperatures, which was consistent with reports at previous study (Voutilainen et al., 2008). Taken together, these data indicated that although the enzymatic characteristics of other cellulase genes in C. thermophilum still need to be identified, the above results are at least proved that better cellulases composition system in C. thermophilum was one of the reasons for its higher cellulose-utilizing efficiency relative to T. reesei.

Replacement of Tr-*cbh1* With Ct-*cbh1* Gene in *T. reesei* Resulted in Increased Production Levels of Most Cellulases Genes

Since the specific activity of Ct-CBH1 was significantly higher than Tr-CBH1, cellobiohydrolase activity in *T. reesei* would be increased if Ct-CBH1 could be expressed in *T. reesei* as a similar level as its native Tr-CBH1. To investigate whether increased cellobiohydrolase activities in *T. reesei* could improve its cellulose utilization, recombinant *T. reesei* strain in which the native *cbh1* gene was replaced with *cbh1* gene from *C. thermophilum* was created and named as Tr-Ct*cbh1* (**Figure 6A**).

Three independent Tr-Ct*cbh1* and C*pyr4* recombinant strains were selected for the measurement of the secreted protein levels, CBH activities, and the filter paper activities under Avicel. It was surprisingly demonstrated that the total secreted protein levels

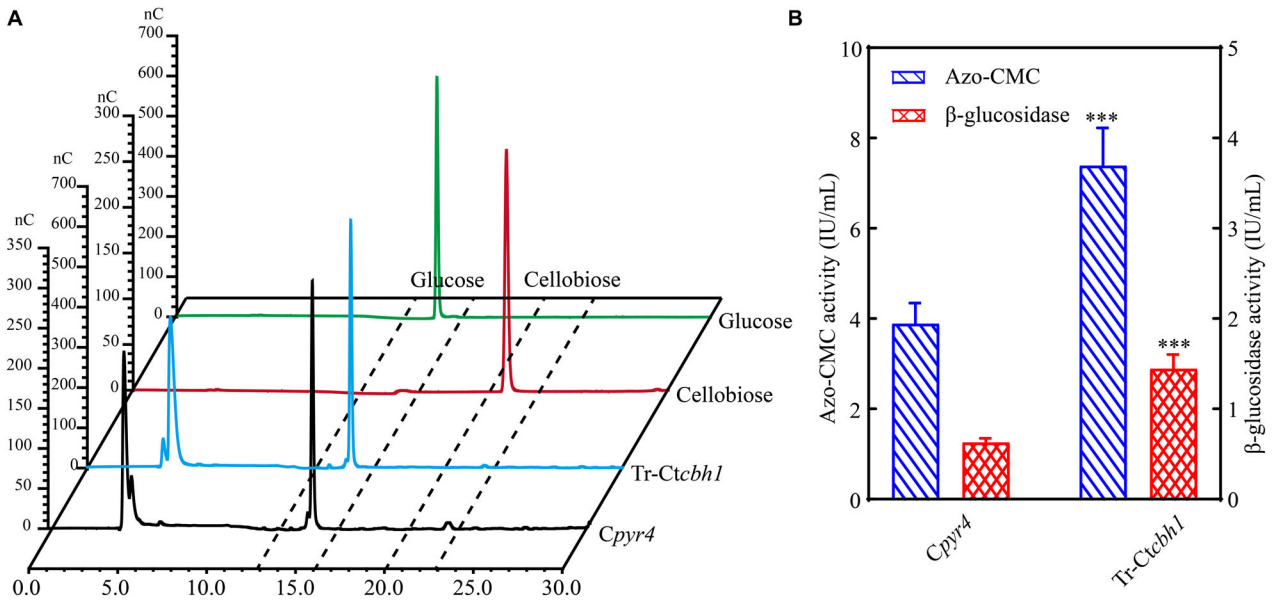

FIGURE 7 | The activities of other cellulases were also increased in Tr-Ct*cbh1* strains. **(A)** HPAEC-PAD analysis of glucose and cellobiose content in the solution of filter paper activity assay (FPA). nC, nano counts, indicating the intensity (abundance) of the signal for each peak. Glucose and cellobiose indicate 100 μM glucose and cellobiose standard sample, respectively. Tr-Ct*cbh1* and C*pyr4* indicate sample taken from the solution of FPA assay with the supernatants of C*pyr4* and Tr-Ct*cbh1* strains under Avicel cultures, respectively. **(B)** Measurements of the endoglucanase activities and β-glucosidase activities of C*pyr4* and Tr-Ct*cbh1* strains in the supernatant of 120-h MM+2% Avicel cultures after transferring from 48 h of MM+2% glucose cultures. The significance of differences between C*pyr4* and Tr-Ct*cbh1* strains was based on *t*-test analysis by the FDR approach. Asterisks indicate significant differences (***$P < 0.001$). ns, not significant.

in Tr-Ct*cbh1* strains were about 1.8-fold higher than those in C*pyr4* strains (**Figure 6B**) and the expression levels of CBH1 in Tr-Ct*cbh1* strains were also significantly higher compared to that in C*pyr4* strains (**Figure 6C**). The cellobiohydrolase activities in Tr-Ct*cbh1* strains were about 4.1-fold higher than those in C*pyr4* strains due to the higher specific activity of Ct-CBH1. In addition, Tr-Ct*cbh1* strains also displayed around 2.2-fold of increased filter paper activities compared to C*pyr4* strains (**Figure 6D**).

Increased CBH1 activities in Tr-Ct*cbh1* strains without any change of ß-glucosidase might cause the accumulation of cellobiose when degrading celluloses. Considering that filter paper activity assays were based on the measurement of the abundance of reducing sugars by DNS method (Xiao et al., 2004), thus the increased filter paper activities in Tr-Ct*cbh1* strains might be caused by the accumulation of cellobiose. To prove this, the amount of glucose and cellobiose in the solution of filter paper activity assay (FPA) was determined by high performance anion exchange chromatography with pulsed amperometric detection (HPAEC-PAD). The data shown in **Figure 7A** unexpectedly revealed that there was no cellobiose accumulation in FPA solutions of both Tr-Ct*cbh1* and C*pyr4* strains, indicating that ß-glucosidase in Tr-Ct*cbh1* strains seemed to be enough to convert the extra cellobiose into glucose. The possible interpretation for this was that more expression of ß-glucosidases might be triggered by the increased CBH1 activity. To investigate whether increased CBH1 activity in *T. reesei* could trigger more expression of other cellulases, besides cellobiohydrolases activities, the activities of ß-glucosidases and endoglucanases of Tr-Ct*cbh1* and C*pyr4* strains under Avicel were measured. As expected, consistent with the above FPA activities data (**Figure 6D**), the activities of endoglucanase and ß-glucosidase of Tr-Ct*cbh1* strains in 120 h Avicel cultures were 1.9 and 2.3-fold greater than that of C*pyr4* strains (**Figure 7B**). Taken together, these data suggested that replacement of Tr-CBH1 with Ct-CBH1 in *T. reesei* not only resulted in increasing CBH1 activities, but also lead to more production of other cellulases. Thus we concluded that increased CBH1 activities in *T. reesei* could contribute to improving the cellulose degradation ability in *T. reesei*.

The Regulation That Increased CBH1 Activities Triggered More Production of Other Cellulases in *T. reesei* Occurred in Transcriptional Level

To further explore the mechanism behind the higher cellulase production in Tr-Ct*cbh1* strains, the transcriptional levels of several major cellulases genes including *eg1* (transcript ID: 122081), *eg2* (transcript ID: 120312), *cbh2* (transcript ID: 72567), and *bgl1* (transcript ID: 76672) under Avicel at different time points were measured by qRT-PCR. As shown in **Figure 8**, at the time point of 12 h, the expression levels of *eg1* and *eg2* in Tr-Ct*cbh1* strains were slightly lower than that in C*pyr4* strains, and the expression levels of the other two tested genes in Tr-Ct*cbh1* strains were similar as in C*pyr4* strains. However, after induction in cellulose condition for 48 h, all these tested genes in Tr-Ct*cbh1* strains were increased at different extent. The mRNA levels of *eg1* and *eg2* genes in Tr-Ct*cbh1* strains were increased

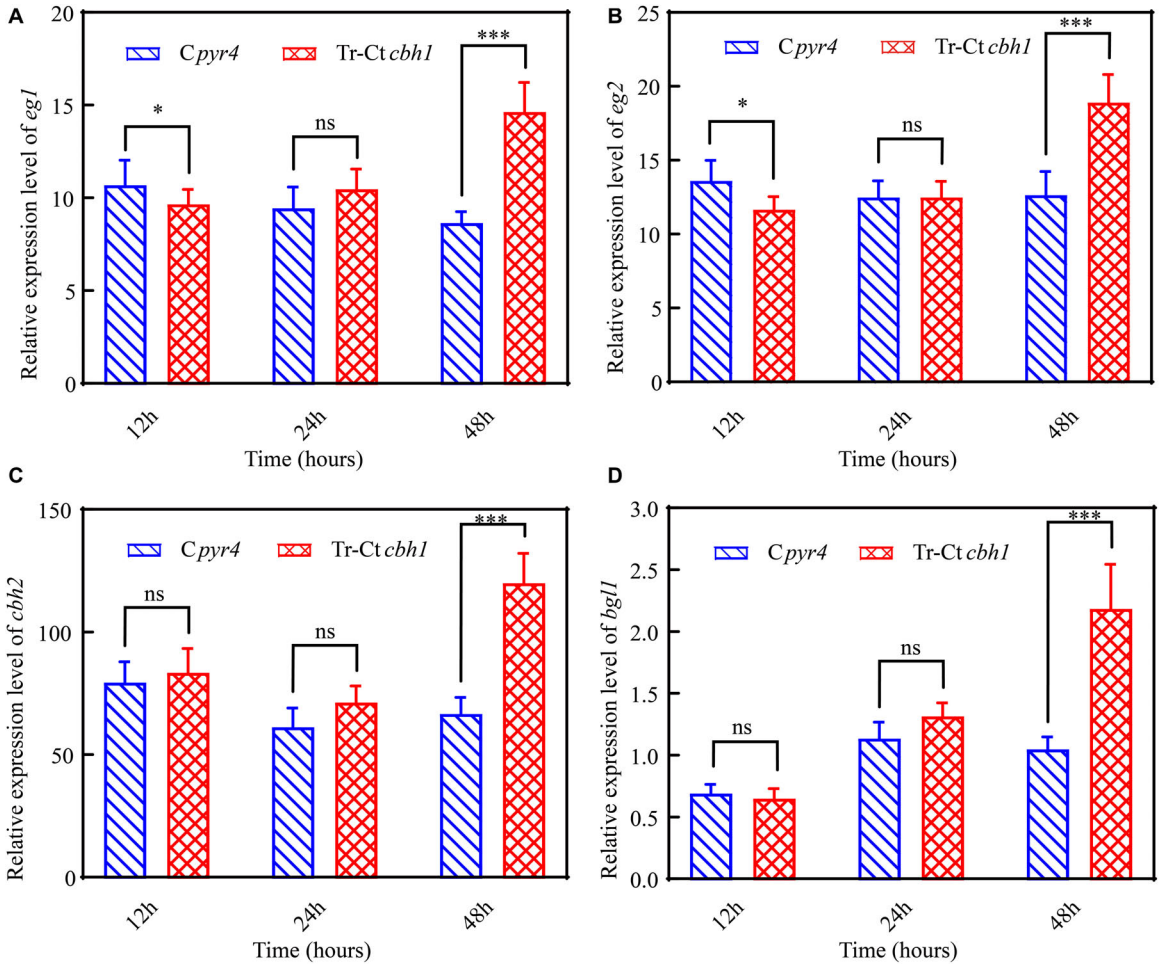

FIGURE 8 | Increased CBH1 activities in *T. reesei* enhanced the induction and expression of the major cellulases genes. Relative quantification of mRNA levels of *eg1* **(A)**, *eg2* **(B)**, *cbh2* **(C)**, and *bgl1* **(D)** genes of C*pyr4* and Tr-Ct*cbh1* strains by qRT-PCR. RNA samples were obtained from the culture of MM+2% Avicel at the indicated time point after a shift of 48 h of MM+2% glucose cultures. The significance of differences between C*pyr4* and Tr-Ct*cbh1* strains was based on *t*-test analysis by the FDR approach. Asterisks indicate significant differences (*$P < 0.05$; ***$P < 0.001$). ns, not significant.

by 1.7 (**Figure 8A**) and 1.5-fold (**Figure 8B**) compared to that in C*pyr4* strains, while the mRNA levels of *cbh2* and *bgl1* genes in Tr-Ct*cbh1* strains were 1.8 (**Figure 8C**) and 2.1-fold (**Figure 8D**) higher than that in C*pyr4* strains. These data suggested that the more expression of cellulases genes in Tr-Ct*cbh1* strains occurred at transcriptional levels.

In *T. reesei*, several major TFs including three activators *xyr1*, *ace2* and *ace3*, and two repressors *cre1* and *ace1* were involved in the regulation of the expression of genes encoding lignocellulases genes (Benocci et al., 2017). To investigate if these TFs were involved in the regulation of the increased production of cellulases in Tr-Ct*cbh1* strains, the expression levels of these TFs in Tr-Ct*cbh1* and C*pyr4* strains under Avicel were also measured by qRT-PCR. The data shown in **Figure 9** demonstrated that the relative mRNA levels of *xyr1*, *cre1*, and *ace3* in Tr-Ct*cbh1* strains were significantly increased over time compared to that in C*pyr4* strains. At the time point of 48 h, the expression levels of *xyr1* and *cre1* in Tr-Ct*cbh1* strains were about 17.4 and 4.5-fold higher than that in C*pyr4* strains (**Figures 9A,B**), while the expression levels of *ace3* were only slightly increased by 1.5-fold (**Figure 9E**). However, the expression levels of *ace1* and *ace2* in Tr-Ct*cbh1* strains exhibited similar levels as that in C*pyr4* strains at all of the time points (**Figures 9C,D**). Considering that the induction of *xyr1* requires *cre1* (Portnoy et al., 2011), it was reasonable that the expression of *cre1* increased along with *xyr1* here. However, the reason for that the expression level of activator *ace2* was not increased in Tr-Ct*cbh1* strains still needs to be investigated. The data here at least indicated that the major regulator *xyr1* was involved in higher cellulase production in Tr-Ct*cbh1* strains.

DISCUSSION

Biorefineries include the sustainable processing of plant biomass into a variety of bioproducts and specialty chemicals. Many of these processes require enzymes that are stable at high temperature to enhance mass transfer and reduce substrate viscosity, with a lower risk of contamination. As natural

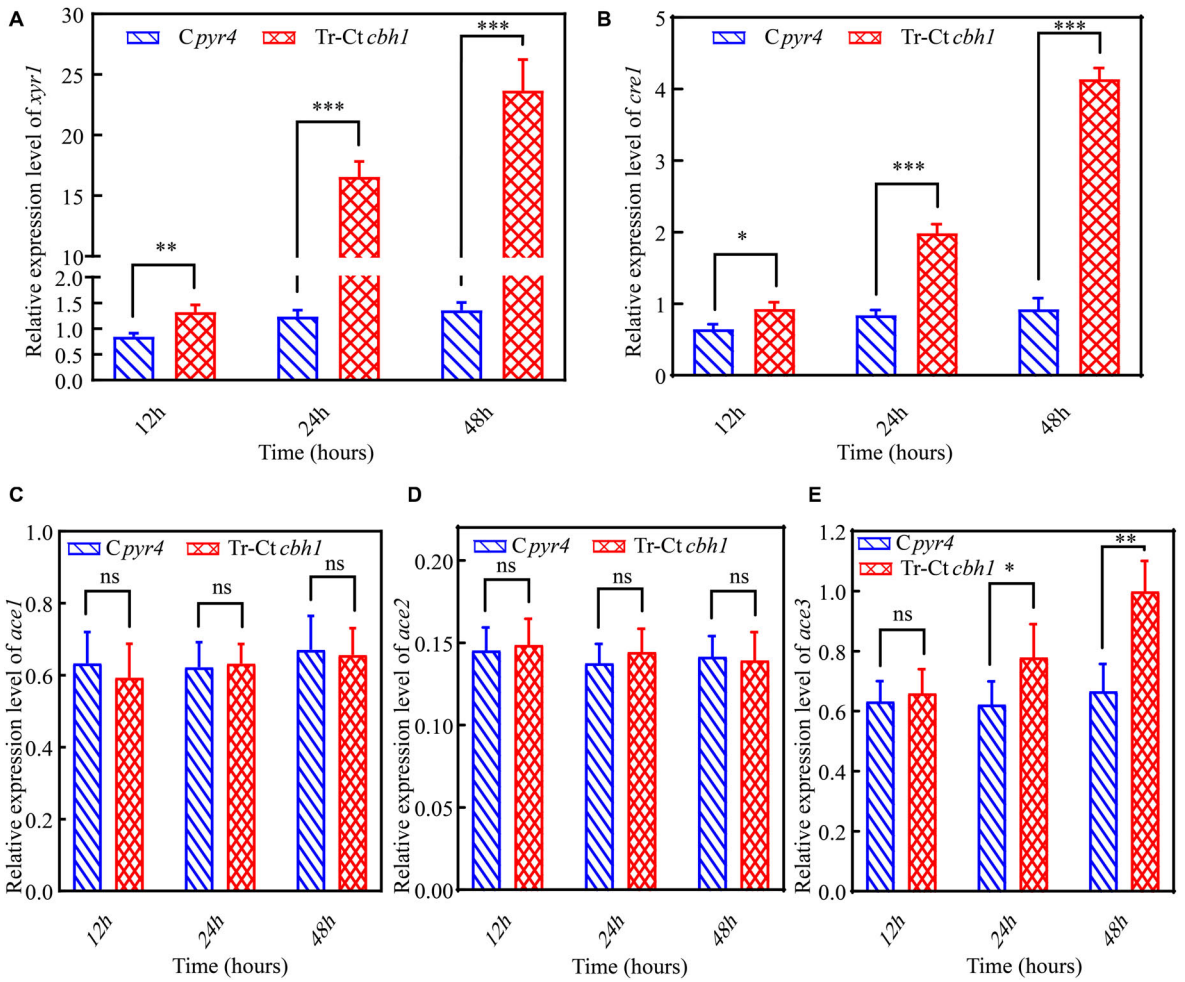

FIGURE 9 | The higher production of cellulases in Tr-Ct*cbh1* strains was caused by increased expression level of *xyr1*. Relative quantification of mRNA levels of *xyr1* **(A)**, *cre1* **(B)**, *ace1* **(C)**, *ace2* **(D)**, and *ace3* **(E)** genes of C*pyr4* and Tr-Ct*cbh1* strains by qRT-PCR. RNA samples were obtained from 12, 24, and 48 h of cultures of MM+2% Avicel after a shift of 48 h of MM+2% glucose cultures. The significance of differences between C*pyr4* and Tr-Ct*cbh1* strains was based on *t*-test analysis by the FDR approach. Asterisks indicate significant differences (*$P < 0.05$; **$P < 0.01$; ***$P < 0.001$). ns, not significant.

plant-biomass degraders, thermophilic fungi must contain thermostable biomass-degrading enzymes. Therefore, in this study, we evaluated the cellulose-utilizing efficiency of a thermophilic fungus *C. thermophilum* and surprisingly found that compared to *T. reesei*, although *C. thermophilum* secreted fewer cellulases, it showed higher efficiency to degrade celluloses. This finding indicated that *C. thermophilum* might contain cellulases with higher specific activities. The characterization and comparison of Ct-CBH1 and Tr-CBH1 further confirmed this hypothesis. However, UPLC-MS/MS analysis of *C. thermophilum* supernatants demonstrated there were many oxidoreductases included in *C. thermophilum* protein secretome. Considering that the certain oxidants could make lignocellulose more susceptible for enzymatic degradation (Zhang et al., 2016; Den et al., 2018), the existence of such amounts of oxidoreductases in the supernatants of *C. thermophilum* culture implied that in addition to contain higher efficient cellulases, *C. thermophilum* might display a different mode of action to degrade lignocelluloses.

In *T. reesei*, it has been generally believed that β-glucosidase is a barrier for its cellulose degradation capacity because the extracellular β-glucosidase comprises only about 1% of the total *T. reesei* cellulases complex (Karkehabadi et al., 2014), based on which, many efforts have been conducted to increase enzyme efficiency of hydrolyzing cellulosic substrates by increasing β-glucosidase amount in the cellulases complex from *T. reesei* (Banerjee et al., 2010; Treebupachatsakul et al., 2016). In the opposite, because of the large amount, studies about increasing enzyme efficiency of cellobiohydrolase in *T. reesei* have been rarely reported. In this study, we first reported that increased cellobiohydrolase activities in *T. reesei* could result in a significant increase of its production of other cellulases and cellulose-utilizing efficiency.

It was worth noting that SDS-PAGE analysis of the supernatants of the Tr-Ct*cbh1* and C*pyr4* strains (**Figure 6C**) showed variations in specific protein levels rather than an

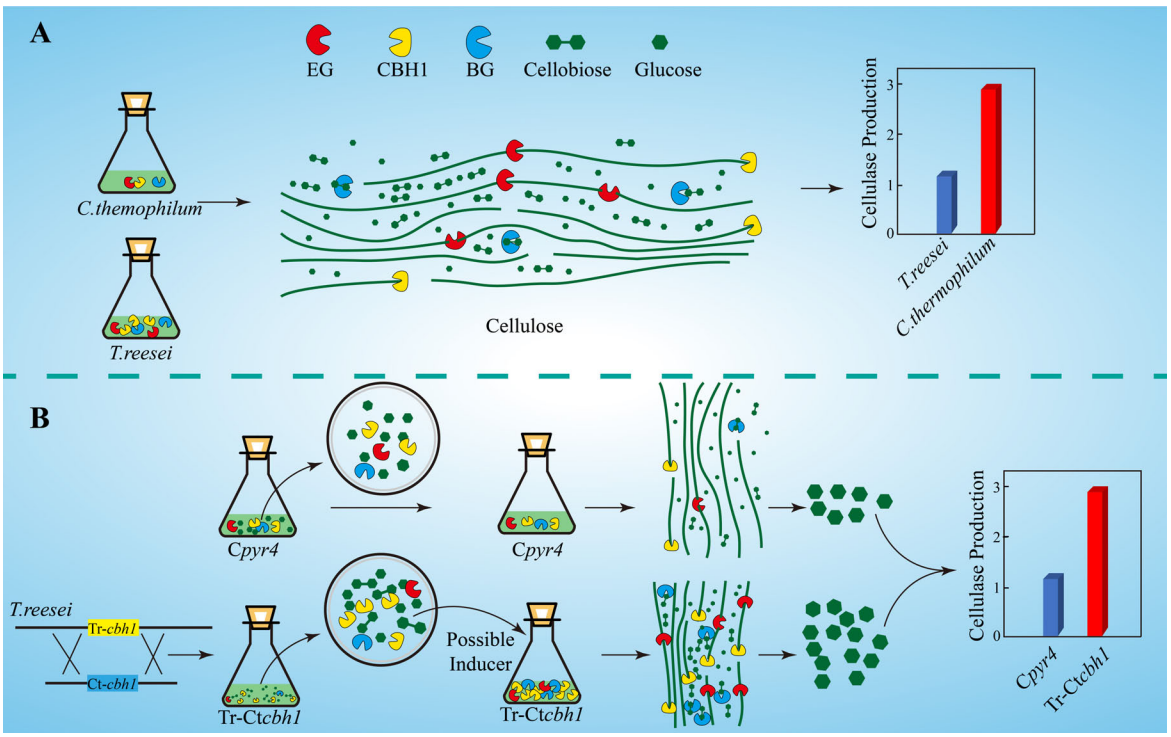

FIGURE 10 | Graphic summary of this study. **(A)** Compared to *T. reesei*, *C. thermophilum* degrades celluloses more efficiently with lower production of cellulases. **(B)** The proposed model of the mechanism for higher production of cellulases in Tr-C*tcbh1* strains. Replacement of Tr-*cbh1* with Ct-*cbh1* gene in *T. reesei* first increased the CBH1 activity, which could cause instantaneous accumulation of cellobiose. This extra cellobiose might function as a possible inducer to trigger more induction and expression of cellulases genes.

overall increase or decrease in the levels of all secreted proteins in Tr-C*tcbh1* strains compared to that in C*pyr4* strains. Relative to C*pyr4* strains, the expression levels of only a few proteins (highlighted with red frame line in **Figure 6C**) were decreased, most of the secreted proteins were increased in Tr-C*tcbh1* strains. Since most of the extracellular proteins in the supernatant of *T. reesei* under cellulose were cellulases and hemicellulases (Herpoël-Gimbert et al., 2008), these data suggested that only improved the function of CBH1 in *T. reesei* might lead to increasing the expression levels of most lignocellulose degradation associated genes. The results that the FPA activities (**Figure 6D**), the Azo-CMC activities and β-glucosidase activities (**Figure 7B**) in Tr-C*tcbh1* strains were significantly higher than those in C*pyr4* strains, and besides, the transcriptional levels of *cbh2*, *eg1*, *eg2*, and *bgl1* genes were also higher in Tr-C*tcbh1* strains (**Figure 8**), which further proved that the induction and expression of most cellulases genes in *T. reesei* could be improved by only enhancing CBH1 activities.

The increased expression levels of *xyr1*, *cre1*, and *ace3* in Tr-C*tcbh1* strains (**Figure 9**) suggested that an extra inducer might be generated in *T. reesei* when response to cellulose with more cellobiohydrolases in its cellulases system. Cellobiohydrolase is an exocellulase, which cleaves cellulose to release cellobiose from the non-reducing ends. Theoretically, increased cellobiohydrolase in *T. reesei* should result in an accumulation of cellobiose when response to cellulose if the expression level of ß-glucosidase was not correspondingly increased. The higher expression levels of most cellulase genes in Tr-C*tcbh1* strains could explain why there was no cellobiose accumulation. A possible interpretation for the increased production levels of cellulases in Tr-C*tcbh1* strains was that the extra cellobiose generated by the increased cellobiohydrolase activities at the very beginning might function as a possible inducer to trigger more expression of cellulases genes (**Figure 10**). It has been previously reported that cellobiose could induce a low level of cellulase gene expression in *T. reesei* (Vaheri et al., 1979). In addition, sophorose, which is widely viewed as the potent inducer of cellulases in *T. reesei,* also could be generated by the transglycosylation of cellobiose by ß-glucosidase (Sternberg and Mandels, 1979). Furthermore, the growth of *Neurospora crassa* under cellobiose could not induce the expression of celluases genes, however, the deletion of three major β-glucosidase genes in *N. crassa* could result in the expression of cellulases under cellobiose (Znameroski et al., 2012). Moreover, deletion of two intracellular β-glucosidase genes (*cel1a* and *cel1b*) and one extracellular β-glucosidase (*cel3a*) gene in *T. reesei* also could increase the expression levels of cellulases genes when response to cellobiose (Zhou et al., 2012). All of these previous reports suggested that cellobiose played an important role in the induction of cellulases genes, especially when the relative ratio of the cellobiohydrolase and ß-glucosidase was enlarged, which was consistent with the phenomenon observed in this study. Therefore, we speculated that the potential temporary

accumulation of cellobiose resulted from the disruption of the synergetic effect of cellobiohydrolase and ß-glucosidase might be able to function as an inducer to trigger the extra induction of cellulases genes in *T. reesei* (**Figure10**).

CONCLUSION

To search for new resources of lignocellulases for plant biomass degradation, here we reported that a thermophilic fungus *C. thermophilum* could degrade celluloses more efficiently with less secreted cellulases compared to *T. reesei,* implying the existence of excellent cellulases genes in its genome. Comparison of the enzyme properties of CBH1 from *C. thermophilum* and *T. reesei* further confirmed this hypothesis. More interesting, our data showed that only raising the function of CBH1 in *T. reesei* could lead to a marked increase in the production levels of other cellulases. Based on the observed phenomenon, we speculated that a certain amount of temporary cellobiose accumulation might play an important role in the process of cellulases genes induction. This study not only provided a new strategy to improve the cellulases yields in *T. reesei,* but also opened the path for fundamental research on thermophilic fungi such as *C. thermophilum*, as well as stimulating investigations into their potential application as sources of commercially important enzymes.

DATA AVAILABILITY STATEMENT

All datasets generated for this study are included in the article/**Supplementary Material**.

AUTHOR CONTRIBUTIONS

XJ and JD participated in the conception of the study and carried out the majority of the experiments. RH and ZZ were involved in evaluating the cellulose-utilizing efficiency of *C. thermophilum* and *T. reesei*. FQ was involved in mass spectrometry analysis. JH was involved in the project leadership and participated in editing the manuscript. LQ was involved in the conception of the study and participated in the guidance with experimental strategies and technical direction. All authors read and approved the final manuscript.

FUNDING

This work was supported by the National Natural Science Foundation of China (31800060 and 31741002); Natural Science Foundation of Fujian Province in China (2019I0009); and by the Scientific Research Innovation Program "Xiyuanjiang River Scholarship" of College of Life Sciences, Fujian Normal University.

ACKNOWLEDGMENTS

We thank Prof. Zhiyang Dong and Dr. Xiuzhen Chen (Institute of Microbiology, Chinese Academy of Sciences) for their assistance with the UPLC-MS/MS experiment. We also thank Xiaoyun Su (Feed Research Institute, Chinese Academy of Agricultural Sciences) for his assistance with HPAEC-PAD experiment.

SUPPLEMENTARY MATERIAL

The Supplementary Material for this article can be found online at: https://www.frontiersin.org/articles/10.3389/fmicb.2020.01633/full#supplementary-material

TABLE S1 | Primers used in this study.

TABLE S2 | UPLC-MS/MS analysis of protein secretome of *T. reesei* under Avicel (Processed data).

TABLE S3 | UPLC-MS/MS analysis of protein secretome of *C. thermophilum* under Avicel (Processed data).

TABLE S4 | UPLC-MS/MS analysis of protein secretome of *T. reesei* under Avicel (Raw data of sample 1).

TABLE S5 | UPLC-MS/MS analysis of protein secretome of *T. reesei* under Avicel (Raw data of sample 2).

TABLE S6 | UPLC-MS/MS analysis of protein secretome of *C. thermophilum* under Avicel (Raw data of sample 1).

TABLE S7 | UPLC-MS/MS analysis of protein secretome of *C. thermophilum* under Avicel (Raw data of sample 2).

REFERENCES

Bailey, M. J., and Tähtiharju, J. (2003). Efficient cellulase production by *Trichoderma reesei* in continuous cultivation on lactose medium with a computer-controlled feeding strategy. *Appl. Microbiol. Biotechnol.* 62, 156–162. doi: 10.1007/s00253-003-1276-9

Banerjee, G., Car, S., Scott-Craig, J. S., Borrusch, M. S., Aslam, N., and Walton, J. D. (2010). Synthetic enzyme mixtures for biomass deconstruction: production and optimization of a core set. *Biotechnol. Bioeng.* 106, 707–720. doi: 10.1002/bit.22741

Benocci, T., Aguilar-Pontes, M. V., Zhou, M., Seiboth, B., and De Vries, R. P. (2017). Regulators of plant biomass degradation in ascomycetous fungi. *Biotechnol. Biofuels* 10:152. doi: 10.1186/s13068-017-0841-x

Bischof, R. H., Ramoni, J., and Seiboth, B. (2016). Cellulases and beyond: the first 70 years of the enzyme producer *Trichoderma reesei*. *Microb. Cell Fact.* 15:106. doi: 10.1186/s12934-016-0507-6

Bock, T., Chen, W. H., Ori, A., Malik, N., Silva-Martin, N., Huerta-Cepas, J., et al. (2014). An integrated approach for genome annotation of the eukaryotic thermophile *Chaetomium thermophilum*. *Nucleic Acids Res.* 42, 13525–13533. doi: 10.1093/nar/gku1147

Cherry, J. R., and Fidantsef, A. L. (2003). Directed evolution of industrial enzymes: an update. *Curr. Opin. Biotechnol.* 14, 438–443. doi: 10.1016/s0958-1669(03)00099-5

Dashtban, M., and Qin, W. (2012). Overexpression of an exotic thermotolerant beta-glucosidase in *Trichoderma* reesei and its significant increase in cellulolytic activity and saccharification of barley straw. *Microb. Cell Fact.* 11:63. doi: 10.1186/1475-2859-11-63

DeCastro, M. E., Rodriguez-Belmonte, E., and Gonzalez-Siso, M. I. (2016). Metagenomics of thermophiles with a focus on discovery of novel thermozymes. *Front. Microbiol.* 7:1521. doi: 10.3389/fmicb.2016.01521

Den, W., Sharma, V. K., Lee, M., Nadadur, G., and Varma, R. S. (2018). Lignocellulosic biomass transformations via greener oxidative pretreatment

processes: access to energy and value-added chemicals. *Front. Chem.* 6:141. doi: 10.3389/fchem.2018.00141

Ghose, T. K. (1987). Measurement of cellulase activities. *Pure Appl. Chem.* 59, 257–268. doi: 10.1351/pac198759020257

Herpoël-Gimbert, I., Margeot, A., Dolla, A., Jan, G., Mollé, D., Lignon, S., et al. (2008). Comparative secretome analyses of two *Trichoderma reesei* RUT-C30 and CL847 hypersecretory strains. *Biotechnol. Biofuels* 1:18. doi: 10.1186/1754-6834-1-18

Himmel, M. E., Ding, S.-Y., Johnson, D. K., Adney, W. S., Nimlos, M. R., Brady, J. W., et al. (2007). Biomass recalcitrance: engineering plants and enzymes for biofuels production. *Science* 315, 804–807. doi: 10.1126/science.1137016

Karkehabadi, S., Helmich, K. E., Kaper, T., Hansson, H., Mikkelsen, N. E., Gudmundsson, M., et al. (2014). Biochemical characterization and crystal structures of a fungal family 3 beta-glucosidase, Cel3A from Hypocrea jecorina. *J. Biol. Chem.* 289, 31624–31637. doi: 10.1074/jbc.M114.587766

Kellner, N., Schwarz, J., Sturm, M., Fernandez-Martinez, J., Griesel, S., Zhang, W., et al. (2016). Developing genetic tools to exploit *Chaetomium thermophilum* for biochemical analyses of eukaryotic macromolecular assemblies. *Sci. Rep.* 6:20937. doi: 10.1038/srep20937

Kubicek, C. P., Starr, T. L., and Glass, N. L. (2014). Plant cell wall-degrading enzymes and their secretion in plant-pathogenic fungi. *Annu. Rev. Phytopathol.* 52, 427–451. doi: 10.1146/annurev-phyto-102313-045831

Li, A. N., Yu, K., Liu, H. Q., Zhang, J., Li, H., and Li, D. C. (2010). Two novel thermostable chitinase genes from thermophilic fungi: cloning, expression and characterization. *Bioresour. Technol.* 101, 5546–5551. doi: 10.1016/j.biortech.2010.02.058

Penttilä, M., Nevalainen, H., Rättö, M., Salminen, E., and Knowles, J. (1987). A versatile transformation system for the cellulolytic filamentous fungus Trichoderma reesei. *Gene* 61, 155–164. doi: 10.1016/0378-1119(87)90110-7

Portnoy, T., Margeot, A., Seidl-Seiboth, V., Le Crom, S., Chaabane, F. B., Linke, R., et al. (2011). Differential regulation of the cellulase transcription factors XYR1, ACE2, and ACE1 in Trichoderma reesei strains producing high and low levels of cellulase. *Eukaryot. Cell* 10, 262–271. doi: 10.1128/EC.00208-10

Qin, L., Jiang, X., Dong, Z., Huang, J., and Chen, X. (2018). Identification of two integration sites in favor of transgene expression in *Trichoderma reesei*. *Biotechnol. Biofuels* 11:142. doi: 10.1186/s13068-018-1139-3

Qin, L. N., Cai, F. R., Dong, X. R., Huang, Z. B., Tao, Y., Huang, J. Z., et al. (2012). Improved production of heterologous lipase in Trichoderma reesei by RNAi mediated gene silencing of an endogenic highly expressed gene. *Bioresour. Technol.* 109, 116–122. doi: 10.1016/j.biortech.2012.01.013

Schuster, A., Bruno, K. S., Collett, J. R., Baker, S. E., Seiboth, B., Kubicek, C. P., et al. (2012). A versatile toolkit for high throughput functional genomics with Trichoderma reesei. *Biotechnol. Biofuels* 5:1. doi: 10.1186/1754-6834-5-1

Sewalt, V., Shanahan, D., Gregg, L., La Marta, J., and Carrillo, R. (2016). The generally recognized as safe (GRAS) process for industrial microbial enzymes. *Ind. Biotechnol.* 12, 295–302. doi: 10.1089/ind.2016.0011

Singh, A., Taylor, L. E. II, Vander Wall, T. A., Linger, J., Himmel, M. E., Podkaminer, K., et al. (2015). Heterologous protein expression in Hypocrea jecorina: a historical perspective and new developments. *Biotechnol. Adv.* 33, 142–154. doi: 10.1016/j.biotechadv.2014.11.009

Stappler, E., Walton, J. D., Beier, S., and Schmoll, M. (2017). Abundance of secreted proteins of *Trichoderma reesei* is regulated by light of different intensities. *Front. Microbiol.* 8:2586. doi: 10.3389/fmicb.2017.02586

Sternberg, D., and Mandels, G. R. (1979). Induction of cellulolytic enzymes in trichoderma reesei by sophorose. *J. Bacteriol.* 139, 761–769. doi: 10.1128/jb.139.3.761-769.1979

Tian, C., Beeson, W. T., Iavarone, A. T., Sun, J., Marletta, M. A., Cate, J. H., et al. (2009). Systems analysis of plant cell wall degradation by the model filamentous fungus Neurospora crassa. *Proc. Natl. Acad. Sci. U.S.A.* 106, 22157–22162. doi: 10.1073/pnas.0906810106

Treebupachatsakul, T., Nakazawa, H., Shinbo, H., Fujikawa, H., Nagaiwa, A., Ochiai, N., et al. (2016). Heterologously expressed Aspergillus aculeatus beta-glucosidase in Saccharomyces cerevisiae is a cost-effective alternative to commercial supplementation of beta-glucosidase in industrial ethanol production using *Trichoderma reesei* cellulases. *J. Biosci. Bioeng.* 121, 27–35. doi: 10.1016/j.jbiosc.2015.05.002

Treebupachatsakul, T., Shioya, K., Nakazawa, H., Kawaguchi, T., Morikawa, Y., Shida, Y., et al. (2015). Utilization of recombinant Trichoderma reesei expressing Aspergillus aculeatus beta-glucosidase I (JN11) for a more economical production of ethanol from lignocellulosic biomass. *J. Biosci. Bioeng.* 120, 657–665. doi: 10.1016/j.jbiosc.2015.04.015

Uzbas, F., Sezerman, U., Hartl, L., Kubicek, C. P., and Seiboth, B. (2012). A homologous production system for *Trichoderma reesei* secreted proteins in a cellulase-free background. *Appl. Microbiol. Biotechnol.* 93, 1601–1608. doi: 10.1007/s00253-011-3674-8

Vaheri, M. P., Vaheri, M. E., and Kauppinen, V. S. (1979). Formation and release of cellulolytic enzymes during growth of Trichoderma reesei on cellobiose and glycerol. *Eur. J. Appl. Microbiol. Biotechnol.* 8, 73–80. doi: 10.1007/bf00510268

Vogel, H. J. (1956). A convenient growth medium for Neurospora (Medium N). *Microb. Genet Bull.* 13, 42–43.

Voutilainen, S. P., Puranen, T., Siika-Aho, M., Lappalainen, A., Alapuranen, M., Kallio, J., et al. (2008). Cloning, expression, and characterization of novel thermostable family 7 cellobiohydrolases. *Biotechnol. Bioeng.* 101, 515–528. doi: 10.1002/bit.21940

Wu, V. W., Dana, C. M., Iavarone, A. T., Clark, D. S., and Glass, N. L. (2017). Identification of glutaminyl cyclase genes involved in pyroglutamate modification of fungal lignocellulolytic enzymes. *mBio* 8:e2231-16. doi: 10.1128/mBio.02231-16

Xiao, Z., Storms, R., and Tsang, A. (2004). Microplate-based filter paper assay to measure total cellulase activity. *Biotechnol. Bioeng.* 88, 832–837. doi: 10.1002/bit.20286

Zhang, J., Presley, G. N., Hammel, K. E., Ryu, J.-S., Menke, J. R., Figueroa, M., et al. (2016). Localizing gene regulation reveals a staggered wood decay mechanism for the brown rot fungus Postia placenta. *Proc. Natl. Acad. Sci. U.S.A.* 113, 10968–10973. doi: 10.1073/pnas.1608454113

Zhang, J., Zhong, Y., Zhao, X., and Wang, T. (2010). Development of the cellulolytic fungus Trichoderma reesei strain with enhanced beta-glucosidase and filter paper activity using strong artificial cellobiohydrolase 1 promoter. *Bioresour. Technol.* 101, 9815–9818. doi: 10.1016/j.biortech.2010.07.078

Zhou, Q., Xu, J., Kou, Y., Lv, X., Zhang, X., Zhao, G., et al. (2012). Differential involvement of β-glucosidases from Hypocrea jecorina in rapid induction of cellulase genes by cellulose and cellobiose. *Eukaryot. Cell* 11, 1371–1381. doi: 10.1128/ec.00170-12

Znameroski, E. A., Coradetti, S. T., Roche, C. M., Tsai, J. C., Iavarone, A. T., Cate, J. H., et al. (2012). Induction of lignocellulose-degrading enzymes in *Neurospora crassa* by cellodextrins. *Proc. Natl. Acad. Sci. U.S.A.* 109, 6012–6017. doi: 10.1073/pnas.1118440109

Conflict of Interest: The authors declare that the research was conducted in the absence of any commercial or financial relationships that could be construed as a potential conflict of interest.

frontiers in Microbiology

ORIGINAL RESEARCH
published: 14 July 2020
doi: 10.3389/fmicb.2020.01617

Diversity of Cellulase-Producing Filamentous Fungi From Tibet and Transcriptomic Analysis of a Superior Cellulase Producer *Trichoderma harzianum* LZ117

*Jia-Xiang Li[1], Fei Zhang[1], Dan-Dan Jiang[2], Jun Li[2], Feng-Lou Wang[2], Zhang Zhang[2], Wei Wang[3] and Xin-Qing Zhao[1]**

[1] State Key Laboratory of Microbial Metabolism, Joint International Research Laboratory of Metabolic and Developmental Sciences, School of Life Sciences and Biotechnology, Shanghai Jiao Tong University, Shanghai, China, [2] R&D Center, JALA Group Co., Shanghai, China, [3] State Key Laboratory of Bioreactor Engineering, East China University of Science and Technology, Shanghai, China

OPEN ACCESS

Edited by:
Jiwei Zhang, University of Minnesota Twin Cities, United States

Reviewed by:
Guangshan Yao, Minjiang University, China
Shuai Zhao, Guangxi University, China

***Correspondence:**
Xin-Qing Zhao
xqzhao@sjtu.edu.cn

Specialty section:
This article was submitted to Fungi and Their Interactions, a section of the journal Frontiers in Microbiology

Received: *15 April 2020*
Accepted: *22 June 2020*
Published: *14 July 2020*

Citation:
Li J-X, Zhang F, Jiang D-D, Li J, Wang F-L, Zhang Z, Wang W and Zhao X-Q (2020) Diversity of Cellulase-Producing Filamentous Fungi From Tibet and Transcriptomic Analysis of a Superior Cellulase Producer Trichoderma harzianum LZ117. Front. Microbiol. 11:1617. doi: 10.3389/fmicb.2020.01617

Filamentous fungi are widely used for producing cellulolytic enzymes to degrade lignocellulosic biomass. Microbial resources from Tibet have received great attention due to the unique geographic and climatic conditions in the Qinghai-Tibet Plateau. However, studies on cellulase producing fungal strains originated from Tibet remain very limited, and so far no studies have been focused on regulation of cellulase production of the specific strains thereof. Here, filamentous fungal strains were isolated from soil, plant, and other environments in Tibet, and cellulase-producing strains were further investigated. A total of 88 filamentous fungal strains were identified, and screening of cellulase-producing fungi revealed that 16 strains affiliated with the genera *Penicillium*, *Trichoderma*, *Aspergillus,* and *Talaromyces* exhibited varying cellulolytic activities. Among these strains, *T. harzianum* isolate LZ117 is the most potent producer. Comparative transcriptome analysis using *T. harzianum* LZ117 and the control strain *T. harzianum* K223452 cultured on cellulose indicated an intensive modulation of gene transcription related to protein synthesis and quality control. Furthermore, transcription of *xyr1* which encodes the global transcriptional activator for cellulase expression was significantly up-regulated. Transcription of *cre1* and other predicted repressors controlling cellulase gene expression was decreased in *T. harzianum* LZ117, which may contribute to enhancing formation of primary cellulases. To our knowledge, this is the first report that the transcription landscape at the early enzyme production stage of *T. harzianum* was comprehensively described, and detailed analysis on modulation of transporters, regulatory proteins as well as protein synthesis and processing was presented. Our study contributes to increasing the catalog of publicly available transcriptome data from *T. harzianum*, and provides useful clues for unraveling the biotechnological potential of this species for lignocellulosic biorefinery.

Keywords: filamentous fungi, cellulase production, *Trichoderma harzianum*, comparative transcriptome analysis, cellulase induction

INTRODUCTION

Lignocellulose biomass is abundant in nature, and represents more than half of the organic matter produced globally via plant photosynthesis. Bioconversion of relatively inexpensive lignocellulosic biomass into biofuels and value-added products can effectively alleviate pressure of energy supply and benefit sustainable development. At present, industrial cellulase preparations for biomass degradation are generally produced from filamentous fungi (Payne et al., 2015) and comprise a mixture of glycoside hydrolases (GHs) as well as other accessory proteins that are required to work synergistically with cellulases (Champreda et al., 2019).

Tibet is regarded as one of the richest areas for biodiversity in China as a consequence of its complex topography and diverse habitats. The Tibetan plateau ecosystem may be subjected to various environmental stresses characterized by low temperature, anoxia and high solar radiation, which endows unique properties of the microbial strains. However, limited studies have been conducted to identify and evaluate potential lignocellulolytic enzyme-producing fungi from this environment. Previously, diversity of cultivable *Trichoderma* strains in Tibet soil samples and diverse fungal strains from permafrost at Qinghai-Tibet Plateau were reported (Sun et al., 2012; Hu et al., 2014), but cellulase producers were not described. It will be of great interest to explore novel filamentous fungal strains from Tibet for cellulase production and biomass degradation.

Trichoderma harzianum is closely related to *T. reesei*, which is widely used for production of cellulolytic enzymes (Bischof et al., 2016; Zhang et al., 2019). Studies on various *T. harzianum* strains showed that they can produce cellulolytic enzyme complex with higher β-glucosidase and endoglucanases activities than that shown by *T. reesei* (de Castro et al., 2010; Benoliel et al., 2013). The secretome of *T. harzianum* and genes encoding carbohydrate-active enzymes in *T. harzianum* were also reported (Rocha et al., 2016; Ferreira et al., 2017; Horta et al., 2018). However, the regulatory mechanisms underlying cellulase production in *T. harzianum* remain unclear. Two related studies have been performed using comparative transcriptome and secretome analysis (Horta et al., 2014, 2018). However, both studies used samples collected at late fermentation stage (96 h). Therefore, information on the regulatory events at early enzyme production stage, especially for cellulase induction, remains to be elucidated. In our previous studies, *T. harzianum* LZ117 was isolated from the surface of a moss collected in Tibet. Compared with the wild-type and mutant strains of the commonly used cellulase producer *T. reesei*, early cellulase induction and high production level of this strain were revealed, suggesting great potential of the strain as a robust cellulase producer (Li et al., 2019). On the other hand, *T. harzianum* LZ117 also serves as a good model to reveal the underlying regulatory mechanisms for cellulase induction and production.

In this report, we present results on isolating filamentous fungal strains from Tibet, with the aim to explore novel cellulase-producing strains. In addition, comparative transcriptome analysis was performed to reveal the mechanisms underlying regulation of cellulase production in *T. harzianum* LZ117. The results here would be helpful to develop better cellulase producers for lignocellulosic biorefinery.

MATERIALS AND METHODS

Description of Sample Collection for Strain Isolation

A total of 36 samples (22 plant samples, 10 soil samples, one melt iceberg water sample from the mountain, two samples from the surface of unknown mushroom and one barley wine starter sample) were collected from different locations in Tibet Autonomous Region of China in August 2018 (details in **Supplementary Table S1**). The soil samples were taken at a depth of 9–10 cm beneath the earth's surface and a distance of 2–3 cm from plant rhizosphere. The samples were placed in sterilized polyethylene bags and stored at 4°C for subsequent fungal isolation.

Isolation of Filamentous Fungal Strains

Serial dilution method was adopted for fungal isolation by using a series of selective media (summarized in **Supplementary Table S2**). Specifically, each sample (0.5–1 g) was immersed in 5 mL of sterile double-distilled H_2O, placed in a centrifuge tube with aseptic glass beads and grinded by Scientz-48 High-Throughput Tissue Grinder (Scientz Bio-tech, Ningbo, China), which was followed by serial dilution using sterilized distilled H_2O. An aliquot of 100 μL of each diluted sample was inoculated onto the Petri-plates containing the selective media supplemented with streptomycin (1%, w/v) to inhibit bacterial growth for primary isolation of fungi. Fungal cultures were incubated at 28°C for 3–5 days, and putative filamentous fungal colonies from the primary isolation agar plates were purified by two rounds of sub-culture on potato-dextrose agar (PDA) and cultured at 28°C. Pure cultures of the fungi were preserved in 20% (w/v) glycerol at −80°C.

Morphological and Molecular Analysis of the Fungal Strains

Filamentous fungal isolates were identified at the genus level via a combination of morphological properties and molecular analysis. Colony characteristics and microscopic morphology of fungal mycelia cultured on malt extract agar (MEA) or Potato Dextrose Agar (PDA) plates were observed following 7-day growth at 28°C. Molecular identification of filamentous fungal species was based on the analysis of the sequence of ITS (Internal Transcribed Spacer, including ITS1-5.8S-ITS2 region sequence of rRNA gene) previously recommended as a universal barcode to identify fungal species (Schoch et al., 2012).

Extraction of total DNA from fungal mycelia was performed according to the method described previously (Zhao et al., 2016). Briefly, mycelia were grinded with 0.4–0.6 mm glass-beads (Magen Biotech Co., Ltd., Guangzhou, China) in a specific amount of lysate reagent (40 mM Tris-HCl, 10 mM ethylenediaminetetraacetic acid, 20 mM sodium acetate, and 1% sodium dodecyl sulfate, pH 8.0),

then centrifuged at 12,000 × *g* for 3 min, followed by transfer of the supernatant into a new centrifuge tube. Subsequently, DNA precipitation was carried out at −20°C by adding isopropanol at a ratio of 1 supernatant: 1 isopropanol (v/v). Genomic DNA was collected after centrifugation at 12000 × *g*, 4°C for 10 min, then washed twice with 70% (v/v) ethanol, and dissolved in 50 μL sterile distilled H_2O.

ITS region was amplified from genomic DNA by PCR using primers ITS4 and ITS5 (White et al., 1990). The purified PCR products were sequenced by Tsingke Biotech Co., Ltd. (Shanghai, China). Identification of fungal isolates was performed via querying the obtained sequences against the NCBI database using BLASTn[1]. The sequences obtained were deposited in National Centre for Biotechnology Information (NCBI) under GenBank accession numbers from MK804322 to MK804409 (**Supplementary Table S1**).

Phylogenetic Analysis of the Fungal Strains

For phylogenetic analysis in MEGA v6.0 software (Tamura et al., 2013), the ITS region sequences of 88 isolates included in 43 filamentous fungal species were used to construct phylogenetic tree according to the neighbor-joining method (NJ tree, Saitou and Nei, 1987) after multiple alignment of sequences data by CLUSTAL_X (Thompson et al., 1997). The corrected evolutionary distance was evaluated according to Kimura's two-parameter model (Kimura, 1980). In order to estimate the consensus of the branching, the bootstrap resampling analysis of phylogenetic tree was employed with 1000 replicates of the data set.

Screening of Cellulolytic Fungi by Agar Culture and Submerged Culture

Extracellular cellulolytic activities were measured both qualitatively and quantitatively. For qualitatively evaluation, the fungi were cultivated on MA (Mandels and Andreotti, 1978) solid medium supplemented with bead-milling cellulose (20 g/L, w/v) as a sole carbon source at 28°C for 7 days. Cellulase activities were observed as transparent zones around the fungal colonies.

In regard to quantitative analysis of cellulase activities, 250 mL Erlenmeyer flasks with 50 mL MA medium [with 2% (m/v) lactose added as the carbon source] supplemented with 0.1% (w/v) peptone were inoculated with fungal spores (1×10^5/mL) collected from the culture in MEA medium, and incubated for 48 h at 28°C and shaking at 180 rpm for mycelial germination. Subsequently, the vigorous hyphal cultures were inoculated respectively with an inoculation size of 10% (v/v) into 250 mL Erlenmeyer flasks containing 50 mL MA mediums supplemented with 0.1% (w/v) peptone and 2% (m/v) microcrystalline cellulose (Merck, Germany) as the sole inducer for cellulase production at 28°C, shaking at 180 rpm.

[1]https://blast.ncbi.nlm.nih.gov/Blast.cgi

T. harzianum Strains and Growth Conditions

Trichoderma harzianum LZ117 was deposited at the China General Microbiological Culture Collection Center (CGMCC) by the strain number CGMCC 17184. *T. harzianum* K223452 (CGMCC 17199) that showed less potent cellulase production profile (Li et al., 2019) was used as the reference strain for comparative transcriptome analysis. The 7-day cultures of the fungal strains grown on MEA plates at 28°C were used to collect conidia. Mature conidia of strains were harvested using 2 mL of sterilized distilled H_2O and the prepared conidia suspensions were stored in sterilized 20% glycerol at −80°C.

Enzyme and Protein Concentration Assays

Sampling was performed at an interval of 24 h and the culture supernatants collected via centrifugation (10,000 rpm for 5 min at 4°C) were used for enzyme and secreted protein concentration assays according to the previously described method (Meng et al., 2020). Briefly, the activities of filter paper (FPA), CMCase and xylanases were measured using Whatman No. 1 filter paper (50 mg, 1.0 × 6.0 cm^2), CMC-Na (Sigma-Aldrich, United States) and beechwood xylan (Sigma-Aldrich) as substrates, respectively. The reaction mixtures contained 50 mg of filter paper, 1.0% CMC-Na or 1.0% xylan with 500 μL of the suitably diluted enzyme fractions. These mixtures were then incubated at 50°C for 60 min (FPA) or 30 min (CMCase and xylanases activities). The amount of reducing sugar released was determined using the DNS method (Ghose, 1987). One unit of enzymatic activity (U) was defined as the amount of enzyme required to produce 1 μmol of reducing sugar per min from the reaction substrates. The activities of cellobiohydrolases (CBHs) and β-glucosidase (BGL) were determined using *p*-nitrophenyl-β-D-cellobioside (*p*NPC) and *p*-nitrophenyl-β-D-glucopyranoside (*p*NPG) (Sigma-Aldrich) as substrates, respectively. The diluted supernatants (100 μL) were incubated with 50 μL of 10 mM *p*NPC or *p*NPG dissolved in 50 mM acetate buffer (pH 5.0) at 50°C for 30 min. Then, 150 μL of each sample was mixed with an equal volume of 10% sodium carbonate to stop the reactions. The absorbance at 405 nm was then measured. One unit of CBHs or BGL activity was defined as the amount of enzyme releasing 1 μmol of *p*NP per minute from the appropriate substrate. Concentration of secreted protein was determined using the Modified BCA Protein Assay Kit (Beyotime Bio-tech, Shanghai, China). All experiments were performed in three biological replicates.

Quantitative Reverse Transcription-PCR (RT-qPCR) Analysis

Due to unknown genomic context or coding sequences of genes to be detected in the naturally isolated *T. harzianum* strains, the primers for RT-qPCR analysis cannot be designed based on the known sequences. Thus, partial CDS sequences of the selected genes, including several cellulase genes, regulators as well as the internal control gene β-*tubulin*, were acquired by PCR with the primers which were designed according to corresponding

CDS sequences from three reference genomes of *T. harzianum* strains (*T. harzianum* TR274 v1.0, *T. harzianum* T22 v1.0, *T. harzianum* M10 v1.0) on the Joint Genome Institute (JGI)-MycoCosm database[2]. Next, the generated CDS fragments were sequenced and aligned by Clustal W[3], then a length of identical CDS sequence for each selected gene between *T. harzianum* LZ117 and the reference strain *T. harzianum* K223452 was used for designing respective quantitative primers. The primers for cloning of CDS fragments and RT-qPCR analysis are listed in **Supplementary Table S3**.

For RNA sampling, mycelia were harvested from *Trichoderma* strains that were cultivated on 2% microcrystalline cellulose at 24 h after a shift from lactose. RNA extraction, reverse transcription, and RT-qPCR were performed as reported previously (Meng et al., 2020). The relative transcription of genes was calculated by the $2^{-\Delta\Delta Ct}$ method (Livak and Schmittgen, 2001), with the β-tubulin gene as the internal reference gene for normalization (da Silva et al., 2017). Two biological replicates and three technical replicates for each reaction were carried out.

Comparative Transcriptomic Analysis

For comparative transcriptomic analysis between *T. harzianum* LZ117 and *T. harzianum* K223452, mycelia of the two strains cultured in MA medium supplemented with 2% microcrystalline cellulose and 0.1% peptone were collected at 24 h, and total RNA was extracted using the Spin Column Plant Total RNA Purification Kit (Sangon Biotech, China). RNA-seq based on Illumina Novaseq 6000 sequencing platform as well as transcriptome analysis was completed by Majorbio Bio-Tech (Shanghai, China) using the standard analysis methods. The reference genome of *T. harzianum* CBS 226.95 (assembly Triha v1.0; taxid: 983964) from NCBI genome database[4] was applied for mapping the sequenced clean reads using the software HISAT2 (Kim et al., 2015), and six major databases were adopted for gene homology and functional annotations (see **Supplementary Table S4**). TPM (Transcripts Per Million reads) (Conesa et al., 2016) was used as an index to analyze the gene expression levels by RSEM v1.2.12 software, and differential expressed genes were selected with the DESeq2 software (Love et al., 2014), with the thresholds: p-adjust < 0.05 and $|\mathrm{Log_2FC}| \geq 1$. CAZymes classification was performed according to the annotation of CAzymes genes in *T. harzianum* CBS 226.95[5]. In addition, the added descriptions of glycoside hydrolase genes and its transcription factor genes were based on the homologues in a model strain *T. reesei* QM6a[6]. Comparative transcriptome data analysis was completed partially using the free online Majorbio Cloud Platform[7]. Two biological replicates were performed, and the transcriptomic data are available at the SRA web site[8] under the accession number PRJNA613881.

[2]https://genome.jgi.doe.gov/mycocosm/home

[3]http://www.ebi.ac.uk/Tools/msa/clustalo/

[4]https://www.ncbi.nlm.nih.gov/genome/2441?genome_assembly_id=370086

[5]https://mycocosm.jgi.doe.gov/mycocosm/annotations/browser/cazy/summary;_Jo0wZ?p=Triha1

[6]https://mycocosm.jgi.doe.gov/pages/search-for-genes.jsf?organism=Trire2

[7]www.majorbio.com

[8]www.ncbi.nlm.nih.gov/sra/

Statistical Analysis

For each experiment, at least two biological replicates were performed with technical duplicates, and reproducible results were presented. All enzyme or protein assay data shown in this paper were carried out at least three times with identical or similar results. The error bars indicate the standard deviation (SD) from the mean of triplicates. Student's t-test was used to compare two samples, and $p < 0.05$ was considered to be significant.

RESULTS AND DISCUSSION

Biodiversity and Phylogenetic Analysis of the Isolated Filamentous Fungi

A total of 88 isolates of filamentous fungi (**Supplementary Table S1**) were isolated from the surface and/or interior of 36 distinct and unique samples collected from Tibet region in China, and the obtained strains were further characterized. Phylogenetic analysis showed that 88 isolates belong to three phyla, six classes, 12 orders, 18 families and 22 genera (**Supplementary Figure S1**).

Among the isolates, 70.5% of strains (62 isolates of 19 genera) were identified as *Ascomycota*, while 3.4% strains (three isolates of two genera) were identified as *Basidiomycota* and 26.1% strains (23 isolates of one genus) were identified as *Mucoromycota* (**Figure 1A**). At the order level, 35.2% of isolates (n = 31) belong to *Hypocreales,* 26.1% to *Mucorales* (n = 23), 13.6% to *Eurotiales* (n = 12), 8.0% to *Mortierellales* (n = 7), and 5.7% to *Pleosporales* (n = 5) (**Figure 1B**). At the genus level, over a half of the whole isolated strains were represented by the *Mucor* sp. (26.1%), *Fusarium* sp. (18.2%), and *Trichoderma* sp. (12.5%) (**Figure 1C**). From the soil samples, a total of 30 fungal strains were obtained, and the dominant groups of genus are *Mucor* sp. (30.0%), *Mortierella* sp. (20.0%) and *Trichoderma* sp. (20.0%); and the other groups are less than 10% for each genus (**Figure 1D**). In contrast, 58 fungal strains were obtained from samples of non-soil origin, and the most frequently isolated groups are *Mucor* sp. (24.1%), *Fusarium* sp. (22.4%), whereas the other groups are less than 10% for each genus (**Figure 1E**).

Strains belonging to the genus of *Mucor* are the most abundant fungal strains that were isolated from Tibet in this study. β-glucosidase from *Mucor circinelloides* have been studied (Kato et al., 2013; Huang et al., 2014), and it will be interesting to further study cellulase production from the isolated *Mucor* strains in the future work. Cellulase-producing *Fusarium* strains, including *F. oryzae* and *F. oxysporum* have been reported in the previous studies (Qin et al., 2010; Zhao et al., 2013; Xu et al., 2015). We did not isolate *Mucor* and *Fusarium* strains of the same species, and due to fewer studies on cellulase production from *Mucor* and *Fusarium* strains than that from *Aspergillus*, *Penicillium, Talaromyces,* and *Trichoderma*, we only tested cellulase activities in some selected strains, which are further discussed as below. However, we cannot exclude the possibility that the *Mucor* and *Fusarium* strains presented here have cellulase-producing ability. On the other hand, we identified these fungal strains based on the ITS sequences, but for more accurate species characterization,

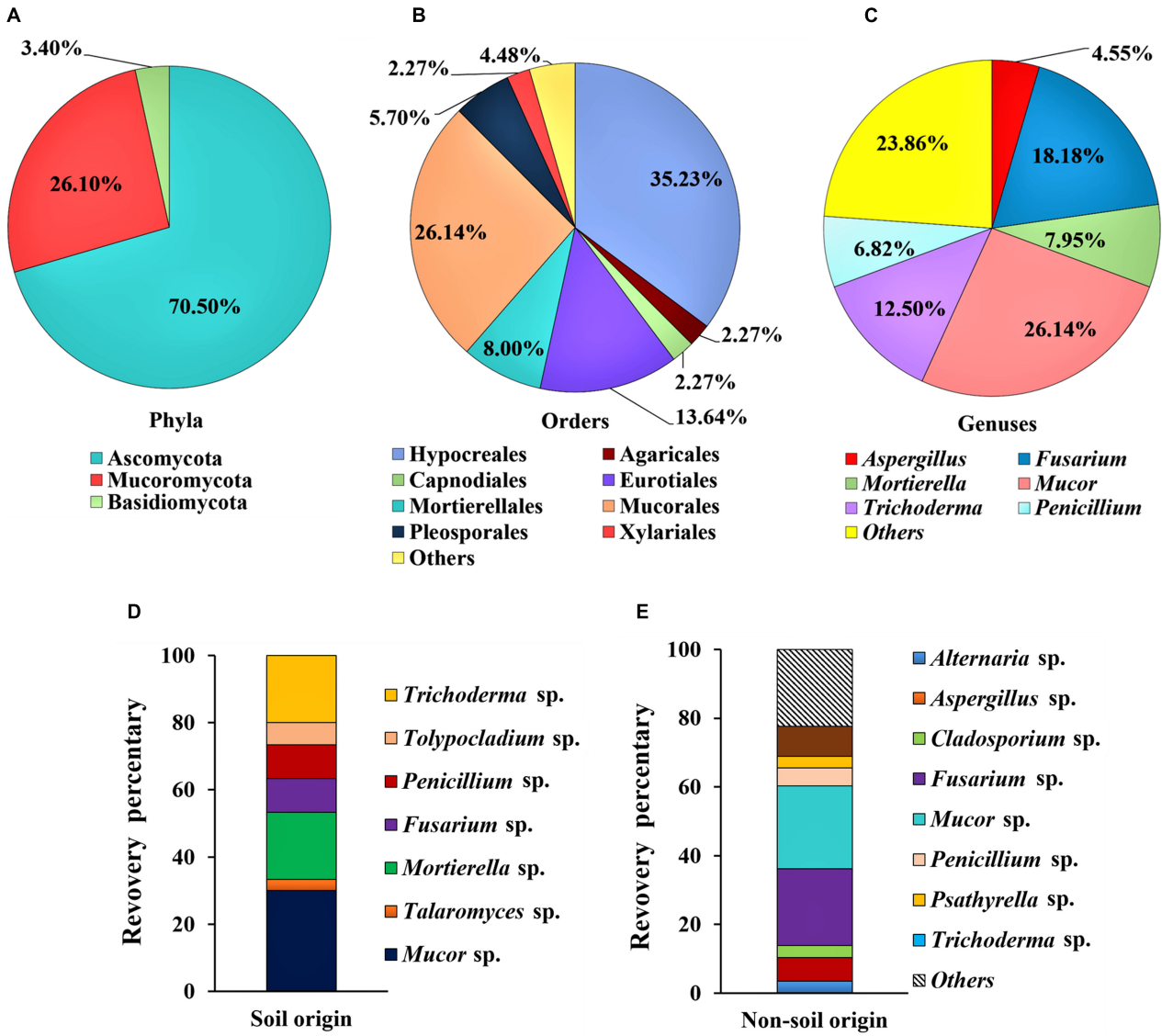

FIGURE 1 | Composition of the dominant filamentous fungal strains isolated from Tibet. The classification was shown at the phyla level **(A)**; order level **(B)**; and genus level **(C)**; and comparison on the diversity of the fungal strains between the soil **(D)** and the non-soil **(E)** samples.

more house-keeping genes should be sequenced, which will be performed in future studies.

Cellulase Activity of the Isolated Fungal Strains

Filamentous fungi, particularly, *Penicillium* sp., *Trichoderma* sp., *Aspergillus* sp., are of great interest due to their great capacity to produce plant cell wall-degrading enzymes (PCWDEs) used to convert lignocellulosic biomass to fermentable sugars (Passos et al., 2018). In addition, the *Talaromyces* genus, early regarded as a teleomorph state of *Penicillium*, forms a monophyletic clade distinct from the other *Penicillium* subgenera (Yilmaz et al., 2014), and *Talaromyces* strains have also been studied as cellulase producers (Liao et al., 2018; Méndez-Líter et al., 2019). Thus, 23 fungal strains that belongs to the genera of *Penicillium*, *Trichoderma*, *Aspergillus* and *Talaromyces* were selected for evaluation of PCWDEs production. An initial transparent zone assay based on cellulose solid plates with above-mentioned strains indicated that they all possessed cellulolytic activities (data not shown). Then, a quantitative assay of extracellular enzyme from the cellulolytic fungi was performed. In liquid culture, the selected fungal strains showed varying activities of cellulases, CMCase, *p*NPCase, *p*NPGase, and xylanase (**Table 1**) in the crude enzyme extracts. It can be seen directly that isolates derived from the same genus showed significant variations in the activities of the exo-cellular enzymes. Three strains, *T. harzianum* LZ117, *Trichoderma* sp. SC56-113 and *Trichoderma* sp. SC13-114, were revealed to produce higher levels of cellulase activities. CBHs (*p*NPCase) production was significantly higher in *Trichoderma*

TABLE 1 | Enzymatic activities of the isolated cellulolytic fungal strains from Tibet*.

Genus	Strain ID	FPase	*p*NPCase	CMCase	*p*NPGase	Xylanase
Trichoderma	C03-11	0.03	0.03	0.19	0.26	1.58
	C03-24	0.04	0	0.06	0.15	1.31
	C03-60	0.06	0.11	2.09	0	0.92
	SC11-65	0	0.03	0.13	0.32	0.3
	SC56-113	0.45	0.47	3.68	0.08	6.43
	SC13-114	0.44	0.44	3.67	0.07	8.5
	SC15-DY53	0.04	0.04	0.16	0.35	0.24
	C01-L2	0.04	0.21	0.16	0	0
	C03-L3	0.11	0.04	0.19	0	0.08
	C03-L4	0.1	0.05	0.23	0	0
	LZ117	0.65	0.31	7.17	2.91	51.87
Aspergillus	SC3_DY9	0	0.37	0.8	0.07	4.28
	SC3-48	0.04	0.42	1.36	0.04	0.74
	SC3-49	0.05	0.19	1.28	0.03	4.1
	SC18-123	0.04	0.16	0.1	0	2.24
Penicillium	SC15-L7	0.08	0.16	0.76	0	0.33
	A06-64	0	0.04	1.43	0	0
	CO3-87	0	0.03	0.9	0.03	0.25
	SC15_DY1	0.15	0.09	0.74	0.03	0.04
	SC15_DY4	0.03	0.25	1.28	0.03	2.93
	A04_DY23	0.04	0.26	0.75	0.03	0.91
Talaromyces	A01-L8	0.18	0.19	0.87	0	0.28
	SB17-DY49	0.13	0.19	0.72	0.03	0.22

**The change of table background color from light to dark in each row represents the transition from low enzyme activities to high enzyme activities.*

TABLE 2 | The main DEGs related to (hemi-) cellulases in *T. harzianum* LZ117*.

Gene ID[a]	Gene name	Description	Log_2FC[b]
486211	Mannosidase	GH76 family endo-1,6-alpha-mannosidase	2.91
441083	*egl2*	GH5 family endoglucanase 2	2.90
488374	*cel61b*	GH61 family AA9 protein	2.64
7497	*cbh1*	GH7 family exoglucanase 1	2.54
512303	*egl1*	GH7 family endoglucanase 1	1.33
6750	*cel5b*	GH5 family endo-1,4-glucanase	1.13
513492	*abf*	GH54 family alpha-L-arabinofuranosidase B	1.11
71613	*bgl1*	GH3 family beta-glucosidase (*cel3a*)	1.00
488862	Mannosidase	GH2 family predicted beta-mannosidase	−7.73
72100	Mannosidase	GH76 family endo-1,6-alpha-mannosidase	−5.51
107669	*bgl2*	GH1 family beta-glucosidase (*cel1a*)	−4.74
503269	*abf*	GH54 family alpha-L-arabinofuranosidase B	−4.19
77214	*cel3g*	GH3 family beta-glucosidase (*bgl3i*)	−3.81

**[a]Gene ID was assigned based on the T. harzianum CBS 226.95 genome database (https://www.ncbi.nlm.nih.gov/genome/2441?genome_assembly_id~=~370086). [b]FC: Ratio of the transcription of genes in T. harzianum LZ117 over that in T. harzianum K223452.*

sp. SC56-113, and other strains including *Trichoderma* sp. SC13-114, *Aspergillus* sp. SC3-DY9, and *Aspergillus* sp. SC3-48 also exhibited comparable *p*NPCase activity. Greater CMCase activity was observed in the case of three strains belonging to *T. harzianum* LZ117, SC56-113 and SC13-114 as compared to that from the other strains. Also, *T. harzianum* LZ117 produced significantly higher β-glucosidase activity (*p*NPGase, 2.91 U/mL) compared to the other strains. *Aspergillus* sp. and *Penicillium* (including *Talaromyces*) sp. isolated in this study showed lower level of β-glucosidase activity than that from the *Trichoderma* sp. strains. Furthermore, among these strains, significantly higher xylanase activity (51.87 ± 2.267 U/mL) was observed for *T. harzianum* LZ117. A notable xylanolytic activity was also observed in the case of *Trichoderma* sp. strains SC56-113 and SC13-114. The reason why certain enzyme activities could scarcely be detected in some strains might be due to the limited enzyme secretion capacity under the conditions employed in this study. Another reason is that enzyme measurement conditions used in this study are not optimal. Additionally, the diversity of cellulase and xylanase production detected might be resulted by different mycelial biomass. It is worth noting that *T. harzianum* LZ117 exhibited the most brilliant enzymatic activities, which renders it a potent source of PCWDEs for lignocellulose conversion.

We assumed that the unique environment such as high altitude in Tibet are inclined to endow local microorganisms special characteristics, including the ability to adapt to low temperature (Hu et al., 2015). It is of great interest to explore cold-adapted cellulase among the fungal strains. Unfortunately, we did not find cold-adapted cellulases using the conditions in this study (data not shown).

Comparative Transcriptome Analysis

T. harzianum LZ117 presented fast kinetic production of cellulase, which was represented by significantly higher Filter paper activity (FPA) and shorter fermentation time as compared to *T. harzianum* K223452, and FPA enzymatic profiles [productivity (FPA/h)] were shown in **Figure 2A**. Regulation of cellulase production *T. harzianum* has been limitedly studied so far, to further understand the mechanisms underlying faster cellulase formation and superior enzymatic activities of *T. harzianum* LZ117, comparative transcriptomic analysis for *T. harzianum* LZ117 and *T. harzianum* K223452 under submerged culture for cellulase production was performed. We believe that the mechanism studies would also provide clues to further engineering other cellulase-producing strains isolated from this work.

Due to the consideration that important molecular events mostly happen at early growth stage, we performed the transcriptome analysis using samples collected at 24 h. Transcriptome data showed a high correlation and consistency between the two biological replicates (**Supplementary Figure S2**). To further verify the reliability of transcriptome data, gene transcription analysis of *T. harzianum* LZ117 over *T. harzianum* K223452 at 24 h was performed by RT-qPCR for several genes, including the transcription factor genes *xyr1* and *cre1*, as well as glycosyl hydrolase genes *cbh1* (*cel7a*), *egl1* (*cel7b*), *egl2* (*cel5a*), and *bgl1* (*cel3a*). The RT-qPCR analysis results reflected that the changing trend in transcriptional levels of these genes was in consistency with those obtained from the comparative transcriptome analysis (**Figure 2B**), indicating that the RNA-seq data are reliable.

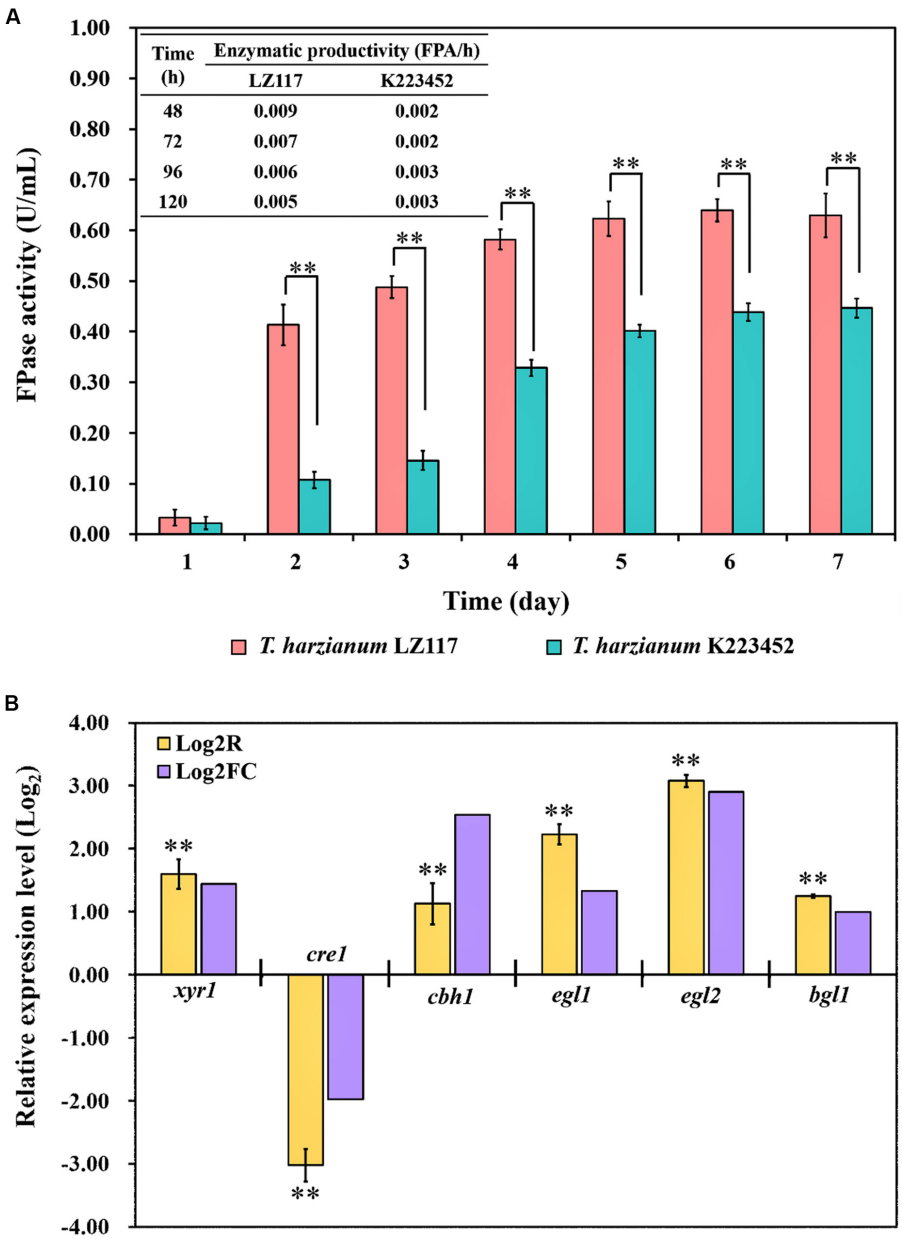

FIGURE 2 | Cellulase production of *T. harzianum* strains and validation of the transcriptome analysis. **(A)** Cellulase production profiles [FPA (U/mL) and productivity (FPA/h)] of *T. harzianum* LZ117 and *T. harzianum* K223452 cultured in shake flask using MA medium supplemented with 0.1% peptone and 2% microcrystalline cellulose. **(B)** Verification of the RNA-Seq data by RT-qPCR analysis using the selected genes encoding cellulolytic enzymes and transcription factors in *T. harzianum* LZ117 at 24 h (Log_2R and Log_2FC indicate results for RT-qPCR and RNA-seq, respectively). Error bars show the standard deviations, and the differences between groups were considered significant at $p < 0.01$ (Student's *t*-test) and are indicated by **.

Functional Enrichment Analysis of Differentially Expressed Genes (DEGs)

A total of 10887 unique transcripts were detected by RNA-seq analysis. Comparative transcriptome analysis showed that there were 1160 DEGs between *T. harzianum* LZ117 and K223452 at 24 h of cellulose induction ($|\log2FC| \geq 1$ and adjusted *p*-values ≤ 0.05), of which 375 genes were up-regulated and 785 genes were down-regulated (**Supplementary File S1**).

Gene ontology (GO) functional enrichment analysis of significantly up-regulated DEGs (**Figure 3A**) showed that not only genes involved in cellular process like protein synthesis, processing and degradation, but also metabolic activities of the cell, including subcategories of purine nucleotide metabolism, carbohydrate biosynthesis, and energy metabolism presented significant enrichment. Genes encoding various carbohydrate-active enzymes (CAZymes) showed increased

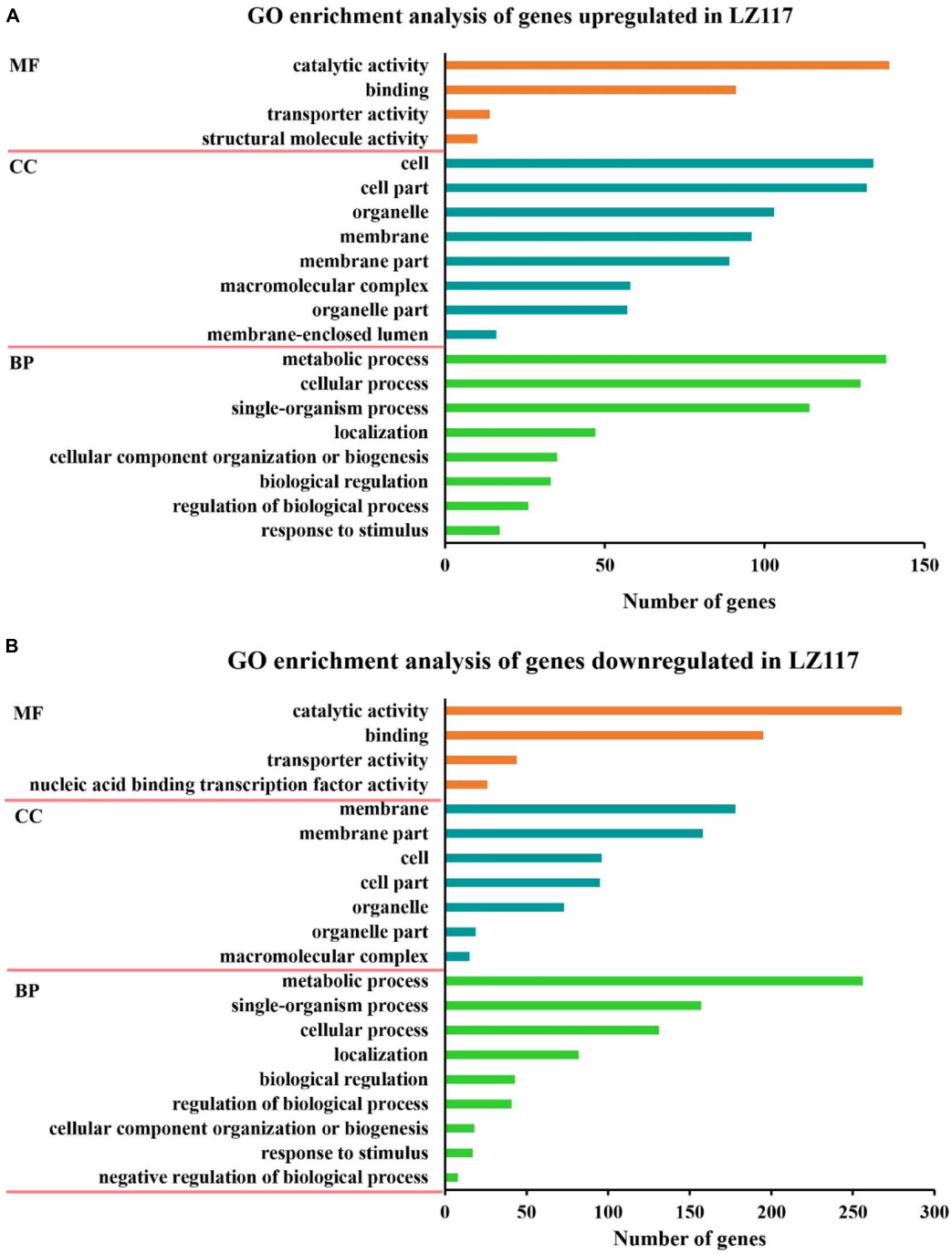

FIGURE 3 | GO enrichment analysis of the changed genes. Results of GO enrichment analysis of the upregulated **(A)** and downregulated **(B)** genes in *T. harzianum* LZ117 relative to *T. harzianum* K223452 were presented. The Y axis represents the name of the most enriched GOs: (MF) molecular function, (BP) biological process, while the *X* axis represents the number of DEGs in each enriched GO.

levels of transcription, and were included in the hydrolase activity sub-term of catalytic activity term in the GO result, which will be further discussed in the following section. Energy metabolism is important for protein synthesis, and we assume that up-regulation of the related genes may benefit cellulase production in LZ117.

On the other hand, the significantly down-regulated DEGs were mainly enriched in the functional categories of membrane, such as transmembrane transport of anions, carboxylic acids, amino acids and organic acids, and the functional genes involved in some sugars (such as chitin and glucosamine) metabolism and genes belonging to catalytic activity group were also significantly

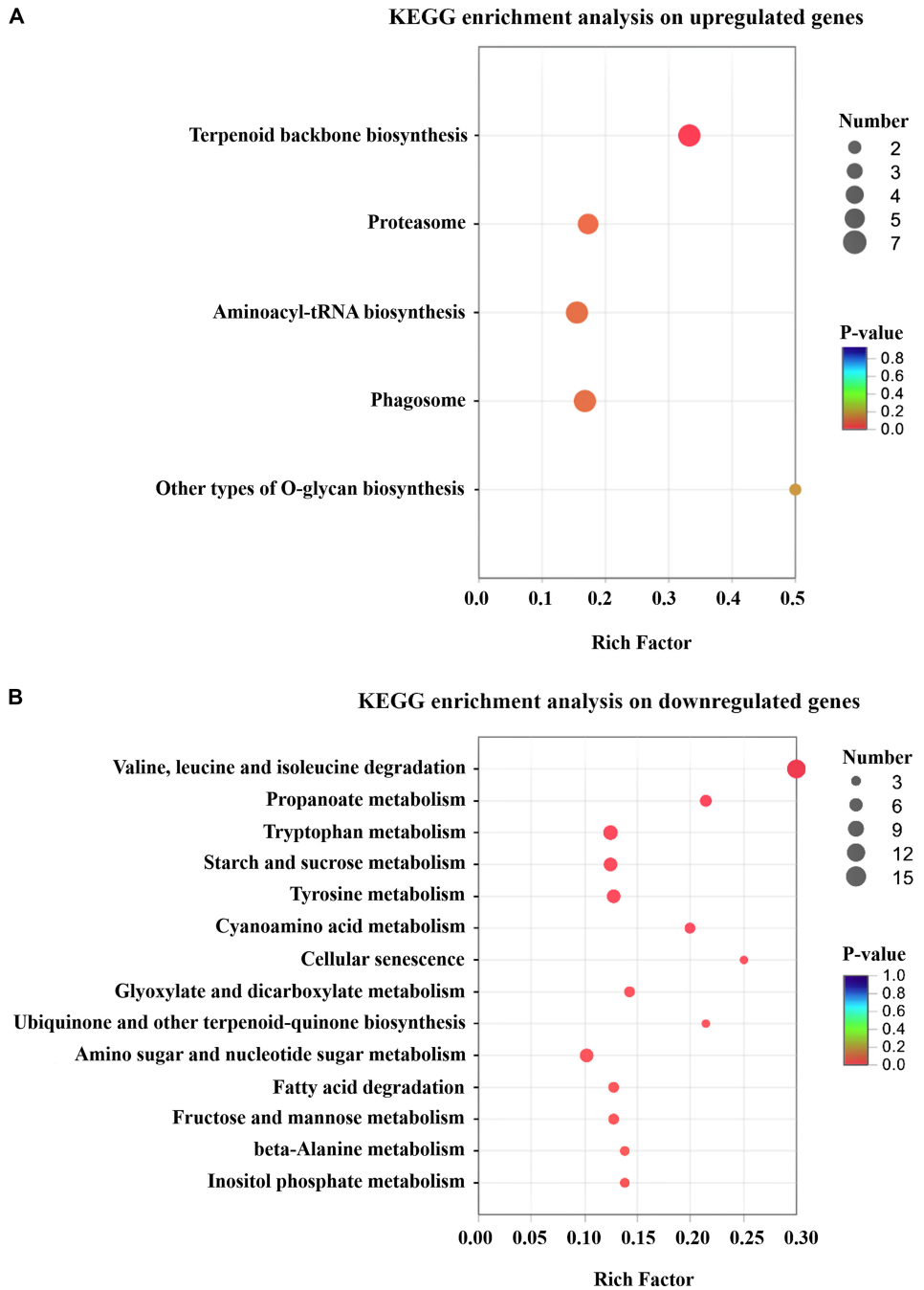

FIGURE 4 | KEGG pathway enrichment analysis of the changed genes. Results of the up-regulated **(A)** and down-regulated **(B)** genes in *T. harzianum* LZ117 relative to *T. harzianum* K223452 were presented. The degree of KEGG enrichment is assessed by the *P*-value and rich Factor. The *X* axis represents Rich factor (the ratio of the number of DEGs (sample numbers) enriched in the pathway to the number of all the annotated genes/transcripts mapped to the corresponding KEGG pathway (Background number). The size of the dot indicates the number of genes in this pathway, and the color of the dot corresponds to a range of different *P*-values (<0.05). The closer the *P*-value is to zero, the greater the Rich factor is, which means that the more the enrichment is significant.

enriched (**Figure 3B**). We deduce that down-regulation of some key metabolism may be helpful to direct more precursors and energy for enzyme biosynthesis.

A total of 199 up-regulated genes were involved in cellular process like protein synthesis, processing and degradation, primary metabolism, small molecule metabolism, such as energy metabolism, cofactors, and vitamin metabolism. Furthermore, *T. harzianum* LZ117 may possess more active anabolism of anabolic secondary metabolites considering the DEGs enrichment in the isoprenoid, terpenoid and polyketides

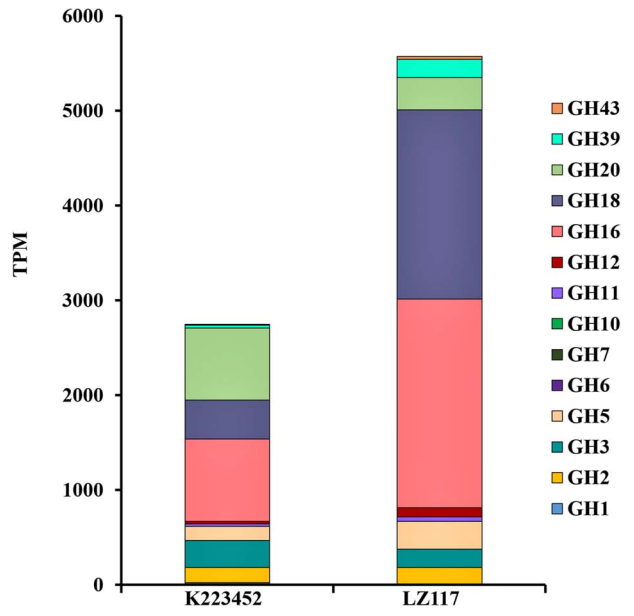

FIGURE 5 | Expression profiles of genes encoding major carbohydrate-active enzymes (CAZymes). The data were extracted from the RNA-seq analysis, which provided the expression values as TPM (Transcripts Per Million reads) mapped for each glycolic hydrolase (GH) family. CAZymes classification was performed according to the annotation of CAzymes genes in *T. harzianum* CBS 226.95 (https://mycocosm.jgi.doe.gov/mycocosm/annotations/browser/cazy/summary;_Jo0wZ?p~=~Triha1).

biosynthetic metabolic pathways (**Figure 4A**). Whereas, down-regulated genes were significantly enriched in valine, leucine, and isoleucine degradation, propanoate metabolism, tryptophan metabolism, starch and sucrose metabolism, as well as tyrosine metabolism (**Figure 4B**). Further exploration of the relationship between these transcriptional changes of pathway genes with cellulase biosynthesis in LZ117 will provide more clues in regulation of cellulase production in this strain.

Transcription Analysis of Glycosyl Hydrolase Genes

In view of the maximum productivity of cellulase achieved by *T. harzianum* LZ117 strain at 48 h, transcriptional pattern of the glycoside hydrolase genes in *T. harzianum* LZ117 was illustrated, in which the lignocellulosic degrading-enzymes were focused (**Supplementary File S2** and **Table 2**). As a whole, the transcription levels of 66 CAZyme genes were significantly changed, of which 19 genes were upregulated and 47 genes were downregulated. The expression of glycoside hydrolase genes from GH5, GH6, GH7, GH11, GH12, GH16, and GH18 families were up-regulated in *T. harzianum* LZ117, and the major cellulase genes were distributed into GH5, GH6, and GH7 families. The total transcription quantity of glycoside hydrolase genes belonging to GH3 and GH20 families decreased (**Figure 5**).

The cellulase cocktail produced by *T. reesei* mainly comprise two cellobiohydrolases (CBHI/Cel7A and CBHII/Cel6A), two endoglucanases (EGI/Cel7B and EGII/Cel5A), and β-glucosidase I (BGLI/Cel3A) that can hydrolyze lignocellulosic complexes synergistically, combined with related hemi-cellulases and auxiliary proteins (Bischof et al., 2016; Druzhinina and Kubicek, 2017). Especially, the major component, CBH1 from *T. reesei* constitutes nearly half of the extracellular protein (Druzhinina and Kubicek, 2017). The transcriptional levels of the major CBH gene *cbh1* and EGs genes *egl1*, *egl2* of *T. harzianum* LZ117 were significantly up-regulated at 24 h comparing with that of K223452 strain, which were essential for robust cellulase production from *T. harzianum* LZ117. Furthermore, the transcription level of *cel5b* gene encoding a GPI anchoring domain-containing membrane-bound protein was also up-regulated in *T. harzianum* LZ117, which is constitutively expressed when cultured on sophorose or lactose, and induced by a small amount under cellulose culture condition in *T. reesei* (Foreman et al., 2003). The transcript of β-glucosidase gene *bgl1* (*cel3a*) in *T. harzianum* LZ117 was increased by around onefold compared with that from *T. harzianum* K223452, which may cause the increased BGL activity of *T. harzianum* LZ117 compared to that of *T. harzianum* K223452. CEL1A has been reported to catalyze transglycosylation of cellobiose to sophorose (sophorose, considered to be the natural strongest inducer of cellulase), which in turn induces *T. reesei* cellulase synthesis (Shida et al., 2015). Surprisingly, the β-glucosidase gene *bgl2* (*cel1a*) of *T. harzianum* LZ117 was down-regulated, whether CEL1A has the similar transglycosylated function as in *T. reesei* for cellulase induction in *T. harzianum* remains to be verified. It is worth noting that the transcription of *cel3g* (*Th_77214*) in *T. harzianum* LZ117 was significantly down-regulated for 14 folds, which may accelerate the initial cellulase induction of *T. harzianum* LZ117, because the present of β-glucosidase gene *cel3g* could affect extracellular lactose absorption and hydrolyze the intracellular sophorose, whose knockout promotes cellulase formation in *T. reesei* (Zou et al., 2018). Increased transcription level of the *cel61b* (*Th_488374*) gene encoding an Auxiliary Activity Family 9 (AA9) protein in *T. harzianum* LZ117 may also help to improve its cellulose hydrolysis efficiency. Even though the transcription level of arabinofuranosidase gene *Th_503269* and two mannosidase genes decreased obviously, no remarkable changes of transcripts of core hemicellulase genes related to xylan degradation in *T. harzianum* LZ117 were observed, such as *xyn1* (*Th_525076*), *xyn2* (*Th_115099*), *xyn3* (*Th_155799*), *axe1* (*Th_94998*), *bxl1* (*Th_502198*), and *cel74a* (*Th_88968*), which resulted in comparable xylanase activities between *T. harzianum* LZ117 and K223452. The downregulated transcripts of gene *Th_133914* encoding extracellular protease (homologous to *tre120998* in *T. reesei*) may contribute to the stability of secreted cellulases from *T. harzianum* LZ117 compared to that in *H. harianum* K223452 (Qian et al., 2019).

Changed Genes That Encode Regulators and Major Transporters

The expression of lignocellulose degrading enzymes in filamentous fungi depends on a regulatory network of multiple positive and negative transcription factors (TFs) (Alazi and Ram, 2018). A total of 660 genes in the *T. harzianum* genome were predicted to function as transcriptional regulators, among which the transcripts of 57 genes changed significantly at 24 h, and five of these genes were up-regulated, whereas 52

genes were down-regulated ($|Log_2FC| > 1$, p-adjust < 0.05) (**Supplementary File S3**). Besides the regulators Xyr1 (Th_1126) and Cre1 (Th_502975) reported to regulate cellulase production by *T. harzianum* (da Silva et al., 2017), the effects of other differentially expressed transcription factors potentially regulating cellulase induction in *T. harzianum* will be discussed below according to their homologues in *T. reesei*.

In the filamentous fungus *T. reesei*, expression of cellulase is tightly regulated by a series of TFs such as transcriptional activators: Xyr1, Ace3, Vib1 and repressors, including Cre1, Ace1, Rce1, and Ctf1 (Zhang et al., 2018; Liu and Qu, 2019; Meng et al., 2020). Among these factors, the homologues of regulator Xyr1 are the most conserved in cellulolytic fungi (Klaubauf et al., 2014). The C2H2-type TF Cre1/CreA functions as the main negative regulator that mediates carbon catabolite repression (CCR) effect (Li et al., 2015; Huberman et al., 2016; Rassinger et al., 2018). Comparative transcriptome analysis showed that the transcription of *xyr1* (*Th_1126*) gene was significantly up-regulated 1.7-fold in *T. harzianum* LZ117, while the transcriptions of the *cre1* (*Th_502975*), *ace1* (*Th_496062*) and *rce1* (*Th_495839*) genes homologous to counterparts in *T. reesei* were significantly decreased to varying degrees, with fold change (Log_2FC) from -1.43 $< Log_2FC < -1.97$ (**Supplementary File S3**). However, the transcripts of *ace3, ctf1*, and *vib1* (*Th_140772*, *Th_469719* and *Th_482779*, respectively) have not changed significantly in *T. harzianum* LZ117. The regulator Rxe1 positively modulates the activator Xyr1 and cellulase gene expression in *T. reesei* (Wang et al., 2019). However, the transcript of *rxe1* homolog (*Th_61248*) in *T. harzianum* LZ117 was dramatically decreased, thus the regulatory relationship between Rxe1 and Xyr1 in *T. harzianum* remains unclear. It was also revealed that Xyr1 recruits SWI/SNF complex through direct interactions with TrSNF12 to remodel chromatin at cellulase gene promoters, thereby activating cellulase gene expression in *T. reesei* (Cao et al., 2019) but no significant change for the transcription of *Trsnf12* homolog (*Th_101097*) in *T. harzianum* LZ117 was found as compared to the control strain. The Velvet family protein Ve1 (Liu et al., 2015) in *T. reesei* plays an important role in the regulation of cellulase expression, while transcriptional level of its homologous gene *veA* (*Th_95531*) in *T. harzianum* LZ117 has not changed significantly. These results imply the elevated transcript level of *xyr1* and reduced transcription of *cre1* may partly account for the faster cellulase induction and higher cellulase activity of *T. harzianum* LZ117 in the early phase of cellulase production, and there are different recruitment mechanisms of Xyr1 function between *T. harzianum* LZ117 and *T. reesei*.

Changes in the levels of the main transcription factors Xyr1 and Cre1 proteins under different induced carbon sources may affect the transporter family proteins in *T. reesei*, especially major facilitator superfamily (MFS) (dos Santos et al., 2014, 2016). About 77 genes in the *T. harzianum* genome are predicted to have sugar transport function, and there are about 11 predicted sugar transporter genes with significant transcriptional changes in transcriptome data ($|Log_2FC| > 1$, p-adjust < 0.05) (**Supplementary Table S5**). Some sugar transporters have the signal transmitting function for extracellular carbon-induced signals. For example, the sugar transporters Cdt1 and Cdt2 (Znameroski et al., 2013) in *Neurospora crassa*, the sugar transporter CltB (dos Reis et al., 2016) in *A. nidulans*, and the sugar transporter Crt1 in *T. reesei* was reported to possess the function of carbon signaling (Zhang et al., 2013). Unexpectedly, the transcript of *crt1* gene (*Th_502689*) decreased remarkably in *T. harzianum* LZ117 over that in *T. harzianum* K223452. The transcript levels of the homologue of *cdt1* and *cdt2* genes, *Th_75576* and *Th_130330* respectively, in *T. harzianum* LZ117 were also similar to that in K223452, so did the transcript of *cltb* homologous gene (*Th_101977*). Cre-1-mediated CCR in *N. crassa* acts through sugar transporter, transcription factor, sugar catabolism, and PCWDE genes to regulate plant cell wall degradation (Wu et al., 2020). In our results, down-regulation of *cre1* did not correlate with enhanced expressions of the master sugar transporters such as *cdt1*, *cdt2*, which demonstrate that regulatory mechanism underlying Cre1-mediated CCR might be varied between different fungal species. Other novel sugar transporters that are crucial for cellulase induction signaling in *T. harzianum* will be further investigated in future studies.

DEGs Related to Protein Synthesis, Sorting and Quality Control

The functional classification analysis for DEGs indicated that the transcriptional levels of 78.6% of the DEGs involved in transcription and protein synthesis in *T. harzianum* LZ117 strains were up-regulated as compared to *T. harzianum* K223452 (**Table 3**). Specifically, RNA polymerase I, II, and III subunit encoding genes (*Th_71797*, *Th_76852*, and *Th_121495*) were up-regulated by 5.2, 3.4, and 7.2 times, respectively, suggesting that rRNA, mRNA and tRNA synthesis activities the LZ117 strain may be enhanced compared with that in K223452 strain. Regarding the DEGs that function in protein translation process, the transcription of eight genes involved in aminoacyl tRNA synthesis in the LZ117 strain was up-regulated by at least 3.4 times, which provided a sufficient amount of related amino acid donors for the enhanced protein synthesis process of *T. harzianum* LZ117. In addition, up-regulation of the mitochondrial ribosomal protein encoding genes *Th_514053* and *Th_504396* indicate that the energy metabolism of *T. harzianum* LZ117 might be more vigorous than that of K223452. Interestingly, the ribosomal protein encoding genes *Th_113828* and *Th_484754*, and two translation initiation factor encoding genes *Th_8152* and *Th_503429* were significantly up-regulated by at least 3.8 times (**Table 3**), indicating that protein synthesis of the *T. harzianum* LZ117 may be increased compared to that of K223452.

Regarding the protein folding processing and sorting pathway (**Table 4**), the transcription of the glucosidase II β subunit-encoding gene (*Th_83575*) in *T. harzianum* LZ117 strain was significantly up-regulated, which may be involved in protein glycosylation modification in the endoplasmic reticulum (Cui et al., 2016). In addition, in *T. harzianum* LZ117, the transcription levels of gene *Th_482508* encoding the molecular chaperone T complex 1β subunit, and gene *Th_92965* encoding the signal recognition particle receptor α subunit were up-regulated by 6.2- and 5.0-fold respectively,

TABLE 3 | The DEGs related to protein synthesis in strain LZ117*.

Gene ID[a]	Functional annotation (Swiss-Prot Description)[b]	Log_2FC[c]
	Transcription	
121495	DNA-directed RNA polymerase III subunit RPC10	3.03
71797	DNA-directed RNA polymerase I subunit RPA12	2.63
76852	DNA-directed RNA polymerase II subunit RPB9	2.13
	Translation	
72064	Phenylalanine-tRNA ligase	8.30
81396	Putative glycine–tRNA ligase	3.94
115899	Aspartate–tRNA ligase, mitochondrial	3.50
113828	40S ribosomal protein S20	3.30
484440	Glutaminyl-tRNA synthase	3.18
514053	54S ribosomal protein L24, mitochondrial	2.87
513968	Ribonucleoprotein-associated protein	2.78
303	Phenylalanine–tRNA ligase alpha subunit	2.77
482810	Putative proline–tRNA ligase	2.59
503429	Eukaryotic translation initiation factor 5A	2.59
500010	Tyrosine–tRNA ligase, cytoplasmic	2.40
504396	54S ribosomal protein subunit img1, mitochondrial	2.29
8152	Eukaryotic translation initiation factor 3 subunit H	2.27
484754	60S acidic ribosomal protein P2	2.26
479650	Glutamate-tRNA ligase, cytoplasmic	2.13
9281	Translation initiation factor eIF-2B subunit gamma	−2.36

*[a]*Gene ID was assigned based on the T. harzianum CBS 226.95 genome database (https://www.ncbi.nlm.nih.gov/genome/2441?genome_assembly_id=370086). [b]Annotation of RNA-seq data against Swiss-Prot database. [c]FC: Ratio of the transcription of genes in strain LZ117 over that in strain K223452.*

TABLE 4 | The DEGs related to protein folding, sorting and degradation in strain LZ117*.

Gene ID[a]	Functional annotation (Swiss-Prot Description)[b]	Log_2FC[c]
83575	Glucosidase II beta subunit	4.33
352623	Proteasome subunit alpha type-6	2.93
482508	Probable T-complex protein 1 subunit beta	2.85
92409	Proteasome subunit beta type-1	2.81
488956	Ubiquitin homeostasis protein	2.66
504589	Proteasome subunit beta type-3	2.63
92965	Signal recognition particle receptor subunit alpha	2.58
510360	Heat shock protein Hsp30	2.58
480080	Proteasome subunit alpha type-7	2.41
505979	Protein transport protein sec13	2.37
511826	Proteasome subunit alpha type-3	2.22
6117	Ubiquitin-activating enzyme E1	2.18
405376	26S proteasome regulatory subunit	2.12
145858	Endoplasmic reticulum chaperone	−6.54

*[a]*Gene ID was assigned based on the T. harzianum CBS 226.95 genome database (https://www.ncbi.nlm.nih.gov/genome/2441?genome_assembly_id~=~370086). [b]Annotation of RNA-seq data against Swiss-Prot database. [c]FC: Ratio of the transcription of genes in strain LZ117 over that in strain K223452.*

which are beneficial for protein folding and exosome-based protein secretion (Wu et al., 2015). Furthermore, significant changes were also observed in genes related to chaperones and ubiquitin-proteasome system for protein quality control (**Table 4**), the transcription of *hacI* gene (*Th_72005*) in *T. harzianum* LZ117 was 1.7 times that of the corresponding transcript of *T. harzianum* K223452, and the transcription of *Th_510360* encoding heat shock protein Hsp30 was up-regulated by 5.0-fold. Meanwhile, the transcription levels of ubiquitin-activating enzyme E1 gene *Th_6117* responsible for misfolded protein degradation, the ubiquitin homeostasis regulatory protein encoding gene *Th_488956*, and genes encoding multiple proteasome subunits were significantly up-regulated. The changes of endoplasmic reticulum marker enzymes and ubiquitin-proteasome proteins indicated increased cellulase synthesis by *T. harzianum* LZ117 at the early cellulase production stage.

Previously, transcriptomic profile analysis of *T. harzianum* underlying biomass degradation has been conducted using *T. harzianum* IOC-3844 induced by sugarcane bagasse and cellulose (Horta et al., 2014). In a recent study, transcriptome of *T. harzianum* was compared with other two *Trichoderma* species (Horta et al., 2018). However, the samples in both studies were collected at 96 h. In the current study, a global transcriptional profile involved in the induction and transcriptional regulation of cellulase was focused, which contributes to the catalog of publicly available transcriptome data from *T. harzianum*, and provides useful clues for unraveling the biotechnological potential of this important *Trichoderma* species for lignocellulosic biorefinery. Genes identified in this study can be further analyzed and used to improve cellulase production in other *T. harzianum* strains as well as *T. reesei* strains. Further studies on cellulase production from *T. harzianum* will unveil more important aspects of this species and enrich the knowledge on cellulase production by filamentous fungi.

In this report, comprehensive analysis of global gene transcription in the promising cellulase producing strain LZ117 at early cellulase-producing stage has been performed. However, the possibility that other mechanisms also exist that affect cellulase production in this strain cannot be excluded, including single nucleotide polymorphism in the genome, post-translational control, and so on. The finding in this study is a reminder that we still have much to learn on the potential of biotechnology applications of microbial strains from Tibet in China, and provide a basis for further exploration of other fungal enzyme producers from specific environments.

CONCLUSION

In this study, 88 filamentous fungal strains were isolated from 36 samples collected from Tibet. Screening for cellulase-producing fungi indicated *T. harzianum* LZ117 is the most potent strain. Comparative transcriptome analysis between *T. harzianum* LZ117 and the control strain revealed significant modulation and quality control of protein synthesis, processing and degradation in *T. harzianum* LZ117 at early cellulase producing stage. Up-regulation of the activator Xyr1 in combination with down-regulation of the repressor Cre1 may lead to early induction of glycoside hydrolases, and global changes in transcriptional regulation, protein production and

processing may also contribute to high cellulase production titer in *T. harzianum* LZ117.

DATA AVAILABILITY STATEMENT

The datasets presented in this study can be found in online repositories. The names of the repository/repositories and accession number(s) can be found in the article/**Supplementary Material**.

AUTHOR CONTRIBUTIONS

J-XL and FZ performed the experiments and analyzed the data. D-DJ, JL, F-LW, and ZZ provided the samples from Tibet and participated in discussion of strain identification. J-XL drafted the manuscript. X-QZ designed the experiments and critically revised the manuscript. WW participated in discussion of the data and revised the manuscript. All the authors read and approved the final version of the manuscript.

FUNDING

This work was financially supported by the National Natural Science Foundation of China (No. 21536006), the Open Funding Project of the State Key Laboratory of Bioreactor Engineering, and State Key Laboratory of Microbial Technology Open Projects Fund (No. M2017-10).

SUPPLEMENTARY MATERIAL

The Supplementary Material for this article can be found online at: https://www.frontiersin.org/articles/10.3389/fmicb.2020.01617/full#supplementary-material

REFERENCES

Alazi, E., and Ram, A. F. J. (2018). Modulating transcriptional regulation of plant biomass degrading enzyme networks for rational design of industrial fungal strains. *Front. Bioeng. Biotechnol.* 6:133. doi: 10.3389/fbioe.2018.00133

Benoliel, B., Torres, F. A. G., and de Moraes, L. M. P. (2013). A novel promising *Trichoderma harzianum* strain for the production of a cellulolytic complex using sugarcane bagasse in natura. *SpringerPlus* 2:656. doi: 10.1186/2193-1801-2-656

Bischof, R. H., Ramoni, J., and Seiboth, B. (2016). Cellulases and beyond: the first 70 years of the enzyme producer *Trichoderma reesei*. *Microb. Cell Fact.* 15:106. doi: 10.1186/s12934-016-0507-6

Cao, Y., Zheng, F., Zhang, W., Meng, X., and Liu, W. (2019). *Trichoderma reesei* XYR 1 recruits SWI / SNF to facilitate cellulase gene expression. *Mol. Microbiol.* 112, 1145–1162. doi: 10.1111/mmi.14352

Champreda, V., Mhuantong, W., Lekakarn, H., Bunterngsook, B., Kanokratana, P., Zhao, X. Q., et al. (2019). Designing cellulolytic enzyme systems for biorefinery: from nature to application. *J. Biosci. Bioeng.* 128, 637–654. doi: 10.1016/j.jbiosc.2019.05.007

Conesa, A., Madrigal, P., Tarazona, S., Gomez-Cabrero, D., Cervera, A., McPherson, A., et al. (2016). A survey of best practices for RNA-seq data analysis. *Genome Biol.* 17:13. doi: 10.1186/s13059-016-0881-8

Cui, J., Chen, B., Wang, H. J., Han, Y., Chen, X., and Zhang, W. (2016). Glucosidase II β-subunit, a novel substrate for caspase-3-like activity in rice, plays as a molecular switch between autophagy and programmed cell death. *Sci. Rep.* 6:31764. doi: 10.1038/srep31764

da Silva, D. P., Rodrigues, G. N., Zubieta, M. P., Ramoni, J., Codima, C. A., Lima, D. J., et al. (2017). The relation between xyr1 overexpression in *Trichoderma harzianum* and sugarcane bagasse saccharification performance. *J. Biotechnol.* 246, 24–32. doi: 10.1016/j.jbiotec.2017.02.002

de Castro, A. M., Ferreira, M. C., da Cruz, J. C., Pedro, K. C. N. R., Carvalho, D. F., Leite, S. G. F., et al. (2010). High-yield endoglucanase production by *Trichoderma harzianum* IOC-3844 cultivated in pretreated sugarcane mill byproduct. *Enzyme Res.* 2010:854526. doi: 10.4061/2010/854526

dos Reis, T. F., de Lima, P. B., Parachin, N. S., Mingossi, F. B., de Castro Oliveira, J. V., Ries, L. N., et al. (2016). Identification and characterization of putative xylose and cellobiose transporters in *Aspergillus nidulans*. *Biotechnol. Biofuels* 9:204. doi: 10.1186/s13068-016-0611-1

dos Santos, C. L., de Paula, R. G., Antoniêto, A. C., Persinoti, G. F., Silva-Rocha, R., and Silva, R. N. (2016). Understanding the role of the master regulator XYR1 in *Trichoderma reesei* by global transcriptional analysis. *Front. Microbiol.* 7:175. doi: 10.3389/fmicb.2016.00175

dos Santos, C. L., Pedersoli, W. R., Antoniêto, A. C. C., Steindorff, A. S., Silva-Rocha, R., Martinez-Rossi, N. M., et al. (2014). Comparative metabolism of cellulose, sophorose and glucose in *Trichoderma reesei* using high-throughput genomic and proteomic analyses. *Biotechnol. Biofuels* 7:41. doi: 10.1186/1754-6834-7-41

Druzhinina, I. S., and Kubicek, C. P. (2017). Genetic engineering of *Trichoderma reesei* cellulases and their production. *Microb. Biotechnol.* 10, 1485–1499. doi: 10.1111/1751-7915.12726

Ferreira, J. A., Horta, M. A. C., Beloti, L. L., dos Santos, C. A., and de Souza, A. P. (2017). Carbohydrate-active enzymes in *Trichoderma harzianum*: a bioinformatic analysis bioprospecting for key enzymes for the biofuels industry. *BMC Genomics* 18:779. doi: 10.1186/s12864-017-4181-9

Foreman, P. K., Brown, D., Dankmeyer, L., Dean, R., Diener, S., Dunn-Coleman, N. S., et al. (2003). Transcriptional regulation of biomass-degrading enzymes in the filamentous fungus *Trichoderma reesei*. *J. Biol. Chem.* 278, 31988–31997. doi: 10.1074/jbc.M304750200

Ghose, T. K. (1987). Measurement of cellulase activities. *Pure Appl. Chem.* 59, 257–268. doi: 10.1351/pac198759020257

Horta, M. A. C., Ferreira Filho, J. A., Murad, N. F., de Oliveira Santos, E., dos Santos, C. A., Mendes, J. S., et al. (2018). Network of proteins, enzymes and genes linked to biomass degradation shared by Trichoderma species. *Sci. Rep.* 8, 1–11. doi: 10.1038/s41598-018-19671-w

Horta, M. A. C., Vicentini, R., Delabona, P., da, S., Laborda, P., Crucello, A., et al. (2014). Transcriptome profile of *Trichoderma harzianum* IOC-3844 induced by sugarcane bagasse. *PLoS One* 9:e88689. doi: 10.1371/journal.pone.0088689

Hu, H., Yan, F. J., Wilson, C., Shen, Q., and Zheng, X. D. (2015). The ability of a cold-adapted *Rhodotorula mucilaginosa* strain from Tibet to control blue mold in pear fruit. *Antonie Van Leeuwenhoek* 108, 1391–1404. doi: 10.1007/s10482-015-0593-1

Hu, W., Zhang, Q., Li, D., Cheng, G., Mu, J., Wu, Q., et al. (2014). Diversity and community structure of fungi through a permafrost core profile from the Qinghai-Tibet Plateau of China. *J. Basic Microbiol.* 54, 1331–1341. doi: 10.1002/jobm.201400232

Huang, Y., Busk, P. K., Grell, M. N., Zhao, H., and Lange, L. (2014). Identification of a β-glucosidase from the *Mucor circinelloides* genome by peptide pattern recognition. *Enzyme Microb. Technol.* 67, 47–52. doi: 10.1016/j.enzmictec.2014.09.002

Huberman, L. B., Liu, J., Qin, L. N., and Glass, N. L. (2016). Regulation of the lignocellulolytic response in filamentous fungi. *Fungal Biol. Rev.* 30, 101–111. doi: 10.1016/j.fbr.2016.06.001

Kato, Y., Nomura, T., Ogita, S., Takano, M., and Hoshino, K. (2013). Two new β-glucosidases from ethanol-fermenting fungus *Mucor circinelloides* NBRC 4572: enzyme purification, functional characterization, and molecular cloning of the

gene. *Appl. Microbiol. Biotechnol.* 97, 10045–10056. doi: 10.1007/s00253-013-5210-5

Kim, D., Langmead, B., and Salzberg, S. L. (2015). HISAT: a fast spliced aligner with low memory requirements. *Nat. Methods* 12, 357–360. doi: 10.1038/nmeth.3317

Kimura, M. (1980). A simple method for estimating evolutionary rates of base substitutions through comparative studies of nucleotide sequences. *J. Mol. Evol.* 16, 111–120. doi: 10.1007/BF01731581

Klaubauf, S., Narang, H. M., Post, H., Zhou, M., Brunner, K., Mach-Aigner, A. R., et al. (2014). Similar is not the same: differences in the function of the (hemi-)cellulolytic regulator XlnR (Xlr1/Xyr1) in filamentous fungi. *Fungal Genet. Biol.* 72, 73–81. doi: 10.1016/j.fgb.2014.07.007

Li, J., Zhang, F., Li, J., Zhang, Z., Bai, F., Chen, J., et al. (2019). Rapid production of lignocellulolytic enzymes by *Trichoderma harzianum* LZ117 isolated from Tibet for biomass degradation. *Bioresour. Technol.* 292:122063. doi: 10.1016/j.biortech.2019.122063

Li, Z., Yao, G., Wu, R., Gao, L., Kan, Q., Liu, M., et al. (2015). Synergistic and dose-controlled regulation of cellulase gene expression in *Penicillium oxalicum*. *PLoS Genet.* 11:e1005509. doi: 10.1371/journal.pgen.1005509

Liao, G. Y., Zhao, S., Zhang, T., Li, C. X., Liao, L. S., Zhang, F. F., et al. (2018). The transcription factor TpRfx1 is an essential regulator of amylase and cellulase gene expression in *Talaromyces pinophilus*. *Biotechnol. Biofuels.* 11:276. doi: 10.1186/s13068-018-1276-8

Liu, G. D., and Qu, Y. B. (2019). Engineering of filamentous fungi for efficient conversion of lignocellulose: tools, recent advances and prospects. *Biotechnol. Adv.* 37, 519–529. doi: 10.1016/j.biotechadv.2018.12.004

Liu, K. M., Dong, Y. M., Wang, F. Z., Jiang, B. J., Wang, M. Y., and Fang, X. (2015). Regulation of cellulase expression, sporulation, and morphogenesis by velvet family proteins in *Trichoderma reesei*. *Appl. Microbiol. Biotechnol.* 100, 769–779. doi: 10.1007/s00253-015-7059-2

Livak, K. J., and Schmittgen, T. D. (2001). Analysis of relative gene expression data using Real-Time quantitative PCR and the 2-ΔΔCt method. *Methods* 25, 402–408. doi: 10.1006/meth.2001.1262

Love, M. I., Huber, W., and Anders, S. (2014). Moderated estimation of fold change and dispersion for RNA-seq data with DESeq2. *Genome Biol.* 15:550. doi: 10.1186/s13059-014-0550-8

Mandels, M., and Andreotti, R. (1978). Problems and challenges in the cellulose to cellulase fermentation. *Proc. Biochem.* 13, 6–13.

Méndez-Líter, J. A., Tundidor, I., Nieto-Domínguez, M., de Toro, B. F., González Santana, A., de Eugenio, L. I., et al. (2019). Transglycosylation products generated by *Talaromyces amestolkiae* GH3 β-glucosidases: effect of hydroxytyrosol, vanillin and its glucosides on breast cancer cells. *Microb. Cell Fact.* 18:97. doi: 10.1186/s12934-019-1147-4

Meng, Q. S., Zhang, F., Liu, C. G., Zhao, X. Q., and Bai, F. W. (2020). Identification of a novel repressor encoded by the putative gene ctf1 for cellulase biosynthesis in *Trichoderma reesei* through artificial zinc finger engineering. *Biotechnol. Bioeng.* 117, 1747–1760. doi: 10.1002/bit.27321

Passos, D. F., Pereira, N., and de Castro, A. M. (2018). A comparative review of recent advances in cellulases production by *Aspergillus*, *Penicillium* and Trichoderma strains and their use for lignocellulose deconstruction. *Curr. Opin. Green Substain. Chem.* 14, 60–66. doi: 10.1016/j.cogsc.2018.06.003

Payne, C. M., Knott, B. C., Mayes, H. B., Hansson, H., Himmel, M. E., Sandgren, M., et al. (2015). Fungal cellulases. *Chem. Rev.* 115, 1308–1348. doi: 10.1021/cr500351c

Qian, Y. C., Zhong, L. X., Sun, Y., Sun, N. N., Zhang, L., Liu, W. F., et al. (2019). Enhancement of cellulase production in *Trichoderma reesei* via disruption of multiple protease genes identified by comparative secretomics. *Front. Microbiol.* 10:2784. doi: 10.3389/fmicb.2019.02784

Qin, Y. L., He, H. Y., Li, N., Ling, M., and Liang, Z. Q. (2010). Isolation and characterization of a thermostable cellulase-producing *Fusarium chlamydosporum*. *World J. Microbiol. Biotechnol.* 26, 1991–1997. doi: 10.1007/s11274-010-0383-x

Rassinger, A., Gacek-Matthews, A., Strauss, J., Mach, R. L., and Mach-Aigner, A. R. (2018). Truncation of the transcriptional repressor protein Cre1 in *Trichoderma reesei* Rut-C30 turns it into an activator. *Fungal Biol. Biotechnol.* 5:15. doi: 10.1186/s40694-018-0059-0

Rocha, V., Maeda, R., Pereira, N., Kern, M., Elias, L., Simister, R., et al. (2016). Characterization of the cellulolytic secretome of *Trichoderma harzianum* during growth on sugarcane bagasse and analysis of the activity boosting effects of swollenin. *Biotechnol. Prog.* 32, 327–336. doi: 10.1002/btpr.2217

Saitou, N., and Nei, M. (1987). The neighbor-joining method: a new method for reconstructing phylogenetic trees. *Mol. Biol. Evol.* 4, 406–425. doi: 10.1093/oxfordjournals.molbev.a040454

Schoch, C. L., Seifert, K. A., Huhndorf, S., Robert, V., Spouge, J. L., Levesque, C. A., et al. (2012). Nuclear ribosomal internal transcribed spacer (ITS) region as a universal DNA barcode marker for fungi. *Proc. Natl. Acad. Sci. U.S.A.* 109, 6241–6246. doi: 10.1073/pnas.1117018109

Shida, Y., Yamaguchi, K., Nitta, M., Nakamura, A., Takahashi, M., Kidokoro, S., et al. (2015). The impact of a single-nucleotide mutation of bgl2 on cellulase induction in a *Trichoderma reesei* mutant. *Biotechnol. Biofuels* 8:230. doi: 10.1186/s13068-015-0420-y

Sun, R. Y., Liu, Z. C., Fu, K., Fan, L., and Chen, J. (2012). Trichoderma biodiversity in China. *J. Appl. Genet.* 53, 343–354. doi: 10.1007/s13353-012-0093-1

Tamura, K., Stecher, G., Peterson, D., Filipski, A., and Kumar, S. (2013). MEGA6: molecular evolutionary genetics analysis version 6.0. *Mol. Biol. Evol.* 5, 1–5. doi: 10.1093/molbev/mst197

Thompson, J. D., Gibson, T. J., Plewniak, F., Jeanmouqin, F., and Higgins, D. G. (1997). The CLUSTAL_X windows interface: flexible strategies for multiple sequence alignment aided by quality analysis tools. *Nucleic Acids Res.* 25, 4876–4882. doi: 10.1093/nar/25.24.4876

Wang, L., Lv, X., Cao, Y., Zheng, F., Meng, X., Shen, Y., et al. (2019). A novel transcriptional regulator RXE1 modulates the essential transactivator XYR1 and cellulase gene expression in *Trichoderma reesei*. *Appl. Microbiol. Biotechnol.* 103, 4511–4523. doi: 10.1007/s00253-019-09739-6

White, T. J., Bruns, T., Lee, S., and Taylor, J. W. (1990). "Amplification and direct sequencing of fungal ribosomal RNA genes for phylogenetics," in *PCR Protocols*, eds M. A. Innis, D. H. Gelfand, J. J. Sninsky, and T. J. White, (New York, NY: Academic Press), 315–322. doi: 10.1016/b978-0-12-372180-8.50042-1

Wu, C. Z., Chang, L. C., Lin, Y. F., Hung, Y. J., Pei, D., and Chen, J. S. (2015). Chaperonin-containing T-complex protein-1 subunit β as a possible biomarker for the phase of glomerular hyperfiltration of diabetic nephropathy. *Dis. Markers* 2015, 1–17. doi: 10.1155/2015/548101

Wu, V. W., Thieme, N., Huberman, L. B., Dietschmann, A., Kowbel, D. J., Lee, J., et al. (2020). The regulatory and transcriptional landscape associated with carbon utilization in a filamentous fungus. *Proc. Natl. Acad. Sci. U.S.A.* 117:201915611. doi: 10.1073/pnas.1915611117

Xu, J., Wang, X., Hu, L., Xia, J., Wu, Z., Xu, N., et al. (2015). A novel ionic liquid-tolerant *Fusarium oxysporum* BN secreting ionic liquid-stable cellulase: consolidated bioprocessing of pretreated lignocellulose containing residual ionic liquid. *Bioresour. Technol.* 181, 18–25. doi: 10.1016/j.biortech.2014.12.080

Yilmaz, N., Visagie, C. M., Houbraken, J., Frisvad, J. C., and Samson, R. A. (2014). Polyphasic taxonomy of the genus *Talaromyces*. *Stud. Mycol.* 78, 175–341. doi: 10.1016/j.simyco.2014.08.001

Zhang, F., Bunterngsookc, B., Li, J. X., Zhao, X. Q., Champreda, V., Liu, C. G., et al. (2019). "Regulation and production of lignocellulolytic enzymes from *Trichoderma reesei* for biofuels production," in *Advances in Bioenergy*, eds Y. B. Li, and X. M. Ge, (Amsterdam: Elsevier), 79–119. doi: 10.1016/bs.aibe.2019.03.001

Zhang, F., Zhao, X. Q., and Bai, F. W. (2018). Improvement of cellulase production in *Trichoderma reesei* Rut-C30 by overexpression of a novel regulatory gene Trvib-1. *Bioresour. Technol.* 247, 676–683. doi: 10.1016/j.biortech.2017.09.126

Zhang, W. X., Kou, Y. B., Xu, J. T., Cao, Y. L., Zhao, G. L., Shao, J., et al. (2013). Two major facilitator superfamily sugar transporters from *Trichoderma reesei* and their roles in induction of cellulase biosynthesis. *J. Biol. Chem.* 288, 32861–32872. doi: 10.1074/jbc.M113.505826

Zhao, S., Yan, Y. S., He, Q. P., Yang, L., Yin, X., Li, C. X., et al. (2016). Comparative genomic, transcriptomic and secretomic profiling of *Penicillium oxalicum* HP7-1 and its cellulase and xylanase hyper-producing mutant EU2106, and identification of two novel regulatory genes of cellulase and xylanase gene expression. *Biotechnol. Biofuels* 9:203. doi: 10.1186/s13068-016-0616-9

Zhao, Z., Ramachandran, P., Kim, T. S., Chen, Z., Jeya, M., and Lee, J. K. (2013). Characterization of an acid-tolerant β-1,4-glucosidase from *Fusarium*

oxysporum and its potential as an animal feed additive. *Appl. Microbiol. Biotechnol.* 97, 10003–10011. doi: 10.1007/s00253-013-4767-3

Znameroski, E. A., Li, X., Tsai, J. C., Galazka, J. M., Glass, N. L., and Cate, J. H. (2013). Evidence for transceptor function of cellodextrin transporters in *Neurospora crassa*. *J. Biol. Chem.* 289, 2610–2619. doi: 10.1074/jbc.M113.533273

Zou, G., Jiang, Y., Liu, R., Zhu, Z., and Zhou, Z. (2018). The putative β-glucosidase BGL3I regulates cellulase induction in *Trichoderma reesei*. *Biotechnol. Biofuels* 11:314. doi: 10.1186/s13068-018-1314-6

Conflict of Interest: D-DJ, JL, F-LW, and ZZ are employed by JALA Group Co.

The remaining authors declare that the research was conducted in the absence of any commercial or financial relationships that could be construed as a potential conflict of interest.

frontiers in Microbiology

ORIGINAL RESEARCH
published: 28 July 2020
doi: 10.3389/fmicb.2020.01646

Functional Genomics, Transcriptomics, and Proteomics Reveal Distinct Combat Strategies Between Lineages of Wood-Degrading Fungi With Redundant Wood Decay Mechanisms

Gerald N. Presley[1], Jiwei Zhang[2], Samuel O. Purvine[3] and Jonathan S. Schilling[4]*

[1] Department of Wood Science and Engineering, Oregon State University, Corvallis, OR, United States, [2] Department of Bioproducts and Biosystems Engineering, University of Minnesota, Saint Paul, MN, United States, [3] Environmental Molecular Sciences Laboratory, Pacific Northwest National Laboratory, Richland, WA, United States, [4] Department of Plant and Microbial Biology, University of Minnesota, Saint Paul, MN, United States

OPEN ACCESS

Edited by:
Monika Schmoll, Austrian Institute of Technology (AIT), Austria

Reviewed by:
Paul Daly, Jiangsu Academy of Agricultural Sciences (JAAS), China
Erika Kothe, Friedrich Schiller University Jena, Germany

***Correspondence:**
Gerald N. Presley
gerald.presley@oregonstate.edu

Specialty section:
This article was submitted to Fungi and Their Interactions, a section of the journal Frontiers in Microbiology

Received: *17 March 2020*
Accepted: *24 June 2020*
Published: *28 July 2020*

Citation:
Presley GN, Zhang J, Purvine SO and Schilling JS (2020) Functional Genomics, Transcriptomics, and Proteomics Reveal Distinct Combat Strategies Between Lineages of Wood-Degrading Fungi With Redundant Wood Decay Mechanisms. Front. Microbiol. 11:1646. doi: 10.3389/fmicb.2020.01646

Wood-degrading fungi vary in their strategies for deconstructing wood, and their competitive successes shape the rate and fate of carbon released from wood, Earth's largest pool of aboveground terrestrial carbon. In this study, one-on-one interspecific interactions between two model brown rot (carbohydrate-selective) fungi, *Gloeophyllum trabeum* and *Rhodonia* (*Postia*) *placenta*, were studied on wood wafers where a clearly resolved interaction zone (IZ) could be generated, reproducibly. Comparative RNAseq and proteomics between the IZ and non-interacting hyphae of each species identified combative strategies for each fungus. Glycoside hydrolases were a relatively smaller portion of the interaction secretome compared to non-interacting hyphae. The interaction zone showed higher pectinase specific activity than all other sampling locations, and higher laminarinase specific activity (branched β-glucan proxy) was seen in the IZ secretome relative to equivalent hyphae in single-species cultures. Our efforts also identified two distinct competitive strategies in these two fungi with a shared nutritional mode (brown rot) but polyphyletic ancestral lineages. *Gloeophyllum trabeum* (Gloeophyllum clade) upregulated more secondary metabolite (SM) synthesis genes in response to a competitor than did *R. placenta*. *R. placenta* (Antrodia clade) upregulated a larger variety of uncharacterized oxidoreductases in interacting hyphae, suggesting that these may play a role in mediating competitor response in this fungus. Both species produced several hypothetical proteins exclusively in the interaction zone, leaving questions as to the function of these proteins. This work supports the existence of multiple interaction strategies among brown rot fungi and highlights the functional diversity among wood decay fungi.

Keywords: fungal interactions, secondary metabolites, brown rot, microbial ecology, wood decay basidiomycetes

INTRODUCTION

Wood-degrading basidiomycetes live in complex microbial communities, sometimes with thousands of other fungal species in a single piece of degrading wood (Rajala et al., 2012). These fungi utilize a variety of combative strategies to compete for resources which impact wood decomposition rates and help modulate global carbon cycles (Hiscox et al., 2015; O'Leary et al., 2018). The physical, biochemical, and chemical responses basidiomycetes produce when confronted with competitors can be replicated in synthetic culture and used to study the mechanistic basis of these interactions (Boddy, 2000). Lab-based study of fungal interspecific interactions can enable a better understanding of fundamental processes that drive forest ecosystem function.

One component of competitor response is the expression of fungal cell wall-degrading enzymes. Fungal cell walls, composed primarily of chitin and branched beta glucans, can serve as a source of nutrients for competing fungi as the "losing" competitor's territory is overtaken (Boddy and Hiscox, 2016). Cell wall beta-glucans and chitin are degraded by extracellular glycoside hydrolases (GHs) belonging to several GH families including GH 16 β-glucanases, GH 18 chitinases, and GH 20 β-N-acetyl-glucosaminidases (Martin et al., 2007; Langner and Gohre, 2016). Elevated GH 18 chitinase expression levels have been shown in secondary colonization of dead fungal hyphae of *Heterobasidion irregulare* by the white rot basidiomycete *Phaneorchaete chrysosporium*, a pattern which may also appear in response to the hyphae of living fungal competitors (Karlsson et al., 2016). This type of response is likely widespread among wood-degrading saprophytes, as hyphal displacement is a common process in natural successional cycles among decay fungi (O'Leary et al., 2018). In contrast, expression levels of other classes of GHs involved in plant cell wall degradation have been shown to remain constant during interspecific interactions, as seen in the white rot fungus *Pycnoporus coccineus* paired against *Coniophora puteana* or *Botrytis cinerea* (Arfi et al., 2013). This pattern, albeit produced from a combination of model species, suggests a diversion of resources away from plant cell wall metabolism and toward fungal cell wall metabolism during interspecific combat.

Basidiomycete oxidoreductases known to participate in lignin decomposition also appear to play a role in mediating interspecific interactions (Hiscox and Boddy, 2017). Laccase activity is widely induced in interspecific interactions of white rot basidiomycetes (Baldrian, 2004; Snajdr et al., 2011) as are ligninolytic peroxidases (Hiscox et al., 2010) and the expression of uncharacterized oxidoreductases (Eyre et al., 2010). The biological function of these enzymes in interactions is not known, but upregulated laccases may be involved in melanin synthesis at the interaction zone, which can serve as a protective barrier between interacting fungi (Silar, 2005; Kuees and Ruehl, 2011; Cordero and Casadevall, 2017). Laccases can also degrade toxic metabolites produced by competitors during interactions (Hiscox and Boddy, 2017), which is an important biological function in interactions laden with antimicrobial metabolites.

In addition to a rich enzymatic diversity, saprotrophic basidiomycetes are also rich sources of secondary metabolites (SMs), and possess a variety of SM-synthesizing genes in their genomes (Quin et al., 2013; Riley et al., 2014). The biological functions of most basidiomycete SM-synthesizing genes are predominantly unknown but could plausibly function as antibiotics against competitor species. Several types of SMs including terpenes and polyketide-derived molecules are produced in response to fungal competitors (Hynes et al., 2007; Evans et al., 2008; El Ariebi et al., 2016; Yao et al., 2016; Hiscox and Boddy, 2017; O'Leary et al., 2019). *Gloeophyllum* sp. are wood-degrading basidiomycetes known to produce several terpenes such as gloeophyllins (Rasser et al., 2000; Han et al., 2015) and orsellinic acid-based polyketides such as oosponols (Sonnenbichler et al., 1997; Rasser et al., 2000) in axenic culture and during interactions (Sonnenbichler et al., 1993, 1994). *Gloeophyllum trabeum* is a well-studied model brown rot fungus whose genome encodes a several SM synthesis genes predicted to produce SM scaffolds of known *Gloeophyllum* metabolites, but their biological role is unknown (Sonnenbichler et al., 1994; Lackner et al., 2012; Wawrzyn et al., 2012). *G. trabeum* has been studied extensively in axenic culture and is an ideal model brown rot system to study the role of these genes in facilitating basidiomycete interactions.

In this study, we investigated the mechanisms of interaction between two model brown rot fungi, *Gloeophyllum trabeum* and *Rhodonia placenta*, both of which are common inhabitants of softwood lumber and could presumably come into contact with one another in this environment. The interactions were facilitated on aspen wood wafers so functional -omics techniques could be used to compare previous interaction cultures to each individual species (Zhang et al., 2016, 2019). The two fungi were grown against one another to simulate interspecific interactions and secreted proteins and RNA were extracted within and around the interacting hyphae. The proteome composition and plant and fungal polysaccharide-degrading activity was compared to actively growing hyphae of single-species cultures as were gene expression profiles from equivalent locations to allow the overlay of transcriptomics, proteomics, and enzyme activity data. This work identifies several proteins that are important in mediating basidiomycete interspecific interactions and identifies two different interaction strategies in the species tested.

MATERIALS AND METHODS

Culture Conditions and Interaction Microcosms

Gloeophyllum trabeum ATCC 11539 and *Rhodonia* (*Postia*) *placenta* MAD 698-R were maintained on malt extract agar and 1 cm diameter agar plugs were used to inoculate soil block microcosms as previously described (Presley and Schilling, 2017). These test strains were chosen for the depth of experimental data associated with them and because they grew at similar rates in the experimental setup used here, which enabled reproducible interactions to be generated. Sterile 19 mm aspen blocks were degraded for 4 weeks in soil block jars for each species and then

were used as inoculum for interaction microcosms. Interactions were simulated by placing one *G. trabeum* and one *R. placenta* block opposing one another in empty soil microcosms and laying a 60 × 23 × 3 mm aspen wafer (largest face in cross section) across the top of the two blocks (**Figure 1**). Fungal hyphae grew together until they met in the center of the wafer, forming an interaction zone which was then sampled along with surrounding hyphae for protein and RNA, as described below.

Protein Extraction and Purification

Interaction wafers were sampled for protein at three sections, one consisting a 10-mm section surrounding the interacting hyphae (IZ), and one 10 mm section 5 mm behind the boundary of the interaction zone toward each species (IZ-5Rp and IZ-5Gt). Non-degraded aspen wood was extracted as a control. For protein extracts, three replicate pools of 15 interaction wafers per poor were extracted with 100 ml of cold extraction buffer (0.5 M NaCl, 0.05 acetate, 0.05% tween 80, pH 5.0) for 24 h at 4°C with gentle shaking. Extracts were filtered through polyester cloth, centrifuged at 4000 × g for 30 min at 4°C, and filtered through 0.2 μm sterile PVDF filters. Extracts were exchanged into 0.05 M citrate pH 5.0 and concentrated using Vivaspin Polyethersulfone (PES) 10 kDa cutoff membranes prior to freezing at −20°C. Protein concentrations of extracts were determined using a BioRad protein assay kit (Hercules, CA, United States).

Biochemical Assays

Protein extracts were assayed for poly, oligo, and disaccharide-degrading activity and compared to previously generated values for single-species cultures on aspen wood 0–5 mm from the advancing hyphal front (Rp/Gt_0–5) and 15–20 mm behind the hyphal front (Rp/Gt_15–20) (Presley et al., 2018). Endoglucanase (EG), xylanase (Xyl), laminarinase (Lam), and pectinase (Pec) activity were measured in triplicate using the DNS assay for reducing sugars (Ghose, 1987). Reactions were done at 50°C in 0.05 M citrate at pH 5.0 using 1.5% carboxymethyl cellulose (EG), 2% birchwood xylan (Xyl), 0.25% laminarin (Lam), and 0.5% polygalacturonic acid (Pec) as substrates. Color was developed at 90°C and absorbance of developed reactions was measured at 540 nm. Units were defined as the amount of enzyme required to liberate 1 μmol of glucose, xylose, glucose, or galacturonic acid reducing equivalents per minute under the above conditions for EG, Xyl, Lam, and Pec activity, respectively.

β-glucosidase (BGL) and β-N-acetylglucosaminidase (BNAG) were measured in triplicate by monitoring the liberation of 4-nitrophenol from 4-nitrophenyl-β-D-glucoside and 4-nitrophenyl-β-D-N-acetylglucosamine, respectively. Reactions were carried out in 10 mM of substrate and 0.05 M citrate, pH 5.0 at 50°C and quenched with 2 volumes of 0.2 M Na_2CO_3. Absorbance at 400 nm of quenched reactions was measured and one unit of activity was defined as the amount of enzyme required to liberate 1 μmol of 4NP per minute in the above conditions.

Mass Spectrometry

Portions of the same protein extracts used for biochemical assays were reserved for proteomics analysis after extraction and purification, as above. Three separate extracts of pools of 15 interaction wafers per pool were analyzed for proteomic studies. Extracts were precipitated in TCA/acetone, pelleted, and reconstituted in saturated guanidine-HCl. The protein concentration of each cellular extract was determined by BCA assay (Smith et al., 1985). For each sample, processing replicates were performed; 50 μg of protein was aliquoted to low-retention Eppendorf tubes for downstream sample processing. All samples were incubated for 30 min at 60°C with tris(2-carboxyethyl)phosphine (Bond-Breaker TCEP, Thermo Fisher Scientific, Rockford, IL, United States) to reduce disulfide bonds. Alkylation of cysteine residues was performed by treatment with 50 mM iodoacetamide, which was added from a 500 mM iodoacetamide, 500 mM ammonium bicarbonate stock solution. After addition of iodoacetamide, all samples were incubated at room temperature in the dark for 40 min on a rocker. Each sample was then diluted to 0.9 M urea with 500 mM ammonium bicarbonate. To each 50 μg sample, 0.1 μg of mass spectrometry grade trypsin (Promega Corp., Madison, WI, United States) was added and incubated overnight at 37°C. Peptides were extracted from each sample using solid phase extraction with Discovery C18 50 mg resin columns (Supelco, St. Louis, MO, United States). Each column was activated with 2 ml of methanol followed by equilibration with 6 ml of 18 mΩ water. The sample was applied to the column and then the column was washed with 8 ml of 50 mM ammonium bicarbonate. Peptides were eluted with two 0.9 ml washes of 40% acetonitrile. Samples were dried using a centrifugal concentrator (Thermo Fisher Scientific, Asheville, NC, United States) and stored at −20°C until LC/MS analysis.

Peptides were solubilized in 150 μl solvent A (0.1% formic acid). For LC/MS analysis, 5 μl of sample was injected onto a Jupiter C18 resin reverse-phase column (3 μm particle size, 35 cm long, 75 μm inner diameter; Phenomenex, Torrance, CA, United States). The peptides were eluted at 0.3 μl min^{-1} with an Agilent (Santa Clara, CA, United States) 1200 high-performance liquid chromatograph with solutions of solvent A and 0.1% formic acid in acetonitrile (solvent B) using the following conditions: 0–30 min, isocratic at 100% solvent A; 30–32 min, linear gradient to 8% solvent B; 32–50 min, linear gradient to 12% solvent B; 50–105 min, linear gradient to 35% solvent B; 105–127 min, linear gradient to 60% solvent B; 127–130 min, linear gradient to 95% solvent B; and isocratic at 95% solvent B for 5 min. Eluted peptides were introduced into an Orbitrap XL mass spectrometer (Thermo Fisher Scientific, Waltham, MA, United States) by electrospray ionization.

Spectra were collected in a data-dependent mode, with the five most intense ions in each survey scan selected for collisional-induced dissociation in the five subsequent scans. Spectra were deconvoluted using the DeconMSn software (Mayampurath et al., 2008) to more accurately assign parent ion mass and ion charge state. Spectra were then searched against predicted peptides derived from the fungal genome sequences via MS-GF+ [software used to analyze tandem mass spectra data, (Kim and Pevzner, 2014)], using a 20 ppm parent ion mass tolerance in searches of tryptic peptides with a variable post-translational modification of oxidized methionine. Peptides from the interaction zone were searched against predicted peptides from each fungus in a single concatenated FASTA file. A Q

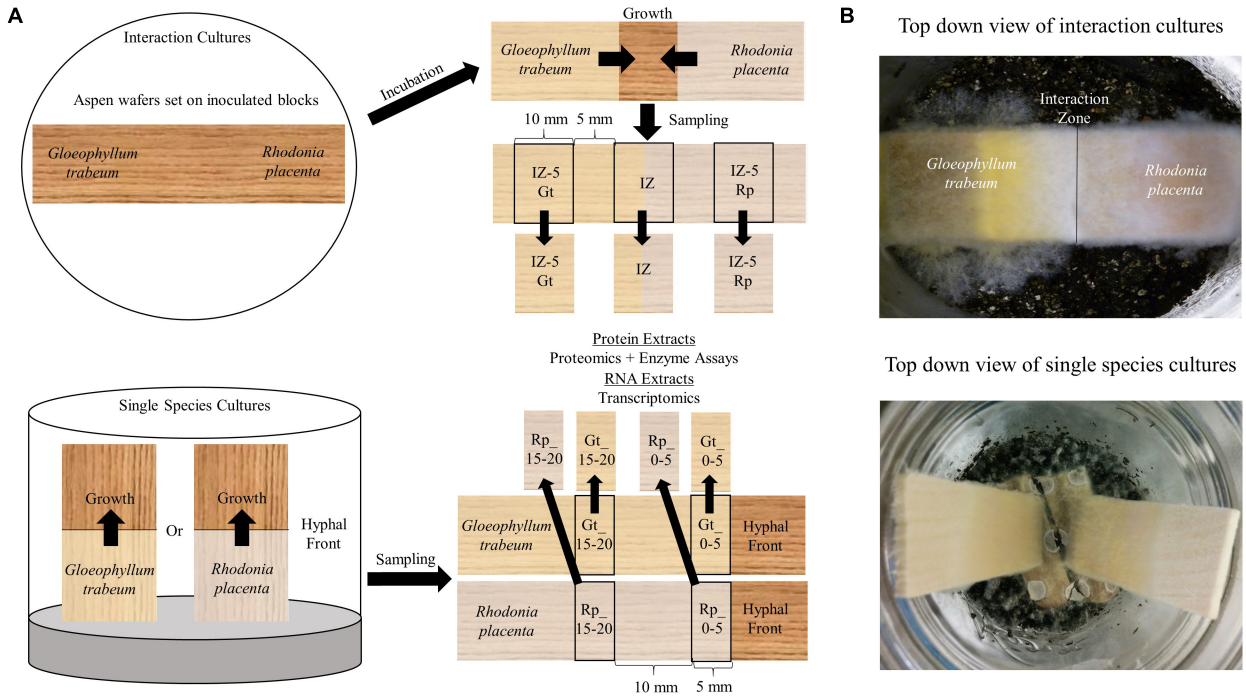

FIGURE 1 | (A) Diagrammatic representation of the two culture types and sampling regime used to generate the different types of decayed wood pieces that were extracted for secretomic or transcriptomic analysis. Competition microcosms used to simulate interspecific interactions between *Gloeophyllum trabeum* and *Rhodonia placenta* in this study. Pre-inoculated wood blocks for each species are used as inocula for each end of a thin aspen wafer placed across them. The two species grow together and contact in the middle of the wafer where the interaction zone and surrounding hyphae 5 mm outside of the interaction zone is sampled for protein and RNA for proteomic and transcriptomic analysis. Single species cultures were the same cultures generated in previous studies (Zhang et al., 2016, 2019; Presley et al., 2018). Gene expression data from single species cultures was adapted from Zhang et al. (2016, 2019) while proteomics data from this culture type was adapted from Presley et al. (2018). **(B)** Pictures of the two culture types from the top down.

value cut off (≤0.01) was utilized to allow a ∼1% false discovery rate (FDR) at each individual data set level, as assessed from a decoy identification search utilizing the reverse fungal genome sequence. Twenty-one peptides mapped to more than one protein in the interaction zone, however, none of these had hits to proteins that were in the opposing species. Spectra that mapped to more than one protein were assigned to the first occurrence of a matching protein in the concatenated FASTA file. The raw proteomics data is deposited in the PRIDE/ProteomeXchange database, project accession: PXD009480 and project doi: 10.6019/PXD009480.

RNA Extraction and RNA-Seq

Five mm sections from equivalent locations on two replicate wood wafers (about 200 mg each) were snap frozen in liquid nitrogen and ground to powder prior to extraction in 2 ml of TRIzol (Life Technologies). Samples were taken from locations equivalent to those used for proteomics analysis. Samples were purified using an RNeasy minikit (Qiagen, Inc.) with on-column DNase digestion. RNA quality was monitored using an Agilent Bioanalyzer (Agilent Technologies) and only RNA samples with RNA integrity >8 were used for RNA-seq. RNA-seq was performed as previously described (Zhang et al., 2016) on a HiSeq 2500 system (Illumina) at the University of Minnesota Genomics Center. Duplicate samples of each type, interaction zone (IZ), 5 mm outside of the interaction toward *G. trabeum* (IZ-5Gt), and 5 mm outside of the interaction toward *R. placenta* (IZ-5Rp) were sequenced.

RNA-seq data analysis was performed on the Galaxy platform[1] using described procedures for differential expression analysis (Trapnell et al., 2012). Raw reads were cleaned with Trimmomatic (v0.3) and mapped against *R. placenta* MAD698-R (v1.0) and *G. trabeum* ATCC11539 (v1.0) genomes together in a single concatenated file using TopHat (v2.0.13). Previously generated RNA-seq data from single-species cultures of both species grown on equivalent on aspen wafers were used for comparison to data generated in this study (Zhang et al., 2016, 2019). Expression levels at the leading hyphal edge of fungal cultures on aspen and 5 mm outside of the interaction zone from hyphae of each of the interacting species were compared to expression levels found at the IZ. Reference transcript models from the JGI database were used to determine differences in expression levels as Reads Per Kilobase Per Million (RPKM) in pairwise comparisons among samples using Cuffdiff (Galaxy Tool Version 2.2.1.3) using geometric normalization. FDR was set at <0.05. Transcripts with fourfold greater RPKM values

[1]https://usegalaxy.org/

in the IZ sample relative to other samples were identified. When the IZ RPKM values were compared to either the *G. trabeum*-only samples or the *R. placenta*-only samples only the reads from the IZ that mapped to the *G. trabeum* or *R. placenta* genome, respectively, were considered for fold-change analysis. Most reads from *G. trabeum* or *R. placenta*-only samples did not map (RPKM = 0) to the opposing fungus's genome, and those that did had RPKM values generally well below 1. The raw RPKM sequence data can be found in **Supplementary Table S1** and in the Gene Expression Omnibus database (GSE151023).

Secondary Metabolite Synthesis Gene Expression Analysis and Cluster Identification

Basidiomycete secondary metabolite (SM) scaffold-synthesizing genes including polyketide synthases (PKSs) (Lackner et al., 2012), sesquiterpene synthases (STSs) (Wawrzyn et al., 2012), non-ribosomal peptide synthases (NRPSs) (Kalb et al., 2013), and NRPS-like reductases (AFRs) (Brandenburger et al., 2016) were identified in the *G. trabeum* and *R. placenta* genomes. SM synthesis gene clusters analysis was performed with anti-smash fungal version (Weber et al., 2015) and gene clusters of upregulated SM genes were identified. Relative expression levels of genes in SM clusters of interest in the IZ were determined relative to levels previously found at the hyphal front of single-species cultures (Zhang et al., 2016, 2019).

Sequence Analysis

Orthologous proteins were identified among those identified in secretomes and among genes fourfold upregulated in the interaction microcosms using the TRIBE-MCL clustering method (Enright et al., 2002). Secretion signal peptides for upregulated and secretome proteins were identified using Signal P prediction server (Armenteros et al., 2019).

RESULTS

Generation of Interaction Microcosms

*Rhodonia placent*a and *Gloeophyllum trabeum* both colonized interaction aspen wafers at similar rates. Once established on the portion of the wafers in contact with the inoculated blocks, in most cases the hyphae advanced on to uncolonized wood in the direction of the opposing fungus and met in the wafer center within 2 weeks. While the location of contact varied somewhat from microcosm to microcosm, the microcosm design was reproducible enough to generate 47 wafers to sample (3 sets of 15 wafers for proteomics and 2 for RNAseq). Interaction outcomes were not measured because the cultures were sampled just as the hyphae came together. However, preliminary observations of longer-incubated cultures indicated that deadlock was the most common outcome under these conditions.

Secretome Composition of Interacting Hyphae Compared to Single-Species Cultures

Secreted proteins isolated from the IZ were compared to those from non-interacting hyphae 5 mm outside of the interaction zone for each species (IZ-5Rp/Gt) and extracts from single-species cultures 0–5 mm (Rp/Gt_0–5) and 15–20 mm (Rp/Gt_15–20) behind an actively growing hyphal front (Presley et al., 2018). Interaction microcosms showed a reduced diversity of secreted protein compared to single-species cultures. Peptides from only 36 different proteins were identified in the IZ, 10 from *R. placenta* and 26 from *G. trabeum*, compared to 42 and 194 proteins identified in Rp_0–5 and Gt_0–5 extracts, respectively. *G. trabeum* proteins were responsible for 74.3% of the spectral counts observed in interactions while *R. placenta* proteins accounted for 25.7%. Fifteen and thirty-three proteins were identified in IZ-5Rp and IZ-5Gt extracts, respectively, whereas equivalent sections in single species cultures of *R. placenta* (Rp_15–20) and *G. trabeum* (Gt_15–20) had 62 and 110 identified proteins, respectively. Glycoside hydrolases (GHs) as a proportion of all proteins identified were lower in IZ extracts (6%) than in extracts outside of the interaction zone (IZ-5Rp/Gt, 21%). All single-species culture extracts had a higher proportion of glycoside hydrolases in than the IZ (15–21%) (**Figure 2**; Presley et al., 2018). Although GH production in the IZ was relatively lower than other extracts, a GH 115 putative α-glucuronidase not found in single-species cultures was produced outside (*G. trabeum* and *R. placenta*) and within (*G. trabeum*) the interaction zone (**Supplementary Tables S1–S3**). One of these (Gt 121308) was produced in particularly high abundance and it constituted 20% of all protein observations of proteins in the IZ-5Gt extracts.

No esterases/lipases were identified in extracts of the IZ while this group of enzymes composed 8% and 6–9% of the proteins found in extracts outside the interaction zone and in single-species cultures, respectively. Extracts from the interaction zone were primarily composed of hypothetical proteins (62%), compared to 48% and 41–47% in non-interacting hyphae and single-species cultures, respectively. Several proteins, eight from *R. placenta* and seven from *G. trabeum*, were found exclusively in the IZ (**Table 1**). The majority of these were uncharacterized hypothetical proteins, but both fungi produced their own putative acid protease exclusive to the interaction zone, both of which contained secretion signals predicted by SignalP (Armenteros et al., 2019).

Enzyme Activities

Specific activities for six enzymes, pectinase (Pec), endoglucanase (EG), xylanase (Xyl), β-glucosidase (BGL), Laminarinase (Lam), and β-N-acetylglucosaminidase (BNAG), were measured on protein extracts from the IZ and outside of the interactions zone (IZ-5Rp/Gt) and were compared to those measured in single-species cultures 0–5 mm (Rp/Gt_0–5) or 15–20 mm (Rp/Gt_15–20) from the advancing hyphal front (**Figure 3**). Extracts of the IZ showed the highest pectinase specific activity, twofold and threefold higher than those found at Rp_0–5 mm and Gt_0–5,

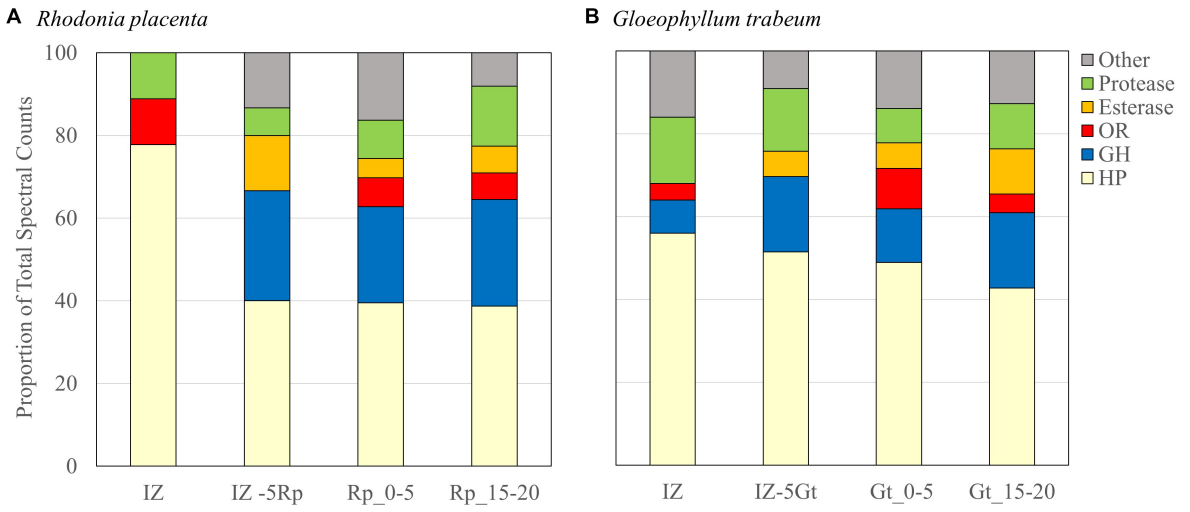

FIGURE 2 | Secretome compositions from *Rhodonia placenta* **(A)** and *Gloeophyllum trabeum* **(B)** isolated from interacting (IZ) and non-interaction interacting hyphae 5 mm outside of the interaction zone (IZ-5Rp/Gt), and 0–5 mm (Rp/Gt_0–5), and 15–20 mm (Rp/Gt_15–20) behind the hyphal front of single species cultures. Protein categories are presented as proportions of the total numbers of spectral counts. HP, hypothetical protein; GH, glycoside hydrolase; OR, oxidoreductase.

TABLE 1 | Proteins found exclusively in the interaction zone (IZ) produced by *Gloeophyllum trabeum* and *Rhodonia placenta*.

Protein ID[a]	Name	Putative function[b]	Observations[c]	Size (kDa)	Signal P[d]
Rhodonia placenta					
105721	FAD-binding protein	FAD-binding protein	4	53.28	18–19
1183565	Hypothetical protein	No strong hits	2	40.45	No
92184	Hypothetical protein	No strong hits	1	85.01	No
99255	Hypothetical protein	No strong hits	7	82.27	No
93455	Hypothetical protein	No strong hits	1	14.97	No
98779	Hypothetical protein	No strong hits	11	79.06	No
96562	Hypothtical protein	No strong hits	36	52.89	No
1127001	Protease, Acid	Polyporopepsin	3	42.22	19–20
Gloeophyllum trabeum					
101772	Hypothetical protein	No strong hits	1	28.76	19–20
91843	Hypothetical protein	Pumilo domain	1	137.06	No
128123	Hypothetical protein	No strong hits	1	22.38	No
108762	Hypothetical protein	No strong hits	7	17.55	17–18
112815	Hypothetical protein	No strong hits	1	32.95	No
136352	Protease, Acid	Acid protease	4	107.7	19–20
81033	Ser/Thr Protein Phosphatase	Ser/Thr Protein Phosphatase	1	66.63	No

[a]*Protein ID numbers from the DOE JGI Mycocosm database (Grigoriev et al., 2014).* [b]*Putative functions determined by BLAST searches of SWISS PROT database (Bateman et al., 2015).* [c]*Number of observations in the interaction zone protein sample (spectral counts).* [d]*Signal peptides identified with Signal P 5.0 (Armenteros et al., 2019).*

respectively. Laminarinase specific activity was also significantly higher ($p < 0.05$, Tukey's HSD) in IZ extracts than all others except IZ-5Gt and Rp_15–20 mm. Only two GHs, both produced by *G. trabeum*, in the IZ, a GH 115 (121308) and a GH 3 (69843) were identified and neither of these are likely endo-laminarinases. All other measured activities were generally low in IZ extracts, but some plant polysaccharide-degrading activities increased to levels equivalent to those found in single-species cultures or IZ-5Rp/Gt extracts (**Figure 3**). The GH 3 produced in non-interacting *R. placenta* cultures was orthologous to those produced in both interacting and non-interacting *G. trabeum* secretomes, suggesting they have a similar function in both species (**Supplementary Data S2**).

Transcriptional Profiling of Interacting Hyphae

RNA-seq was used to compare gene expression levels in the IZ to surrounding hyphae and single-species cultures for each species. In the interaction zone, 65.5% of the reads mapped to the *G. trabeum* genome, while 36.5% mapped to the *R. placenta* genome. Of the genes that are upregulated at least fourfold in the

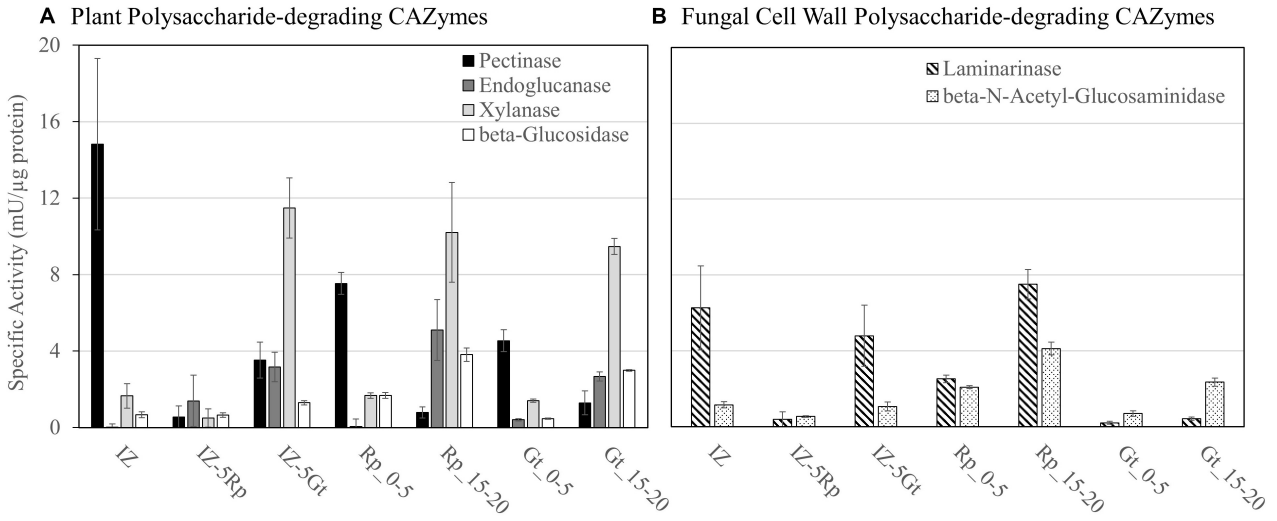

FIGURE 3 | Enzyme specific activities for **(A)** plant polysaccharide-degrading CAZymes and **(B)** fungal cell wall polysaccharide-degrading enzymes in protein extracts from interacting (IZ) and non-interacting hyphae 5 mm outside of the interaction zone (IZ-5Rp/Gt), and 0–5 mm (Gt/Rp_0–5) and 15–20 mm (Rp/Gt_15–20) behind the advancing hyphal front in single species cultures.

IZ relative to Rp_0–5 and Gt_0–5, 34.6% (79) and 16.0% (41) were oxidoreductases (ORs), respectively, indicating a significant role for this enzyme group in the IZ (**Figure 4A**). *G. trabeum* upregulated a greater number of secondary metabolite (SM) synthesizing genes (eight) at least fourfold in the interaction zone relative to Gt_0–5 than *R. placenta* did relative to Rp_0–5 (one). *R. placenta* upregulated more proteases at least fourfold in the interaction zone relative to Rp_0–5 (eight) than *G. trabeum* did relative to Gt_0–5 (three) (**Figure 4A**). Similar patterns were seen when gene expression levels in the interaction zone were compared to non-interacting hyphae around it (IZ-5Rp/Gt). Of the genes that are fourfold upregulated in the interaction zone relative to IZ-5Rp and IZ-5Gt, 19.0% (116) and 14.2% (26) were putative oxidoreductases, respectively (**Figure 4B**).

The 25 most highly upregulated genes in the interaction zone relative to the *R. placenta* hyphal front (Rp_0–5) included 5 hypothetical proteins, 14 uncharacterized ORs including putative cytochrome p450s, an aryl alcohol dehydrogenase and a protease (**Table 2**). One of these, Rp105721 a putative FAD-binding protein, was also identified in interaction secretomes and it also had no orthologs among upregulated genes in *G. trabeum*. Of the 25 most highly upregulated genes in the interaction zone relative to Gt_0–5, the majority (17) were hypothetical proteins. Four of these hypothetical proteins, Gt101772, 44870, 92695, and 129354 were also found in the interaction secretomes. The 25 most highly upregulated genes also included a laccase, an oxalate decarboxylase, an O-methyl transferase, a polyketide synthase, and a hydrophobin (**Table 2**). Only a few GHs were upregulated in the interaction zone vs. non-interacting hyphae for *R. placenta* (4) or *G. trabuem* (1). In the interaction zone, both species upregulated a GH 16 protein and *R. placenta* also upregulated two GH 18 chitinase domain-containing proteins, as well as a GH 5 β-1,3-glucanase. Hypothetical proteins were the largest category of upregulated proteins among all comparisons, ranging from 51.3 to 70.5% of all genes upregulated at least fourfold in the interaction zone (**Figure 4**). This is likely not due to any specific enrichment in hypothetical proteins in the interaction, but probably due to the general high abundance of hypothetical proteins in basidiomycete genomes.

Secondary Metabolite Synthesizing Genes in *G. trabeum*

G. trabeum upregulated several SM-synthesizing genes in the interaction zone whereas *R. placenta* upregulated fewer members of this group in the same sample. Proteins upregulated in the interaction zone by *G. trabeum* included two polyketide synthases (PKSs), four sesquiterpene synthases (STSs), one non-ribosomal peptide synthases (NRPSs)-PKS hybrid, and two NRPS-like proteins (**Figure 5**). AntiSMASH (Weber et al., 2015) SM cluster analysis identified seven gene clusters in which these nine upregulated proteins are located in the *G. trabeum* genome and most are located near cytochrome p450s, other ORs, and/or membrane transporters. One of the PKSs, Gt116317, shares high homology with characterized basidiomycete orsellinic acid synthases (Lackner et al., 2012). Upregulated sesquiterpene cyclases share greatest homology with protoilludene synthases (Gt117331 and Gt78472) and sativene synthases (Gt131990 and Gt79917).

DISCUSSION

Rhodonia placenta and *Gloeophyllum trabeum* are two model brown rot fungi commonly found on softwood lumber and while this interaction may not be likely without human intervention, it is presumed to occur in lumber. The interactions generated in this study were also generated on aspen wood, which is not a native or preferred substrate for these fungi (Krah et al., 2018). However,

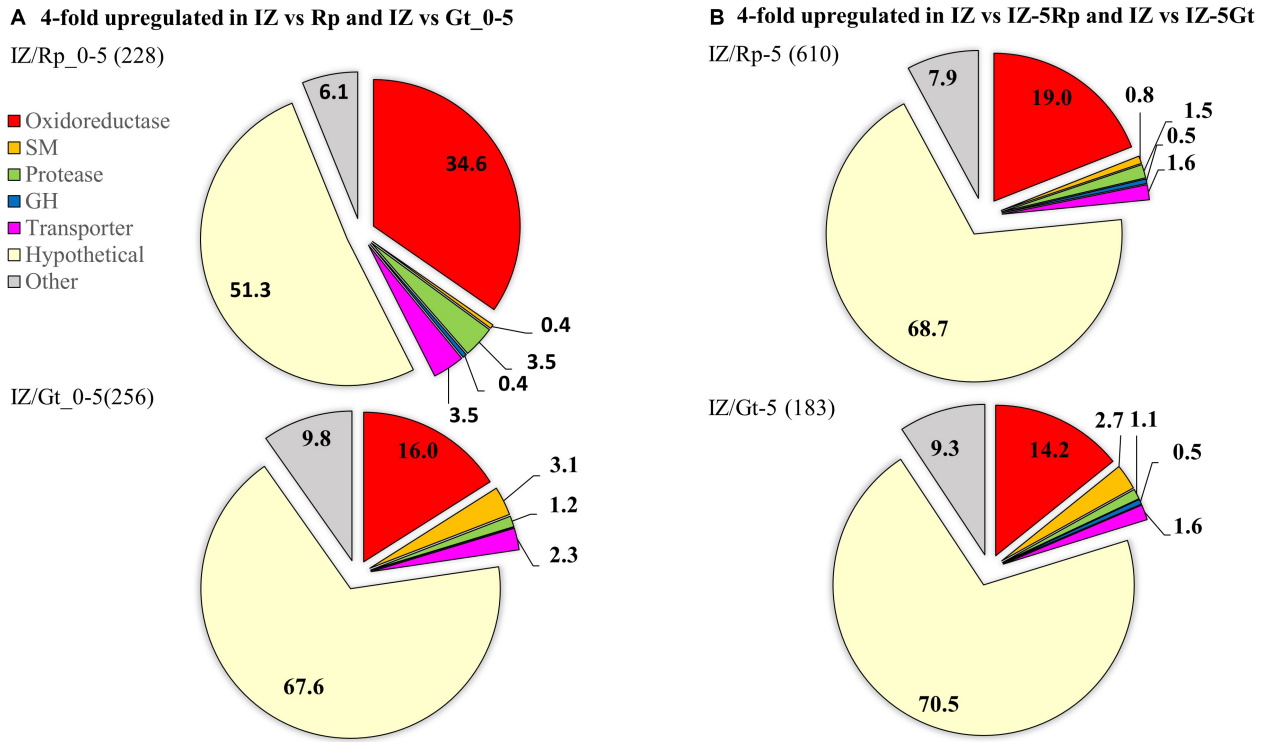

FIGURE 4 | Genes fourfold upregulated in interacting hyphae (IZ) compared to non-interacting hyphae **(A)** at the leading hyphal front of single species cultures (Rp/Gt_0–5) and **(B)** outside of the interaction zone (IZ-5Rp/Gt) of *Rhodonia placenta* and *Gloeophyllum trabeum*. Categories are represented as proportions of all genes fourfold upregulated and the total number of genes upregulated are in parentheses. SM, secondary metabolite scaffold-synthesizing genes; GH, glycoside hydrolase.

aspen wood is a widely used model substrate for these two fungi and it was used here to maintain continuity with previous work that was used as a single species control for this study (Zhang et al., 2016, 2019; Presley et al., 2018). The single species cultures used here were also used in a different orientation than the interaction microcosms, which may have caused some differences in gene expression and protein secretion and must be considered when interpreting the results.

Wood-degrading basidiomycete fungi have several tactics to deal with competitors in wood, each characterized by specific morphological and/or biochemical alterations to fungal cultures (Boddy and Hiscox, 2016). This study identifies characteristic differences in protein secretion and gene expression in response to a fungal competitor in the two model brown rot fungi, *Rhodonia placenta* and *Gloeophyllum trabeum*. Secretomes of interacting hyphae showed a general reduction in the prevalence of common decay-related genes such as glycoside hydrolases (GHs) and carbohydrate esterases (CEs) compared to non-interacting hyphae and single-species cultures (**Figure 2** and **Supplementary Tables S1–S7**; Presley et al., 2018). Most of the GHs and CEs previously shown to be secreted by these two fungi in single-species cultures were either downregulated or not significantly changed in the interaction zone (**Supplementary Data S1**) compared to non-interacting hyphae or single-species cultures. This is similar to the white rot fungus *Pycnoporus coccineus*, which did not upregulate plant cell wall-degrading enzymes when confronted with competitors (Arfi et al., 2013), indicating they were not important in mediating the interaction.

The GHs upregulated fourfold or more in the interaction zone in this study included one GH 16 in both *G. trabeum* and *R. placenta*, two GH 18 chitinases from *R. placenta*, none of which were likely involved in plant cell wall degradation. Both GH 16 proteins have putative transmembrane regions (Krogh et al., 2001), indicating they may be involved in cell wall reorganization within the fungus. The GH 18 proteins upregulated in *R. placenta* interactions are not transmembrane proteins, and one of them, Pp118230, contains a secretion signal suggesting an extracellular localization. These may play a similar role as GH 18 chitinases in *Phanerochaete chrysosporium* which were differentially expressed during contact with living and dead competitor hyphae, presumably to recycle competitor cell wall components (Karlsson et al., 2016). Laminarinase activity was also higher in the interaction zone than hyphal fronts of single-species cultures (**Figure 3**), suggesting that branched beta-glucan metabolism is induced in by the interaction.

Plant polysaccharide degrading-enzyme activities were not markedly reduced in the interaction zone compared to equivalent non-interacting hyphae and single species cultures (**Figure 3**), but these are known to be generally low at the leading hyphal edge of fungal cultures except for pectinase (Zhang et al., 2016;

TABLE 2 | Top 25 genes most highly upregulated in interacting hyphae (IZ) compared to the leading hyphal edge (Rp/Gt_0–5) of single-species cultures of *Gloeophyllum trabeum* (Gt) and *Rhodonia placenta* (Rp).

Most upregulated in IZ/Gt_0–5						Most upregulated in IZ/Rp_0–5					
Protein ID[a]	**Name[b]**	**RPKM IZ**	**RPKM Gt_0–5[c]**	**Log_2 IZ/Gt_0–5**	**Signal P[d]**	**Protein ID[a]**	**Name[b]**	**RPKM IZ**	**RPKM Rp_0–5[e]**	**Log_2 IZ/Rp_0–5**	**Signal P[d]**
137245	Hypothetical protein	492.6	0.4	10.1	No	63488	Oxidoreductase	211.1	0.7	8.3	No
92695	Hypothetical protein	3599.5	8.8	8.7	19–20	60565	Oxidoreductase	129.4	0.5	8.0	No
103366	Oxalate decarboxylase	463.5	1.5	8.2	19–20	105320	Hypothetical protein	65.6	0.3	7.9	22–23
44870	Hypothetical protein	721.6	3.9	7.5	21–22	105721	Oxidoreductase	257.9	1.5	7.4	No
48004	Vacuolar protein	14.4	0.1	7.4	No	47260	Oxidoreductase	389.2	2.6	7.2	No
95418	Hypothetical protein	203.6	1.4	7.2	15–16	35307	Oxidoreductase	545.3	4.3	7.0	No
134059	Hypothetical protein	5481.2	69.5	6.3	23–24	54275	Hypothetical protein	94.8	1.0	6.6	20–21
95488	Hypothetical protein	130.7	1.8	6.2	No	48020	Cytochrome p450	154.3	1.8	6.4	No
114641	O-methyl transferase	3051.3	45.2	6.1	No	45365	Uncharacterized transporter	49.1	0.8	5.9	No
134822	Hypothetical protein	404.2	6.3	6.0	19–20	126377	Oxidoreductase	156.9	2.9	5.8	No
104526	Hypothetical protein	245.2	3.9	6.0	19–20	92340	Cytochrome p450	77.6	1.5	5.7	27–28
96525	Hypothetical protein	159.9	2.8	5.8	No	46594	Aryl alcohol dehydrogenase	79.3	1.5	5.7	No
104708	Oxidoreductase	741.1	13.8	5.7	No	116256	Potassium channel	45.0	0.9	5.7	No
112738	Hypothetical protein	500.8	9.4	5.7	No	126381	Protease, acid	82.2	1.6	5.6	26–27
129354	Hypothetical protein	587.6	11.3	5.7	19–20	105719	Cytochrome p450	68.3	1.6	5.5	27–28
113399	Oxidoreductase	840.4	16.9	5.6	No	106360	Hypothetical protein	69.5	1.7	5.4	No
45373	Hypothetical protein	98.3	2.0	5.6	21–22	103283	Expansin-like protein	25.3	0.6	5.3	20–21
67066	Hypothetical protein	1826.5	37.4	5.6	No	99672	Oxidoreductase	31.1	0.8	5.2	No
94357	Hypothetical protein	58.7	1.2	5.6	17–18	100325	Hypothetical protein	150.3	4.0	5.2	20–21
50822	Polyketide synthase I	184.0	4.0	5.5	No	63451	Oxidoreductase	67.6	2.0	5.1	No
19724	Hydrophobin	2085.5	46.0	5.5	No	45316	Hypothetical protein	121.7	4.1	4.9	No
50761	Hypothetical protein	695.6	15.5	5.5	No	61173	Oxidoreductase	188.3	6.4	4.9	No
101772	Hypothetical protein	372.3	8.8	5.4	25–26	91006	Alcohol dehydrogenase	125.1	4.3	4.9	No
130426	Laccase 2	47.0	1.1	5.4	20–21	115141	Lipase	204.6	7.2	4.8	26–27
17704	Hypothetical protein	149.8	3.8	5.3	No	45371	Oxidoreductase	33.2	1.2	4.8	No

RPKM values for each gene at each condition is shown with the log2 of the ratio of IZ. [a]Protein ID numbers from the DOE JGI Mycocosm database (Grigoriev et al., 2014). [b]Putative functions determined by BLAST searches of SWISS PROT database (Bateman et al., 2015). [c]Gt_0–5 RPKM value adapted from Zhang et al. (2019). [d]Secretion signals for detected protein sequences were detected using Signal P algorithm (Armenteros et al., 2019). [e]Rp_0–5 RPKM values adapted from Zhang et al. (2016).

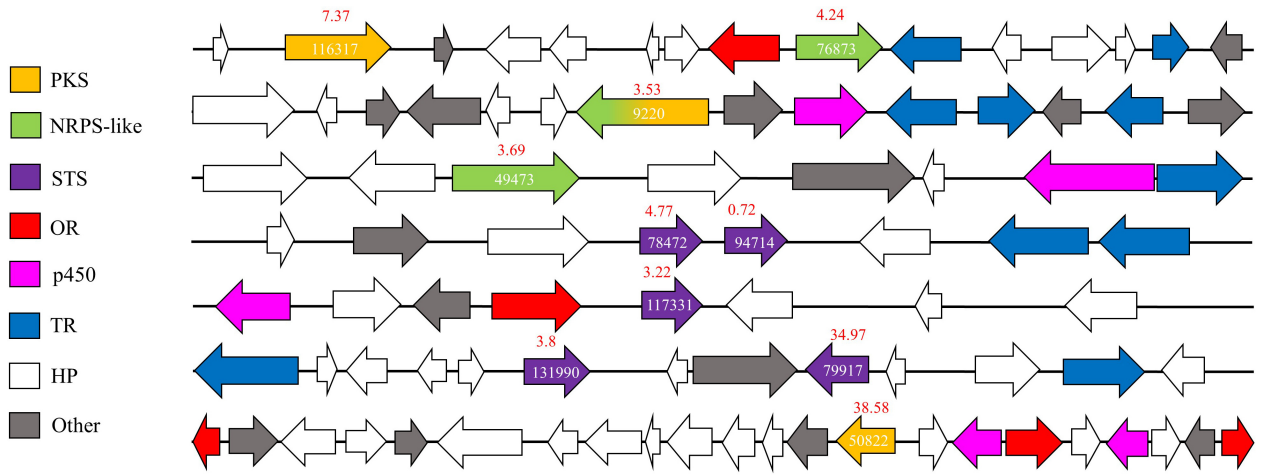

FIGURE 5 | Secondary metabolite (SM) synthesis clusters in *Gloeophyllum trabeum* that contain at least one SM-synthesizing gene that is upregulated in interacting hyphae relative to 0–5 mm behind the leading hyphal front of single species cultures. Arrows represent genes with JGI protein ID number over relevant genes. Fold changes in expression levels (IZ/Gt_0–5) are shown in red over each SM synthesis-related gene. JGI protein ID numbers are shown on each annotated gene on the secondary metabolite synthesis cluster. PKS, Polyketide synthases; OR, oxidoreductases; p450, Cytochrome p450; STS, sesquiterpene synthases; NRPS, Non-ribosomal peptide synthase; TR, Transporter.

Presley and Schilling, 2017). Pectinase activity was increased in the interaction zone compared to other samples, but no GH 28 pectinases were identified using proteomics analysis or were upregulated at least fourfold compared to non-interacting hyphae (**Supplementary Table S1** and **Supplementary Data S1**). Pectinases in the interaction zone may have gone undetected by our proteomics analysis, as the total number of proteins detected in the interaction was low compared to single-species cultures (**Supplementary Table S1**; Presley and Schilling, 2017; Presley et al., 2018). Pectinase activity is also performed by some other carbohydrate active enzyme families such as carbohydrate esterase families 8 and 12 and polysaccharide lyase family 1, however, none of these were found to be upregulated in the interaction zone. Furthermore, the polygalacturic acid substrate used to detect pectinase activity in this assay was only guaranteed to be ≥90% (Sigma Aldrich), so some of the activity detected here could be due to the degradation of other cell wall polysaccharides. One way basidiomycetes compete in wood is by capturing more resources than their competitors (Boddy, 2000). Heightened IZ pectinase activity may be an attempt by fungi to "outmaneuver" competitors by overexpressing early stage colonization enzymes including pectinases (Zhang et al., 2016, 2019) and oxidant-producing enzymes (Hori et al., 2014) to facilitate rapid resource capture (Hiscox et al., 2010; Boddy and Hiscox, 2016).

Transcriptomics and proteomics of the interaction zone identified differing strategies for interaction in *G. trabeum* and *R. placenta*. *G. trabeum* appeared to rely more heavily on SM synthesis gene upregulation in response to competitors than *R. placenta* (**Figure 4** and **Table 2**). Interestingly, *G. trabeum* was previously shown to produce pore-forming endotoxin-like proteins in single-species cultures (Presley and Schilling, 2017), but these were not identified in this study and were not upregulated in the interaction. This suggests these putative pore-forming enzymes are not involved in mediating fungal-fungal interactions, but instead may be part of a general anti-herbivory strategy in *G. trabeum* as are homologous proteins in other organisms (Jaquet et al., 1987; Weng et al., 2004). Both fungi upregulated several ORs in the interaction which has been observed previously in interacting hyphae (Arfi et al., 2013). *R. placenta* upregulated more ORs in the IZ than *G. trabeum*, which suggests this species relies more heavily on enzymatic oxidants to facilitate interactions. Xenobiotic-metabolizing ORs are major secretome components in wood-degrading basidiomycetes and some of the oxidoreductases upregulated in the interaction in this study may have similar functional roles (Moody et al., 2018). One OR, Rp105721, was both found exclusively in protein extracts of the interaction (**Table 1**) and was the 3rd most highly upregulated *R. placenta* gene in the interaction (**Tables 1**, **2**). Rp105721 contains a Rossman-fold NAD(P)-binding domain as well as an FAD-binding domain and shares homology to several other uncharacterized fungal putative FAD-binding proteins. Further characterization of this enzyme may provide insight into interaction mechanisms in this fungus.

Basidiomycetes are rich sources of SMs and several studies have demonstrated the importance of SMs in mediating interspecific interactions in wood decay fungi (Hynes et al., 2007; Evans et al., 2008; Peiris et al., 2008; El Ariebi et al., 2016; O'Leary et al., 2019). *Gloeophyllum* species are known to produce several classes of SMs, including terpenoids (Rasser et al., 2000; Han et al., 2015) and polyketides (Sonnenbichler et al., 1997), that have mild antibacterial and antifungal activity. *G. trabeum* upregulated several SM-synthesis genes in the IZ, implicating the products of these genes in mediating fungal-fungal interactions (**Figure 4**). Fewer orthologous terpene synthases were also upregulated in

R. placenta in the IZ, but had generally lower RPKM values than those in *G. trabeum*. In *G. trabeum*, nine upregulated SM-synthesis genes were identified on seven SM-synthesis clusters that were identified using AntiSMASH SM cluster analysis (**Figure 5**; Weber et al., 2015). Some of these genes, such as the putative orsellinic acid synthase Gt116317, share high homology to characterized SM-synthesizing genes (Lackner et al., 2012, 2013). These SM clusters also contain IZ-upregulated ORs and cytochrome p450s may perform oxidations necessary to produce orsellinic acid-derived metabolites and contribute to the overall greater proportion of ORs upregulated in the IZ (**Figure 5**). Our study suggests that antimicrobial orsellinic acid-derived SMs may help mediate interspecific interactions in *G. trabeum*, however, this must be confirmed via metabolomics analysis.

Laccases are oxidoreductases that have been widely implicated in basidiomycetes interactions, where they can play a role in melanization (Cordero and Casadevall, 2017) or metabolite detoxification (Hiscox and Boddy, 2017). Brown rot secretomes are generally characterized by a lack of phenol oxidase activity but some do contain these proteins in their genomes (Riley et al., 2014) and produce them in low quantities (Wei et al., 2010). In this study, a laccase in *G. trabeum* was highly upregulated (Gt130426) in the IZ (**Table 2**), as is seen in protein extracts of the interacting hyphae of several white rot fungi (Baldrian, 2004; Hiscox et al., 2010). However, no laccase activity was found in this test (ABTS assay, data not shown) and no laccase peptides were identified in protein extracts from interaction microcosms, indicating they are not part of the secretome in amounts detectable with our methods. Some secretion signal-containing ascomycete laccases localize to fungal cell walls (Liu and Free, 2016), but Gt130426 does not contain any transmembrane sequences or GPI anchoring sites that would suggest it is localized there.

Basidiomycete interspecific interactions are ubiquitous processes necessary for the survival of these organisms. This study identifies general strategies utilized by wood-degrading basidiomycetes during interspecific combat and identifies interspecific variation in combative mechanisms in two brown rot species. Both species divert resources away from GH and CE production except for pectinase and laminarinase activity, the latter likely to target fungal cell wall β-glucanases. In addition, several orthologous genes were upregulated in the interaction in both species, which suggests an overlap in functionality for these genes which include some cytochrome p450s, proteases, uncharacterized oxidoreductases, hypothetical proteins, terpene synthases and several others. However, there were also patterns unique to each species. *G. trabeum* appeared to exhibit an SM-based interaction strategy by upregulating more SM-synthesis genes than *R. placenta*, while *R. placenta* upregulated a larger proportion of oxidoreductases in the interaction. Several oxidoreductases, including those that could be involved in SM synthesis, metabolite degradation, and cell wall melanization were upregulated in the IZ, indicating they may be important in facilitating interactions. This work provides evidence for the broader functional role of a variety of uncharacterized genes in two model brown rot fungi.

DATA AVAILABILITY STATEMENT

The raw proteomics data is deposited in the PRIDE/ProteomeXchange database, project accession: PXD009480 and project doi: 10.6019/PXD009480. The raw RPKM sequence data can be found in **Supplementary Table S1** and in the Gene Expression Omnibus database (GSE151023).

AUTHOR CONTRIBUTIONS

GP generated the cultures, extracted protein, performed proteomics experiment prep, extracted RNA for RNAseq, performed enzyme assays, and wrote the manuscript. JZ performed the RNAseq analysis, data workup for this portion, and edited the manuscript. Ellen Panisko was not listed as an author but she was the technical specialist that performed the LC-MS and data analysis for this portion. SP performed the data analysis for the proteomics. JS was the PI at the time this work was done, directed and funded the research, and edited the manuscript. All authors contributed to the article and approved the submitted version.

FUNDING

This work was funded in part by the U.S. Department of Energy (DOE) Office of Science (Early Career Grant DE-SC0004012 to JS, from the Office of Biological and Ecological Research (BER) and BER Grant DE-SC0012742 to JS and Ellen Panisko. This work was also funded by the National Science Foundation Graduate Research Fellowship Programs under Grant No. 00039202 to GP. Any opinions, findings, and conclusions or recommendations expressed in this material are those of the authors and do not necessarily reflect the views of the DOE or NSF.

SUPPLEMENTARY MATERIAL

The Supplementary Material for this article can be found online at: https://www.frontiersin.org/articles/10.3389/fmicb.2020.01646/full#supplementary-material

REFERENCES

Arfi, Y., Levasseur, A., and Record, E. (2013). Differential gene expression in Pycnoporus coccineus during interspecific mycelial interactions with different competitors. *Appl. Environ. Microbiol.* 79, 6626–6636. doi: 10.1128/aem.02316-13

Armenteros, J. J. A., Tsirigos, K. D., Sonderby, C. K., Petersen, T. N., Winther, O., Brunak, S., et al. (2019). SignalP 5.0 improves signal peptide predictions using deep neural networks. *Nat. Biotechnol.* 37, 420–423. doi: 10.1038/s41587-019-0036-z

Baldrian, P. (2004). Increase of laccase activity during interspecific interactions of white-rot fungi. *FEMS Microbiol. Ecol.* 50, 245–253. doi: 10.1016/j.femsec.2004.07.005

Bateman, A., Martin, M. J., O'Donovan, C., Magrane, M., Apweiler, R., Alpi, E., et al. (2015). UniProt: a hub for protein information. *Nucleic Acids Res.* 43, D204–D212. doi: 10.1093/nar/gku989

Boddy, L. (2000). Interspecific combative interactions between wood-decaying basidiomycetes. *FEMS Microbiol. Ecol.* 31, 185–194. doi: 10.1111/j.1574-6941.2000.tb00683.x

Boddy, L., and Hiscox, J. (2016). Fungal ecology: principles and mechanisms of colonization and competition by saprotrophic fungi. *Microbiol. Spectr.* 4:0019-2016. doi: 10.1128/microbiolspec.FUNK-0019-2016

Brandenburger, E., Braga, D., Kombrink, A., Lackner, G., Gressler, J., Künzler, M., et al. (2016). Multi-genome analysis identifies functional and phylogenetic diversity of basidiomycete adenylate-forming reductases. *Fungal Genet. Biol.* 112, 55–63. doi: 10.1016/j.fgb.2016.07.008

Cordero, R. J. B., and Casadevall, A. (2017). Functions of fungal melanin beyond virulence. *Fungal Biol. Rev.* 31, 99–112. doi: 10.1016/j.fbr.2016.12.003

El Ariebi, N., Hiscox, J., Scriven, S. A., Muller, C. T., and Boddy, L. (2016). Production and effects of volatile organic compounds during interspecific interactions. *Fungal Ecol.* 20, 144–154. doi: 10.1016/j.funeco.2015.12.013

Enright, A. J., Van Dongen, S., and Ouzounis, C. A. (2002). An efficient algorithm for large-scale detection of protein families. *Nucleic Acids Res.* 30, 1575–1584. doi: 10.1093/nar/30.7.1575

Evans, J. A., Eyre, C. A., Rogers, H. J., Boddy, L., and Muller, C. T. (2008). Changes in volatile production during interspecific interactions between four wood rotting fungi growing in artificial media. *Fungal Ecol.* 1, 57–68. doi: 10.1016/j.funeco.2008.06.001

Eyre, C., Muftah, W., Hiscox, J., Hunt, J., Kille, P., Boddy, L., et al. (2010). Microarray analysis of differential gene expression elicited in Trametes versicolor during interspecific mycelial interactions. *Fungal Biol.* 114, 646–660. doi: 10.1016/j.funbio.2010.05.006

Ghose, T. K. (1987). Measurement of cellulase activities. *Pure Appl. Chem.* 59, 257–268. doi: 10.1351/pac198759020257

Grigoriev, I. V., Nikitin, R., Haridas, S., Kuo, A., Ohm, R., Otillar, R., et al. (2014). MycoCosm portal: gearing up for 1000 fungal genomes. *Nucleic Acids Res.* 42, D699–D704. doi: 10.1093/nar/gkt1183

Han, J. J., Bao, L., Tao, Q. Q., Yao, Y. J., Liu, X. Z., Yin, W. B., et al. (2015). Gloeophyllins A-J, Cytotoxic ergosteroids with various skeletons from a chinese tibet fungus *Gloeophyllum abietinum*. *Org. Lett.* 17, 2538–2541. doi: 10.1021/acs.orglett.5b01080

Hiscox, J., Baldrian, P., Rogers, H. J., and Boddy, L. (2010). Changes in oxidative enzyme activity during interspecific mycelial interactions involving the white-rot fungus Trametes versicolor. *Fungal Genet. Biol.* 47, 562–571. doi: 10.1016/j.fgb.2010.03.007

Hiscox, J., and Boddy, L. (2017). Armed and dangerous – chemical warfare in wood decay communities. *Fungal Biol. Rev.* 31, 169–184. doi: 10.1016/j.fbr.2017.07.001

Hiscox, J., Savoury, M., Vaughan, I. P., Muller, C. T., and Boddy, L. (2015). Antagonistic fungal interactions influence carbon dioxide evolution from decomposing wood. *Fungal Ecol.* 14, 24–32. doi: 10.1016/j.funeco.2014.11.001

Hori, C., Gaskell, J., Igarashi, K., Kersten, P., Mozuch, M., Samejima, M., et al. (2014). Temporal alterations in the secretome of the selective ligninolytic fungus *Ceriporiopsis subvermispora* during growth on aspen wood reveal this organism's strategy for degrading lignocellulose. *Appl. Environ. Microbiol.* 80, 2062–2070. doi: 10.1128/aem.03652-13

Hynes, J., Muller, C. T., Jones, T. H., and Boddy, L. (2007). Changes in volatile production during the course of fungal mycelial interactions between *Hypholoma fasciculare* and *Resinicium bicolor*. *J. Chem. Ecol.* 33, 43–57. doi: 10.1007/s10886-006-9209-6

Jaquet, F., Hutter, R., and Luthy, P. (1987). Specificity of *Bacillus thuringiensis* delta-endotoxin. *Appl. Environ. Microbiol.* 53, 500–504. doi: 10.1128/aem.53.3.500-504.1987

Kalb, D., Lackner, G., and Hoffmeister, D. (2013). Fungal peptide synthetases: an update on functions and specificity signatures. *Fungal Biol. Rev.* 27, 43–50. doi: 10.1016/j.fbr.2013.05.002

Karlsson, M., Stenlid, J., and Lindahl, B. (2016). Functional differentiation of chitinases in the white-rot fungus *Phanerochaete chrysosporium*. *Fungal Ecol.* 22, 52–60. doi: 10.1016/j.funeco.2016.04.004

Kim, S., and Pevzner, P. A. (2014). MS-GF plus makes progress towards a universal database search tool for proteomics. *Nat. Commun.* 5:5277. doi: 10.1038/ncomms6277

Krah, F.-S., Baessler, C., Heibl, C., Soghigian, J., Schaefer, H., and Hibbett, D. S. (2018). Evolutionary dynamics of host specialization in wood-decay fungi. *BMC Evol. Biol.* 18:119. doi: 10.1186/s12862-018-1229-7

Krogh, A., Larsson, B., von Heijne, G., and Sonnhammer, E. L. L. (2001). Predicting transmembrane protein topology with a hidden Markov model: application to complete genomes. *J. Mol. Biol.* 305, 567–580. doi: 10.1006/jmbi.2000.4315

Kuees, U., and Ruehl, M. (2011). Multiple multi-copper oxidase gene families in basidiomycetes – what for? *Curr. Genomics* 12, 72–94. doi: 10.2174/138920211795564377

Lackner, G., Bohnert, M., Wick, J., and Hoffmeister, D. (2013). Assembly of melleolide antibiotics involves a polyketide synthase with cross-coupling activity. *Chem. Biol.* 20, 1101–1106. doi: 10.1016/j.chembio1.2013.07.009

Lackner, G., Misiek, M., Braesel, J., and Hoffmeister, D. (2012). Genome mining reveals the evolutionary origin and biosynthetic potential of basidiomycete polyketide synthases. *Fungal Genet. Biol.* 49, 996–1003. doi: 10.1016/j.fgb.2012.09.009

Langner, T., and Gohre, V. (2016). Fungal chitinases: function, regulation, and potential roles in plant/pathogen interactions. *Curr. Genet.* 62, 243–254. doi: 10.1007/s00294-015-0530-x

Liu, L. Z., and Free, S. J. (2016). Characterization of the *Sclerotinia sclerotiorum* cell wall proteome. *Mol. Plant Pathol.* 17, 985–995. doi: 10.1111/mpp.12352

Martin, K., McDougall, B. M., McIlroy, S., Chen, J. Z., and Seviour, R. J. (2007). Biochemistry and molecular biology of exocellular fungal beta-(1,3)- and beta-(1,6)-glucanases. *FEMS Microbiol. Rev.* 31, 168–192. doi: 10.1111/j.1574-6976.2006.00055.x

Mayampurath, A. M., Jaitly, N., Purvine, S. O., Monroe, M. E., Auberry, K. J., Adkins, J. N., et al. (2008). DeconMSn: a software tool for accurate parent ion monoisotopic mass determination for tandem mass spectra. *Bioinformatics* 24, 1021–1023. doi: 10.1093/bioinformatics/btn063

Moody, S. C., Dudley, E., Hiscox, J., Boddy, L., and Eastwood, D. C. (2018). Interdependence of primary metabolism and xenobiotic mitigation characterizes the proteome of *Bjerkandera adusta* during wood decomposition. *Appl. Environ. Microbiol.* 84:e01401-17. doi: 10.1128/aem.01401-17

O'Leary, J., Eastwood, D., Muller, C., and Boddy, L. (2018). Emergent properties arising from spatial heterogeneity influence fungal community dynamics. *Fungal Ecol.* 33, 32–39. doi: 10.1016/j.funeco.2018.02.001

O'Leary, J., Hiscox, J., Eastwood, D. C., Savoury, M., Langley, A., McDowell, S. W., et al. (2019). The whiff of decay: linking volatile production and extracellular enzymes to outcomes of fungal interactions at different temperatures. *Fungal Ecol.* 39, 336–348. doi: 10.1016/j.funeco.2019.03.006

Peiris, D., Dunn, W. B., Brown, M., Kell, D. B., Roy, I., and Hedger, J. N. (2008). Metabolite profiles of interacting mycelial fronts differ for pairings of the wood decay basidiomycete fungus, Stereum hirsutum with its competitors *Coprinus micaceus* and *Coprinus disseminatus*. *Metabolomics* 4, 52–62. doi: 10.1007/s11306-007-0100-4

Presley, G. N., Panisko, E., Purvine, S. O., and Schilling, J. S. (2018). Coupling secretomics with enzyme activities to compare the temporal processes of wood metabolism among white and brown rot fungi. *Appl. Environ. Microbiol.* 84, e159–e118. doi: 10.1128/AEM.000159-18

Presley, G. N., and Schilling, J. S. (2017). Distinct growth and secretome strategies for two taxonomically divergent brown rot fungi. *Appl. Environ. Microbiol.* 83:e02987-16. doi: 10.1128/AEM.02987-16

Quin, M. B., Flynn, C. M., Wawrzyn, G. T., Choudhary, S., and Schmidt-Dannert, C. (2013). Mushroom hunting by using bioinformatics: application of a predictive framework facilitates the selective identification of sesquiterpene synthases in basidiomycota. *Chembiochem* 14, 2480–2491. doi: 10.1002/cbic.201300349

Rajala, T., Peltoniemi, M., Pennanen, T., and Makipaa, R. (2012). Fungal community dynamics in relation to substrate quality of decaying Norway spruce (*Picea abies* L. Karst.) logs in boreal forests. *FEMS Microbiol. Ecol.* 81, 494–505. doi: 10.1111/j.1574-6941.2012.01376.x

Rasser, F., Anke, T., and Sterner, O. (2000). Secondary metabolites from a Gloeophyllum species. *Phytochemistry* 54, 511–516. doi: 10.1016/s0031-9422(00)00137-0

Riley, R., Salamov, A. A., Brown, D. W., Nagy, L. G., Floudas, D., Held, B. W., et al. (2014). Extensive sampling of basidiomycete genomes demonstrates inadequacy of the white-rot/brown-rot paradigm for wood decay fungi.

Proc. Natl. Acad. Sci. U.S.A. 111, 9923–9928. doi: 10.1073/pnas.1400592111

Silar, P. (2005). Peroxide accumulation and cell death in filamentous fungi induced by contact with a contestant. *Mycol. Res.* 109, 137–149. doi: 10.1017/s0953756204002230

Smith, P. K., Krohn, R. I., Hermanson, G. T., Mallia, A. K., Gartner, F. H., Provenzano, M. D., et al. (1985). Measurement of protein using bicinchoninic acid. *Anal. Biochem.* 150, 76–85. doi: 10.1016/0003-2697(85)90442-7

Snajdr, J., Dobiasova, P., Vetrovsky, T., Valaskova, V., Alawi, A., Boddy, L., et al. (2011). Saprotrophic basidiomycete mycelia and their interspecific interactions affect the spatial distribution of extracellular enzymes in soil. *FEMS Microbiol. Ecol.* 78, 80–90. doi: 10.1111/j.1574-6941.2011.01123.x

Sonnenbichler, J., Dietrich, J., and Peipp, H. (1994). Secondary fungal metabolites and their biological-activities, .5. Investigations concerning the induction of the biosynthesis of toxic secondary metabolites in basidiomycetes. *Biol. Chem. Hoppe. Seyler.* 375, 71–79. doi: 10.1515/bchm3.1994.375.1.71

Sonnenbichler, J., Peipp, H., and Dietrich, J. (1993). Secondary fungal metabolites and their biological-activities .3. Further metabolites from dual cultures of the antagonistic basidiomycetes *Heterobasidion annosum* and *Gloeophyllum abietinum*. *Biol. Chem. Hoppe. Seyler.* 374, 467–473. doi: 10.1515/bchm3.1993.374.7-12.467

Sonnenbichler, J., Sonnenbichler, I., and Schwarz, D. (1997). Biosynthesis of oosponol and oospoglycol elucidated by C-13 NMR. *Phytochemistry* 44, 267–269. doi: 10.1016/s0031-9422(96)00469-4

Trapnell, C., Roberts, A., Goff, L., Pertea, G., Kim, D., Kelley, D. R., et al. (2012). Differential gene and transcript expression analysis of RNA-seq experiments with TopHat and Cufflinks. *Nat. Protoc.* 7, 562–578. doi: 10.1038/nprot.2012.016

Wawrzyn, G. T., Quin, M. B., Choudhary, S., Lopez-Gallego, F., and Schmidt-Dannert, C. (2012). Draft genome of *Omphalotus olearius* provides a predictive framework for sesquiterpenoid natural product biosynthesis in Basidiomycota. *Chem. Biol.* 19, 772–783. doi: 10.1016/j.chembiol.2012.05.012

Weber, T., Blin, K., Duddela, S., Krug, D., Kim, H. U., Bruccoleri, R., et al. (2015). antiSMASH 3.0: a comprehensive resource for the genome mining of biosynthetic gene clusters. *Nucleic Acids Res.* 43, W237–W243. doi: 10.1093/nar/gkv437

Wei, D. S., Houtman, C. J., Kapich, A. N., Hunt, C. G., Cullen, D., and Hammel, K. E. (2010). Laccase and its role in production of extracellular reactive oxygen species during wood decay by the brown rot basidiomycete *Postia placenta*. *Appl. Environ. Microbiol.* 76, 2091–2097. doi: 10.1128/aem.02929-09

Weng, Y. P., Lin, Y. P., Hsu, C. I., and Lin, J. Y. (2004). Functional domains of a pore-forming cardiotoxic protein, volvatoxin A2. *J. Biol. Chem.* 279, 6805–6814. doi: 10.1074/jbc.M308675200

Yao, L., Zhu, L. P., Xu, X. Y., Tan, L. L., Sadilek, M., Fan, H., et al. (2016). Discovery of novel xylosides in co-culture of basidiomycetes *Trametes versicolor* and *Ganoderma applanatum* by integrated metabolomics and bioinformatics. *Sci. Rep.* 6:33237. doi: 10.1038/srep33237

Zhang, J., Silverstein, K. A. T., Castano, J. D., Figueroa, M., and Schilling, J. S. (2019). Gene regulation shifts shed light on fungal adaption in plant biomass decomposers. *mBio* 10:e02176-19. doi: 10.1128/mBio.02176-19

Zhang, J. W., Presley, G. N., Hammel, K. E., Ryu, J. S., Menke, J. R., Figueroa, M., et al. (2016). Localizing gene regulation reveals a staggered wood decay mechanism for the brown rot fungus *Postia placenta*. *Proc. Natl. Acad. Sci. U.S.A.* 113, 10968–10973. doi: 10.1073/pnas.1608454113

Conflict of Interest: The authors declare that the research was conducted in the absence of any commercial or financial relationships that could be construed as a potential conflict of interest.

frontiers in Microbiology

ORIGINAL RESEARCH
published: 28 January 2021
doi: 10.3389/fmicb.2021.552301

Trichoderma reesei Isolated From Austrian Soil With High Potential for Biotechnological Application

*Wolfgang Hinterdobler[1], Guofen Li[1], Katharina Spiegel[1], Samira Basyouni-Khamis[1,2], Markus Gorfer[1] and Monika Schmoll[1]**

[1] Center for Health and Bioresources, AIT Austrian Institute of Technology GmbH, Tulln, Austria, [2] Department of Sustainable Agricultural Systems, Institute of Agricultural Engineering, University of Natural Resources and Life Sciences Vienna, Tulln, Austria

Fungi of the genus *Trichoderma* are of high importance for biotechnological applications, in biocontrol and for production of homologous and heterologous proteins. However, sexual crossing under laboratory conditions has so far only been achieved with the species *Trichoderma reesei*, which was so far only isolated from tropical regions. Our isolation efforts aimed at the collection of *Trichoderma* strains from Austrian soils surprisingly also yielded 12 strains of the species *T. reesei*, which was previously not known to occur in Europe. Their identity was confirmed with *tef1*- and *rpb2*-sequencing and phylogenetic analysis. They could clearly be distinguished from tropical strains including the common laboratory wildtypes by UP-PCR and genetic variations adjacent to the mating type locus. The strains readily mated with reference strains derived from CBS999.97. Secreted cellulase and xylanase levels of these isolates were up to six-fold higher than those of QM6a indicating a high potential for strain improvement. The strains showed different responses to injury in terms of induction of sporulation, but a correlation to alterations in the *nox1*-gene sequence was not detected. Several synonymous SNPs were found in the sequence of the regulator gene *noxR* of the soil isolates compared to QM6a. Only in one strain, non-synonymous SNPs were found which impact a PEST sequence of NoxR, suggesting altered protein stability. The availability of sexually fertile strains from middle Europe naturally producing decent amounts of plant cell wall degrading enzymes opens up novel perspectives for non-GMO strain improvement and biological pretreatment of plant biomass for bioethanol production. Moreover, the varied response of these strains to injury in terms of sporulation, which is independent of Nox1 and NoxR suggests that additional regulators impact this phenomenon in *T. reesei*.

Keywords: *Trichoderma reesei*, *Hypocrea jecorina*, sexual development, pretreatment for biofuels and biogas, cellulases and xylanases, biocontrol, plant cell wall degradation, strain improvement

OPEN ACCESS

Edited by:
Jiwei Zhang,
University of Minnesota Twin Cities, United States

Reviewed by:
Xinqing Zhao,
Shanghai Jiao Tong University, China
Minou Nowrousian,
Ruhr University Bochum, Germany

****Correspondence:***
Monika Schmoll
monika.schmoll@ait.ac.at

Specialty section:
This article was submitted to Fungi and Their Interactions, a section of the journal Frontiers in Microbiology

Received: *15 April 2020*
Accepted: *12 January 2021*
Published: *28 January 2021*

Citation:
Hinterdobler W, Li G, Spiegel K, Basyouni-Khamis S, Gorfer M and Schmoll M (2021) Trichoderma reesei Isolated From Austrian Soil With High Potential for Biotechnological Application. Front. Microbiol. 12:552301. doi: 10.3389/fmicb.2021.552301

INTRODUCTION

The genus *Trichoderma* comprises fungi with widespread ecological functions, which are of high interest in research. Species of this genus include a considerable number of efficient biocontrol agents (Harman et al., 2004; Harman, 2011), the biotechnological workhorse *T. reesei* (Bischof et al., 2016) and species know to comprise pathogenic strains impacting mushroom farming (Komon-Zelazowska et al., 2007) or even threatening human health (Hatvani et al., 2013). Roughly 260

species are documented from this genus in current literature (Atanasova et al., 2013; Bissett et al., 2015), with a total of 443 species listed in Mycobank for *Trichoderma*[1] (access on July 31st, 2020).

Among *Trichoderma* spp., *T. reesei* is among the best studied species (Schmoll et al., 2014, 2016), predominantly due to its broad application in biotechnology (Gudynaite-Savitch and White, 2016; Arnau et al., 2020). After the isolation of the wild-type strain QM6a from the Solomon Islands during World War II, its efficient production of cellulolytic enzymes was recognized (Bischof et al., 2016). Since then, decades of research, including mutation programs were aimed at improvement of cellulase production as well as optimization of *T. reesei* as a host for heterologous protein production (Seiboth et al., 2011; Paloheimo et al., 2016). The enhanced strains from these efforts are all derived from the original isolate QM6a.

The natural habitat of *Trichoderma reesei* is known to be a tropical rain forest with abundant decaying plant material (Druzhinina et al., 2011). The teleomorph of *T. reesei* was initially known as *Hypocrea jecorina*, a name which was frequently used in literature of this species as well, until the one fungus = one name nomenclature ended the century old practice of naming sexual and asexual forms independently (Bissett et al., 2015). Since then, only the name *T. reesei* is accepted. Phylogenetically the species *T. reesei* belongs to the *Longibrachiatum* clade, which comprises 26 putative species (Druzhinina et al., 2012) with the closest relatives being *Trichoderma parareesei*, *Trichoderma orientalis*, and *Trichoderma longibrachiatum*. Most analyzed isolates originate from tropical or subtropical regions like the Solomon Islands, French Guiana, Brazil, or Peru (Druzhinina et al., 2012). Genome analysis revealed that *T. reesei*, representing the *Longibrachiatum* clade is evolutionarily one of the youngest species of *Trichoderma* (Kubicek et al., 2011). The same study indicated that the rather poor performance of *T. reesei* in most biocontrol applications compared to other *Trichoderma* species may be due to the loss of multiple genes associated with antagonism and mycoparasitism.

As a highly efficient producer of homologous and heterologous proteins, manipulation of the genome of *T. reesei* is supported by optimized tools like non-homologous end joining deficient (NHEJ) strains and genome wide deletion primer design (Schuster et al., 2012), transient knock down of NHEJ (Chum et al., 2017), or CRISPR/Cas9 mediated genome editing (Liu et al., 2015). The genome of *T. reesei* is sequenced in high quality (Martinez et al., 2008; Marie-Nelly et al., 2014; Li et al., 2017) and manually annotated (Druzhinina et al., 2016; Schmoll et al., 2016; Li et al., 2017). Despite the broad array of versatile tools for genome manipulation, a common drawback for strain improvement lies in the fact that either the genes responsible for an improvement has to be known or that deleterious mutations are introduced by random mutagensis along with the desired mutations leading to an overall suboptimal result. The latter drawback can be avoided by the use of sexual crossing for strain improvement (Ashton and Dyer, 2016).

Breeding of industrial fungi for high efficiency production has been an aim for decades. Although the sexually propagating *H. jecorina* was identified as the teleomorph of *T. reesei* (Kuhls et al., 1996) and fruiting bodies were seen with an isolate from French Guiana (Lieckfeldt et al., 2000), fruitless attempts to achieve mating led to the assumption that *T. reesei* is a clonal species. Only about 11 years ago, after the discovery of peptide pheromone precursor genes in the genome, sexual development under laboratory conditions was achieved (Schmoll et al., 2004, 2010; Seidl et al., 2009; Hinterdobler et al., 2020). *T. reesei* is a heterothallic fungus with a common mating type structure of three mat-genes in the MAT1-1 locus and one mat-gene in the MAT1-2 locus (Seidl et al., 2009). Its pheromone system comprises two pheromone receptors HPR1 and HPR2 as well as two associate peptide pheromone precursors, HPP1 and PPG1 (Schmoll et al., 2010; Seibel et al., 2012). Additionally, also chemical communication is involved in mate recognition (Bazafkan et al., 2015). In contrast to many other fungal species, mating in *T. reesei* occurs on rich media like malt extract and is facilitated by light (Schmoll, 2013; Hinterdobler et al., 2020). Unfortunately, the parental strain of all strains currently used in industry and academia, QM6a, was found to be female sterile (Seidl et al., 2009). This defect is due to mutations in the *ham5* gene, causing erratic splicing and loss of function (Linke et al., 2015; Tisch et al., 2017). While this mutation can now be complemented, it still causes a considerable obstacle in industrial strain improvement by crossing.

Here, we identified and analyzed twelve *T. reesei* strains of both mating types unexpectedly isolated in the temperate climate zone in Austria (Central Europe), which readily mate with common *T. reesei* lab strains and each other. They show production of plant cell wall degrading enzymes and different inducibility of asexual development by injury. Their application for strain improvement by crossing renders them a valuable resource for diverse plant cell wall degrading enzymes using diverse substrates. Fungal strain improvement and/or GMO-free optimization of production is moreover crucial if the resulting strains are to be distributed in nature (biocontrol applications) or due to labeling requirements of products from GMO organisms by the EU[2].

RESULTS

Trichoderma reesei Occurs in Austrian Soil

In the course of a collection project aimed at isolation of novel *Trichoderma* strains from agricultural soil, we surprisingly found *T. reesei* strains in four independent locations in Austria (for GPS data see **Table 1**). The phylogenetic species concept (PSC) determines a species as a monophyletic group based on evolutionary history (Lee et al., 2010). Hence, species identification for the isolates from Austria was performed by sequence analysis of the *tef1* diagnostic region (Samuels et al., 2002; Chaverri et al., 2003) and BLAST search against the

[1] www.mycobank.org

[2] https://ec.europa.eu/food/plant/gmo/legislation_en

TABLE 1 | Origin and identification of Austrian soil isolates.

Strain	Mating type	Isolation from	GPS Coordinates (isolation)	GenBank Accession number		
				tef1	*rpb2*	INDEL/SNP region
AIT_TRKH1a1	MAT1-1	Soil	47.03273, 15.37634	MT317221	MT809491	MW345895
AIT_TRKH1c1	MAT1-1	Soil	47.03273, 15.37634	MT317222	MT809492	MW345896
AIT_TRKH1d1	MAT1-1	Soil	47.03273, 15.37634	MT317223	MT809493	MW345897
AIT_TRKH1h1	MAT1-1	Soil	47.03273, 15.37634	MT317224	MT809494	MW345898
AIT_TRLF1e1	MAT1-1	Soil	47.45514, 16.25114	MT317225	MT809495	MW345899
AIT_TRLF4a1	MAT1-1	Soil	47.46148, 16.25278	MT317226	MT809496	MW345900
AIT_TRLF4a2	MAT1-1	Soil	47.45514, 16.25114	MT317227	MT809497	MW345901
AIT_TRLF4d2	MAT1-1	Soil	47.45514, 16.25114	MT317228	MT809498	MW345902
AIT_TRLF4e1	MAT1-1	Soil	47.45514, 16.25114	MT317229	MT809499	MW345903
AIT_TRLF4f1	MAT1-1	Soil	47.45514, 16.25114	MT317230	MT809500	MW345904
AIT_TRLF4h1	MAT1-1	Soil	47.45514, 16.25114	MT317231	MT809501	MW345905
AIT_TRMS44c2	MAT1-2	Soil	47.89873, 16.88850	MT317232	MT317233	MW345906

NCBI nucleotide database. Phylogenetic analysis confirmed that the *tef1* sequences amplified from the 12 strains tentatively assigned to *T. reesei* indeed clustered with *T. reesei* QM6a and several other *T. reesei* strains. The closely related *T. parareesei* strains clustered separately (**Figure 1**). The diagnostic *rpb2* gene (Jaklitsch et al., 2008; Jaklitsch and Voglmayr, 2015) was used for additional confirmation for species identity, particularly because the pattern for AIT_MS44c2 in universal primers (UP-PCR) was divergent from the other strains (see also below). This analysis confirmed the species identity as *T. reesei* (**Supplementary Figure 1** in **Supplementary File 1**). The 12 isolates showed clearly distinguishable phenotypes upon growth on plates with malt extract medium (**Figure 2**).

Twelve Novel and Unique *T. reesei* Strains Are Distinguishable by Molecular Methods

Previously, strains of the species *T. reesei* were not found in Europe and hence, *T. reesei* was assumed to be adapted to tropical climate. Consequently, we considered it of utmost importance to rule out any contamination by laboratory strains. In order to unequivocally distinguish these strains from our reference strains routinely used in the lab, we performed UP-PCR (Naeimi et al., 2011) using five different primers under different PCR conditions. All our isolates showed patterns distinct from the wild-type strains we are routinely using in the lab (**Figure 3A**, **Supplementary Figure 2** in **Supplementary File 1**). The difference of QM6a from AIT_TRKH1a1, AIT_TRKH1c1, AIT_TRKH1d1, and AIT_TRKH1h1 is more subtle, but obvious in **Figure 3A**, showing one additional band migrating more slowly (green triangle) in QM6a. Moreover, these isolates also showed phenotypic differences with respect to cellulase regulation and injury response (see following sections). The differences between the individual isolates were not sufficiently clear in some cases and needed additional support (**Figure 3A**). Hence, we compared the banding patterns of all strains against each other and used additional criteria from our analyses for clarification (**Figure 3B**). Applying alternative primers, we could find characteristic patterns for most of the strains compared to the others (**Supplementary Figures 3, 4** in **Supplementary File 1**). However, UP-PCR did not allow for clear separation of AIT_TRKH1a1, AIT_TRKH1c1, AIT_TRKH1d1, and AIT_TRKH1h1 from each other (**Figure 3B**). Therefore we compared the behavior of these strains in cellulase and xylanase production as well as injury response (see below). We found clear differences confirming that these strains are individuals rather than re-isolations of one and the same strain (**Figure 3B**). For further confirmation of the distinct origin of these strains, we screened the rapidly evolving region of the mating type locus for characteristics variations. We found a four base pair long INDEL and a SNP in the region adjacent to the mating type idiomorphs[3], both of which are specific for the isolated strains and distinct from QM6a, RutC30, and CBS999.97 (**Table 1** and **Figure 3C**).

Austrian Isolates Are Sexually Fertile and Compatible Among Each Other

The biological species concept (BSC) supports the concept that sexually compatible individuals belong to the same species, while two populations that cannot mate represent different species (Lee et al., 2010). Sexual reproduction between strains of different species has not been shown for fungi previously and would contradict the BSC. Hence, the ability to mate with known and confirmed *T. reesei* strains can add further confirmation to species identity of the 12 strains investigated here.

Additionally, *T. reesei* strains with an origin in middle Europe and the potential of breeding for strain improvement would have a high potential for applications under natural conditions in this region. Consequently, we explored the prerequisites for that and found solid support for the strains belonging to the species *T. reesei*: Using mating type specific primers (Seidl et al., 2009) for *T. reesei*, we found that of the 12 new isolates, eleven strains comprised the MAT1-1 idiomorph and one strain was of MAT1-2. All strains showed efficient sporulation with

[3]https://mycocosm.jgi.doe.gov/Trire_Chr/Trire_Chr.home.html; scaffold 3:3896980-3896983 and scaffold 3:3897139.

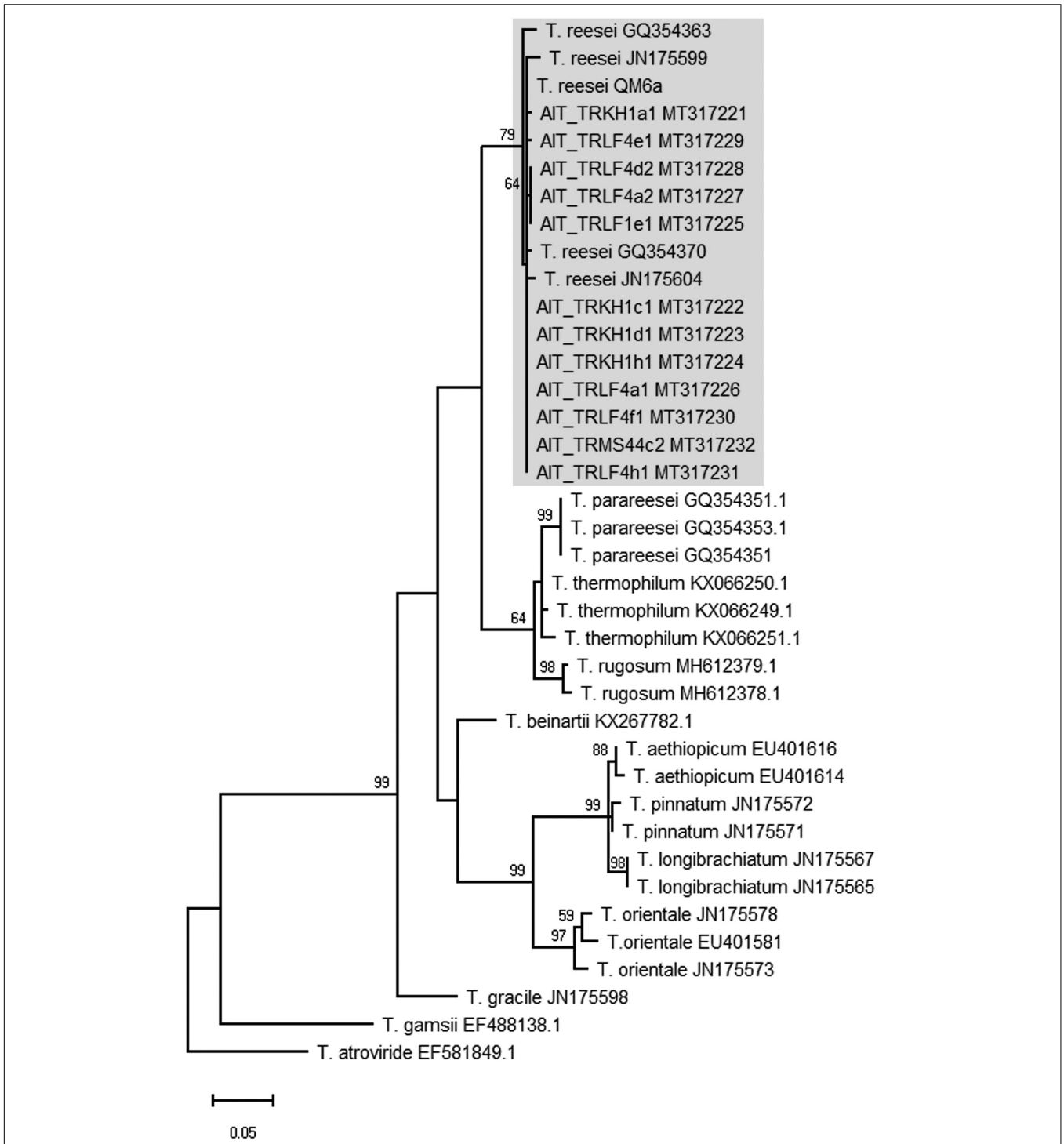

FIGURE 1 | Phylogram obtained from an alignment of the *tef1* locus. The evolutionary history was inferred by using the Maximum Likelihood method and Tamura-Nei model (Tamura and Nei, 1993). The tree with the highest log likelihood (–1894.50) is shown. The bootstrap test was carried out with 1,000 replicates (Felsenstein, 1985) and values >50 are shown. Species names are given along with the GenBank accession number of the sequence (as retrieved from the NCBI nucleotide database) used for the analysis.

a preference for asexual development in light, i.e., increased production of conidia in light compared to darkness. Due to the biotechnological importance of sexual development we tested all strains for mating (Schmoll, 2013) with fully fertile *T. reesei* strains under daylight conditions (**Figure 2A**).We found that all strains were able to undergo sexual development with CBS999.97

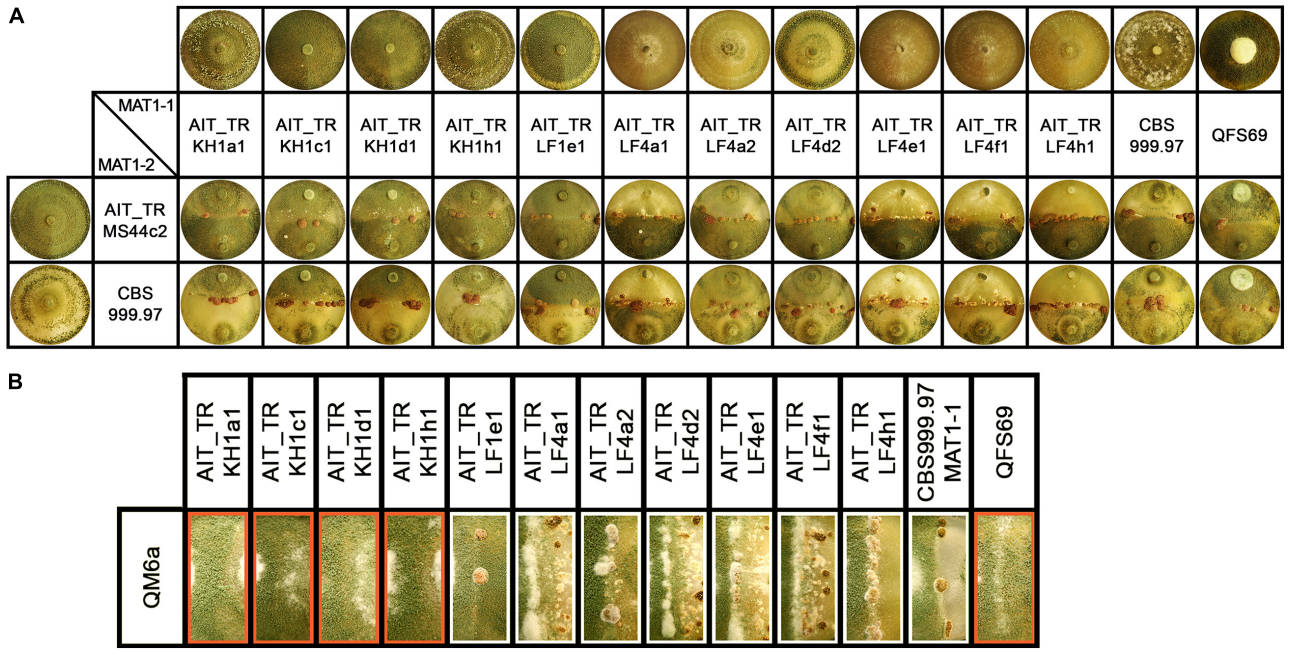

FIGURE 2 | Growth and development of *T. reesei* strains isolated from Austrian soil. **(A)** Axenic growth and crossings of Austrian strains of MAT1-1 with AIT_TRMS44c2 (MAT1-2) and CBS999.97 MAT1-2 (wild-type control, female fertile). **(B)** Analysis of female fertility by crossing of Austrian soil isolates of MAT1-1 with the female sterile strain QM6a (MAT1-2). Abolished fruiting body formation indicates female sterility of the tested strains (Hinterdobler et al., 2020). Female sterile strains are indicated by red boxes. Strains were grown on malt extract agar plates (3% w/v) at 22°C with light-dark cycles. Phenotypes and fruiting body development are shown for day 14 after inoculation. One representative of three biological replicates is shown.

representing a fully fertile partner of opposite mating type under usual mating conditions.

Fruiting body formation of the new isolates with fully fertile strains started at 4–5 days after inoculation, which is roughly at the same time or even slightly earlier as seen with the control crossing of CBS999.97 MAT1-1 and CBS999.97 MAT1-2, our model strains for sexual development (**Figure 2A**). As female sterility was found to occur in natural strains of *T. reesei*, most importantly with QM6a (MAT1-2) (Seidl et al., 2009), we also tested whether our strains are female fertile by confrontation of the strains with the female sterile QM6a (MAT1-2). Indeed we found female sterility for four of our isolates (**Figure 2B**): AIT_TRKH1a1, AIT_TRKH1c1, AIT_TRKH1d1, and AIT_TRKH1h1. The only MAT1-2 strain, AIT_TRMS44c2, was crossed with a female sterile derivative of QM6a bearing the MAT1-1 locus, QFS69. Together with the fact that AIT_TRMS44c2 readily crossed with the obviously female sterile strains mentioned above, confirmed that AIT_TRMS44c2 is female fertile.

Interestingly, crossing of the MAT1-2 isolate AIT_TRMS44c2 with strains that could not form fruiting bodies with QM6a (**Figure 2B**, red boxes) was significantly delayed to 7–8 days for AIT_TRKH1c1, AIT_TRKH1d1 and AIT_TRKH1h1 as well as the control strain QFS69 or even 9 days with AIT_TRKH1a1. Also AIT_TRLF1e1 showed a delay to 6 to more than 7 days in all crossings. Consequently, the ability of all our new isolates to mate with different, known and confirmed *T. reesei* strains further confirmed species identity.

Production of Cellulases and Xylanases

For *T. reesei* as an important species in biotechnological industry, production of enzymes is of particular interest. Therefore we tested our strain for production of cellulases and xylanases upon growth on Mandels Andreotti minimal medium with cellulose as carbon source. While the majority of the strains produced cellulases in the range of QM6a, some of the strains were considerably more efficient with up to a six-fold increase in cellulase efficiency (**Figure 4A**). Also for xylanase expression we found a considerably higher efficiency in some strains compared the QM6a (**Figure 4B**). As these strains showed also high cellulase production, they are the most interesting ones for further studies.

A Strain Specific Response to Mycelial Injury

Asexual development is regulated in response to environmental conditions in fungi and is of high importance for application in biotechnology. Usually, sporulation in *T. reesei* is enhanced in light and diverse carbon sources modulate its efficiency (Friedl et al., 2008; Steyaert et al., 2010a,b). However, in some *Trichoderma* species, also injury was shown to induce sporulation (Casas-Flores et al., 2004). In the reference strain QM6a, we could not previously observe this phenomenon. Therefore we wanted to evaluate if this is a species specific characteristic or merely dependent on the strain.

The strains were grown in constant darkness for two days and then injured by cutting (**Figure 5A**). *T. atroviride* IMI206040 and

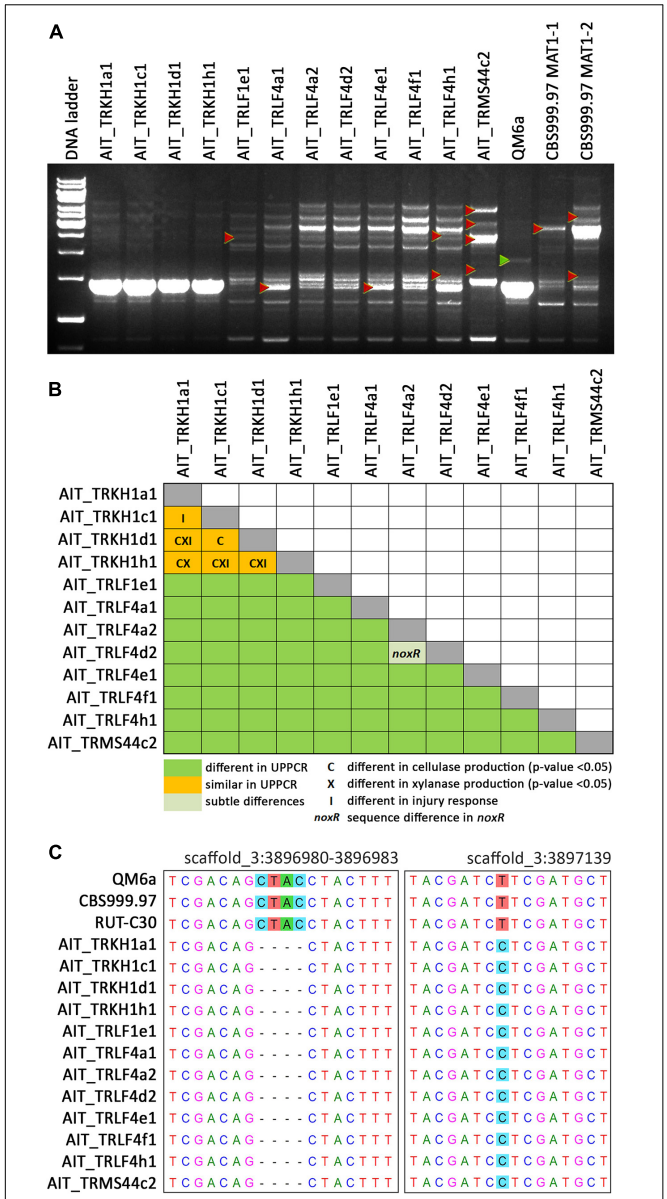

FIGURE 3 | UP-PCR analysis, phenotypic differentiation and genetic alterations of strains. **(A)** UP-PCR of Austrian isolates along with QM6a and CBS999.97 MAT1-1 and MAT1-2 using as15inv as primer. For analysis with additional primers resulting in different patterns for separation of individual strains see also **Supplementary Figures S2–S4** in **Supplementary File 1**. Triangles indicate bands indicative of differences to other strains. **(B)** Schematic representation of comparison of individual strains. UP-PCR band patterns and **Supplementary Figures S2–S4** were used for evaluation. If no difference was found for band patterns, we considered sequence differences in noxR, altered enzyme production or injury response as well. **(C)** INDEL and SNP in the sequence flanking the mating type locus and specific for Austrian strains compared to laboratory strains in chromosome 3 (https://mycocosm.jgi.doe.gov/Trire_Chr/Trire_Chr.home.html; scaffold 3).

P1, for which a strong response to injury in terms of conidiation is well known was used as a control (Casas-Flores et al., 2004; Hernandez-Oñate et al., 2012). In many cases, the growth front at the time of injury became clearly distinguishable, because growth after the injury commenced with mycelium, in which no premature sporulation was induced (**Figures 5B,C**). We observed a strong response in some, but not all strains (**Figures 5–7**). In QM6a and CBS999.97 we found weak, but detectable induction of sporulation by injury (**Figure 5**).

Our results showed that the reaction to injury is highly strain-specific in *T. reesei*, and we could assign four distinguishable types of responses. We found a range from no reaction up to strong sporulation in the young mycelium present at the timepoint of injury (**Figure 5**). The reaction of *T. atroviride* IMI206040 with no sporulation close to the inoculum indicates a fast, coordinated signal transduction within the mycelium before the colony continues its radial growth (**Figure 5C**). While the morphological changes associated with sporulation are close to the injured mycelial areas in some strains, in other strains, injury triggers sporulation in the adjacent mycelium. Comparison between *type III* and *type IV* injury response (**Figure 5C**) suggests intracellular signal transduction in both directions for *type III* and only in direction toward the growth margin in *type IV*. Injury response of *type IV* shown here only for *T. atroviride* IMI206040 seems in addition to be medium dependent as a previous study (Hernandez-Oñate et al., 2012) described rather *type II* sporulation on PDA and minimal medium. Further research regarding the influence of the provided nutrients on intercellular injury signaling is need for a better understanding of the observed phenomenon.

Since growth and sporulation after injury were altered, we analyzed the site of injury shortly after cutting and the expected, thinner hyphae emerged from injured mycelial cells (**Figure 6**). Additionally, we were interested whether this growth after injury would be permanently and consistently altered. Therefore, we injured the young mycelium with one cut to be able to monitor further growth for a longer time (**Figure 7A**).

Interestingly, the separation of a small part of the young mycelium by injury as shown in **Figure 7** did not affect the macroscopic phenotype of the emerging mycelium in all tested strains. In two strains, AIT_TRLF4d2 and *T. atroviride* P1 (**Figures 7B,C**), the separated, younger mycelium close to the growth margin at the timepoint of injury shows less sporulation than the emerging mycelium and the older mycelium close to the inoculum. This indicates a different influence of an injury event, either on young hyphae currently exploring new food sources compared to older hyphae, or an influence of the general size and energy reserves of the colony needed to react properly.

Altered Response to Injury Is Not Due to Variations in Nox1, NoxR, or MAPkinase Genes

Since we saw differences in the injury response between many strains, also from the same locations, were interested if this might be reflected in the genome. Injury induced conidiation was found to be associated with an oxidative response and triggers NADPH oxidase (Nox)-dependent ROS production (Hernandez-Oñate et al., 2012). Fungi have between one and three NADPH oxidases (Aguirre et al., 2005), which are regulated by NoxR.

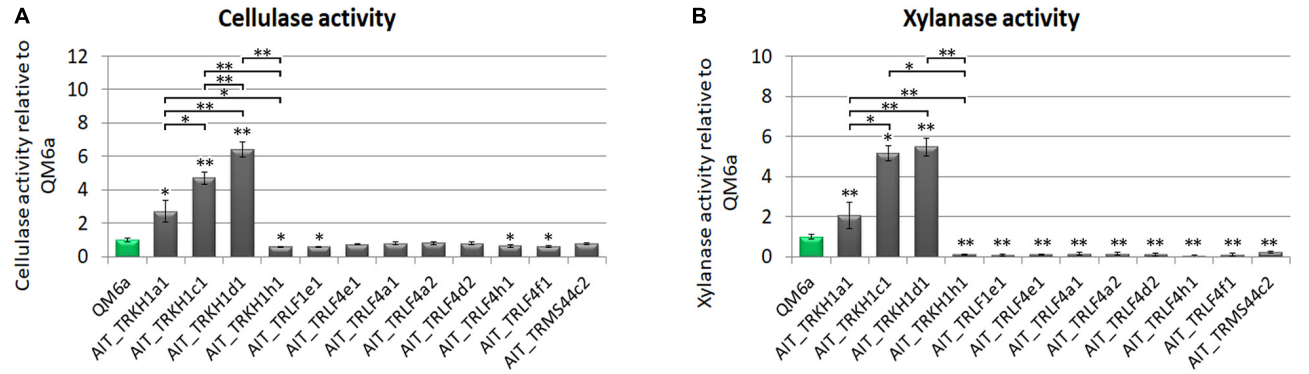

FIGURE 4 | Enzyme production. **(A)** Cellulase activity and **(B)** xylanase activity represented by measurement of reducing sugars as released by enzymes secreted into the culture supernatant relative to wildtype strain QM6a. Strains were grown on Mandels Andreotti minimal medium with 1% (w/v) cellulose as carbon source in constant darkness for 72 h in 24-well plates with shaking. Error bars show standard deviations from three biological replicates. Statistically significant differences to wildtype are indicated by asterisks. Comparisons between individual strains are shown with brackets. *p-value < 0.05, **p-value < 0.01.

Presence of the biosynthetic gene responsible for this process, *noxR* is required for fruiting body formation in *Aspergillus nidulans* (Lara-Ortiz et al., 2003). A function of *nox1* in female fertility and asexual development was reported for *Neurospora crassa* (Cano-Dominguez et al., 2008). Therefore we evaluated whether the varied response in our strains would be due to different gene variants of the NADPH oxidase encoding *nox1* or the regulator gene *noxR* in the strains of this study versus QM6a and CBS999.97.

For *nox1*, sequence analysis showed no alterations between QM6a, CBS999.97 and the 12 new isolates. However, the nucleotide sequences of *noxR* from the new isolates showed only a 98% identity to QM6a, but practically complete similarity with CBS999.97 (**Supplementary File 1**). Testing for SNPs in this sequence, which would alter the protein sequence, we found that despite numerous SNPs at the nucleotide level, the protein sequence remained the same for most strains. Or in other words, all of the SNPs were synonymous.

Interestingly, for one strain, AIT_TRLF4a2, we found alterations in the encoded protein sequence of NoxR in close proximity. In this region, no characteristic domains for NoxR are located. Also no phosphorylation sites were altered. However, testing for PEST regions, which are crucial for protein stability (Rechsteiner and Rogers, 1996) we found a potential PEST motif in QM6a and all other strains (SNAFPPTPPPEND, position 230-244, hydrophobicity index 29.94, and PEST score 8.84). In AIT_TRLF4a2, this sequence (nts marked in green in **Supplementary File 1**) is altered to SNVFPPTPPAEND, which causes a decrease in the PEST score to only 2.79 rendering it now a poor PEST motif. Due to the relevance of such PEST motifs for protein stability (Rechsteiner and Rogers, 1996), NoxR in AIT_TRLF4a2 may be more stable than in other strains. Since the phenotypic differences after injury are not limited to this strain, but are similar in other strains as well, the altered PEST sequence is unlikely to significantly contribute to characteristic injury response in *T. reesei*. Moreover, we also could not find indications that the minor sequence alterations would have an influence on sexual development in these strains.

Previously, the MAPkinase genes *tmk1* and *tmk3* were shown to be required for enhanced sporulation upon injury in *T. atroviride* (Medina-Castellanos et al., 2014). Therefore we analyzed the gene sequences of *tmk1* and *tmk3* for selected strains with different injury types (AIT_TRKHa1, AIT_TRKH1c1, AIT_TRLFe1, and AIT_TRMS44c2) in comparison with QM6a, RUTC30, and CBS999.97 (see **Supplementary Material**). Although these sequences formed groups according to their SNP patterns, they did not correlate with injury types in these strains.

We conclude that the differences in injury response that we observed for our isolates is not due to specifically altered alleles of *nox1, noxR, tmk1*, or *tmk3*.

DISCUSSION

Trichoderma spp. are among the few ascomycetes for which extensive reports on distribution in many areas all over the world are available (Druzhinina et al., 2006; Atanasova et al., 2013). These species are most commonly isolated, which has been attributed to their often mycoparasitic lifestyle and efficient enzyme production, which increase competitiveness in nature (Schuster and Schmoll, 2010; Druzhinina et al., 2011; Atanasova et al., 2013). [Early isolates originate from tropic areas, but detailed research in Europe revealed that the diversity of *Trichoderma/Hypocrea* in Europe consists of at least 75 holomorphic species (Jaklitsch, 2009, 2011) as well as several anamorphic species (Friedl and Druzhinina, 2012) and references therein]. Consequently, *Trichoderma* spp. are a major element of the mycoflora also in temperate regions. Due to their broad distribution, but also because of their efficiency in mycoparasitism and biocontrol of plant pathogens, *Trichoderma* spp. are included in commercial products for plant protection, which are applied in Europe as well. So far, no studies are available with investigations, whether strains applied with commercial biocontrol agents were possibly re-isolated during screening studies.

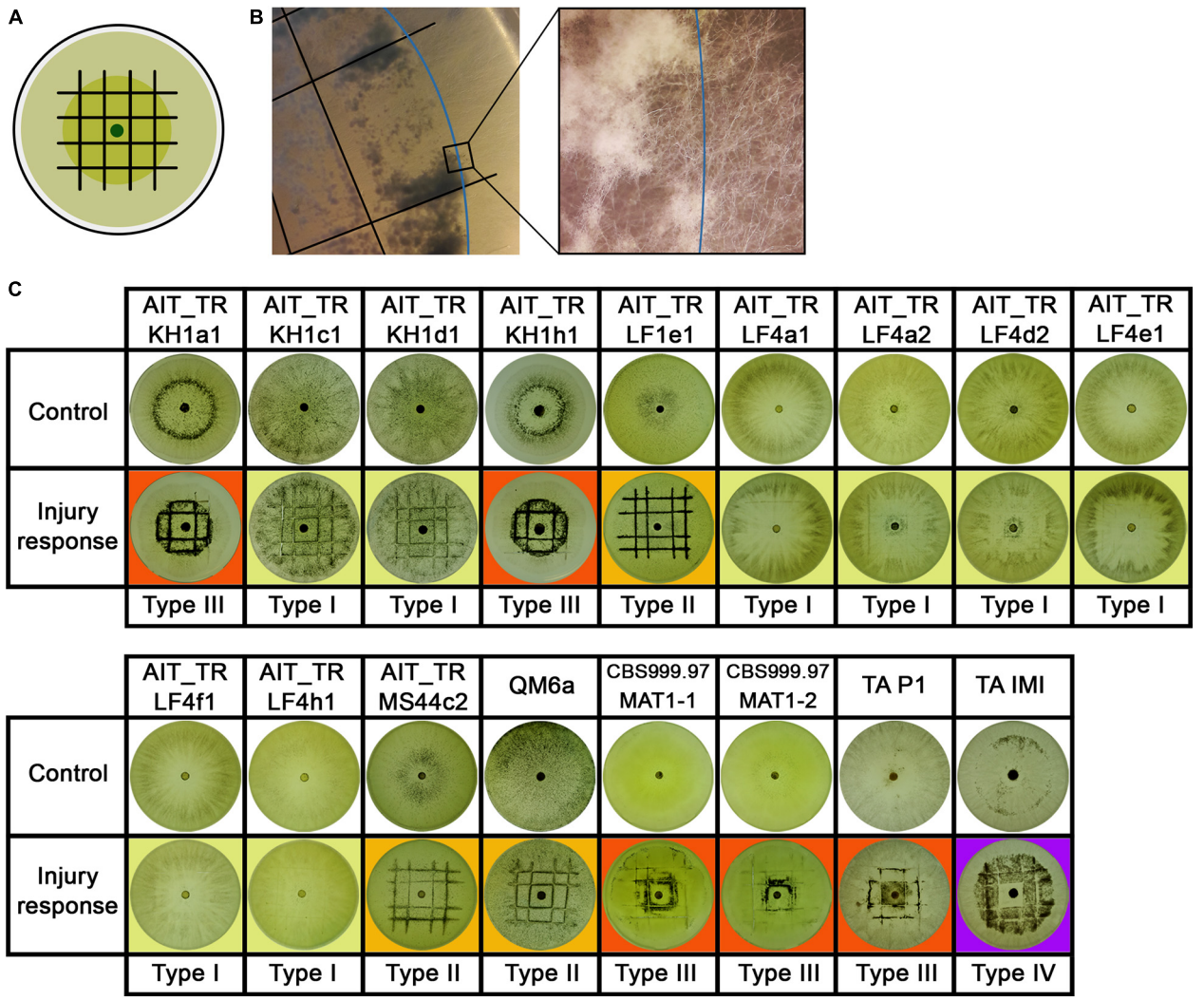

FIGURE 5 | Injury response. **(A)** Illustration of the experimental setup. Strains were inoculated with an agar plug in the center of the petri dish. After 2 days of growth at 28°C in darkness, the mycelium (dark green) was injured under red safety light (black lines). Phenotypic changes of the young and developing (light green) mycelium were monitored 24 h after injury. **(B)** Shows the control strain *T. atroviride* IMI206040 (TA IMI). After injury (black lines) the young mycelium (blue line marks growth margin at timepoint of injury) grew dense, formed aerial mycelium and sporulated. The developing mycelium (right of blue line) shows undifferentiated morphology without sporulation after injury. **(C)** Shows response to injury of the tested strains. Four types of injury responses were observed: *Type 1* (yellow background) strains show slight to no response to injury. Strains of *type 2* (orange background) show clear sporulation close to the injury site. In *type 3* (red background), the young mycelium shows a widespread response to the injury. *Type 4* (purple background), represented only by TA IMI, shows a pattern similar to *type III* but with no sporulation around the inoculum.

Trichoderma reesei only showed poor performance in mycoparasitism and biocontrol (Seidl et al., 2006) and is hence not commercially applied or thereby artificially distributed in nature. Consequently, isolation of *T. reesei* of non-natural origin would be due to an accidental contamination from labs working with this species and subsequent broad distribution, which is extremely unlikely. Actually, strains of *T. reesei* were not previously reported from screening studies in Austria (Wuczkowski et al., 2003; Friedl and Druzhinina, 2012) or in Europe (Jaklitsch, 2009, 2011). Unequivocal determination of species is of high and increasing importance due to the rising numbers of novel and interesting fungal isolates for diverse sources. Phylogenetic analysis using ITS sequences alone is not reliable and reproductive isolation is often difficult to confirm if sexual development cannot be achieved under laboratory conditions (Lücking et al., 2020). The strains we now describe here were confirmed to be *T. reesei* first by molecular methods using two diagnostic markers recommended for species identification, *tef1* and *rpb2* (Lücking et al., 2020) and phylogenetic analysis and second by crossing with known and accepted *T. reesei* strains. Although unisexual reproduction is known from some species and well-studied in *Cryptococcus neoformans* (Ni et al., 2011; Sun et al., 2014) there are no hints that this might occur in *T. reesei* or any other *Trichoderma* species.

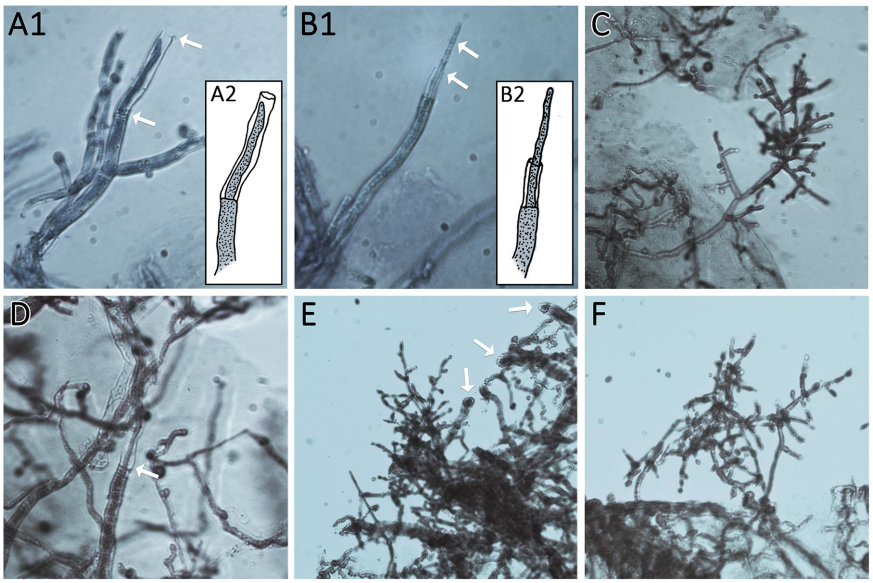

FIGURE 6 | Thin regeneration hyphae and conidiophores emerge at the agar margin as response to previous injury. Edges of cut agar plugs are shown. (**A1,2** and **B1,2**) Show regenerating hyphae of AIT_LF4a1 growing from the last intact septum of the cut hyphae. Arrows mark thin regenerating hyphae and empty cell walls of cut hyphae. **(A2,B2)** Show illustrations of **(A1,B1)** for better visualization. **(C,D)** Show AIT_LF4a2. **(C)** Shows an emerging conidiophore from the agar margin. **(D)** Shows a regenerating hypha growing in the empty cell wall of a cut hypha (arrow). **(E,F)** show AIT_LF4e1 with emerging conidiophores. Arrows in **(E)** point at the cutting sites of hyphae at the agar margin. All images were taken at 400× magnification. Samples were stained with methylene blue solution.

Complex phylogenies and reproductive strategies that render the reproductive mode unreliable for species determination are only known from lichen-associated fungi (Lücking et al., 2020), a case which is not comparable with *Trichoderma* spp. Hence, even if the molecular identification would leave room for interpretation, cross-species sexual development under laboratory conditions yielding fruiting bodies typical for *T. reesei* (Hinterdobler et al., 2020) would be an absolute novelty and can practically be excluded. Consequently, these 12 strains belong to the species *T. reesei*.

The fact that the 12 strains we investigated, originate from four individual samples raised the question whether they might be just re-isolations of one and the same strain from the respective location. Moreover, since *T. reesei* was never found in Europe before, it was important to unequivocally ensure that our screening study did not contain unwanted contaminants from *T. reesei* strains we routinely use in the lab. Also the potential introduction of *T. reesei* by the application of biocontrol products, which may be relevant for other taxonomic studies as outlined above, can rather be excluded for *T. reesei*, since commercial products are only known for the highly efficient *Trichoderma* species like *T. asperellum*, *T. harzianum* etc. UP-PCR and specific mutations clearly showed that no contaminations with lab strains had occurred and that these isolates indeed originated from Austrian agricultural soil. UP-PCR also showed that the isolates from different sites showed clearly different patterns. However, strains from the same site showed very similar patterns. In some cases, we therefore included also enzyme expression, injury response and phenotype in our analyses, which eventually allowed for discrimination between strains (**Figure 2B**). Therefore, we assume that the multiple strains from the separate sites are indeed individuals, albeit closely related, which suggests that sexual development and recombination likely have occurred in the past. This is particularly interesting with the female sterile strains, which are also clearly distinguishable. As they all are of the same mating type, strains of the opposite mating type can also be expected to occur in this habitat and should be female fertile.

Already in the initial study reporting sexual development with *T. reesei* under laboratory conditions (Seidl et al., 2009), the issue of female sterile strains in this species was broached. Early studies with *T. reesei* on the topic came to the conclusion, that it would be an asexually propagating, clonal species (Kuhls et al., 1996). However, the existence and evolutionary survival of exclusively clonal species was questioned (Taylor et al., 1999) and considered a rather transient phenomenon aimed to avoid the efforts to reproduce sexually. Thereby, both sexual and asexual propagation bear costs and benefits for fungi (Nieuwenhuis and James, 2016). The strains we isolated here represent interesting examples for such a strategy. We isolated both female fertile and female sterile strains, suggesting that strategies to avoid the costs of sex are occurring naturally and are unlikely to be associated with climate or a specific habitat. However, previously also loss of female fertility after repeated asexual propagation was reported and this loss was assumed to be genetic rather than epigenetic (Saleh et al., 2012). The emerging female sterile strains then propagated more efficiently via asexual reproduction without investing energy in mating and fruiting body formation and invaded the whole population (Saleh et al., 2012). Consequently, the isolation of female sterile strains could also be due to an

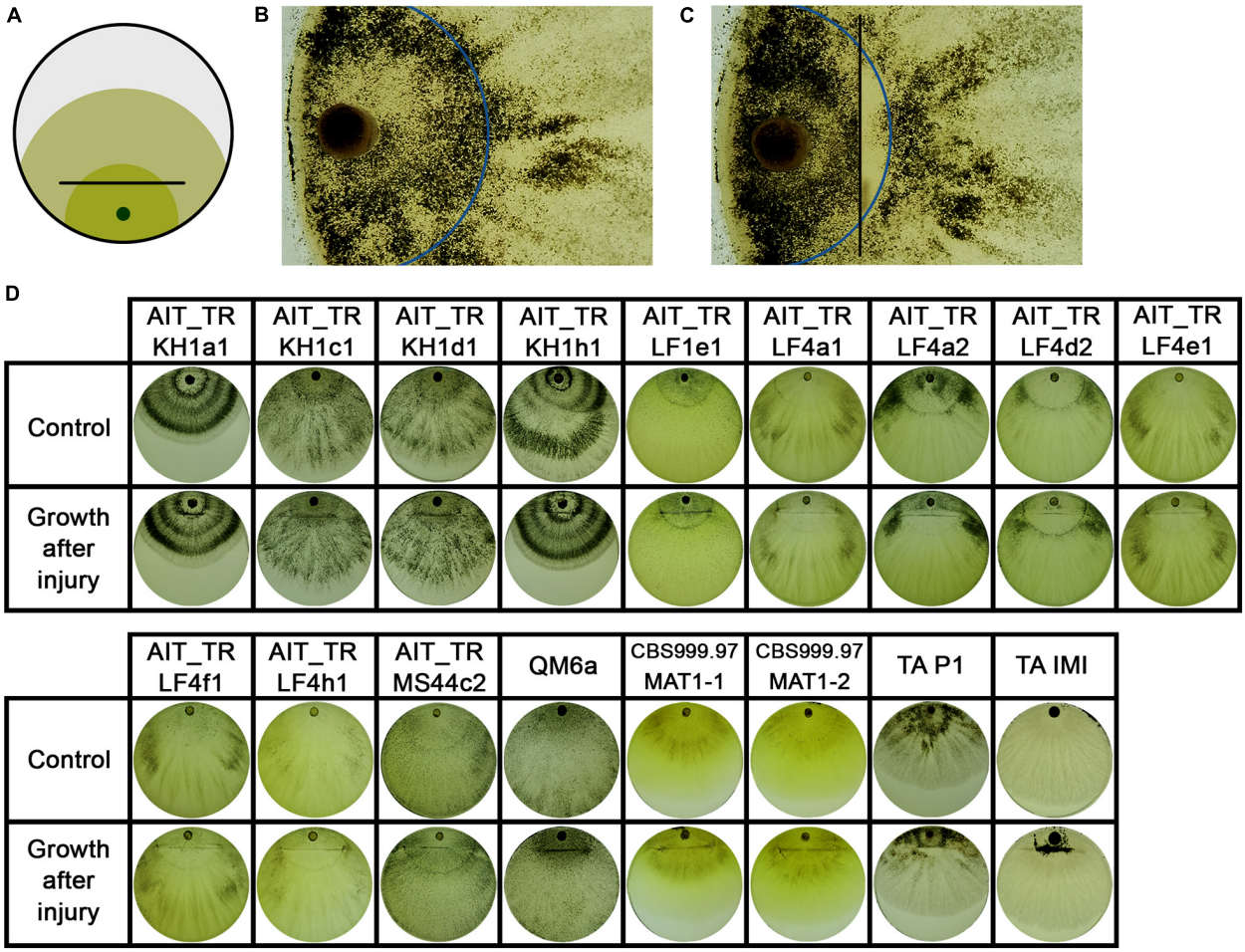

FIGURE 7 | Growth after injury. **(A)** Illustration of the experimental setup. Strains were inoculated with an agar plug close to the border of the petri dish. After 2 days of growth at 28°C in darkness, the mycelium (dark green) was injured by cutting under red safety light (black line). Phenotypic changes were monitored 24 h after injury (light green). **(B, C)** The control strain *T. atroviride* P1 showed different sporulation pattern of the older compared to the younger colony area separated by the injury. Blue line indicates the growth margin at the timepoint of injury. In **(C)** the area between injury (black line) and the colony margin shows less sporulation compared to the old mycelium. **(D)** Shows phenotypic effects of early injury on the developing colonies compared to non-injured controls.

environment in which the conditions for sexual development were not met and female fertility was lost. Thereafter the resulting female sterile strains could have been more successful in colonization of the respective habitat.

The achievement of sexual development under laboratory conditions for *T. reesei* (Seidl et al., 2009) represented already an important innovation in the field of strain improvement. However, initially the application was mainly seen with proprietary industrial strains and in academia for fungal genetics and strain improvement. With the strains we introduce here, a novel opportunity opens up. We can now use natural strains from Europe, which we can improve for their degradative performance without genetic manipulation, which is still seen critically. Particularly with (decentralized) pretreatment for biogas and biofuel production from agricultural cellulosic waste these strains will be a valuable resource. Deposition of waste does then not cause environmental issues with GMO distribution and pretreatment could even be done on site on the field. Moreover, in-process production of enzymes can be supported by natural strain improvement while alleviating environmental issues of waste disposal.

Last but not least, for the broad applications of enzymes in customer products the market pull for non-GMO ingredients is rising, and EU regulations for labeling of GMO use in production processes[4] increase customer awareness. Hence, production without the use of GMO organisms can be an interesting future perspective for the use of natural enzyme producer strains like those introduced in this study. We could already achieve a proof of concept for natural strain improvement by crossing of these strains for enhanced enzyme production (Basyouni-Khamis and Schmoll, unpublished), which supports the applicability of this approach. First steps in this direction were previously reported for *Myceliophthora heterothallica* (Aguilar-Pontes et al., 2016). Besides practical application, we can thereby also follow up which

[4]https://ec.europa.eu/food/plant/gmo/legislation_en

natural mechanisms become enhanced when enzyme production is increased due to natural recombination.

While the use of these strains for improvement of enzyme production is most straight forward with *T. reesei*, also the potential for biocontrol applications should be considered. *Trichoderma* spp. have a long history in safe application in agriculture worldwide and are known as beneficial plant symbionts (Guzman-Guzman et al., 2019). Also *T. reesei* was previously shown to be effective in plant protection (Seidl et al., 2006), albeit with lower performance than known biocontrol agents, which is why it was not used commercially for this purpose so far. Moreover, previously only tropical strains of *T. reesei* were known, which were not assumed to survive in the European climate. Obviously, this assumption has to be revised, since we could isolate *T. reesei* independently from different locations in Austria. Therefore, the possibility to adapt *T. reesei* to antagonism against plant pathogens by sexual development warrants exploration, particularly with respect to oomycetes for which the cellulosic cell wall should be subject to efficient degradation by the potent enzyme machinery of *T. reesei*. First studies with *T. reesei* reference strains against *Pythium ultimum* (Seidl et al., 2006) and *Phytophthora infestans* (Schmoll, unpublished), showed already promising results.

MATERIALS AND METHODS

Strains and Cultivation Conditions

Trichoderma reesei (syn. *H. jecorina*) wildtype strains QM6a [female sterile (Linke et al., 2015; Tisch et al., 2017)], MAT1-2, ATCC 13631; (Martinez et al., 2008), CBS999.97 [female fertile, both mating types; (Lieckfeldt et al., 2000; Seidl et al., 2009)] and QFS69 [female sterile, MAT1-1; (Bazafkan et al., 2015)] were applied as controls and mating partners. Strains were maintained on malt extract agar.

For determination of enzyme production, strains were grown in 24-well plates with 2 mL of Mandels Andreotti minimal medium (Mandels and Andreotti, 1978) with 1% (w/v) microcrystalline cellulose as carbon source for 72 h at 28°C in darkness. Enzyme activity was determined as described previously (Mellitzer et al., 2012) from three biological and tree technical replicates with QM6a as control. Statistical significance was calculated using Student's *t*-Test in RStudio (compare_means, ggpubr v0.3.0). Sexual crossing was performed as described previously (Seidl et al., 2009; Schmoll, 2013). Strains were inoculated in similar distances to enable analysis of delays in fruiting body formation. Differences in growth rates between strains, which could alter the time to fruiting body formation, were negligible. Crossings were performed in three biological replicates and fruiting body formation was monitored daily.

All chemicals mentioned were supplied by Roth Lactan (Karlsruhe, Germany) unless stated otherwise.

Isolation of Strains From Soil

Soil samples in which *T. reesei* strains were detected originated from four different locations in Austria (**Table 1**). One gram of soil was suspended in 10 mL of phosphate buffered saline (PBS) containing 0.1% (w/v) Triton X-100. After homogenization of 50 rpm for 30 min, the suspension was diluted 1:100 and 1:1000 with PBS and 100 μL were applied to malt extract agar (Merck, Darmstadt, Germany) containing 50 mg/L Rose Bengal sodium salt (Sigma, Steinheim, Germany). After incubation at room temperature under daylight conditions, appearing fungal colonies were isolated and subjected to single spore separation to obtain pure cultures. The strains are available for non-commercial academic use.

Nucleic Acid Isolation and Analysis

DNA extraction from young mycelia grown on malt extract agar plates was performed as described previously (Liu et al., 2000). Mating type determination of isolates was performed by PCR as described previously (Seidl et al., 2009). A diagnostic fragment of the genomic region encoding translation elongation factor 1 alpha (*tef1*) was amplified using the primers EF1-728F

TABLE 2 | Oligonucleotides used in this study.

Purpose	Name	Sequence	References
UP-PCR	L45	5′-GTAAAACGACGGCCAGT-3′	Bulat et al., 1998
UP-PCR	3-2	5′-TAAGGGCGGTGCCAGT-3′	Bulat et al., 1998
UP-PCR	AA2M2	5′-CTGCGACCCAGAGCGG-3′	Lübeck et al., 1998
UP-PCR	AS15inv	5′-CATTGCTGGCGAATCGG-3′	Bulat et al., 1998
UP-PCR	L15/AS19	5′-GAGGGTGGCGGCTAG-3′	Lübeck et al., 1998
nox1 amplification	nox1F1	5′-ATCAAGAGGAGGGATTCC-3′	This study
nox1 amplification	nox1R1	5′-TTGAGAGGCATAAAGTCAG-3′	This study
noxR amplicication	noxRF1	5′-AGCGAGAGATTAGGTTAAAG-3′	This study
noxR amplicication	noxRR1	5′-AGGGCAGTAACGTACCTC-3′	This study
tef1 amplification	EF1-728F	5′-CAT CGA GAA GTT CGA GAA GG-3′	Carbone et al., 1999
tef1 amplification	TEF1rev	5′-GCC ATC CTT GGA GAT ACC AGC-3′	Samuels et al., 2002
rpb2 amplifiation	rpb2v3F	5′-CATTTCCCAGACAGAAGGTAG-3′	This study
rpb2 amplification	rpb2v3R	5′-GGAATAGTTGGTGAGGAAGAAA-3′	This study
INDEL/SNP region	MATovF	5′-GTCTCCCCCACAAGTTCTCG-3′	This study
INDEL/SNP region	MATovR	5′-TGATCCACCTGCGTTACGAC-3′	This study

(Carbone et al., 1999) and TEF1 rev (Samuels et al., 2002). Primers for amplification of *rpb1* and the INDEL/SNP containing region were designed based on the genome sequence publicly available at JGI (Martinez et al., 2008; Grigoriev et al., 2014; Li et al., 2017).

Amplification of sequences of *nox1* and *noxR* was performed using primers nox1F1, nox1R1, noxRF1, and noxRR1. For primer sequences see **Table 2**.

Sequences were aligned using MUSCLE and adjusted in MEGA-X [Version 10.0.5, (Kumar et al., 2018)]. Phylogenetic analysis was done using the Maximum Likelihood method and Tamura-Nei model (Tamura and Nei, 1993). Trees with highest log likelihood are shown in **Figure 1** and **Supplementary Figure 1** for *tef1* and *rpb1* marker sequences, respectively. The bootstrap test was carried out with 1,000 replicates (Felsenstein, 1985). Sequences were retrieved from the NCBI nucleotide database for *T. reesei*, *Trichoderma thermophilum* (Qin and Zhuang, 2016), *T. parareesei*, *Trichoderma rugosum*, *Trichoderma beinartii*, *Trichoderma aethiopicum*, *Trichoderma gracile*, *Trichoderma orientale*, *Trichoderma pinnatum*, *T. longibrachiatum*, *Trichoderma Gamsii*, and *T. atroviride*. The diagnostic sequences for *tef1* and *rpb2* of the strains investigated in this study are deposited at GenBank, for accession numbers see **Table 1**.

Analysis of Injury Response

For the injury assays, round agar plugs of well grown cultures were used as inoculum. *T. atroviride* strains P1 (ATCC 74058) and IMI206040 (Kubicek et al., 2011) as well as *T. reesei* strains CBS999.97 (MAT1-2 and MAT1-1) and QM6a (Martinez et al., 2008) were used as control. For both assays, 90 mm petri dishes containing 3% (w/v) malt extract medium were used. Strains were grown in constant darkness at 28°C for two days, injured as shown in **Figures 5A**, 7A under red safety light. Consequences of injury were documented and analyzed 24 hours after injury. Three biological replicates were performed.

UP-PCR Fingerprinting

For PCR using UP-PCR, DNA was isolated using the DNAeasy plant mini kit (QIAGEN, Heidelberg, Germany). UP-PCR was performed essentially as described earlier (Naeimi et al., 2011). Primers were tested individually and in combinations using gradient PCR with annealing temperatures ranging from 50–65°C. AS15inv, L45, 3-2 and a combination of L15/AS19 showed best results and were used for PCR amplification with DreamTaq Green Polymerase (ThermoFisher Scientific, Waltham, MA, United States).

DATA AVAILABILITY STATEMENT

All datasets relevant for this study are included in the article/**Supplementary Material**. Sequence information is available either online under the provided GenBank accession numbers or in supplementary material as noted in the text.

AUTHOR CONTRIBUTIONS

WH contributed to injury analysis, analysis of phenotype, and sexual development, phylogenetic analyses, statistical evaluations, and MAPkinase analysis as well as to figure design, interpretation, and writing of the manuscript. GL isolated and identified strains, and contributed experimental work for UP-PCR analysis, injury analysis, and amplification of *nox1* and *noxR* sequences. KS performed analysis of sexual development. SB-K performed analysis of enzyme production. MG performed analysis of *nox1* and *noxR* sequences. MS conceived of the study and designed experiments, contributed to analysis of *nox1*, *noxR*, and MAPkinase sequences, to figure design, interpreted results, and wrote the manuscript. All authors read and agreed to publication of the final manuscript.

FUNDING

WH was supported by the NFB (Science Fund of Lower Austria; grant LC16-04 to MS). Work of GL was supported by the Austrian Science Fund (FWF; projects P26935). KS was supported by a fellowship of the Austrian research promotion agency (FFG; FEM-tech fellowship for female talents). SB-K was supported by the FFG, the Austrian Research Promotion Agency (e!MISSION project 848780 to MS).

ACKNOWLEDGMENTS

We are grateful to Christina Paiato, Ida Aglaia Gisella Scalmani, and Sabrina Beier for technical assistance.

SUPPLEMENTARY MATERIAL

The Supplementary Material for this article can be found online at: https://www.frontiersin.org/articles/10.3389/fmicb.2021.552301/full#supplementary-material

REFERENCES

Aguilar-Pontes, M. V., Zhou, M., van der Horst, S., Theelen, B., de Vries, R. P., and van den Brink, J. (2016). Sexual crossing of thermophilic fungus *Myceliophthora heterothallica* improved enzymatic degradation of sugar beet pulp. *Biotechnol. Biofuels* 9:41. doi: 10.1186/s13068-016-0460-y

Aguirre, J., Rios-Momberg, M., Hewitt, D., and Hansberg, W. (2005). Reactive oxygen species and development in microbial eukaryotes. *Trends Microbiol.* 13, 111–118. doi: 10.1016/j.tim.2005.01.007

Arnau, J., Yaver, D., and Hjort, M. C. (2020). "Strategies and challenges for the development of industrial enzymes using fungal cell factories," in *Grand challenges in Fungal Biotechnology*, ed. H. Nevalainen (Cham: Springer Nature Switzerland AG), 179–210. doi: 10.1007/978-3-030-29541-7_7

Ashton, G. D., and Dyer, P. (2016). "Sexual development in fungi and its uses in gene expression systems," in *Gene Expression Systems in Fungi: Advancements and Applications*, eds M. Schmoll and C. Dattenböck (Cham: Springer International Publishing), 335–350. doi: 10.1007/978-3-319-27951-0_15

Atanasova, L., Druzhinina, I., and Jaklitsch, W. M. (2013). "Two hundred *Trichoderma* species recognized on the basis of molecular phylogeny," in *Trichoderma – Biology and Applications*, eds P. K. Mukherjee, B. A. Horwitz, U. S. Singh, M. Mukherjee, and M. Schmoll (Wallingford: CAB International), 10–42. doi: 10.1079/9781780642475.0010

Bazafkan, H., Dattenböck, C., Böhmdorfer, S., Tisch, D., Stappler, E., and Schmoll, M. (2015). Mating type dependent partner sensing as mediated by VEL1 in *Trichoderma reesei*. *Mol. Microbiol.* 96, 1103–1118. doi: 10.1111/mmi.12993

Bischof, R. H., Ramoni, J., and Seiboth, B. (2016). Cellulases and beyond: the first 70 years of the enzyme producer *Trichoderma reesei*. *Microb. Cell. Fact* 15:106. doi: 10.1186/s12934-016-0507-6

Bissett, J., Gams, W., Jaklitsch, W., and Samuels, G. J. (2015). Accepted *Trichoderma* names in the year 2015. *IMA Fungus* 6, 263–295. doi: 10.5598/imafungus.2015.06.02.02

Bulat, S. A., Lübeck, M., Mironenko, N. V., Jensen, D. F., and Lübeck, P. S. (1998). UP-PCR analysis and ITS1 ribotyping of *Trichoderma* and *Gliocladium* fungi. *Mycol. Res.* 102, 933–943. doi: 10.1017/s0953756297005686

Cano-Dominguez, N., Alvarez-Delfin, K., Hansberg, W., and Aguirre, J. (2008). NADPH oxidases NOX-1 and NOX-2 require the regulatory subunit NOR-1 to control cell differentiation and growth in *Neurospora crassa*. *Eukaryot Cell* 7, 1352–1361. doi: 10.1128/EC.00137-08

Carbone, I., Anderson, J. B., and Kohn, L. M. (1999). Patterns of descent in clonal lineages and their multilocus fingerprints are resolved with combined gene genealogies. *Evolution* 53, 11–21. doi: 10.1111/j.1558-5646.1999.tb05329.x

Casas-Flores, S., Rios-Momberg, M., Bibbins, M., Ponce-Noyola, P., and Herrera-Estrella, A. (2004). BLR-1 and BLR-2, key regulatory elements of photoconidiation and mycelial growth in *Trichoderma atroviride*. *Microbiology* 150(Pt 11), 3561–3569. doi: 10.1099/mic.0.27346-0

Chaverri, P., Castlebury, L. A., Overton, B. E., and Samuels, G. J. (2003). *Hypocrea/Trichoderma:* species with conidiophore elongations and green conidia. *Mycologia* 95, 1100–1140. doi: 10.1080/15572536.2004.11833023

Chum, P. Y., Schmidt, G., Saloheimo, M., and Landowski, C. P. (2017). Transient silencing of DNA repair genes improves targeted gene integration in the filamentous fungus *Trichoderma reesei*. *Appl. Environ. Microbiol.* 83:e00535-17. doi: 10.1128/AEM.00535-17

Druzhinina, I. S., Komon-Zelazowska, M., Ismaiel, A., Jaklitsch, W., Mullaw, T., Samuels, G. J., et al. (2012). Molecular phylogeny and species delimitation in the section Longibrachiatum of *Trichoderma*. *Fungal. Genet. Biol.* 49, 358–368. doi: 10.1016/j.fgb.2012.02.004

Druzhinina, I. S., Kopchinskiy, A. G., and Kubicek, C. P. (2006). The first 100 *Trichoderma* species characterized by molecular data. *Mycoscience* 47, 55–64. doi: 10.1007/s10267-006-0279-7

Druzhinina, I. S., Kopchinskiy, A. G., Kubicek, E. M., and Kubicek, C. P. (2016). A complete annotation of the chromosomes of the cellulase producer *Trichoderma reesei* provides insights in gene clusters, their expression and reveals genes required for fitness. *Biotechnol. Biofuels* 9:75. doi: 10.1186/s13068-016-0488-z

Druzhinina, I. S., Seidl-Seiboth, V., Herrera-Estrella, A., Horwitz, B. A., Kenerley, C. M., Monte, E., et al. (2011). *Trichoderma*: the genomics of opportunistic success. *Nat. Rev. Microbiol.* 9, 749–759. doi: 10.1038/nrmicro2637

Felsenstein, J. (1985). Confidence limits on phylogenies: an approach using the bootstrap. *Evolution* 39, 783–791. doi: 10.2307/2408678

Friedl, M. A., and Druzhinina, I. S. (2012). Taxon-specific metagenomics of *Trichoderma* reveals a narrow community of opportunistic species that regulate each other's development. *Microbiology* 158(Pt 1), 69–83. doi: 10.1099/mic.0.052555-0

Friedl, M. A., Kubicek, C. P., and Druzhinina, I. S. (2008). Carbon source dependence and photostimulation of conidiation in *Hypocrea atroviridis*. *Appl. Environ. Microbiol.* 74, 245–250. doi: 10.1128/aem.02068-07

Grigoriev, I. V., Nikitin, R., Haridas, S., Kuo, A., Ohm, R., Otillar, R., et al. (2014). MycoCosm portal: gearing up for 1000 fungal genomes. *Nucleic Acids Res.* 42, D699–D704. doi: 10.1093/nar/gkt1183

Gudynaite-Savitch, L., and White, T. C. (2016). "Fungal biotechnology for industrial enzyme production: focus on (hemi)cellulase production strategies, advances and challenges," in *Gene Expression Systems in Fungi: Advancements and Applications*, eds M. Schmoll and C. Dattenböck (Cham: Springer International Publishing Switzerland), 395–435. doi: 10.1007/978-3-319-27951-0_19

Guzman-Guzman, P., Porras-Troncoso, M. D., Olmedo-Monfil, V., and Herrera-Estrella, A. (2019). *Trichoderma* species: versatile plant symbionts. *Phytopathology* 109, 6–16. doi: 10.1094/PHYTO-07-18-0218-RVW

Harman, G. E. (2011). Multifunctional fungal plant symbionts: new tools to enhance plant growth and productivity. *New Phytol.* 189, 647–649. doi: 10.1111/j.1469-8137.2010.03614.x

Harman, G. E., Howell, C. R., Viterbo, A., Chet, I., and Lorito, M. (2004). *Trichoderma* species–opportunistic, avirulent plant symbionts. *Nat. Rev. Microbiol.* 2, 43–56. doi: 10.1038/nrmicro797

Hatvani, L., Manczinger, L., Vagvölgyi, C., and Kredics, L. (2013). "*Trichoderma* as a human pathogen," in *Trichoderma – Biology and Applications*, eds P. K. Mukherjee, B. A. Horwitz, U. S. Singh, M. Mukherjee, and M. Schmoll (Wallingford: CAB International), 202–313.

Hernandez-Oñate, M. A., Esquivel-Naranjo, E. U., Mendoza-Mendoza, A., Stewart, A., and Herrera-Estrella, A. H. (2012). An injury-response mechanism conserved across kingdoms determines entry of the fungus *Trichoderma atroviride* into development. *Proc. Natl. Acad. Sci. U.S.A.* 109, 14918–14923. doi: 10.1073/pnas.1209396109

Hinterdobler, W., Beier, S. S. K., and Schmoll, M. (2020). "Sexual development, its determinants and regulation in *Trichoderma reesei*," in *Recent Developments in Trichoderma Research*, eds S. Zeilinger, I. Druzhinina, H. B. Singh, and V. K. Gupta (Amsterdam: Elsevier), 185–206. doi: 10.1016/b978-0-12-819453-9.00009-x

Jaklitsch, W. M. (2009). European species of *Hypocrea* Part I. The green-spored species. *Stud. Mycol.* 63, 1–91. doi: 10.3114/sim.2009.63.01

Jaklitsch, W. M. (2011). European species of *Hypocrea* part II: species with hyaline ascospores. *Fungal Divers.* 48, 1–250. doi: 10.1007/s13225-011-0088-y

Jaklitsch, W. M., Gruber, S., and Voglmayr, H. (2008). *Hypocrea seppoi*, a new stipitate species from Finland. *Karstenia* 48, 1–11. doi: 10.29203/ka.2008.423

Jaklitsch, W. M., and Voglmayr, H. (2015). Biodiversity of *Trichoderma* (Hypocreaceae) in Southern Europe and Macaronesia. *Stud. Mycol.* 80, 1–87. doi: 10.1016/j.simyco.2014.11.001

Komon-Zelazowska, M., Neuhof, T., Dieckmann, R., von Dohren, H., Herrera-Estrella, A., Kubicek, C. P., et al. (2007). Formation of atroviridin by *Hypocrea atroviridis* is conidiation associated and positively regulated by blue light and the G protein GNA3. *Eukaryot Cell* 6, 2332–2342. doi: 10.1128/ec.00143-07

Kubicek, C. P., Herrera-Estrella, A., Seidl-Seiboth, V., Martinez, D. A., Druzhinina, I. S., Thon, M., et al. (2011). Comparative genome sequence analysis underscores mycoparasitism as the ancestral life style of *Trichoderma*. *Genome Biol.* 12:R40. doi: 10.1186/gb-2011-12-4-r40

Kuhls, K., Lieckfeldt, E., Samuels, G. J., Kovacs, W., Meyer, W., Petrini, O., et al. (1996). Molecular evidence that the asexual industrial fungus *Trichoderma reesei* is a clonal derivative of the ascomycete *Hypocrea jecorina*. *Proc. Natl. Acad. Sci. U.S.A.* 93, 7755–7760. doi: 10.1073/pnas.93.15.7755

Kumar, S., Stecher, G., Li, M., Knyaz, C., and Tamura, K. (2018). MEGA X: molecular evolutionary genetics analysis across computing platforms. *Mol. Biol. Evol.* 35, 1547–1549. doi: 10.1093/molbev/msy096

Lara-Ortiz, T., Riveros-Rosas, H., and Aguirre, J. (2003). Reactive oxygen species generated by microbial NADPH oxidase NoxA regulate sexual development in *Aspergillus nidulans*. *Mol. Microbiol.* 50, 1241–1255. doi: 10.1046/j.1365-2958.2003.03800.x

Lee, S. C., Ni, M., Li, W., Shertz, C., and Heitman, J. (2010). The evolution of sex: a perspective from the fungal kingdom. *Microbiol. Mol. Biol. Rev.* 74, 298–340. doi: 10.1128/MMBR.00005-10

Li, W. C., Huang, C. H., Chen, C. L., Chuang, Y. C., Tung, S. Y., and Wang, T. F. (2017). *Trichoderma reesei* complete genome sequence, repeat-induced point mutation, and partitioning of CAZyme gene clusters. *Biotechnol. Biofuels* 10:170. doi: 10.1186/s13068-017-0825-x

Lieckfeldt, E., Kullnig, C. M., Samuels, G. J., and Kubicek, C. P. (2000). Sexually competent, sucrose- and nitrate-assimilating strains of *Hypocrea jecorina* (*Trichoderma reesei*) from South American soils. *Mycologia* 92, 374–380. doi: 10.2307/3761493

Linke, R., Thallinger, G. G., Haarmann, T., Eidner, J., Schreiter, M., Lorenz, P., et al. (2015). Restoration of female fertility in *Trichoderma reesei* QM6a provides the basis for inbreeding in this industrial cellulase producing fungus. *Biotechnol. Biofuels* 8:155. doi: 10.1186/s13068-015-0311-2

Liu, D., Coloe, S., Baird, R., and Pederson, J. (2000). Rapid mini-preparation of fungal DNA for PCR. *J. Clin. Microbiol.* 38:471.

Liu, R., Chen, L., Jiang, Y., Zhou, Z., and Zou, G. (2015). Efficient genome editing in filamentous fungus *Trichoderma reesei* using the CRISPR/Cas9 system. *Cell Discov.* 1:15007. doi: 10.1038/celldisc.2015.7

Lübeck, P. S., Alekhina, I. A., Lübeck, M., and Bulat, S. A. (1998). UP-PCR genotyping and rDNA analysis of *Asochyta pisi* Lib. *J. Phytopathol.* 148, 109–115. doi: 10.1046/j.1439-0434.2000.00467.x

Lücking, R., Aime, M. C., Robbertse, B., Miller, A. N., Ariyawansa, H. A., Aoki, T., et al. (2020). Unambiguous identification of fungi: where do we stand and how accurate and precise is fungal DNA barcoding? *IMA Fungus* 11. doi: 10.1186/s43008-020-00033-z

Mandels, M., and Andreotti, R. (1978). Problems and challenges in the cellulose to cellulase fermentation. *Proc. Biochem.* 13, 6–13.

Marie-Nelly, H., Marbouty, M., Cournac, A., Flot, J. F., Liti, G., Parodi, D. P., et al. (2014). High-quality genome (re)assembly using chromosomal contact data. *Nat. Commun.* 5:5695. doi: 10.1038/ncomms6695

Martinez, D., Berka, R. M., Henrissat, B., Saloheimo, M., Arvas, M., Baker, S. E., et al. (2008). Genome sequencing and analysis of the biomass-degrading fungus *Trichoderma reesei* (syn. *Hypocrea jecorina*). *Nat. Biotechnol.* 26, 553–560.

Medina-Castellanos, E., Esquivel-Naranjo, E. U., Heil, M., and Herrera-Estrella, A. (2014). Extracellular ATP activates MAPK and ROS signaling during injury response in the fungus *Trichoderma atroviride*. *Front. Plant Sci.* 5:659. doi: 10.3389/fpls.2014.00659

Mellitzer, A., Glieder, A., Weis, R., Reisinger, C., and Flicker, K. (2012). Sensitive high-throughput screening for the detection of reducing sugars. *Biotechnol. J.* 7, 155–162. doi: 10.1002/biot.201100001

Naeimi, S., Kocsube, S., Antal, Z., Okhovvat, S. M., Javan-Nikkhah, M., Vagvolgyi, C., et al. (2011). Strain-specific SCAR markers for the detection of *Trichoderma harzianum* AS12-2, a biological control agent against *Rhizoctonia solani*, the causal agent of rice sheath blight. *Acta Biol. Hung* 62, 73–84. doi: 10.1556/ABiol.61.2011.1.8

Ni, M., Feretzaki, M., Sun, S., Wang, X., and Heitman, J. (2011). Sex in fungi. *Annu. Rev. Genet.* 45, 405–430. doi: 10.1146/annurev-genet-110410-132536

Nieuwenhuis, B. P., and James, T. Y. (2016). The frequency of sex in fungi. *Philos. Trans. R. Soc. Lond. B Biol. Sci.* 371:20150540. doi: 10.1098/rstb.2015.0540

Paloheimo, M., Haarmann, T., Mäkinen, S., and Vehmaanperä, J. (2016). "Production of industrial enzymes in *Trichoderma reesei*," in *Gene Expression Systems in Fungi: Advancements and Applications*, eds M. Schmoll and C. Dattenböck (Heidelberg: Springer International), 23–58. doi: 10.1007/978-3-319-27951-0_2

Qin, W., and Zhuang, W. (2016). Four species of *Trichoderma* with hyaline ascospores from central China. *Mycol. Prog.* 15, 811–815. doi: 10.1007/s11557-016-1211-y

Rechsteiner, M., and Rogers, S. W. (1996). PEST sequences and regulation by proteolysis. *Trends Biochem. Sci.* 21, 267–271. doi: 10.1016/s0968-0004(96)10031-1

Saleh, D., Milazzo, J., Adreit, H., Tharreau, D., and Fournier, E. (2012). Asexual reproduction induces a rapid and permanent loss of sexual reproduction capacity in the rice fungal pathogen *Magnaporthe oryzae*: results of in vitro experimental evolution assays. *BMC Evol. Biol.* 12:42. doi: 10.1186/1471-2148-12-42

Samuels, G. J., Dodd, S. L., Gams, W., Castlebury, L. A., and Petrini, O. (2002). Trichoderma species associated with the green mold epidemic of commercially grown *Agaricus bisporus*. *Mycologia* 94, 146–170. doi: 10.2307/3761854

Schmoll, M. (2013). "Sexual development in *Trichoderma* – scrutinizing the aspired phenomenon," in *Trichoderma: Biology and Applications*, eds P. K. Mukherjee, B. A. Horwitz, U. S. Singh, M. Mukherjee, and M. Schmoll (Wallingford: CAB International), 67–86. doi: 10.1079/9781780642475.0067

Schmoll, M., Dattenböck, C., Carreras-Villasenor, N., Mendoza-Mendoza, A., Tisch, D., Aleman, M. I., et al. (2016). The genomes of three uneven siblings: footprints of the lifestyles of three *Trichoderma* species. *Microbiol. Mol. Biol. Rev.* 80, 205–327. doi: 10.1128/MMBR.00040-15

Schmoll, M., Seibel, C., Tisch, D., Dorrer, M., and Kubicek, C. P. (2010). A novel class of peptide pheromone precursors in ascomycetous fungi. *Mol. Microbiol.* 77, 1483–1501. doi: 10.1111/j.1365-2958.2010.07295.x

Schmoll, M., Seiboth, B., Druzhinina, I., and Kubicek, C. P. (2014). "Genomics analysis of biocontrol species and industrial enzyme producers from the genus *Trichoderma*," in *The Mycota XIII*, eds K. Esser and M. Nowrousian (Berlin: Springer), 233–266. doi: 10.1007/978-3-642-45218-5_10

Schmoll, M., Zeilinger, S., Mach, R. L., and Kubicek, C. P. (2004). Cloning of genes expressed early during cellulase induction in *Hypocrea jecorina* by a rapid subtraction hybridization approach. *Fungal Genet. Biol.* 41, 877–887. doi: 10.1016/j.fgb.2004.06.002

Schuster, A., Bruno, K. S., Collett, J. R., Baker, S. E., Seiboth, B., Kubicek, C. P., et al. (2012). A versatile toolkit for high throughput functional genomics with *Trichoderma reesei*. *Biotechnol. Biofuels* 5:1. doi: 10.1186/1754-6834-5-1

Schuster, A., and Schmoll, M. (2010). Biology and biotechnology of *Trichoderma*. *Appl. Microbiol. Biotechnol.* 87, 787–799. doi: 10.1007/s00253-010-2632-1

Seibel, C., Tisch, D., Kubicek, C. P., and Schmoll, M. (2012). The role of pheromone receptors for communication and mating in *Hypocrea jecorina* (*Trichoderma reesei*). *Fungal Genet. Biol.* 49, 814–824. doi: 10.1016/j.fgb.2012.07.004

Seiboth, B., Ivanova, C., and Seidl-Seiboth, V. (2011). "*Trichoderma reesei*: a fungal enzyme producer for cellulosic biofuels," in *Biofuel Production – Recent Developments and Prospects*, ed. M. A. dos Santos Bernardes (Rijeka: Intech), 309–340.

Seidl, V., Schmoll, M., Scherm, B., Balmas, V., Seiboth, B., Migheli, Q., et al. (2006). Antagonism of *Pythium* blight of zucchini by *Hypocrea jecorina* does not require cellulase gene expression but is improved by carbon catabolite derepression. *FEMS Microbiol. Lett.* 257, 145–151. doi: 10.1111/j.1574-6968.2006.00157.x

Seidl, V., Seibel, C., Kubicek, C. P., and Schmoll, M. (2009). Sexual development in the industrial workhorse *Trichoderma reesei*. *Proc. Natl. Acad. Sci. U.S.A.* 106, 13909–13914. doi: 10.1073/pnas.0904936106

Steyaert, J. M., Weld, R. J., and Stewart, A. (2010a). Ambient pH intrinsically influences *Trichoderma* conidiation and colony morphology. *Fungal Biol.* 114, 198–208. doi: 10.1016/j.funbio.2009.12.004

Steyaert, J. M., Weld, R. J., and Stewart, A. (2010b). Isolate-specific conidiation in *Trichoderma* in response to different nitrogen sources. *Fungal Biol.* 114, 179–188. doi: 10.1016/j.funbio.2009.12.002

Sun, S., Billmyre, R. B., Mieczkowski, P. A., and Heitman, J. (2014). Unisexual reproduction drives meiotic recombination and phenotypic and karyotypic plasticity in *Cryptococcus neoformans*. *PLoS Genet.* 10:e1004849. doi: 10.1371/journal.pgen.1004849

Tamura, K., and Nei, M. (1993). Estimation of the number of nucleotide substitutions in the control region of mitochondrial DNA in humans and chimpanzees. *Mol. Biol. Evol.* 10, 512–526. doi: 10.1093/oxfordjournals.molbev.a040023

Taylor, J., Jacobson, D., and Fisher, M. (1999). The evolution of asexual fungi: reproduction, speciation and classification. *Annu. Rev. Phytopathol.* 37, 197–246.

Tisch, D., Pomraning, K. R., Collett, J. R., Freitag, M., Baker, S. E., Chen, C. L., et al. (2017). Omics Analyses of *Trichoderma reesei* CBS999.97 and QM6a indicate the relevance of female fertility to carbohydrate-active enzyme and transporter levels. *Appl. Environ. Microbiol.* 83:e01578–17. doi: 10.1128/AEM.01578-17

Wuczkowski, M., Druzhinina, I., Gherbawy, Y., Klug, B., Prillinger, H., and Kubicek, C. P. (2003). Species pattern and genetic diversity of *Trichoderma* in a mid-European, primeval floodplain-forest. *Microbiol. Res.* 158, 125–133. doi: 10.1078/0944-5013-00193

Conflict of Interest: The authors declare that the research was conducted in the absence of any commercial or financial relationships that could be construed as a potential conflict of interest.

Frontiers in Microbiology

Explores the habitable world and the potential of microbial life

The largest and most cited microbiology journal which advances our understanding of the role microbes play in addressing global challenges such as healthcare, food security, and climate change.

Discover the latest Research Topics

See more →

Frontiers

Avenue du Tribunal-Fédéral 34
1005 Lausanne, Switzerland
frontiersin.org

Contact us

+41 (0)21 510 17 00
frontiersin.org/about/contact